UNIVERSITY OF HULL

Modelling the Morphodynamics of Sandy Coastal Systems under a Changing Climate

By

Chloe Sarah Morris

BSc (*Hons*), University of Chester

A THESIS SUBMITTED FOR THE DEGREE OF DOCTOR OF PHILOSOPHY (PHD) IN THE UNIVERSITY OF HULL

March 2019

Abstract

Coasts are vulnerable to changing environmental conditions and are likely to be affected by predicted sea level rise and wave climate variations over the next century. Predicting the likely response of coastal systems to these changes, including altering erosional patterns and flood potentials, is complex and involves understanding their morphodynamics and key sensitivities. Whilst numerical models can be powerful tools for the exploration and prediction of environmental behaviours, mesoscale coastal models tend towards one-line approaches that are unable to simulate the combined effects of wave action and sea level rise (e.g. COVE and CEM).

In this thesis the development and application of a new two-dimensional numerical model is presented, designed to simulate coastal morphodynamics at the mesoscale to a higher resolution than afforded by existing models of its kind. The Coastline Evolution Model 2D (CEM2D) has been built upon the core principles of the one-line Coastline Evolution Model but with increased complexity in the domain structure and representation of sediment transport processes. CEM2D has shown to simulate fundamental cause-effect relationships in coastal environments and demonstrated its ability to evolve key shoreline shapes

according wave-driven sediment transport processes (including cuspate headlands, sand waves and spits). The results of the modelling exercises reinforce the theory of high angle wave instability and compare well to the planform morphology of natural coastal environments worldwide, including the Carolina Capes (USA) and Spurn Point Spit (UK).

Insightful dynamics are observed in the evolution of the simulated coastal environments when subject to sea level rise. Coastal landforms show a varying ability to keep pace with rates of rise at 1 m and 2 m per 100 years, representative of relatively extreme values of change over the coming century. The results suggest that there is a sensitive balance between the wave energy delivered to the shoreline, the balance of cross- and longshore sediment transport, the sediment budget and the level of geomorphic activity that occurs in the systems. These factors determine whether the shoreline erodes, landforms are submerged or progradation occurs and whether remnant morphologies can be preserved in the bathymetric profile. Whilst it is observed that sea level rise plays a significant role in coastal evolution, the wave climate conditions remain the principal agent in defining their planform morphology.

Acknowledgements

Of all the words written in this thesis, it is hard to find the right ones to thank all those who have supported me throughout this journey. There have been many people who have influenced me and helped me along the way. For each and everyone one, I am grateful.

To my supervisors Tom Coulthard, Dan Parsons, Andy Barkwith and Sue Manson. Thank you for all your guidance and for the hours you spent sharing your expertise. Tom, thank you for helping me to explore who I am a researcher and for giving me the freedom and encouragement to develop my ideas, whilst making sure that I stayed on track. I would also like to gratefully acknowledge the support of my funders including the University of Hull, The Environment Agency and the British Geological Survey.

To my friends. Thank you for all the cakes, coffees, tears and beers! I am so very grateful to have been surrounded and supported by you all.

To my family. Thank you for always supporting me and continually encouraging me along the way. I always knew you were just a phone call or a car ride away and if I needed it, you would be there with bells, whistles and a bag full of goodies to keep me going.

Thank you to Adam. Thank you for your unfading faith in me and your continual encouragement and support in all that I do. In your very own words, which I cannot argue with, your emotional support has been a full-time job that has required your skills as a comedian, editor in chief, domestic goddess, sandwich maker, tea maker and chef – and that is just a small sample of what you have done for me throughout this PhD.

Table of Contents

Table of Figures

Chapter 4

Chapter 5

Chapter 6

Chapter 7

Chapter 8

Table of Tables

Chapter 6

Chapter 7

Chapter 8

Table of Equations

Chapter 1

A General Introduction

1.1 Introduction

Coastal systems are amongst the most dynamic environments on the planet, with their form and behaviour being highly sensitive to changes in environmental conditions, over a range of spatial and temporal scales (Wong *et al.*, 2015). It is predicted that climate change is likely to cause large-scale, long-term changes to to the evolution of coastal systems through sea level rise, variations in wave climate conditions and intensified storm activity (IPCC, 2013a). These processes can alter energies in the coastal environment and the level of geomorphic activity that occurs.

The Fifth Assessment Report of the Intergovernmental Panel on Climate Change (IPCC) states that globally, coastal beaches have experienced net erosion during the last century (Solomon *et al.*, 2007; IPCC, 2013a). It is suggested that this has been caused by increased rates of erosion and submergence that is attributed to a rising sea level. Sea level is predicted to continue rising, with global projections

of between 0.28-0.98 m by 2100: this has the potential to alter shoreline evolution and lead to an increased risk of erosion and flooding in vulnerable localities (IPCC, 2013a). Considering the increasing social and economic importance of coasts, with over 40% of the world's population living in these environments (Bird, 2011; Ranasinghe, 2016), understanding their behaviour and potential future evolution is essential for the development of suitable and sustainable management (Wong *et al.*, 2015).

Whilst we know that coasts are sensitive to environmental change, research into their evolution over the mesoscale (10's to 100's km and 10's to 100's years) and predictions of the influence of sea level rise is relatively limited in the literature, as will become apparent in Chapter 2. However, numerical models are increasingly being used for understanding and predicting the behaviour of coastal systems, providing powerful tools that can give an insight into their complex morphodynamics and sensitivities (e.g. Ashton *et al.*, 2001; Nam *et al.*, 2009; Nicholls *et al.*, 2012). Nevertheless, many of these existing models are unable to simulate the effects of climate change, such as sea level rise, due to their one-dimensional nature. Mesoscale models are also still in their infancy since modelling processes at this scale presents many challenges relating to the parameterisation of key processes (Murray, 2007). Not all processes can be simulated since each adds an element of uncertainty and computational expense, which can be multiplied over long simulated timescales.

In this thesis, the development and application of the Coastline Evolution Model 2D (CEM2D) is presented which provides a step forward in the field of coastal geomorphology and modelling. CEM2D has been developed according to the underlying assumptions and mathematical framework of the established one-

contour model, the Coastline Evolution Model (CEM), but applied over a two-dimensional grid and with the addition of cross-shore sediment transport processes. With these additional functionalities, CEM2D is capable of simulating fundamental cause-effect relationships in coastal systems and exploring the influence of a variable water level on their evolution over meso-spatiotemporal scales. The model sits between one-dimensional and three-dimensional models, with the advantage of increased complexity and detail in model outputs compared to the former, but with more efficiency and less computational expense than the latter. The model could be used to inform coastal management and adaption decisions that will be sustainable over the long-term.

1.2 Thesis Structure

This thesis is divided into eight Chapters, including this general introduction, the contents of which are each described below. Each chapter from Chapter 3 (methodology) to Chapter 7 (research results) contains literature reviews and methodologies specific to the themes of each chapter, in addition to the general literature survey given in Chapter 2.

Chapter 2 | Sandy, Wave-Dominated Coastal Systems: *A Literature Survey*

This chapter sets the context for this research, giving a general overview of the current literature relating to coastal systems with a specific focus on wave-dominated, open sandy environments. Our current understanding of the drivers of change in these systems is outlined, highlighting the key processes that influence the way in which coastal systems behave and evolve. The literature survey is concluded with the overarching aim of this study and the key research objectives.

Chapter 3 | Development of the Coastline Evolution Model 2D (CEM2D)

This methods based chapter details the development of a mesoscale numerical model named the Coastline Evolution Model 2D (CEM2D). A review of numerical modelling techniques in environmental science is given, followed by an in-depth description of the features of CEM2D which highlights its ability to simulate fundamental coastal processes, including sea level rise.

Chapter 4 | Development of CEM2D, Part II: A Sensitivity Analysis and Selection of Model Parameters

This chapter continues the work on the development of CEM2D presented in Chapter 3. It details the rigorous testing conducted on CEM2D, to determine the sensitivity of the model in terms of the relationship between variations in the output of the model to the input data. This is an important step in the development of a model to ensure that it is configured sensitively and fulfils its purpose.

Having tested the model in terms of its mathematical structure in the first half of this chapter, the second half details the parameterisation of the key, or sensitive, inputs to CEM2D. This is to ensure that the set-up of the model is suitable, according to our understanding of the behaviour of coastal systems and the results of the empirically tested CEM.

Chapter 5 | The Influence of Wave Climate Conditions on Shoreline Shape and Evolution

This chapter assesses the influence of wave climate conditions on the behaviour of coastal systems. A comparison of model results between the empirically tested CEM and CEM2D is initially given to determine similarities and difference in the results. The results are also compared to natural coastal systems to determine

whether CEM2D is capable of simulating observed shoreline shapes according to the site-specific driving wave conditions.

Chapter 6 | The Two-Dimensional Evolution of Coastal Systems: An Application of CEM2D

This chapter builds upon the findings of Chapter 5 and details how the topographic and bathymetric profiles of the coastal systems evolve throughout each simulation, driven by the wave conditions outlined in the previous chapter. The dynamic evolution of the beach surface and bathymetry are analysed according to different wave climate conditions and the results compared to well-known theories of coastal behaviours.

Chapter 7 | Sea Level Rise: A Driver of Change in Coastal Environments

This chapter investigates how the simulated coastal system responds to a variable water level, with reference to sea level rise at a rate of 1 m and 2 m per 100 years. The results focus on the evolution of the cross-shore coastal profile, the topographic and bathymetric profile and specifically, differences in how landforms evolve when subject to a changing water level.

Chapter 8 | Synthesis

This chapter draws together the key findings from each chapter of this thesis, with reference to the wider implications of this research. An acknowledgement of the limitations is also given, of which are addressed in the summary of future work. The chapter is concluded with a succinct summary of how the overarching aim of this study and each research objective outlined in Chapter 2 have been addressed.

Bibliography

A complete bibliography for this thesis.

Appendix

Appendices referenced in this thesis.

1.3 Publications

It is intended that the main findings of this research will be published and some progress towards this goal has been made during this PhD course. Below is a list of publications currently in preparation.

- Morris, C., Coulthard, T., & Parsons, D. (in Prep.) *The Coastline Evolution Model 2D (CEM2D).*
- Morris, C., Coulthard, T. (in Prep.) *Development of CEM2D, Part II: A Sensitivity Analysis and Selection of Model Parameters*.

Chapter 2

Sandy, Wave-Dominated Coastal Systems

A Literature Survey

2.1 Introduction

In Chapter 1, a general introduction was given to provide the context for this research. This thesis has been constructed so Chapter 3 to Chapter 7 each contain a methodology and review of relevant literature that is specific to its theme. These specific literature reviews are intended to provide a detailed account of the current state of knowledge relevant to each chapter, to accompany the results and discussion. The themes are relatively distinct and therefore, segregation of the relevant literature ensures a focused critical review and discussion of findings.

This chapter provides a general literature survey that discusses current knowledge of coastal systems, intended to support the more specific and critical literature reviews given in each of the subsequent chapters. Context is given to the overarching theme of this research, including nomenclature, descriptions of widely accepted characteristics of coastal environments and processes that

influence their morphodynamics, as well as environmental modelling research methodologies. Having identified areas of coastal science where further research is of interest, this chapter is concluded with an overarching aim and a defined set of research objectives, on which this study and thesis is based.

2.2 The Coastal Zone

The coastal zone is defined as an area where land, water and air meet; it describes a host of environments each formed and governed by different processes, including open coasts, deltas, estuaries, embayment's and so forth (Haslett, 2009). Of interest to this research are open coastal systems which comprise approximately 40% of the world's shorelines (Short, 1996; Bird, 2011; Ranasinghe, 2016), but more specifically, sandy environments with a mean grain size of between 0.063 – 2 mm found along approximately 20% of shorelines (Finkl, 2004). Sandy, open coasts are highly dynamic zones which evolve over micro to macro scales, according to changes in environmental conditions, including sea level rise (Ranasinghe, 2016). From this point forward, the term coast and other synonyms will be used to describe open sandy coastal environments.

2.2.1 Defining the Coastal Zone

Zonations and nomenclature used to describe different areas of the coastal zone vary throughout the literature and are particularly dependent on the types of environments being discussed (Haslett, 2009). The cross-sectional schematic shown in Figure 2.1 labels common coastal terms taken from Bird (2011) and those which will be used in this thesis.

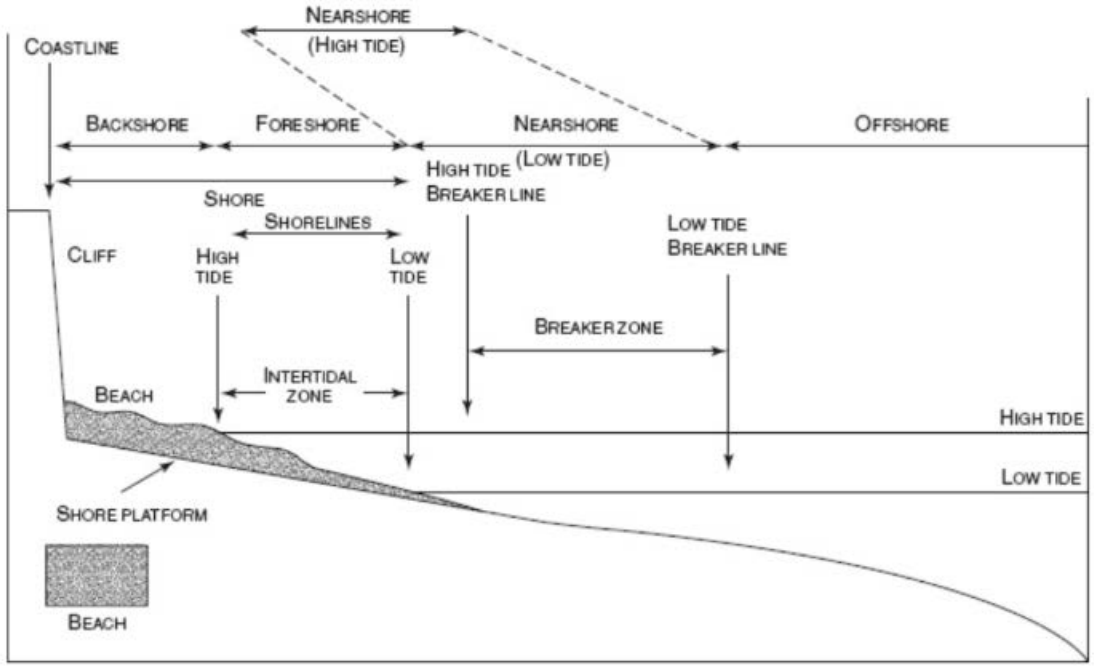

Figure 2.1 Coastal Terminology (Bird, 2011, p. 2)

The coastal zone can be divided into the offshore, nearshore and beach (or shore) (Figure 2.1). The transition between the offshore and nearshore marks the broad location where wave-driven sediment transport is considered negligible, often known as the Depth of Closure (DoC) (Ashton and Murray, 2006a). The term nearshore and shoreface are often used synonymously to describe the area where wave action dominates and which migrates cross-shore with the water line (Bird, 2011). The nearshore can be further subdivided into the surf and swash zones, which describe the types of wave processes that occur; wave breaking occurs in the surf zone and the swash and backwash motion of broken waves occurs in the so-termed swash zone (Haslett, 2009; Bird, 2011). The beach or shore can be subdivided into the foreshore that delineates the area between low and high water and the backshore which lies landward of the high water mark and is rarely affected by hydrological processes (Bird, 2011). The shoreline and the coastline are distinctly different terms, which respectively describe the continually migrating position of the water and land interface and the relatively

fixed position of the land margin at the high spring tide mark as shown in Figure 2.1 (Haslett, 2009; Bird, 2011). However, these terms are often used synonymously and in this thesis, will be used to describe the migrating boundary.

2.2.1.1 *Types of Open Sandy Coastal Systems*

Coastal systems have been classified in many different ways, including being defined according to the dominant physical, biological, evolutionary or geological characteristics; and there has been much debate about classifications and whether such dynamic systems can be confined to such general taxonomies (Finkl, 2004). No comprehensive and accepted scheme has yet been devised and this may never come to fruition given the diverse and complex nature of coasts and the range of disciplines interested in the systems. However, classifications allow us to organise our knowledge and theories, which can be used to further our understanding and make predictions about their future state (Finkl, 2004; Masselink, Hughes and Knight, 2014).

Sandy coastlines are commonly classified according to the driving hydrodynamic conditions (Finkl, 2004). Waves and tides are considered the principal physical processes acting in the nearshore zone and as such, coasts are often classified as wave-dominated or tide-dominated, or as mixed energy environments (Davis and Hayes, 1984; Anthony and Orford, 2002).

Wave-dominated environments are typically characterised by beaches or barrier systems with micro-tidal ranges from 0-2 m and tide-dominated environments (such as estuaries) are commonly macro-tidal, with ranges in excess of 4 m (Davis and Hayes, 1984; Masselink, Hughes and Knight, 2014). A third classification termed mixed energy environments are influenced by a subequal combination of wave and tidal processes and typical exhibit meso-tidal ranges,

from 2-4 m (Davis and Hayes, 1984). These types of environments are often considered as a hybrid, but Anthony and Orford (2002) argue of their existence in their own right.

The dominant mechanism acting along the coast is controlled by the relative forcing generated by the waves and tides (Hayes, 1979). Therefore, for instance, a micro-tidal coast could be classified as tide-dominated, if the wave energy and fluvial influences are low in relative terms (Hayes, 1979). Few coasts are devoid of both waves and tides, and it is estimated that approximately 50% and 44% of the energy dissipated around the world's coasts is derived from these respective processes (Anthony and Orford, 2002). Waves are often considered the dominant force and have hence received greater attention in the field, although globally both waves and tides provide a relative balance of energy to the coastal zone (Anthony and Orford, 2002).

Whilst these hydrodynamic-based classifications can suggest the dominant mechanisms that induce morphological evolution along specific coastlines, it is important to understand how waves and tides influence sediment transport, regardless of their dominance in any one environment. A further consideration for long-term coastal change is the influence of sea level rise and how a gradual change in the position of the shoreline, distinct from tidal fluctuations, can induce morphological change. These processes are each discussed in Section 2.3.

2.3 Coastal Morphodynamics

The morphodynamics of coastal environments describes the three-dimensional evolution of their shape and form, which is primarily driven by the non-linear interactions between sediments and fluids (Cowell and Thom, 1994; Carter,

2013). How a coast behaves and the landforms that evolve is determined by such interactions, in addition to site-specific environmental conditions, external forcings and boundary conditions (Figure 2.2) (Masselink, 2008; Bird, 2011).

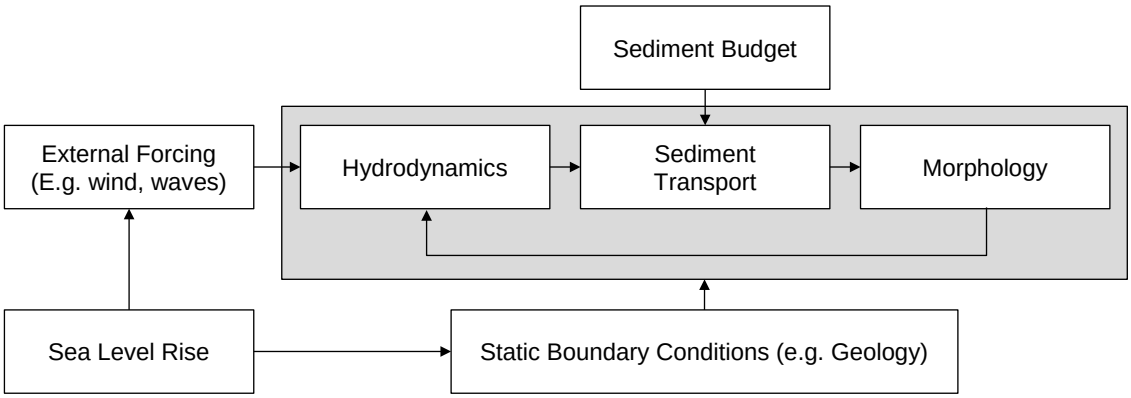

Figure 2.2 Coastal morphodynamic system (after Masselink, 2008)

Coastal systems are observed to tend towards a dynamic equilibrium according to the predominant environmental conditions (Woodroffe, 2002). A dynamic equilibrium state is defined as the fluctuation of a system around an average form; coastal systems will exhibit short-term changes and seasonal variations but will tend towards an average state over the long-term given relatively consistent environmental conditions (Bruun, 1962; Dean, 1991). If significant changes occur to these conditions, however, the form of the environment will adjust accordingly within its means which may be restricted, for instance, by human interventions.

Shorelines are punctuated by erosional and depositional features that form from the interaction of hydrodynamic processes which induce sediment transport (Van Den Berg, Falqués and Ribas, 2012). Of particular interest to this research, as will become clear in the results presented in this thesis, are four principle coastal features or shoreline shapes. These include cuspate headlands, alongshore sand waves, reconnecting spits and flying spits (Ashton *et al.*, 2001). Each of these landforms are described in more detail in Chapter 5. There is much difficulty in

identifying the mechanisms responsible for the formation of these features, but research has highlighted a number of key processes that are likely to be responsible or influential, as described in Section 2.4 (Ashton *et al.*, 2001; Van Den Berg, Falqués and Ribas, 2012).

2.4 Coastal Processes

The coastal system is governed by processes that act over multiple spatial and temporal scales. In reference to the relevant scale of this research, here we focus on key sedimentological and hydrodynamic processes that influence these systems over mesoscales.

2.4.1 Coastal Sediments

The morphological characteristics of a coastal system can be influenced by its sediment budget, which refers to the relative balance of sources, sinks and stores of material; environments with a surplus of sediment tend to be accretional and where there is a deficit of material, erosion occurs (Rosati, 2005). The physical properties of sediments can influence their transport potential, which ultimately affects the sediment budget (Lick and Mcneil, 2001; Sawczyński and Kaczmarek, 2014). For example, the density of particles relative to the velocity of fluids influences whether the material is transported and the mode of transportation, including as bed load or as suspended material (Davis Jr., 2012). Coarse, non-cohesive sediments are typically moved along the bed, whilst finer particles are more readily transported in suspension (Davis Jr. and Dalrymple, 2011).

The flux of material in the sediment budget is influenced by the movement of material in cross-shore or longshore directions, which plays a role in determining the evolution of the coastal system (Rosati, 2005). The cross-shore component

describes the onshore and offshore transport of material and the longshore by the shore parallel movement along the coastline. It is argued that waves are the primary drivers determining the proportion of longshore and cross-shore sediment transport, which act to distribute sediment and induce morphological evolution (Zenkovitch, 1959; Ashton *et al.*, 2001). This concept is known as the theory of high angle wave instability and is explored in greater detail in Chapter 5.

The sediment budget and transport direction can be influenced by both natural and anthropogenic factors, including the driving environmental conditions and human interventions. For instance, evidence suggests that sea level change (see Section 2.5) has increased rates of coastal erosion globally during the last century (IPCC, 2013a). This has contrasting effects on the sediment budget depending on other environmental conditions at play; in some locations erosion leads to a reduction in sediments supply and shoreline retreat (Dickson, Walkden and Hall, 2007) whereas in others, a surplus afforded by the eroded volumes leads to accretional behaviours (Jarmalavičius *et al.*, 2013). In terms of anthropogenic influence, the implementation of engineering structures to protect vulnerable locations from coastal hazards can alter the sediment budget and transport processes (Bird, 2011). Traditionally, hard engineered structures have been used to artificially fix the coastline in place and defend against wave attack which in the case of groynes, prevents the longshore transport of material. However, over the past few decades management has migrated to ‘softer’ techniques which use native materials and techniques that mimic natural processes (Finkl, 2012; National Trust, 2015). Regardless of the technique used, many defences alter the

sediment budget by disturbing the natural movement of material or hydrodynamics processes (French, 2002).

2.4.2 Coastal Hydrodynamics

Coastal hydrodynamics are principally governed by a combination of wave and tidal processes, with storm activity also considered to drive significant episodic changes to coastal environments (Masselink and Short, 1993; Short, 1996). It is these three processes that will be explored in more detail in this section. However, it is noted that there are many processes and site-specific conditions that play a role in the formation and evolution of coastal systems and hence why a large range of coastal types exist (Short, 1996).

2.4.2.1 *Wind-Waves*

Wind-waves are often considered to be the principal contributor to morphodynamic change in coastal environments, providing the greatest source of energy to induce sediment transport processes (Woodroffe, 2002). It is estimated that approximately half of the energy delivered to coastal systems is derived from wave processes, but this is dependent on site-specific conditions (Anthony and Orford, 2002).

Wind-driven waves are the most common type of waves observed on the ocean, but which are more specifically termed according to additional driving forces such as ‘gravity waves’ to describe those maintained by gravitational forces (Woodroffe, 2002; Ahmed *et al.*, 2010). As the wind blows over a water surface, it transfers energy to the water particles and sets waves in orbital motion (Ahmed *et al.*, 2010). At the peak of the orbit, a wave crest is formed, with the water particles rising and advancing with the motion (Figure 2.3) (Ahmed *et al.*, 2010). As the particles lose energy, they sink in the water column forming the trough of

the wave. The particles translate backwards as the trough advances, completing the orbit. As the crest forms, the particles rise and continue the orbital motion, as illustrated in Figure 2.3 (Ahmed *et al.*, 2010).

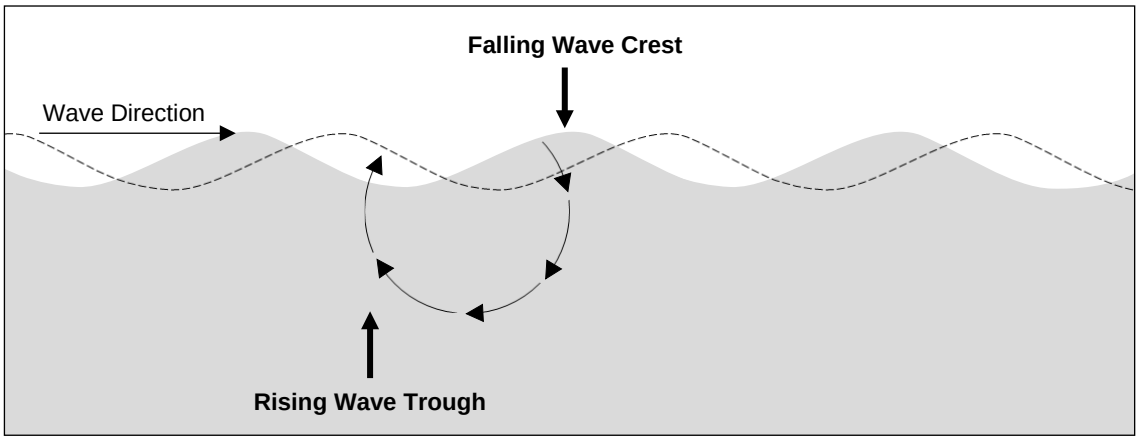

Figure 2.3 An illustration of the orbital movement of water particles and the formation of waves (after Ahmed *et al.*, 2010).

In deep water where the waves are not influenced by interactions with the bed, the orbital paths are circular and show a decrease in radial size with increasing water depth (Figure 2.4) (Ahmed *et al.*, 2010). In shallow water, such as in the nearshore, interactions with the bed cause the orbits to become increasing elliptical with shallower depths, decreasing in radius along the vertical axis (Figure 2.4) (Ahmed *et al.*, 2010).

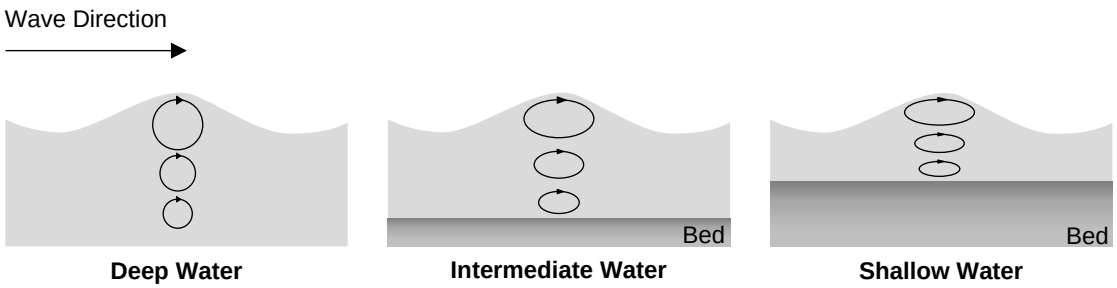

Figure 2.4 An illustration of wave orbital motion in deep to shallow water and the transformation of orbitals from circular to elliptical induced by interaction with the bed (after Ahmed *et al.*, 2010)

As wind-waves approach shallow water in the nearshore zone and the orbital path of water particles change (Figure 2.4), the characteristics of the waves are

transformed in response to their interaction with the bed and physical characteristics of the coast (Ahmed *et al.*, 2010). Measuring the transformation of a waves geometry is complex as it involved high resolution spatial and temporal monitoring to capture rapid changes that occur at fluctuating locations across the dynamic surf zone (Butt *et al.*, 2007; Martins *et al.*, 2017). Each wave behaves differently according to, for instance, varying rates of motion, non-linear interactions and a varying point at which wave transformation or breaking occurs (spatially and temporally) (Larson, Kubota and Erikson, 2004). Attempts have been made to gain greater insight into these processes, but with limited success due to complexity in the deployment of instrumentation and of monitoring this dynamic zone (Larson, Kubota and Erikson, 2004; Martins *et al.*, 2017).

Although there is complexity in understanding processes in the surf and swash zones, studies have shown that they have a significant influence on sediment transport processes and the net sediment budget, which influences morphodynamics and the overall evolution of the systems (Butt *et al.*, 2007). This understanding has been gained from improved technologies (e.g. LiDAR) that are able to extract data at higher spatial and temporal resolutions than previously achieved (Blenkinsopp *et al.*, 2012; Martins *et al.*, 2016; Martins *et al.*, 2017).

According to currently accepted theories of wave transformations in the surf zone, the process is principally controlled by refraction, diffraction and shoaling (Holthuijsen, 2007). Refraction and diffraction describe changes in the propagation direction of approaching waves by different mechanisms. Refraction occurs as waves enter decreasing water depth. With an unchanged wave period, the wavelength and speed of propagation decreases and as a consequence, the wave direction is turned towards shallower regions (Dean and Dalrymple, 2004a).

Diffraction describes the change in wave direction due to abrupt changes in the height of waves, often caused by interactions with obstacles such as headlands, around which the waves may contort (Dean and Dalrymple, 2004b; Holthuijsen, 2007). The change in height results in waves changing direction, which can cause them to propagate into shadow regions formed by the obstacles with which they interacted (Dean and Dalrymple, 2004b).

Shoaling is a process by which waves steepen as they propagate into shallow water (Holthuijsen, 2007). If the wave base, defined according to its depth of influence, is deeper than the water depth then the interaction of the rotating particles with the bed pushes the water column up and increases the wave height. Descriptions of the depth of influence in the literature are synonymous with the DoC, which is located at the interface of the offshore and nearshore zone (Ashton and Murray, 2006a). The depth is estimated to be half the wavelength and seaward of the cross-shore location of this point, negligible cross-shore sediment transport occurs (Ashton and Murray, 2006a). As the waves approach the shoreline and the water column is raised, wave motion and propagation slows at the front of the wave field. The waves further back in the field continue their rate of motion and cause the projection of waves to bend perpendicular to the shore through refraction, as described previously (Holthuijsen, 2007). With increasing height and decreasing wavelength, the waves become increasingly unstable and eventually break in the surf zone (see Figure 2.1). The point of breaking is estimated by a steepness ratio of 0.147 calculated by the wave height divided by the wavelength (Woodroffe, 2002).

When waves break, their energy is dissipated into the swash zone where the water ebbs and floods across the beach face (Bakhtyar *et al.*, 2009). Four

principal types of wave breaking are described in the literature, including spilling, plunging, collapsing and surging, although intermediate types occur in nature (Figure 2.5) (Holthuijsen, 2007).

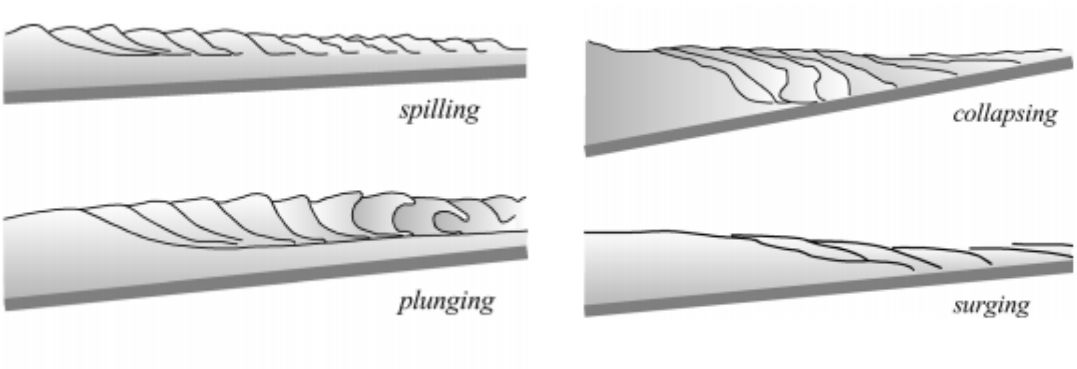

Figure 2.5 Four principal types of wave breaking processes (Holthuijsen, 2007, p. 243).

The swash and backwash motion of broken waves in the swash zone, as aptly named, determines whether sediment is accreted or eroded; if material is returned to the surf zone by a sufficiently strong backwash, the combined motion of waves and tides can transport it along- or cross-shore (Bakhtyar *et al.*, 2009). The volume of sediment transported is a function of the energy at the shoreline and the sediment metrics, including availability and density.

An offshore wave climate may be transformed in a number of ways according to the geometry and physical characteristics of specific localities and can influence how a shoreline behaves and evolves, through the transport of sediment, induced by the energy transferred by the waves (Wright and Short, 1984; Short, 2006; Butt *et al.*, 2007). Accordingly, Wright and Short (1984) defined three broad beach states of wave-dominated sandy coastal environments to distinguish between highly energetic dissipative types typically characterised by fine-grained material and more reflective low energy systems which tend to consist of coarse-grained material (Wright and Short, 1984; Short, 2006). These classifications are described in greater detail in Chapter 6.

2.4.2.1.1 The Wave Climate

According to the metrics of transformed waves, the wave climate is principally defined by the angle of approach, the wave height, the fetch and periodicity (Barkwith *et al.*, 2014b). Of these descriptors, the wave angle is considered as having a primary role in the morphodynamics of many types of coastal systems and very few systems are devoid of their influence (Anthony and Orford, 2002; Dickson, Walkden and Hall, 2007; Barkwith *et al.*, 2014b).

Barkwith *et al.* (2014b) investigated the influence of changing wave angles and heights on the movement of sediment along the Holderness Coast located along the UK's east coast and identified that erosion rates have a greater correlation to wave angle than wave height, although an increase in sediment transport rates was found to occur with greater wave heights and periods (Barkwith *et al.*, 2013, 2014a). Barkwith *et al.,* (2014b) used the Coastline Evolution Model (CEM) for this study, driven by a historic wave climate. The wave angle is perturbed by up to $\pm 20^{o}$ and the wave height by up to $\pm$0.4 m, as selected at random for each simulation. The spread of results demonstrates a sensitivity of the Holderness Coast to these wave climate conditions, with both an increase and decrease in erosion rates observed according to the wave conditions (Barkwith *et al.*, 2014b).

Whilst a weak relationship was observed between the wave height and relative rates of erosion by Barkwith *et al.* (2014b), an anticlockwise rotation of the wave climate (relative to the baseline) from -20^{o} to 0^{o} showed a reduction in erosion rates along the Holderness Coast and an increased rate where the wave angle is rotated clockwise, up to 18^{o}; beyond 18^{o} a reduction in relative erosion is observed (Barkwith *et al.*, 2014b).

Murray *et al.,* (2013) and Ashton *et al.,* (2001), also identified the significance of wave angles on coastal evolution and morphology. Both authors suggest that low angle waves (angles smaller than the optimum for alongshore transport) approaching straight coasts create smooth planform shorelines, whilst high angle waves (angles greater than the optimum for alongshore transport) tend to form small perturbations (Ashton *et al.*, 2001; Murray *et al.*, 2013). Where waves approach perpendicular to the shore, cross-shore sediment transport dominates (Hoefel and Elgar, 2003).

The approaching wave angle is further shown to influence embayed coastlines, as well as open coasts. Whilst embayed coasts are not the focus of this research, it highlights the influence that the wave climate can have on sediment transport. Hurst *et al.,* (2015) use a vector-based one-line model (COVE) to simulate the evolution of coastlines between two fixed headlands with zero sediment flux. The shoreline responds to the approaching wave angle and the spread of angles to generate straight, bay and crenulated bay morphologies according to the wave conditions (Figure 2.6). The authors note that the wave direction and spread of approaching wave angles are able to dictate how the bays form and evolve (Hurst *et al.*, 2015).

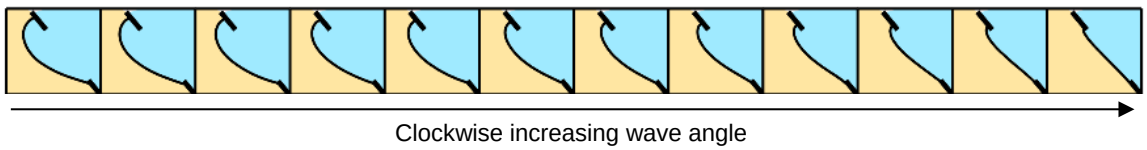

Figure 2.6 Bay morphologies generated under high to low angle waves (from left to right) (Hurst *et al.*, 2015).

Conversely, a study completed by Cartier and Héquette (2011) along a macro-tidal coast identified that longshore sediment transport rates are more closely related to the wave height; no significant relationship was found between sediment transport and the wave approach angle. The authors reasoned this to

the greater influence of tidal forcing on the longshore movement of material at the three sites in Northern France that were investigated (Cartier and Héquette, 2011). This emphasises the importance of considering site-specific conditions in coastal science, as all systems will evolve differently according to the specific environmental conditions.

A further consideration of the influence of waves on the coastal system is that protruding sections of coastline (e.g. headlands) can create wave shadowed regions that are sheltered from the dominant wave direction (Ashton *et al.*, 2001; Barkwith *et al.*, 2014b). This shadowing protects the coast from wave-induced erosion, according to the angle of wave approach. For instance, wave shadowing effects in the northernmost portion of the Holderness coastline, created by the chalk promontory known as Flamborough Head, creates a broad north-south divide in the relative rates of erosion (Barkwith *et al.*, 2014b). Relative erosion rates are lowest in the lee of the headland at the most northern point of the coastline that is shadowed from the dominant wave approach. Immediately south of the shadow region, the greatest rate of erosion occurs (between approximately 10 km and 30 km south of the headland) which gradually reduces towards the southern end of the ~60 km coastline (Barkwith *et al.*, 2014b). However, the transformation of waves in the nearshore zone and particularly the processes of diffraction around protruding features can result in wave energy propagating into the shadow zones (Daly et al., 2014).

2.4.2.2 *The Tidal Regime*

Whilst wave conditions are often considered the principal agent in coastal environments, the influence of tides is recognised particularly in macro-tidal or tide-dominated environments. However, these processes are relatively less well

understood than wave processes (Masselink and Short, 1993; Anthony and Orford, 2002). It is, however, suggested by Anthony and Orford (2002) that approximately half of the energy delivered to the coast is from tidal processes, regardless of the range, which imposes an influence on coastal morphodynamics.

Tides are formed by the combined gravitational forces exerted on the earth's water masses by the sun and moon (Schwartz, 2006). These forces cause the water bodies to bulge in the direction of greatest gravitational attraction, which depends on the location and alignment of the earth, moon and sun. There are three primary types of tidal patterns: diurnal, semidiurnal and mixed semi-diurnal (Figure 2.7) (NOAA, 2017). Semidiurnal are the most common and are defined by two high and two low water levels in 24 hours, whilst diurnal tides have one low and one high tide in a 24 hour period (NOAA, 2017). If two high and two low tides occur at differing heights, they are termed mixed semidiurnal.

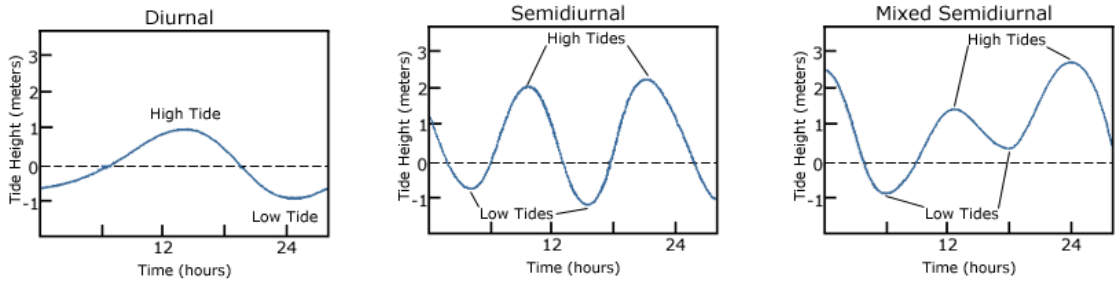

Figure 2.7 Three primary types of tidal patterns: diurnal, semidiurnal and mixed semidiurnal (NOAA, 2017).

The difference in vertical height of the tides, known as the tidal range, depends on the alignment of the earth, moon and sun and the force this exerts on the water masses (Figure 2.8). The forces are strongest when all are aligned and give the largest tidal ranges, known as Spring Tides. When they are not aligned and the tidal range is at its minimum, Neap Tides occur.

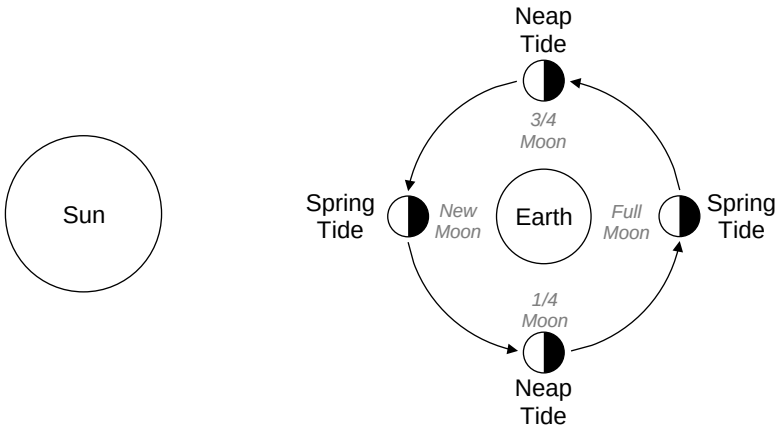

Figure 2.8 Diagram showing the astronomical tidal cycle that occurs concurrently with phases and alignment of the sun, earth and moon (after NOAA, 2018).

It is often surmised that the fluctuation of sea level caused by the horizontal and vertical tidal range determines a coast's exposure to hydrodynamic processes, including wave action (Short, 1996; Anthony and Orford, 2002). The tides act to shift the location of zones in the coastal environment, including the surf and swash, succumbing the intertidal zone to wave transformation and breaking processes (Masselink and Short, 1993). To generalise this point, larger tidal ranges tend to expose larger cross-sections of the coast to wave action, resulting in greater volumes of sediment transport (Masselink and Short 1993).

The tidal asymmetry, referring to both the flow rate and period of the rising and falling vertical tide, influences tidal currents in the nearshore zone and the dynamics of sediment transport (Bolle *et al.,* 2010). The rising tide creates a landward current known as the 'flood' and the falling tide creates an 'ebb' current that flows seawards. If the flood and ebb have different energies and durations, the net transport of material will occur in the direction of greatest flow velocity or period (Davis Jr. and Dalrymple 2011; Bolle *et al.,* 2010). For instance, a flood-dominated coast is likely to transport a greater amount of material in the landward direction. At the turn of the tide, a period of 'slack water' can occur when the flow

ceases as it begins to change direction. Slack water can last from seconds to minutes and typically encourages sediment deposition in the low (or no) velocity water (Dalrymple and Choi, 1978). Large tidal ranges are often associated with strong flood and ebb currents which can influence the volume and type of material that is transported.

The importance of tidal processes on coastal morphodynamics and particularly on the cross-shore profile of these systems led to the beach classification system of Masselink and Short (1993). The system is concurrent with Wright and Short's (1984) classifications according to wave processes (see Section 2.4.2.1), but with the inclusion of tidal influences on coastal morphology. As noted previously, these classifications are discussed in more depth in Chapter 6.

Tidal cycles and ranges are highly predictable, but the difference in predicted and observed patterns can often be attributed to location-specific meteorological conditions (Haslett, 2009). This includes, for instance, atmospheric pressures, storm surge and strong onshore winds which can each act to increase or decrease water level on top of the tidal fluctuations (Haslett, 2009). Strong winds during storms can hold back or push forward tides, resulting in abnormally low or high levels respectively (Brown, 2013). This can influence the potential for inundation, flooding and/or breaching in vulnerable localities (Haslett, 2009; Wragg, 2014; Skinner *et al.*, 2015). This was observed in the Humber Estuary in December 2013 (Wragg, 2014), as described in Section 2.4.2.3.

2.4.2.3 *Storm Activity*

Storm activity can cause significant volumes of material to be eroded from the coastal zone (Bird, 2011). The characteristics of these events and their impact on coastal environments depend on the non-linear interactions between the surge,

tidal conditions and the wave climate (Spencer *et al.*, 2015). Zhang *et al.,* (2004) suggest that the increase in sea level, whether this is surge or tide-induced, combined with energetic surges and waves can erode large amounts of sediment from a coastline. The material that is removed is transported into the offshore zone before being returned or redistributed along the coast during 'normal' conditions (Zhang, Douglas and Leatherman, 2004).

The 1953 storm along the east coast of the UK illustrates the important relationship between sea level, waves and surges. This event caused "one of the worst cases of flooding in the UK in recent history" (Wolf, 2008, p. 19). According to the Met Office (2016), the tidal surge in the North Sea exceeded 5.6 m above mean sea level along the coast and winds of 126 mph were recorded in Orkney, north-east Scotland. This, combined with high spring tides and high wind-waves resulted in the overtopping or breaching of many defences and extensive flooding in east coast communities (Wolf, 2008). During the storm surge of 2013, where one of the largest storms since the 1953 event propagated down the east coast of the UK, the peak of the event occurred approximately 30 minutes before the predicted high tide mark (Wragg, 2014). The combined effects of the surge and tide resulted in around 40 km of defences breaching, widespread flooding on the north and south banks of the Humber Estuary and breaching of Spurn Point spit (Raynor and Chatterton, 2014; Wragg, 2014).

2.5 Climate Change and Sea Level Rise

The climate influences processes that shape and dictate the behaviours of natural coastal environments (Bird, 2011). A change in these conditions, therefore, has

the ability to influence hydrodynamics and sediment transport patterns, and cause a shift in the morphodynamic behaviours of coastal systems.

Amongst all major climate drivers, coastal systems are particularly vulnerable to the effects of sea level rise (Masselink and Russell, 2013; Kopp *et al.*, 2014). It has been reported that net erosion has occurred along beaches globally during the last century, and flooding and inundation have increased due to a more rapid rate of sea level rise (Solomon *et al.*, 2007; Wong *et al.*, 2015). Low Elevation Coastal Zones of up to 10 m in elevation are the most at risk of increased erosion, submergence and flooding.

According to the IPCC's Fifth Assessment Report (AR5), since the late 19th and early 20th centuries, the mean rate of sea level rise has increased beyond the relatively low rates of rise observed over the past two millennia (IPCC, 2013b). It is predicted that global sea levels rose at an average rate of 1.7 mm yr^{-1} between 1901 and 2010, by 2.0 mm yr^{-1} between 1971 and 2010 and by 3.2 mm yr^{-1} between 1993 and 2010 (IPCC, 2013b). Climatologists believe that approximately 75% of this rise since the 1970s is as a result of melting glaciers and the thermal expansion of the oceans caused by climate warming (IPCC, 2013b).

The IPCC predicts that sea levels will continue to rise throughout the 21st century, but that rates of rise will be not felt homogenously, nor will the impacts (IPCC, 2013a). Rates of rise are predicted globally to be between 0.26-0.82 m by 2081-2100 relative to 1986-2005 levels, depending on the future emissions scenario (IPCC, 2013a). A high risk, but low probability scenario (termed H++) has also been calculated for the coastline around the UK, which predicts a rise of between 0.93-1.9 m by 2081-2100 (Jenkins *et al.*, 2009).

However, it is important to consider that erosion and shoreline change is not exclusively as a consequence of rising sea levels but due to the combined influence of local environmental conditions on sediment dynamics (Wong *et al.*, 2015). The morphologies and behaviours of these systems are as a consequence of multiple cause-effect relationships acting across many spatial and temporal scales. In fact, site-specific conditions have led to the progradation of the shoreline in some localities, facilitated by an abundant sediment supply (Dickson, Walkden and Hall, 2007; Jarmalavičius *et al.*, 2013).

2.6 Environmental Modelling

Many types of modelling techniques exist which aim to simplify real-world systems and allow us to study their complex behaviour. These include conceptual, physical, analytical, numerical and visual models (Murray, 2007). Physical and numerical types are the most commonly used in geomorphology, with numerical techniques proving to be the most cost-effective, efficient and reliable of the two (Trenhaile and Lakhan, 1989; Thomas and Dwarakish, 2015).

Numerical models are mathematical representations of behaviours and processes in given systems; in this case, coastal environments. The advance of computer processing power over recent years has seen this technique become commonplace amongst geoscientists who use this technology to represent, explore and improve our process-based understanding of environmental systems and predict how they may evolve (Tucker and Hancock, 2010).

Mesoscale models are less common in geomorphology than other earth science fields since they sit between more traditionally used reduced complexity reductionist studies and more complex synthesis investigations (van Maanen *et*

al., 2016). Examples of numerical models in published literature include one-line models such as COVE (Hurst *et al.*, 2014) and CEM (Ashton *et al.*, 2001) and more complex three-dimensional models such as Delft3D (Lesser *et al.*, 2004). The one-line models are highly efficient and can simulate large spatial areas and long time periods to a limited level of detail and the more complex two- to three-dimensional models can simulate a high level of detail but over a limited time and spatial scale.

Many existing models which are capable of simulating the evolution of coastal systems over relatively long time periods over which sea level rise will become more apparent (e.g. the mesoscale) are unable to simulate the combined effect of wave climate conditions and sea level rise due to their one-dimensional nature. As has been shown in this literature survey, these two environmental conditions are the key factors that should be considered to understand coastal morphodynamics at this scale of study.

2.7 Research Aims and Objectives

The literature survey has facilitated in highlighting key areas in the field of coastal geomorphology where the advancement of science is required to better understand the morphodynamics and evolution of coastal systems. In Section 2.2 common nomenclature used to describe coastal systems was given to define the terms that will be used throughout this thesis. In Sections 2.3 to 2.4 the processes that are currently understood to control the behaviour of coastal systems were discussed, in particular highlighting the role of wave climate conditions. In Section 2.5 the potential influence of climate change and particularly the role of sea level rise in changing the behaviour of coastal systems and inducing or enhancing

erosion, flooding and submergence (and progradation) was highlighted. Finally, in Section 2.6, the application of numerical models to the study of coastal morphodynamics was highlighted and the current lack of tools to be able to simulate the combined effects of environmental conditions (e.g. waves) and sea level rise on their evolution. From these findings, an overarching aim and four principal research objectives have been formulated.

The overall aim of this research is:

to improve our understanding of the morphodynamic behaviour of wave-dominated sandy coastal systems and predict their likely response to changing environmental conditions, including the wave climate and sea level rise.

This will be facilitated by the development of a meso-spatiotemporal numerical model which represents fundamental process-form relationships in these environments. Our current understanding of how coastal systems may behave over mesoscales is relatively limited since existing numerical models, which are commonly used in such studies, lack development in this field. The following research objectives have been defined to guide this project:

Objective 1: To develop and test a two-dimensional coastline evolution model which can be used to understand the behaviour of coastal systems according to the driving wave conditions and their likely response to climatic changes over meso-spatiotemporal scales.

Objective 2: To examine the relationship between coastal planform and wave climate conditions, which drive sediment transport processes in the environments under consideration, by comparison of the two-dimensional coastline evolution model with an existing model as well as to natural systems.

Objective 3: To investigate the topographic evolution of coastal systems, according to changes in environmental conditions, including the dynamics of the beach surface and nearshore profile under different wave climate conditions.

Objective 4: To investigate the effects of sea level rise on the two-dimensional evolution and behaviour of coastal systems at the mesoscales, including the influence on landforms.

In reference to these research objectives, each will be addressed by specific chapters of this thesis are shown in Table 2.1. In Chapter 8 of this thesis, the primary findings of this research will be synthesised, and the final conclusions will be drawn. This will include a summary of how the overarching aim and each of the research objectives have been met.

Table 2.1 A list of the research objectives, paired with the chapters that address each of them

Research Objective	**Chapter(s) Which Address the Research Objective**
1	**Chapter 3** Development of the Coastline Evolution Model 2D (CEM2D) **Chapter 4** Development of CEM2D, Part II: A Sensitivity Analysis and Selection of Model Parameters
2	**Chapter 5** The Influence of Wave Climate Conditions on Shoreline Shape and Evolution

3	**Chapter 6** The Three-Dimensional Evolution of Coastal Systems: An Application of CEM2D
4	**Chapter 7** Sea Level Rise: A Driver of Change in Coastal Environments

2.8 Conclusion

In this Chapter, key concepts relating to the processes which influence the morphodynamic behaviour of coastal systems over the mesoscale have been surveyed. This has provided a basis for the context of this research and justification of choices on the types of coastal systems and processes that will be considered in this thesis.

Whilst it is important to consider the effects of tidal processes in wave-dominated, sandy coastal systems, even if micro-tidal, over meso-temporal scales their effects are less influential to the large-scale long-term behaviour of these environments compared to processes such as the wave climate. The mesoscale nature of this study necessitates that the influence of sea level rise is considered. Over these time periods, the effects associated with increasing water levels will likely drive morphodynamic change in these systems.

In the following Chapter, the methods employed to study the driving forces and sensitivities of wave-dominated sandy coastal systems will be outlined.

Chapter 3

Development of the Coastline Evolution Model 2D (CEM2D)

Research Methodology

3.1 Introduction

In the previous chapter, our current understanding of the behaviour of coastal systems in terms of their morphological dynamism and evolution was surveyed (with more detailed literature reviews given in the subsequent chapters). As outlined in Chapter 2, the overarching aim of this research is to build upon this understanding and explore how coastal systems might evolve over meso-spatiotemporal scales and the influence that changing environmental conditions may have.

In this Chapter, the methods used to conduct this research are presented. Following a more detailed review of the model development process and of existing coastal models, a full description is given of the development of the Coastline Evolution Model 2D (CEM2D) developed for this project. CEM2D has been built from the fundamental concepts of the established CEM model and is

capable of simulating key cause-effect relationships in coastal systems. Additional functionalities within CEM2D, notably the change from one-dimensional (e.g. CEM) to a two-dimensional model, means it is also capable of exploring the influence of a variable water level on sediment transport and the formation and evolution of morphological features and landforms at the scale of interest. In subsequent chapters, the model will be tested (see Chapter 4) and be used to address the research questions outlined in Chapter 2 (see Chapter 5 to Chapter 7).

This chapter specifically addresses Research Objective 1, as outlined in Chapter 2 and reiterated in the conclusion of this chapter (Section 3.8).

3.2 Numerical Models and the Model Development Process

Modelling environmental systems is complex and can involve the representation of a large number of processes that act at varying spatial and temporal scales (Trenhaile and Lakhan, 1989; Coulthard *et al.*, 2013). Numerical models can be used to delve into various systems and subsystems that constitute given environments, branching into a range of different disciplines (e.g. biology, geology, geomorphology, socio-economics). Modelling all these processes could be impracticable and expensive, both monetarily and computationally and it is, therefore, important to define and limit the bounds of a model to the purpose of the study. There is a balance to be found between model complexity and efficiency (Chau, 2010). Trenhaile and Lakhan (1989) recommend nine key steps for developing a credible and parsimonious numerical model, which guides the use of as fewer parameters and processes as possible whilst accomplishing the necessary level of detail. These steps include:

1. Define the problem that needs to be solved
2. Outline the specification of the system to be developed
3. Distinguish the processes that need to be represented, relevant to the problem
4. Data collection and preparation
5. Translation of theories and equations into the computational model
6. Program verification
7. Model validation
8. Run simulations
9. Analysis and interpretation of results

Underpinning steps 1 – 3 are three key questions (Hutton, 2012):

1. What are the relevant form-process interactions at the scale of enquiry?
2. How can these processes be represented mathematically?
3. Are there appropriate data to constrain model parameters and evaluate model predictions?

The steps and key questions outlined above can be used to guide the development of a numerical model that is specific to the field of research.

3.2.1 Model Design

Numerical models can be classified according to their design and structure (though such classifications are not mutually exclusive). A number of key types are explored subsequently.

3.2.1.1 Empirical vs Process-Based Models

Numerical models can be broken down into two main types; empirical and process-based models (Wainwright and Mulligan, 2013). Empirical models are

designed from observations of given systems, whereas process (or physical) based models aim to quantify physical mechanisms through the explicit understanding of processes. Two main types of process models exist: static and dynamic. Static models simulate systems in a steady state condition, whereas dynamic models account for changes in variables over time.

Both empirical and process-based models can be further classified as deterministic or stochastic. Deterministic models generate results from defined processes, meaning outputs from the same input configuration will produce identical results. Stochastic (or probabilistic) models include elements of uncertainty and randomness in the processes and calculations.

3.2.1.2 Raster and Vector-Based Models

Environmental models are typically designed to represent systems using either raster or vector-based techniques. Raster-based models discretise the modelling domain into a grid of usually regular, equally spaced square or hexagonal cells. Vector models represent the environment as a series of points, connected by lines, as in a Triangular Irregular Network (TIN). Whilst vectors can provide a comparatively more accurate representation of hydrological and sedimentological processes, as common in coastal models, regular grids are more popular due to their computational and mathematical simplicity (Wainwright & Mulligan 2013)

3.2.1.3 Dimensionality

The appropriate dimensionality of a model is dependent upon the purpose of the study; one-, two- and three-dimensional types are common in geomorphology. One-dimensional models provide the most simplistic representation of a system in the cross-shore direction and do not include a vertical component (Kondolf and Piegay, 2016). In geomorphological modelling, one-dimensional models are

typically used to represent flow and basic sediment transport processes (Kondolf and Piegay, 2016). Two-dimensional models represent both cross-shore and cross-stream processes meaning they can model systems in greater detail, including flow paths around depositional features (Kondolf and Piegay, 2016). The vertical dimension can also be modelled, but processes tend to be depth-averaged. Three-dimensional models are used far less frequently than two-dimensional models due to their complexity (Kondolf and Piegay, 2016). Three-dimensional models simulate processes in a more complex way by including cross-shore, cross-stream and vertical components of a system (Kondolf and Piegay, 2016). They often provide a higher level of detail (spatially and of processes) compared to one- and two-dimensional models, making them more suited to smaller spatial and temporal scale studies.

3.2.1.4 Resolution

The spatial and temporal resolution of a model is dependent upon its application. Mesoscale modelling, from 10^1 to 10^2 km and 10^1 to 10^2 years, is suggested to be the most suitable and widely used resolution for management practices, into which a large amount of research falls (Nicholls *et al.*, 2012; French *et al.*, 2015). This scale allows general trends to be identified through the observation of large-scale and long-term processes, without compromising computational efficiency (Barkwith *et al.*, 2014b).

The resolution can vary throughout a model to accommodate areas of the domain that require more attention (Murray, 2007). For example, within the hydrodynamic model CAESAR-Lisflood, the erosion and deposition components operate on a different time step to the flow model (Coulthard *et al.*, 2013). This concentrates

model time and detail in areas of greatest need, which can improve the efficiency of the program.

3.2.1.5 Parameterisation

Parametrisation is a term used to describe the assignment of numerical equations to the representation of real-world processes. The complexity of multi-scale systems necessitates parameterisation, so only key processes relevant to the study are represented in the model (Murray, 2007; Hutton, 2012; Zangiabadi *et al.*, 2015). Reducing the complexity of the model in this way can make the simulations more reliable, efficient and reduce the uncertainty that is inherent in each variable and process included (Ramming and Kowalik, 1980). The first choice in parameterisation is, therefore, to define which key processes to include in the model environment and the second to determine the equations and parameters used to represent these processes.

3.2.2 Governing Equations

The governing equations used in numerical models are designed to mathematically represent physical processes in systems. They determine how variables are changed throughout the simulation, according to the equations imposed on them. In coastal evolutionary modelling, the key processes to consider are sediment transport and hydrological processes (Cowell and Thom, 1994; Carter, 2013). The hydrology of the system drives the movement of sediment that results in its morphodynamic evolution.

There are a range of sediment transport and wave transformation equations in the literature, but the choice of methods for this research was largely guided by the techniques used in the base model, from which the numerical model designed

for this study was built (as will become apparent in Section 3.4). Therefore, the subsequent review will be based on the equations relevant to this study.

As will become apparent later in this chapter, the Coastline Evolution Model (CEM) was chosen as the base model from which the Coastline Evolution Model 2D (CEM2D) was built for this study. CEM uses Linear Wave Theory to calculate the transformation of waves as they approach the nearshore (e.g shoaling and refraction) with depth-limited breaking and the CERC formula to drive longshore sediment transport. These formulas were chosen to be used in CEM2D for their common usage and their adoption in the CEM; it was not within the scope of this research to adopt these formulas from the base model but future revisions are suggested for future versions of CEM2D, as outlined in Chapter 8.

3.2.2.1 Linear Wave Theory

Wave theories describe the form and dynamics of waves, including how they are affected by the changing water depth as they propagate onshore in coastal areas (Holthuijsen, 2007). Whilst complex theories can be used to describe wave behaviours, such as the Navier-Stokes set of equations, linear wave theory provides a more appropriate method for cases where computational efficiency and simplicity outweigh the advantages of a more accurate approach (Soulsby, 2006).

Linear wave theory was developed in 1845 by George Airy and is often referred to as ‘Airy Wave Theory’ (Holthuijsen, 2007). In the nearshore coastal zone, as is the focus of this study, the theory describes the way in which water waves transform as they enter shallower water. The transformation processes were described in Chapter 2 and include the shoaling, refraction and diffraction of waves.

Where the water depth in the nearshore zone is shallower than is suitable for Linear Wave Theory equations, the shallow-water Boussinesq methods offer a more complex alternative (Holthuijsen, 2007). These equations further include non-linear interactions between waves and depth-induced breaking, although the latter is poorly understood at present (Holthuijsen, 2007).

3.2.2.2 The CERC Equation

Sediment Transport equations are abundant in the literature, each taking account of different variables that influence the movement of material. The most commonly used is the CERC formula, which is based on the concept that longshore sediment transport rates are attributed to the energy flux according to the breaking waves, per length of the beach (Equation 3.1) (Komar, 1971). Sediment transport rates can be written as:

$$Q_s = \left[\frac{{K_{\rho g}}^{\frac{1}{2}}}{(\rho_s - \rho)(1-p)}\right] {H_b}^{\frac{5}{2}} \cos(\phi_b - \theta) \sin(\phi_b - \theta)_b$$

Equation 3.1

Where Q_s is the volume of longshore sediment transport (m^3/s), K is an empirical constant, ρ *is water density,* g is gravitational forces (m^2/s), ρ_s is sediment density (g/cm^3), p is sediment porosity (~0.4), H_b is the breaking wave height (m), ϕ_b is the breaking wave angle (º) and θ is the shoreline orientation (º). The CERC formula does not take into account the influence of particle size and beach slope on sediment transport rates, but these variables are included in the refined equations of Kamphuis (1991) (Equation 3.2).

$$Q_s = \left(2.27 m^{0.75}\ {d_{50}}^{-0.25}\ T^{1.5}\right) {H_b}^2\, cos^{0.6}(\phi_b - \theta) sin^{0.6}(\phi_b - \theta)$$

Equation 3.2

Where *T* is the wave period (s), *d* is the median grain size (mm) and *m* is the beach slope. Both the CERC and Kamphuis equations are more suited to sandy coastal systems than those with gravel or shingle lithologies, although they can be applied to these sorts of coastlines by altering the *K* value. They also require that the input wave conditions be representative of breaking wave characteristics, calculated by the wave equations.

3.3 Coastal Numerical Models

Since the 1950s and 1960s, numerical models have been used to explore and predict the behaviour of a wide range of systems (Pilkey *et al.*, 2013). Many different environmental models have been developed and as such, there is a large variety available which are aimed at solving different problems.

Numerical models are increasingly being used to simulate coastal behaviours, providing powerful tools that can give an insight into their complex morphodynamics and sensitivities (e.g. Ashton *et al.*, 2001; Nam *et al.*, 2009; Nicholls *et al.*, 2012). Simulating changes in these environments over the mesoscale is highly relevant for coastal management and also fits with our historical frame of observation for model validation and calibration (French, Thornhill and Burningham, 2014; van Maanen *et al.*, 2016). This mesoscale sits between reductionist studies (‘bottom-up’, small-scale) and synthesist (‘top-down’, large-scale) investigations, which have traditionally been the focus of research into coastal behaviours (Figure 3.1) (van Maanen *et al.*, 2016).

Reductionist or ‘bottom-up’ models are designed to investigate small-scale processes that act over relatively short timescales (Figure 3.1) (van Maanen *et al.*, 2016). They typically simulate complex behaviours to a high level of detail

and attempt to include a large range of processes that could influence the evolution of the system (van Maanen *et al.*, 2016). Using these types of models for mesoscale applications can be impracticable since there are a large number of processes that can be simulated over relatively long timescales, multiplying computational expensive (van Maanen *et al.*, 2016).

Synthesist or 'top-down' models are designed to simulate large-scale behaviours that act over longer time periods and often include only a few parameterised processes (Figure 3.1) (Murray, 2007; van Maanen *et al.*, 2016). They are intended to represent general behaviours and patterns in natural systems, rather than answer specific research questions (Murray, 2007). As such, synthesist models are relatively limited in their ability to provide a level of understanding and prediction of coastal behaviours that are required for mesoscale research (Murray, 2007).

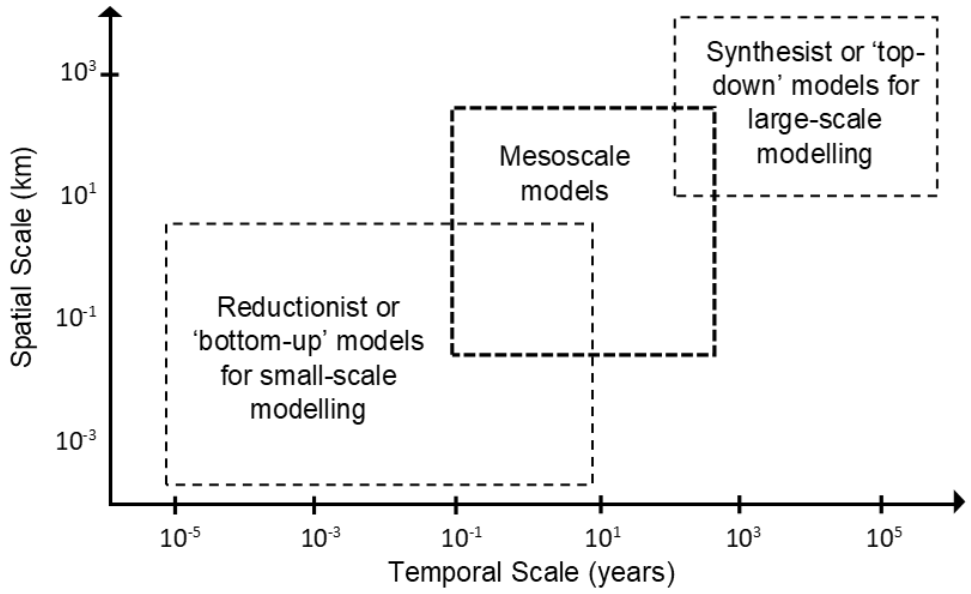

Figure 3.1 Spatial and temporal ranges for traditionally reductionist and synthesist models, with mesoscale models within the scale appropriate for coastal management (adapted from Gelfenbaum and Kaminsky, 2010; van Maanen et al., 2016)

One of the challenges of mesoscale modelling is parameterising key processes that act over much longer or shorter time periods, but which also influence behaviours at the mesoscale. Decisions have to be made about which processes to include in these models since each process can add computational expense and uncertainty, which can propagate errors or inaccuracies over long simulated timescales (Murray, 2007; Hutton, 2012). Therefore, mesoscale morphodynamic coastal models need to be parsimonious and include only fundamental processes that capture the main physical dynamics of a system, thus minimising model uncertainty.

Mesoscale models are less commonplace in geomorphology compared to those that address smaller or large-scale systems and processes. Examples of existing mesoscale coastline models are shown in Table 3.1 and are discussed in the following sections. The list given in Table 3.1 is not comprehensive but includes a number of relevant models commonly cited in the literature and which are representative of the current methods used for simulating the behaviour of coastal environments. They are classified here according to their one-, two- or three-dimensionality, into which a large proportion of these models fall. Due to cost, access or availability constraints, a number of these models could not be sourced and so the review is based on model documentation, literature and current applications of the software.

Table 3.1 A summary of popular mesoscale coastline evolution models that currently exist within published literature. The list is not exhaustive but highlights a number of commonly cited, relevant models.

Model Name	Description	Domain Structure	Spatial Scale	Temporal Scale	Reference
COVE	The Coastal One-line Vector Evolution (COVE) model is designed to investigate the geomorphic evolution of coastal features, over decadal to centennial scales.	Vector (Links and nodes)	$10^1 – 10^2$ kms	Decades to millennia	(Hurst *et al.*, 2014)
CEM	The Coastline Evolution Model (CEM) is a one-contour line sediment transport model that is designed to simulate the planform evolution of coastal systems.	Cellular	$10^1 – 10^2$ kms	Years to millennia	(Ashton *et al.*, 2001)
GENESIS	The GENEralized Model for SImulating Shoreline Change (GENESIS) is a one-line, grid-based model designed to simulate wave-induced shoreline change.	Cellular	$10^1 – 10^2$ kms	Monthly to yearly	(Hanson, 1989; Hanson and Kraus, 1989)
MIKE 21	MIKE 21 is a modular two-dimensional coastal modelling tool that can simulate complex hydrodynamic and sediment transport processes, amongst others, in coastal systems.	Cellular	Multiple	Multiple	(Warren and Bach, 1992)
Delft3D	The Delft3D package integrates various modules that are designed to simulate hydrodynamic flow and sediment transport, amongst other processes.	Cellular	Multiple	Days to centuries	(Lesser *et al.*, 2004)

3.3.1 One-Dimensional Coastal Models

The Coastal One-line Vector Evolution (COVE) model is a one-line model designed to investigate the evolution of coastal features over decadal to millennial scales (Hurst *et al.*, 2014). COVE is a vector-based model that depicts the coastline as a series of nodes and divides the area into polygonal, trapezoid or triangular cells depending on the shoreline's geometry (Hurst *et al.*, 2014). The cross-shore profile of a coastline is assumed to be constant over the long term and its position is dictated by alongshore sediment transport processes (Hurst *et al.*, 2014). Sediment transport is a function of the breaking wave height and angle of approach, calculated according to the diffraction and refraction of offshore waves (Hurst *et al.*, 2014). The COVE model is a relatively new model and has limited applications at present. However, it has successfully been used to investigate the sensitivity of crenulated bays to different wave climates (Hurst *et al.*, 2015). The authors argue that the vector approach, which is distinct from the other cellular-based models discussed here, is more suited to modelling concave or convex coastlines and the complex topographies of spits, bays and islands.

The Coastline Evolution Model (CEM) is a one-contour line sediment transport model that is designed to simulate the planform evolution of coastal systems via wave-driven alongshore sediment transport (Ashton *et al.*, 2001; Ashton and Murray, 2006; Valvo *et al.*, 2006). The model is designed to simulate the mesoscale evolution of coasts in predominately wave-dominated, sandy environments. Being one-dimensional and reduced complexity, the CEM's purpose is not to accurately replicate and predict the evolution of specific coastal areas, but rather explore fundamental cause-effect relationships using as fewer processes, that are represented in their simplest form. It is typically used to investigate the evolution of shoreline shapes under a range of wave climate

conditions, considering the asymmetry and angle of approaching waves (Ashton *et al.,* 2001). A lithological component in the model can be used to limit the erodibility of cells and the material available for transport, allowing the simulation of, for example, fixed sections of coastlines and headlands (Valvo, Murray and Ashton, 2006). Whilst the CEM is able to give an insight into the one-line evolution of a given shoreline, its one-dimensionality prevents the exploration of more complex geomorphological processes. The dynamics of the shoreface and bathymetry as the shoreline retreats or advances is not simulated and the water level is kept at a constant, preventing it from being used to investigate the effects of sea level change (Ashton and Murray, 2006).

The CEM has been used extensively to explore how wave conditions can influence the planform shape of shorelines. Ashton and Murray (2006) identified five key shoreline responses to an ensemble of wave climates, as defined by their asymmetry and proportion of high angle waves: (1) a flattened shoreline; (2) migrating alongshore sand waves; (3) cuspate bumps; (4) flying spits and (5) reconnecting spits. The relationship found between the wave climate and shoreline shape has been compared to a number of coastlines around the world, including the Carolina Capes, North America (Ashton and Murray, 2006); Long Point Flying Spit, Canada (Ashton and Murray, 2006); and the crenulate shaped Holderness Coast and Spurn Point spit feature, UK (Barkwith *et al.*, 2014b). Further studies have investigated how rapid changes in the wave climate, as induced by climate change, could affect rates of shoreline change along cuspate coasts, such as the southeast US coast (Slott *et al.*, 2006). The lithological components in the model have also been used to investigate how a coastline's geological structure can affect how it is shaped and evolves (Valvo *et al.*, 2006).

As further explored in Chapter 6, the CEM has also been used to investigate hysteresis in coastal systems and the theory that antecedent environmental conditions can influence the future evolution of the shoreline (Thomas *et al.*, 2016).

Similar to the CEM, the GENEralized Model for SImulating Shoreline Change (GENESIS) is a one-line, grid-based model designed to simulate wave-induced shoreline change (Hanson, 1989). It is capable of simulating coastline evolution over monthly or yearly timescales and has been applied to a variety of environments due to its generalised approach to modelling (Hanson, 1989; Young *et al.*, 1995). A primary use of GENESIS is modelling coastal engineering structures and their effect on shoreline change (Hanson and Kraus, 1989; Gravens, Kraus and Hanson, 1991). In accordance with the other models, GENESIS assumes that the beach profile remains constant over the long term, with the advance or retreat of a coastline dictated by sediment transport processes that are determined primarily by the wave height and direction (Hanson, 1989; Young *et al.*, 1995). The ability of GENESIS to simulate the influence of engineered structures gives it an advantage over some coastline evolution models (Hanson, 1989). Using simplified equations, the model can calculate the diffraction, refraction and shoaling of waves around a structure and the influence of barriers on the movement of sediment (Hanson, 1989).

Young et al., (1995) dispute the accuracy of the GENESIS model and its ability to predict coastline evolution due to its generalised assumptions about coastal processes. However, it has been successfully used to model shoreline change at Lakeview Park in Ohio (Hanson, 1989), Oarai beach in Japan (Kraus and Harikai,

1983) and it is the official model used by the US Army Corps of Engineers (Hanson and Kraus, 1989; Gravens *et al.*, 1991).

3.3.2 Two-Dimensional Coastal Models

MIKE 21 is a two-dimensional, modular coastal model designed to simulate physical, chemical and biological processes in these environments (Warren and Bach, 1992). Within the basic package, the model is capable of simulating flows, water levels, waves and sediment transport, amongst other processes which can be purchased as add-on modules (Warren and Bach, 1992). There are a range of hydrodynamic, wave and sediment transport modules designed to represent different types of processes. For instance, wave modules range from spectral wind-waves to detailed Boussinesq wave simulations with surf and swash processes (DHI, 2017). Each of these processes are modelled on a rectilinear grid, using one of three domain modes; single grid, multiple grids and a flexible mesh (DHI, 2017). The single and flexible meshes can take advantage of parallel processing which can improve the performance of the model (DHI, 2017). The intended spatial and temporal scale of model simulations is not explicitly stated in MIKE 21's documentation, suggesting that it is flexible depending on the study in question.

Many applications within the literature focus on relatively short-term processes and use time steps from seconds to minutes. For instance, Wang *et al.*, (2012) used MIKE 21 to investigate the combined effects of sea level rise, land subsidence and storm surges on low-lying areas of Shanghai's Coastline in China. Using predicted data as inputs to the model, three sets of simulation were run to explore likely effects in 2030, 2050 and 2100 (Wang *et al.*, 2012). Each simulation was run for 48 simulated hours with a 30 second time step (Wang *et*

al., 2012). However, there are some applications over wider spatial and temporal timescales, including to investigate the impact of groynes on littoral drift over yearly to decadal scales (Kristensen *et al.*, 2016), but these appear less common.

3.3.3 Three-Dimensional Coastal Models

The Delft3D package is a three-dimensional morphodynamic modelling package that incorporates the most processes and the highest level of physical realism of the models summarised here. It integrates modules that simulate hydrodynamic flow, wave generation and propagation, the transport of water-borne elements (e.g heat), sediment transport, ecological processes, water quality parameters and morphological change (Lesser *et al.*, 2004). Each module in the model is discretised into either a Cartesian rectangular, orthogonal curvilinear or spherical grid (Lesser *et al.*, 2004). It uses layers or a staggered grid, referred to as the Arakawa C-grid, to organise each variable. The FLOW module within Delft3D is fundamental to modelling sediment transport processes and morphological change (Lesser *et al.*, 2004). It solves the shallow water equations and is designed to predict flow dynamics in a wide range of environments, including coasts and estuaries (Lesser *et al.*, 2004). Waves can be simulated in the model through a separate WAVE module, which calculates wave heights, peak spectral period, wave direction and so forth (Lesser *et al.*, 2004). These wave processes drive sediment transport and move material as either suspended or bed-load (Lesser *et al.*, 2004). However, Delft3D is complex to set up and implement and can have very long computation run times. This presents a fundamental limitation in applying Delft3D to large spatial extents and/or simulating long time scales of mesoscale environments.

3.4 Model Development

The development of a suitable model for this research was guided by a set of criteria to ensure that the model fulfilled the aims of this research, as outlined in Chapter 2. The criteria are as follows:

1. The model should simulate coastal systems at the mesoscale, from 10^1 – 10^2 years and 10^1 – 10^2 kms.
2. Sandy coastal systems are the focus of this research, so the model should be able to simulate fundamental behaviours in these environments.
3. The model should represent longshore sediment transport, which is suggested to be highly influential to coastal morphodynamics at the mesoscale.
4. A theoretical representation of coastal systems is preferred, so the model can be applied to a variety of sandy coastal systems rather than be site-specific.
5. A cellular structure is preferred to allow for integration with other software and modules in future developments of the model.

All of the approaches described in Section 3.3 have limitations, in terms of their suitability for this research according to the criteria above. COVE, GENESIS and CEM are one-dimensional, meaning the coastline is represented simply as a line with little accommodation for the nearshore shape or bathymetry. This means the models are relatively parsimonious and fast but are limited in their application to investigate the effects of sea level rise on coastal geomorphology. Conversely, the two-dimensional model MIKE 21 and the three-dimensional model DELFT3D can represent the nearshore and bathymetry to a high level of detail and simulate complex hydrodynamics and sediment transport along coasts, but their

complexity and long model run times mean exploring the effects of sea level rise over decadal to millennial time scales is presently impracticable. Therefore, there is a gap for a more reduced complexity two-dimensional coastal models that can simulate coastal features along with the nearshore bathymetry but are parsimonious enough to enable short run times to answer research questions about coastal evolution at mesoscales.

With the model development criteria and existing coastal models in mind, the Coastline Evolution Model 2D (CEM2D) has been developed for this study. It is based on the underlying assumptions of the one-dimensional CEM, but which has been adapted to apply sediment transport processes over a two-dimensional grid. This allows the representation of the morphology of coastlines in more detail and also incorporates changing water levels. A key aim of model development is to create a tool to improve our understanding of the mesoscale morphodynamic behaviour of coastal systems, their sensitivities and the influence that climate change may have on their evolution over decadal to centennial timescales. The model's operation and parameterisations are described in full in the remainder of this chapter.

3.4.1 The Coastline Evolution Model (CEM)

As CEM2D is based on many concepts developed for CEM, it is important to first describe the operation of the CEM in more detail. The model is grid-based, dividing a planform coastline into a grid of regular square cells of a user-defined size (m). Each of these cells contains a fractional proportion of sediment (F_i) that represent its horizontal fill across the domain. Cells containing Fi values equal to 1 constitute the land; values greater than 0, but less than 1 represent the shore; and values equal to 0 represent the sea (Ashton *et al.*, 2001). The F_i values are

updated according to the longshore transport of sediment and the landward or seaward migration of the shoreline (Ashton *et al.*, 2001). Each cell's erodibility (defined as fast or slow) can also be defined to represent the basic lithological characteristics of a coastline.

The one-dimensional shoreline is located at the interface of cells with F_i values between 1 (land) and 0 (sea). A shoreline search technique is used to locate these shoreline cells, as illustrated in Figure 3.2. The initial shoreline cell on the left side of the domain is located by iterating through the first column of cells from the top to the bottom of the domain until a land cell is found. A clockwise search is then used around the first shoreline cell to locate the next cell. This is then repeated until all shoreline cells are found. This method is also used in CEM2D.

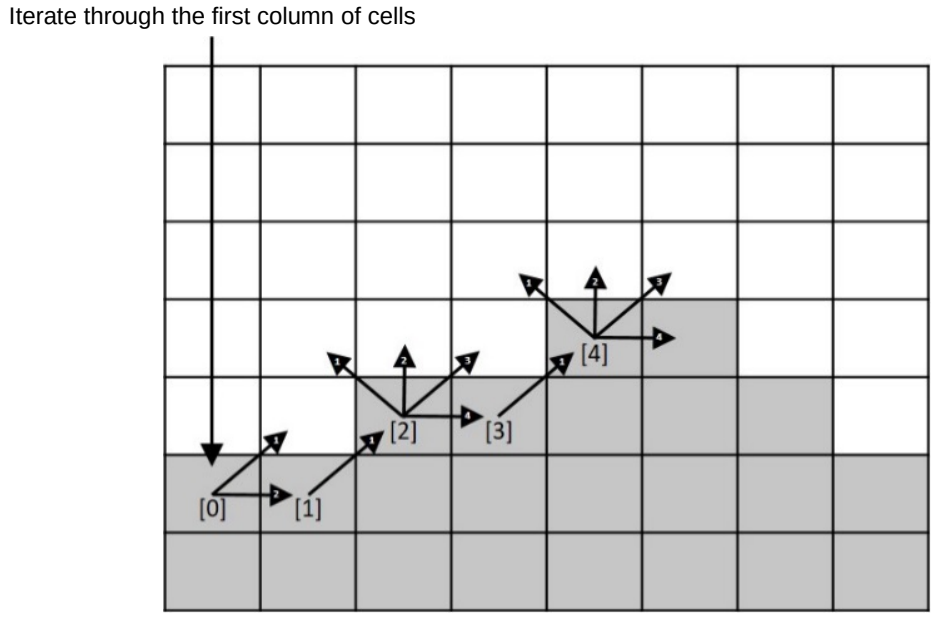

Figure 3.2 A schematic of the shoreline search technique used in CEM (and CEM2D) to map the X and Y location of shoreline cells. The shoreline cell number is given in square brackets and the number on each arrow is the iteration of the clockwise search from the shoreline cell where it originates.

The sediment flux and net erosion or accretion of material in each cell determines the cross-shore movement of the shoreline. The flux is controlled by wave-induced sediment transport calculated using an adapted and more simplistic

version of the CERC formula (also commonly referred to as the Komar (1971) formula), written in terms of breaking wave quantities (Equation 3.3):

$$Q_s = KH_b^{\frac{5}{2}} \sin(\phi_b - \theta) \cos(\phi_b - \theta)$$

Equation 3.3

Here, Qs is the sediment flux (m^3/day), K is a calibration coefficient, H_b is the breaking wave height (m), φ_b is the breaking wave angle (º) and θ is the local shoreline orientation (º). Unlike the CERC formula given in Equation 3.1, Equation 3.3 does not include direct terms for sediment porosity, sediment density or gravitational forces.

Breaking wave characteristics are calculated from an offshore wave climate that is transformed over assumed shore-parallel contours, using Linear Wave Theory (Ashton *et al.,* 2001). An arbitrary offshore water depth is iteratively reduced, and the offshore wave angle and height recalculated until the waves break. The wave climate characteristics at the point of breaking are then used to compute the sediment flux between each cell and the net erosion or deposition of sediment using Equation 3.4 (Ashton *et al.,* 2001).

$$Q_{s,net}: \Delta F_i = Q_{s,net} \Delta t / (W^2 D_i)$$

Equation 3.4

Where W is the cell width and D_i the depth to which significant sediment transport occurs, known as the Depth of Closure (DoC). The DoC is defined as the location from the shore where the depth of water is greater than the depth of wave influence and therefore, the flow has a negligible impact on cross-shore sediment transport; this depth is often approximated as half the average wavelength (Hallermeier, 1978; Nicholls, R.J., Birkemeier, W.A. and Hallermeier, 1997; Pinet, 2009). The assumed location of the DoC in CEM is the point where the

continental shelf and the linear shoreface slope intersect (Figure 3.3) (Ashton *et al.,* 2001). The slope of the shoreface is kept constant and does not evolve morphologically throughout simulations; it is implicit in the model and does not vary in profile. Sediment is not transported out of cells that are shadowed by protruding sections of coastline since they are protected from incoming waves (Figure 3.4).

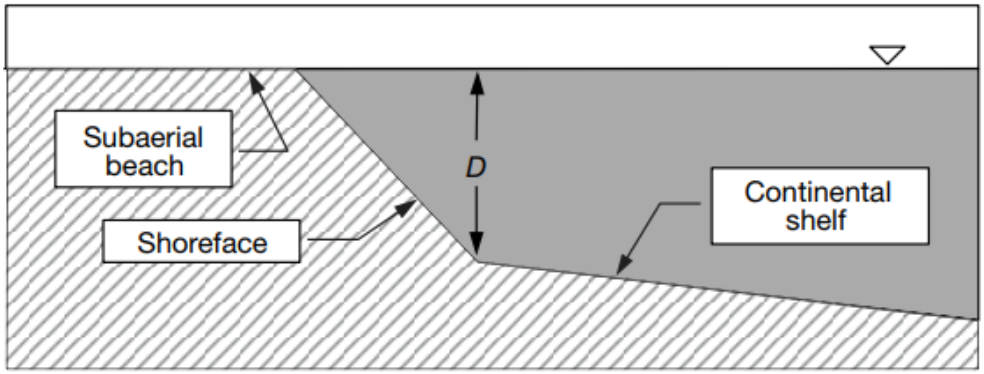

Figure 3.3 Cross-sectional profile of CEM showing the location of the depth of closure, where the shoreface slope intersects the continental shelf slope (Ashton et al., 2001, p. 297)

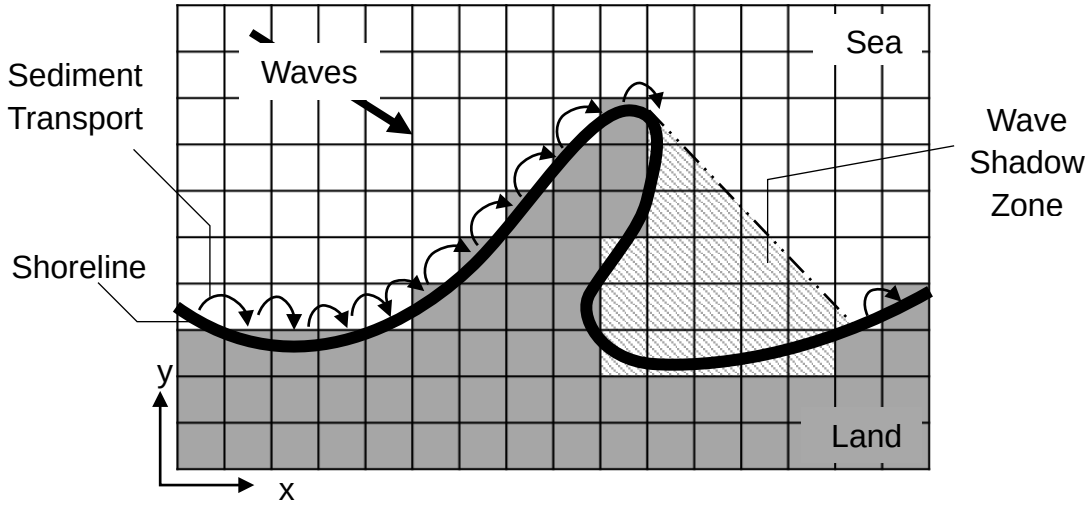

Figure 3.4 Plan-view schematic of CEM2D showing the shadow zone that is formed when protruding sections of coastline prevent waves from approaching the shoreline (Ashton et al., 2001, p. 297)

Where a shoreline cell overfills with sediment, the excess material is deposited in the surrounding empty cells that have a F_i value equal to 0. As cells become

active land cells, the shoreline advances. As CEM is one dimensional, this redistribution of material has no effect on the topographic profile of the coastline, but simply shifts the location of the shoreline to where cells have filled with sediment. If all material in a cell is eroded, but further needs to be transported according to the sediment flux, sediment is removed from full ($F_i = 0$), or partially full cells ($F_i > 0$) landward of the shoreline cell. The shoreline cell is given a F_i value of 0 and the shoreline retreats. In effect, the water level in the model is held constant and cannot be varied, which limits its application to studies interested in the influence of sea level change on coastal evolution.

The initial set-up of the model involves altering values within the source code. There is no Graphical User Interface (GUI) in the model and some understanding of programming is required in order to effectively run the program. The model outputs ASCII (.asc) files containing the rock type and F_i value of each cell in the domain.

3.5 The Coastline Evolution Model 2D (CEM2D)

A number of modifications were made to the concepts of the original CEM to enable it to model the evolution of more complex two-dimensional coastal features and the influence of a variable water level. Here, each stage of the development is discussed and justified.

3.5.1 Model Domain

As per the CEM, in CEM2D the domain is divided into regular square cells of a user-defined size (m), however, each cell contains values for the depth of sediment to a base level (used to represent the continental shelf) (Figure 3.5, F), elevation of sediment above the water level (Figure 3.5, C) or depth of water

(Figure 3.5, C). These values are input into the model from an ASCII file containing either elevation or water depth data for each cell. Having these additional values enables CEM2D to include a two-dimensional representation of the beach and nearshore topography (Figure 3.6).

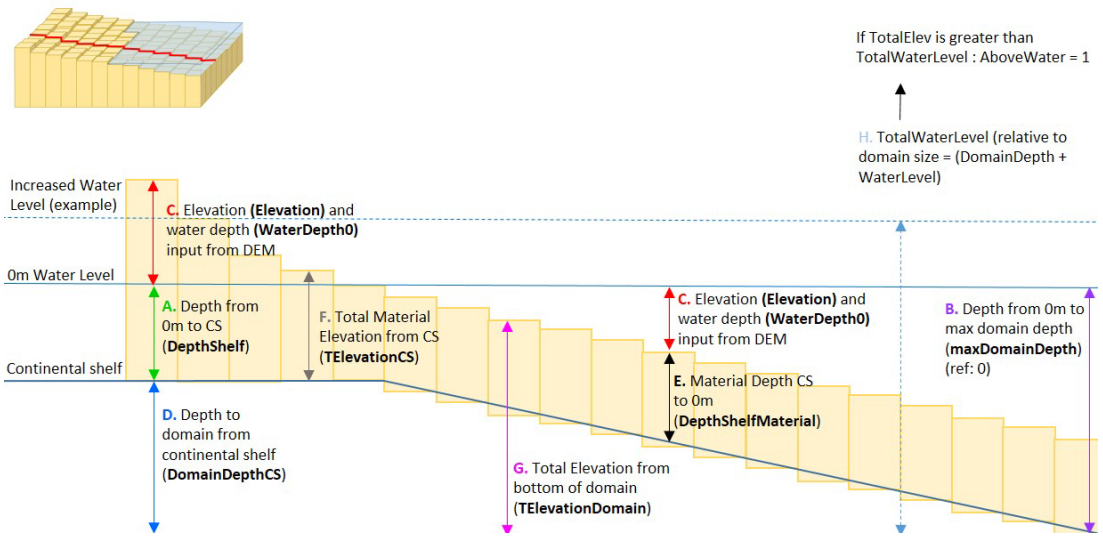

Figure 3.5 Cross-section of CEM2D showing calculations used to derive each cell's sediment metrics from the input DEM.

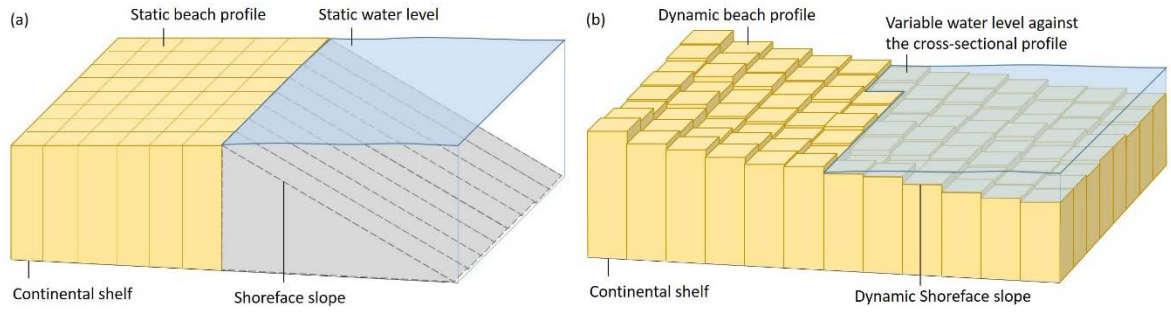

Figure 3.6 Schematics of CEM (a) and CEM2D's (b) profiles, illustrating the difference in structure and dimensionality of the two models

In CEM2D the elevation of each cell above the continental shelf and the water level of the current iteration is used to classify cells as either wet or dry. The interface between these environments is used to locate the one-line shoreline, using the same shoreline search technique as CEM (see Figure 3.2). As the

sediment transport equations are taken from the CEM, it was necessary that this shoreline search technique be retained in CEM2D.

3.5.2 Governing Equations

3.5.2.1 Longshore Sediment Transport

As per CEM, Linear Wave Theory is used to transform the offshore wave climate and the CERC formula to calculate sediment flux between shoreline cells in CEM2D (Ashton and Murray, 2006) (Equation 3.3 and Equation 3.4). A value of 0.4 is used for the calibration coefficient K to represent quartz density sandy. It was not within the scope of this research to alter these equations, although it is understood that there are caveats to their use in CEM2D. This is particularly in relation to the wave breaking equations, which do not take account of the water depth and bathymetric profile in the transformation of waves as they approach the shore. Possibly, other sediment transport equations may prove more suitable for CEM2D, such as the Kamphuis equation outlined in Section 3.2.2.2. This will be considered in future developments of the software, as discussed further in Chapter 8.

3.5.2.2 Sediment Distribution

In natural coastal systems, sediment is redistributed across the coastal profile by the flow of water and by gravitational forces acting on sediment grains. This limits the formation of deep depressions and piling of sediment, contingent upon the material properties. The CEM contains a basic function to prevent too much material being transported between cells that would result in sediment piling or pits forming across the domain. The flux of sediment between shoreline cells and the amount of material that can be removed or deposited is dependent on a cell's percentage fill, whereby a cell cannot exceed 0% or 100% capacity. If it exceeds

100% then the material is distributed to the neighbouring cells and if it is below 0% the shoreline recedes (see Section 3.4.1). However, this technique is not compatible with the two-dimensional domain and sediment handling technique in CEM2D, since the material is stored as volumes or elevations of material on a two-dimensional grid as opposed to percentage capacities. It was, therefore, necessary to develop an alternative method to represent the natural distribution of sediment across the shoreface.

The sediment distribution method was modified in CEM2D to allow longshore and cross-shore sediment transport. Various methods were tested before the implemented technique was chosen, based on a critical evaluation of the results. A description of the chosen method is given subsequently, and details of other techniques can be found in Appendix 1.

The sediment distribution method implemented in CEM2D is a simple threshold-based landslide model that acts to diffuse sediment across the domain. Similar techniques are widely implemented in landscape evolution models, such as SIBERIA (Willgoose, Bras and Rodriguez-Iturbe, 1991) and GOLEM (Tucker and Slingerland, 1994) (Coulthard, 2001). A relationship exists between the properties of coastal material (e.g. sand, gravel) and it's slope angle (McLean and Kirk, 1969) and we can assume that in general, coastal profiles will maintain an average slope angle consistent with the properties of beach material (McLean and Kirk, 1969). Based on this concept, the method implemented prevents material piling or depressions unnaturally forming across the domain and allows the subaerial beach and shoreface profiles to evolve dynamically whilst maintaining an average slope consistent with defined lithological characteristics. This also partially replicates the natural distribution of sediment across coastal

profiles (McLean and Kirk, 1969), induced by a range of processes including currents, waves and swash motions (Aagaard, 2014) that are not simulated in CEM or CEM2D.

In CEM2D, the algorithm checks the entire model domain and identifies where a given angle of repose has been reached between a cell and its neighbour. The material is redistributed, taking account of the elevation and repose angles of the orthogonal surrounding cells (Figure 3.7). The sediment metrics are then updated accordingly, including the total volume of material and the cell's elevation above a reference point. The rules defining *when* sediment redistribution should occur are important parameters that can significantly alter the model outcomes and have therefore been thoroughly tested.

The time interval at which sediment redistribution occurs is controlled by (1) the threshold angle between cells that instigates transport and (2) the frequency that the domain is analysed for these thresholds.

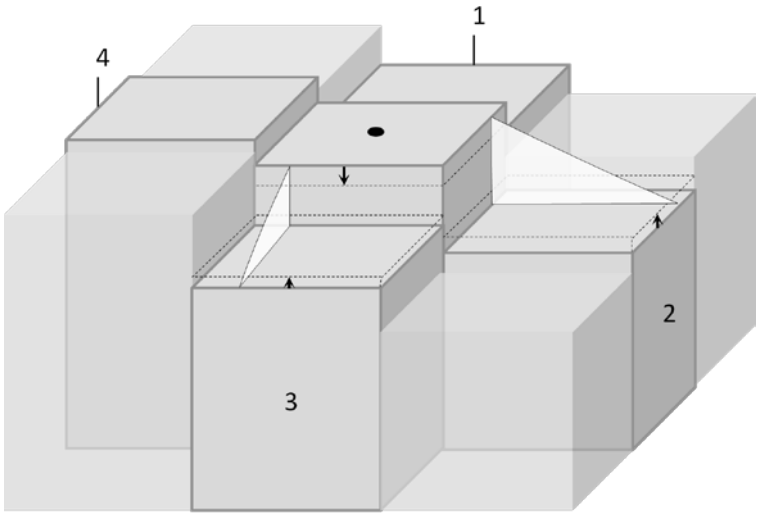

Figure 3.7 Schematic of the sediment distribution technique used to distribute sediment to cells with lower elevations. In the example, the angle between the central cell and cells [2] and [3] exceeds the threshold for diffusion. Sediment is removed from the central cell and redistributed to these cells. Cells [1] and [4] are not readjusted in this iteration but may be in subsequent sweeps of the coastline.

3.5.2.2.1 Sediment Distribution Threshold

The threshold for sediment movement is defined according to slight fluctuations around the average slope of the coastline, which is assumed to reflect the properties of the sediments as discussed (McLean and Kirk, 1969). Various thresholds were tested, including defining two different values for wet and dry material, to reflect the cohesivity of sediments when saturated and the greater angle of repose they are likely to possess compared with dry equivalents (Komar, 1978). However, the two different thresholds created a boundary between wet and dry zones that prevented the smooth transition of material and formed irregularities in the profile.

A further method tested involved two thresholds to define (1) an angle which would instigate the sediment distribution method and (2) the angle between cells to which the equation would attempt to achieve. The purpose of this exercise was to allow sediment to build up in the cells, so enough sediment would be moved each time the method was employed. This proved particularly important when the method was employed at high frequencies, as explored further subsequently. For instance, when the domain is scanned on every iteration, relatively small amounts of material are moved between the shoreline cells, as per the technique in the CEM. If this is then redistributed, one of two processes can occur. Firstly, on the next iteration, this sediment can be moved back to the cell if sufficiently eroded below the threshold for redistribution. The material can then continue to be flicked between these two cells, potentially creating an infinite loop within the operation of the model. Secondly, the material could be transported offshore which reduces the availability of material to form depositional features along the shoreline, resulting in a straight planform shoreline forming regardless of the wave climate.

The experiments using two sediment distribution thresholds reveal a facet of CEM2D and CEM in that accumulations of sediment are required in order to build features along the shoreline that in turn instigate the wave shadowing effects and allow the further development of coastal features. The model needs to have the ability to generate accumulations of sediment to form, sustain and drive the evolution of coastal features. Without these accumulations, no planform morphologies develop regardless of the wave climate.

Based on these findings, a single sediment redistribution threshold was implemented. Using this simplistic setup allows a configuration of sediment threshold and frequency that allows sediment to accumulate in cells and induce suitable instabilities to driven shoreline evolution.

3.5.2.2.2 Sediment Distribution Frequency

The frequency at which sediment is redistributed in the model was found to have a similar role as the sediment distribution threshold outlined in Section 3.5.2.2.1, by enabling sediment to accumulate and create necessary instabilities in the modelled environment. Running the algorithm every iteration smoothed the domain as described above and it is also computationally expensive. Various frequencies were tested against different thresholds, to identify how the model responded to these input parameters. After testing various settings, a 1% threshold and frequency of 10 iterations proved the most suitable combination for the experimental set-up used. This combination allows the coastal slope to dynamically evolve around the mean angle and proved the most effective and realistic when compared to observations of nature, as presented in the results of this thesis. The periodic smoothing of the profile induced by the method at this

frequency reflects the effect of tidal processes that would occur at the timescale of model operation.

It is noted that the threshold and frequency at which sediment distribution occurs should be calibrated according to the characteristics of the coastline being represented. It was found that different frequencies could be used with different wave climate conditions, due to the rate of sediment transport and the balance of cross- and longshore currents. However, for this research, it was deemed important that these values remain consistent throughout the model simulations to allow the results to be compared across this piece of research.

3.5.3 Variable Water Level

CEM2D's two-dimensional structure allows the water level to be changed. Cells with an elevation greater than the current water level are defined as dry cells and those below, as wet cells. By default, the water level is at 0 m elevation but this can easily be increased or decreased by the user. Either a static water level can be defined or a dynamic level that updates throughout the simulation. There are two water level modes within the model which can be run independently or in combination. The 'tidal' mode continually fluctuates the water level, according to a specified cycle, including minimum and maximum water levels and the cycle length (days). This is not intended as an accurate depiction of daily tidal cycles, but as a signal that can be used to represent a varying water level and its influence on cross-shore morphology. The 'sea level' mode gradually increases or decreases the water level over a defined time period, calculating equal increments of change for every time step according to the run duration.

3.5.4 Graphical User Interface

The model also differs from the original CEM as it features a graphical user interface (GUI) that guides users through the initial set-up of the model and the input of key user-defined variables and conditions rather than command line operation (Figure 3.8). The GUI also allows real-time graphic visualisations to monitor how the simulated environment evolves throughout the model run. The graphics window can be updated automatically at user-defined intervals, or manually at any point during the simulations and the graphics shown can be changed according to the user's preference. This can be useful not only for instant analysis but also to identify whether the model is behaving as expected and the variables are suitable for the simulation and environment used. Model outputs (image files and DEM data) can be output at user-defined intervals. CEM2D is written in C# and is freely available from the following repository: https://sourceforge.net/projects/coastline-evolution-model-2d/ (see Appendix 2 for CEM2D's source code).

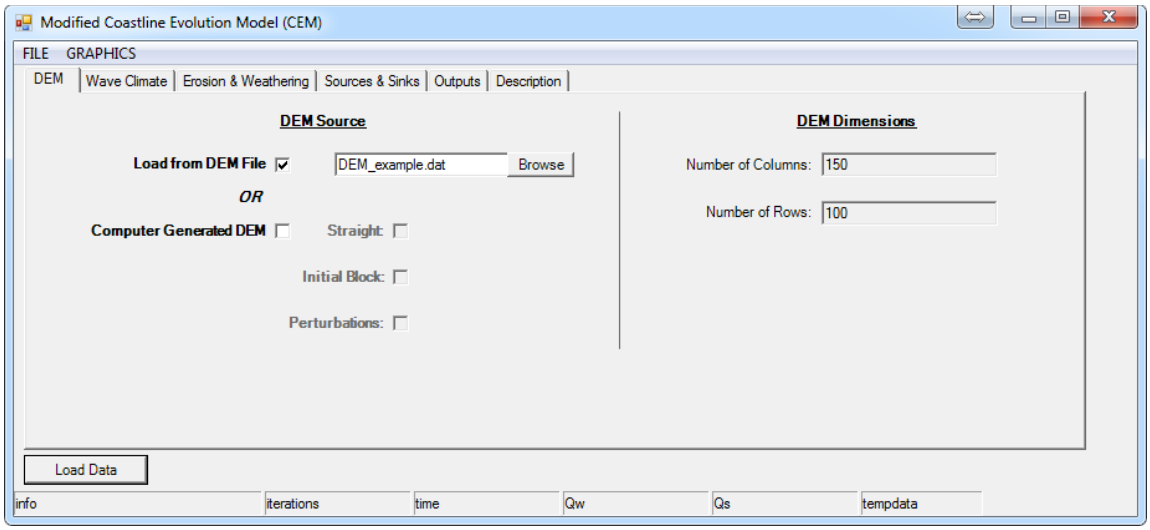

Figure 3.8 Visual of CEM2D's Graphical User Interface (GUI)

3.5.5 Model Structure

The flow diagram shown in Figure 3.9 illustrates the operational structure of CEM2D and an overview of the key processes the model completes on each iteration, or at defined intervals. Data is loaded into the model from external files or according to information entered into the GUI. The wave climate and water level are then set for the current iteration. The position of the one-contour shoreline is located where land and water cells meet, using the shoreline search technique outlined above. Cells within wave shadow zones are found, according to the incoming wave angle and shape of the shoreline. The sediment flux between cells is calculated using the CERC formula and distributed across the coastal profile at defined intervals. If the option is selected, data is output from the model and saved to file. The process repeats until the defined endpoint is reached. If the model is running in batch mode, the model will restart and the input data is reloaded automatically.

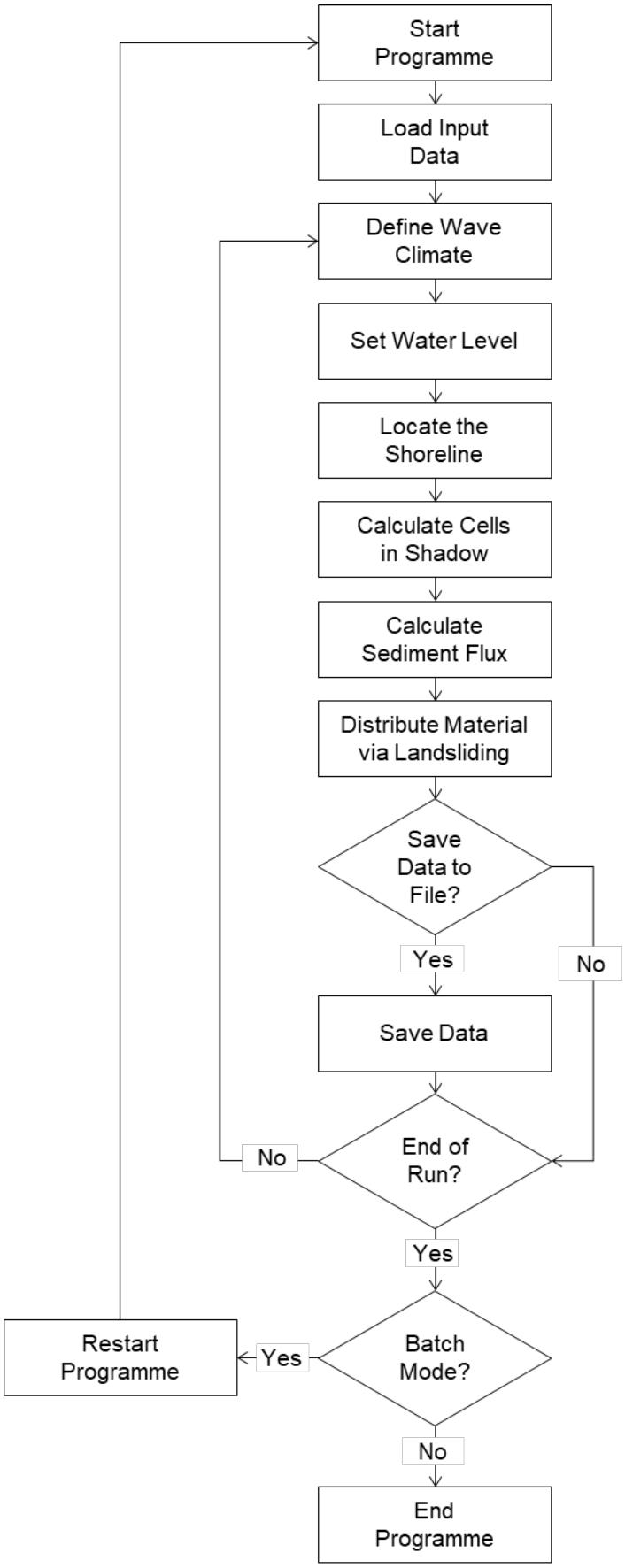

Figure 3.9 Operational flow diagram of CEM2D, listing key processes in the model.

3.6 Model Testing

As part of the development processes, the functions of models must be tested in terms of their ability to represent the system in question and fulfil the aims of the research. This is often a difficult process since no model is capable of accurately representing natural systems without error or uncertainty.

There are three types of tests that should be conducted: (1) a sensitivity analysis to determine which input factors have a significant or negligible influence on model outputs, (2) calibration to refine the key parameters to the system being modelled and (3) validation to determine the fit of model results to the system being represented. These are distinctly different but essential assessments that were each applied to CEM2D throughout its development.

3.6.1 Sensitivity Analysis

Sensitivity analyses are designed to determine how variations in model inputs influence the outputs. They identify the relative importance of variables which can be used to guide the developer or user how the model should be set-up, in order to yield the most accurate results achievable. It also ensures that the model is fit for purpose and is capable of producing results which address the research objectives.

A sensitivity analysis is completed for CEM2D in Chapter 4. A range of input factors are tested including the wave climate, sediment distribution parameters, the domain size, the shape of the initial shoreline and the water level. As reported in Chapter 4, the results of this test varied depending on the behavioural indices used to assess model sensitivity. However, the wave angle and height consistently showed relatively high sensitivity whilst the shape of the initial shoreline has a relatively negligible influence.

3.6.2 Model Calibration

Model calibration refers to the processes of altering input values in the model to improve the comparison between modelled and observed data (Oreskes *et al.*, 1994). The calibration of processes in this research is informed from the sensitivity analysis in Chapter 4 and initial model testing. Knowledge of the sensitive input factors and of the accuracy of model results to natural coastal systems informs how the model should be tuned to provide a more accurate representation of the systems.

3.6.3 Model Validation

Model validation refers to the processes of legitimising the model in question and determining whether it provides a suitable representation of the studied system (Oreskes et al., 1994). However, a valid model does not necessarily denote an accurate model but indicates that the internal processes are consistent with the test data, most commonly derived empirically or from laboratory results (Oreskes *et al.,* 1994).

Validating numerical models is a complex process and one that is impossible to complete accurately, to provide an exact representation of the studied system (Oreskes *et al.*, 1994). Common limitations associated with model validation include the lack of data to compare to model results, lack of understanding of how the actual system in question behaves, issues associated with scaling processes between the actual system and the model processes and lastly, limitations induced by the tools or method used (Oreskes *et al.,* 1994; Valters, 2016). Limitations associated with the tools and methods are commonly related to computational efficiency and the ability to simulate only a limited number of processes over a given time period (Oreskes *et al.*, 1994; Valters, 2016).

Considering the exploratory nature of the numerical model developed and the limitations listed above, for this research, we refer to model validation in terms of how well results of CEM2D fit with observations of natural coastal systems and with the empirically tested CEM. During the development of CEM2D, the ability of the model to simulate fundamental processes in natural systems was assessed. Further validation was also conducted alongside the generation of results for this thesis, as part of the research analysis. The results of these tests are presented within each results chapter.

3.7 Discussion

The new features in CEM2D described above enable it to model complex two-dimensional coastal profiles and evolve their morphology according to wave-induced sediment transport processes. The ability of the coastal system in CEM2D to evolve dynamically across the entire domain provides a more realistic representation of the morphodynamic behaviour of these systems, as will be demonstrated in subsequent chapters.

Importantly, restructuring and increasing the dimensionality of the model allows us to explore how the profile of the coastal systems changes with the shape of the shoreline. In many one-line models, the cross-shore profile of the coastline is kept constant and it is assumed that its core geometric properties are retained over meso-spatiotemporal scales. Whilst this is a well-used and scientifically grounded concept, there are advantages to modelling the two-dimensional morphodynamics of the beach and shoreface and it is necessary if we are to consider the influence of a variable water level.

The sediment storage and handling technique allow complex landforms and features to develop. The topographic profile of coastal landforms is indicative of their formation and evolution, highlighting patterns in sedimentation and drift processes. How this profile changes over time can inform the stability and future behaviour of the feature. The formations both influence and are influenced by the surrounding environment. As a landform evolves, it alters the bathymetry and sediment availability within and around itself. Where depositional features migrate longshore or evolve, remnants of the features can be left behind creating a morphological ‘memory’ or ‘inheritance’ that is preserved within the system. This can interact with other features as they form and evolve (Thomas *et al.*, 2016).

A key component of CEM2D is its variable water level. We can use this functionality to explore the response of coastal systems to fluctuating water levels, including the influence of fundamental climate change effects such as sea level rise. If we are to explore coastal evolution over the mesoscale, being able to model the effect of rising sea levels is essential. The power of this tool is vast and will be particularly useful for coastal managers who must plan for the dynamic evolution of these systems over time periods that will be highly influenced by the effects of climate change.

Whilst the developments of CEM2D boast many advantages, there are also a number of caveats that should be noted, but which are explored further in Chapter 8. The methods used to redistribute sediment across the two-dimensional coastal profile would preferably be employed on every iteration, consistent with the timestep of the model. However, as discussed, this smoothes the shoreline and prevents instabilities in the model that are required to form and evolve the

shoreline shapes. This is inherited from the CEM since much of its structure has been retained in the current version of CEM2D. In future developments, the structure of the model and sediment handling techniques could be reviewed and improved further to mimic natural processes. However, the results generated by the current version are suitable for the purpose of the study here.

3.8 Conclusion

In this Chapter, an overview of the development of CEM2D from the one-dimensional CEM has been presented. The structure and governing mathematical equations that drive model simulations have been described and their uses justified. The model sits between more traditionally developed one- and two-dimensional models that explore smaller and larger scale processes respectively. This mesoscale two-dimensional model is capable of simulating more complex systems than synthesist models but with greater computational efficiency than reductionist models.

With its additional functionalities and increased complexity, it is apparent that the model will enable us to conduct interesting and insightful investigations to answer research questions including how entire coastal profiles behave under changing environmental conditions and how sea level change might influence their morphodynamic behaviour.

Through the development of CEM2D, a two-dimensional mesoscale numerical model capable of simulating wave-driven coastal evolution and a variable water level, this chapter has contributed to addressing Research Objective 1:

> *"To develop and test a two-dimensional coastline evolution model which can be used to understand the behaviour of coastal systems according to*

the driving wave conditions and their likely response to climatic changes over meso-spatiotemporal scales" (see Chapter 2).

In the following chapter (Chapter 4), CEM2D will be tested to determine its functionalities through a sensitivity analysis as well as parameterised to select the optimum set-up conditions for this research.

Chapter 4

Development of CEM2D, Part II: A Sensitivity Analysis and Selection of Model Parameters

Research Results

4.1 Introduction

In the previous chapter, a detailed description of the Coastline Evolution Model 2D (CEM2D) and the development processes was given. The use of numerical models such as CEM2D in environmental science is becoming more commonplace, as the advance of technology improves our ability to simulate complex systems and understand their behaviours (Tucker and Hancock, 2010). Our increasing reliance on the outputs of these models warrants that the tools be suitably and thoroughly tested to ensure results are as reliable as can be achieved (Campolongo *et al.*, 2007). Sensitivity Analyses (SA) are designed for this purpose and should be completed before a numerical model is applied.

This chapter is divided into two main parts. First (Section 4.2), a review is given of different types of SA and a suitable method is chosen to test the sensitivity of model outputs to key input variables, which can inform how CEM2D should be set-up (Saltelli *et al.*, 2008). This is an essential process in the development of CEM2D and is completed here before the model is used to answer questions of the simulated coastal environment. The second part of this chapter (Section 4.3) uses the results from the SA (Section 4.2) to refine the values of the tested model inputs and ensure that sensitive factors are suitably defined.

This chapter, in combination with Chapter 3, will address Research Objective 1 of this study, which is outlined in Chapter 2 and reiterated in Section 4.4.

4.2 A Sensitivity Analysis

The first section of this chapter focuses on selecting and completing a suitable SA for CEM2D.

4.2.1 Sensitivity Analyses

Saltelli (2002, p. 579) defined SA as *"the study of how the uncertainty in the output of a model (numerical or otherwise) can be apportioned to different sources of uncertainty in the model input"*. This practice ensures that the user fully understands the abilities of the model, its limitations, its assumptions and its fit to the intended purpose (Saltelli *et al.*, 2008). Since numerical models are coarse representations of reality, regardless of the detail they provide, no environmental model can accurately represent and simulate the behaviour of a given system. Therefore, it is important to understand how the models work in order to interpret and apply the results.

There is a clear distinction between model sensitivity as described here, using a given model to identify the sensitivity of an environment to changing conditions and conducting an uncertainty analysis (UA) to generate a probabilistic measure of model fit to empirical or observed data. The SA presented in this Chapter aims to identify the sensitivity of a model as a mathematical entity and ascertain whether variations in the input values can be accredited to variation in the outputs (Yang, 2011; King and Perera, 2013; Iooss and Lemaître, 2015). Inputs that are identified as being highly influential to the outputs of the model are important to set-up accurately, as they can have a greater bearing on how the model performs and processes data. It does not necessarily suggest that those factors are key drivers in the environmental system, only that they influence how the model behaves numerically.

There are a number of key questions that can be asked of the relationship between model inputs and outputs including, but not limited to (Campolongo *et al.*, 2007; Iooss and Lemaître, 2015; Skinner *et al.*, 2018):

1. Which input variables have the greatest influence on models outputs?
2. Which input variables have a negligible influence on model outputs?
3. Which variable interactions amplify and which lessen variance in the outputs?

Using these questions as a basis, SA methods are typically designed to either rank, screen or map input variables against the outputs (Pianosi *et al.*, 2016). Ranking methods assess the relative influence of inputs factors on the outputs of a model, screening is often used as a preliminary analysis to identify which, if

any, inputs have a negligible impact on the model outputs and mapping is used to visualise the spread of outputs and identify any outliers in the input space.

Performing an SA is an important step in the development and use of a numerical model (Ziliani *et al.*, 2013). However, whilst this concept is widely accepted, there are few examples of their application (Ziliani *et al.*, 2013; Skinner *et al.*, 2018). No single accepted method for conducting an SA exists and there is limited guidance on how they should be performed (Mccarthy *et al.*, 1995; Beres and Hawkins, 2001).

4.2.1.1 Types of Sensitivity Analyses

A whole range of SA techniques exists, each designed to answer specific questions of different models. Pianosi *et al.* (2016) proposed a systematic classification scheme for SA methods according to the purpose of the analysis and the number of evaluations required or preferred, as shown in Figure 4.1. The illustration in Figure 4.1 is populated with some of the most widely used SA types in environmental modelling, although it is not an exhaustive list. Each of the five SA classes are explored subsequently and further details on these classifications can be found in Pianosi *et al.* (2016). The techniques used are most commonly classified as being either ‘Local’ or ‘Global’ methods, which use either a ‘One-At-a-Time (OAT)’ or ‘All-At-a-Time (AAT)’ sampling technique (Pianosi *et al.*, 2016).

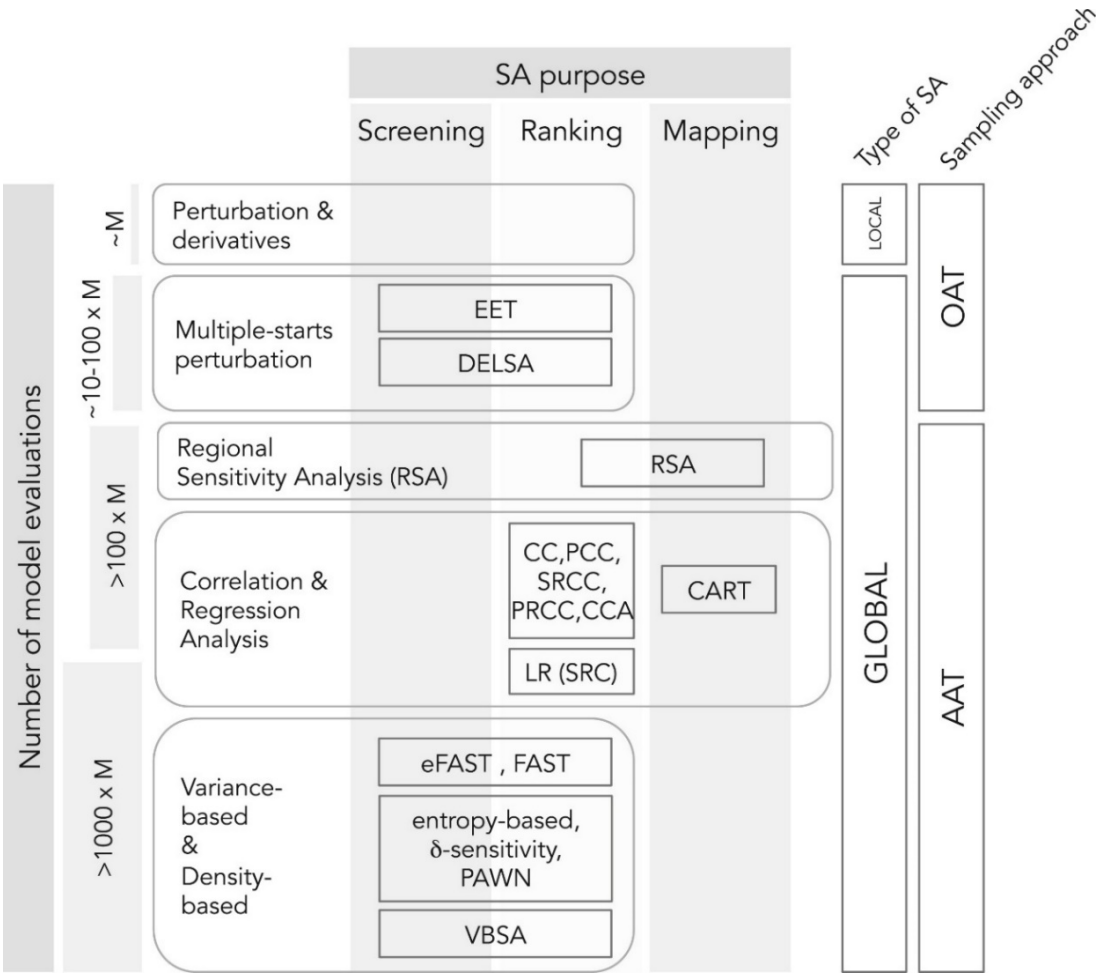

Figure 4.1 Sensitivity Analysis (SA) classification scheme according to the computational complexity and purpose of use. M on the y-axis denotes the number of input factors (adapted from Pianosi *et al.*, 2016, p. 219).

4.2.1.1.1 Global and Local SA

Local SA methods tend to alter one variable per simulation and assess their relative impact on model outputs, and hence often use OAT sampling techniques (Gan *et al.*, 2014; Pianosi *et al.*, 2016). Conversely, Global SA methods are designed to vary a whole range of inputs per simulation and most commonly use AAT sampling techniques, although few use the OAT method (Gan *et al.*, 2014; Pianosi *et al.*, 2016).

4.2.1.1.2 OAT and AAT SA

The distinction between OAT and AAT methods is made according to the input sampling technique used in the analysis. OAT techniques are the simplest form

of sampling techniques used in sensitivity analyses; they are designed to perturb key input variables one-at-a-time and identify the impact each has on model outputs (Pianosi *et al.*, 2016). Changing just one variable each simulation has its limitations in terms of capturing nonlinear interactions between model inputs, but it provides a computationally cost-effective method of pre-screening a model and identifying sensitive input factors for further analysis (Yang, 2011).

AAT methods vary multiple inputs per simulation and are capable of identifying the influence of individual variables as well as the combined influence of many variables on model outputs. Whilst more complex and less cost-effective, Global methods explore nonlinear interactions between variables and typically generate more reliable results compared to Local SA techniques (Yang, 2011; Skinner *et al.*, 2018).

4.2.1.1.3 Perturbation & Derivative SA

The simplest and most common Local SA types are termed Perturbations or Derivative methods (Figure 4.1). Using OAT sampling techniques, these methods are designed to screen or rank input variables according to their relative influence on model outputs (Pianosi *et al.*, 2016). The number of model evaluations is equal to the number of input factors plus one, making them relatively quick to execute and cheap computationally, but with the compromise of only a Local evaluation (Pianosi *et al.*, 2016).

4.2.1.1.4 Multiple-Starts Perturbation SA

Multiple-Starts Perturbation methods are Global types of the Perturbation techniques discussed in Section 4.2.1.1.3. They maintain the OAT sampling technique but combine individual sensitivity results to measure Global input-

output relationships (Pianosi *et al.*, 2016). Hence, they are more computationally expensive than truly Local methods but less-so than full Global techniques, providing a balance between efficiency and detail. The most established form of Multiple-Start SA is the method of Morris (Morris, 1991), also known as the 'Elementary Effects Test' (EET) (Saltelli *et al.*, 2008; Pianosi *et al.*, 2016).

4.2.1.1.5 Regional Sensitivity Analysis (or Monte-Carlo Filtering)

Regional Sensitivity Analyses (RSA) are Global methods that utilise AAT techniques to map the input space which generates extremes in model outputs (Pianosi *et al.*, 2016). Using Monte Carlo Simulations, whereby model input data is derived from repeated random sampling, model outputs are typically classified as 'behavioural' or 'non-behavioural' according to whether they fall within or outside expected results (Saltelli *et al.*, 2008; Pianosi *et al.*, 2016). The inputs that generate non-behavioural outputs are considered most influential in the SA (Saltelli *et al.*, 2008).

4.2.1.1.6 Correlation and Regression SA

Correlation and Regression based SA also use Monte Carlo simulations to measure the relationship between model inputs and outputs through statistical analysis (Pianosi *et al.*, 2016). This sampling technique is categorised as an AAT method, used to assess Global sensitivity for ranking or mapping purposes (Pianosi *et al.*, 2016). Common types of Correlation and Regression based sensitivity analyses include using the Pearson Correlation Coefficient (CC), the Partial Rank Correlation Coefficient (PRCC) and the Standardised Regression Coefficients (SRC) (Pianosi *et al.*, 2016).

4.2.1.1.7 Variance-Based SA

Variance-based sensitivity analyses are based on the assumptions that the model output distribution can be attributed to variance in stochastic input variables and be used to measure sensitivity (Norton, 2015; Pianosi *et al.*, 2016). As a Global method that uses an AAT sampling technique, the influence of inputs and groups of interacting inputs can be measured (Pianosi *et al.*, 2016). Variance-based methods were first introduced in the 1970s by Cukier *et al.,* (1973) who developed the Fourier Amplitude Sensitivity Test (FAST). However due to its computational intensity, the application of FAST is relatively limited (Saltelli *et al.*, 2008). A high number of model runs are often required, particularly for models with large parameter spaces (Saltelli *et al.*, 2008).

4.2.1.1.8 Density-Based SA

Density-Based methods are similar to variance techniques discussed in Section 4.2.1.1.7, but consider the influence of inputs on the Probability Density Function (PDF) of model outputs as well as the variance (Pianosi *et al.*, 2016). They boast advantages over Variance techniques since they can suitably measure the sensitivity of different distribution types, including those which are highly skewed (Pianosi and Wagener, 2015). However, as with other Global AAT methods, they can be highly computationally expensive (Pianosi and Wagener, 2015).

4.2.2 Methodology

The choice of SA should be based on the questions being asked by the sensitivity investigation, the type of model being analysed, and the purpose of the overall study (Pianosi *et al.*, 2016). A number of methods have been outlined in Section 4.2.1, highlighting the difference between complex Global types and more simplistic, computationally inexpensive Local techniques. Multi-Starts

Perturbation methods sit between these categories, providing an SA that is efficient but can assess model sensitivity across the Global parameter space. For this research, Multi-Starts Perturbation methods provide a suitable level of analysis by screening key input factors and highlighting those that require attention during model set-up. As the most common type of Multi-Starts Analysis, the Morris Method (1991) will be applied here to CEM2D.

4.2.2.1 The Morris Method

The SA method proposed by Max Morris in 1991 (Morris, 1991), also termed the 'Elementary Effects Test' and which was adapted by Campolongo *et al.* (2007), uses multiple Local SA to approximate model sensitivity across a Global parameter space. The primary aim of this method is to identify whether the relationship between individual model inputs and outputs are (a) negligible, (b) linear, (c) nonlinear or (d) are influenced by other input factors (Morris, 1991). Each input factor is ranked, according to their relative influence on model outputs (Brockmann and Morgenroth, 2007b). The results are often used as a pre-screening test to highlight factors which require more rigorous assessments or which should be given attention during the parameterisation of key inputs to the model (Ziliani *et al.*, 2013; Skinner *et al.*, 2018). For the purpose of this study, it is intended as a pre-screening test to inform the model's set-up.

The Morris Method's design of experiment uses a defined set of values for each input factor, which are discretised into equal intervals and constrained by upper and lower boundaries (Morris, 1991; Ziliani *et al.*, 2013). According to the one-at-a-time sampling technique, each value is altered incrementally per model sensitivity simulation and the elementary effect of each factor on model outputs is calculated according to the variance of performance indices, by Equation 4.1:

$$d_{ij} = \left(\frac{y\left(x_1 x_2 \ \ldots, x_{i-1,}\ x_i + \Delta_i,\ x_{i+1}, \ldots, x_k\right) - y\left(x_1 x_2 \ \ldots, x_{i-1,}\ x_i,\ x_{i+1}, \ldots, x_k\right)}{\Delta_i} \right)$$

Equation 4.1

Where d_{ij} denotes the value of the *j*-th elementary effect (j = 1,…,r) of the *i*-th input factor (and where r is the number of repetitions), $y(x_1 x_{2,\ldots,} x_k)$ is the value of the performance measure, k is the number of factors investigated and Δ is the incremental step value. The main effect is then calculated according to the mean (μ) of multiple elementary effects computed randomly from the parameter space. This measure is used to indicate the relative influence of each input factor on model outputs (Ziliani *et al.*, 2013). The standard deviation ($б$) is also calculated and used to determine which, if any, input factors have nonlinear effects or which have an influence on model output but in combination with other unspecified inputs (Ziliani *et al.*, 2013). Nonlinear behaviour and input-input interactions are complex and challenging to predict. The standard deviation is therefore not intended to specify what these behaviours are or which two or more specific input factors have complex and/or nonsequential interactions, only highlight those individuals that exhibit these sorts of behaviours. For instance, if the wave angle has a high standard deviation, this indicates that it has a non-linear influence on the behavioural index used (e.g. sediment transport rate) or that it influences the index through interactions with other unspecified inputs (e.g. the interaction of the wave angle with the wave height, although this second factor is not identified in the result).

The Morris Method has proven to be a successful compromise between relatively simplistic Local methods and more complex Global techniques (Campolongo *et al.*, 2007). Its design is efficient and relatively computationally inexpensive but

allows for a comparatively large parameter space to be screened to identify the relative influence of inputs factors and depict those that have a negligible effect (Brockmann and Morgenroth, 2007a). However, as a qualitative assessment, input factors are ranked according to their relative importance and no quantification is given of their sensitivity (Brockmann and Morgenroth, 2007a).

4.2.2.2 Design of Experiments for CEM2D

As well as selecting a suitable model, designing the analysis involves choosing the input variables to be perturbed, defining the boundaries of these inputs and setting up the outputs to be analysed (Pianosi, 2015, 2016). The design of experiments can influence model outputs, for instance through the definition of the boundaries of input factors, and so should be considered carefully in terms of the model being assessed and the environmental system it represents.

The Morris Method varies a single input factor per repeat run of the model and so the number of total simulations is dependent upon the number of input factors tested and the number of repeats. Typically, between 10 and 50 repeats are completed (Campolongo *et al.*, 2007) and here, 10 repetitions are used to limit computational expense.

Performance indices are used in the Morris Method as a measure of assessing variations in model outputs from expected results according to data taken from the natural environment. However, this is often not the most suitable approach where there is a lack of data to populate the performance indices and so a more qualitative approach can be used (Skinner *et al.*, 2018). As demonstrated by Skinner *et al.,* (2018) behavioural indices can be used in the place of performance indices. The results can be used to assess how input factors influence model outputs behaviourally, rather than how well it can represent physical processes

in the natural environment. This more qualitative approach is adopted in this thesis.

4.2.2.3 Input Factors

A multitude of inputs factors and processes are used to drive CEM2D, but to test the sensitivity of each using the Morris Method with 10 repeats according to the available resources would be computationally expensive; as shown later in this chapter (see Section 4.3.2.1 and Section 4.3.3.1) the runtimes vary according to the parameters used but at the largest domain size of x = 90 km, the model takes approximately 38 hours to compute 100 simulated years' worth of data. Further, through the continual exploratory tests completed during the development of the model there are a number of input factors known to have a negligible effect on model performance and including these in the sensitivity test would render no additional information or understanding. Hence, few input factors are selected based on their known importance in driving key processes in the model or due to their unknown influence. This includes the conditions of the wave climate, sediment distribution behaviours, the water level and the set-up of the domain. The minimum and maximum levels selected for each of the input factors are within the bounds relevant to this research, as explained subsequently. Since this sensitivity test ranks factors relatively, driving the model with extreme values that would not be used in the subsequent experiments could skew the results and not provide a suitable representation of model sensitivity relevant to the study. Each input factor used in the sensitivity test is listed in Table 4.1 and justified below.

Table 4.1 A table listing the 8 input factors used in the Morris Method.

Code	Factor	Intervals	Minimum	Maximum
1	Wave Angle (º)	5	1	5
2	Wave Height (m)	5	1	6
3	Wave Period (s)	5	1	14
4	Sediment Redistribution Frequency (iterations)	5	10	50
5	Sediment Redistribution Threshold (%)	5	1 (%)	100 (%)
6	Water Level Change (m)	5	0	2
7	Initial Shoreline Shape	3	1	3
8	Domain Width (km)	3	1	3

4.2.2.3.1 The Wave Climate

The first three factors in Table 4.1 define the primary characteristics used to define the wave climate conditions. The purpose and foundations of the CEM and inherently CEM2D are to understand the influence of the wave climate on the behaviour of coastal systems and so it would be expected that these inputs would have an influence on model outputs. Prior exploratory modelling supports this theory. The wave angle is defined according to a Probability Distribution Function (PDF) defined in Chapter 3, defining the proportional wave asymmetry (*A*) and

proportion of high angle waves (*U*) approaching the coastline. Five wave angle conditions were selected, based on the spread of values used throughout this thesis, as shown in Table 4.3. The maximum values used for the wave height and wave period represent the average Global values, with the minimum set at 1 m and 1 s respectively (Young, 1999).

Table 4.2 A list of the 5 wave climates used in the Morris Method, according to values of A and U.

Number	**Proportional Asymmetry (*A*)**	**Proportion of High-Angle Waves (*U*)**
1	0.7	0.55
2	0.5	0.65
3	0.7	0.65
4	0.9	0.65
5	0.7	0.75

4.2.2.3.2 Sediment Distribution Method

One of the primary developments in CEM2D, necessitated from the increased dimensionality of the model and complexity of sediment transport processes, is the addition of the sediment redistribution method that allows the transport of sediment cross-shore (Chapter 3). The frequency that the method is employed in the model and the threshold defining when distribution should occur are the fundamental inputs controlling the process. As a new function in the model that has shown to influence model outputs during exploratory testing, the frequency

and threshold of sediment distribution are included in the sensitivity test (Table 4.1, factor number 4 and 5).

The minimum and maximum values chosen for the sediment distribution factors were informed by the exploratory tests completed during the development of CEM2D. As stated in Chapter 3, according to the experimental set-up conditions a threshold of 1% allows the morphology of the coastline to evolve dynamically around the mean slope angle with a maximum of 100%, to provide an extreme value for comparison purposes. A minimum frequency of 10 iterations was chosen as it enables sediment to accumulate which was necessary for the shoreline and its features to form, sustain and evolve. A maximum of 50 iterations was chosen, as prior modelling has shown that the lower the frequency the greater the nonlinearity of the system due to sediment piling up.

4.2.2.3.3 Water Level

The increased dimensionality of the domain in CEM2D allows the influence of a change in water level to be assessed and is an important factor to consider in the sensitivity test (Table 4.1, factor number 6). This will ensure that it is set-up suitably and the outputs are interpreted in accordance with its known sensitivity.

In this study, a rate of water level change will be induced between 1 m and 2 m elevation from the base level per 100 years (see Chapter 7) and so these values were chosen as the minimum and maximum values for the SA. Positive values were chosen since the influence of a rising sea level on the morphodynamics of coastal systems is explored in this study.

4.2.2.3.4 Initial Conditions

Factors 7 and 8 in Table 4.1 define some initial conditions in the model that define the geometry of the initial shoreline shape and the size of the domain. Ashton and Murray (2006a, 2006b) completed tests on CEM and revealed that it is not sensitive to these conditions. However, Thomas *et al.,* (2016) demonstrated that under some conditions the evolution of the shoreline simulated in CEM is influenced by initial or remnant morphologies. It is currently unknown whether CEM2D is sensitive to the initial conditions, but it could be induced by the increased complexity of sediment handling techniques and is therefore included in the sensitivity test.

Three shoreline shapes were chosen for the test: (1) a straight shoreline, (2) a perturbed shoreline as used in the studies of Ashton and Murray (2006a, 2006b) and (3) a spun-up shoreline. The spun-up shoreline was generated from the final geometry of a simulated coastline after 3,000 simulated years (or when in a quasi-equilibrium state prior to the premature termination of the run) assumed to be at equilibrium, driven by the exacting environment conditions but from a slightly perturbed shoreline. This decision to use a perturbed shoreline when creating the spin-up condition was based on modelling of the CEM and exploratory tests with CEM2D which gave the understanding that sediment transport and the formation of features is delayed or halted when the shoreline is straight due to the coarse sediment transport techniques. Three domain sizes were tested within the mesoscale, as relevant to this study including (1) 10 km (2) 30 km and (3) 60 km longshore shoreline length.

4.2.2.4 Behavioural Indices

The behavioural indices chosen for this study are listed in Table 4.3, with the frequency at which the data is recorded.

Table 4.3 A table showing the 4 behavioural indices used in the Morris Method and the frequency that data is recorded in each simulation.

Number	**Behavioural Index**	**Recording Frequency**
1	Longshore sediment transport rate (m^3 / 10 years)	3650 model iterations (10 simulated years)
2	Coastal sinuosity	3650 model iterations (10 simulated years)
3	The ratio of wet-dry areas	300 model iterations (300 simulated days, to align with each diffusion frequency tested)
4	Run duration (simulated years)	1095000 model iterations (3,000 simulated years)

Each behavioural index describes a core element of CEM2D's behaviour and outputs which can be used to demonstrate its sensitivity to the input factors listed in Table 4.1. Longshore sediment transport is a key element which is fundamental to evolving the coastal system. The sinuosity of the coastline is an indicator of the types of shorelines that evolve and can be used to determine the amount of potential morphodynamic change. The ratio of wet and dry cells can be used to indicate erosional or depositional behaviours. The run duration (in simulated

years) is a measure of a number of model behaviours including nonlinearity and dynamism, which can show both sensitivities and model error.

4.2.3 Results of the Morris Method

Figure 4.2 shows the aggregated mean and standard deviations for each of the elementary effects, calculated for each of the four behavioural indices (Table 4.3). The aggregated scores for both the mean and standard deviation are calculated from the sum of the ranking position (1-8) of each input factor, for each behavioural index. The higher the mean, the greater the influence of that factor on model outputs and the higher the standard deviation, the greater the nonlinearity (Ziliani *et al.*, 2013; Skinner *et al.*, 2018). As described in Section 4.2.2.1 this nonlinearity refers to the nonsequential effects of the given factor on model sensitivity or that it influences model behaviour through complex input-input interactions (Ziliani *et al.*, 2013). In the legend of Figure 4.2, the ranking of each input factor is also given according to the means of each behavioural index. A ranking of 1 denotes a factor with the most relative influence on variations in the outputs and a ranking of 8 showing the least influence.

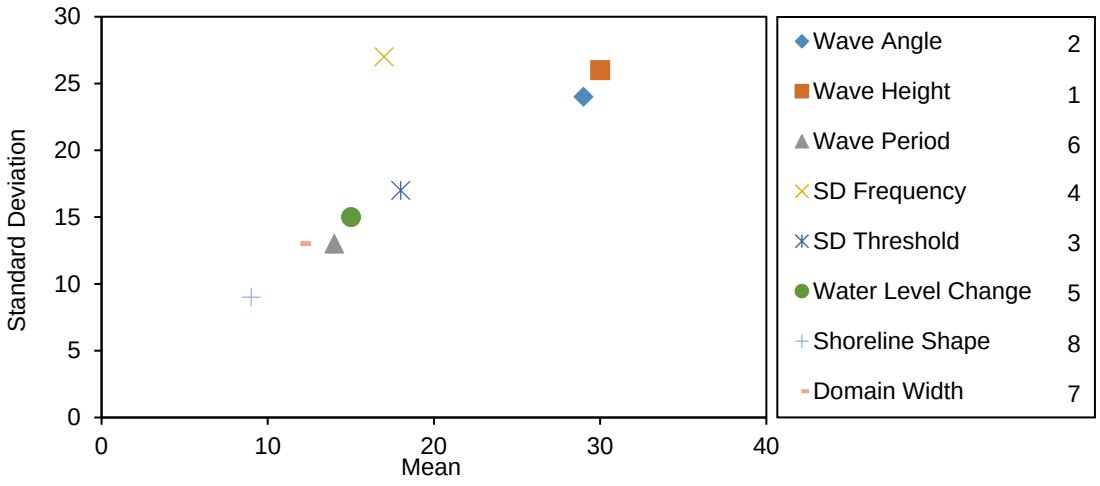

Figure 4.2 Aggregated means and standard deviations for each elementary effect, calculated according to each of the four behavioural indices (SD: Sediment Distribution). In the legend, each factor is ranked according to its influence on model sensitivity (1 = most sensitive, 8 = least sensitive)

The wave height is ranked as the most influential to the sensitivity of CEM2D, with the wave angle ranked second with a mean difference of just 1. The set-up of the domain in terms of both the domain width and initial shoreline shape shows the least influence on model sensitivity.

There is a trend which shows that with increasing mean, factors show increasing standard deviation (Figure 4.2). The sediment distribution frequency is an outlier, showing a mean ranking of 4/8 but a relatively high standard deviation. This suggests that it has an average influence on model sensitivity compared to the other factors, but generates complex nonlinear behaviours when combined with other factors.

4.2.3.1 Model Performance According to the Behavioural Indices

Figure 4.3 shows the mean and standard deviation of each of the input factors according to the four behavioural indices individually. As shown in the aggregated results, the greater the influence of input factors on model outputs, the greater the nonlinear or complexity of interactions with other inputs (Figure 4.3). The results do not reveal, however, what nonlinear behaviours occur or which input-input interacts influence model behaviour. However, there is only a weak relationship between the mean and standard deviation for results according to the ratio of wet-dry areas (Figure 4.3c). The sediment distribution frequency shows a relatively low influence on model sensitivity when assessed according to the ratio of wet-dry areas, with the other factors clustered at a higher mean and standard deviation.

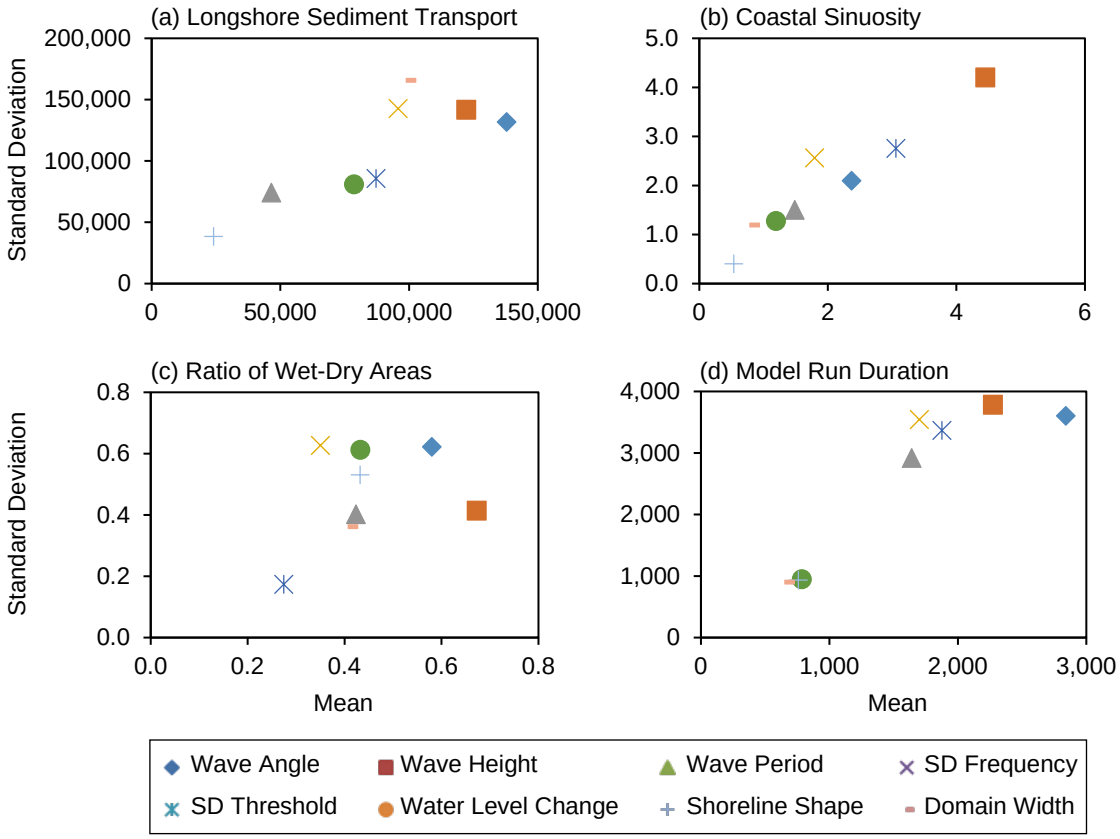

Figure 4.3 The mean and standard deviation of results from the input factors, according to the four behavioural indices labelled a-d.

Across all behavioural indices, there is a pattern observed in where input factors rank according to the mean, as reflected in the aggregated scores (Table 4.4). The aggregate results show that the wave angle and height have the highest ranking influence on model behaviours, followed by sediment distribution factors and the domain set-up is considered the least influential. Considering the rankings according to the individual performance indices, a similar pattern is observed (Table 4.4).

Table 4.4 Summary table of input factor rankings from CEM2D, including those calculated from four behavioural indices and aggregated scores. The behavioural indices including the longshore sediment transport rate (LSTR), coastal sinuosity, the ratio of wet-dry areas and the model run duration.1 = Most Sensitive, 8 = Least Sensitive.

Code	Input Factor	Aggregate Rank	LSTR	Sinuosity	Wet-Dry	Run Duration
1	Wave Angle	2	1	3	2	1
2	Wave Height	1	2	1	1	2
3	Wave Period	6	7	5	5	5
4	Sediment Distribution Frequency	4	4	4	7	4
5	Sediment Distribution Threshold	3	5	2	8	3
6	Water Level Change	5	6	6	3	6
7	Shoreline Shape	8	8	8	4	7
8	Domain Width	7	3	7	6	8

The principal differences are in the ranking of sediment distribution parameters and domain set-up characteristics when assessed according to changes in the wet-dry ratio of cells (Figure 4.3 and Table 4.4). The sediment distribution factors rank average or above average according to the other behavioural indices, but rank lowest for the wet-dry area ratio. Other exceptions include the wave period, which ranks lower than average when calculated according to the longshore sediment transport rate. The change in water level has a below average influence in general but ranks higher according to the ratio of wet to dry cells. The set-up of the domain (shoreline shape and domain size) consistently ranks low, but the shoreline shape has an average influence on the ratio of wet to dry cells and the size of the domain shows a relatively high influence on longshore transport rates.

The variation in the ranking of input factors according to the behavioural index also induces a change in those factors which show nonlinear behaviours; some factors show a high standard deviation when analysed according to one behavioural index, but have a low value when analysed according to a different index. This is with exception to the ratio of wet-dry areas and run duration indices where a relatively large proportion of input factors demonstrate nonlinear behaviours regardless of their sensitivity ranking.

The raw data recorded for the model run duration behavioural index can further indicate patterns of model behaviour and sensitivities between model inputs and outputs. Since the Morris Method is a one-at-a-time technique, differences in the sequential pattern of run durations can highlight sensitive factors which cause the model to terminate prematurely.

The graph in Figure 4.4 shows the run duration of each of the 90 model simulations. The maximum run duration was set at 1095000 iterations, representing 3,000 years. Only 28 of the 90 simulations reached this maximum simulation time with the other runs terminating prematurely, giving an average run duration of 1,437 years.

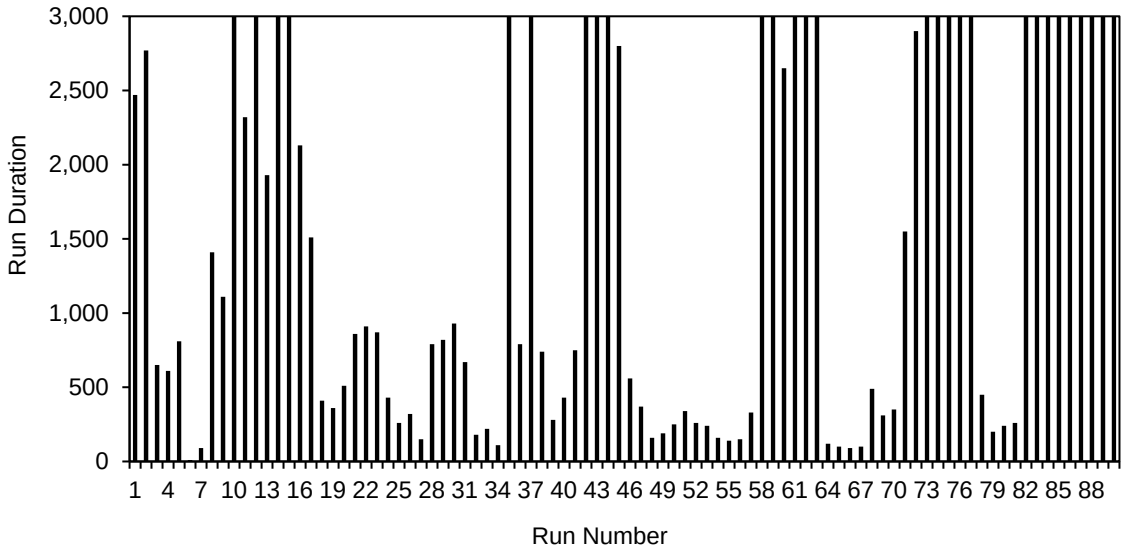

Figure 4.4 A graph showing the run durations (years) for each of the 90 model simulations.

A sharp increase or decrease in model run duration is observed between simulations, for instance between run number 34 and 35 which have total run durations of 110 years and 3,000 years respectively. The factor that has been incremented between these runs is assumed to have a significant influence on the behaviour of the model. Since this pattern is observed recurrently in Figure 4.4, it is suggested that there are input factors which do have a significant influence on model outputs (whether independently or in combination with other inputs), indicated through significant changes in model run durations.

An analysis of the pattern of run durations in Figure 4.4 shows that the most significant changes, both in terms of a significant increase or decrease in model run duration from the previous simulation, occur where the wave angle, wave

height or sediment distribution threshold are altered. This is concurrent with the findings in Figure 4.3 and Table 4.4, as these three factors rank as the top three influential inputs to variations in model outputs.

4.2.4 Discussion

The SA presented in this chapter demonstrates the influence of a selection of key model input factors on model outputs in CEM2D. The results identify the inputs that have a greater influence on the behaviour of the model and also those which lead to nonlinear, possibly complex interactions with other factors. A correlation was also found between inputs which induced variations in model outputs and those which exhibit nonlinear behaviour or complex input-input interactions.

It was found that the rankings of the various input factors differ according to the behavioural indices used to assess model sensitivity, each of which describes a different behaviour in the model. For instance, the water level shows a high influence on model behaviour when assessed against the ratio of wet to dry cells but according to the sinuosity of the shoreline, is ranked just below average (Figure 4.3, Figure 4.5 and Table 4.4).

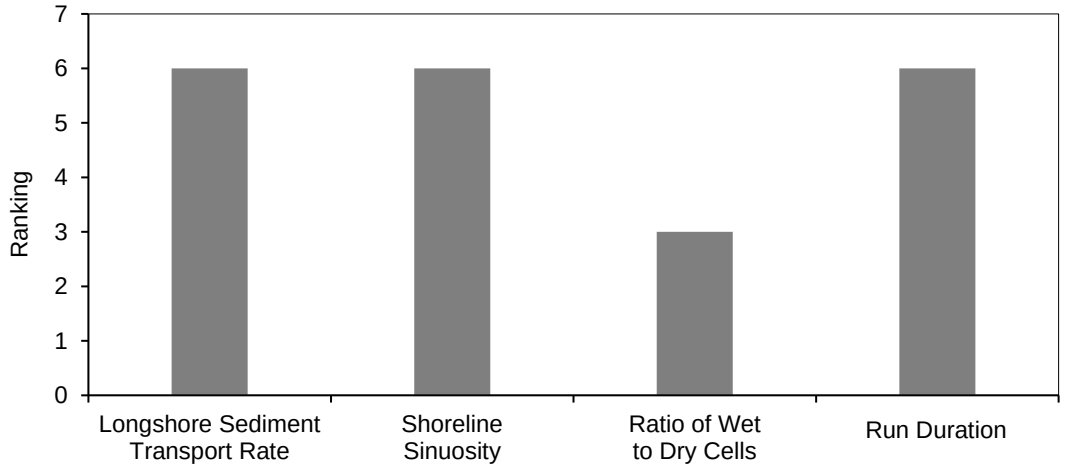

Figure 4.5 Water level ranking, in terms of the factors relative influence on model outputs compared to the other input factors used in the Morris Method, according to the ratio of wet to dry cells (1 = Most Sensitive, 8 = Least Sensitive).

To illustrate this, Figure 4.6 compares outputs from simulations after a period of 300 simulated years where the water level has been incremented by (a) 0 m per 100 years and (b) 0.5 m per 100 years; no other factors have been altered. The shape of the shoreline remains relatively consistent, whilst the shoreline shows a greater level of recession at a higher rate of water level increase (Figure 4.6b). The sinuosity of the shoreline is therefore not influenced significantly by changes in this factor with a greater rate of sea level rise. The ratio of wet-to-dry areas increases in the example given in Figure 4.6, denoting that a change in water level has a greater influence on this behavioural index.

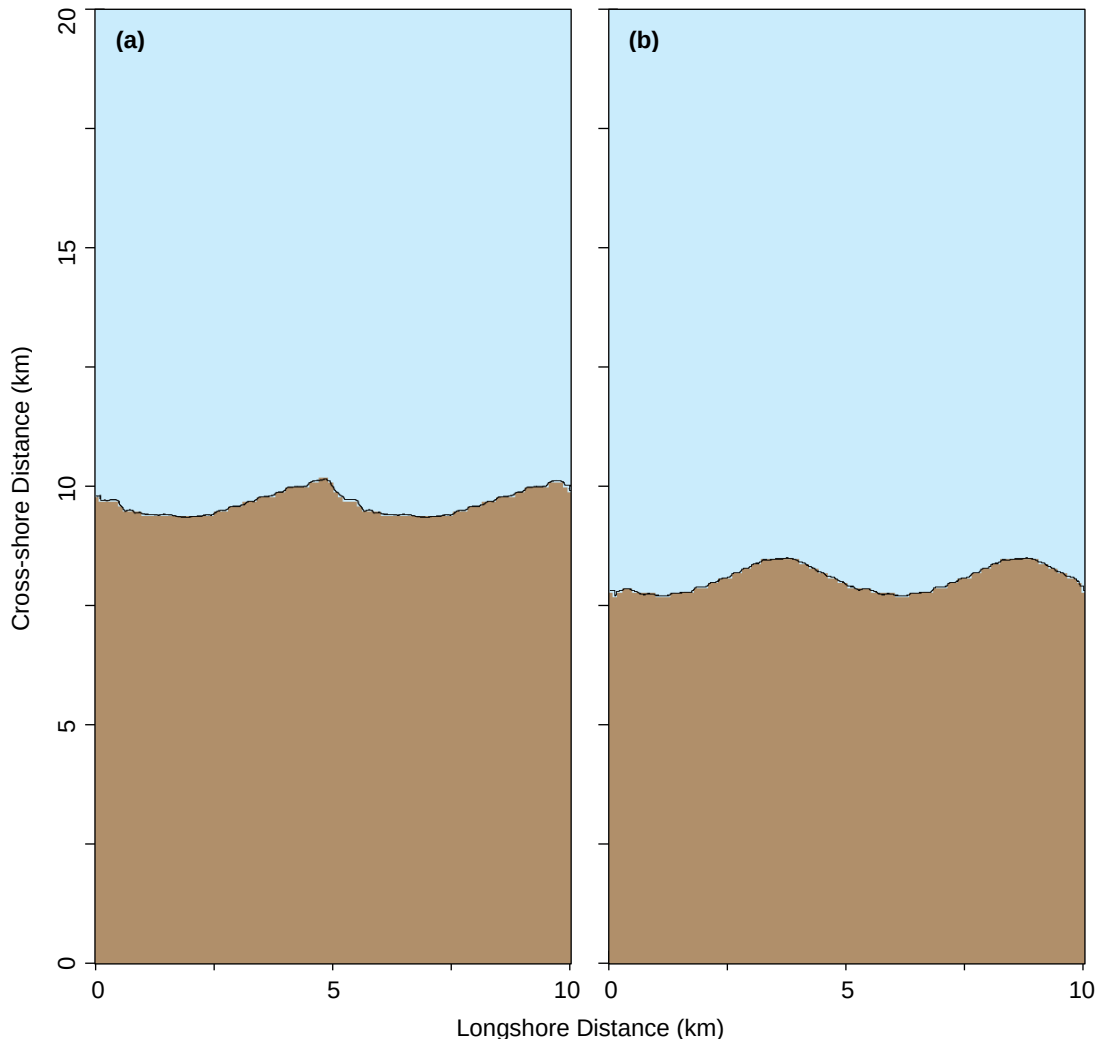

Figure 4.6 Comparison of model outputs after 300 simulated years where the rate of water level change is (a) 0 m per 100 years and (b) +0.5 m per 100 years.

These results demonstrate the complexity of SA tests and highlight that the results can be skewed or highly influenced by the input factors used, the range of values and the behavioural indices that are chosen to assess sensitivity. Care should be taken when constructing an SA and the spread of behavioural indices should be selected to cover the array of model behaviours. This should ensure that major sensitivities in the model are detected and that outlying results are identified. Similar results were found by Skinner *et al.,* (2018) who discussed how different model metrics identified different sensitivities in the Landscape Evolution Model the authors were evaluating. Specifically, their SA ranked input factors differently according to whether sediment yield or geomorphological behavioural indices were used to assess model sensitivity, even though the sediment yield is often considered a suitable proxy for changes in geomorphology (Skinner *et al.*, 2018).

The results generated for the SA are skewed by the varying spread of run durations with approximately 69% of the simulations terminating prematurely. The primary reasons for this termination are due to (1) the complexity of the shoreline and its evolution beyond the capabilities of the model to simulate or (2) the position of the shoreline and its accretion or erosion beyond the domain boundaries (top and bottom). These limitations are inherent from the CEM but have been considered and addressed where possible in the development of CEM2D. However, further developments are required to prevent the premature termination of the model, which is currently beyond the scope of this project. This is discussed further in Chapter 8.

Whilst the premature termination of the model is a limitation in many respects, it can indicate (1) instability in the model (2) nonlinearity, (3) sensitivities or (4)

errors. The results can, therefore, be informative and used to support the findings of the Morris Method. The ranking of input factors according to the run duration has been discussed previously in Section 4.2.3.1, but are comparable to the aggregated score of all behavioural indices presented in Table 4.4.

The results presented in this section have successfully answered the key questions intended of an SA (Campolongo *et al.*, 2007; Iooss and Lemaître, 2015; Skinner *et al.*, 2018), outlined in Section 4.2.1. It has highlighted the principle input factors which (1) have the greatest influence on model sensitivity, (e.g. wave angle, wave height, sediment distribution factors) (2) those which have a negligible influence (e.g. wave period and domain characteristics) and (3) those which show nonlinear behaviours or interactions which can amplify variance in model outputs (those which also have the greatest influence on model behaviour, e.g. the wave angle). The results further highlighted input factors that can have an influence on model outputs, but only according to specific behavioural indices (e.g. water level and domain characteristics). As discussed in Chapter 8, further sensitivity and model testing could be conducted on CEM2D including repeat model runs to determine the influence of stochasticity on the results.

The results of the SA are considered as a pre-screening and are used to inform part two of this chapter, intended for the selection of model parameters and set-up of CEM2D for this thesis. This is to ensure that the inputs which induce a change in the model are as accurately represented as achievable.

4.3 Selection of Model Parameters

Section 4.2 highlighted the sensitivity of CEM2D to key input factors. In this section, the most appropriate model parameters are selected for the simulations

described in the subsequent chapters. These parameters are selected in light of the SA, previous parameter choices in the CEM and on preliminary modelling and exploratory runs to test the influence that different parameters sets could have on model outputs. Attention is given to the wave climate conditions, the sediment distribution input factors and the domain characteristics, for reasons given in the following sections.

4.3.1 The Wave Climate

The wave period shows little influence on the sensitivity of the model, whilst the wave angle and wave height showed a relatively high influence on outputs. Since much of the results are compared to the findings of the empirically tested CEM and particularly the results of Ashton *et al.,* (2001; 2006a, 2006b), the set-up of these inputs were guided by the set-up used by these authors; the wave period is held at a constant value of 8 seconds and the wave height at 1.7 meters. The wave angle is defined according to a Probability Distribution Function (PDF), as used by Ashton *et al.,* (2001; 2006a, 2006b) which provides a value for the proportional wave asymmetry (*A*) and for the proportion of high angle wave (*U*) approaching the shoreline. Details of this method are described in Chapter 3.

4.3.2 Sediment Distribution

The threshold and frequency for sediment distribution show a higher than average influence on model outputs, according to the majority of behavioural indices used in the Morris Method. Through the development of the model, as described in Chapter 3, it was found that the accumulation of sediment in cells is necessary in order to induce change and build features along the shoreline. The threshold and frequency inputs both have the ability to create these accumulations. Since the sediment distribution method in CEM2D is a very

coarse representation of natural processes, these inputs cannot be set-up with empirical values and values must be selected more subjectively based on knowledge of the model and with an understanding of the behaviour of natural systems.

The relationship between the threshold and frequency of sediment distribution is such that a high threshold requires a high frequency in order to prevent accretion or erosion of sediment beyond what would be found in natural systems. A low threshold, therefore, requires a low frequency to allow significant changes in sediment volume in each cell, including accumulations necessary for the development of features. Since it was found that a high frequency is computationally expensive, a preference for a low frequency and therefore a low threshold was given. A threshold of 1% was chosen, which allows the slope to fluctuate whilst maintaining a mean angle; this is applied over the entire model domain.

With a slope threshold of 1% selected, the frequency at which sediment distribution occurs was tested. The sediment distribution technique was tested in the SA using a frequency of every 10 and every 50 iterations, for purposes described in Section 4.3.2.1. The tests were completed using a 60 km coastline, which proved to generate results comparable to the CEM (Ashton, Murray and Arnault, 2001; Ashton and Murray, 2006a, 2006b) as discussed later in this chapter, as well as being an intermediate size at the mesoscale.

4.3.2.1 Frequency Testing

At higher sediment distribution frequencies than those explored here, instabilities occur in the model. This is due to the continual shift of material back and forth between cells; the volume of material in each cell causes the slope angle to

exceed the threshold criteria but not significantly enough to cause more permanent changes. This is illustrated in the results in Figure 4.7, showing the planform shoreline after 3 simulated years with a diffusion frequency of 1 iteration (denoting 1 day). Beyond this timestep, the shoreline continued to exhibit instability, particularly noticeable through the checkerboard effect along the shoreline. The wave climate used in this example is defined by A = 0.7, U = 0.65 which drives both cross-shore and longshore sediment transport.

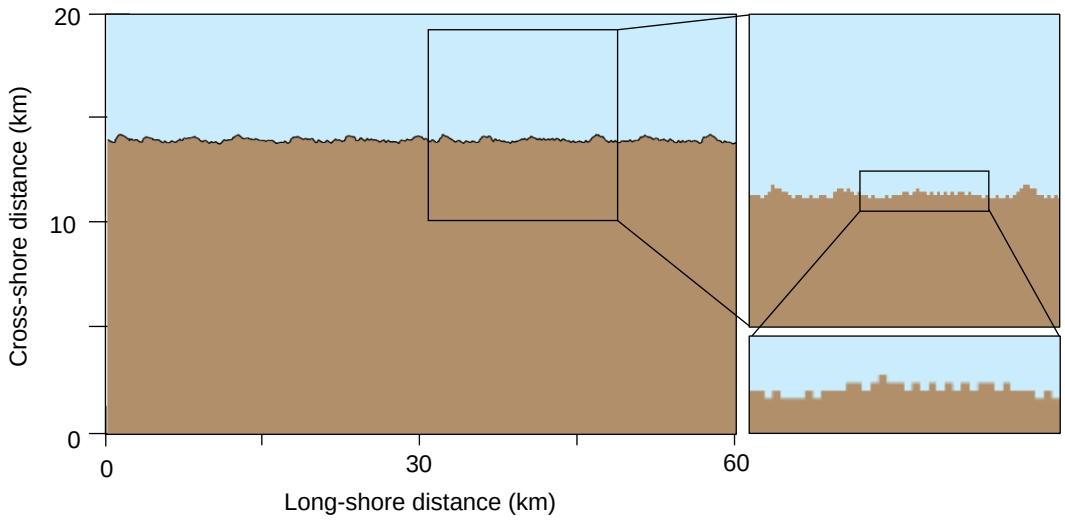

Figure 4.7 Results showing model instability resulting from a high sediment distribution frequency of every iteration. The shoreline is driven by a wave climate defined by A = 0.7, U = 0.65 and the output is recorded after 3 simulated years.

Allowing the one-contour line cells to retain or lose a significant volume of sediment before calculating the volume and direction that it is redistributed reduces the instability observed in Figure 4.7. For this reason, a maximum frequency of every 10 iterations (as used in the SA in Section 4.2) was employed in the investigation here, since this value was devoid of similar levels of instability and checker-boarding.

When the sediment distribution method is employed every 50 simulated years (as used in the SA in Section 4.2), the accumulation of a large amount of material in

the shoreline cells can result in peaks and cliffs forming across the domain. The image in Figure 4.8 illustrates this and shows an output from CEM2D under the same wave climate as in Figure 4.7 but with a sediment distribution frequency of 50 iterations.

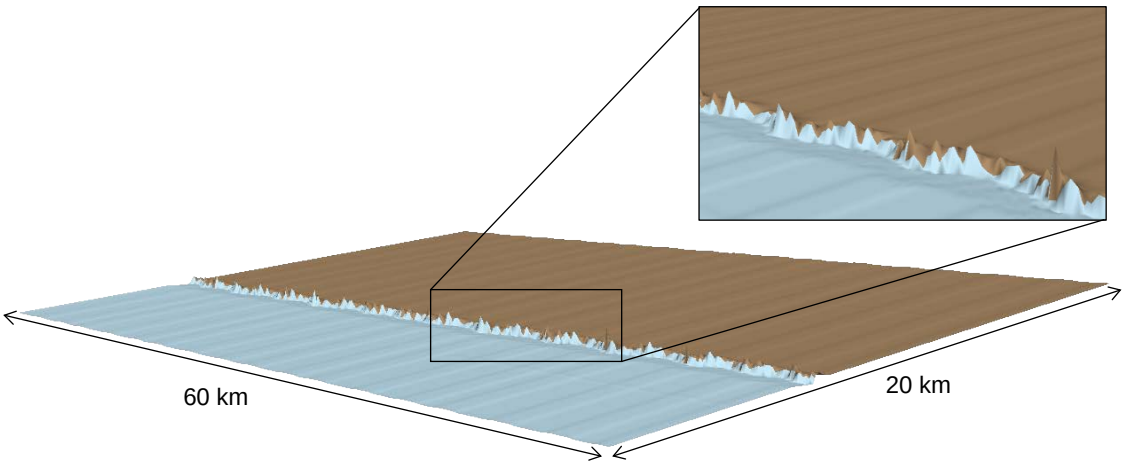

Figure 4.8 Results showing model instability resulting from a low sediment distribution frequency of every 50 iterations. The shoreline is driven by a wave climate defined by A = 0.7, U = 0.65 and the output is recorded after 3 simulated years. The output has been exaggerated by a factor of 10 to emphasize the change in slope.

As noted in Chapter 3, the sediment distribution technique is designed to prevent significant depressions and peaks, as seen in Figure 4.8, forming across the domain. It was therefore considered that a high frequency is required in the set-up of the model. A minimum value of 30 iterations, denoting a monthly cycle, is selected for comparison of results with the maximum defined frequency of every 10 iterations.

The following results compare outputs from CEM2D with the sediment distribution frequency at every 10 iterations and at every 30 iterations (Figure 4.9). Four wave climate conditions are tested which represent a range of scenarios used later in this research and include PDF values where: (1) A = 0.7, U = 0.55, (2) A = 0.5, U = 0.65, (3) A = 0.9, U = 0.65 and (4) A = 0.7, U = 0.75 (Figure 4.9).

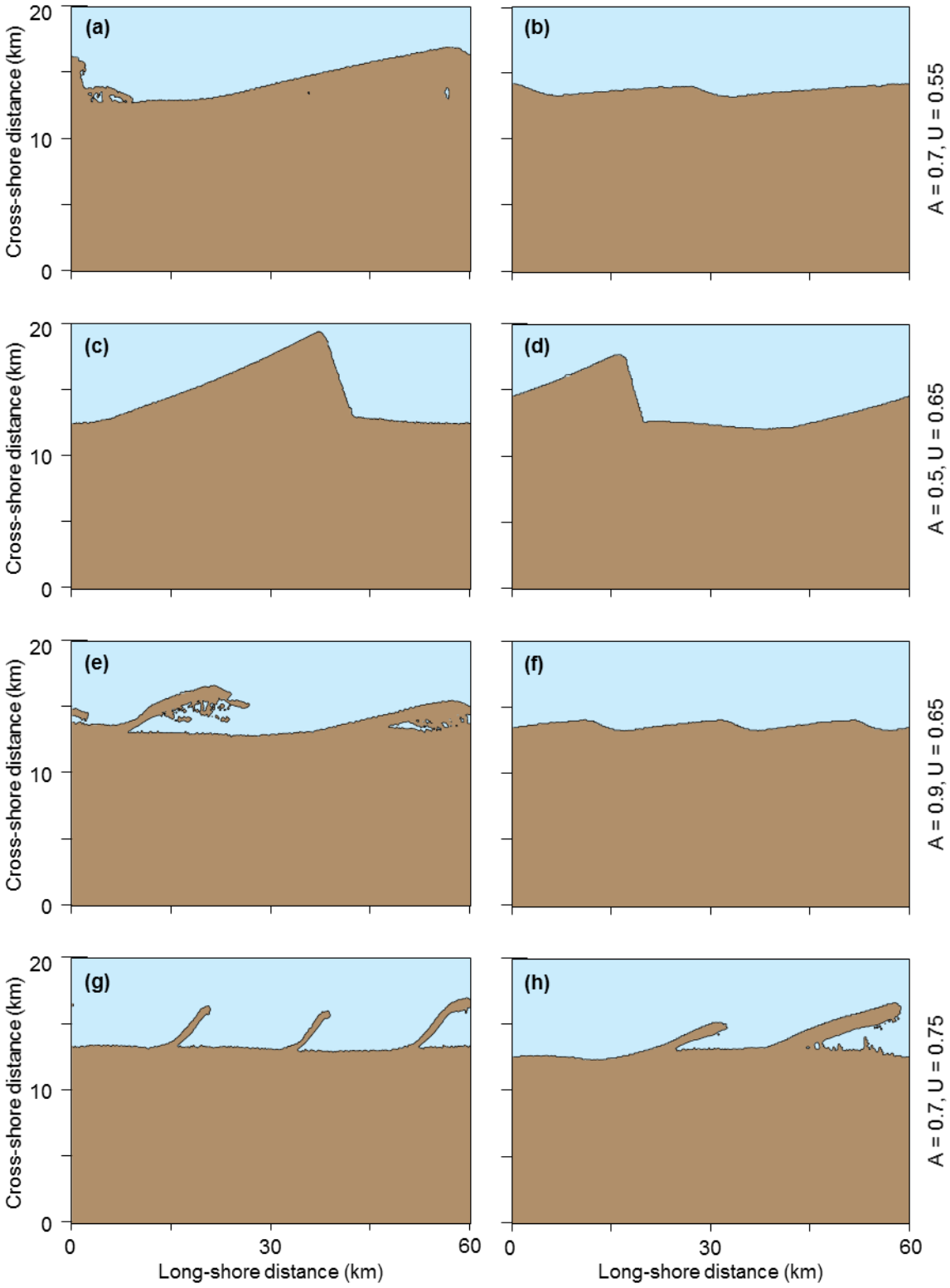

Figure 4.9 Comparison of results where the sediment distribution frequency is employed every 10 (left) and every 30 (right) iterations, under four different wave climate conditions according to the proportional wave asymmetry (A) and the proportion of high angle waves (U).

Certain types of shoreline features (e.g. cusps) are likely to form in coastal environment according to the driving wave climate conditions given in Figure 4.9, as proposed by the theory of high angle wave instability (Zenkovitch, 1959) and the model results of Ashton *et al.,* (2001; 2006a, 2006b). For instance, sand waves typically form in environments where there is a slight asymmetry in wave angle of approach (e.g. A = 0.7, U = 0.55 - Figure 4.9a-b). Cusps are likely to form in natural systems governed by a relatively symmetrical wave climate conditions (e.g. A = 0.5, U = 0.65 - Figure 4.9c-d). Where the wave climate is highly asymmetric and dominated by high angle waves (e.g. A = 0.9, U = 0.65 - Figure 4.9e-f, and A = 0.7, U = 0.75 - Figure 4.9g-h), flying spits form. Further descriptions of these features and the theory of high angle wave instability are given in Chapter 5.

Where the sediment distribution method occurs every 10 iterations, the expected shoreline features (e.g. cusps) evolve along the shorelines according to the driving wave conditions (as described above) (Zenkovitch, 1959; Ashton *et al.*, 2001, 2006a, 2006b). Where the frequency is every 30 iterations, the expected shoreline shapes evolve but with a lower amplitude. This is with exception to where the wave climate is highly asymmetric (A = 0.9, U = 0.65 - Figure 4.9e-f) and sand waves form along the shoreline as opposed to flying spits (Ashton *et al.*, 2001, 2006a, 2006b).

It is noted that where the wave climate is dominated by high angle waves or is highly asymmetric, the features show a lower amplitude when the sediment distribution method is employed at a low frequency of every 30 iterations (Figure 4.9g-h). For instance, spit features form under a wave climate where 70% of waves approach the shoreline from the left of the domain and 75% of waves are

of a high angle (A = 0.7, U = 0.75), with sediment distribution frequencies of both 10 and 30 iterations (Figure 4.9g-h). However, features which develop where the frequency is every 10 iterations extend further offshore and have a limited curvature at the tip compared to those which form with a frequency of 30 iterations, which align relatively shore-parallel although there is significant cross-shore transport.

This result suggests that the lower frequency is acting to dampen the amplitude of features and smooth the planform shoreline. The continual accumulation of material in a cell for long iteration periods, causes large volumes of sediment to be distributed across the entire domain and also offshore when the method is employed. This can prevent the development of features that rely on cross-shore sediment transport to form, such as spits, as shown in Figure 4.9. Whilst these features are still noted, their form is less obvious and in some cases could be mistaken for other landforms, such as cuspate bumps which form under different environmental conditions. This smoothing effect can, therefore, be misleading for the types of features that form and develop. This is contrary to the previously discussed findings where a frequency of 50 iterations is employed. Under these even lower frequencies, the volume of sediment that accumulates cannot be suitably processed by the model and significant peaks in the topography, particularly along the shoreline, form (Figure 4.8). The balance of sediment is, therefore, a sensitive but crucial component in the model that influences coastal evolution.

The sediment distribution frequencies tested here produce similar results, although at a frequency of 10 iterations the landforms are more defined compared to the diffusive nature of the shorelines with frequencies of 30 iterations. The

computational efficiency of the model reduces with a lower frequency, with an average runtime of 16 hours per 100 simulated years with a frequency of 10 iterations and 8 hours with a frequency of 30 iterations. Taking these points into consideration, it is suggested that the greater similarity of features to results of the empirically tested CEM outweighs the computational expense and hence, a sediment distribution frequency of every 10 iterations is preferable in the experimental set-up used in this thesis.

4.3.3 Domain Characteristics

The shoreline shape consistently showed a low influence on model outputs in the results in Section 4.2. A shoreline shape with initial perturbations, required to induce sediment transport in the model, was therefore selected to be used throughout the thesis. The size of the domain demonstrated a below average influence but shows a relatively high influence on model outputs when assessed using the longshore sediment transport rate behavioural index. The domain size was therefore investigated further in order to determine the optimum size for the experimental set-up.

The domain size directly relates to the length of the coastline in the longshore direction (denoted by x). Since the objective of this study is to understand the mesoscale behaviour of coastal systems, the domain lengths tested are within the bounds of this scale which ranges from 10 km – 100 km. Four different sizes were chosen at equal intervals to limit computational expense, whilst representing a full range of shoreline lengths, including 10 km, 30 km, 60 km and 90 km. These lengths are inclusive of the periodic boundaries in the model.

4.3.3.1 Domain Size Evaluation

The shape of the shoreline and the development and evolution of landforms differs depending on the length of the coastline. As a qualitative measure, the planform morphology of the shorelines are compared, according to four different PDF wave climate conditions as in Section 4.3.2.1, where: (1) A = 0.7, U = 0.55 (Figure 4.10), (2) A = 0.5, U = 0.65 (Figure 4.11), (3) A = 0.9, U = 0.65 (Figure 4.12) and (4) A = 0.7, U = 0.75 (Figure 4.13). Under these four wave conditions, the shoreline is expected to respond in a given way according to the theory of high angle wave instability as discussed in Section 4.3.2.1 (e.g. Zenkovitch, 1959; Ashton *et al.*, 2001, 2006a, 2006b). This current understanding of how natural systems behave under particular wave climate condition is used as a comparison to the model results.

Under a wave climate where A = 0.7, U = 0.55, sand wave features typically form in natural coastal systems, due to the asymmetry in the angle of approach and slight dominance of high angle waves (Ashton and Murray, 2006a). As shown in Figure 4.10, the larger domain sizes, measuring 90 km and 60 km, generate shoreline shapes that most resemble sand wave features (Figure 4.10a and Figure 4.10b respectively). The sand waves that form along the 60 km shoreline are more developed than those on the 90 km shoreline, which have a limited amplitude cross-shore. Under the smallest domain with a length of 10 km more symmetrical or cuspate sand wave features form which may, over a longer simulation period, develop into sand waves as observed in the transition from cusps to sand waves for the longer coastlines (Figure 4.10d). The 30 km coastline performs less comparatively to natural systems under this wave climate, generating a diffusive shoreline (Figure 4.10c). The relatively straight planform

shoreline would not be expected to occur where cross-shore sediment transport is induced by the dominance of high angle waves in this wave climate (Ashton and Murray, 2006a).

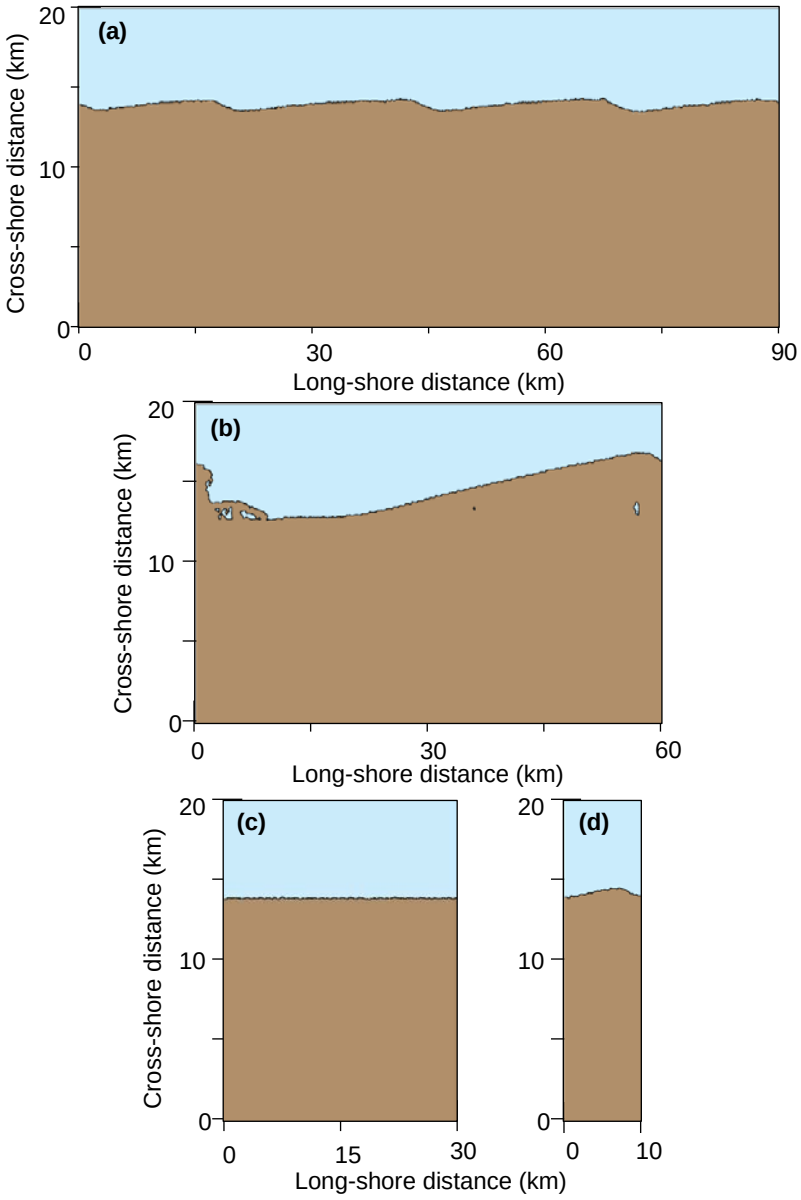

Figure 4.10 Comparison of model outputs with domain sizes of 10 km, 30 km, 60 km and 90 km under PDF wave climate condition (1) where A = 0.7, U = 0.55.

Where the wave climate is symmetrical but there is a dominance of high angle waves, where A = 0.5, U = 0.65, cuspate features would typically form in natural systems (Ashton and Murray, 2006a). Whilst these features form initially in the coastal environment with a domain length of 30 km and 10 km (Figure 4.11c and

Figure 4.11d respectively), they develop further into sand waves throughout the simulations (Figure 4.11). Significant accretion of the shoreline is also observed along the 10 km shoreline (Figure 4.11d). The behaviour of the shorelines with 90 km and 60 km domain lengths show similar results with both producing cusps along their length (Figure 4.11a and Figure 4.11b respectively). It is noted however that with a 60 km coastline, the sand waves are more mature and also skew towards the right of the domain due to directional bias in the model (Chapter 8). The mechanism driving the formation of these features is indicative of cusps, however.

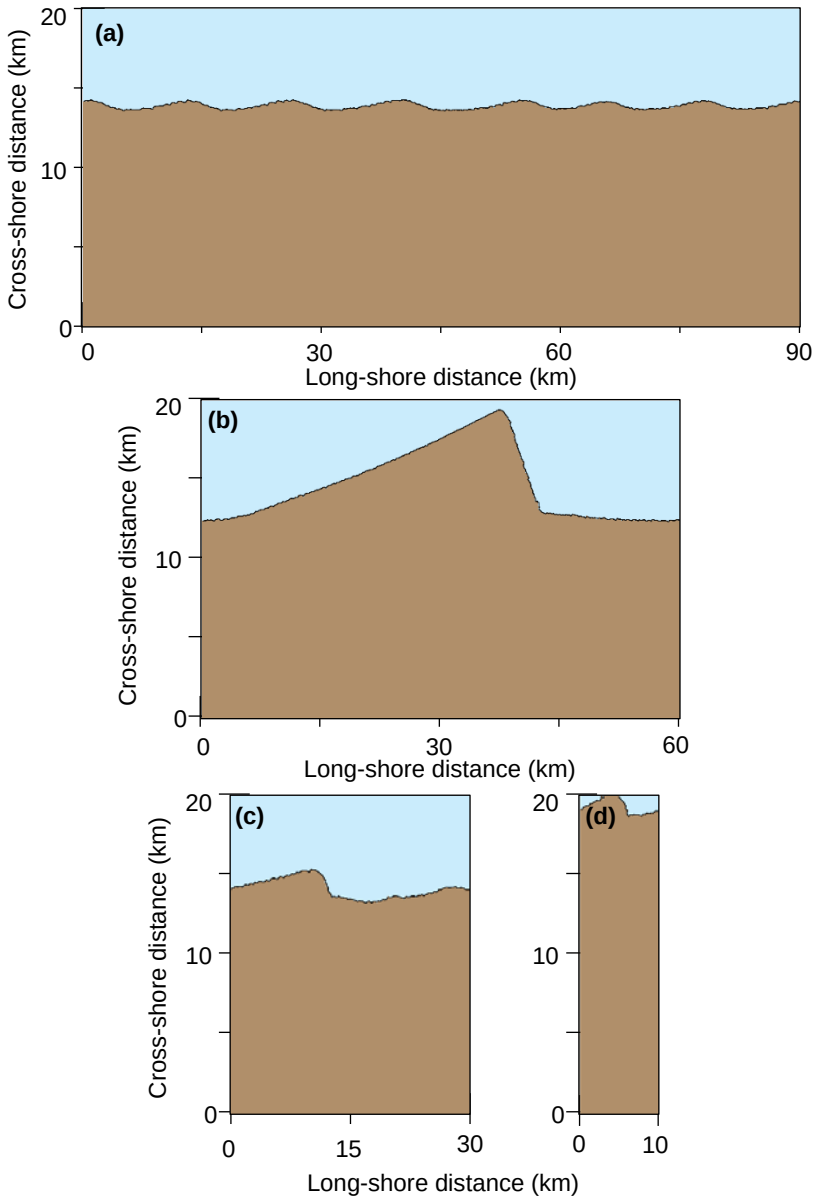

Figure 4.11 Comparison of model outputs with domain sizes of 10 km, 30 km, 60 km and 90 km under PDF wave climate condition (2) where A = 0.5, U = 0.65.

Under wave climate conditions with a high directional dominance and high angle wave instability (where A = 0.9, U = 0.65), spit features would typically form in natural environments (Ashton and Murray, 2006a). Cuspate landforms form along the shoreline where the domain is 90 km, 30 km and 10 km in length (Figure 4.12a, Figure 4.12c and Figure 4.12d respectively). There is some indication of reconnecting spit formation in the 10 km shoreline, but these features do not develop to a stable form. Where the domain is 60 km in length, reconnecting spit

features develop and evolve throughout the simulation and form features most expected under the driving wave climate conditions (Figure 4.12b).

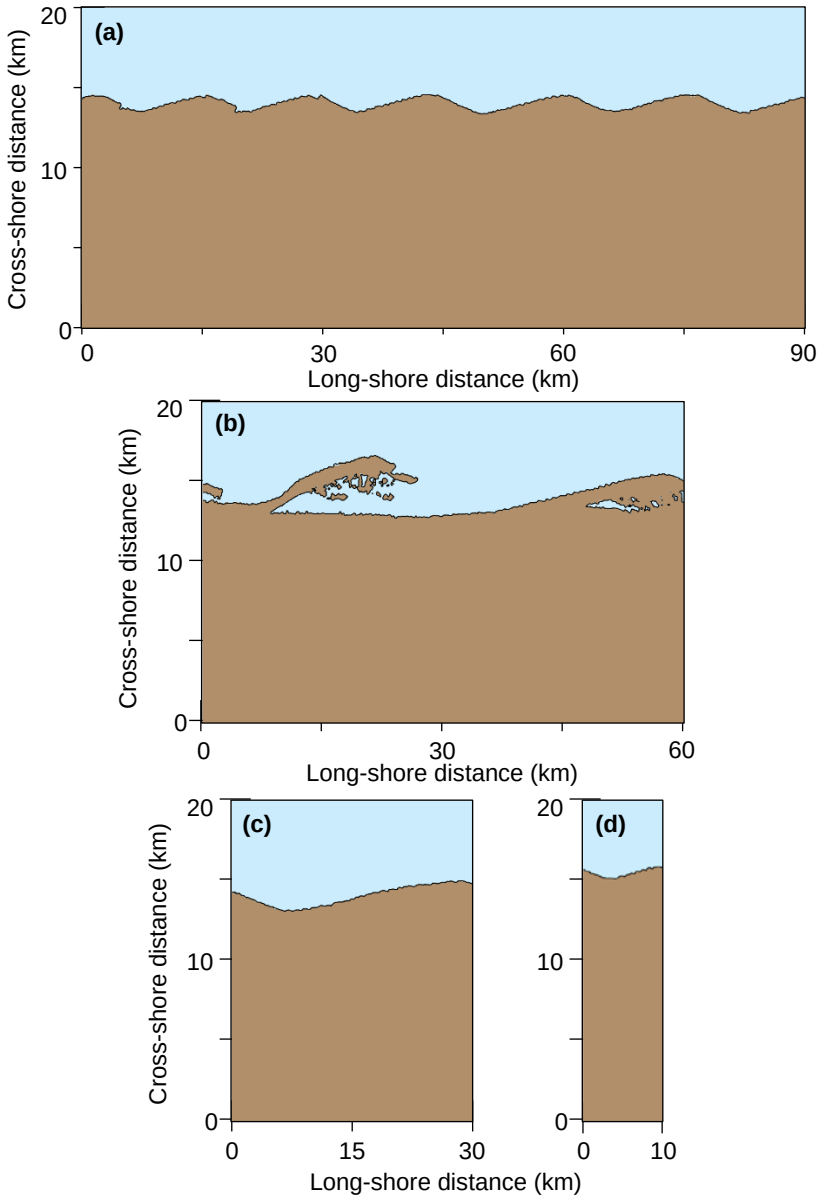

Figure 4.12 Comparison of model outputs with domain sizes of 10 km, 30 km, 60 km and 90 km under PDF wave climate condition (3) where A = 0.9, U = 0.65.

Finally, a wave climate dominated by 70% of waves from the left of the domain and 75% from a high angle (where $A = 0.7$, $U = 0.75$) would also typically produce spit features in natural environments (Ashton and Murray, 2006a). Here, for each of the domain sizes, varying forms of spit features are generated along the shoreline (Figure 4.13). The spit forms are comparable particularly between the

90 km, 30 km and 10 km coastal lengths which evolve characteristic reconnecting spits (Figure 4.13a, Figure 4.13c and Figure 4.13d respectively). Along the shoreline with a domain length of 60 km the spits show a greater resemblance to flying spit features, as observed in the model results of Ashton *et al.,* (2001; 2006a, 2006b).

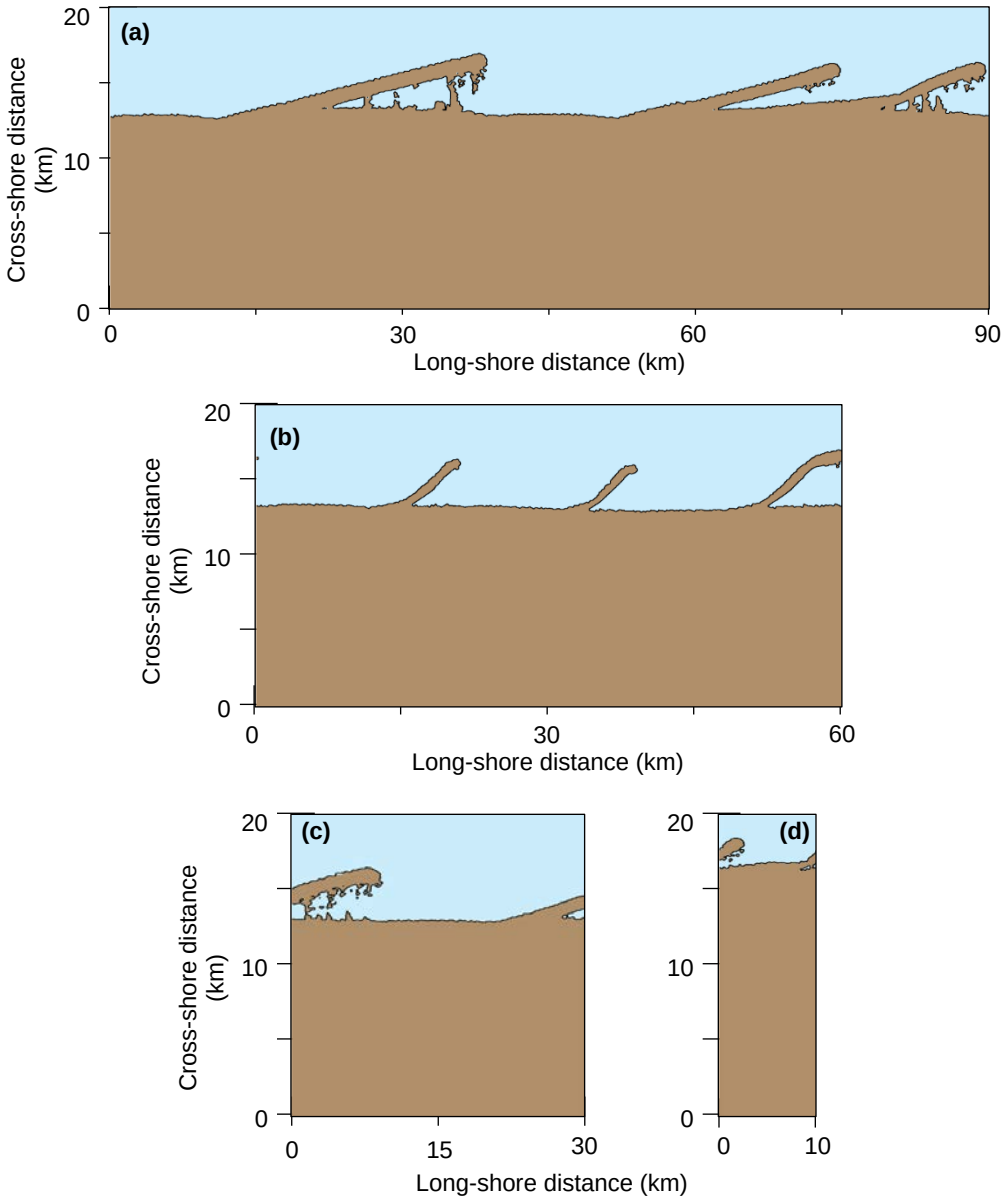

Figure 4.13 Comparison of model outputs with domain sizes of 10 km, 30 km, 60 km and 90 km under PDF wave climate condition (4) where A = 0.7, U = 0.75.

It is apparent from these results that the size of the domain has a nonlinear effect on the evolution of the shoreline and on the sensitivity of the model to this

condition. The characteristics of the 10 km and 30 km shorelines show some similarities. Under these wave climate conditions, the shoreline shapes generated are the least comparable to expected behaviours according to the theory of high angle wave instability (Zenkovitch, 1959) and results of Ashton *et al.,* (2001; 2006a, 2006b).

Each of the shoreline shapes produced closely resembles the landforms that are characteristics of the driving wave conditions, according to current scientific understanding of high angle wave instability. This is with the exception of the 90 km domain size under a wave climate where A = 0.9, U = 0.65 which generates cuspate sand waves as opposed to spits (e.g. Zenkovitch, 1959; Ashton *et al.*, 2001, 2006a, 2006b). At the 60 km and 90 km scales, the coastal systems are more dynamic and produce more prominent features that show a relatively linear growth of maturity throughout the simulation periods. It is observed however that for the larger domain size of 90 km, the landforms are slightly less developed and show a smaller amplitude than the 60 km coasts. Further, the computational expense increases with increasing domain size with an average runtime of 16 hours per 100 simulated years with a domain size of 60 km and 38 hours with a 90 km domain.

The reasoning for domain size sensitivity is unclear, however, it could be attributed to the behaviour of the periodic boundaries and processes such as wave shadowing in the model domain. It is further noted that the cell size could have an influence on the sensitivity of the model to the domain size, although this factor was not evaluated in this study; a cell size of 100 by 100 m was adopted throughout this research, consistent with the standard set-up of the CEM and investigations of Ashton *et al.,* (2001). However, it is shown in the results of the

Morris Method that the model's sensitivity to the domain size is relatively low and so further analysis is not necessary at this stage. Based on the results presented in this section, a 60 km domain size was chosen as the preferable size for this research. The outputs are comparable to natural systems and research of Ashton *et al.,* (2001; 2006a, 2006b) and with greater computational efficiency than the 90 km coastline.

4.4 Conclusion

In the first section of this Chapter, the Morris Method was applied to CEM2D to determine the sensitivity of the model in terms of the influence that input factors have on model outputs. The sensitivity analysis provides an assessment of the mathematical structure and processes in the model, as opposed to an analysis of environmental behaviours. A total of eight input factors were presented, each of which was assessed against four behavioural indices to generate results which are representative of core processes in the model. The results suggest that the wave climate, primarily the angle and height of waves are the most sensitive input factors and the shoreline shape the least sensitive, with the other factors showing a varied influence according to the behavioural indices analysed. Comment is given on the limitation of such sensitivity analyses in that the choice of both the input factors and behavioural indices is subjective and therefore liable to skewing the results.

The results of the SA in Section 4.2 are subsequently used in Section 4.3 of this chapter to design the experimental set-up of CEM2D for this thesis. The focus of this section was the wave climate conditions, sediment distribution factors and the domain size. Completing the SA and defining suitable values for sensitive

inputs in CEM2D is a necessary step in the development of CEM2D and its use as a tool in investigating the behaviour of coastal systems in this thesis.

Through completing a sensitivity test and selecting suitable model parameters for CEM2D, this chapter (along with Chapter 3) has contributed to addressing Research Objective 1 of this study:

> *"To develop and test a two-dimensional coastline evolution model which can be used to understand the behaviour of coastal systems according to the driving wave conditions and their likely response to climatic changes over meso-spatiotemporal scales"* (see Chapter 2).

In the following chapter (Chapter 5), the application of CEM2D to understanding the influence of the wave climate conditions on coastal systems will be presented.

Chapter 5

The Influence of Wave Climate Conditions on Shoreline Shape and Evolution

Research Results

5.1 Introduction

In the previous two Chapters, Chapters 3 and 4, the development of the Coastline Evolution Model 2D (CEM2D) was presented. Having gained an understanding of its structure and sensitivities, here the model is applied to understanding the planform evolution of coastal systems according to the driving wave conditions. This specifically addresses Research Objective 2, as outlined in Chapter 2 and reiterated in Section 5.6.

The volume of sediment moved in a coastal system is a function of the energy delivered to the shoreline, which is principally defined in many coastal systems by the wave climate (Barkwith *et al.*, 2014a, 2014b). The wave conditions, therefore, play a significant role in shaping coastal environments, particularly in wave-dominated systems. We focus here on the wave angle as it has been shown to have a greater influence on coastal morphodynamics compared to the

height and period of waves in many locations; it is recognised however that the wave height and period can be dominating conditions in some environments such as in diffusive systems (Dickson *et al.,* 2007; Barkwith *et al.*, 2014b).

There are a number of key studies that use the CEM to investigate the influence of wave climate conditions on coastal behaviours in a one-line modelling environment (see Section 5.2). To conduct this investigation, a model-model comparison is instrumented between the empirically tested CEM and CEM2D and the results are compared to the behaviour of natural coastal systems. The conclusions drawn will either reinforce or dispute our current understanding of the ways in which these systems behave and will be used to inform research in subsequent chapters of this thesis.

5.2 Waves and Coastal Geomorphology

The mechanisms driving the formation of landforms along shorelines has been of interest to scientists over many decades. As previously discussed in Chapter 2, it is understood that the development of landforms is a product of the movement of sediments by hydrodynamic processes (Cowell and Thom, 1994; Carter, 2013). In particular, the breaking of waves along a coastline influences the direction and volume of sediment transport (Komar and Inman, 1970). This, in turn, determines the types of shorelines that develop (e.g. diffusive or anti-diffusive, erosional or accretional etc), the presence of accretional and/or depositional landforms and how these features evolve. Chapter 2 gave an overview of this concept and the influence of other hydrodynamic processes, but here the focus is specifically on the wave angle which, as discussed, has a

dominant influence on coastal evolution in many locations (Barkwith *et al.*, 2014b).

The wave angle of approach is suggested to be influential to the types of features and landforms that evolve along a shoreline, such as cusps (Ashton *et al.,* 2001). Fisher (1955) claims to be one of the first to conduct a detailed investigation of the formation of cuspate spit features on a barrier beach within the lagoons of St. Lawrence Island, Alaska. Fisher (1955) attempts, in reference to similar studies, to provide a qualitative theory for their formation by a number of mechanisms including tidal eddies, deposition in wave shadows, lagoon breaching and longshore drift, but concluding that the most likely explanation is over wash of the barrier by storm activity. This theory is debated by Zenkovitch (1959) who suggests that the primary mechanism in the formation of the cuspate forelands is related to longshore sediment transport. Zenkovitch (1959) was one of the first authors to identify a relationship between high angle waves and coastal instability that results in the growth of perturbations and irregularities along shorelines; the author further suggests that longshore transport rates are maximised at an angle of 45^{o} (Zenkovitch, 1959).

The study by Zenkovitch's (1959) is focused on the formation and evolution of cuspate forelands that occur in enclosed coastal systems, which may differ from the behaviour of those which form in open coastal environments (Price and Zenkovitch, 1964), as is the focus of this research. However, these studies are some of the first examples of detailed qualitative investigations from which current research into these landforms stem or cite a reference to (e.g. Ashton *et al.,* 2001).

Through the progression of research in this field, there has been a recent increase in scientific understanding of the influence of wave climates, particularly the distributed angle of approach, on shoreline shapes. The theory of 'High Angle Wave Instability' postulates that gradients in wave-induced alongshore sediment transport can influence the planform shape of shorelines (Ashton and Murray, 2006a; Valvo *et al.,* 2006). The balance of the sediment budget and net transport in or out of a system determines whether a shoreline erodes or accretes (Valvo *et al.,* 2006). Shoreline instability is suggested to be highly attributed to the angle of wave approach and more weakly correlated to the wave period (Ashton and Murray, 2006a). This is contrary to traditional studies that have paid less attention to the wave climate, but attributed shoreline change to other processes in coastal systems as discussed previously (Fisher, 1955; Ashton and Murray, 2006a).

Whilst debate continues into the mechanisms responsible for the evolution of shoreline shapes and landforms, the focus of this research and specifically this chapter is the wave climate. Of interest is whether the wave angle and high angle wave instability are responsible or influential to the erosional and depositional patterns found along many shorelines globally. It is understood, however, that in natural systems, there are many complex drivers that act in combination to control the behaviour of these environments.

5.2.1 High Angle Wave Instability

In 2001, Ashton *et al.,* (2001) presented the Coastline Evolution Model (CEM) which was one of the first applications of numerical models to test the theory of high angle wave instability from which a wealth of studies have stemmed (Ashton *et al.,* 2003, 2006a, 2006b, 2015; Serizawa *et al.,* 2012; Barkwith *et al.*, 2014b; Hurst *et al.,* 2015). Since CEM2D is built upon many of the fundamental principles

of CEM and a model-model comparison will be conducted in this chapter, a detailed review of the principle studies using the CEM is completed here; in particular, a review is given of the work by Ashton *et al.,* (2001, 2006a, 2006b).

In the original study by Ashton *et al.,* (2001), the CEM is driven by wave conditions according to a Probability Distribution Function (PDF) of the proportional wave asymmetry (*A*) and proportion of high angle waves (*U*) approaching the shoreline. As waves approach near-parallel to the local shoreline orientation, longshore currents are produced which tend to diffuse and smooth the planform shape of the shoreline (Ashton *et al.,* 2001, 2003, 2006a). Where the wave angle is dominated by high angle waves that are greater than the angle which maximises sediment transport, approximated to 45º-42º, perturbations along the shoreline form and grow (Zenkovitch, 1959; Ashton *et al.,* 2001).

Under a symmetrical wave climate, cusps grow. As the local shoreline orientation changes along the edges of these features, sediment transport rates decrease and sediment is deposited at the tip of landforms (Figure 5.1a) (Ashton *et al.,* 2001). Where the wave climate is asymmetric, features will skew in the direction of net longshore drift and as sediment is transported along the updrift edges and deposited at the crest, spit-like features will grow (Figure 5.1b) (Ashton *et al.,* 2001). If the asymmetry creates a sufficiently strong net longshore transport rate, features migrate and merge to form larger landforms (Ashton *et al.,* 2001).

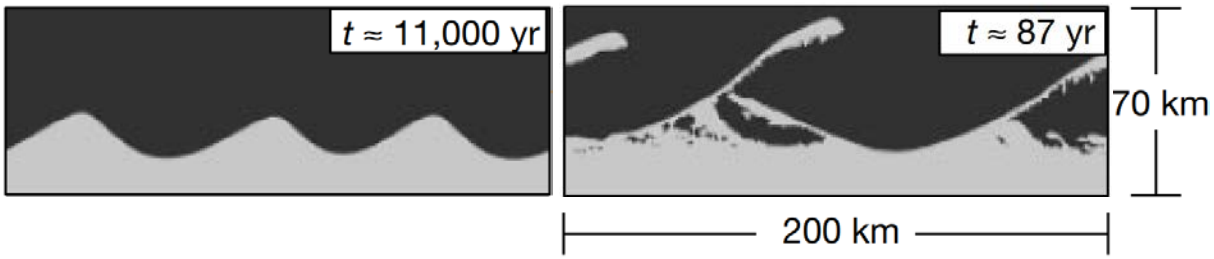

Figure 5.1 Outputs from CEM showing (a) the formation of cusps in a symmetrical wave climate dominated by high angle waves and (b) the formation of spits in an asymmetric wave climate dominated by high angle waves (Ashton *et al.*, 2001, p. 298).

The growth of features can be exaggerated by wave shadowing effects which shelter sections of the shoreline, creating a dominance of low-angle waves in these zones (Figure 5.2) (Rosen, 1975; Ashton *et al.,* 2001). Wave shadowing effects are well demonstrated in CEM, showing smaller features diffusing in the shelter of larger landforms (Ashton *et al.,* 2001).

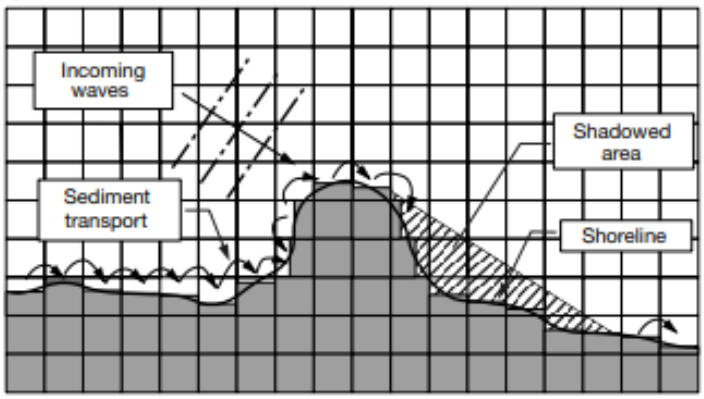

Figure 5.2 Schematic showing the process of wave shadowing (Ashton *et al.*, 2001, p. 297)

Ashton and Murray (2006a, 2006b) further investigate the relationship between high angle waves and the shape of the shoreline, originally explored by Ashton *et al.,* (2001). Using the same PDF method to generate wave climate conditions as Ashton *et al.,* (2001), the authors discuss the formation of four basic planform shoreline shapes; (1) cuspate bumps, (2) alongshore sand waves, (3) reconnecting spits and (4) flying spits (Ashton and Murray, 2006a). Support is given to the theory of high angle wave instability and the formation of these four

types of shoreline shapes by Serizawa *et al.,* (2012). In their study, Serizawa *et al.,* (2012) use the three-dimensional model 'BG' to simulate the influence of high angle waves on shorelines over relatively short time periods (3 years), where the wave direction is symmetrical with 0.5:0.5 probabilities and where it is asymmetrical with 0.65:0.35 probabilities (Serizawa *et al.*, 2012).

The BG model and its documentation are not available to view or download and hence, the model was not considered as a viable option for this research; it is therefore not included in the review of available models in Chapter 3. It is also apparent that the model is used for microscale studies, as opposed to the mesoscale which is of interest here (Serizawa *et al.,* 2012). Nevertheless, the results from the model reinforce the theory of high angle wave instability and the formation of the four fundamental shoreline shapes, each of which are discussed in detail subsequently.

5.2.1.1 *Cuspate Bumps*

Shorelines dominated by symmetrical wave climate conditions where waves approach in equal proportions from the left and right, accrete cuspate features (Gulliver, 1897; Rosen, 1975; Carter, 1982; Ashton and Murray, 2006a). Where there is a balance between opposing wave directions, sediment is deposited and features grow offshore in a relatively symmetrical fashion (Rosen, 1975). The rate of growth and size of these formations are a function of sediment availability and the amount of energy delivered to the shoreline (Carter, 1982). This is determined by the strength of cross-shore sediment transport and the proportion of high angle waves (Carter, 1982). With an increasing proportion of high angle waves and cross-shore sediment transport, cusps translate from sinusoidal to pointed features (Ashton and Murray, 2006a).

Results of the study by Serizawa *et al.,* (2012) also suggests that under a symmetrical wave climate, high angle waves form rhythmic cuspate landforms that are triangular in planform morphology (Figure 5.3). As the landforms grow over time through the deposition of sediment at the cape tips, wave shadowing and sediment starvation to smaller landforms result in them being absorbed by the larger features. The number of features found along the shoreline, therefore, decreases in time which increases the wavelength (Serizawa *et al.*, 2012).

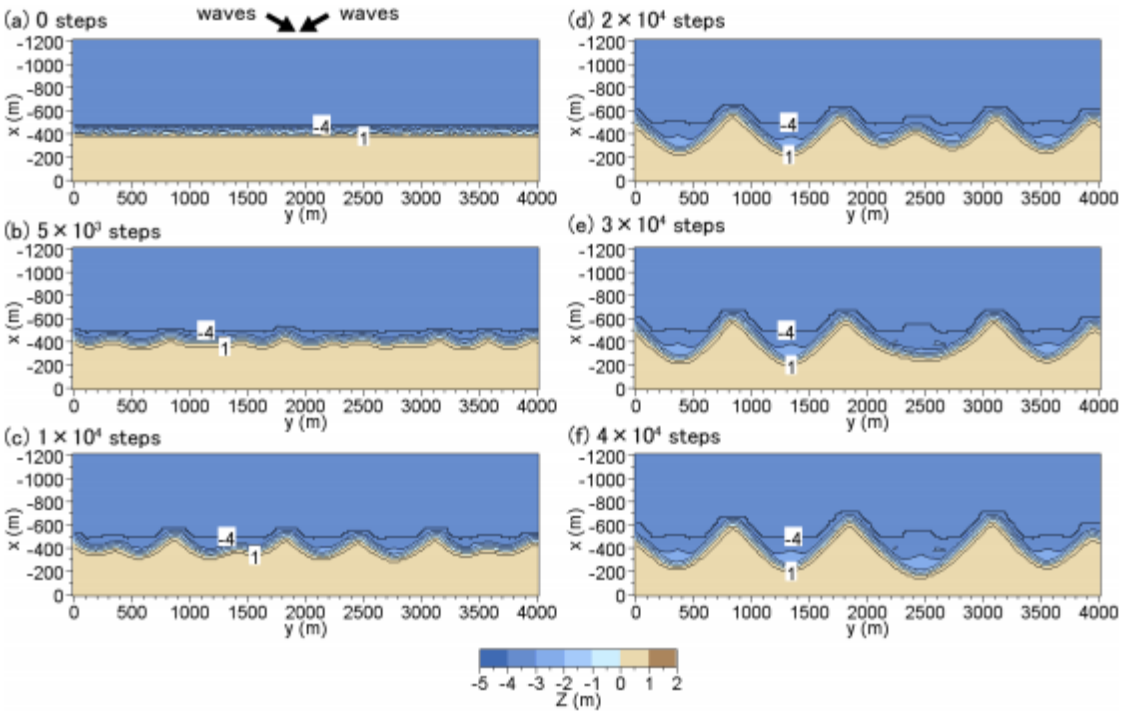

Figure 5.3 Temporal development of cuspate landforms under a symmetrical wave climate, dominated by high angle waves (Serizawa *et al.*, 2012).

The Carolina Capes that span parts of North and South Carolina's coast in the USA (Figure 5.4) are exemplary of these cuspate features. Whilst there is continuing debate regarding the formation of the capes, the symmetrical wave approach and dominance of high angle waves is suggested to be a key driver in evolving their planform shape (McNinch and Luettich, 2000; Ashton and Murray, 2006a). Further, wave processes are suggested to account for approximately

80%-90% of overall sand transport according to a study at Cape Lookout (Figure 5.4) (McNinch and Luettich, 2000). Opposing wave approaches transport material along the capes towards the crests and the material is deposited seaward of the tip, which also contributes to the formation of the cape shoals (McNinch and Luettich, 2000; Park and Wells, 2005). The slight skew of the tips towards the south is driven by the slightly stronger southerly current (Park and Wells, 2005).

Modelling results by Ashton *et al.,* (2006b) using the CEM also generate cuspate forelands according to wave climate data derived from the Carolina Coast. Similar observations are made for Nantucket Harbour whereby opposing wave angles drive sediment transport towards the crest of cusps and offshore, with features showing minimal longshore migration (Rosen, 1975; Ashton and Murray, 2006b).

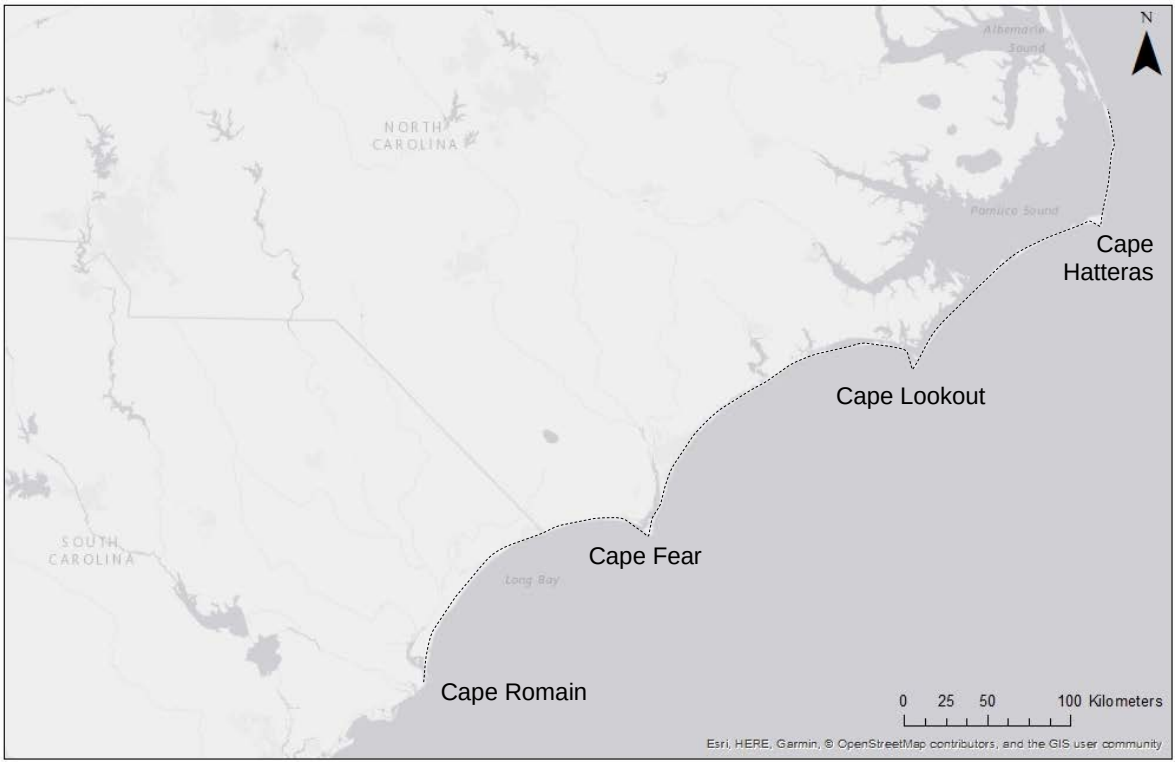

Figure 5.4 Map of the Carolina Capes along North and South Carolina's coastline, USA. The dashed line highlights the three primary capes (ESRI, 2018).

5.2.1.2 *Alongshore Sand Waves*

Where the wave climate has some directional asymmetry and sufficient high angle wave instability, alongshore sand waves form and migrate in the direction of net longshore transport (Ashton and Murray, 2006a). Ashton and Murray (2006b) liken these features to the humps found along Long Point Spit in Ontario, Canada (Figure 5.5). The environment is dominated by an asymmetric wave climate and a slight dominance of high angle waves that form shallow undulations along the length of the spit, as highlighted in Figure 5.5 (Ashton and Murray, 2006b). The asymmetry of the wave climate drives the longshore transport of material that skews the form of the undulations. High angle waves induce cross-shore transport which determines the amplitude of the sand waves (Ashton and Murray, 2006a). Using wave climate approximations for Long Point Spit, Ashton and Murray (2006b) generate these sand wave features but suggest that given time, these will continue developing into spits.

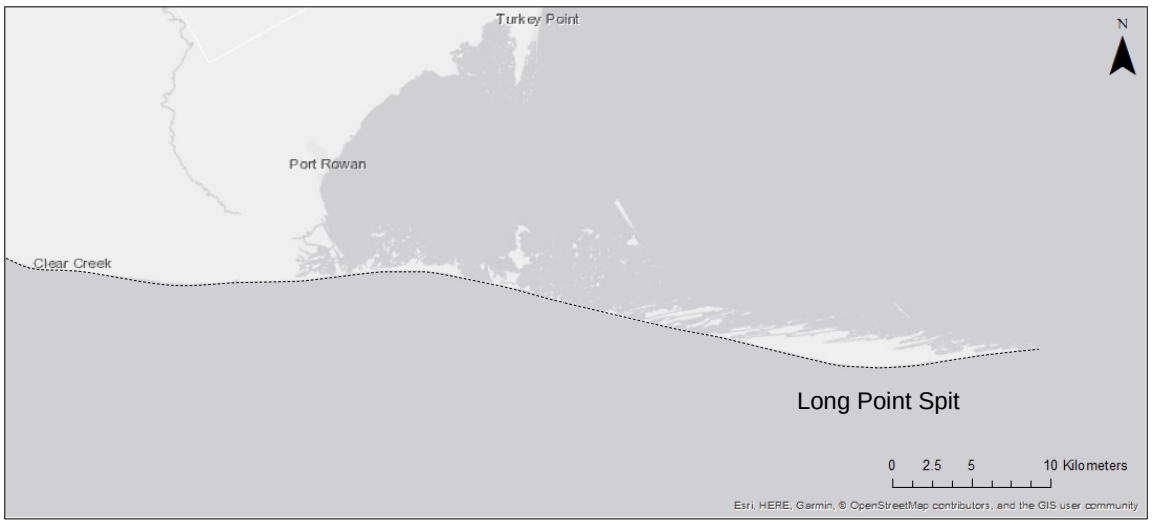

Figure 5.5 Map of Long Point Spit in Ontario, Canada. The dashed line highlights the sand wave undulations that migrate along the landform (ESRI, 2018).

Following on from, and in response to the research of Ashton *et al.,* (2001), Davidson-Arnott and Van Heyningen (2003) present a continuation and further

analysis of work previously carried out by Stewart and Davidson-Arnott (1988). The original research by Stewart and Davidson-Arnott (1988) investigated the mechanisms responsible for the formation and longshore migration of sand waves found along the Long Point Spit. Whilst supporting the theory that high angle wave instability plays a role in the evolution of these sand waves, as suggested by Ashton *et al.,* (2001), Davidson-Arnott and Van Heyningen (2003) hold to the theory published previously (Stewart and Davidson-Arnott, 1988) that their migration longshore, particularly when rapid, is related to the onshore migration of nearshore bars which attach to the downdrift section of the coastline and elongate their form. The authors dispute further modelling results of Ashton *et al.,* (2001), on the basis that the regular spacing of the features, their simultaneous generation and the growth of smaller sand waves over time in the numerical model are not evident in their investigation of a natural system.

Ashton and Murray (2006b) address some of the latter points made by Davidson-Arnott and Van Heyningen (2003) regarding the extent to which their modelling results and those of their predeceasing studies represent natural systems. The authors note that the model's initial and boundary conditions, including the set-up of the domain and its longshore extent, contribute to a number of behaviours that the author's reference, such as the regular spacing or simultaneous growth of features. Whilst the significance of this point is noted, Ashton and Murray (2006b) stress that the model (CEM) is capable of simulating the fundamental processes even if it does not exactly replicate the natural system and can still be used to understand the formation and behaviour of these features. Further, Ashton and Murray (2006b) give credit to the theory proposed by Davidson-Arnott and Van Heyningen (2003) that bar welding could contribute to the formation of

these features, along with many other mechanisms, but that the scale of the numerical modelling is much larger than the scale of this process and is therefore not intended to be modelled. Rather, the sum of such events is considered to contribute to the overall long-term evolution of the sand waves (Ashton and Murray, 2006b).

5.2.1.3 *Reconnecting and Flying Spits*

With a high proportional wave asymmetry, spit features develop along an initially perturbed shoreline (Ashton and Murray, 2006a). Serizawa *et al.,* (2012) suggest that these sand spits form where the direction of wave approach is asymmetric, due to the net longshore transport of sediment. Over time, the perturbations grow and develop hooks at the spit tips, towards the downdrift direction (Figure 5.6). According to the asymmetry of the wave climate, the features migrate longshore and merge together to create larger features (Serizawa *et al.,* 2012).

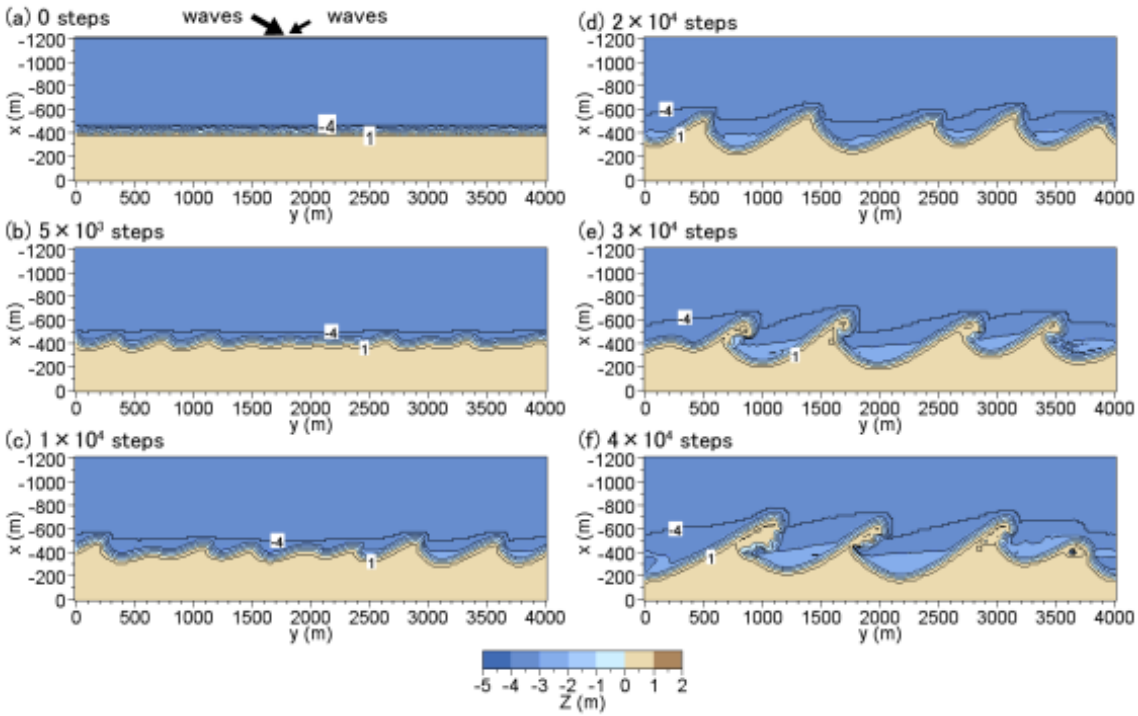

Figure 5.6 Temporal development of sand spits under an asymmetric directional wave climate, dominated by high angle waves (Serizawa *et al.*, 2012)

Reconnecting spit features form where the extension of the tip is constrained by low or high angle waves approaching from downdrift which causes sediment pathways to be formed between the spit and mainland (Ashton and Murray, 2006a). Flying spits that are largely disconnected from the mainland except at their neck are formed where the wave climate has a directional and high-angle dominance (Ashton and Murray, 2006a). These features are likened to natural spits found globally including along the coastline of Ukraine, in the Sea of Azov and the Long Point Spit itself in Lake Erie, Canada (Ashton and Murray, 2006a; Ashton *et al.,* 2007). The authors successfully compute the response of shorelines to high-angle wave instabilities, comparing the results of their simulations to natural systems to give confidence in model results (Ashton and Murray, 2006b).

Ashton *et al.,* (2015) delve deeper into the relationship between the wave angle and the formation of spit features. Following concepts of Ashton *et al.,* (2001), on the basis of numerical modelling results the authors conclude that the shape and curvature of these landforms is controlled by gradients in longshore sediment transport, as induced by the approaching wave angle relative to the local shoreline orientation (Ashton *et al.,* 2015). Sediment supply from the mainland or headland is transported to the “Fulcrum Point” which marks the interface between the largely eroding neck of the spit and the accreting hook. The Fulcrum Point, originally noted by David (1896) migrates along the spit according to the wave angle, which alters the extent of eroding and accreting morphological segments (Ashton *et al.,* 2015). The change in wave angle also alters sediment supply and the combination of these factors can influence the shape and curvature of the spit (Ashton *et al.,* 2015).

Serizawa *et al.,* (2012) further explore how at oblique wave angles of 40º and 50º, the net longshore transport of material combined with limited cross-shore transport pathways that are induced by high angle waves, leads largely to shoreline smoothing. With a wave approach of 40º finite undulations are observed (Figure 5.7) and at 50º shore parallel spits evolve (Figure 5.8).

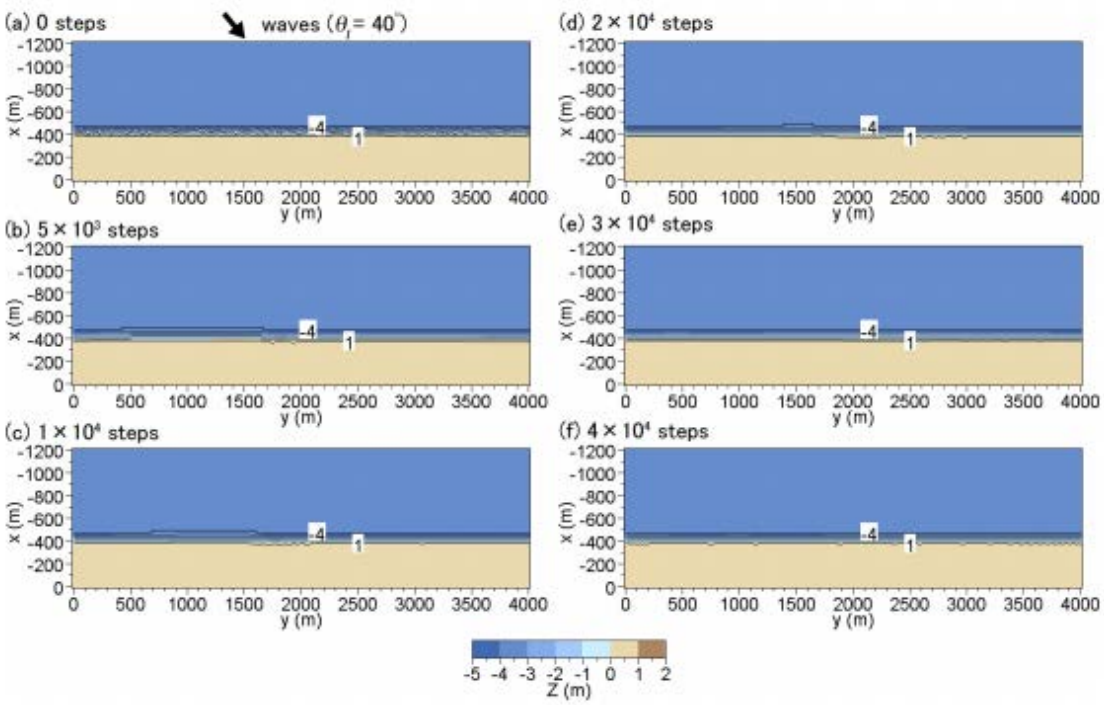

Figure 5.7 Temporal evolution of the shoreline under an oblique wave angle of 40º (Serizawa *et al.*, 2012).

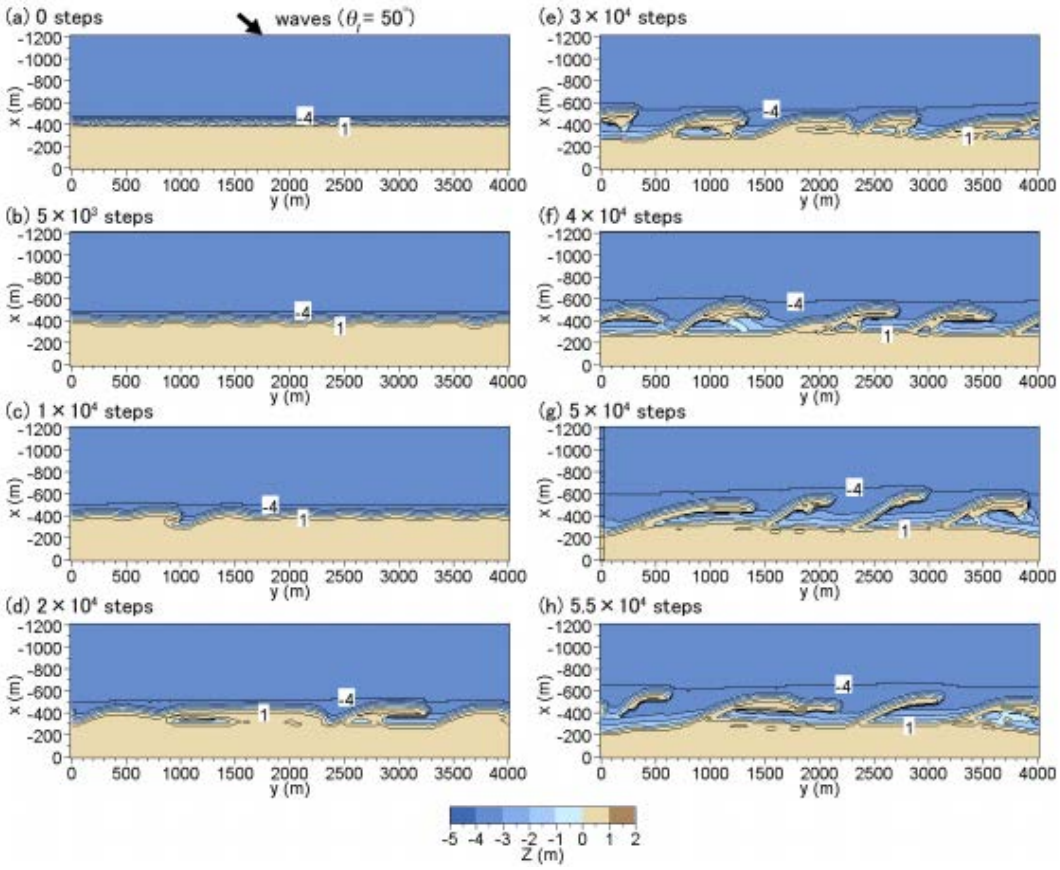

Figure 5.8 Temporal evolution of the shoreline under an oblique wave angle of 50° (Serizawa *et al.*, 2012)

5.3 Experimental Set-Up

The experimental set-up used in this Chapter is replicated throughout this thesis. Whilst some of the input variables used will differ between chapters, the basic set-up of the model remains consistent. Rather than repeating a description of this set-up in each subsequent results chapter, a detailed account is given here and where relevant, reference is given to this Section in other Chapters. In each individual Chapter, any changes made to this basic experimental set-up including input environmental conditions are described. In this chapter, as we are comparing CEM to CEM2D, there is also a description of CEM set up variables.

5.3.1 Initial Conditions

CEM and CEM2D are initially set-up with a uniform gridded domain measuring 200 (cross-shore) by 600 (longshore) cells, with a cell size of 100 by 100 m (Figure 5.9). The length of the domain is such that the fixed boundary conditions at the top and bottom of the domain have minimal influence on the evolution of the shoreline. The width of the domain is set wide enough to allow features to develop and migrate before being captured by the periodic boundaries but is short enough to minimise model runtimes (Figure 5.9). The width of the domain was selected after the development and testing of the model (Chapter 4).

A straight planform shoreline is used, with a number of uniform undulations along its length (Figure 5.9). Perturbations along the planform shoreline represent unconformities in natural systems and are necessary within the numerical model, which is limited by its cellular structure, for the initiation of sediment transport. The initial conditions used here were tested and justified in Chapter 4.

The coastal profile is characterised by a fixed continental shelf slope of 0.1 and an average coastal profile slope of 0.01 (Figure 5.9). These values were chosen for consistency with the study of Ashton *et al.,* (2001) and it's representation of many coastlines globally (Komar *et al.*, 1991; Ranasinghe *et al.*, 2007). Within CEM, these average slopes are applied across the domain but a flat profile is maintained across the beach surface as per the structure of the model (see a full explanation of the structure of CEM in Chapter 3). Within CEM2D, the average slopes are imposed across the two-dimensional domain via the input DEM, including the beach profile and bathymetric profiles which are built to replicate an average coastal profile slope of 0.01 (Figure 5.9).

The left and right boundaries of CEM and CEM2D's model domains are governed by periodic boundary conditions, to allow a constant flux of sediment from one end to the other in order to conserve the volume of material in the system (Figure 5.9). No-flow conditions are set at the seaward end of the domain to again, conserve sediment and prevent any gain or loss of material (Figure 5.9). The boundary conditions can influence the behaviour of the system and so it was concluded that a conservation of sediment approach would be the most applicable and relevant here.

A daily model time step is used for all simulations. The models are run over a simulated period of 3,000 years, to allow time for the model to spin-up, to reduce the potential influence of initial conditions and to allow sufficient time for the coastal systems to evolve. It also allows for patterns to be observed in the behaviour of the system, once they reach their equilibrium form. Some conditions initiate a faster evolution towards equilibrium than others, but a standard model run time that exceeds the lengthiest developments proves the best approach.

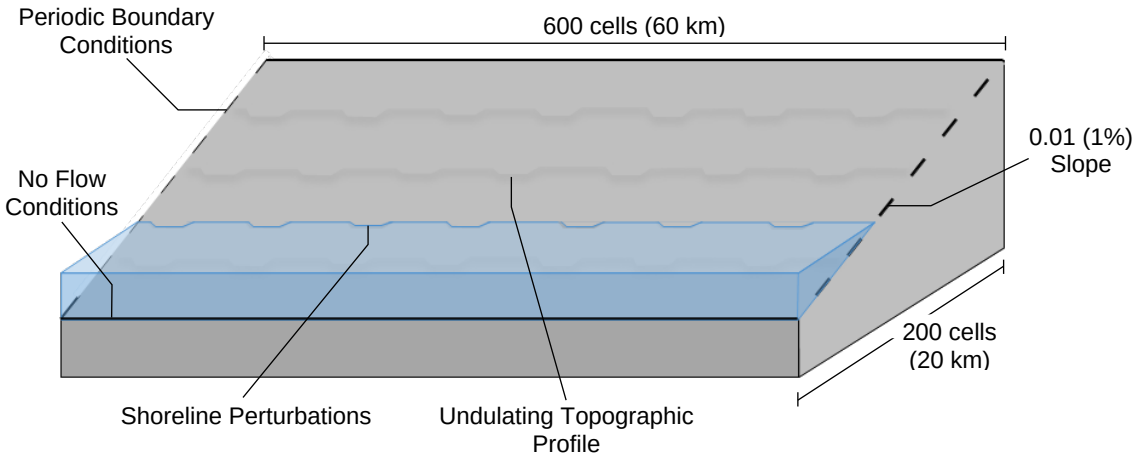

Figure 5.9 A schematic of CEM2D's model set-up and initial conditions used for simulations presented in this chapter.

5.3.2 Wave Climate

An ensemble of wave climates is used to drive the model in order to explore the influence of wave conditions on the morphology and evolution of coastal systems. The four binned Probability Distribution Function (PDF) of Ashton and Murray (2006) is used to define the asymmetry (*A*) of the wave climate and the proportion of high angle waves (*U*) approaching the coastline, relative to the wave crest and average shoreline orientation (Figure 5.10). The wave angle is randomly generated on each iteration, according to these proportional values. In each simulation, the wave height and period are held constant, at 1.7 m and 8 s respectively, guided by the experimental set-up of Ashton *et al.,* (2001, 2006a, 2006b) as discussed in Chapter 4.

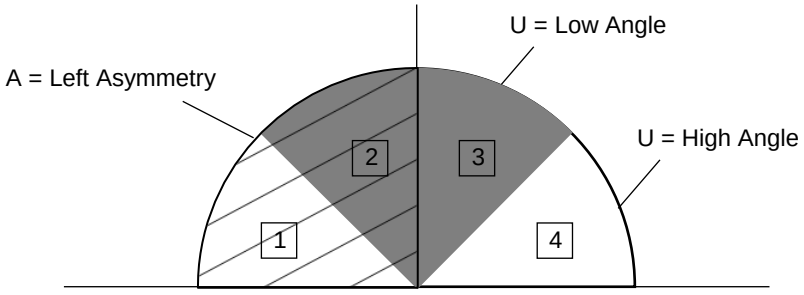

Figure 5.10 Schematic showing the wave angle direction, defined by the wave climate asymmetry (A) and the proportion of high to low angle waves (U) with the numbers denoting the four bins.

The *U* and *A* values used in this research replicate those of Ashton and Murray (2006) so results can be compared to the original study; as per the aims of this chapter (see Section 5.1). The ensemble of wave climates also represents a wide range of conditions which allow the evolution of fundamental shoreline shapes to be explored, including cusps, sand waves, flying spits and reconnecting spits. Twenty-five simulations are run with *A* values between 0.5-0.9 at increments of 0.01 and *U* values between 0.55-0.75 at increments of 0.05 (Table 5.1).

Table 5.1 Wave climate ensembles used to investigate the influence of wave climate conditions on coastal morphodynamics according to the wave climate asymmetry (A) and proportional highness of waves (U).

Run Number	Asymmetry (A)	High Angle (*U*)	Run Number	Asymmetry (A)	High Angle (*U*)
1	0.5	0.55	**14**	0.8	0.65
2	0.6	0.55	**15**	0.9	0.65
3	0.7	0.55	**16**	0.5	0.7
4	0.8	0.55	**17**	0.6	0.7
5	0.9	0.55	**18**	0.7	0.7
6	0.5	0.6	**19**	0.8	0.7
7	0.6	0.6	**20**	0.9	0.7
8	0.7	0.6	**21**	0.5	0.75
9	0.8	0.6	**22**	0.6	0.75
10	0.9	0.6	**23**	0.7	0.75
11	0.5	0.65	**24**	0.8	0.75
12	0.6	0.65	**25**	0.9	0.7
13	0.7	0.65			

5.3.3 Water Level

In this chapter, the influence of a variable water level on coastal morphodynamics is not explored. A static water level is therefore used, which by default in CEM2D is set at 0 m elevation; the water level cannot be altered in CEM.

5.3.4 Output Data

CEM2D outputs a number of files at user-defined intervals that can be used to analyse the behaviour and evolution of the simulated coastline. Descriptions of each of these outputs are given in Table 5.2.

Table 5.2 Output data from CEM2D used to analyse the behaviour and evolution of the simulated coastline.

Output	**Description**	**File Type**	**Frequency**
Image	Image of the planform coastal profile, at the defined time step.	PNG	10 years
DEM	Digital elevation model of the coast to produce 3D models and contour maps.	ASC	10 years
Average Beach Slope	The average slope of the dry beach is calculated according to the average of three regularly spaced transects.	TXT	10 years
Average Shoreface Slope	The average slope of the shoreface, calculated according to the average of three regularly spaced transects.	TXT	10 years

5.4 A Comparison of Results from CEM and CEM2D

A detailed analysis of individual results from CEM and CEM2D is given in Appendix 3, which explores the influence of the wave climate asymmetry and the proportion of high angle waves on shoreline evolution. Attention has been focused on the evolution of the shoreline shape and the types of features that develop under different wave climate conditions, including cusps, sand waves, reconnecting spits and flying spits. Specifically, an analysis is given of how the planform size, wavelength and aspect ratio of landforms change over time according to the input wave climate conditions.

In this section, outputs from both CEM and CEM2D are compared to identify similarities and differences in the evolution of the shorelines. CEM has been

validated and used to understand the behaviour of many natural systems (Ashton *et al.,* 2001, 2006a, 2006b; Barkwith *et al.*, 2014b) and there is confidence in its outputs. Since CEM2D is based on many of the assumption and processes used in CEM, similar results should be obtained particularly concerning the generation of fundamental shoreline shapes. However, differences in outputs do not necessarily nullify results of CEM2D but can show increased detail and complexity afforded by the model. The results are also compared to natural coastal systems, to determine whether the shoreline shapes generated by both CEM and CEM2D are found in the natural environment according to the driving wave conditions.

During preliminary investigations, outputs from CEM showed slight variations from the findings presented in Ashton *et al.,* (2001, 2006a). The differences observed are most likely to be attributed to: differences in initial and driving conditions that were not discussed in the papers meaning that the experimental set-up was not identical, due to variation in the source code since the original development of the model or due to differences in the presentation of results[1] (e.g. Ashton *et al.*, 2001, 2006a). The sensitivity of the model could result in large differences in outputs with only slight differences in the input parameters. Reproducing the simulations using the CEM, therefore, ensures that the experimental set-up used for CEM and CEM2D in this thesis are consistent and comparable.

[1] These reasonings are supported by correspondence with the original authors and subsequent developers of CEM (Ashton A., Murray, A., Barkwith, A.).

The ensemble plots in Figure 5.11 and Figure 5.12 show final coastal morphologies produced from CEM and CEM2D respectively, where the asymmetry (*A*) and proportion of high angle waves (*U*) have been varied according to the values in Table 5.1. Enlarged copies of these matrices are given in Appendix 4. Increasing wave asymmetry is shown along the x-axis and increasing proportion of high angle waves along the y-axis. Both results demonstrate a sensitivity of shorelines to different wave climate scenarios, as previously demonstrated by Ashton and Murray (2006a). It is important to note that the purpose here is not to replicate this study, but to compare the results of the two models as an initial test of CEM2Ds behaviour and to highlight differences in the outputs.

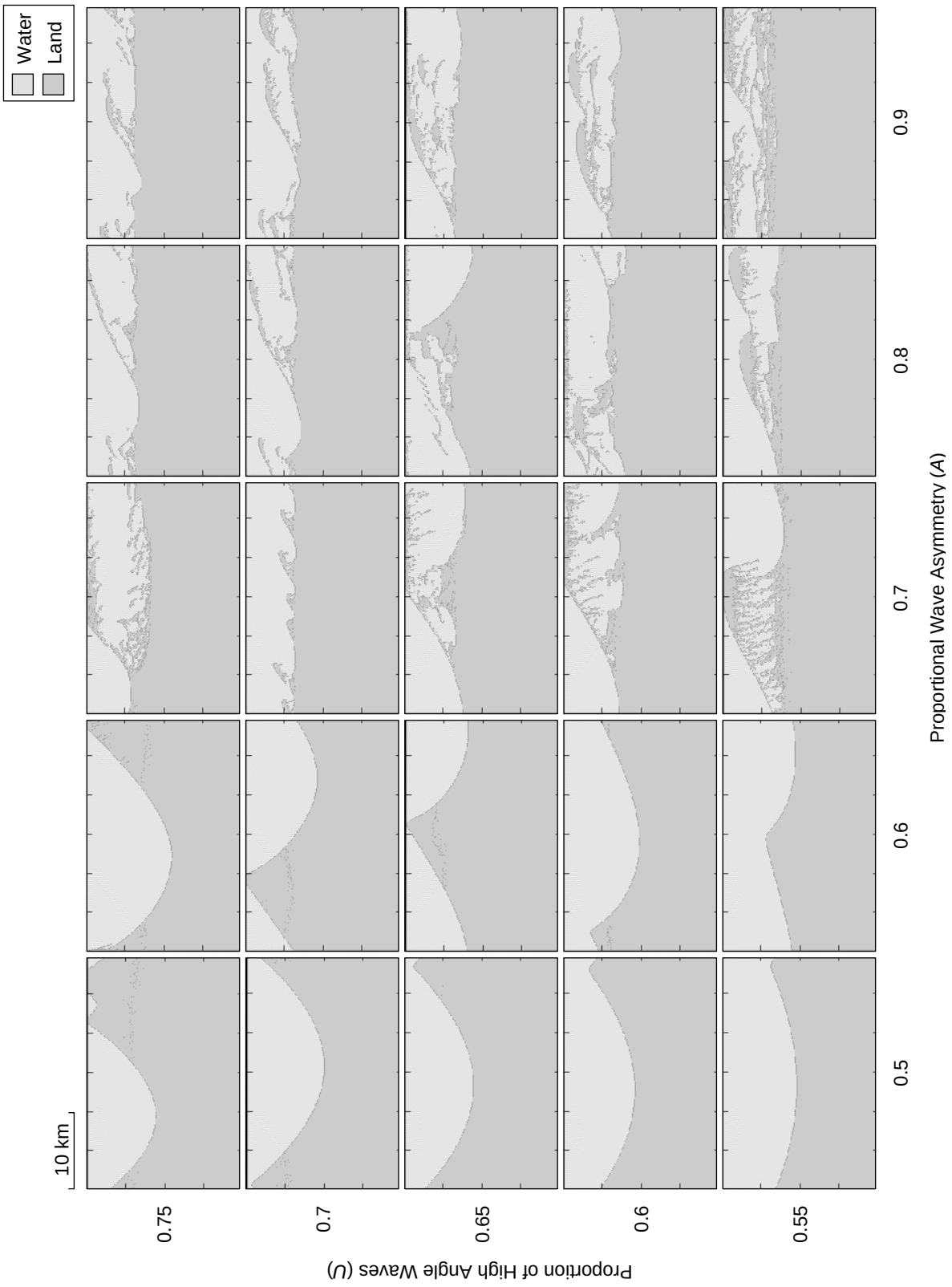

Figure 5.11 A matrix of results from CEM showing final shoreline morphologies as a function of the wave angle asymmetry (A) and proportion of high angle waves (U) approaching the coast relative to the local shoreline orientation. The outputs measure 20 km width and 30 km in length and are not inclusive of the periodic boundaries.

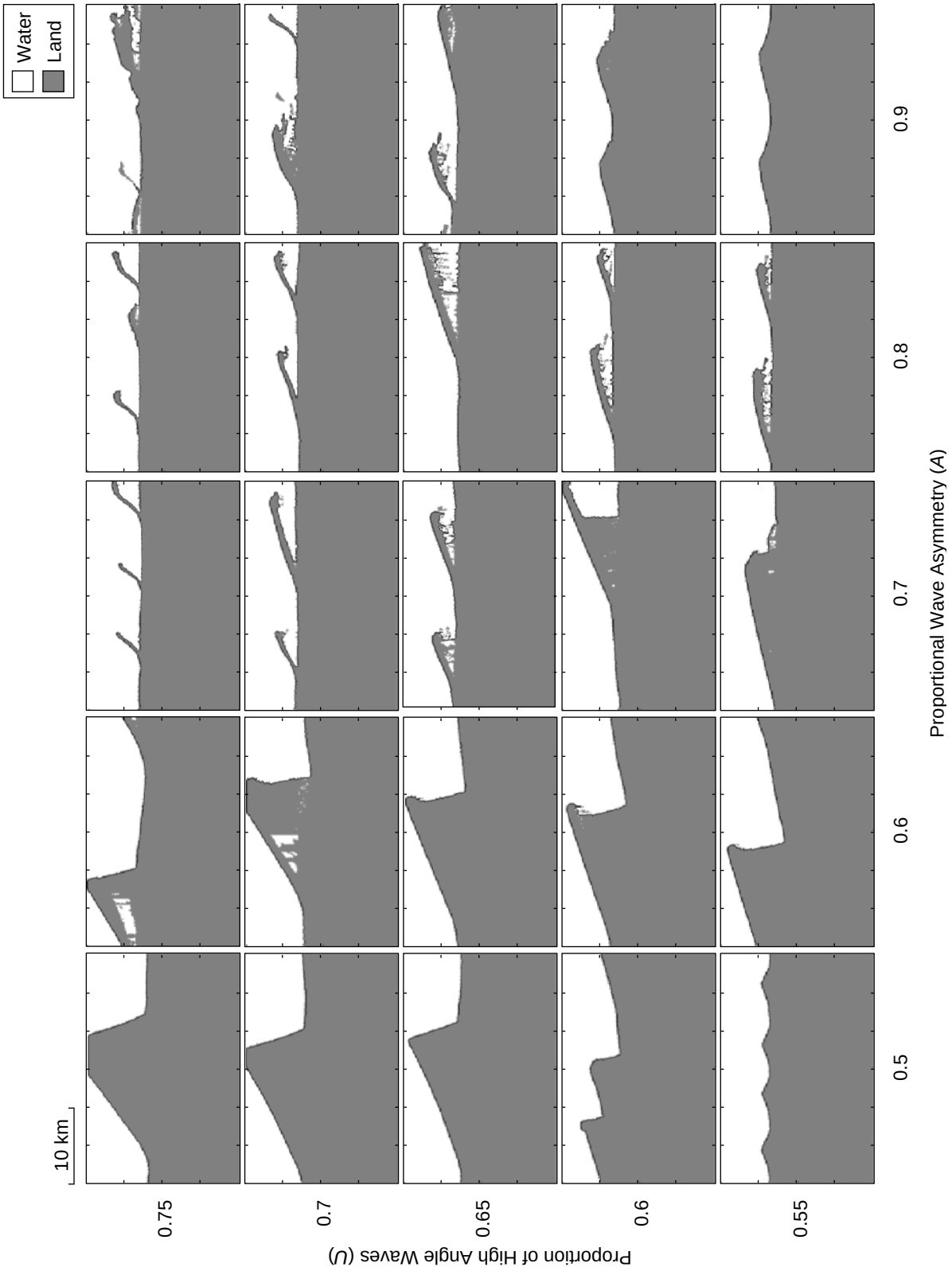

Figure 5.12 A matrix of results from CEM2D showing final shoreline morphologies as a function of the wave angle asymmetry (A) and proportion of high angle waves (U) approaching the coast relative to the local shoreline orientation. The outputs measure 20 km width and 30 km in length and are not inclusive of the periodic boundaries.

Whilst the majority of simulations in both CEM and CEM2D completed the 3,000 years maximum simulation period, several runs terminate prematurely (Figure 5.13). This occurs predominantly with greater wave climate asymmetry (*A*) and proportion of high angle waves (*U*), forming reconnecting and flying spits which tend to evolve relatively rapidly compared to cusps and sand wave features. With the rapid development of features, the complexity of the landforms and their amplitude increases. This reduces the ability of the shoreline search method (described in Chapter 3) to locate a continuous shoreline, as necessary for sediment transport processes to be employed. If the shoreline cannot be found after a given number of attempts, the program terminates.

The runtime of simulations in CEM2D are generally longer than those in CEM, as shown in Figure 5.13. The plot is configured with proportional wave asymmetry along the x-axis and the proportion of high angle waves along the y-axis as in Figure 5.11 and Figure 5.12. With the increased complexity of sediment handling techniques in CEM2D, the model has an improved ability to simulate more complex shorelines as well as additional debugging processes to prevent premature termination of the model. However, the issues are still inherent in the model and projections of future solutions in forthcoming versions are discussed in Chapter 8.

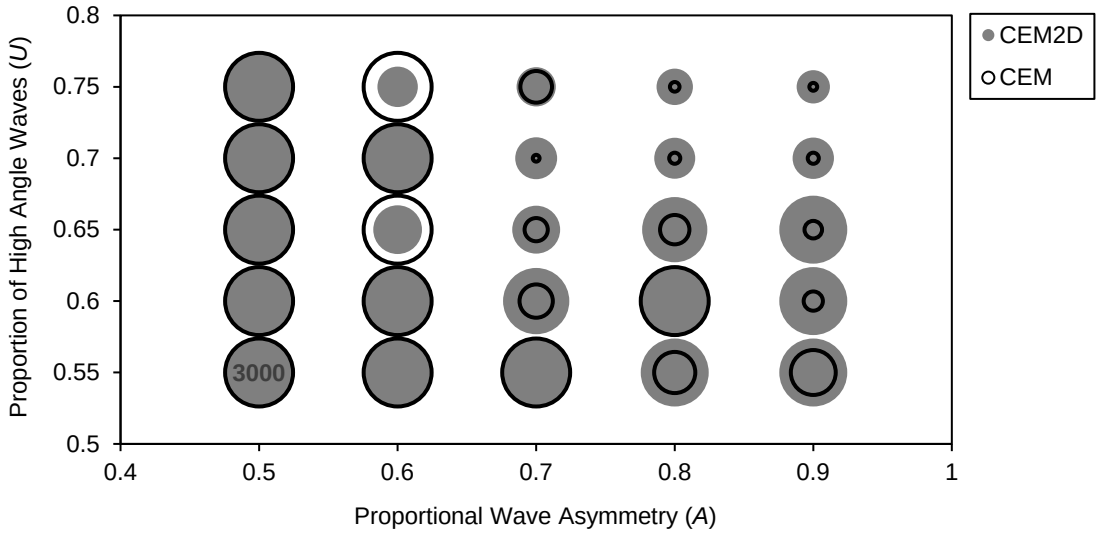

Figure 5.13 A plot showing the relative runtimes of CEM and CEM2D simulations where A ranges from 0.5 to 0.9 and U ranges from 0.55 to 0.75. The area of the scatter points denotes the runtime, with larger circles representing longer runtimes to a maximum of 3,000 simulated

5.4.1 Sensitivity to Wave Climate Conditions

Results of CEM and CEM2D demonstrate a sensitivity of shorelines to both the wave asymmetry and the proportion of high angle waves (Figure 5.11 and Figure 5.12). This compliments findings of other authors who investigate the role of high angle wave instability on the behaviour of these systems, including Ashton *et al.,* (2001, 2006a, 2006b) and Zenkovitch (1959).

It is apparent that the proportion of high angle waves influences cross-shore sediment transport and the extent to which landforms accrete seaward, whilst the wave asymmetry determines the balance of cross- to longshore transport and the skew of features. With increasing wave asymmetry and proportion of high angle waves, landforms show greater rates of development in terms of both planform area (Figure 5.14) and wavelength (Figure 5.15), concurrent with findings of Ashton and Murray (2006a).

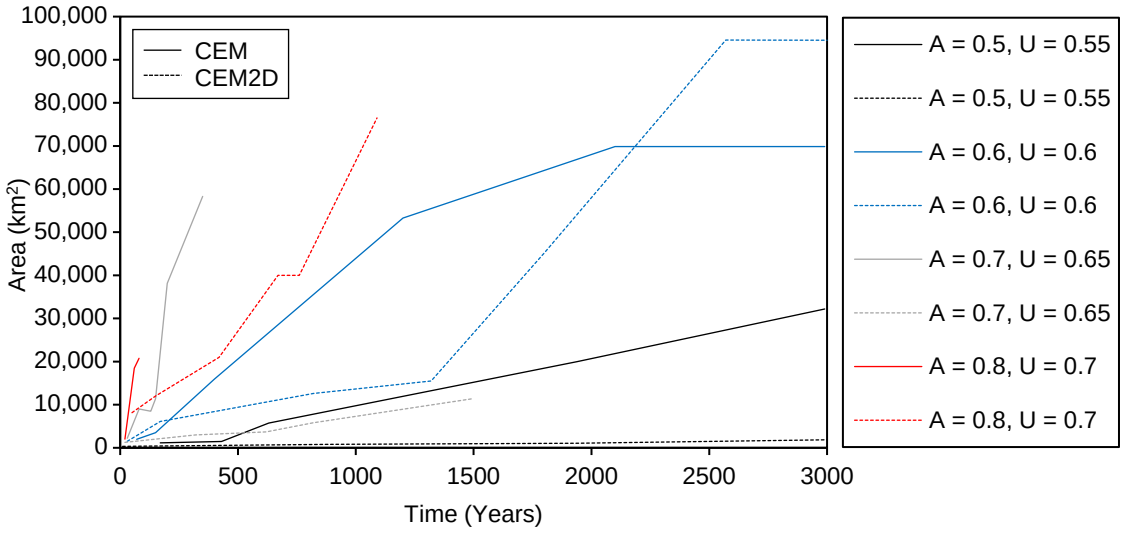

Figure 5.14 A graph showing the average area of landforms over time, with increasing wave asymmetry (A) and proportions of high angle waves (U). Simulation using CEM are marked with solid lines and for CEM2D by dashed lines.

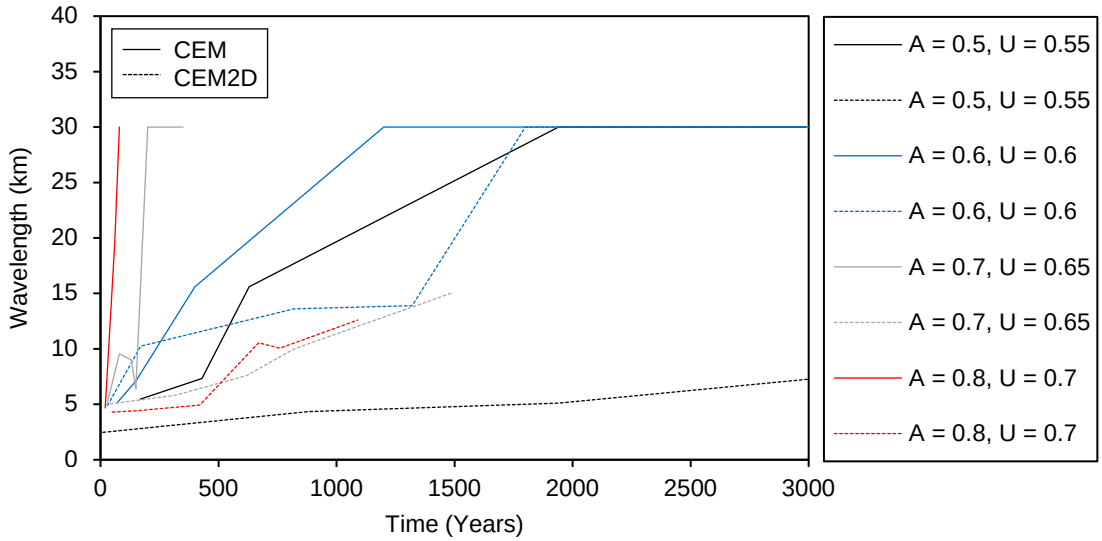

Figure 5.15 A graph showing the average wavelength of landforms over time, with increasing wave asymmetry (A) and proportions of high angle waves (U). Simulation using CEM are marked with solid lines and for CEM2D by dashed lines.

A comparison of the planform area (Figure 5.14) and wavelength (Figure 5.15) of landforms shows that features generated in CEM are generally larger than those produced in CEM2D. Differences in how sediment is represented in the model and the two-dimensional transport processes can alter the way sediment behaves and is distributed across the entire domain in CEM2D. However, while the scale and dimensions of the landforms differ, the focus of this analysis is the types of

features that are evolve and their mechanisms of formation and the results show that the planform morphologies are largely comparable between the two models.

With greater asymmetry in the wave climate, the rate at which landforms migrate longshore increases in results of both CEM and CEM2D (Figure 5.16); a relationship previously observed by Ashton and Murray (2006a). Where the wave climate is symmetrical (A = 0.5), little to no longshore migration of landforms should occur (Rosen, 1975). However, the results presented from CEM and CEM2D show some translation of symmetrical cuspate features longshore under these conditions, even though there is no directional dominance in the wave climate. It is found that there is some directional bias in the source code that drives a longshore current independent of the wave climate conditions; this occurrence is more noticeable in simulations where the wave climate is symmetrical.

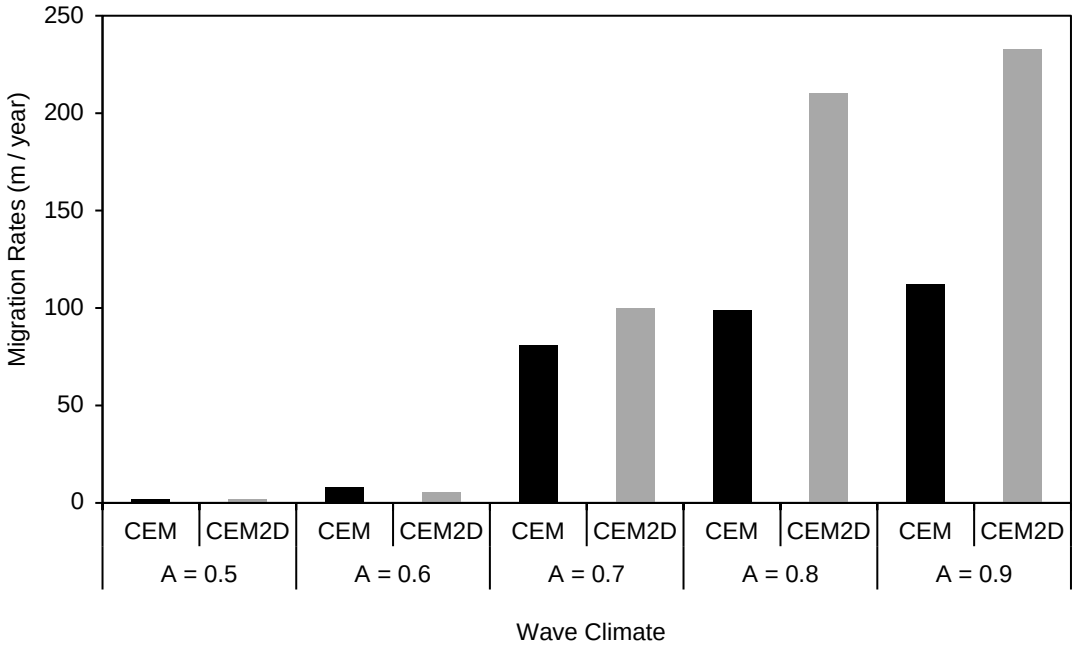

Figure 5.16 A bar chart showing the average migration rates of landforms generated in CEM and CEM2D after relative equilibrium, where the proportion of high angle waves is held constant at U = 0.6 and the wave asymmetry increases from A = 0.5 to A = 0.9.

A comparison of migration rates shows that typically, landforms generated in CEM2D migrate at a greater rate compared to those in CEM and increasingly so with greater wave asymmetry (Figure 5.16). Ashton and Murray (2006a) suggest that smaller features migrate faster than larger landforms since they trap and accumulate sediment at the same rate but a larger volume is required to translate the larger landforms. This pattern is observed in the results presented here, with the features in CEM2D generally showing smaller morphologies (Figure 5.14) and faster migration rates (Figure 5.16) compared to those in CEM. The differences observed here could be related to changes in the representation of sediment transport processes, as noted previously, and also in the formation of remnant morphologies (see Chapter 6) which could influence how the shoreline behaves and evolves (Thomas *et al.*, 2016).

In CEM2D, where A = 0.9, U = 0.55-0.6 cuspate sand waves evolve along the shoreline, contrary to the pattern of results in the matrix which shows that the wave asymmetry skews the planform of morphological features. Throughout the simulations, the strong longshore sediment transport component and only slight dominance of high angle waves generate a smoothing effect along the shoreline. Whilst spits do form along the shoreline as shown in Figure 5.17 after 2540 simulates years, they develop relatively shore-parallel and are highly reconnective. An in-depth analysis of the evolution of this coastal system is given in Appendix 3.

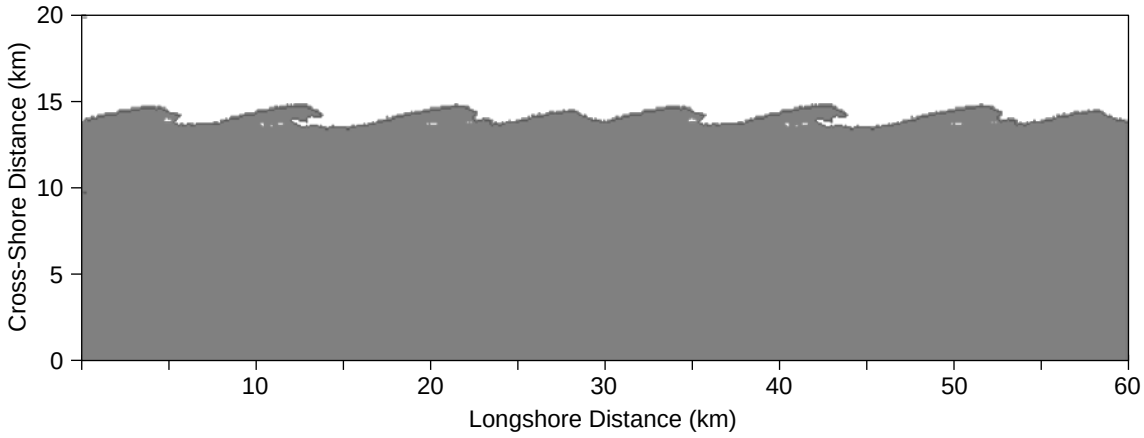

Figure 5.17 An image showing an output of CEM2D after 2540 simulated years (T), where the coastal system is driven by a wave climate where A = 0.9, U = 0.6.

5.4.2 Fundamental Shoreline Shapes

According to the wave climate conditions, both CEM and CEM2D generate four principal planform shoreline shapes including cuspate bumps, sand waves, reconnecting spits and flying spits (Figure 5.11 and Figure 5.12), as per the comparable study by Ashton and Murray (2006a). CEM2D shows a greater sensitivity to inputs variables compared to the CEM, apparent in the development of these four feature types. The spatial pattern of cusps, alongshore sand waves, reconnecting spits and flying spits in the results of both models do not map identically and the landforms show differing amplitudes and timescales of development. Further, a greater distinction is made between reconnecting spits and flying spits in CEM2D than observed in CEM.

Increasing the asymmetry and proportion of high angle waves from a symmetrical climate (where $A = 0.5$, $U = 0.55$) to a highly asymmetric climate (where $A = 0.9$, $U = 0.75$) shows a progression of landforms from cusps, to sand waves, reconnecting spits and flying spits in both CEM and CEM2D (Figure 5.11 and Figure 5.12). Where the asymmetry value is held constant and the proportion of high angle waves increases, cross-shore sediment transport increases the

amplitude of landforms. Increasing the wave asymmetry and maintaining the proportion of high angle waves drives longshore sediment transport, producing landforms which skew in the downdrift direction (Figure 5.11 and Figure 5.12). These findings reinforce the theory of high angle wave instability outlined in Section 5.2.1, proposed by authors including Zenkovitch (1959), Ashton *et al.,* (2001, 2006a, 2006b), Serizawa *et al.,* (2012) and Hurst *et al.,* (2015).

The planform area, wavelength and aspect ratio of features show coincidence in many of the simulations and their pattern of change over time is influenced by the balance of cross and longshore sediment transport. It is further observed that the greater the asymmetry and proportion of high angle waves, the faster the evolution of landforms (Ashton and Murray, 2006a). These relationships are explored further in subsequent sections, according to the four fundamental shoreline shapes identified.

5.4.2.1 *Cuspate Bumps*

Under a symmetrical wave climate (A = 0.5*)* cuspate features form along the shoreline in CEM and CEM2D (Figure 5.11, Figure 5.12 and Figure 5.18). With an increasing proportion of high angle waves, cross-shore sediment transport drives an increase in amplitude (Figure 5.19) and planform area (Figure 5.20).

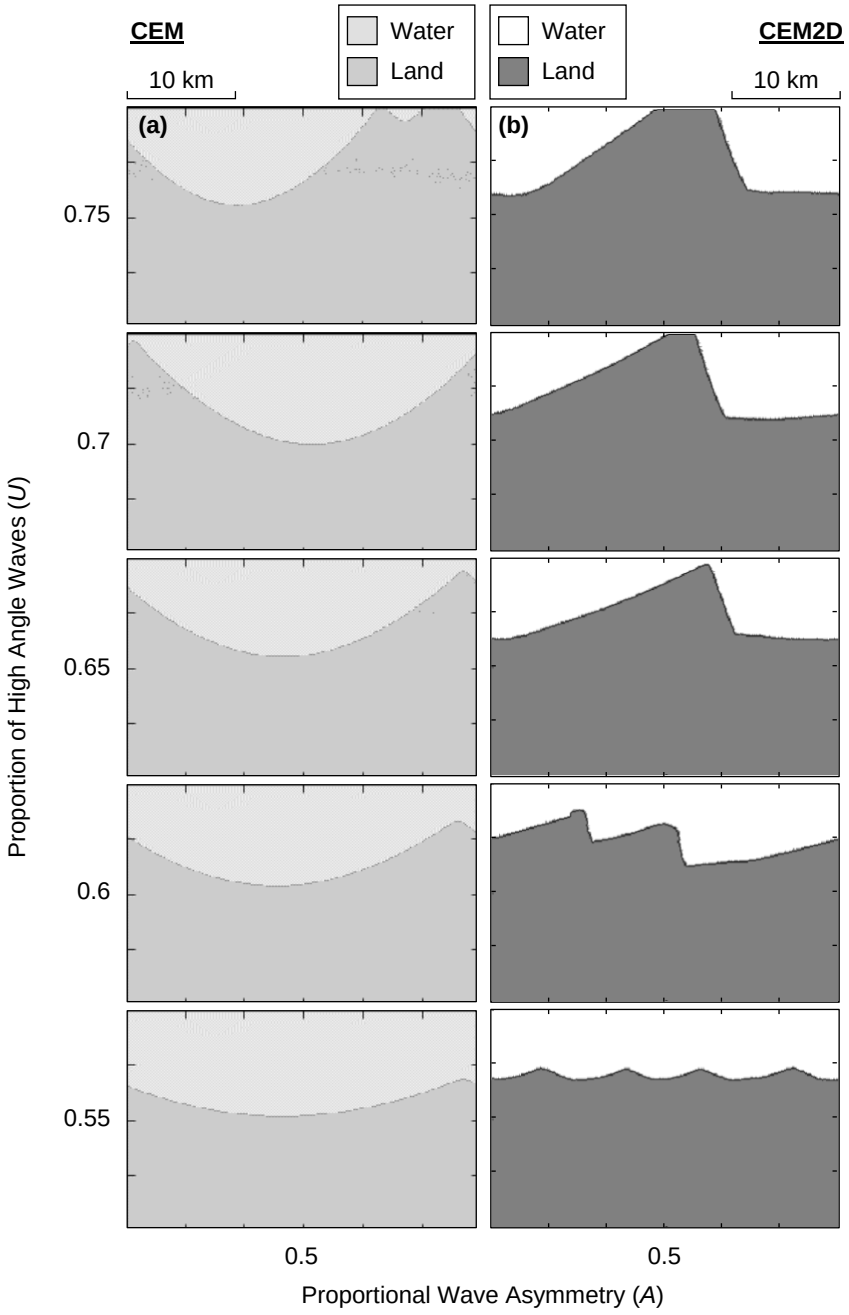

Figure 5.18 A series of images showing the difference in amplitude of cuspate landforms that form under a symmetrical wave climate (A = 0.5) with an increasing proportion of high angle waves (U). The outputs measure 20 km width and 30 km in length and are not inclusive of the periodic boundaries. Results from CEM are shown on the left (a) and from CEM2D on the right (b).

There is a significant correlation found in results of CEM and CEM2D, between the proportion of high angle waves approaching the shoreline and (1) the amplitude (average R^2 = 0.65) (Figure 5.19) and (2) average planform area (average R^2 = 0.68) (Figure 5.20) of the cusps at the end of the simulation.

Consistent with the results in Section 5.4.1, the average amplitude and area of cuspate features are greater in results of CEM than in CEM2D. To reiterate however, the focus is on the evolutionary patterns as opposed to the scales of features generated by the two models.

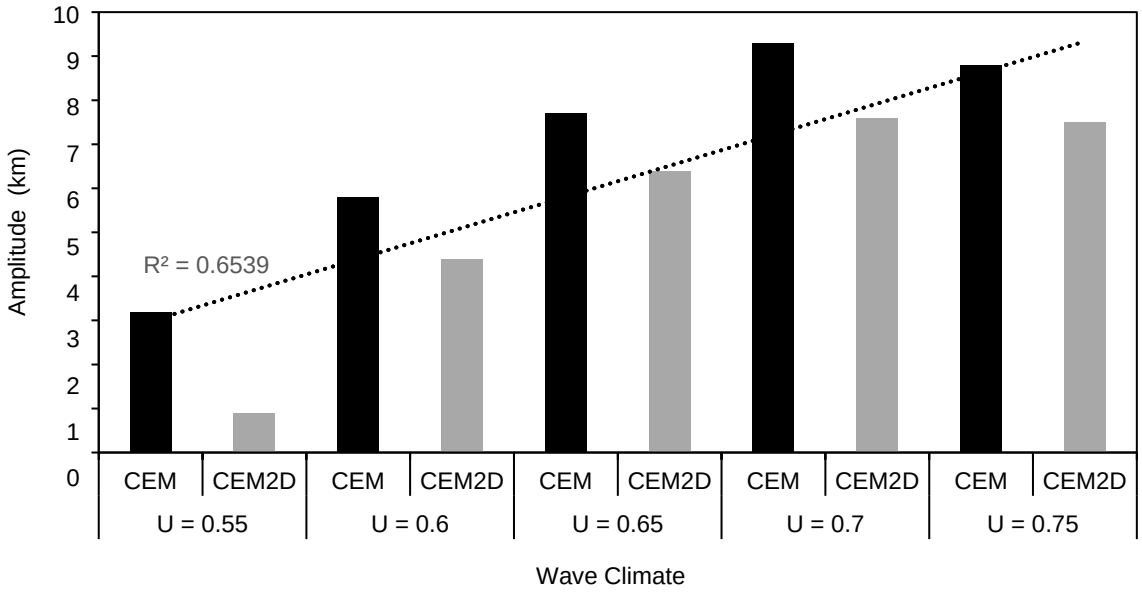

Figure 5.19 A bar chart showing the average amplitude of cuspate landforms that evolve under a symmetrical wave climate (A = 0.6), with increasing proportions of high angle waves (U), generated by CEM and CEM2D.

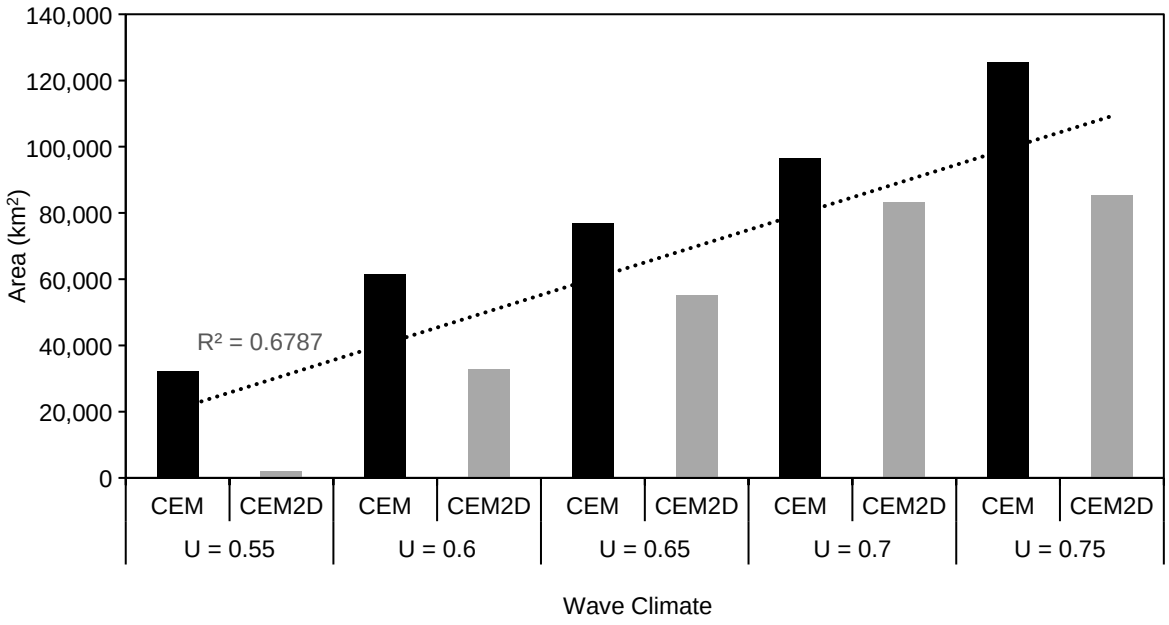

Figure 5.20 A bar chart showing the average planform area of cuspate landforms that evolve under a symmetrical wave climate (A = 0.6), with increasing proportions of high angle waves (U), generated by CEM and CEM2D.

Comparing results of the temporal change in planform area and wavelength of cusps over time, there is a correlation between outputs from CEM (Figure 5.21, solid lines) and CEM2D (Figure 5.21, dashed lines). It is observed that the sizes of features are generally larger when simulated in CEM, but the trend of change over time is concurrent. As the amplitude of cusps increases over time, larger features shadow and absorb smaller features. The areal extent of the larger cusps grows as they are fed sediment from the smaller landforms (Figure 5.21) and the number of objects along the shoreline reduces, which increases the wavelength (Figure 5.22).

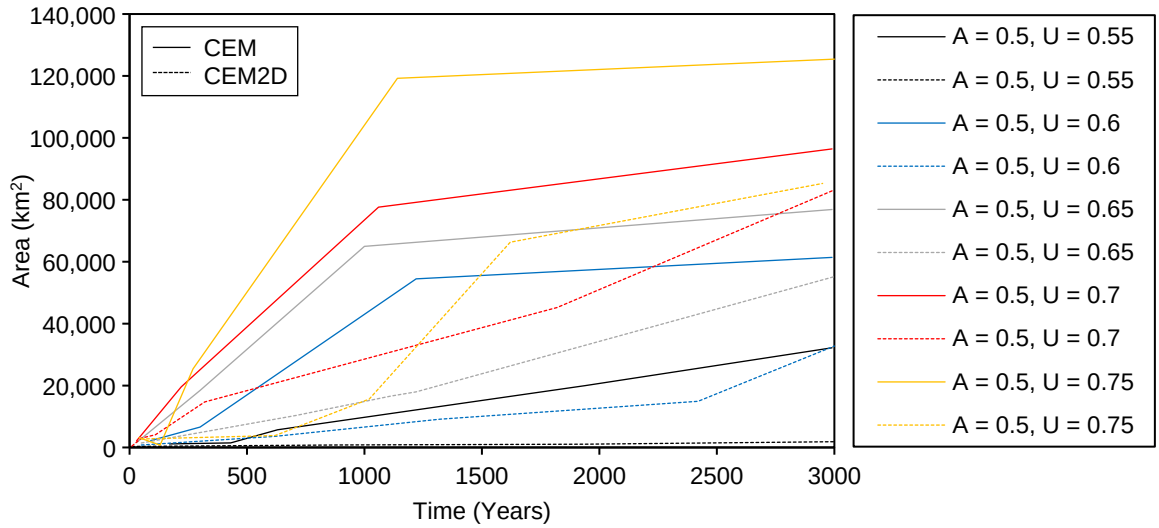

Figure 5.21 A graph showing the average area of cuspate landforms over time, where A = 0.5 and U varies from 0.55 to 0.75. Simulation generated using CEM are marked with solid lines and for CEM2D by dashed lines.

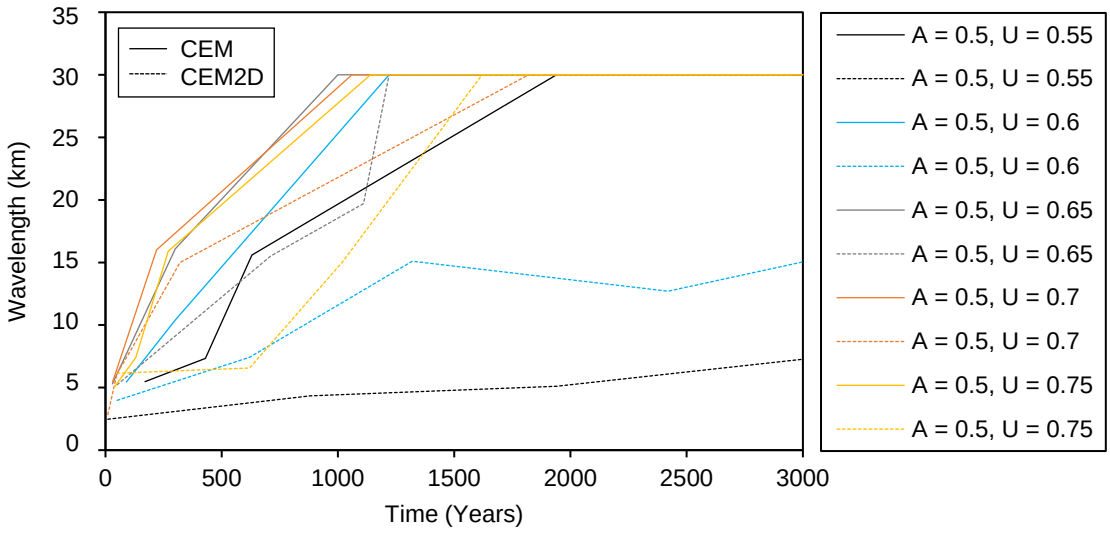

Figure 5.22 A graph showing the average wavelength of cuspate landforms over time, where A = 0.5 and U varies from 0.55 to 0.75. Simulation generated using CEM are marked with solid lines and for CEM2D by dashed lines.

In the results from CEM, it is clearly observed where the landforms reach a dynamic equilibrium, by the stabilisation of growth rates in terms of planform area and wavelength (Figure 5.21 and Figure 5.22). However, this is not so clearly defined in results from CEM2D. The landforms show a more gradual development over time and develop smaller features, as noted previously, due to more complex sediment handling and transport processes. In both models, the growth of landforms overtime and their ability to reach an equilibrium form is dictated by the sediment and energy budget (Carter, 2013). Therefore, with a slower rate of growth, a longer period may be necessary to allow features in CEM2D to develop to a state of equilibrium. However, a visual analysis of the outputs of CEM2D show that whilst the landforms continue to develop in planform area, their shape and form remain relatively consistent for the majority of simulations. This suggests that a dynamic equilibrium has been achieved and that the area and wavelength cannot, therefore, be used exclusively as an indicator of stabilisation.

Shoreline evolution in CEM2D shows a bias towards the longshore transport of sediment to the right of the domain, which is typically considered as downdrift in the asymmetric wave climate simulations in this thesis (and also by Ashton and Murray (2006a)). Even where the wave climate is symmetrical (*A* = 0.5*)* and cuspate features form, the tips of landforms show some directional skew and migration downdrift. The reasoning for this behaviour was suggested in Section 5.4.1 to be related to directional bias in the numerical model. Once features begin to skew, wave shadowing and sediment distribution processes can act to exaggerate the asymmetry (Rosen, 1975; Ashton *et al.*, 2001). This then continues in the model simulations and the morphological evolution is influenced by this exaggerated directional skew. It is observed however that the effect is more pronounced in simulations driven by symmetrical wave climate conditions. This is likely due to the internal operation of the model which dominantly works from left to right across the domain. To resolve this, the shoreline search and sediment transport processes in the numerical model need to be re-reviewed and updated to remove any bias. This could be addressed in future versions of CEM2D, as explored in Chapter 8. In the current version of CEM2D, an analysis of the results should consider this limitation in the model.

The results relating to the formation of cuspate features in CEM and CEM2D are comparable. They reinforce findings of previous studies (e.g. Zenkovitch (1959), Ashton *et al.,* (2001, 2006a, 2006b), Hurst *et al.,* (2015) and Serizawa *et al.,* (2012)) which suggest that wave-driven sediment transport under a symmetrical wave climate can form cusps along sandy shorelines. As demonstrated in the results, it is understood that the size and offshore accretion of the crests are related to sediment availability and the energy of waves, determined by high

angle wave instability (Carter, 1982). The results show that with an increasing proportion of high angle waves, the cusps exhibit greater amplitudes and encompass larger planform areas.

Cuspate forelands such as those generated by CEM and CEM2D occur along many shorelines globally. The Carolina Capes span parts of north and south Carolina's coast in the USA (Figure 5.4) and are used as a case site by Ashton and Murray (2006b) to validate model results generated by CEM (see Section 5.2.1). The wave climate along this stretch of coastline is characterised by high angle waves of relative symmetry, which broadly equate to PDF values of A = 0.55 and U = 0.6 (Ashton and Murray, 2006b). Placing the Carolina Capes into the context of the results shown in Figure 5.12, CEM2D would predict that under the driving wave climate conditions a cuspate coastline would be generated with a slight skew induced by the 5% dominance of waves approaching from the left of the domain (Park and Wells, 2005). The wave direction plays a significant role in the formation of the features, with the slightly stronger southerly current skewing the tips of the landforms (Park and Wells, 2005). Considering that all site-specific conditions controlling the evolution of capes are not represented in CEM2D, the model is able to predict a comparable shoreline type to that observed in this natural system.

5.4.2.2 *Alongshore Sand Waves*

Slight asymmetry in the wave climate (where A = 0.6) generates alongshore sand wave features in both CEM (Figure 5.11) and CEM2D (Figure 5.12). The results presented in Figure 5.23 are examples of these features, generated where A = 0.6, U = 0.6. The outputs show differences in the formation of these sand waves with the CEM developing more cuspate-type sand waves and CEM2D showing

the early development of a hook at the downdrift tip of the landform; this could be influenced by the extension of the feature to the seaward boundary of the domain (Figure 5.23). As noted previously, final outputs are not always representative of the evolution of the shorelines and the temporal development of these features can be found in Appendix 3.

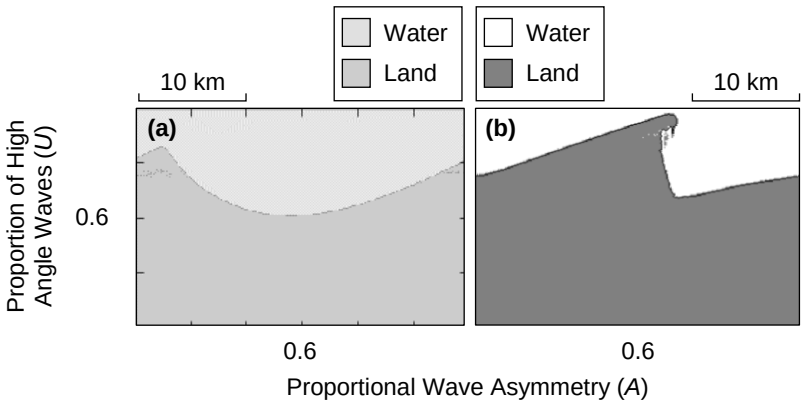

Figure 5.23 Outputs from CEM (left) and CEM2D (right) after 3,000 simulated years where A = 0.6, U = 0.6. The outputs measure 20 km in width and 30 km in length and are not inclusive of the periodic boundaries.

It is apparent from the results that CEM2D is more sensitive to the wave asymmetry and sand waves show a greater percentage of skew downdrift compared to those which form in CEM (Figure 5.24). As shown in Figure 5.24, where A = 0.6 and U ranges from 0.55 to 0.65 features in CEM skew downdrift by approximately 40% whereas in CEM2D a 96% skew is observed; a 0% skew would denote a symmetrical feature, with a positive value indicating how much the landform skews towards the right of the domain ("downdrift"). The differences in model results are attributed to the directional bias in the numerical model described previously in this section, as well as the more complex representation of the coastal system and the influence of the two-dimensional topographic and bathymetric profile. This is investigated further in Chapter 6, where the evolution of the two-dimensional profile and its influence on coastal behaviours is explored.

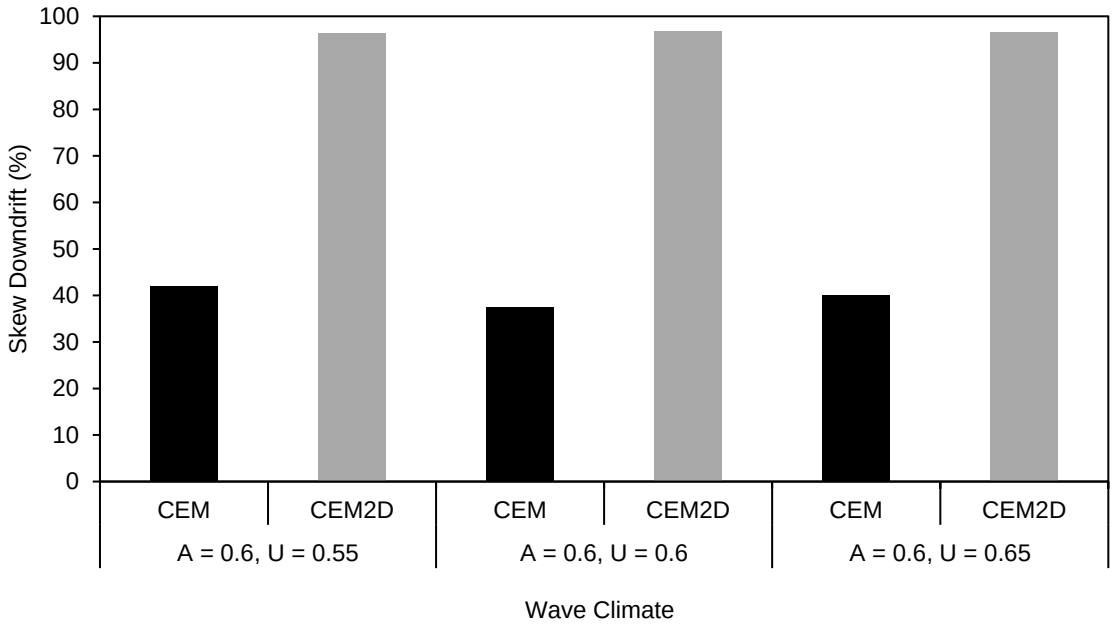

Figure 5.24 A bar chart showing the percentage skew of sand wave features downdrift, in CEM and CEM2D against three different wave climates. A 0% skew denotes a symmetrical landform and 100% where the downdrift flank is vertical or concaved.

Figure 5.25 and Figure 5.26 compare the results from CEM and CEM2D showing the development of sand waves in terms of their planform area and wavelength over time. The sand waves in CEM show a relatively linear development compared to CEM2D which alternates between periods of rapid and gradual growth. The total areas of the landforms that evolve in CEM and CEM2D after the 3,000 year simulation period are approximately 70,000 km^2 and 95,000 km^2 respectively (Figure 5.25). This is contrary to findings of cuspate features which generally show a smaller planform area when generated by CEM2D than by CEM. The wavelength for both simulations reaches the maximum of 30 km according to the size of the domain, after 1,200 simulated years for CEM and more slowly after 1,800 years in CEM2D (Figure 5.26). Although there is a difference in the evolutionary patterns of these features, they exhibit similar mechanisms of development over time.

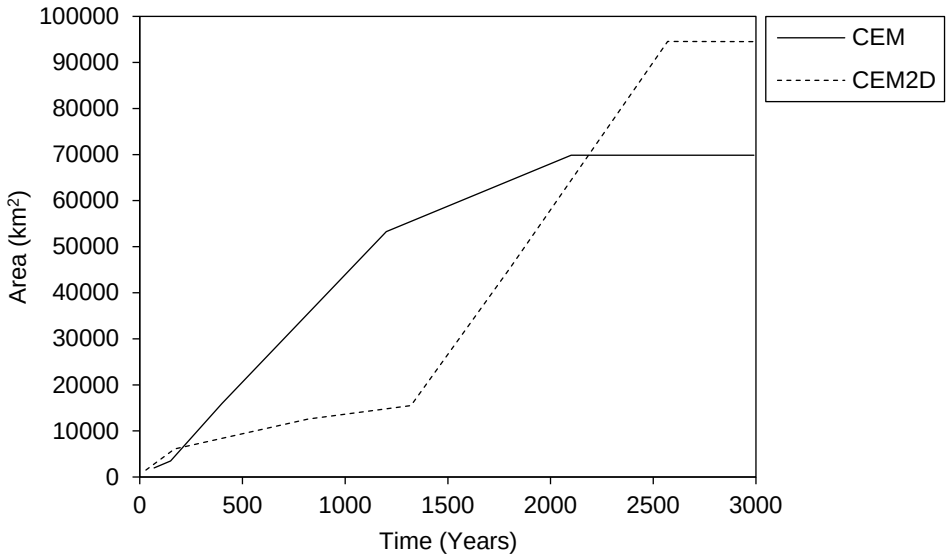

Figure 5.25 A graph showing the average area of sand waves over time, where A = 0.6 and U = 0.6. The simulation generated using CEM is marked with a solid line and for CEM2D by a dashed line.

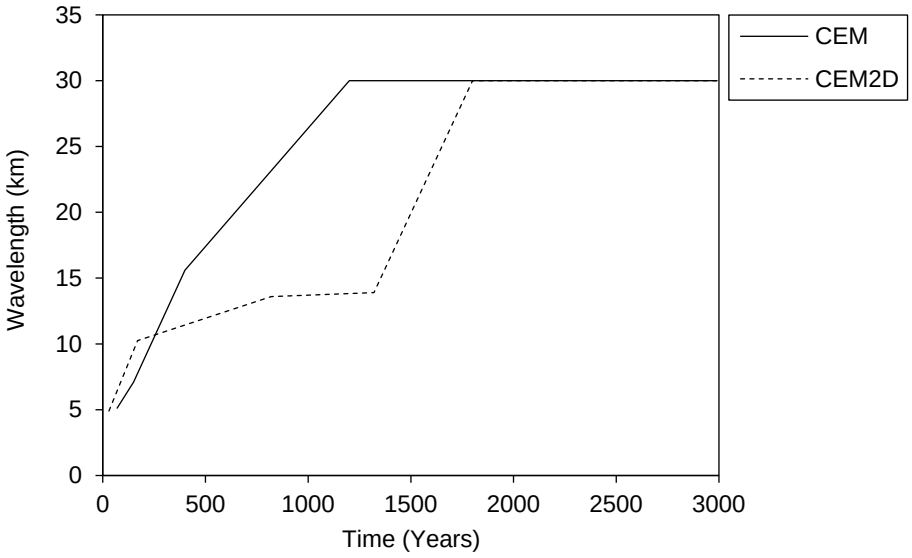

Figure 5.26 A graph showing the average area of sand waves over time, where A = 0.6 and U = 0.6. The simulation generated using CEM is marked with a solid line and for CEM2D by a dashed line.

The sand wave features generated in CEM and CEM2D can be likened to such termed landforms found in nature. As discussed in Section 5.2.1, Ashton and Murray (2006b) make reference to the sand waves along Long Point Spit in Ontario, Canada (Figure 5.5). The focus here is on the sand wave formations along the length of the spit, as opposed to the spit itself. The site has a highly

asymmetric wave climate, which here we assume to be *A* = 0.8-0.9 and a high value of *U* between 0.6-0.7 (Ashton and Murray, 2006b).

The results of CEM (Figure 5.11) suggest that for all four of the potential *A* and *U* combinations listed above, reconnecting spit features develop from initial sand waves along the shoreline. Ashton and Murray (2006b) note that the continued development of spit features in the model is not observed at Long Point currently, but suggest that they could form in time, as the model predicts. This is contrary to previous findings of Davidson-Arnott and Van Heyningen (2003) who argue that high angle wave instability is not the sole processes influencing the formation of features found at Long Point, however.

The results of CEM2D (Figure 5.12) when driven by wave climate conditions similar to those found along Long Point Spit, generate both sand wave features and spits. Where the asymmetry of the wave climate (*A*) is 0.8 and the proportion of high angle waves (*U*) is either 0.6 or 0.7, relatively shore-parallel spit features form that are elongated downdrift. Where the asymmetry is 0.9 and again, the proportion of high angle waves is either 0.6 or 0.7, cuspate sand waves form along the shoreline. Whilst these features show resemblance to cusps or sand waves, they develop as spit-like features concurrent with the high wave asymmetry. However, due to the dominance of wave from the left of the domain and the relative balance of high and low wave approaches, there is a strong net longshore current that tends to drive features towards the shoreline. This process could be influencing the shape of the sand waves along Long Point Spit, forming undulations as opposed to spit features under the highly asymmetric wave climate.

Taking an example from the UK, Benacre Ness is a migrating longshore sand wave feature located along the Suffolk coastline, in eastern England (Figure 5.27).

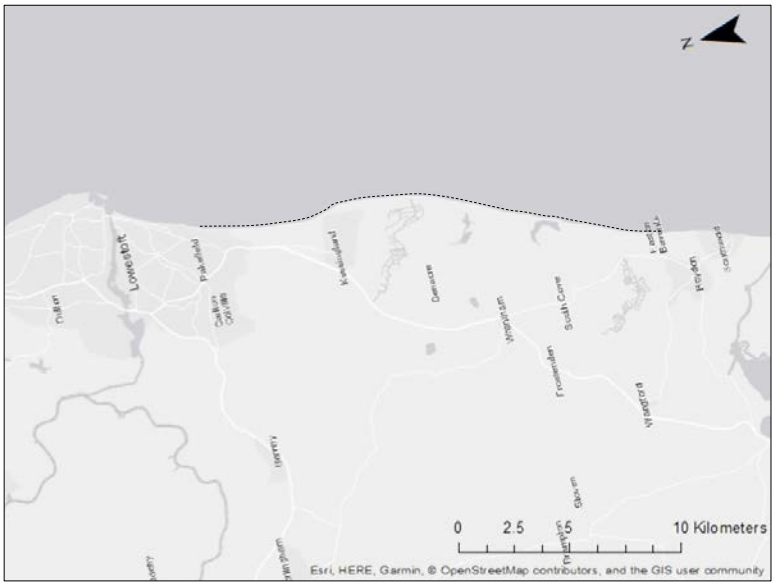

Figure 5.27 Map of Benacre Ness along the Suffolk Coastline, UK. The dashed line highlights the sand wave feature (ESRI, 2018).

An analysis of the wave climate data from the Southwold Buoy suggests that the coastline is subject to a slightly asymmetric wave climate dominated by high angle waves. Processing the data into PDF values generates a wave climate where A = 0.6 and U = 0.8 (Figure 5.28). The wave climate is calculated from data recorded between January 2010 and January 2018 by the Southwold Wave Buoy, made available by CEFAS Wave Net data hub (CEFAS, 2018). Considering the local shoreline orientation, the peak wave angle is binned according to the four categories shown in Figure 5.28, from which the PDF values are calculated.

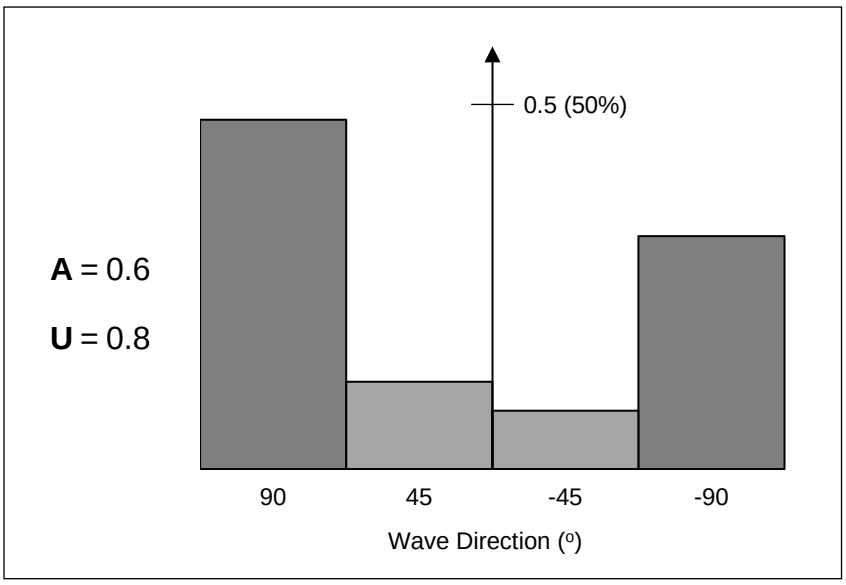

Figure 5.28 Probability distribution function (PDF) calculated for Benacre Ness, where A represents the asymmetry of the wave climate and U represents the proportion of high angle waves. Data were taken from the Southwold Approach WaveNet Site between 2010 and 2018, sourced from the CEFAS data hub (CEFAS, 2018).

The shoreline simulated in CEM under these wave conditions produces alongshore sand waves features that map onto the planform morphology of Benacre Ness (Figure 5.12). Comparatively, the CEM2D generates features which are more spit-like in shape as opposed to the shallow amplitude perturbations observed in the natural system (Figure 5.11). It is noted that site-specific environmental and boundary conditions play a role in the formation and evolution of Benacre Ness which are not modelled by either software.

5.4.2.3 *Reconnecting and Flying Spits*

Where the wave climate is asymmetric (A = 0.7-0.8) and dominated by high angle waves (U = 0.65-0.7), spit features form along shorelines simulated in both CEM (Figure 5.11) and CEM2D (Figure 5.12). However, CEM2D shows greater sensitivity to the input wave climate and a greater distinction is made between the formation of reconnecting and flying spits. In results of CEM, where spits form along the shoreline the majority resemble reconnecting spits with islands and

sediment paths connecting the neck with the mainland, whereas in CEM2D both reconnecting and flying spits are identified in the results. This is one of the points of difference between the results of CEM in this research and previous studies using this model, and one of the justifications for reproducing the results (as stated in Section 5.1). Ashton and Murray (2006a) differentiate between the two types of spit features, although they note that landforms can evolve between these types given longer runtimes. In the results discussed here, wave climate conditions where A = 0.7 and U = 0.65 are used to exemplify the behaviour of reconnecting spits and A = 0.8, U = 0.7 for flying spits in both models (Figure 5.29).

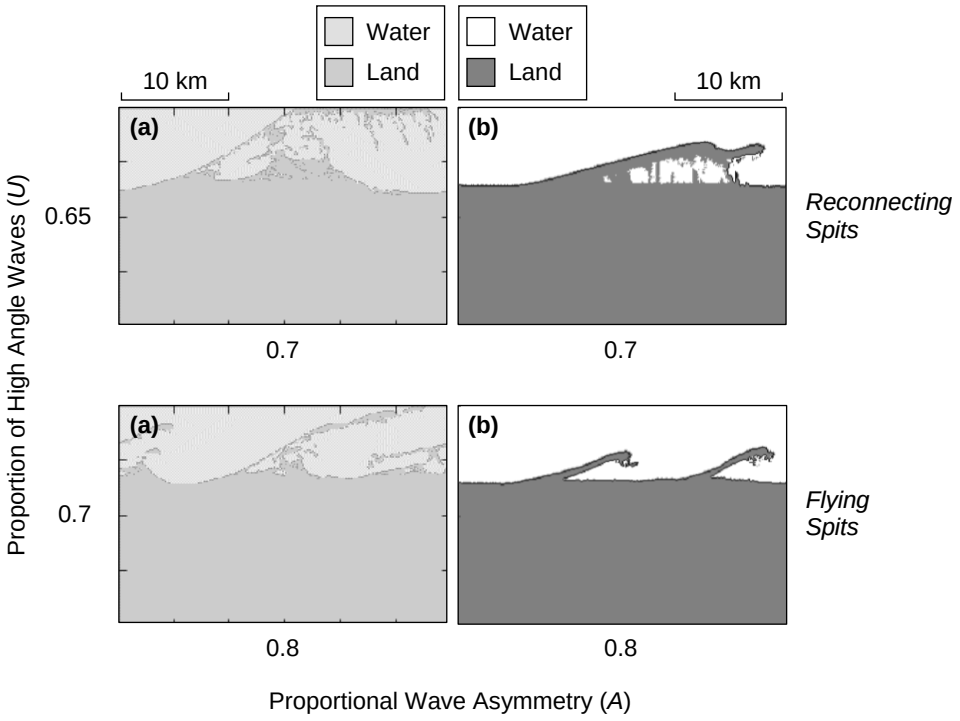

Figure 5.29 Outputs from CEM (a, left) and CEM2D (b, right) where A = 0.7, U = 0.65 (top, reconnecting spit) and where A = 0.8, U = 0.7 (bottom, flying spit). The total runtime of the simulation in years is given by 'T'. The outputs measure 20 km in width by 30 km in length and are not inclusive of the periodic boundaries.

Figure 5.30 and Figure 5.31 shows how the planform area and wavelength of these features change over the simulation period. As shown in the graphs in these figures, the landforms exhibit different patterns of development when

simulated in CEM and CEM2D. It is also of note that both models terminate prematurely as the development of the landforms create a shoreline shape that is too complex for the simplified shoreline search technique to detect and process (Figure 5.30 and Figure 5.31). This is a limitation noted previously in this chapter and which is discussed in more detail in Chapter 8.

Since the forms in CEM2D are more refined and the sediment handling techniques are more complex, the simulation runs for a greater period of time than CEM. The final shorelines in both models at the end of each simulation show well-developed landforms and so the premature termination of the models is not considered a major limitation and is rather an indication of the rapid development of these types of landforms compared to the other types investigated in this study.

The reconnecting and flying spits that evolve in CEM2D do so at a relatively gradual rate of approximately 0.02 km^2 and 0.2 km^2 respectively per simulated day (Figure 5.30). In CEM, the landforms develop at a greater rate of approximately 0.4 km^2 and 0.8 km^2 per day for reconnecting and flying spits respectively (Figure 5.30). A similar pattern is observed in the change in wavelength of spits over time, as shown in Figure 5.31. Spits generated in CEM2D gradually increase in wavelength and multiple features pertain along the shoreline at the end of the simulation, whereas in CEM a rapid increase in wavelength to the maximum is observed with only a single feature remaining.

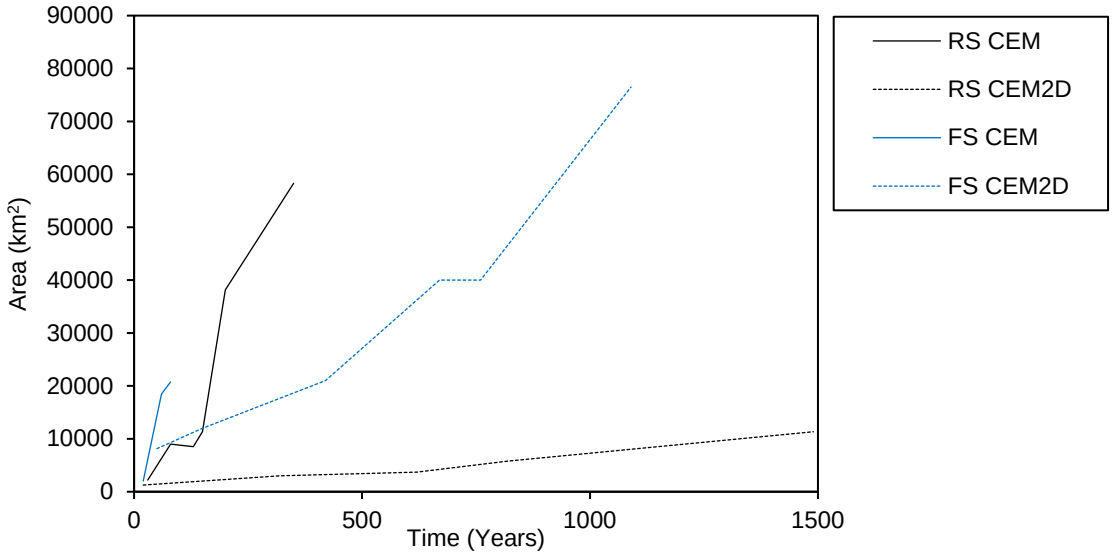

Figure 5.30 A graph showing the average area of spits over time, where A = 0.7 and U = 0.65 (Reconnecting Spits, RS) and where A = 0.8 and U = 7 (Flying Spit, FS). The simulations generated using CEM are marked with a solid line and or CEM2D by dashed lines.

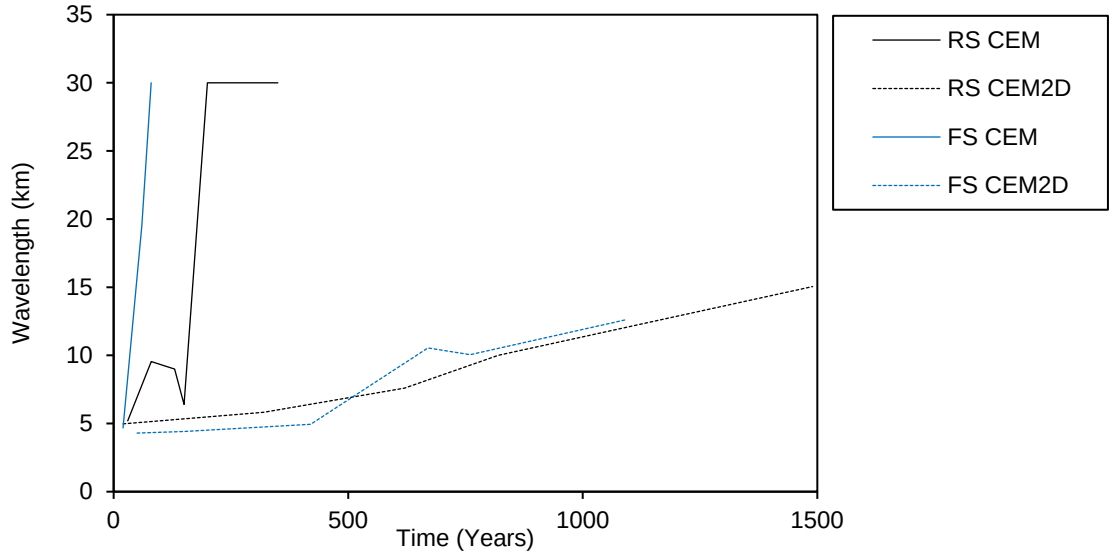

Figure 5.31 A graph showing the average wavelength of spits over time, where A = 0.7 and U = 0.65 (Reconnecting Spits, RS) and where A = 0.8 and U = 7 (Flying Spit, FS). The simulations generated using CEM are marked with a solid line and for CEM2D by dashed lines.

The differences in the growth rate and pattern of spit features observed in CEM and CEM2D are predicted to be attributed to the change in sediment handling, storage and transport techniques in the latter model. In particular, the sediment distribution method in CEM2D, that prevents material piling or pits forming in any

given cell, will affect dry cells even if they are not connected to the shoreline. This includes the island and sediment paths that exist between the spit neck and mainland. In CEM, if these accumulations occur and become disconnected from the primary shoreline, they will not be found in the shoreline search method and will therefore not evolve, but remain static until new pathways are formed to the shoreline. This is illustrated by outputs from CEM in Figure 5.32. In natural systems, these accumulations (e.g. offshore bars) evolve independently unlike those generated by the CEM. Therefore, whilst the method of sediment distribution in CEM2D is a simplification and does not represent all processes that influence sediment movement in the nearshore, it allows sediment to be dynamic and deters the formation of static accumulations.

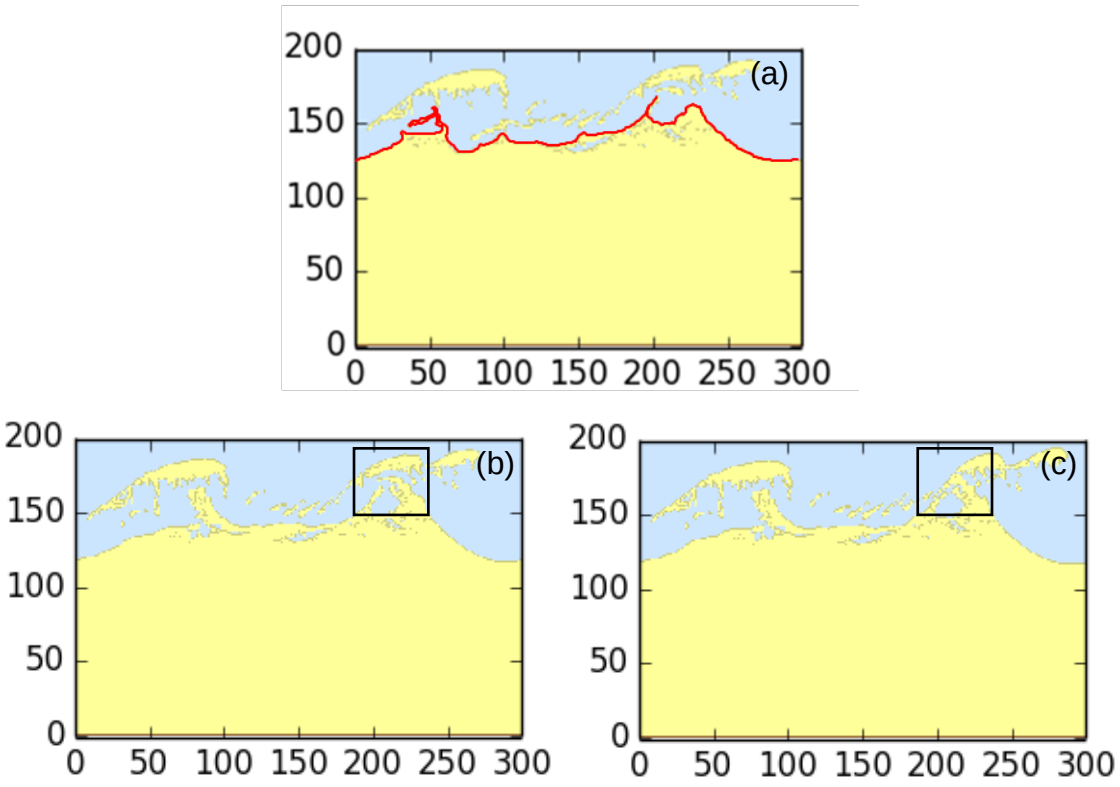

Figure 5.32 A time series of images from CEM, where A = 0.8, U = 0.6. Image (a) shows the model output at 500 simulated years with the position of the shoreline according to the model's algorithm marked in red. Image (b) shows model outputs at 2800 simulated years and (c) at 2810 simulated years. The black box in images (b) and (c) shows where the reconnecting spit is detached (b) and then reconnects with the shoreline (c).

Concurrent with the results of the study by Ashton *et al.,* (2001, 2006b), when CEM2D is driven by wave climate conditions similar to those found where natural spits evolve, similar features form in the model. As discussed in Section 5.2.1, Ashton and Murray (2006b) use Long Point Spit in Lake Erie, Canada to compare model results of CEM to the behaviour and development of this natural system. The wave climate conditions in this location have been previously stated in Section 5.4.2.2, where the formation of sand waves along the spit was discussed. The climate is characterised by high asymmetry (A = 0.8-0.9) and high angle wave dominance (U = 0.6-0.7) (Ashton and Murray, 2006b). Under these wave climate conditions reconnecting spit features form in CEM (Figure 5.11), whereas in CEM2D (Figure 5.12) either sand waves or reconnecting spits form depending on the combination of A and U values (as discussed in Section 5.4.2.2). Ashton and Murray (2007) suggest that the wave climate is favoured towards an asymmetry (A) of 0.8 along the entire spit; under these conditions, reconnecting spits form in CEM2D, as per the natural system (Figure 5.12).

Taking an example from the UK, Spurn Point is a spit formation located on the east coast in the East Riding of Yorkshire, extending off the southern end of the Holderness Coast (Figure 5.33). The narrow sandy spit follows the trajectory of the Holderness before curving south-west across the mouth of the Humber Estuary. Resampling recorded peak wave direction data into the four PDF bins shown in Figure 5.34 and considering the local shoreline orientation (from Withernsea to the tip of Spurn Point), gives wave climate values where A = 0.75, U = 0.35. The wave climate data is taken from the Hornsea Wave Rider buoy between January 2010 and January 2018 and has been made available by the Channel Coastal Observatory (Channel Coastal Observatory, 2018).

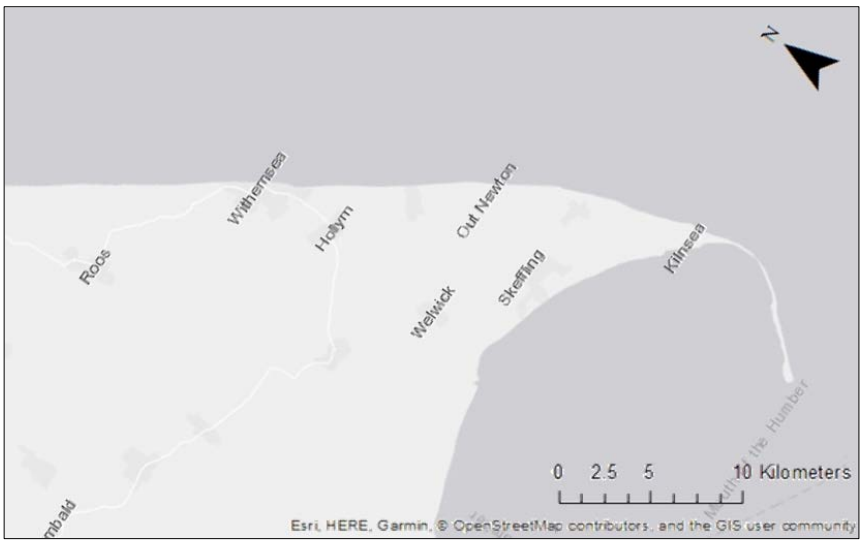

Figure 5.33 Map of Spurn Point Spit along the east coast of the UK (ESRI, 2018).

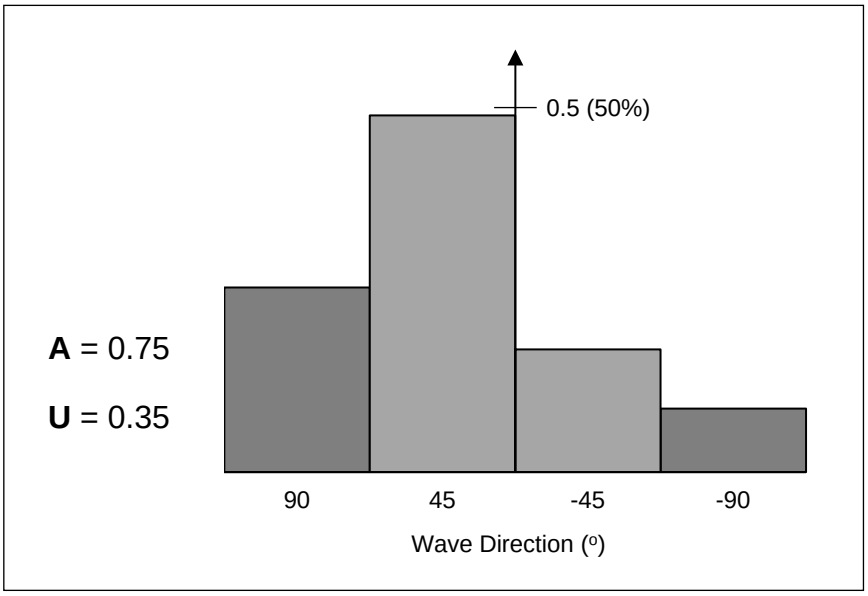

Figure 5.34 Probability distribution function (PDF) calculated for the southern Holderness Coast, where A represents the asymmetry of the wave climate and U represents the proportion of high angle waves. Data is taken from the Wave Rider between 2010 and 2018, sourced from the Channel Coastal Observatory (Channel Coastal Observatory, 2018).

Following the pattern of results from CEM (Figure 5.11) and CEM2D (Figure 5.12), if driven by the wave climate conditions at the southern end of Spurn Point, the models would generate spit features. In both models where there is proportional asymmetry (*A*) of between 0.7 and 0.8, net longshore sediment transport forms these types of landforms. However, in CEM2D these features

fluctuate between spits and sand waves owing to the strong longshore current generated by the low angle waves and high asymmetry.

The ability of CEM and CEM2D to generate shorelines with proportions of high angle waves less than 0.55 is a limitation when comparing outputs to the Holderness and Spurn Point. However, the data suggest that with decreasing *U* values, the amplitude of features decreases. This is particularly apparent in the results of CEM2D. As shown in Figure 5.33, the cross-shore extension of Spurn Point is relatively limited, but it projects approximately 6km longshore as it forms across the mouth of the Humber Estuary. This behaviour and the growth of the spit which follows the trajectory of the shoreline is explained in the model results by the proportion of low-angle waves which drives a strong longshore sediment transport rate. Also not considered in either CEM or CEM2D is the influence of estuary flows in the formation of Spurn Point.

5.5 Synthesis

The purpose of this chapter was to demonstrate the functions of CEM2D in terms of its ability to simulate fundamental planform shoreline shapes according to the driving wave climate conditions, as per the CEM. The results presented show that there are many similarities in the outputs of CEM2D and the empirically tested CEM under a range of PDF wave climate scenarios. The results are also shown to compare to observations of several natural systems and shoreline shapes according to the driving wave conditions.

CEM2D demonstrates that under various wave asymmetries (*A*) and proportions of high angle waves (*U*), the model can predict the evolution of cusps, sand waves, reconnecting spits and flying spits as previously demonstrated in the CEM

(Ashton *et al.*, 2001, 2006a, 2006b). The results are compared in this chapter to exemplary shorelines, showing how outputs from CEM2D align with natural coastal systems including the Carolina Capes (USA), Long Point sand waves and Long Point Spit (Canada), Benacre Ness (UK) and Spurn Point spit (UK). Compiling the model with PDF values representing the conditions at each of these sites generates similar types of shoreline features.

The findings demonstrate that shorelines generated in CEM2D show greater comparison to natural systems, than those formed by CEM. From the examples given in this chapter, where there is a slight asymmetry in the wave climate (A = 0.6, U = 06), CEM2D forms sand waves or shallow reconnecting spits alike those of Long Point Spit sand waves (Canada) or Benacre Ness (UK) which are driven by similar wave climates; in CEM, spits form under these conditions. Increasing the asymmetry and proportion of high angle wave further generates spits in both models. The formation and trajectory of spits which evolve in CEM2D are more comparable to the example location (Spurn Point, UK), compared to the results of CEM.

Where the wave climate is relatively symmetrical and cuspate-type features form in natural systems, such as the case of the Carolina Capes, the CEM underestimates the skew of features according to the slight directional dominance in the wave climate and CEM2D overestimates this skew. The results here are attributed to the directional bias in the models which are exaggerated in CEM2D due to the more complex representation of processes and domain structure.

An analysis of the phase spaces produced for the CEM (Figure 5.11) and CEM2D (Figure 5.12) show the influence of wave conditions on the planform morphology

of the simulated coastline. A smooth transition is observed between landform types in CEM2D, depicting the role of wave asymmetry and high angle wave instability on cross-shore and longshore sediment transport. Less distinction is made between spit types in CEM and the landforms show a transition between the two types at high values of wave asymmetry (*A*) and high angle wave instability (*U*). It is argued that where a greater distinction is made between these landforms types as shown in CEM2D, a clearer understanding of the influence of wave conditions on shoreline evolution can be gained as is the intention of these exploratory models.

An anomaly to the results discussed so far is the formation of cuspate sand waves in CEM2D, where the wave climate is highly asymmetric with only a slight dominance of high angle waves (A = 0.9, U = 0.55-0.6). As noted in the results, the strong longshore sediment transport generated by these wave climate conditions creates a smoothing effect along the shoreline. This process reinforces similar theories proposed by Serizawa *et al.,* (2012). These features are not observed in the CEM, where spits develop according to the high asymmetry in the wave climate with no evidence of shoreline smoothing.

Whilst the types of landforms generated according to the driving wave conditions are comparable between the two models, in general CEM exhibits a greater rate of development and produces landforms with larger planform areas, except where sand waves form. This is particularly the case for spit features in CEM, where the total landform area includes the static accumulations between the spit neck and mainland, which increases the area of the landforms artificially. As discussed in Section 5.4.2.3, these accumulations form and sustain due to the simplistic shoreline search technique employed and the limited or inability of the

model to redistribute the material unless it is connected to the shoreline. This is a limitation in the CEM and which has been improved upon in CEM2D through the addition of the sediment distribution method (see Chapter 3). The improvements here are not only noted in the definition of landforms that develop but also in the run durations, which are longer for CEM2D and do not terminate as prematurely as in CEM. It is important to reiterate that whilst the scale of planform features differs between the two models, the focus of this study is on the types of features and shoreline shapes that evolve. Therefore, although consideration is given to the differing scale of landforms and explanation is given associated with the different sediment handling and transport procedures, the types of landforms and their evolutionary patterns are given precedence in this analysis.

The patterns and rates of landform development are more complex in the outputs of CEM2D. Again, this can be attributed to the sediment handling methods which generate greater feedbacks between various processes in the model. For instance, the beach and nearshore profile evolve dynamically in CEM2D and can store remnant morphologies, or morphological memories in the profile which can influence the morphology and evolution of the coastal system[2] (Thomas *et al.*, 2016). Such feedbacks are not captured in CEM but could prove important in the long-term behaviour and evolution of these systems. It is, therefore, a useful component of CEM2D that provides a representative insight into the behaviour of

[2] The concept of morphological memories is acknowledged in this chapter, but a more in depth discussion is given in Chapter 6.

the coastal system. For instance, in the example of Long Point sand waves and Spit in Sections 5.4.2.2 and 5.4.2.3, CEM2D is able to more accurately represent the natural system than the CEM, perhaps owing to the more complex representation of processes and process interactions in the model.

Directional bias is observed in simulations where the wave climate is symmetrical in CEM2D (where A = 0.5). As can be seen in Figure 5.12, under these wave climate conditions some of the cuspate landforms skew downdrift although the process of their formation is exemplary of cusps. Many of the techniques inherited in CEM2D from CEM induce some bias of net longshore transport towards the right of the domain; for instance, many domain search methods process from the left to the right. Due to the more complex and refined sediment handling and transport techniques in CEM2D as well as the addition of sediment distribution in the model, these effects become more noticeable. Once the directional skew is induced, processes such as wave shadowing exaggerate the behaviour (Rosen, 1975; Ashton *et al.*, 2001).

Modelling bias is a limitation of CEM2D and addressing it will involve making significant changes to the structure of the model. This was not possible within the constraints of this research project but are intended for future versions of the model (see Chapter 8). The influence that this has on the behaviour and evolution of modelled shorelines is taken into account in this thesis and a detailed review of future work to address the behaviour is given in Chapter 8. In other cases, the sensitivity of CEM2D leads to greater clarity of landform types particularly concerning reconnecting and flying spit features (Figure 5.11 and Figure 5.12). As previously stated, greater clarity can lead to a clearer understanding or analysis of behaviours, as is the intention of this research.

The findings of this chapter demonstrate that CEM2D is more sensitive to input environment conditions than the CEM. This occurs as a result of the more complex domain structure and representation of processes in CEM2D, particularly with regards to sediment transport and distribution methods. As described in Chapter 3, the new model transports sediment across the two-dimensional domain, allowing the topographic and bathymetric profile of the entire modelled system to evolve dynamically and instituting a more calculated dispersal of material across the nearshore profile. Changes to environmental conditions in the model which alter cross-shore and longshore sediment transport rates, therefore, have a greater influence on the evolution of the entire domain in CEM2D than is achievable in the one-line CEM. The sensitivity of the model is evident in the results from CEM2D, which generates shorelines with greater definition of planform types (e.g. cusps, sand waves, spits), particularly those which form under highly asymmetric wave climates that are dominated by high angle waves (e.g. reconnecting and flying spits). Model sensitivity is also shown in the more complex evolution of shoreline features and the relationship between high angle wave instability and the planform types which are generated. As has been discussed in the results, differences in model results between CEM and CEM2D are observed where the wave climate is highly asymmetric but has little dominance from high angle waves (A = 0.9, U = 0.55-0.6). This wave climate drives a smoothing effect along the shoreline in CEM2D, also observed by authors including Serizawa *et al.,* (2012), which is not found in the results of CEM. The sensitivity of CEM2D to input wave climate conditions shown in this chapter reinforces results from the sensitivity analysis completed in Chapter 4.

The results from CEM2D highlight that there is a more complex relationship between shoreline evolution and high angle wave instability than has previously been explored within this theory. It shows that the inclusion of more complex sediment transport processes across the two-dimensional domain is advantageous for investigating the role of wave climate conditions on the behaviour of the coastal system. In the results presented in this chapter, the focus has intentionally been on the one-line shoreline in CEM2D, extracted from the results and there has been little discussion of the two-dimensional features of the model; this has been for the purpose of model-model comparison with the one-line CEM. In the following chapter, the two-dimensional behaviour of CEM2D will be explored in greater depth, reinforcing the theories discussed here regarding the influence that the more complex domain structure and process representation has on modelled shorelines.

5.6 Conclusion

In this Chapter, outputs from CEM and CEM2D are presented and compared giving evidence of CEM2D's ability to simulate fundamental shoreline shapes according to the empirically tested CEM, as well as the behaviour natural coastal systems (e.g. Carolina Capes (USA) and Spurn Point (UK)). There are many similarities found between the results of both models and any differences have been justified against behaviours of natural coastal systems or modelling behaviours which have been taken into account. The results have also shown however that under a number of wave climate conditions, such as where there is an asymmetry in the directional wave climate, the CEM2D performs better than

CEM in representing the form of natural shorelines according to the examples given.

This chapter has explored the planform response of coastal systems to driving wave climate conditions, supporting and disputing current theories presented by Ashton *et al.,* (2001; 2006a, 2006b) with reference to the behaviour of natural systems. In doing so, this chapter has addressed Research Objective 2 of this study, as given in Chapter 2:

> *"To examine the relationship between coastal planform and wave climate conditions, which drive sediment transport processes in the environments under consideration, by comparison of the two-dimensional coastline evolution model with an existing model as well as to natural systems"* (see Chapter 2).

In the following chapter (Chapter 6), the additional functionalities of CEM2D including its ability to simulate the topographic evolution of coastal systems will be explored.

Chapter 6

The Two-Dimensional Evolution of Coastal Systems: An Application of CEM2D

Research Results

6.1 Introduction

In the previous Chapter, results generated by CEM and CEM2D were presented which showed how the wave climate, specifically the wave asymmetry and proportion of high angle waves, can drive shoreline evolution as evidenced in natural coastal systems. The additional functionalities and two-dimensional structure of CEM2D mean that further exploration of these behaviours can be conducted. Not only can the planform shoreline be analysed (Chapter 5), but also the dynamic behaviour of the bathymetry and beach topography under different wave climates conditions.

Understanding the two-dimensional dynamics of the coastal profile is important for predicting coastal evolution over the long term, particularly considering the effects of changing water levels and sea level rise (Pacheco *et al.*, 2015; Ortiz

and Ashton, 2016). Pacheco *et al.,* (2015, p. 102) suggests that the “nearshore bathymetry is likely to be the coastal variable that most limits the investigation of coastal processes and the accuracy of numerical models”. Changes occurring particularly in the nearshore zone can affect a multitude of processes including wave transformations, longshore and cross-shore sediment transport, the sediment budget and sediment distribution (Hequette and Aernouts, 2010). Each of these processes plays a role in the morphodynamic behaviour and evolution of coastal environments.

Wave transformations in CEM2D are not influenced by the dynamic bathymetry and resulting changes in the water depth, but the model is capable of exploring cross-shore behaviours and sediment pathways nevertheless. The development of more complex wave transformations is not within the scope of this research but could be integrated into future versions of the software (see Chapter 8). Two-dimensional modelling of mesoscale coastal processes is still in its infancy and software development is an iterative process that will generate ever-improving results as our understanding of these systems and modelling methods progress.

In this Chapter, the same experimental set-up described in Chapter 5 is applied, but the results of CEM2D are used to investigate how the beach and bathymetric profiles evolve concurrently with the shoreline shape. In doing so, this chapter will contribute to Research Objective 3 of this study, as outlined in Chapter 2 and reiterated in the conclusion of this chapter in Section 6.8.

6.2 Coastal Classifications

Classifications of coastal systems are widespread in the literature and are useful for describing principle modal two- and three-dimensional morphologies that are dictated by the driving environmental conditions (Scott *et al.*, 2011). The most

prevalent classifications were developed and adapted by a multitude of authors, with the most common adaption refined by Wright and Short (1984). Drawing on previous work (Wright *et al.*, 1978, 1979, 1982a, 1982b, 1982c), Wright and Short (1984) define three key beach states of wave-dominated sandy coastal systems; dissipative, intermediate and reflective (Figure 6.1). The state of the shoreline is determined by the dimensionless fall velocity (Ω) according to the wave and sediment characteristics, which is calculated using Equation 6.1:

$$\Omega = H_b \,/\, (W_s T)$$

Equation 6.1

Where H_b is the wave breaker height (m), W_s is the fall velocity of sediments (m/s) and T is the period of waves (s). A dimensionless fall velocity less than 1 denotes a reflective beach, between 1 and 6 an intermediate beach type and greater than 6, a dissipative beach type (Wright and Short, 1984).

High-energy dissipative beaches are typically characterised by fine sandy material and high waves which tend towards a relatively planar or concave beach profile with shallow slope gradients (Figure 6.1) (Wright and Short, 1984; Short, 2006). Low-energy reflective beaches tend to form under low wave conditions and are composed of coarser sediments and steeper profiles, often with a step in the profile at the base of the dry beach (Figure 6.1) (Wright and Short, 1984; Short, 2006). The four intermediate states are characterised by both dissipative and reflective behaviours, including Longshore Bar-Trough, Rhythmic Bar and Beach, Transverse Bar and Beach, and Ridge-Runnel or Low Tide Terrace types (Figure 6.1). These intermediate states are defined by decreasing dimensionless fall velocities and exhibit more complex morphologies compared to the extremes of dissipative and reflective beaches.

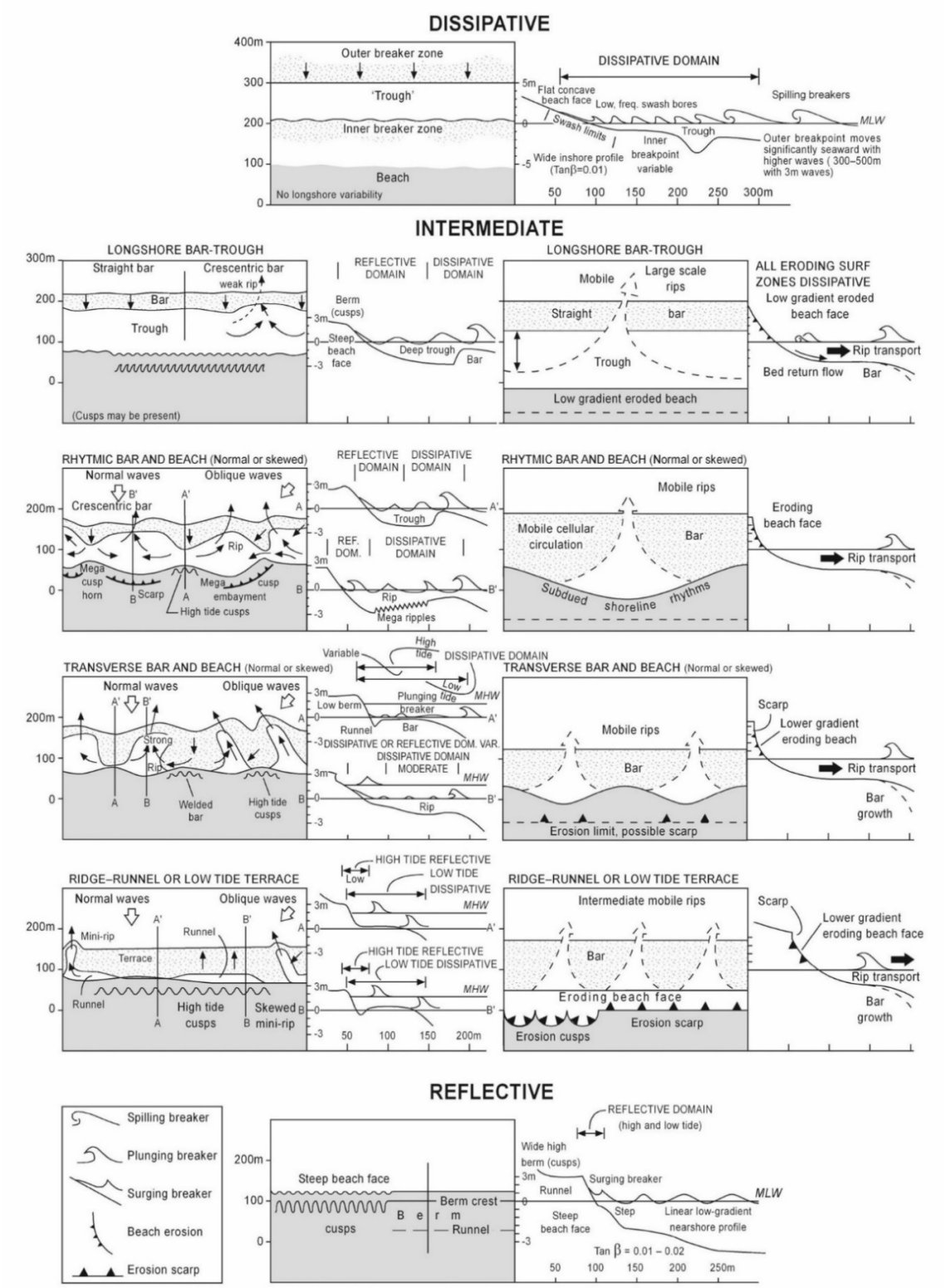

Figure 6.1 Types of Wave-Dominated Sandy Coastal Systems as per Wright and Short (1984) (Short, 2006)

Masselink and Short (1993) support the classifications proposed by Wright and Short (1984) but assert the importance of tidal processes and wave-tide interactions in determining beach state. They hence added an additional term into Wright and Short's (1984) equation, to represent the relative tidal range (RTR)

(Davis and Hayes, 1984; Masselink and Short, 1993). The RTR is calculated according to the ratio of the tidal range and breaker height, where a large value denotes a tide-dominated system and a low value, a wave-dominated system (Masselink and Short, 1993):

$$RTR = TR/H_b$$

Equation 6.2

Where *RTR* is the relative tidal range (m), *TR* is the tidal range (m) and H_b is the wave breaker height (m). Combining Equation 6.1 and Equation 6.2 generates eight conceptual beach types according to the dimensionless fall velocity and tidal range, as shown in Figure 6.2.

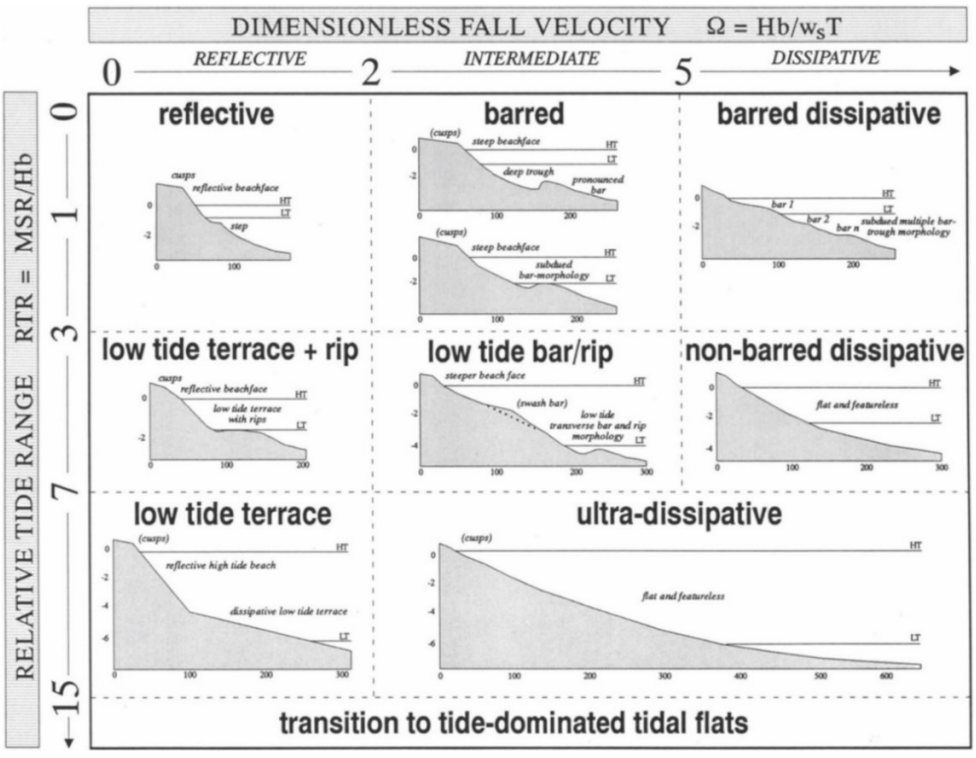

Figure 6.2 Coastal classifications affording to the dimensionless fall velocity and tidal range (Masselink and Short, 1993, p. 791)

Concurrent with Wright and Short's (1984) classifications, reflective beach types are characterised as those with steep beach face particularly on the upper beach which is subject to less tidal and wave energy, as well as an increasingly featureless lower beach with greater *RTR* (Figure 6.2) (Masselink and Short,

1993). For intermediate types, reflective and dissipative behaviours shape a steeper upper beach profile and shallower lower slopes. These types are also characterised by undulating morphologies (e.g. bars and rips), but which are increasingly muted with greater tidal range (Figure 6.2). Dissipative beach types are characterised by flat wide beaches, which show increasingly low gradients and fewer morphological features with increasing *RTR* (Masselink and Short, 1993).

Both Wright and Short (1984) and Masselink and Short (1993) demonstrate how the dimensionless fall velocity, as well as the tidal range, influence the morphology of the cross-shore coastal profile. With increasing fall velocity and tidal range, beach types transition from steep, reflective forms with bar and step morphologies to non-barred dissipative types with a relatively low gradient, featureless profiles (Figure 6.1 and Figure 6.2) (Wright and Short, 1984; Masselink and Short, 1993). Using evidence from 92 beaches around England and Wales, Scott *et al.,* (2011) further suggest that the wave energy flux should be considered as a control on beach state, particularly for the formation of different morphologies within intermediate groupings.

A switch in beach states can occur if sediment and hydrological conditions change, including varying sediment supply or the amount of energy delivered to the coastline (French *et al.*, 2015). During summer and winter months, or during periods where the wave energy is different from the modal conditions (e.g. storm conditions), such-termed ‘summer’ and ‘winter’ profiles can form. Reflective coastal types are often synonymous with ‘summer’ profiles where there is typically less energy along the shoreline and dissipate types with ‘winter’ or ‘storm’ profiles (Wright and Short, 1984). It is a well-accepted theory that whilst over the short-term or on a seasonal basis the coastal profile will exhibit a complex

dynamic behaviour, over the long term (from months to years), it will maintain a quasi-equilibrium profile (Wright and Short, 1984; Gao and Collins, 1998; Falqués and Calvete, 2005; Schwartz, 2006).

6.3 Numerical Modelling of Cross-Shore Coastal Profiles

The concept that the coastal profile will remain consistent over long time periods is the foundation of many mesoscale numerical models (see Chapter 3). One-line models are prevalent in mesoscale coastal studies and aim to represent complex processes in a relatively simplistic way, that is less computationally expensive than two- and three-dimensional modelling solutions (Hanson *et al.*, 2003). These one-line models are often designed to investigate gradients in longshore sediment transport, assuming that the cross-shore maintains an equilibrium form (e.g. CEM (Ashton *et al.*, 2001), GENESIS (Hanson and Kraus, 1989) and COVE (Hurst *et al.*, 2015)[1]). The modal or equilibrium coastal profile and its variability are defined by the environmental conditions, which are assumed to be relatively consistent over the long-term (Wright and Short, 1984).

6.3.1 Equilibrium Cross-Shore Coastal Profiles

The concept of an equilibrium coastal profile was first suggested in the late 19th century and postulates that the cross-shore geometry of sandy coastal environments will fluctuate around an average profile over long timescales (Gao and Collins, 1998; Schwartz, 2006). The Bruun Rule (Bruun, 1954, 1988) and Dean's Equilibrium Profile (Dean, 1991) are commonly used laws for determining the equilibrium beach profile for a given location. In particular, the Bruun Rule is

[1] Each of these models are reviewed in Chapter 3.

used to predict the geometric response of coastal environments to sea level change (see Chapter 7).

The specific shape of the equilibrium profile and its response time to formation depends upon driving environmental conditions, including sedimentology, hydrology, mean slope, storm response, and so forth (Dean, 1991; Pilkey *et al.*, 1993; Gao and Collins, 1998). However, there are four well-accepted characteristics of equilibrium beach profiles, as listed below (Dean, 1991):

1. They tend to be concave upwards,
2. The slope is determined by the sediment size; small grain sizes produce milder slopes and larger grain sizes, steeper slopes,
3. The slope is also determined by the wave steepness; steeper waves produce milder slopes and tend to form bar features,
4. The beach face is typically a planar surface.

According to the driving environmental conditions, Dean (1991) suggests five primary equilibrium profiles, as calculated by Equation 6.3, which can form relative to the initial cross-shore slope:

$$h = Ax^n$$

Equation 6.3

Where *h* is the profile depth (m), *A* is a profile scaling parameter, x is the cross-shore distance (m) and *n* is a profile shape parameter. As shown in Figure 6.3, the average slope of the shoreline decreases from Type 1 to 5. With decreasing slope angle the sediment transport regime across the beach switches from predominantly erosion to depositional, showing retreat and advance of the shoreline respectively. The wave climate also plays a significant role in the cross-shore shape of the shoreline with high energy waves forming gentler profiles and

lower-energy waves forming steeper profiles (Wright and Short, 1984; Dean, 1991).

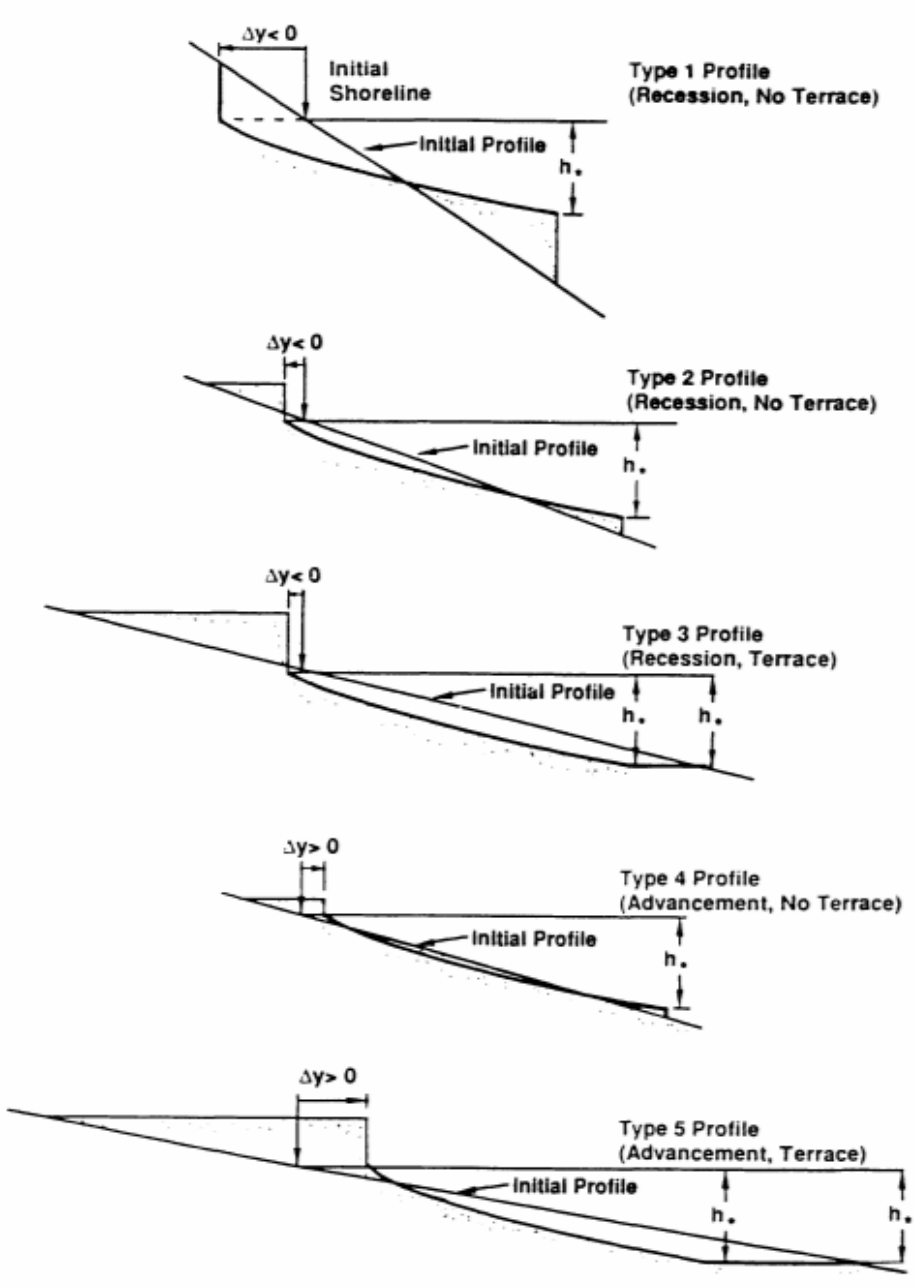

Figure 6.3 Five primary types of equilibrium coastal profile from an initial linear slope, with the slope angle decreasing from Type 1-5 (Dean, 1991).

The equilibrium profiles presented by Dean (1991) have been shown to map onto natural coastal systems (Karunarathna *et al.*, 2016). Using Equation 6.3, Karunarathna et al., (2016) computed average profile shapes that are comparable to four natural coastal systems (Figure 6.4). The authors further

classify each of the sites according to Wright and Short's (1984) beach states; Narrabeen Beach in New South Wales (Australia) and the Joetsu-Ogata Coast (Japan) exhibit intermediate profiles, Milford-on-Sea Beach in Christchurch Bay (UK) is reflective and Hasaki Coast (Japan) is classically dissipative (Karunarathna *et al.*, 2016).

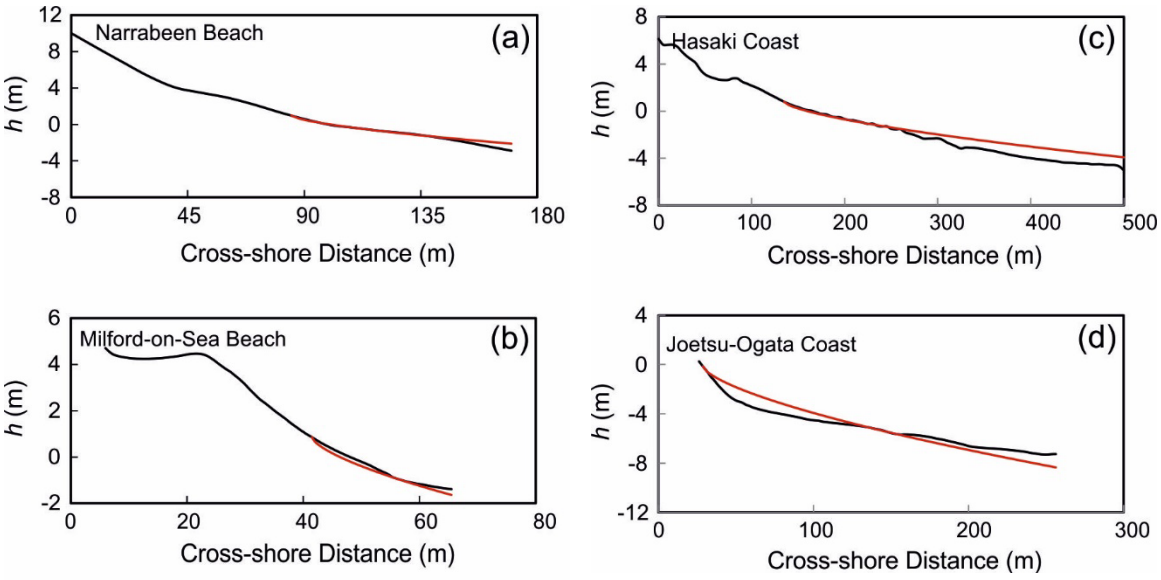

Figure 6.4 Measured mean beach profiles (black lines) and calculated Dean Equilibrium Profiles (red lines) for four coastal sites (Karunarathna *et al.*, 2016, p. 200).

An understanding of the cross-shore equilibrium coastal profile is an important concept in holistic studies of coastal behaviours (Dean, 1991). However, there are a number of assumptions made, which should be considered in its application (Pilkey *et al.*, 1993):

1. Sediment transport is primarily a function of the interaction of waves with a sandy shoreface,
2. Conservation of mass should be employed, where there is no net loss or gain or material,
3. A depth of closure must exist, beyond which there is negligible sediment transport,

4. The entire shoreface is composed of sandy material,
5. The underlying geology plays no role in the development and dynamics of the coastal profile.

Whilst the theory of equilibrium profiles is shown to be applicable to some natural coastal systems at large spatiotemporal scales, there is much criticism amongst the geoscience community about its degree of simplicity and therefore its accuracy in practice (Pilkey *et al.*, 1993; French *et al.*, 2015). Even on sand-rich coastlines the concept is oversimplified and fails to account for conditions and morphologies which can play a significant role in the shape and behaviour of the shoreface (e.g. underlying geology, sediment loss and gain, the existence of bars and troughs). Pilkey et al., (1993) use the sandy shoreline of the Gold Coast, Australia to illustrate this point. A lack of geological control allows the coastal systems to be highly dynamic, so no beach state can be attributed to the modal conditions. Whilst the wave climate plays a significant role in the formation of the cross-shore profile along the Gold Coast as suggested by the equilibrium theory, the influence of morphological features and so termed “memory effects” are not considered (Pilkey *et al.*, 1993)]. The less dynamic lower shoreface is primarily affected by high energy events and has the ability to store a memory of predeceasing morphologies, although some modifications are made by diffusional processes and currents (Pilkey *et al.*, 1993). These memories can present in the form of storm bars seaward of the highly dynamic shoaling zone in the upper shoreface, dictating the shape of the coast’s cross-shore profile (Pilkey *et al.*, 1993). The influence of the dynamic bathymetric profile on the evolution of coastal systems, particularly in terms of morphological memories, is of interest for further research in this field (Nicholls *et al.*, 2012; Van Den Berg, Falqués and Ribas, 2012).

6.3.2 Dynamic Cross-Shore Coastal Profiles

There is limited scope to assess the cross-shore dynamics of a coastal system with a one-line modelling approach, as used by many scientists to predict behaviours at the mesoscale of interest (Hanson *et al.*, 2003). Two and three-dimensional models prove too complex for such purposes since they are typically limited in terms of time and spatial scales due to the computational expense and process representation or parameterisation (Hanson *et al.*, 2003). Nearshore processes, in particular, are highly dynamic overt short-time periods which makes them difficult to analyse or upscale to the mesoscale (Aagaard *et al.*, 2004; French *et al.*, 2015). There is a particular interest in the behaviour of the bathymetry since it is understood that the nearshore profile can influence the evolution of the shoreline and coastal dynamics due to its influence on sediment transport and wave processes (Falqués and Calvete, 2005; Hequette and Aernouts, 2010; Ortiz and Ashton, 2016).

The studies of Serizawa *et al.,* (2007, 2009; 2012) were discussed previously in Chapter 5, as part of the literature review into the behaviour of the shoreline under differing wave climate conditions. The authors show how the angle of wave approach influences longshore sediment transport patterns and the formation of key shoreline features including cusps and spits (Serizawa *et al.*, 2009, 2012). Of interest to this chapter, their study also shows how the three-dimensional beach and nearshore profile respond to driving wave climate conditions. Using the BG Model, Serizawa *et al.,* (2007, 2009, 2012) compare their results to the physical wave tank experiments of Uda and Yamamoto (1991) which show similarities in the evolution of the bathymetric profiles, particularly for spit formations. Shown in Figure 6.5 are a comparison of Uda and Yamamoto's (1991) wave tank experiments after 30 minutes of simulation with the three-dimensional numerical

simulations of Serizawa *et al.,* (2009), after a simulated time period of approximately 80 days (4000 steps x 0.5hr time interval). Serizawa *et al.,* (2007, 2009, 2012) further compares results of their simulations to natural systems globally and found a likeness between the bathymetric profile of the Wada-misaki sand spit in Lake Kasumiga-ura (Japan) (Figure 6.6), results of the wave tank experiment and the numerical simulation. A further analogous comparison can be made between these results and the bathymetric profile of the Sand Engine (The Netherlands), as illustrated in Figure 6.7 (Luijendijk *et al.*, 2017).

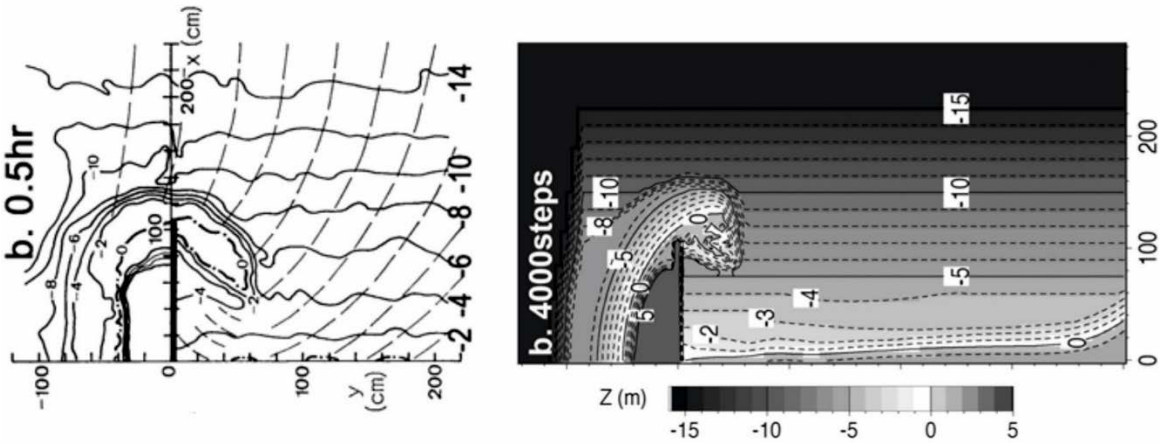

Figure 6.5 Topographies of sand spits generated in a wave tank (left, Serizawa et al.*, 2009, p. 1060) and using a numerical model (right, Serizawa* et al.*, 2009, p. 1063).*

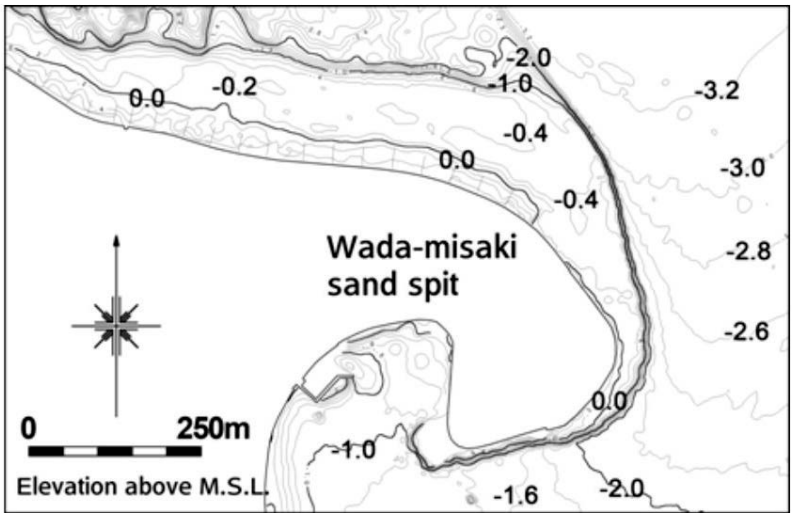

Figure 6.6 Bathymetry of the Wada-misaki sand spit in Lake Kasumiga-ura, Japan (Serizawa et al.*, 2009, p. 1064).*

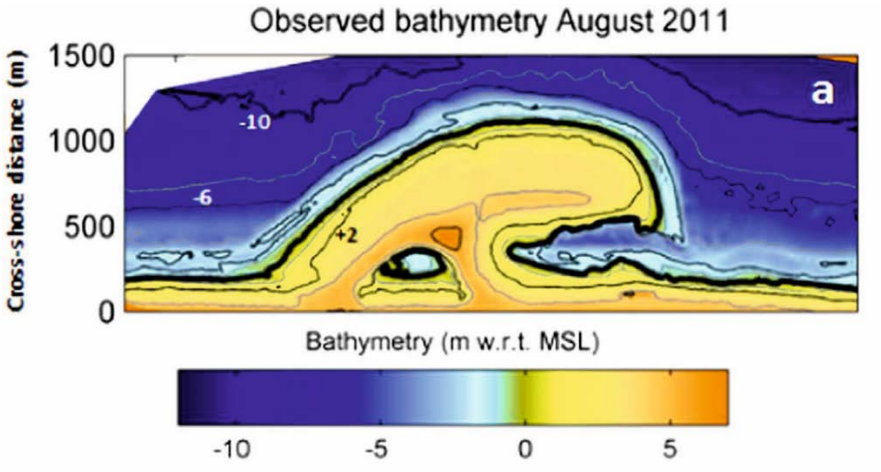

Figure 6.7 Topographic and bathymetric profile of the Sand Engine, The Netherlands (Luijendijk et al.*, 2017, p. 7)*

Similar characteristics are observed in the evolution of the bathymetry surrounding the sand spits in each of the studies described above, including the wave tank experiment (Uda and Yamamoto, 1991; Serizawa *et al.*, 2009), the numerical simulations (Serizawa *et al.*, 2007, 2009) and observations of the natural sand spit features (Serizawa *et al.*, 2009; Luijendijk *et al.*, 2017). The nearshore bathymetry at the tip or head of the spit is relatively steep as the feature extends offshore into deeper water. Offshore of the features, a shallower gradient or wave cut platform develops along the updrift edge and a similar nearshore platform also exists downdrift in the numerical experiment (Figure 6.5, right) and for the Sand Engine (Figure 6.7).

The volume stack shown in Figure 6.8 illustrates that the downdrift tip of the Sand Engine and the updrift shoreline are characterised by zones of deposition, whilst the central portion and downdrift region are subject to erosion (Luijendijk *et al.*, 2017). The data is recorded over a 160 day time period, showing relatively short term evolution of this feature, but it indicates the spatial pattern of evolution. According to the model data, the majority of morphological changes that occur across the landform are induced by wave processes (Luijendijk *et al.*, 2017).

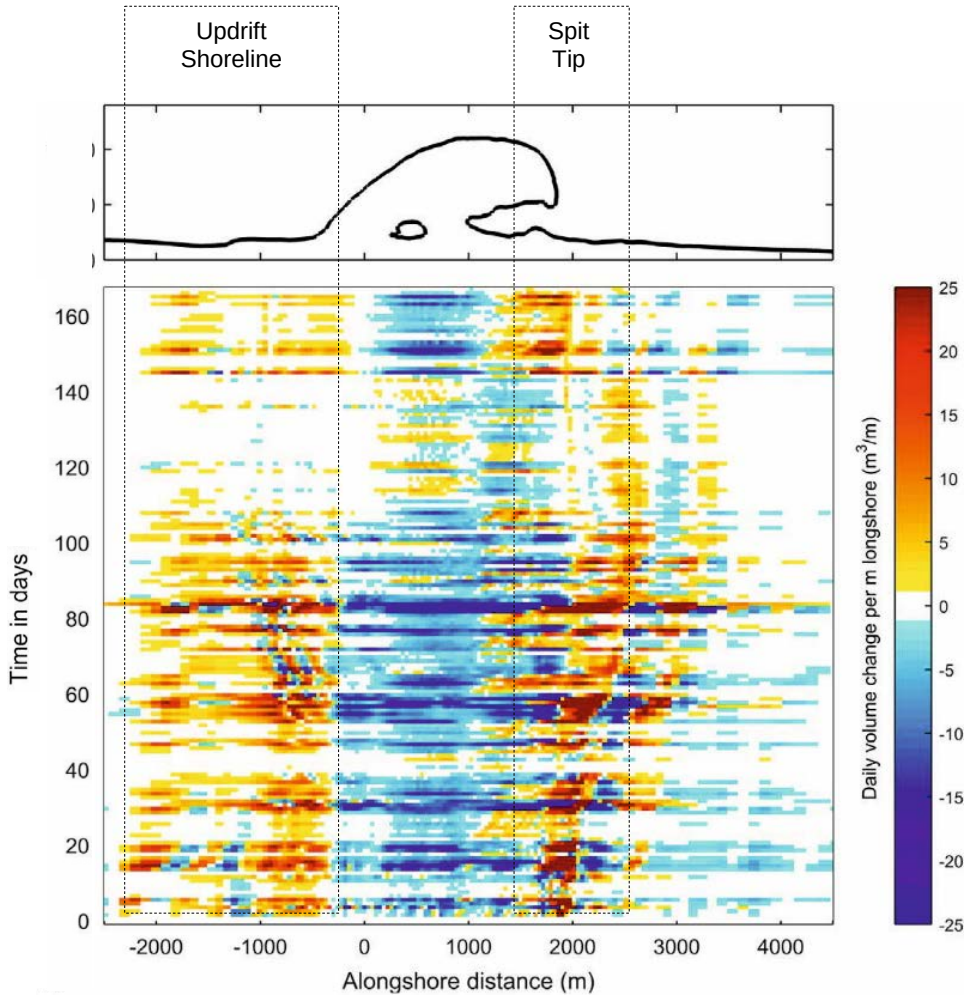

Figure 6.8 Volume stack of daily volume changes for the Sand Engine, The Netherlands (Luijendijk *et al.*, 2017, p. 11).

A similar bathymetric pattern was computed for cuspate features by Serizawa *et al.,* (2012), under a symmetrical wave climate over an approximate simulated time period of 2 years. As shown in Figure 6.9, the gradients of the contours around the tip of the cuspate headlands are relatively steep in the zone of deposition compared to the bathymetric profiles in the bay areas, particularly during the mature stages of growth (Figure 6.9d-f). Morphological memories, or remnants of previous cusps, are also observable in these results, although there is no discussion of these forms in the literature. Highlighted by the dashed box in Figure 6.9, at time step 1 x 10^4 (Figure 6.9c) a cusp is observed along the shoreline with relatively steep contours at its tip. As this foreland is gradually diffused throughout the simulation, the bathymetric contours retain their shape

whilst the foreland retreats and creates a shallow platform in the bay. At time step 4 x 10^4 (Figure 6.9f), no indication of the feature is found along the shoreline, but an impression remains in the bathymetry. A one-contour line model would not be capable of modelling this occurrence, although as mentioned, there is no discussion of it in the text (Serizawa *et al.*, 2012).

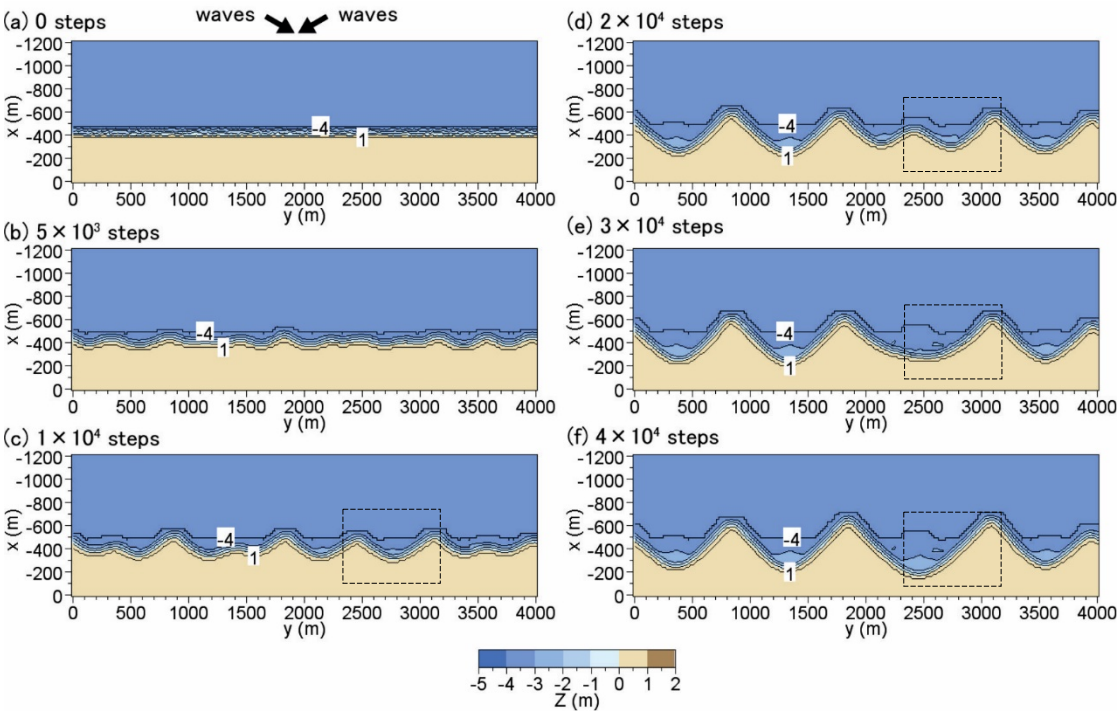

Figure 6.9 Development of cuspate features under a symmetrical wave climate, generated by the BG Model (Serizawa *et al.*, 2012).

The nearshore bathymetry also affects the transformation of waves as they approach the shoreline. Falqués and Calvete (2005) extended a one-line model to include the simulation of a curvilinear shoreline and a fixed bathymetric profile that mirrors the shape of the shoreline to the depth of closure (DoC), but which affects wave transformation processes. The authors support the theory of high angle wave instability discussed by Ashton *et al.,* (2001, 2006a, 2006b) (see Chapter 5), but suggest that instability also depends on a number of other factors. Instability is particularly enhanced by small waves with limited height and period since their transformation is more greatly affected by shallowing in the nearshore

compared to larger waves which tend to break close to the Depth of Closure[2] (Falqués and Calvete, 2005). This is supported in later research by Ashton *et al.,* (2006b, 2006a), who suggest that this mechanism could be responsible for the behaviour of nearshore bar welding during short-period storm waves in the winter season along Long Point Spit in Lake Eerie, Canada (Falqués and Calvete, 2005). Falqués and Calvete (2005) further suggest that the topographic profile of the nearshore influences instability, with shallower profiles owing to a more stable shoreline. A major caveat of this study is the use of a single wave height, angle and period which is unrealistic in unnatural systems. It also assumes that the bathymetry responds instantaneously to changes in the shape of the shoreline (Van Den Berg *et al.*, 2012). As shown in the previous discussion, the bathymetric contours do not always mirror the shoreline shape as assumed by Falqués and Calvete (2005).

Highlighting the importance of the bathymetric profile on the evolution of coastlines, particularly where high-angle wave instability is concerned, Van Den Berg *et al.,* (2011, 2012) developed the model of Falqués & Calvete (2005) into a quasi-two-dimensional form where sediment transport is driven in two horizontal directions. The authors support already discussed theories of high angle wave instability (e.g. Ashton *et al.*, 2001) and the greater instability induced by short period waves (Falqués and Calvete, 2005), but further attribute the role of the bathymetry. The bathymetric profile is shown to influence the characteristics of waves upon breaking which induces variations in alongshore sediment transport and the occurrence, or absence, or instabilities (van den Berg *et al.*, 2011, 2012). The study provides a more in-depth investigation into the quasi-two-dimensional

[2] The depth of closure is defined as the depth beyond which only negligible cross-shore sediment transport occurs (Ashton and Murray, 2006a).

evolution of these simulations but its application is limited by the temporal scale it is designed to simulate due to its complexity (days to decades) (van den Berg *et al.*, 2011, 2012).

It is clear from the discussion above that studies into the long-term behaviour of the cross-shore coastal profile is relatively limited at present. Short-term studies that draw conclusions about the bathymetric profile relative to the shoreline shape give an indication of how these two sections of the coastline are connected. However, feedbacks between the beach profile, shoreline and bathymetry at the mesoscale have received little attention in the literature to date. These feedbacks are an important next step in our scientific understanding of how coastal systems behave and evolve and further research into the longer-term dynamics of the bathymetric profile, in particular, is required.

6.3.2.1 Morphological Memories

Apparent from the previously reviewed literature in this chapter, morphological memories preserved particularly in the lower nearshore profile (Pilkey *et al.*, 1993) can store a record of past environmental conditions and influence the future behaviour of coastal environments (Masselink and Short, 1993; Nicholls *et al.*, 2012; Van Den Berg *et al.*, 2012; French *et al.*, 2015; Thomas *et al.*, 2016). Surmised from these studies, morphological memories are commonly defined as any remnants of depositional or erosion features along in the coastal zone that records characteristics of the historical morphology of the system. If, for instance, a perturbation exists in the bathymetry, perhaps due to the prior formation of a spit that has since migrated longshore or has been diffused by changes to the wave climate, its existence can influence how this section of coastline evolves. The minor perturbation could act as a sediment trap, or as a barrier blocking the longshore flow of material down the coast for instance.

With changing environmental conditions, particularly considering the predicted effects of climate change, the concept of morphological memories could be of great interest and importance to mesoscale coastal science. In reference to climate change, large-scale forces such as sea level rise and storm patterns are likely to change sediment pathways and in turn, coastal morphology (Thomas *et al.*, 2016). However, the response will not be instantaneous but will propagate through the system at varying rates (Thomas *et al.*, 2016). The rate of change is related to the rate of change in the offending environmental conditions, the type of change that occurs and the ability of the system to adjust. In some cases, the resilience of the system due to natural geological conditions or because of man-made interventions can also alter these responses.

Wright and Short (1984) suggest that memories are an important driver in the way geomorphological systems behave and evolve. The authors suggest that antecedent conditions and beach states influence the current behaviour and morphology of a coastline, but also advocate that modal conditions may still prevail over the long term (Wright and Short, 1984). It could be suggested that the coastal behaviours and planform shapes noted in the current timeframe could, in fact, be reflecting historical environmental conditions as opposed to current conditions. This theory is supported by the work of Thomas *et al.,* (2016), who demonstrate that antecedent environmental conditions can be important drivers of present behaviours. Thomas *et al.,* (2016) use the CEM in their study and focus on two primary shoreline shapes, spits and cuspate capes that form under two different types of wave climates with different levels of wave asymmetry, but both with significant high angle wave instability. The wave climates in the two environments are gradually adjusted over a 100 year time period to be more diffusive, by decreasing the proportion of high angle waves approaching the

coastline. The timescales of readjustment to the wave climate vary between these two initial morphologies and shoreline shapes. The capes adjust to the wave climate conditions within this 100 year period and eventually, the coastline is smoothed. The spit features have a slower response rate as some of the morphology of the landforms are preserved in the environment as the wave climate changes. Although this wave climate becomes diffusive, the shoreline does not smooth completely and retains sand wave features or undulations that are indicative of the previous spit morphology. Thomas *et al.,* (2016) note that the response time of the spit features from when the wave climate is adjusted to when the shoreline reaches a more diffusive morphology (even if not completely smooth) and is quasi-dynamic, is twice that of the time it took for the original features to form; some 750 simulated years. It is important to note however that Thomas *et al.,* (2016) focus exclusively on the response of the one-line shoreline to changing environmental conditions and do not consider changes across the beach or nearshore profile since this is not achievable in CEM.

Whilst the present behaviours of a coastal system can be influenced by antecedent conditions, French *et al.,* (2015) suggest that due to the vast changes in behaviour and sediment supply over the long-term (e.g. during the latter part of the Holocene), as well as the increasing influence of human activities, the past is not necessarily a proxy for the future in natural environments (French *et al.*, 2015). Further, interactions and feedbacks between features along a coastline can influence patterns of sediment flux and the evolution of features (French *et al.*, 2015). Therefore, it cannot be assumed that current conditions reflect either present or historical conditions. The shoreline is modified as a consequence of long- and short-term processes, making it difficult to decipher the environmental conditions responsible for its shape and form.

The literature suggests that the presence of residual morphologies has the potential to influence how coastal systems behave and evolve. Some authors suggest a more simplistic relationship whereby historic conditions can be calculated from present morphologies, whilst others suggest that it is a complex relationship and that it is difficult to decipher the relationship between current morphologies and the historic or present environmental conditions. In any case, there is an agreement that residuals can influence morphodynamics and this could have implications for the way we make predictions concerning the future evolution of these systems, particularly when considering the potential influence of climate change.

6.4 Methodology

The methodology used in this chapter mirrors the experimental set-up used in Chapter 5. The reader is therefore referred to Section 5.3 for a full explanation of CEM2D's initial set-up to compliment the brief overview given here.

Figure 6.10 (also Figure 5.9 in Chapter 5), shows the initial conditions used for the experiments in CEM2D. In Figure 6.11, the contours show the regular topographic and bathymetric profile of the coast at the start of each simulation.

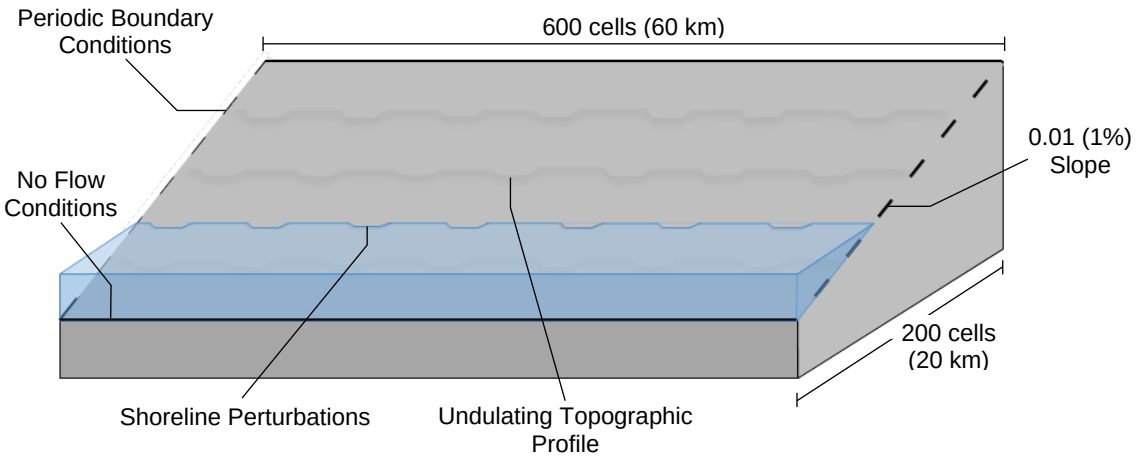

Figure 6.10 A schematic of CEM2D's model set-up and initial conditions used for simulations presented in this chapter.

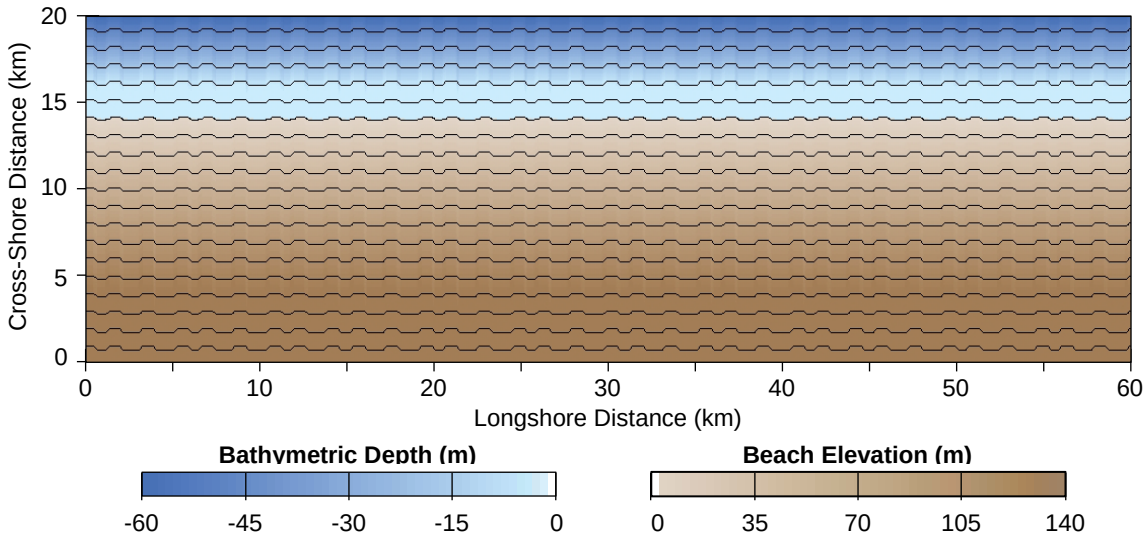

Figure 6.11 Initial Conditions of all simulations presented in this Chapter, showing bathymetric and topographic profile with 10 m contours.

A total of twenty-five simulations were run under different wave climate conditions using a four binned Probability Distribution Function (PDF) which defines the proportion of high angle waves (*U*) and the wave asymmetry (*A*). Table 6.1 (also Table 5.1 in Chapter 5) lists the wave climates used for each simulation. The wave period is kept consistent at 8 s, the wave height at 1.7 m and the water level at 0 m.

Table 6.1 Wave climate ensembles used to investigate the influence of wave climate conditions on coastal morphodynamics according to the wave climate asymmetry (A) and proportional highness of waves (U).

Run Number	Asymmetry (A)	High Angle (*U*)	Run Number	Asymmetry (A)	High Angle (*U*)
1	0.5	0.55	**14**	0.8	0.65
2	0.6	0.55	**15**	0.9	0.65
3	0.7	0.55	**16**	0.5	0.7
4	0.8	0.55	**17**	0.6	0.7
5	0.9	0.55	**18**	0.7	0.7
6	0.5	0.6	**19**	0.8	0.7
7	0.6	0.6	**20**	0.9	0.7
8	0.7	0.6	**21**	0.5	0.75
9	0.8	0.6	**22**	0.6	0.75
10	0.9	0.6	**23**	0.7	0.75
11	0.5	0.65	**24**	0.8	0.75
12	0.6	0.65	**25**	0.9	0.7
13	0.7	0.65			

6.5 The Evolution of the Coastal Profile

The ensemble plot in Figure 6.12 (see Appendix 5 for a larger print) shows final coastal morphologies, including topographic and bathymetric profiles for each of the twenty-five simulations. Along the x-axis, the proportional asymmetry of the wave climate increases from 50% to 90% (0.5 to 0.9) of waves approaching from the left of the domain and along the y-axis, the proportion of high angle waves approaching the shoreline increases from 55% to 75% (0.55 to 0.75). Contour lines and isobaths are drawn at 10 m intervals from the water line and the colour gradients remain consistent across all the images, for comparison across the matrix.

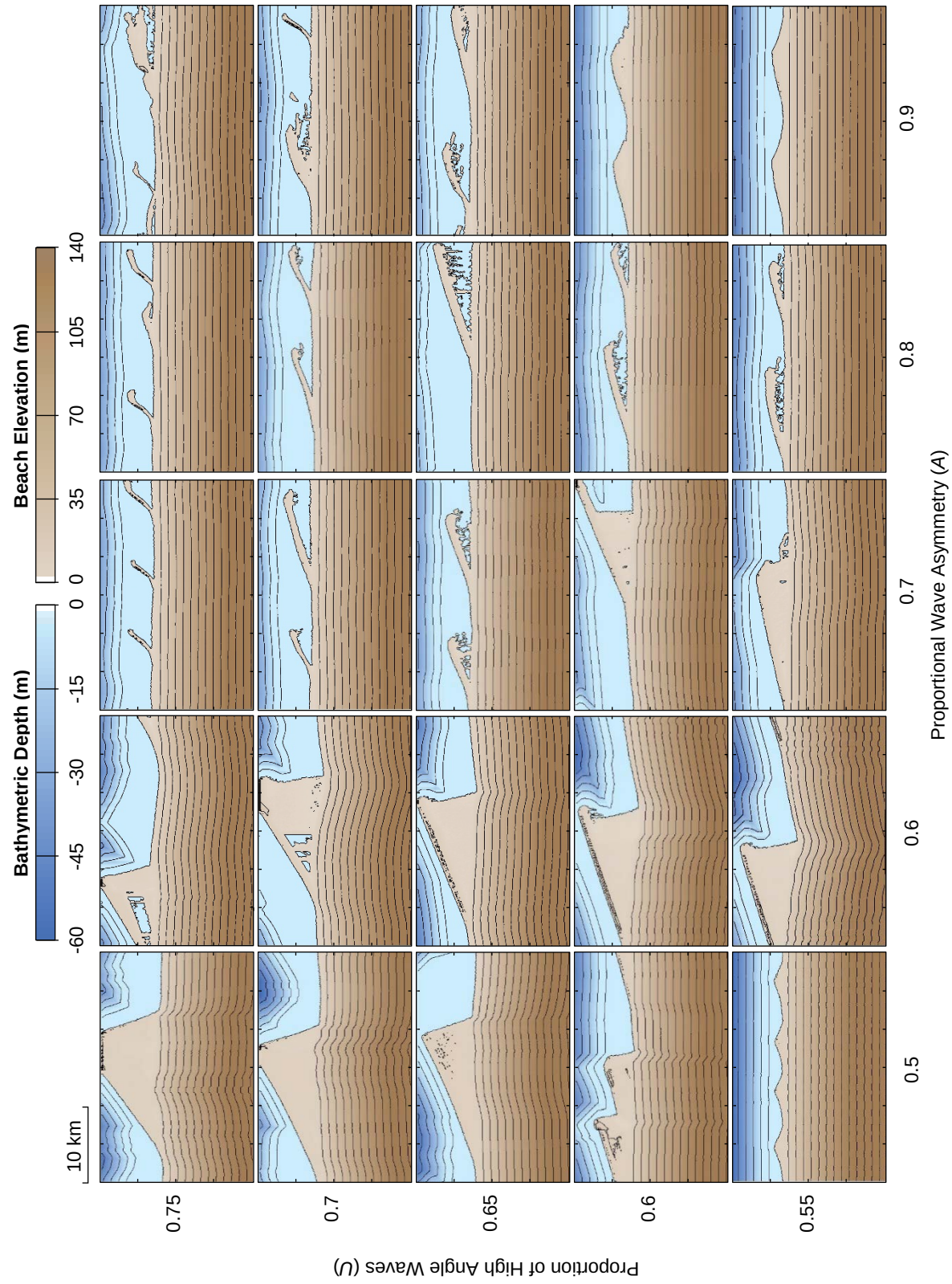

Figure 6.12 A matrix of results from CEM2D showing two-dimensional final shoreline morphologies as a function of the wave angle asymmetry (A) and proportion of high angle waves (U) approaching the coast relative to the local shoreline orientation. The outputs measure 20 km width and 30 km in length and are not inclusive of the periodic boundaries.

6.5.1 Coastal Contours

In several simulations, the shape of the shoreline is reflected in the beach and nearshore profile, with the latter showing more agreement to the shoreline shape (Figure 6.12). This is more prevalent in simulations with greater symmetry in the wave climate (A = 0.5-0.6) and is observed more clearly where there is a balance of high and low angle waves (U = 0.55). Where high angle waves dominant, the shoreline shape mirrors the planform shoreline but is also influenced by morphological remnants.

For example, as shown in Figure 6.13, where A = 0.6 and U = 0.6 the bathymetric contours curve along the updrift slope of the spit, around the tip and into the bays, mirroring the planform shoreline shape. The beach surface shows a relatively muted dynamism compared to the nearshore profile, curving seaward along the updrift edge of the spit and landward where the feature reconnects with the mainland downdrift.

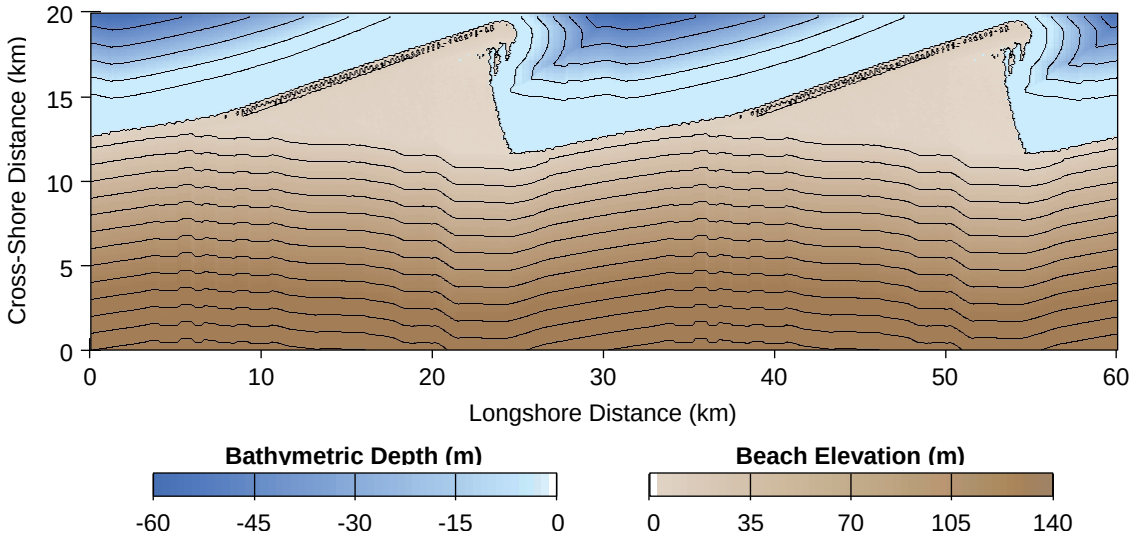

Figure 6.13 A contour plot showing results after 3,000 simulated years, where the wave climate is defined by A = 0.6 and U = 0.6. The plot shows 10 m contours across the coastal domain.

However, in most simulations, the beach and nearshore profiles do not wholly reflect the shape of the shoreline, most notably where there is greater wave

climate asymmetry (Figure 6.12). Where *A* = 0.8 and *U* = 0.7 (Figure 6.14) the beach profile is planar, and the bathymetry undulates but the contours do not align shore-parallel. Whilst the bathymetric profile is largely smoothed in this example, subtle remnant features are preserved further offshore. The previous locations of spits are preserved where the offshore contours are out of synchronisation with the planform of the current features. It should be noted that this simulation terminated prematurely after 1,090 simulated years, due to instability that occurred in the model.

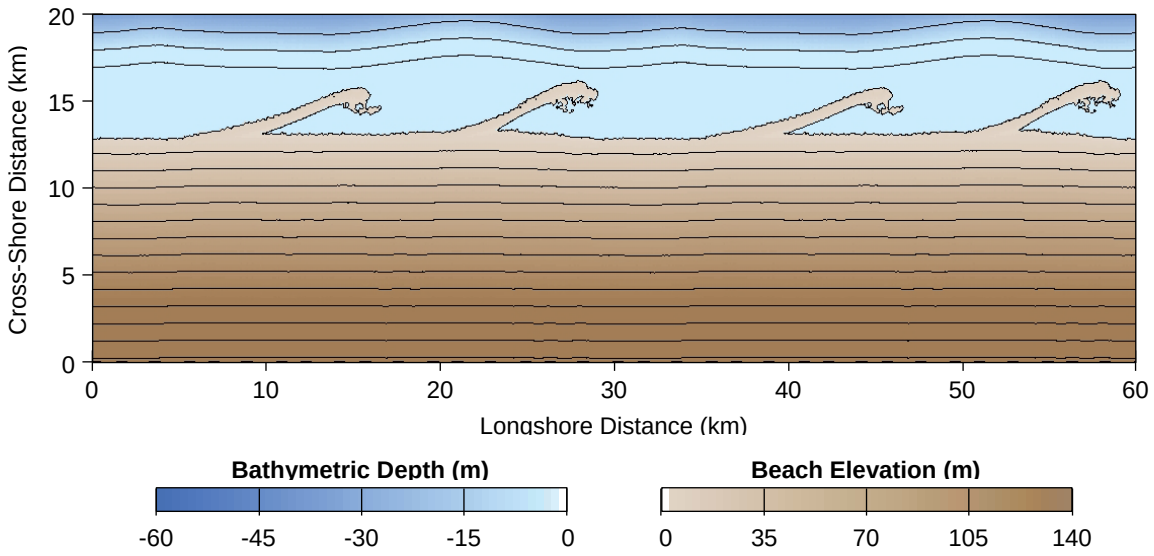

Figure 6.14 A contour plot showing results after 3,000 simulated years, where the wave climate is defined by A = 0.8 and U = 0.7. The plot shows 10 m contours across the coastal domain.

However, there are exceptions to this trend including where *A* = 0.5 and *U* = 0.55 (Figure 6.15). Although the wave climate is relatively symmetrical, the coastal profile is not shore-parallel. The contours across the entire profile are relatively planar compared with the undulating cuspate shoreline. There are some slight undulations across the beach profile, but these are remnants from the initial conditions, indicating that limited sediment transport has occurred across the beach surface.

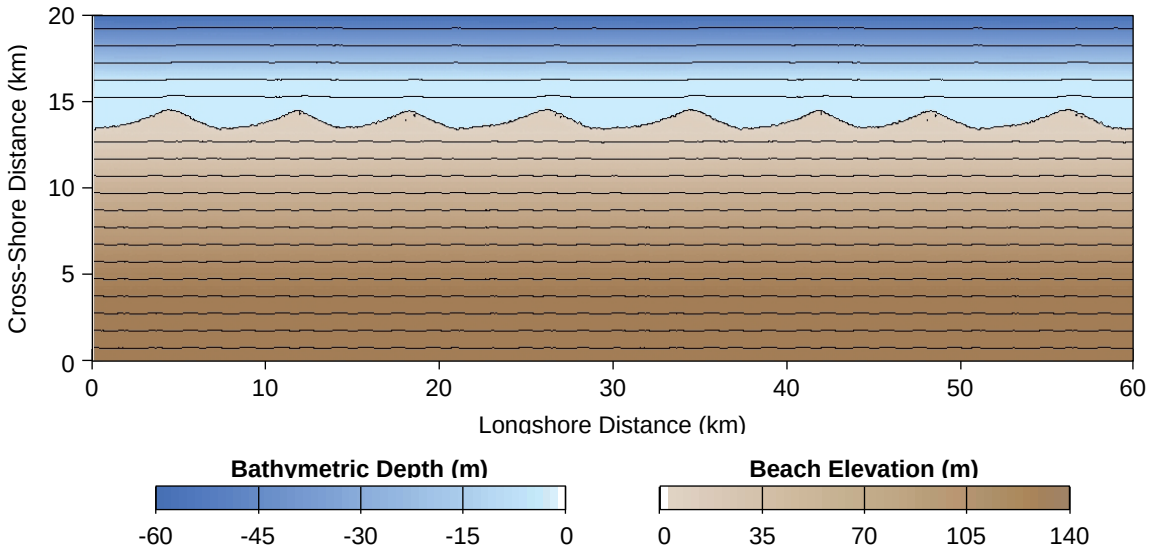

Figure 6.15 A contour plot showing results after 3,000 simulated years, where the wave climate is defined by A = 0.5 and U = 0.55. The plot shows 10 m contours across the coastal domain.

6.5.2 Cross-Shore Profiles

Figure 6.16 and Figure 6.17 show the cross-shore profile of each simulated coastline according to differing wave asymmetries (*A*) and proportions of high angle waves (*U*). Figure 6.16 examines the profiles in two-dimensions and Figure 6.17 in a three-dimensional form, to show individual transects in greater detail. Each transect was recorded across sections of the coastal profiles where the cross-shore position of the shoreline represents the average location for the given simulation and time step. This reduced the influence of depositional landforms on the profile's shape, which induces relatively short-term fluctuations in its form. The cross-shore profiles have been cropped to the most active zone surrounding the shoreline in Figure 6.16 and the position of the shoreline in each of the transects is marked by a white line in Figure 6.17.

.

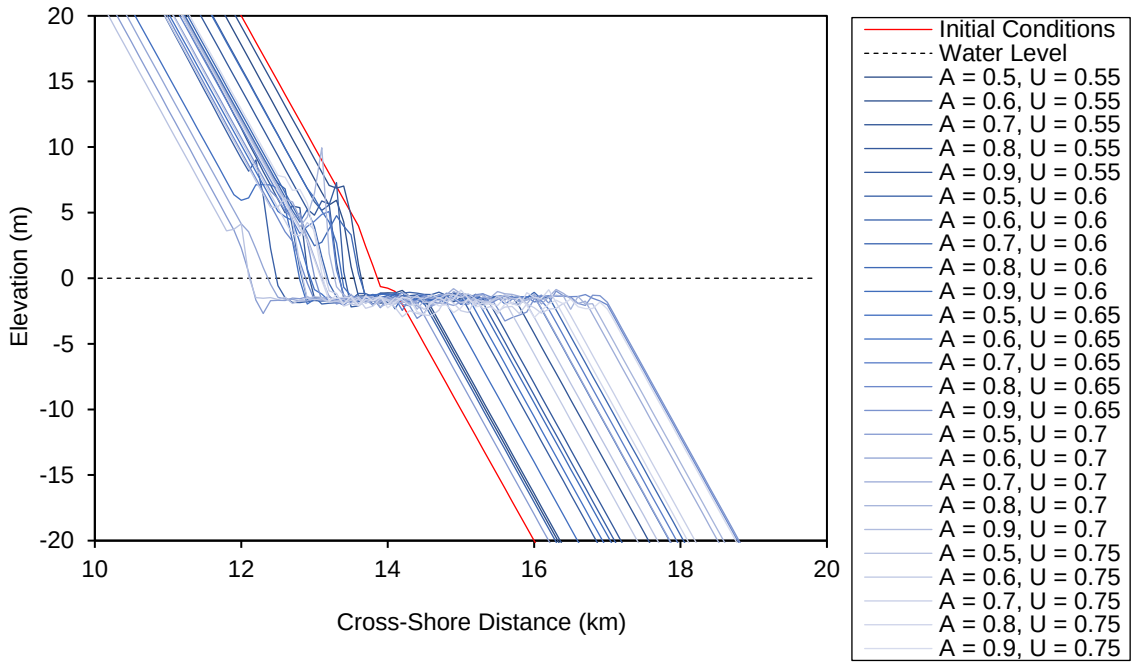

Figure 6.16 Cross-shore profiles taken for each of the twenty-five simulations shown in 2D.

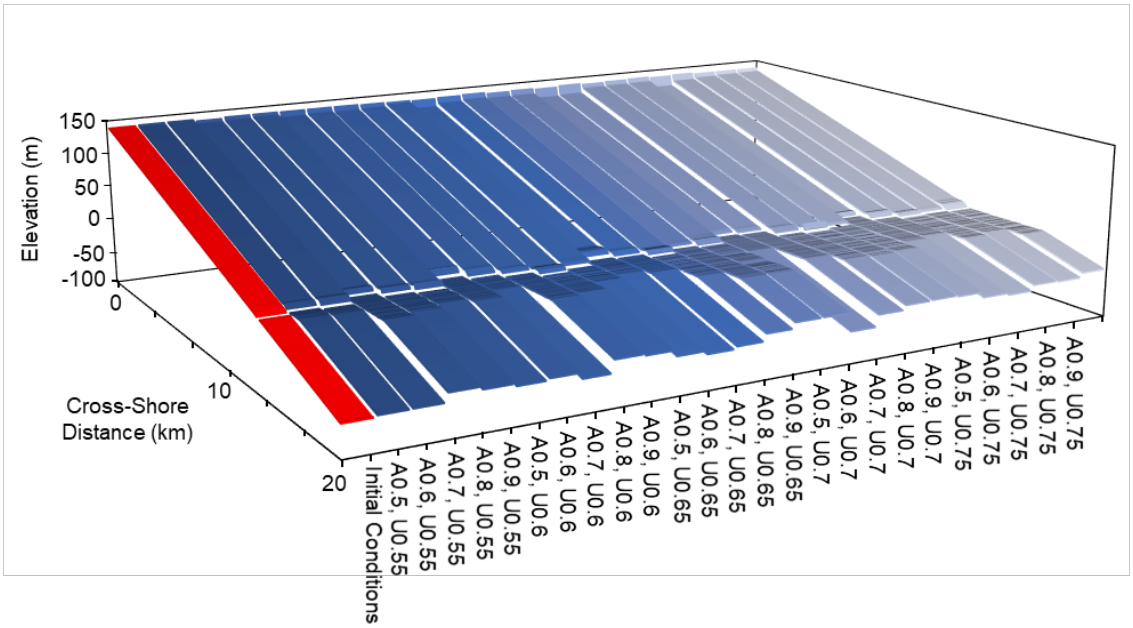

Figure 6.17 Cross-shore profiles taken for each of the twenty-five simulations shown as a 3D line graph, with water level shown as a white band across the transect.

6.5.2.1 Beach Profile

The two- and three-dimensional plots of the cross-shore coastal profiles (Figure 6.16 and Figure 6.17) show that the beach profiles retains an average slope of approximately 0.01 (1%), consistent with the initial conditions imposed in the model. Regardless of the wave climate conditions, minimal change is observed across the beach throughout the simulations. This agrees with the outputs in Figure 6.12, which show that each of the simulated shorelines exhibits a relatively planar surface at the end of the model runs.

6.5.2.2 Shoreline Position

The initial location of the shoreline is positioned 13.9 km from the edge of the domain (the upper beach). At the end of each simulation, the shoreline position ranges from 11.8 km to 13.6 km from the edge of the domain, with each of the coastlines, therefore, receding to some extent and representing the re-working of material from the shore to the nearshore as the morphologies develop (Figure 6.16 and Figure 6.17). It is observed that with increasing wave asymmetry, less recession occurs along the shoreline according to the average value of 'Y'. For instance, where the proportion of high angle waves is 60% (U = 0.6) and the wave climate is symmetrical (A = 0.5), the shoreline recedes by 1.5 km from the initial average shoreline position (Figure 6.18). Where the wave approach is highly asymmetric with 90% ($A = 0.9$) of waves approaching from the left of the domain, the shoreline recedes by 0.5 km. Each run with 60% high angle waves (U = 0.6) completed the 3,000 year simulation period, aside from where the wave asymmetry is 60% ($A = 0.6$) which completed 2,870 simulated years. There is therefore only a negligible influence of run duration on these results.

However, the theory that higher wave asymmetries lead to lower shoreline recession distances is challenged by few simulations where there is a dominance

of high angle waves (*U* = 65% - 75%) and is highly asymmetric (*A* > 70%) (Figure 6.18). For instance, where *U = 0.75* the recession distance decreases from 1.7 km from the initial average shoreline position to 0.7 km where *A = 0.5* to *A = 0.7* but increases to 0.9 km where *A = 0.9.* The run duration reduces for this set of simulations from 2950 to 720 simulated years with increasing wave asymmetry and this, therefore, could skew the results and relationships observed.

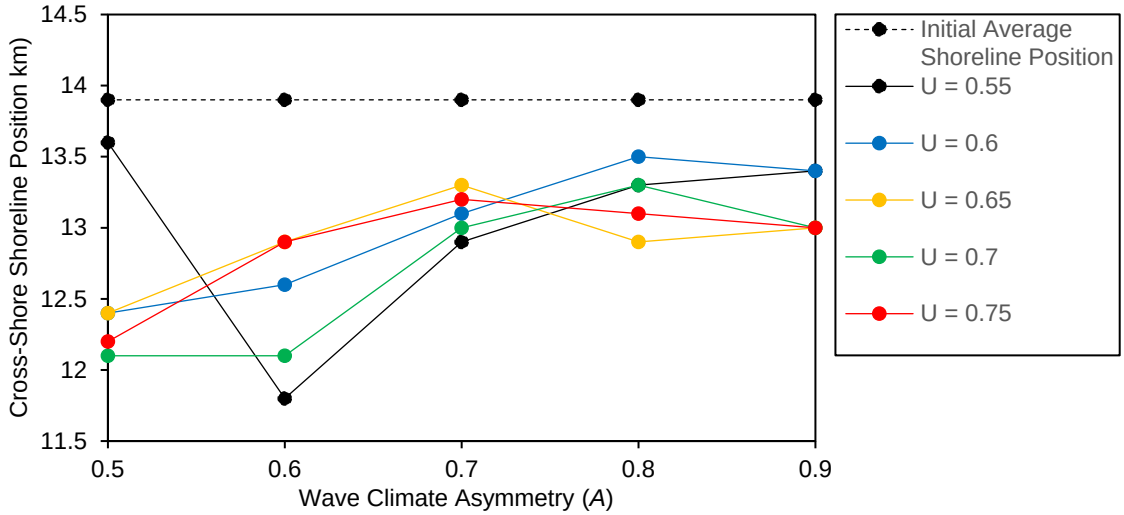

Figure 6.18 The average recession distance (m) attained throughout the duration of each twenty-five simulations, according to the initial average shoreline position. The legend denotes the proportion of high angle waves (U) for each simulation.

6.5.2.3 Nearshore Profile

Across the upper nearshore profile, a shallow shelf develops with an undulating bathymetry. The width of the shelf varies across the results (Figure 6.19), from 1 km to 2.7 km with the data suggesting that the shelf width decreases with increasing wave asymmetry. Plotting these results against the shoreline position (Figure 6.19) shows that the recession distance and shelf width have a relationship; the greater the recession distance, the larger the shelf width. The plot also shows however that the shelf width is always larger than the recession distance in the simulations, demonstrating that they form through both erosional and accretional processes.

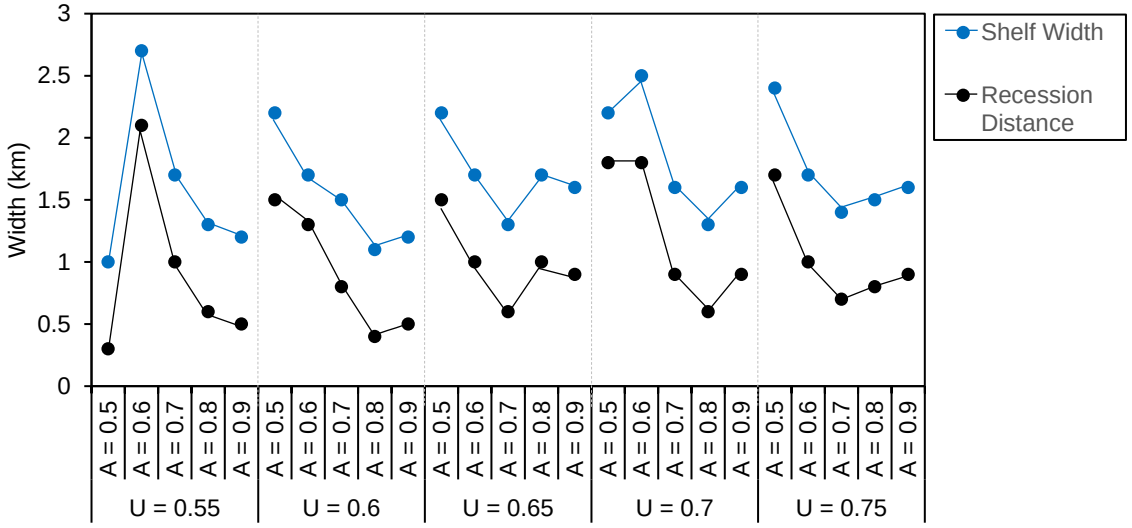

Figure 6.19 A plot showing the relationship between the position of the shoreline and the width of the nearshore shelf.

Beyond the nearshore shelf, the bathymetry slopes increasingly towards an average slope angle of 0.01 (1%), as imposed by the initial conditions. The position of the break of slope marks the offshore boundary of the nearshore shelf discussed previously. The cross-shore location of this point is a function of the change in the position of the shoreline and the width of the shelf, both of which are influenced by the asymmetry of the wave climate.

6.1.1 Dynamic Regions of the Coastal Profile

Whilst the beach and nearshore profile both respond to the wave climate conditions with changes in their morphology occurring according to sediment transport patterns (Figure 6.16 and Figure 6.17), volume stacks can be used to depict the most dynamic regions of the coastal profile. These stacks show the change in sediment volume of each cell of the cross-section (corresponding to the cross-sections used in Figure 6.16 and Figure 6.17). Transects are recorded every 30 simulated years, to provide 100 datasets for each 3,000 year simulation. Select volume stacks are discussed here which represent the spread of results, but stacks for each of the simulations are provided in Appendix 6.

The volume stack in Figure 6.20 shows the change in volume of a cross-section at x = 30 km (from the left of the domain). The figure is cropped to a relatively thin section of the cross-shore profile, showing the most active area (smaller than -5 km^3 or greater than 5 km^3 every 30 years). The results demonstrate that the most active area of the shoreline is a 2 km section which spans the shoreline but primarily constitutes the upper nearshore. There are alternating periods of erosion and deposition across this transect averaging between -130 km^3 to 130 km^3 per 30 simulated years in individual cells.

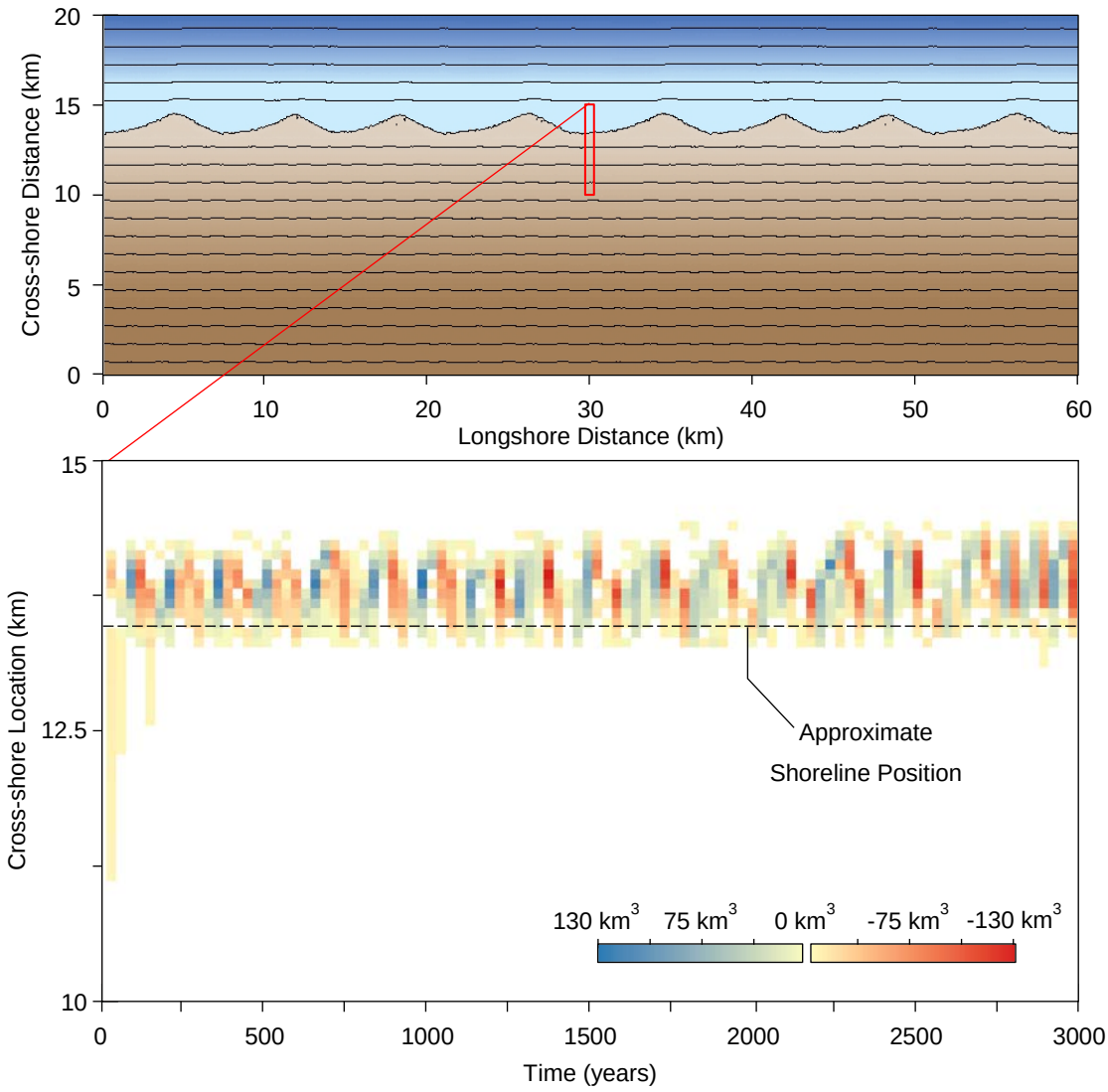

Figure 6.20 Volume stack of change in sediment volume (km^3) cross-shore over 3,000 simulated years, where A = 0.5, U = 0.5. The DEM shows the final shoreline morphology after 3,000 years where the location of the transect is depicted by the red line and the segment with the greatest morphodynamics by the red box.

The volume stack in Figure 6.21 shows results where A = 0.8 and U = 0.7, which after 1,090 simulated years generates spits along the shoreline. The simulation terminates prematurely when the model can no longer find the position of the shoreline; this is a model limitation that is discussed further in Chapter 8. Again, the transect has been cropped to show the most dynamic section of the coastline, which is located across the lower beach and nearshore profile, with the latter showing the greatest dynamism. In the nearshore between 10 km to 17.5 km from the edge of the domain along the upper beach (Figure 6.21), there are alternating periods of deposition up to 130 km^3 per 30 simulated years and erosion down to -130 km^3. The zone further offshore typically experiences net deposition of between 5 km^3 to 50 km^3 per 30 simulated years and the lower beach experiences erosion of between -5 km^3 to -50 km^3.

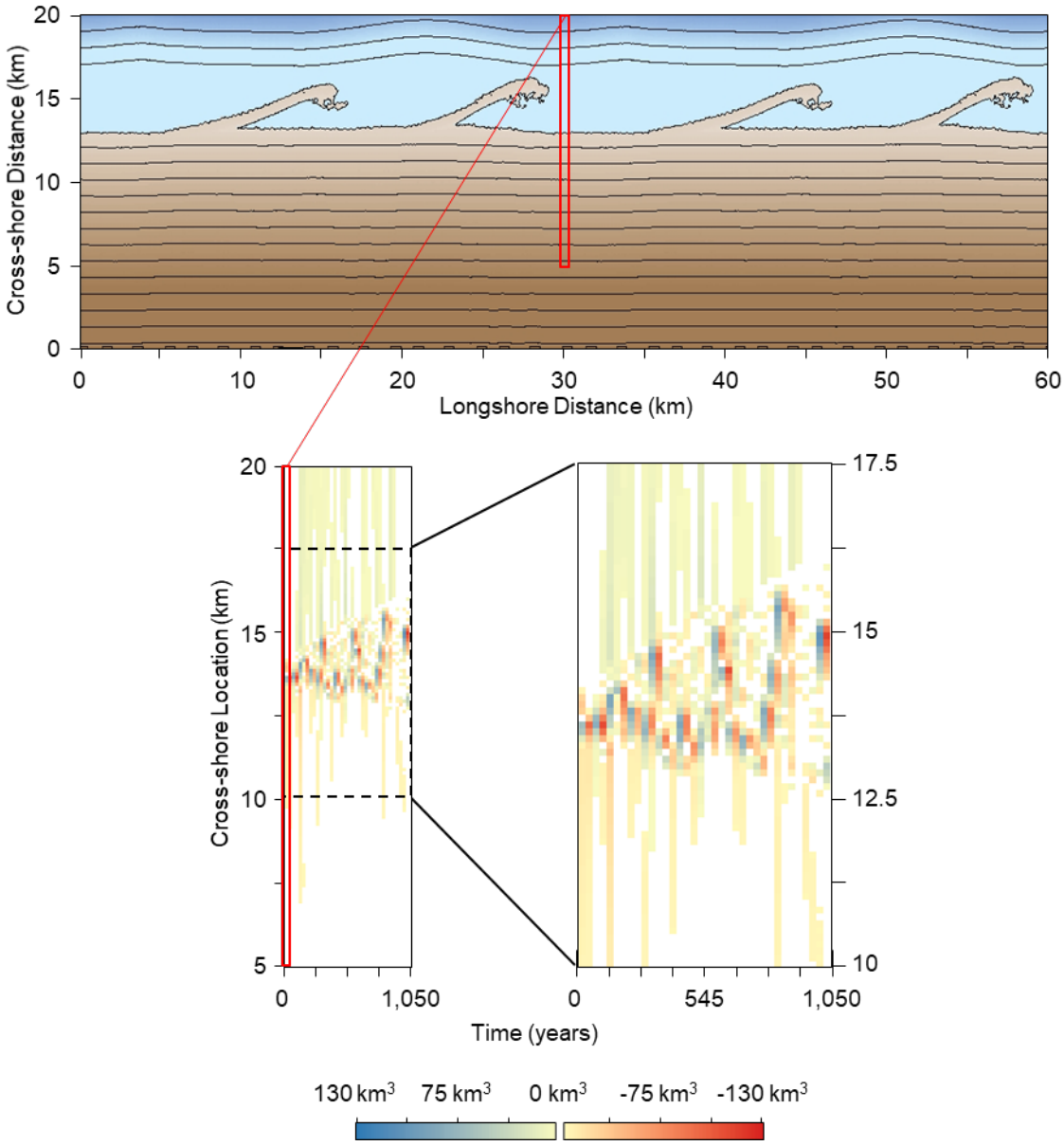

Figure 6.21 Volume stack of change in sediment volume (km^3) cross-shore over 1,050 simulated years, where A = 0.8, U = 0.7. The DEM shows the final shoreline morphology after 1,050 years.

The maximum values of erosion and deposition occur in the nearshore profile (Figure 6.21), but the defined location fluctuates cross-shore due to the influence of migrating spits along the shoreline. Shown in Figure 6.22 are coastal morphologies generated under wave climate conditions where A = 0.8 and U = 0.7 after (a) 450 and (b) 600 simulated years. Below the volume stack, originally given in Figure 6.21, with the location of the transect depicted by the blue and black line. Also shown is the position of the shoreline at each time step, marked by red dashed lines on the morphology plots and the volume stack.

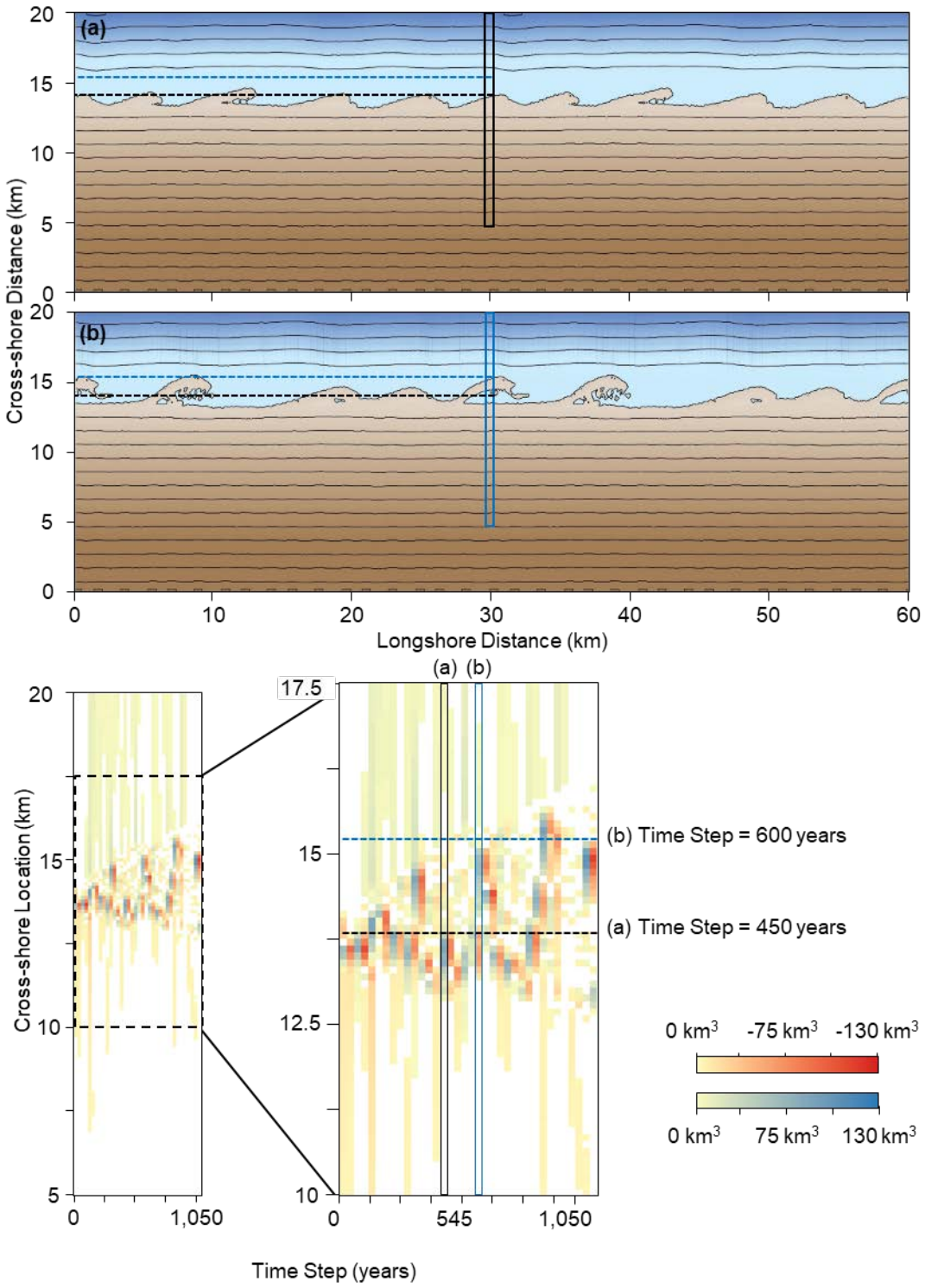

Figure 6.22 A plot showing the coastal morphology after 450 iterations (a) and after 600 (b) iterations. The dashed lines mark the cross-shore extent of the beach at the transect location, which is also marked on the volume stack.

The spit formed along the coastline after 600 simulated years (Figure 6.22b) extends the shoreline approximately 1 km offshore from its location after 450 simulated years (Figure 6.22a). This is reflected in the volume stack which shows the zone deposition further offshore for plot (b). Also observable in the data for

plot (b) are two distinct regions of relative volume change, with erosion in the bay behind the spit and deposition along the spit's neck, compared to the previous 30 years (Figure 6.22).

6.6 The Influence of Depositional Landforms on the Evolution of the Coastal Profile

An overview of results showing the evolution of the cross-shore coastal profile from initial conditions has been presented in Section 6.5. In this section, a review of the morphodynamic evolution of the coastal profile is considered in more detail, under four wave climate conditions. The wave climate conditions and the resulting planform shoreline morphologies for each of these runs are listed in Table 6.2. The time steps evaluated correspond with when significant morphological changes occur in the simulations, for instance, a change from one state to another and correlate with those used in Chapter 5.

Table 6.2 A table listing the wave climate conditions and resulting shoreline morphologies for the four simulations presented in this section.

	Wave Climate Asymmetry (*A*)	**Proportion of High Angle Waves (*U*)**	**Resulting Planform Shoreline Morphology**
1	0.5	0.55	Cusps
2	0.6	0.6	Alongshore Sand Waves
3	0.7	0.65	Reconnecting Spits
4	0.8	0.7	Flying Spits

As highlighted in Figure 6.23, a relatively small section of the coast is focused on in more detail in this Section, to show the morphodynamics of the systems more clearly. The initial conditions (Figure 6.23) for each of the simulations where T

(time) = 0, is consistent across all runs. The shoreline has regular planform undulations and this profile is mirrored in the topographic and bathymetric contours. In Figure 6.23 the contours are regularly spaced, shown at 10 m (black) and 2 m (grey) intervals.

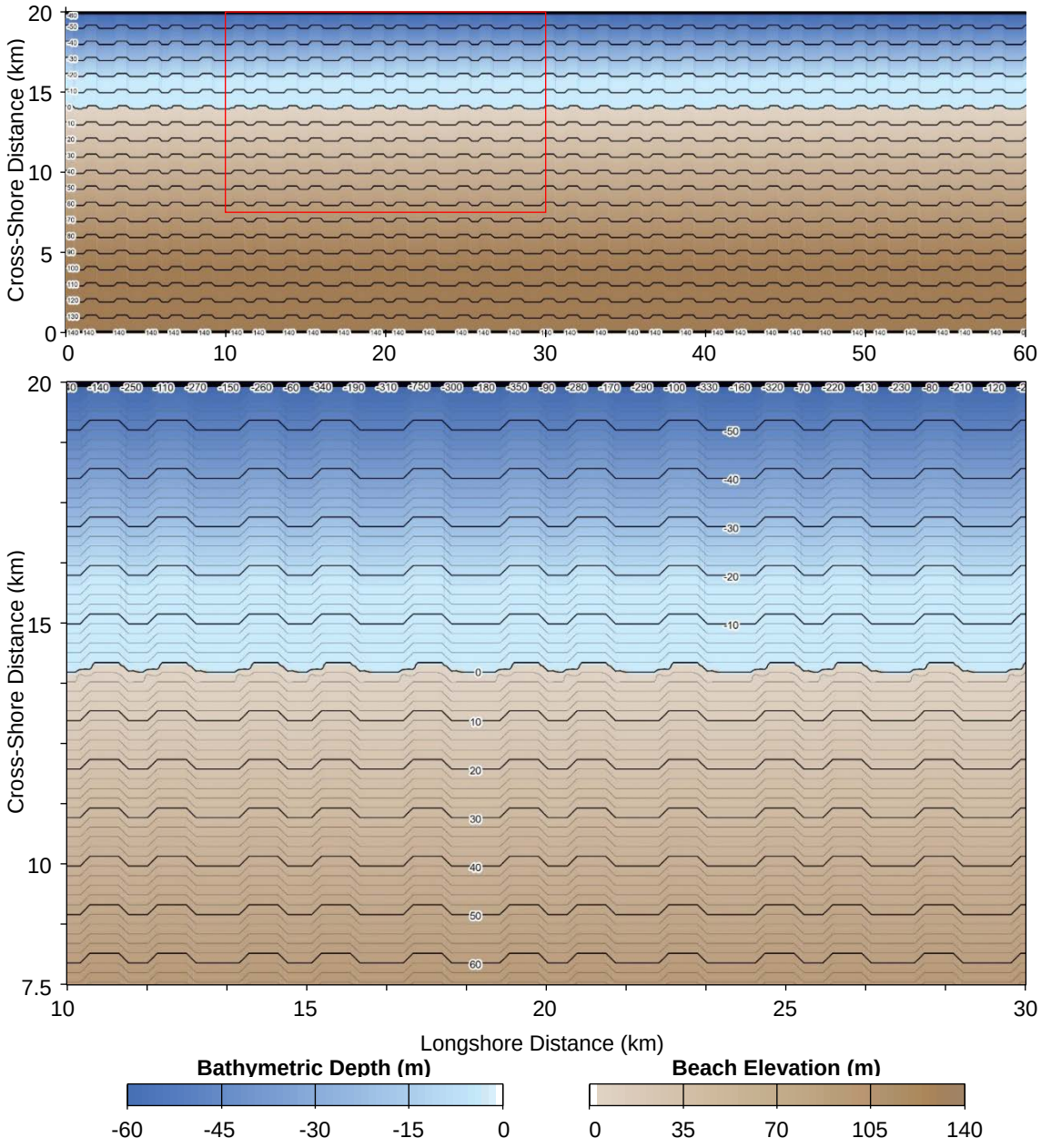

Figure 6.23 Topographic map showing the initial conditions of the coastal profile. The red square in the top image delimits the location of the study area, shown in the bottom image.

6.6.1 Cuspate Features

Where the wave climate is symmetrical (A = 0.5) and there is only a 5% dominance of high angle waves (U = 0.5), cuspate features develop along the

simulated shoreline as explored previously in Chapter 5. Figure 6.24 shows how the coastal profile evolves throughout the 3,000 year simulation according to these driving wave conditions.

During the first 10 simulated years, minimal changes occur across the coastal profile (Figure 6.24a). The beach and the nearshore maintain a form consistent with the initial conditions, with the majority of morphodynamics occurring near the shoreline between 8 m and -4 m elevation. The initial perturbations along the shoreline where T = 0 (Figure 6.23) smooth and form larger but fewer undulations. A topographic peak forms on the emergent cuspate feature, offset to the left of its centre denoting some directional dominance in the wave climate from the left of the domain. Since the wave climate is symmetrical this dominance is concomitant to the directional bias in CEM2D which has been noted previously and discussed further in Chapter 8. The bathymetry between 0 m and -4 m elevation does not align shore-parallel as the coastline evolves, but is marginally disturbed from the initial conditions.

The shoreline continues to evolve as the cuspate landforms develop and after 880 simulated years (Figure 6.24b) extensive smoothing occurs across the entire coastal profile. The topography of the beach retains remnants of the initial undulations across the profile, but which increasingly smooth towards the shoreline. The nearshore exhibits a smooth profile with regularly spaced contours sloping approximately 0.01 (1%) offshore, consistent with the initial imposed slope angle in the model environment. Neither the beach nor nearshore develops shore-parallel contours. Across the section of coastline where the cuspate features are situated, the topographic peaks observed after 10 simulated years (Figure 6.24a) increase in spatial extent and remain offset to the left of the landform’s centre point. The shoreline slopes steeply towards the water on the

left of the landform and more gently on the right side of the cusp. The -2 m contour is located approximately 0.2 km offshore of the cusp tips, maintaining the average 1% slope and approximately 0.7 km from the shoreline within the bay, creating a wide nearshore shelf or platform.

After 1,940 simulated years (Figure 6.24c), further smoothing occurs across the beach surface. As the cuspate headlands develop and extend further offshore, the position of the shoreline and the nearshore shelf is gradually relocated approximately 0.65 km seaward of its position at 880 simulated years (Figure 6.24b). The size of the nearshore shelf to -2 m depth and the distance from the shoreline to this depth contour remains consistent with that found at 880 simulated years. Morphodynamic changes elsewhere across the domain are negligible.

At the end of the simulation after a 3,000 year time period, the tip of the cuspate headlands are more pointed than observed throughout their development (Figure 6.24d). This peak extends further offshore and disturbs the planar contours that were observed previously between 880 and 1,940 years. The contours are shore-parallel around the distal point of the cusp, gradually becoming planar approximately 2.2 km from the shoreline. The morphology of the cusp retains a peaked topography offset to the left of the central point but is of a lower amplitude to that observed previously, having been subject to diffusional processes. The landform exhibits steep slopes from this point towards the water and a more gently sloping morphology landward. Further smoothing is observed across the beach surface compared to its form after 1,940 simulated years, although it is relatively negligible particularly considering the time step.

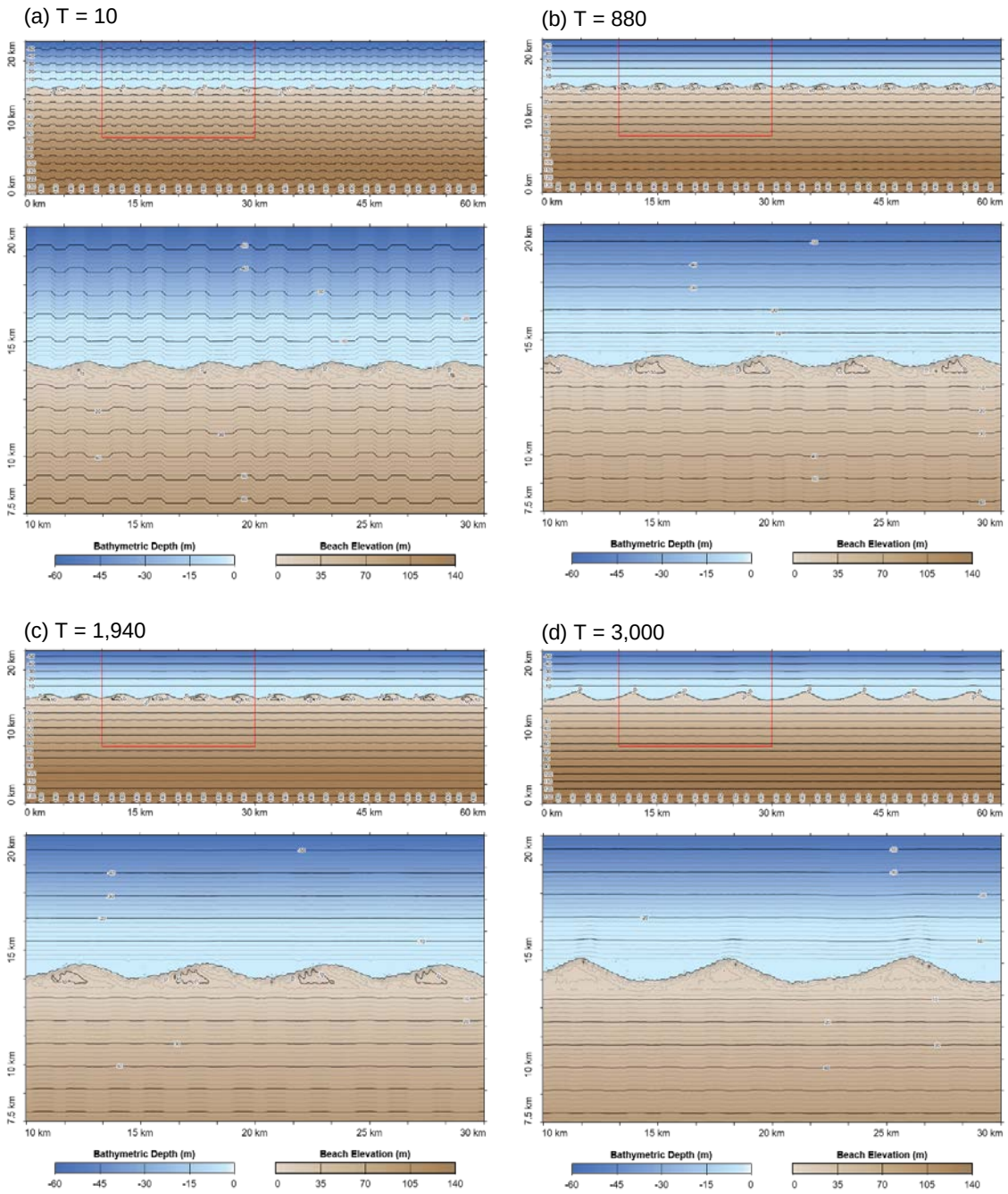

Figure 6.24 Two-dimensional temporal evolution of the coastal profile under wave climate conditions where A = 0.5, U = 0.55 which generates cuspate features along the shoreline.

6.6.2 Alongshore Sand Waves

Where the wave climate is driven by a slight asymmetry (A = 0.6) and there is a 10% dominance of high angle waves (U = 0.6), alongshore sand waves develop along the simulated shoreline as explored previously in Chapter 5. Figure 6.25a-

d and Figure 6.26e-g show how the coastal profile evolves throughout the 3,000 year simulation according to these driving wave conditions.

During the initial 30 simulated years, the cuspate features develop along the shoreline (Figure 6.25a) from the initial perturbations (Figure 6.23). Around the tip of the cuspate landforms, the contours across the nearshore align shore-parallel but maintain an average slope of 0.01 (1%), imposed from the initial conditions. A shallow bay is formed to the -2 m depth contour measuring approximately 0.6 km. The sand wave exhibits a gently undulating topography, with steeper slopes towards the water along the updrift flank, on the left of the landform. Smoothing of the beach surface occurs cross-shore between the bays. The remainder of the beach and nearshore profile are largely undisturbed and retain an average cross-shore slope of 1% and the longshore undulations, imposed from the initial conditions.

After 170 simulated years, the sand waves merge and develop further in size (Figure 6.25b). The profile of the nearshore aligns shore-parallel around the headland of the sand waves, creating a marginally steeper slope along the updrift edge. A shallow shelf is retained in the bay, that extends further offshore in the central portion than at the edge of the bay. The planform shape of the contours in this location align with those at 30 simulated years, that were formed by the existence of a smaller sand wave feature that has since diffused or merged to create a larger landform. This is suggestive that remnant of the morphology of this predeceasing landform has been retained in the bathymetric profile. The beach profile does not exhibit a similar memory mechanism but is smoothed in accordance with the profile of the existing sand waves and the shape of the shoreline. The sand wave itself exhibits a similar morphology to that observed at

30 simulated years, with a gently undulating morphology and steeper slopes seaward.

The concept of a morphological memory is further observed at 820, 1,320 and 1,800 simulated years (Figure 6.25c-d and Figure 6.26e). Whilst the profile of the beach and nearshore translate downdrift towards the right of the domain and the contours elongate marginally with this migration, the coastal profile retains a consistent morphological form. However, there is a lag time between the evolution of the beach and nearshore profile with the movement of the sand wave features. Hence, the contours, whilst replicating the shape of the shoreline, are not shore-parallel.

From 1,800 to 3,000 simulated years (Figure 6.26e-g) the sand wave shows minimal migration longshore and the contours align shore-parallel with the feature. The contours are steepest in the nearshore at the tip of the sand wave, which shows some premature development of a spit hook. A shallow nearshore shelf forms in the sheltered region downdrift of the sand wave, in the bay of the developing spit hook. At the end of the simulation, a shallower shelf also forms along the updrift edge of the feature. This, however, is the steepest part of the sand wave, which exhibits a more gradually sloping leeward side, towards the water within the bay. The morphology of the beach surface is influenced by the presence of the sand wave, with the contours receding landward where the feature reconnects with the shoreline and seaward where the shoreline begins to accrete offshore. It is of note that in Figure 6.26 the landforms increase is size towards the end of the simulation, encompassing a large proportion of the model domain. This could constrain the behaviour of the system and be influencing the evolution of the landform during these final timesteps.

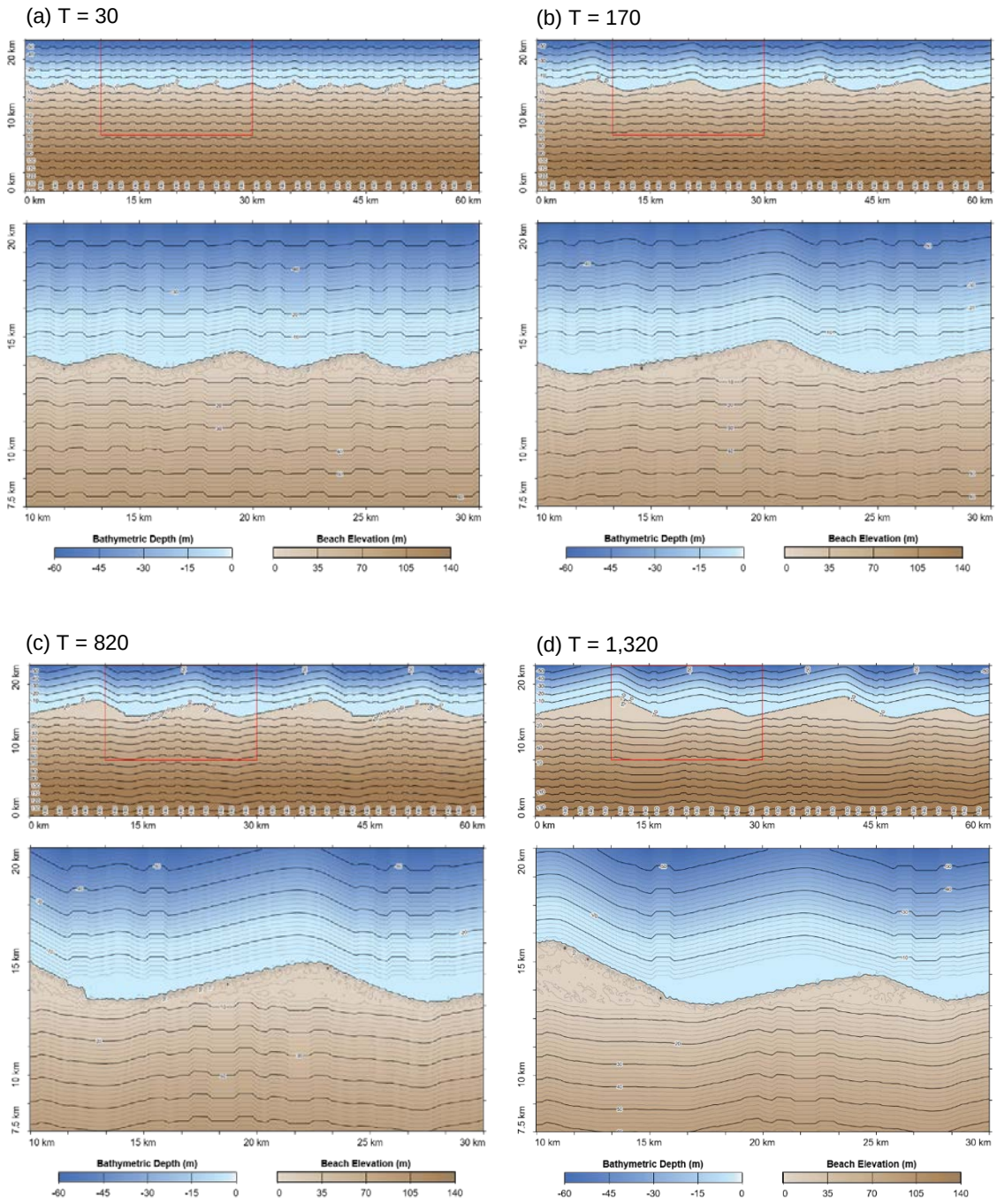

Figure 6.25 Two-dimensional temporal evolution of the coastal profile under wave climate conditions where A = 0.6, U = 0.6 which generate sand waves features along the shoreline (Images a-d).

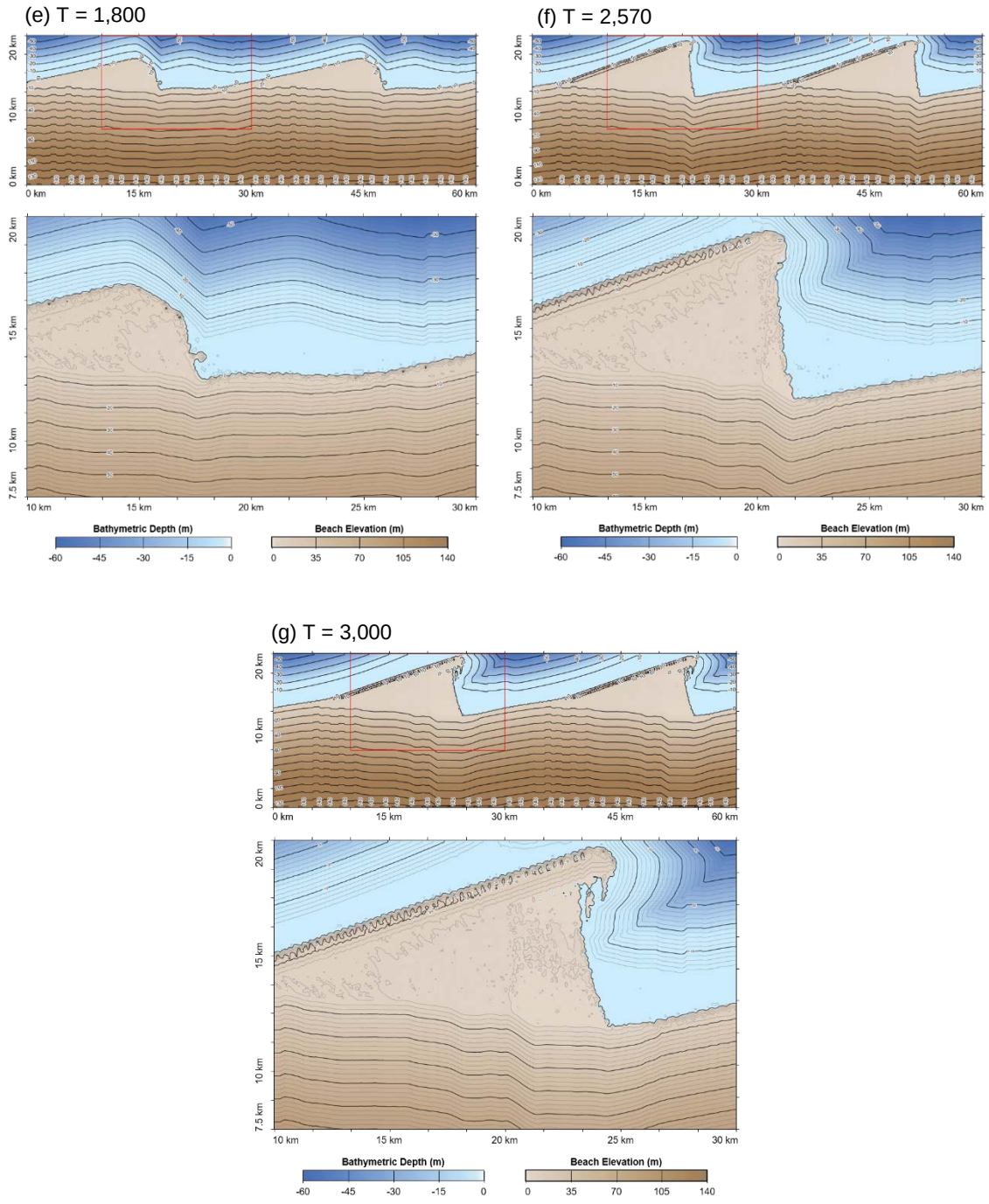

Figure 6.26 Two-dimensional temporal evolution of the coastal profile under wave climate conditions where A = 0.6, U = 0.6 which generate sand waves features along the shoreline (Images e-g).

6.6.3 Reconnecting Spits

Where the wave climate is dominated by waves approaching from the left of the domain (A = 0.7) and by high angle waves (U = 0.65), reconnecting spits develop along the simulated shoreline as explored previously in Chapter 5. Figure 6.27a-

d and Figure 6.28e shows how the coastal profile evolves throughout the 1,489 year simulation according to these driving wave conditions.

After 20 simulated years, cuspate bumps form along the initially perturbed shoreline (Figure 6.27a). The cuspate landforms are characterised by steep sloping profiles seawards along the edges of the feature, with a more gently undulating central topography. The beach and nearshore profile are largely undisturbed by the changes to the shoreline shape, with the most dynamic region between 10 and -4 m elevation. Within this band of coastline, the beach surface in the area which aligns with the location of the bays between cuspate features shows some smoothing. The contours of the bathymetry in this segment begin to align shore-parallel with the tips of the cusps but remain consistent with the initial conditions within the bays, creating a shallow shelf.

Extensive changes occur across the coastal profile by 320 simulated years. The cuspate features have evolved into larger sand wave features that skew downdrift, towards the right of the domain (Figure 6.27b). The features exhibit steeper slopes and higher topographies along their updrift edges and more gentle slopes and lower topographies across the centre of the landforms, towards the downdrift edge. A shallow shelf is retained in the bay area between the features to -2 m depth but with finite amplitude topographic peaks formed just offshore of the updrift edge. Beyond this, the nearshore profile exhibits significant smoothing, creating relatively planar contours which maintain an average slope of 0.01 (1%), consistent with the initial conditions. The upper beach at 50 m elevation remains relatively undisturbed, with the profile of the contours maintaining their original form. The beach surface is increasingly smoothed longshore towards the water level, particularly the areas which align with the bays, whilst maintaining an average slope of 0.01 (1%).

After 620 simulated years, reconnecting spits are observed along the shoreline (Figure 6.27c). The updrift edge of the features exhibit the steepest slopes, as observed in the predeceasing landforms, with the slopes shallowing towards the downdrift edge to below the water level. The nearshore bathymetry is influenced by the growth of the spit, creating steeper contours around the offshore tip which gradually shallows back to a 1% slope over approximately 0.7 km. The beach surface continues to smooth cross-shore, whilst maintaining an average slope of 1% which steepens at the shoreline.

Similar patterns of morphodynamic evolution are observed after 820 (Figure 6.27d) and 1,489 (Figure 6.28e) simulated years. The reconnecting spits continue to develop further, creating peninsulas that extend increasingly offshore with sediment paths intermittently reconnecting the landform to the shoreline. The increasing amplitude of the landforms creates an increasingly wide shallow bay between the features. The bay is punctuated by peaks in the bathymetry, which are not confined to the updrift edge but are found across the entire bay area. The nearshore bathymetry retains a planar longshore profile with a 1% cross-shore slope, but which is disturbed and steepens around the tips of the landforms.

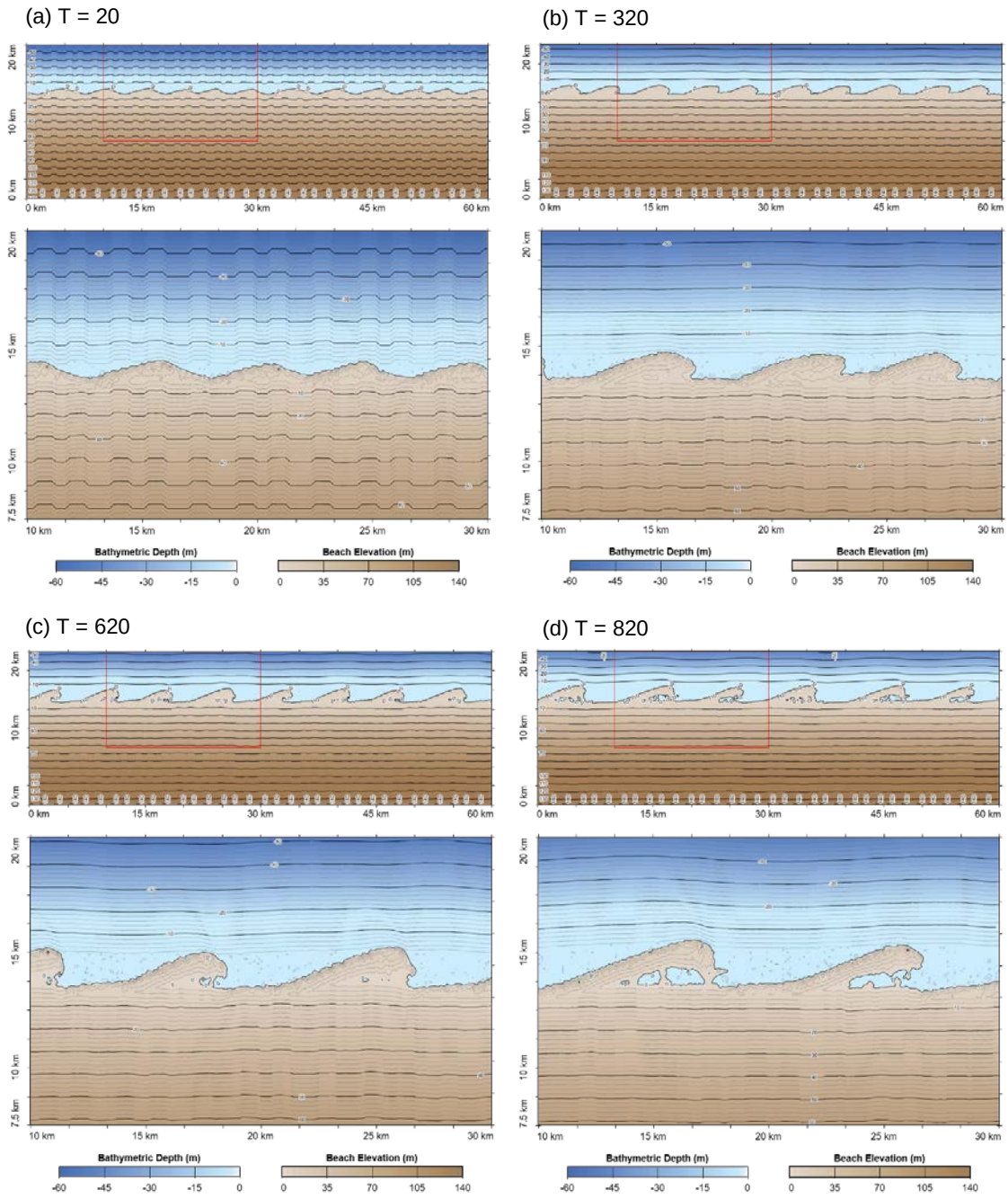

Figure 6.27 Two-dimensional temporal evolution of the coastal profile under wave climate conditions where A = 0.7, U = 0.65 which generates reconnecting spits along the shoreline (Images a-d)

(e) T = 1,489

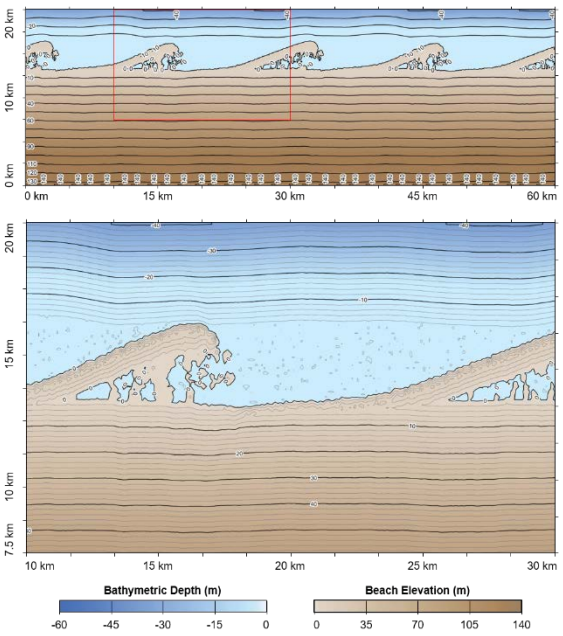

Figure 6.28 Two-dimensional temporal evolution of the coastal profile under wave climate conditions where A = 0.7, U = 0.65 which generates reconnecting spits along the shoreline (Image e)

6.6.4 Flying Spit

Where the wave climate is highly dominated by waves approaching from the left of the domain (A = 0.8) and from high angles (U = 0.7), flying spits develop along the simulated shoreline as explored previously in Chapter 5. Figure 6.29a-d and Figure 6.30e-f show how the coastal profile evolves throughout the 1,090 year simulation according to these driving wave conditions.

After 50 simulated years (Figure 6.29a), the coastal profile evolves in a similar manner to that observed for reconnecting spits (Figure 6.27 and Figure 6.28). Cuspate features develop from the initial perturbations along the shoreline, which are gently sloping from their central point towards more steeply sloping edges at the water line. A shallow bay forms between the landforms, which is punctuated by peaks in the undulating bathymetry. The nearshore and beach surface remain largely undisturbed with the contours retaining their original form.

Developed flying spit features are observed along the shoreline after 150 simulated years (Figure 6.29b). The narrow peninsulas exhibit higher topographies along the updrift edges, which slope more gently towards the bay within the hook of the spits. Down to -2 m depth, the bathymetric profile reflects the general shape of the shoreline. Between -10 m and 10 m elevation, the shape of the coastal profile is influenced by the presence of the spits, but this is increasingly negligible further offshore across the bathymetry and further landwards across the beach surface. The uppermost beach surface is relatively undisturbed above 50 m elevations, with the profile of the contours retaining their original form.

The flying spits become increasingly perpendicular after 420 simulated years (Figure 6.29c) and retain a steeper profile along the updrift edge. The nearshore profile is smoothed longshore with gentle undulations offset from the headlands of the spits. A slightly steeper profile is observed from the shoreline to depths of -4 m around the tips of the headlands and a complex undulating bathymetry is observed in the bay between the spits. The beach surface exhibits a relatively planar longshore bathymetry, although remnants of the original profile are observed in the upper beach above 50 m elevation.

Between 670 and 1,090 simulated years (Figure 6.29d and Figure 6.30e-f) the profile of the beach surface remains relatively undisturbed, with only negligible changes in the location of undulations in the topography. The spit features cycle through periods of extending relatively shore-parallel and perpendicular to the local shoreline orientation, which influences the nearshore profile. The bathymetry becomes increasingly undulated longshore, whilst maintaining an average slope of 0.01 (1%) in the cross-shore direction. However, after 1,090 simulated years, the undulations in the planform contours do not align parallel

with the shape of the shoreline and the position of the extruding headlands of the spits. At 760 (Figure 6.30e) and 1,090 (Figure 6.30f) simulated years, the distal point of the flying spits punctuate the relative planar contours at -2 m to -10 m depths, creating steeper profiles offshore. The bays between each spit continue to exhibit complex undulating bathymetries.

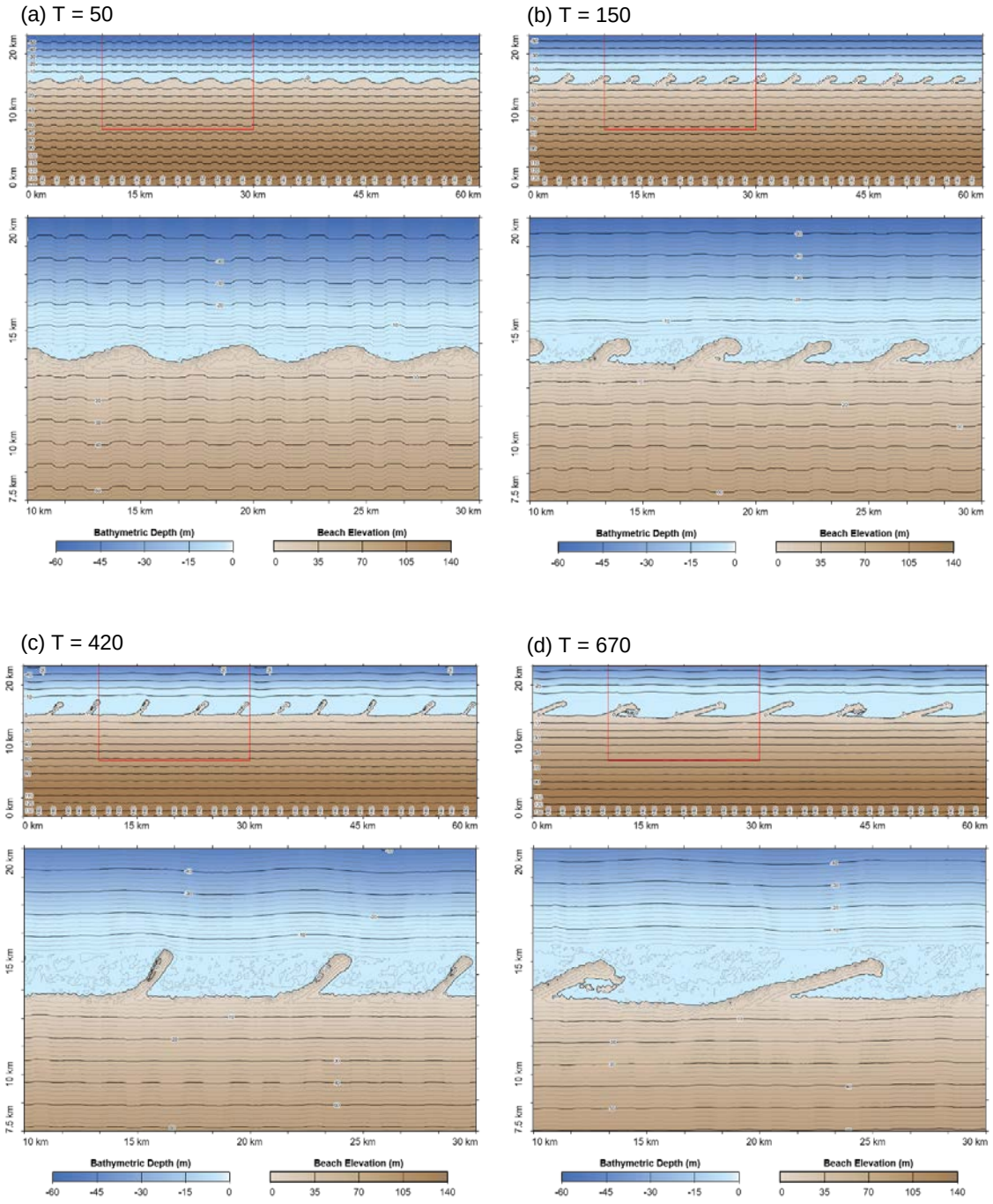

Figure 6.29 Two-dimensional temporal evolution of the coastal profile under wave climate conditions where A = 0.8, U = 0.7 which generates flying spits along the shoreline (images a-d).

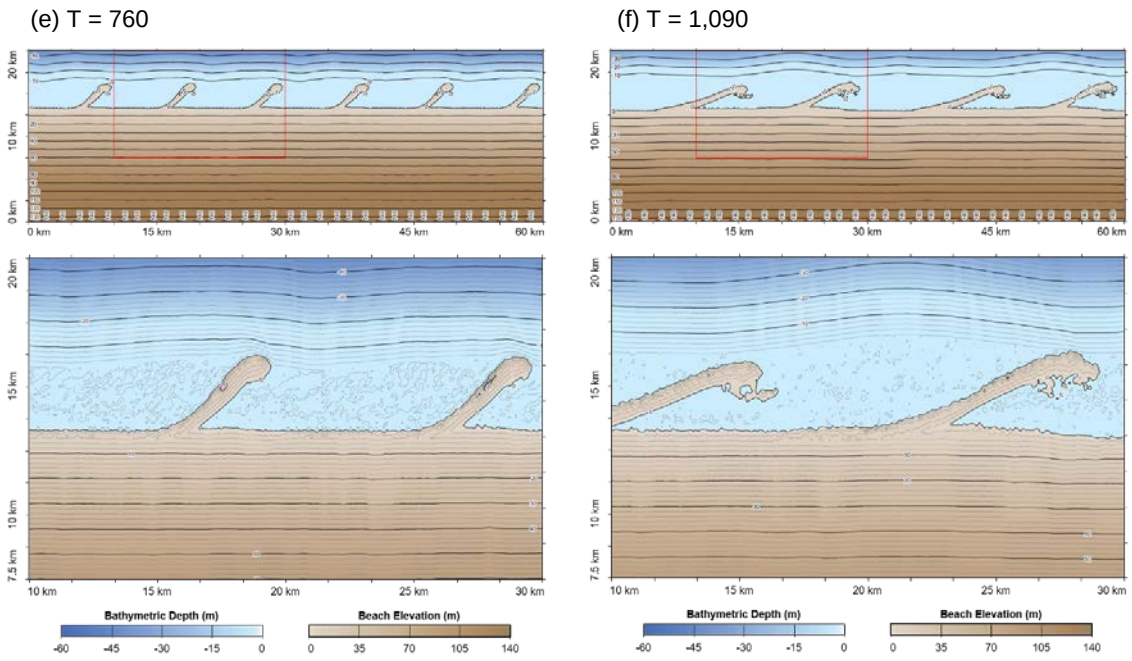

Figure 6.30 Two-dimensional temporal evolution of the coastal profile under wave climate conditions where A = 0.8, U = 0.7 which generates flying spits along the shoreline (images e-f)

6.6.5 Rates and Patterns of Change in Landform Formation

As has been discussed in Section 6.6.1 to Section 6.6.4, the dynamics of the coastal profile differs depending on the driving wave conditions and the consequential formation and behaviour of depositional landforms. The volume stacks in Figure 6.31 show change in net erosion and deposition patterns in a cross-shore transect of the coastal systems (where x = 30 km) for the four wave climate conditions discussed in Section 6.6.1 to Section 6.6.4. To reiterate, the wave climates are as follows: (a) A = 0.5, U = 0.55, (b) A = 0.6, U = 0.6, (c) A = 0.7, U = 0.65 and (d) A = 0.8, U = 0.7. The cross-shore transects are recorded every 30 simulated years and are cropped to the first 1,050 years, which is the shortest run duration of the simulations presented. The transects have also been cropped to the most active area of the profile, between 12-17 km cross-shore and 25-32 km longshore (Figure 6.31).

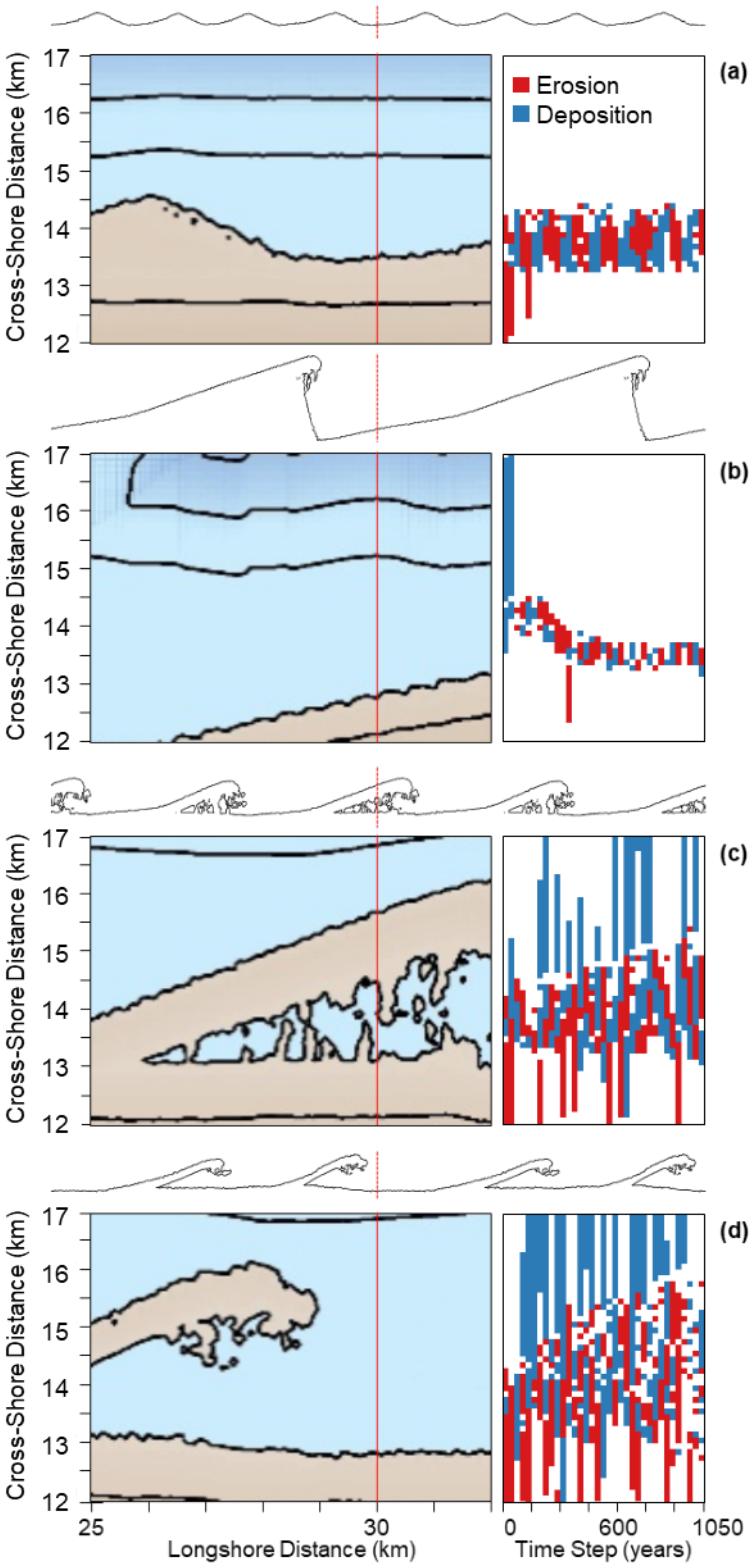

Figure 6.31 Shoreline Morphologies (left) and volume stacks (right) for four simulations where the wave climate is defined by (a) A = 0.5, U = 0.55, (b) A = 0.6, U = 0.6, (c) A = 0.7, U = 0.65 and (d) A = 0.8, U = 0.7. The red line marks the cross-shore transect where the change in volume at 30 year time intervals is recorded.

The volume stacks are shown to the right of the plot in Figure 6.31 and to the left are images showing the morphology of the shoreline at the end of each simulation. The location of the transect is highlighted in red in these images, portraying both the cross-shore and longshore extent of the results shown in the volume stacks. The shape of the shoreline is shown above each image and volume stack, with a red dotted line marking the longshore location of the transect; the cross-shore extent is not given accurately on this outline (Figure 6.31). A visual analysis of the results shows a general increase in activity with increasing wave asymmetry (*A*) and proportion of high angle waves (*U*) (Figure 6.31a-d). Each simulation shows a different pattern of change over time and varying proportions of total erosion and deposition throughout the simulations.

Where the wave climate is symmetrical with only a 5% dominance of waves approaching from high angles (Figure 6.31a), the volume stack shows a relatively consistent pattern of erosion and deposition over the 1,050 year period. This is exemplary of the behaviour of the shoreline which gradually develops relatively finite amplitude cuspate features that gradually migrate alongshore (see Section 6.6.1 and Chapter 5). Under a symmetrical climate such as this, cusps would not tend to migrate significantly longshore in a natural system due to the relatively equal proportion of waves approaching from both directions (Rosen, 1975). The behaviour observed in CEM2D is therefore attributed to the sensitivity of the model to the angle of wave approach (see Chapter 4) which changes daily, or due to directional dominance in the model which is explored further in Chapter 8. Net accretion is observed on the plot (Figure 6.31a) where a depositional cuspate feature is positioned on the transect and net erosion where the cusps migrate across the transect. Over time, the zone of activity migrates gradually seaward as the shoreline accretes, but by a relatively negligible amount.

Where the wave climate has a slight asymmetry (Figure 6.31b) and alongshore sand waves develop along the shoreline, the zone of significant net erosion and deposition along the shoreline is relatively limited spatially compared to the results under a symmetrical wave climate (Figure 6.31a). The shoreline shows a very narrow band of change that gradually recedes landward over time. A notable change occurs after 360 simulated years, where the dynamic zone retreats from an average location where y = 14 km to y = 13.5 km over a period of approximately 180 years. An analysis of the shoreline morphology and shoreline position is coincident with this finding, showing the recession of the shoreline by comparable amounts between 240 and 390 simulated years across the transect (Figure 6.32). The volume stack is dominated by periods of erosion, but activity overall decreases throughout the simulation. The results discussed are to some extent influenced by the location of the transect relative to the most active section of the profile longshore; this is discussed further subsequently.

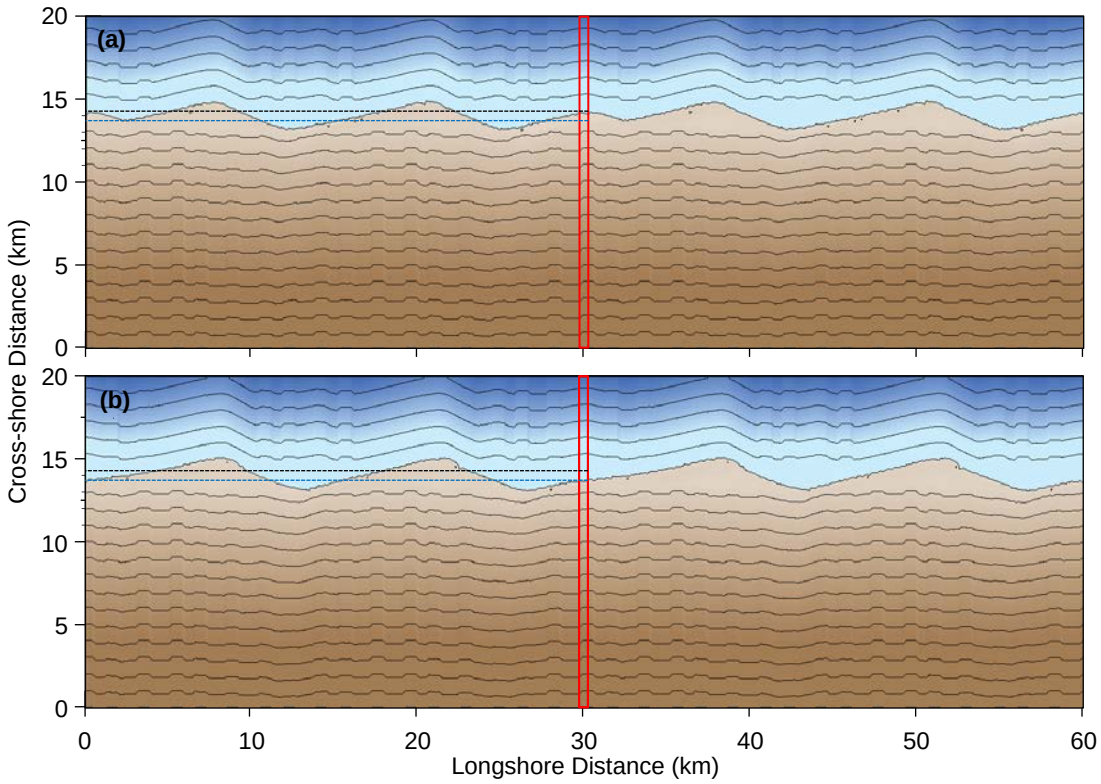

Figure 6.32 Images showing the morphology of the coast where A = 0. 6, U = 0.6 after (a) 240 and (b) 390 simulated years, corresponding with the period showing in Figure 6.31 where the shoreline shows rapid recession. The location of the transect where data has been extracted for Figure 6.31 is shown in the red box (x = 30 km).

Where the wave climate is highly asymmetric and spit features form along the shoreline (Figure 6.31c-d), the zone of erosion and deposition is larger spatially than observed under a symmetric wave climate (Figure 6.31a). In Figure 6.31c-d, alternating patterns of erosion and deposition are observed coincident with the migration of landforms along the shoreline. The average cross-shore extent of the active zone migrates offshore over time as the reconnecting (Figure 6.31c) and flying (Figure 6.31d) spits increase in amplitude, with the flying spits showing a greater increase in amplitude induced by greater proportions of high angle waves (*U*) approaching the shoreline. A distinct difference between the two results shows that for flying spits (Figure 6.31d) there are segments of the transects that show negligible activity within the active zone; this is not observed for reconnecting spits (Figure 6.31c), which show a greater spatial coverage of activity across the transects in this area. This is representative of the types of

features forming along the shorelines with the paths of sediment between the spit neck and mainland causing changes in sediment volumes across the profile.

As shown in Figure 6.31, across a single transect individual cells show either an increase, decrease or no change in the volume of material compared to the volumes recorded 30 simulated years previously. In Figure 6.33, the total volume of material accreted in a given time step is summed (shown in green) and the total volume eroded is summed (shown in red) and presented in the graph. The net change at each time interval across the transect is shown by the black line. These results show the temporal pattern of sediment erosion, deposition and net change, according to the four different wave climate conditions.

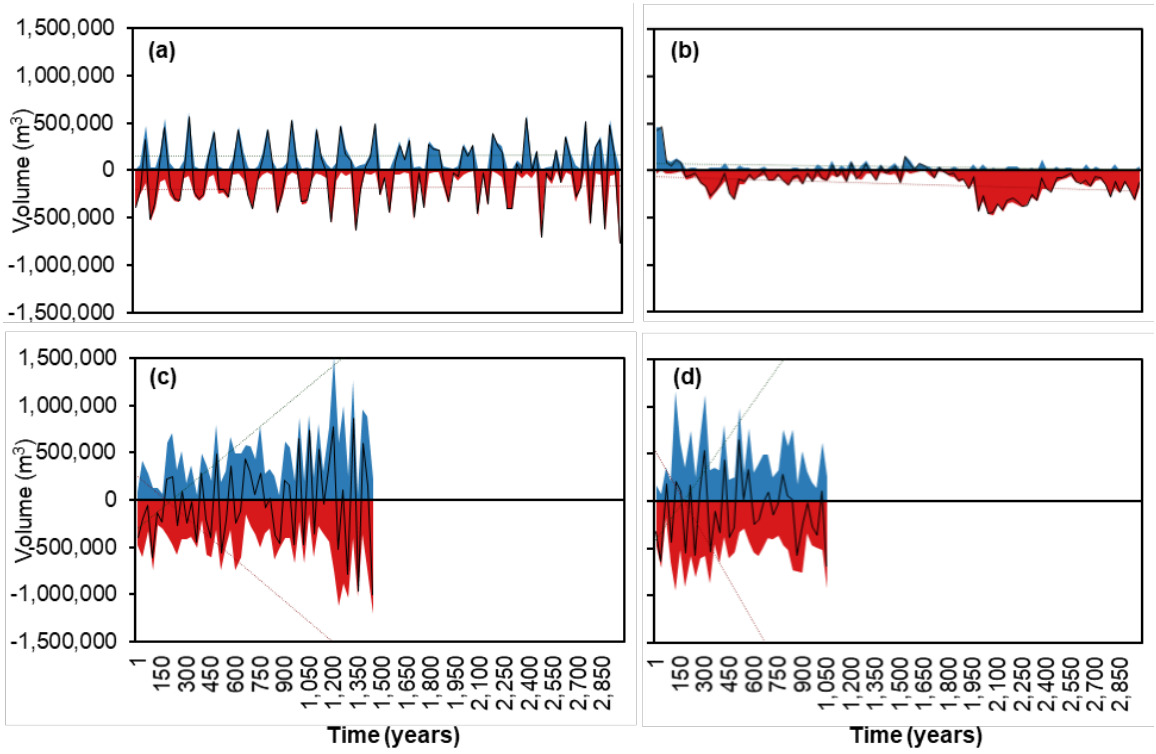

Figure 6.33 Sum of change in erosion and deposition across the cross-shore transect (where x = 30 km) at each 30 year time interval over the 3,000 year time period. Net erosion and deposition is a measure of change in each cell between the 30 year intervals. Results of four simulations are presented where the wave climate is defined by (a) A = 0.5, U = 0.55, (b) A = 0.6, U = 0.6, (c) A = 0.7, U = 0.65 and (d) A = 0.8, U = 0.7.

The temporal pattern of erosion and deposition of material varies according to the wave climate conditions (Figure 6.33). Where the wave climate is symmetrical

(Figure 6.33a) a regular and alternating pattern of erosion and deposition is observed. As discussed previously, this is induced by the evolution of relatively finite amplitude cuspate features along the shoreline that gradually migrate throughout the simulation. Minimal change in the total volume of eroded and accreted material is observed, remaining relatively consistent throughout the simulation.

Where the wave climate has a slight asymmetry (Figure 6.33b) the transect is dominated by erosional behaviours. Limited deposition occurs and over time, the zone of deposition extends further landward as the shoreline recedes (as discussed previously, see Figure 6.32). An analysis of the morphological evolution of the shoreline shows that at the location of the transect (shown in Figure 6.31b) the larger sand wave features show minimal longshore migration across this point. Relocating the transect to where x = 22 km (Figure 6.34), which crosses through the sand waves feature at the end of the simulation as opposed to in the bay, generates different volumes and patterns of change as shown in Figure 6.35.

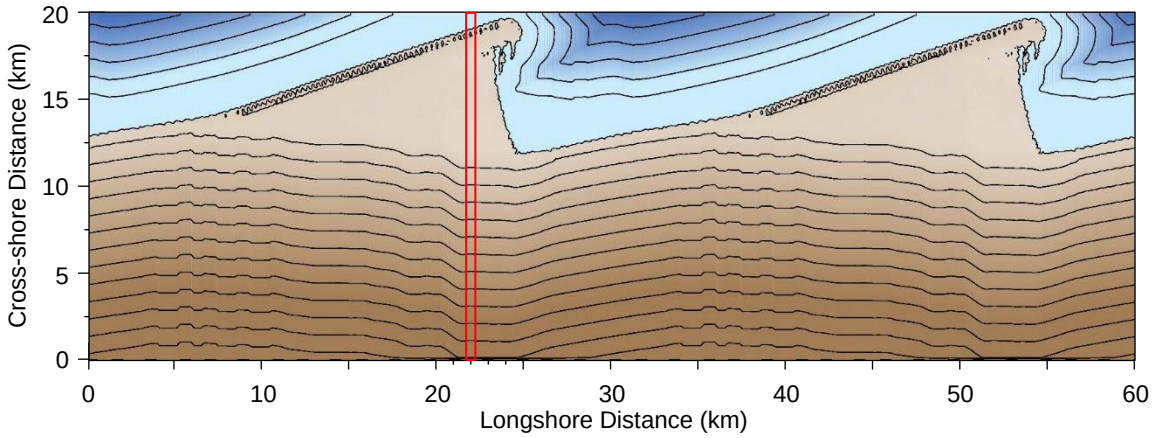

Figure 6.34 Planform morphology of the coast where A = 0.6, U = 0.6 after 3,000 simulated years. The location of the cross-shore transect located at x = 22 km, used to record volume change, is shown by the red box.

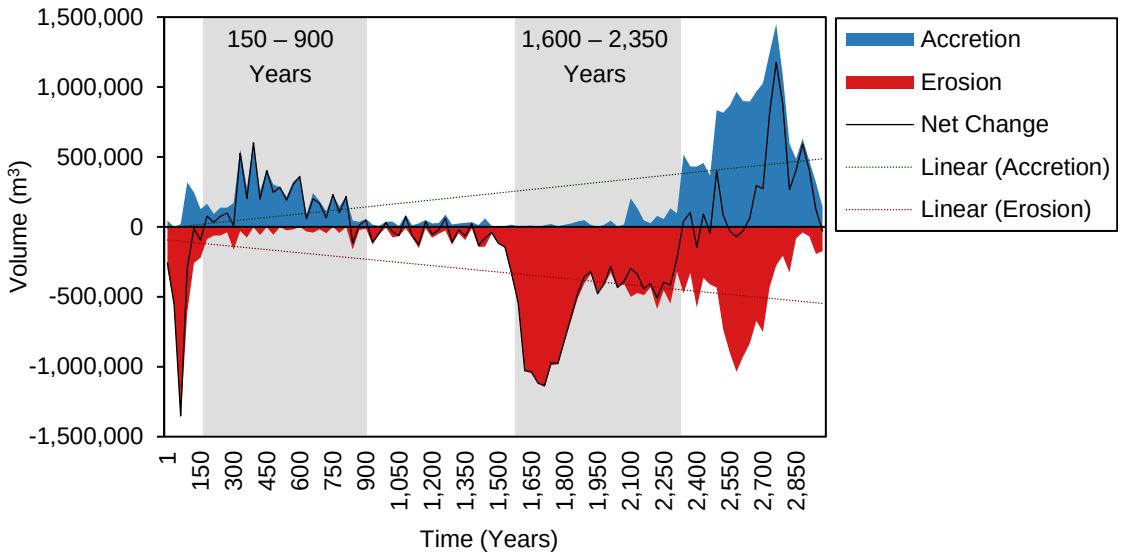

Figure 6.35 Sum of change in erosion and deposition across the cross-shore transect (where x = 22 km) at each 30 year time interval over the 3,000 year simulation period. Net erosion and deposition is a measure of change in each cell between the 30 year intervals. Results presented where the wave climate is defined by *A = 0.6, U = 0.6*.

As shown in Figure 6.35, erosional behaviours remain dominant when the location of the transect is repositioned from x = 30 km to x = 22 km. The period of accretion between approximately 150 and 900 simulated years is coincident with the formation of a sand wave feature at the location of the transect, which thereafter is gradually diffused. After approximately 1,600-1,650 simulated years, two principle sand waves exist at the shoreline and begin to increase in cross-shore amplitude rapidly and form large bays which gradually retreat landward. At this point, the transect is located within the bay and as shown in Figure 6.35, relatively high net erosion occurs. As the sand waves migrate alongshore, it crosses the transect after approximately 2,350 simulated years and net accretion is observed (Figure 6.35).

Where the wave climate is asymmetric and spit features form along the shoreline (Figure 6.33c-d), the volume of material transported (according to net erosion and deposition) is relatively high in comparison to the simulations with greater symmetry in the wave climate (Figure 6.33a-b). The pattern of change in the total

volume of material also shows more dynamism, driven by the more rapid growth, evolution and migration of landforms.

Under a wave climate where *A = 0.7, U = 0.65*, over the simulation period the net rate of change in terms of both erosion and deposition of sediment across the transect increases (Figure 6.33c). However, where *A = 0.8, U = 0.7*, a decrease in erosion and deposition volumes is observed (Figure 6.33d). In Chapter 5 it was shown that the average planform area of the former, which generates reconnecting spits, is smaller than of the latter, which generates flying spits. However, recording change across a transect shows more complexity in the morphodynamic evolution of the entire cross-shore coastal profile than the planform area alone denotes.

The spacing of peak accretion volumes in the results presented in Figure 6.35 can be used to illustrate relative rates of change in the simulations, according to the driving wave conditions. Figure 6.36 shows results of the sum of the change in deposition only for each of the four simulations taken from Figure 6.33 (where x = 30), to support the subsequent analysis.

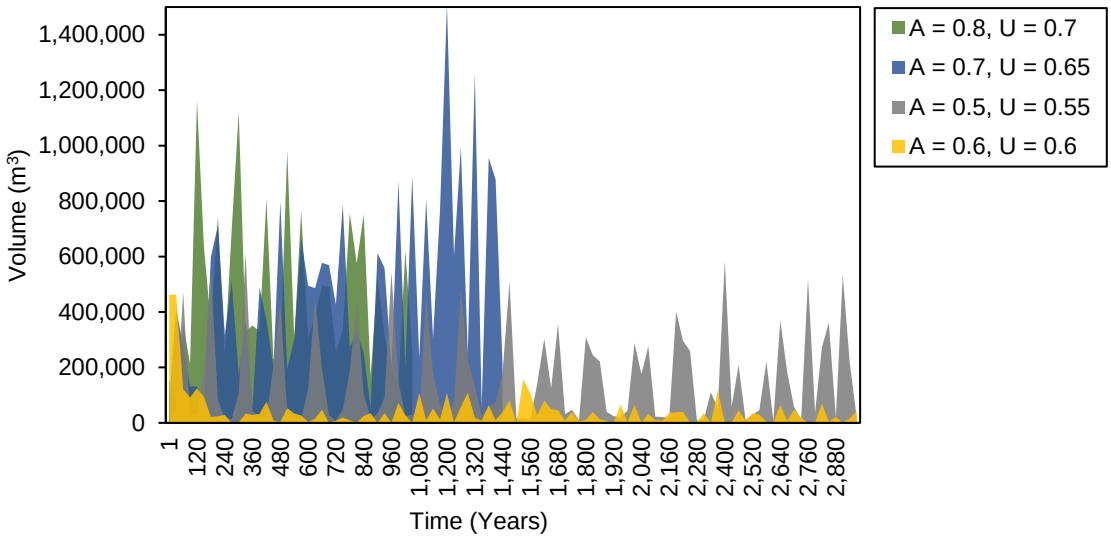

Figure 6.36 Sum of change in deposition across the cross-shore transect (where x = 30 km) at each 30 year time interval over the 3,000 year time period, for four wave climate conditions.

Shown in Figure 6.37 is the average time frame (recorded in years) between major peaks in sediment deposition across the transects for the four wave climate scenarios, taken from results in Figure 6.36. The wave climate with greater symmetry shows the highest average time frame between major sediment deposition peaks, denoting the lowest rates of change. The rate of change rapidly increases with greater wave asymmetry as the directional dominance in the wave climate drives the longshore transport of material, which is captured in the cross-shore transect.

However, where the wave climate is defined by $A = 0.8$, $U = 0.7$, the rate of change slows. This is complementary to findings presented previously in Chapter 5 which showed that high directional dominance in the wave climate and relatively equal proportions of low and high angle waves can act to smooth the shoreline by inducing a strong longshore component and limiting cross-shore sediment transport. In the instance shown here under an asymmetric wave climate and a significant proportion of high angle wave, the relatively strong cross-shore component counters longshore sediment transport processes and slows the rate of change in this direction. Since the cross-section principally records changes in the longshore, the results show the reduced rate of change in longshore sediment transport.

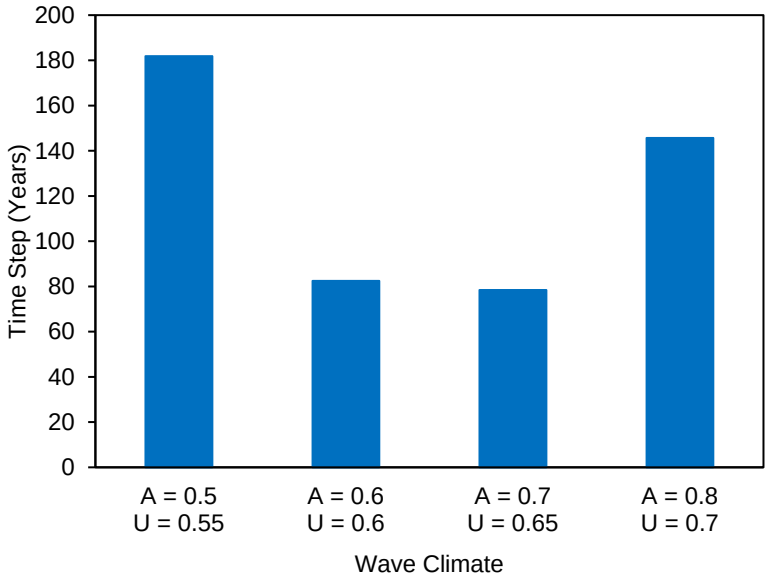

Figure 6.37 Average time frame (years) between peaks in the total volume of deposited sediment in the cross-shore transect (where x = 30 km), according to four wave climate conditions. Transects are recorded at 30 year intervals and show a change in sediment volumes of each cell compared to the previous time intervals.

The irregularity of the peaks and patterns of erosion and deposition shown in Figure 6.33 (see also Figure 6.36 and Figure 6.38) can also infer the dynamics of the system. It is apparent that with increasing wave climate asymmetry and proportion of high angle waves, the sediment transport regime becomes more irregular and non-linear. This is in terms of both the spacing of peaks showing changes in the rate of change and variations in the total volume of material being transported.

The total volume of eroded and accreted material across the transects in each of the simulations presented in Figure 6.33 is shown in Figure 6.38 and can infer relative activity in the coastal systems, according to the driving wave conditions. The results are for the period up to 1,050 simulated years, which is the shortest run duration of the simulations presented, so the data can be compared over the same timeframe. The trend shows that with increasing wave climate asymmetry and high angle waves, the level of activity occurring in the system increases.

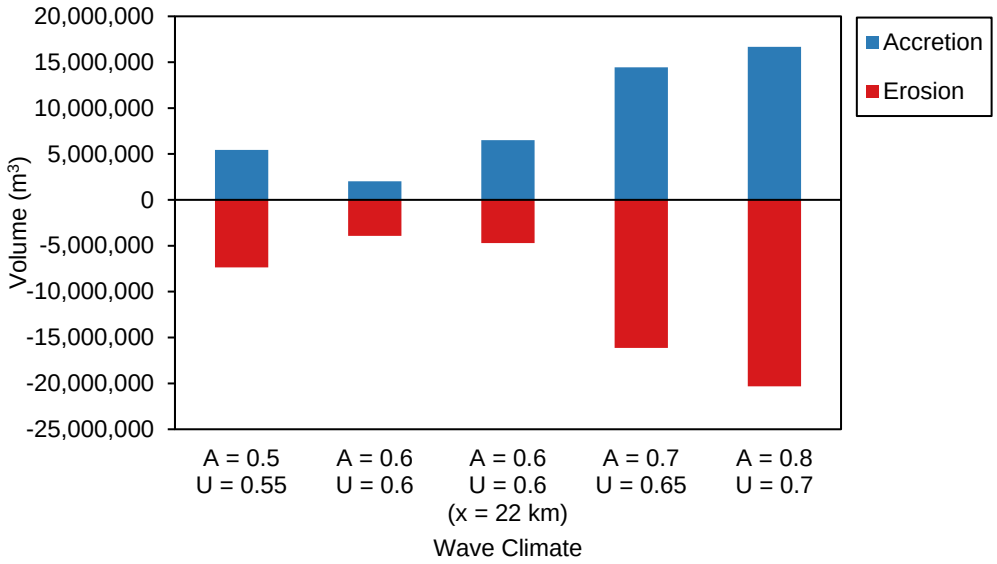

Figure 6.38 Total volume of sediment eroded or deposited, calculated from changes in the volume of material in each cell of the transect (at x = 30km, unless otherwise stated), for four simulations (including for A = 0.6, U = 0.6 at X = 22 km) with varying wave climates. Results are generated from the initial 1,050 year simulated time period, being the shortest run duration of the four simulations.

The results where A = 0.6, U = 0.6 shows a smaller total change in eroded and deposited sediment than the trend would suggest (Figure 6.38). Even where the transect is relocated to x = 22 km to capture the evolution of the mature sand waves (as previously discussed), relatively low values are observed under these wave climate conditions. The volume of sediment transported is influenced by the balance of longshore and cross-shore sediment transport which in this case is driving the movement of sediment cross-shore. This dynamic is not well captured by the cross-shore transect.

6.7 Discussion

The existence of quasi-equilibrium forms in coastal systems has led to the use of static modal profiles in many one-line models, as discussed in Section 6.3. The beach is represented as a planar surface and the bathymetry as a shore-parallel slope (e.g. CEM (Ashton *et al.*, 2001), GENESIS (Hanson and Kraus, 1989) and COVE (Hurst *et al.*, 2015)). The results presented in this Chapter reinforce the

use of this method for the beach surface only, which has shown to smooth throughout most simulations to create a planar surface. The subaerial beach shows relatively limited dynamism, regardless of the input wave conditions used in the experiments and has little influence on the long-term evolution of the systems.

In few simulations, the profile of the nearshore reflects the shape of the shoreline and creates shore-parallel contours (e.g. low values of *A*), which further supports the use of equilibrium profiles (Bruun, 1962; Dean, 1991) in mesoscale modelling. However, in most simulations, the use of equilibrium profiles is disputed as the coastal profile does not align shore-parallel and is not solely influenced by current environmental conditions but by previous states and morphological residuals. This effect has been previously suggested by authors including Wright and Short (1984), French et al., (2015) and Thomas *et al.,* (2016) and is discussed further in Section 6.7.3.

The results show that where the wave climate is asymmetric and landforms migrate, they exhibit a periodic influence on the nearshore profile as they translate longshore (Ashton *et al.*, 2001). This alternating supply of sediment influences how the nearshore evolves and can create interesting morphologies in the profile. Conversely, in highly symmetrical wave climates, landforms found along the shoreline show minimal change and migration longshore and also show relatively shore-parallel nearshore slopes (Ashton *et al.*, 2001). Their growth is concentrated in the cross-shore direction, driven by the incident wave angles. The zone influenced by sediment transport is therefore concentrated on these areas surrounding the landforms. Modelling the dynamic nature of the nearshore profile could, therefore, be important for understanding how coastal profiles

behave over the long-term, particularly in highly dynamic coastal areas with longshore transport components.

The dynamics of the beach and nearshore profiles could be influenced, or even controlled, by the sediment distribution method which is not employed on every iteration of the model (see Chapter 3). This is particularly the case for the nearshore profile; there is limited transport potential across the beach and so the evolution of morphological features is constrained more-so by sediment availability than its distribution per se. For instance, in the case where the bathymetric profile responds to the formation of sand waves and creates shore-parallel contours if these features begin to migrate rapidly at a rate greater than the sediment distribution method is employed, remnants of the sand waves could be held in the profile. Whilst this could describe the natural processes of morphological memories (see Section 6.7.3), it could also be related to the frequency at which sediment distribution occurs relative to the transport rate and patterns. It is recognised that ideally the sediment distribution method would be employed on every iteration consistent with other processes in the model, but further development of the sediment transport technique is required before this can be tested further (see Chapter 8).

6.7.1 Beach States and Equilibrium Coastal Profiles

To quantitatively compare the coastal profiles generated by CEM2D against the widely accepted beach states of Wright and Short (1984) and equilibrium coastal profiles of Dean (1991) would require calculating Equation 6.1 or Equation 6.2, and/or Equation 6.3. Equation 6.1 calculates the dimensionless fall velocity which can be used to classify a beach as dissipative, intermediate or reflective, Equation 6.2 adds a tidal range factor into Equation 6.1 and Equation 6.3 computes the evolution of a cross-shore profile. Unreliable assumptions would be required to

populate these equations due to the reduced complexity of the model and its limited precision on wave breaking metrics, hydrodynamics, sediment properties and fall velocities. This is a limitation of many mesoscale coastal models that are required to compromise on such details for the benefit of longer term exploratory modelling, compared to more complex short-term models. A qualitative assessment of the resulting coastal profiles is, therefore, the focus of this section.

6.7.1.1 Beach States

The simulated coastline is comprised of fine-grained sand (0.4 mm) and a gently sloping profile with a gradient of 0.01 (1%). This dissipative beach form is retained throughout the simulations, consistent with the descriptions given by Wright and Short (1984) and Masselink and Short (1993). Further, the outputs align with the more descriptive classifications given by Scott *et al.,* (2011), including characteristics of the wave climate conditions typically found along a range of dissipative beach types in England and Wales. Scott *et al.,* (2011) describes a non-barred dissipative type of coastline, which forms a featureless intertidal zone with a slope angle of 0.5-1^{o} (0.87% – 1.75%). The wave climate conditions in these types of systems are characterised by significant wave heights of between 1-1.2 m and mean wave periods of 8 s, similar to the experimental conditions used in this study (see Section 6.4). However, Scott *et al.,* (2011) also note that coasts in this classification are typically macrotidal, unlike the simulated environment, which does not explicitly include tidal processes[3]. The incorporation of tides into the simulations would fluctuate the location of the shoreline and would have a smoothing effect across the shoreline. It is therefore anticipated

[3] A tidal signal can be simulated in CEM2D, but it is not used in the simulations presented in this chapter.

that even if tidal fluctuations were to be included in these simulations, the overall profile would remain dissipative.

Whilst the average profile of the slope is influenced by the experimental setup and sediment distribution thresholds, the model can override these numerical rules given suitable conditions. For instance, the threshold for distribution is such that the average 0.01 slope is retained, but the angle can fluctuate around this mean and topographic undulations can develop and sustain given suitable sediment supply. However, it is important to consider the role of the model and parameterisations in the simulations and the model's sensitivities and limitations as discussed in Chapter 4.

6.7.1.2 Equilibrium Coastal Profiles

Cross-shore coastal profiles simulated under each wave climate condition in CEM2D generate similar patterns of evolution throughout the duration of the simulations (Figure 6.16 and Figure 6.17). The profiles exhibit a landward recession of the beach face and shoreline, the formation of a shallow nearshore shelf or platform and the seaward migration of the nearshore profile beyond this platform (Figure 6.39).

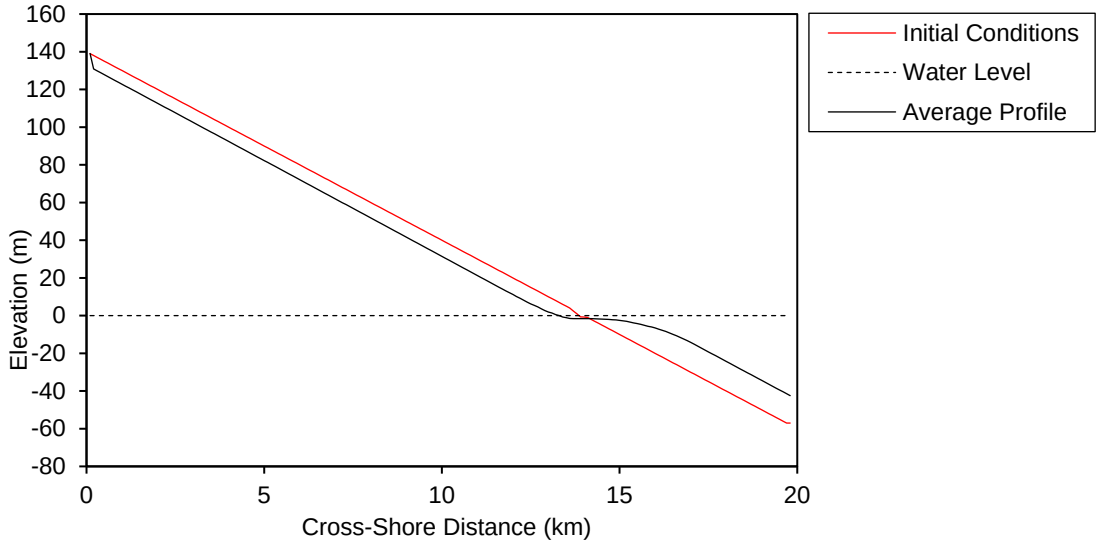

Figure 6.39 A Graph showing the average change in the cross-shore profiles in CEM2D according to twenty five different wave climate conditions, based on results presented in Figure 6.16 and Figure 6.17.

At this scale, there are similarities between the shape of the evolved cross-shore profiles and the equilibrium forms of Dean (1991). However, a more detailed exploration of the most dynamic areas of the coastline shows interesting morphologies particularly in the nearshore which are not captured by these classifications (French et al., 2015; Pilkey et al., 1993). The results therefore largely disagree with the use of these classifications and of equilibrium profiles in modelling coastal morphodynamics.

6.7.2 Spatial Variations in the Dynamic Behaviour of the Coastal Profile

The most dynamic areas of the profile are the beach surface constituting the depositional landform and the upper nearshore profile which responds more rapidly to short-term changes in the environment. This is illustrated by a single volume stack plot in Figure 6.40. These areas are subject to greater sediment flux and redistribution of material compared to the beach surface, which experiences a gradual change over time in response to changes in the shape of the shoreline. This is in agreement with studies of Falqués and Calvete (2005), Hequette and Aernouts (2010) and Ortiz & Ashton (2016).

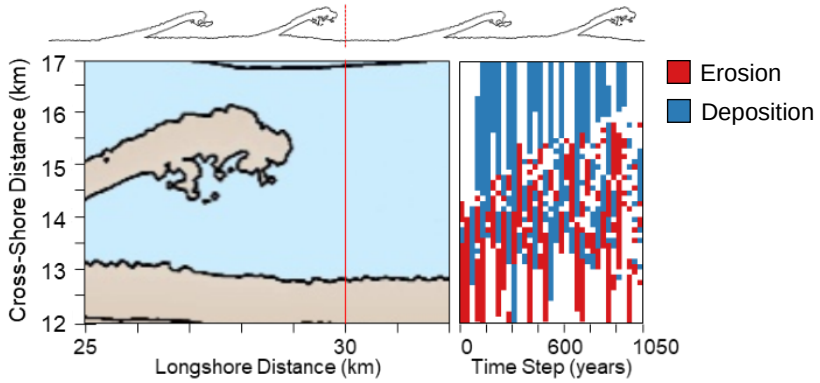

Figure 6.40 Diagram showing the morphology of the coastal systems where A = 0.8, U = 0.7 after 1,050 simulated years (left) and volume stack showing the temporal change in erosion and deposition hotspots across a transect at x = 30 km and y = 12 km to 17 km (right) which is marked by a red line on the morphology plot on the left. Above these diagrams is an outline of the shoreline shape, also marked with a red line where the transect is recorded.

The lower nearshore profile evolves, but at a relatively slower rate compared to the upper nearshore profile. These findings are consistent with those of Pilkey *et al.,* (1993) who suggests that the lower nearshore has the ability to record previous morphological states due to its lower rate of change, compared to the upper nearshore profile and shoreline which undergoes rapid morphodynamics.

In the results of this chapter, an analysis is given of the more specific behaviours of cusps, sand waves, reconnecting spits and flying spits. Trends are found in the evolution of the profile, which further highlights the dynamic nature of the depositional landforms and upper nearshore profile (Pilkey *et al.*, 1993). Each of the landforms develops with peaked topographies and steeper slopes on their updrift sides, compared with a more gently sloping leeward side. This is even found on cuspate features, although formed under a symmetrical wave climate, suggestively due to directional bias in the model as discussed further in Chapter 8.

Focusing therefore on features formed in asymmetric wave climates, sediment is transported and deposited along the updrift edge of landforms to form the seaward extending peninsula. The downdrift slope or bay influenced by

proportionally fewer waves according to the asymmetry of the wave climate and/or due to being wave shadowed by protruding peninsulas, which leads to a lower sediment availability (Ashton *et al.*, 2001). Steeper profiles are found at the distal point of sand waves and spits in the zone of deposition. Shallower profiles and terraces form along the updrift flanks of the landforms and within the bays. This is consistent with findings of physical experiments (Uda and Yamamoto, 1991), short-term numerical simulations (Serizawa et al., 2007, 2009) and empirical evidence taken from natural sand spits (Serizawa et al., 2009; Luijendijk et al., 2017).

Rates of morphological change in coastal systems according to the driving wave conditions are difficult to extract from the data and would provide unreliable results where obtained. As a mesoscale exploratory model, it is not designed to accurately simulate coastal evolution but to highlight patterns of behaviour and the response of systems to different wave climate conditions. However, the volume stacks presented in Section 6.6.5 show some relationships between rates of relative morphological change and both the direction (*A*) and angle (*U*) of wave approach. It was observed that with increasing values of *A* and *U* the active cross-shore zone shows greater dynamism and greater volumes of net longshore transport occurs. This compliments findings of Chapter 5 and the results of Ashton and Murray (2006a), showing that landforms along the shoreline show greater rates of development, in terms of both planform area (Chapter 5, Figure 5.14) and wavelength (Chapter 5, Figure 5.15) with greater wave asymmetry.

Further, more complex patterns are observed where there are competing processes of cross-shore and longshore sediment transport. For instance, the rate of change increases with greater wave asymmetry except in the case where *A = 0.8, U = 0.7* (Figure 6.41). It is suggested that the proportion of high versus

low angle waves induces strong cross-shore sediment transport components and reduces long-shore transport. However, the sum of the change in erosion and deposition volumes is greatest for this simulation demonstrating that large volumes of material are moved overall (Figure 6.41). Whilst this does not necessarily suggest patterns of landform migration, it could be interpreted that as the landforms increase in size, particularly in terms of amplitude, the rate of migration reduces as the cross-shore sediment transport component dominates over longshore transport. This compliments the study of Ashton and Murray (2006a) who suggests that landforms show a reduction in longshore transport rates with increasing area.

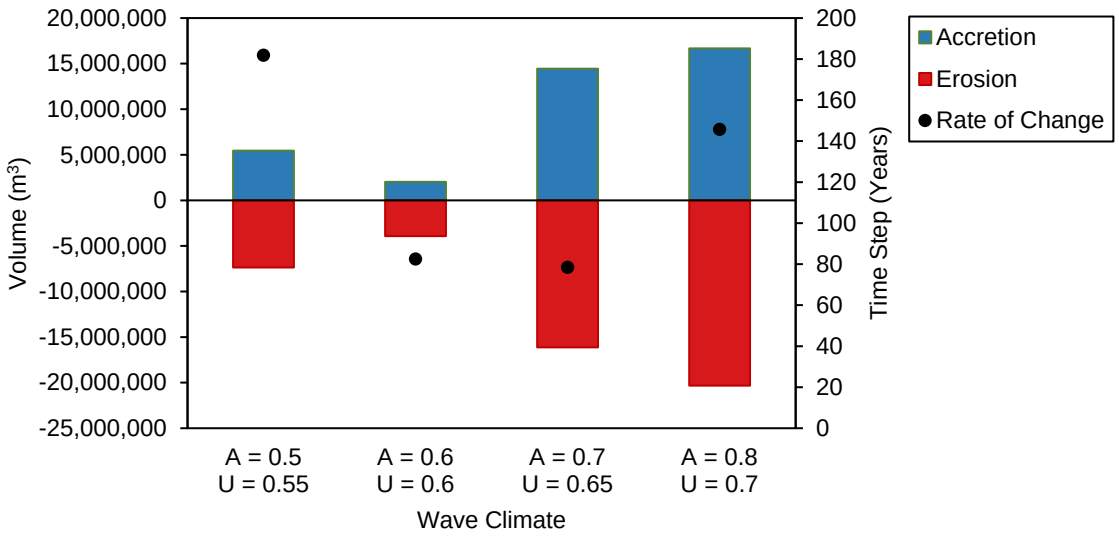

Figure 6.41 The sum of the change in erosion and deposition volumes over 1,050 simulated years for four wave climates scenarios (taken from Figure 6.38) and the average rate of change calculated by the average timeframe between peaks in deposition volumes (taken from Figure 6.37).

The results presented in Figure 6.41 show that there is a relationship between the dynamics of coastal systems and the driving wave conditions. However, it also shows that these systems have complex, non-linear behaviours that emerge from the balance of longshore and cross-shore sediment transport. This supports previous findings discussed in Section 6.6, particularly in relation to Figure 6.33.

In Figure 6.33, it is shown that the cusps, sand waves, reconnecting spits and flying spits which form under the four different want climate conditions (as in Figure 6.41) have different evolutionary signatures. This is observed in the total volume of sediment eroded and deposited across a single transect at each 30-year interval. For example, in Figure 6.33a it is shown that under symmetrical wave climate conditions the pattern of erosion and deposition is regular over time with relatively low sediment exchange. This can be compared to coastlines that evolve in highly asymmetric wave climate conditions (Figure 6.33b) which exhibit more irregular patterns of sediment transport and exchange larger volumes of sediment in total. With each landform exhibiting relatively unique signatures, as explored in more detail in Section 6.6 , these patterns can be used to infer how particular landforms behave over time, the rate and amount of volumetric growth and the stability of the landforms. This type of information can be valuable for informing management decision, particularly if a transition from one landform type to another can be identified using these unique signatures. A transition or change in state could, for instance, be linked to changes in sediment supply or driving environmental conditions such as the wave climate or sea level change.

6.7.3 Morphological Memory

Many of the results presented have noted the presence of remnant features or states in the coastal profile, particularly in the nearshore zone. The types of features found or preserved in the coastal profiles are described in the literature as morphological memories (Wright and Short, 1984; French *et al.*, 2015; Thomas *et al.*, 2016) and could prove important for understanding the nearshore dynamics of coastal environments, particularly under changing environmental conditions.

In its simplest form, initial conditions used in the experimental set-up of CEM2D are preserved in the coastal profile for varying durations in each of the simulations along the upper beach profile, as exemplified in Figure 6.42a.

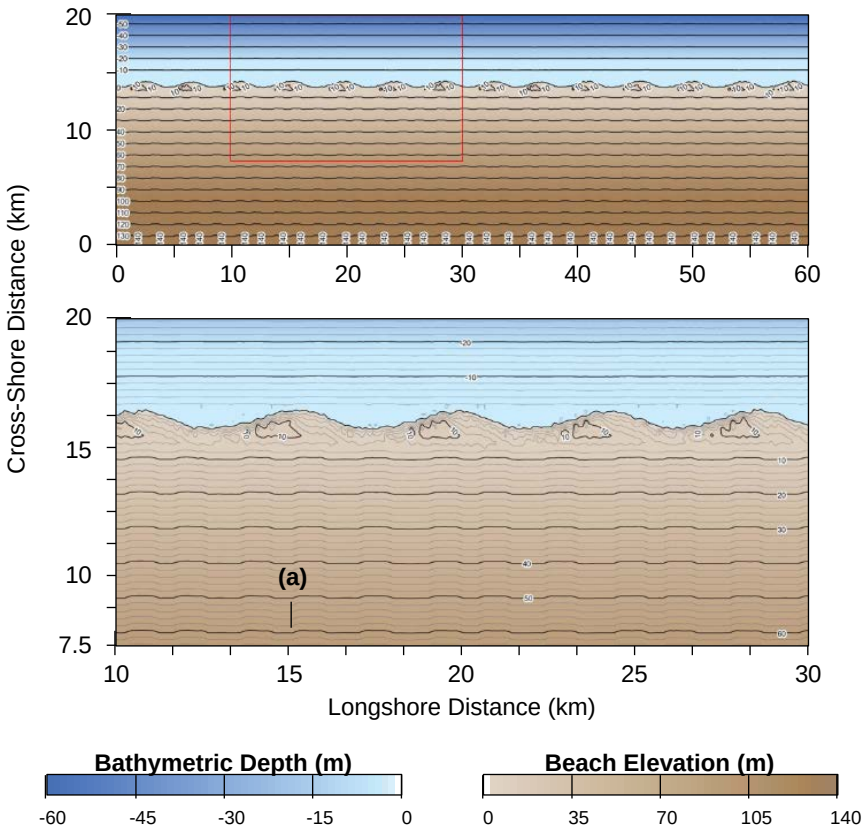

Figure 6.42 Two-dimensional coastal profile under wave climate conditions where A = 0.5, U = 0.55, after 880 simulated years, showing the formation of cuspate features along the shoreline and the preservation of the initial coastal profile in the upper beach (a).

Morphological memories occur in two other ways in the results presented; by the formation of a wide nearshore shelf or platform and by the preservation of prior features in the bathymetric profile. The formation of a shelf or preservation of features is attributed to the rate of change and balance of cross- and longshore sediment transport. It was found that under highly symmetrical wave climates with relatively low rates of change, a shallow nearshore shelf forms and the contours develop a relatively planar form (Figure 6.43a). With increasing rates of change and sediment transport, sand waves form along the shoreline and remnants of their morphological form remain in the bathymetric profile. The rate of change is

such that the longshore movement of landforms makes an impression in the profile that is significant enough to be sustained in the bathymetry as the feature migrates (Figure 6.43b). Where reconnecting spits form along the shoreline, the rapid rate of longshore and cross-shore sediment transport act to smooth the profile and create a shallow shelf (Figure 6.43c). Where the wave asymmetry is increased further and cross- and longshore sediment transport processes compete to reduce rates of longshore change (as observed in Section 6.6.5), morphological memories are found to be preserved in the bathymetry (Figure 6.43d).

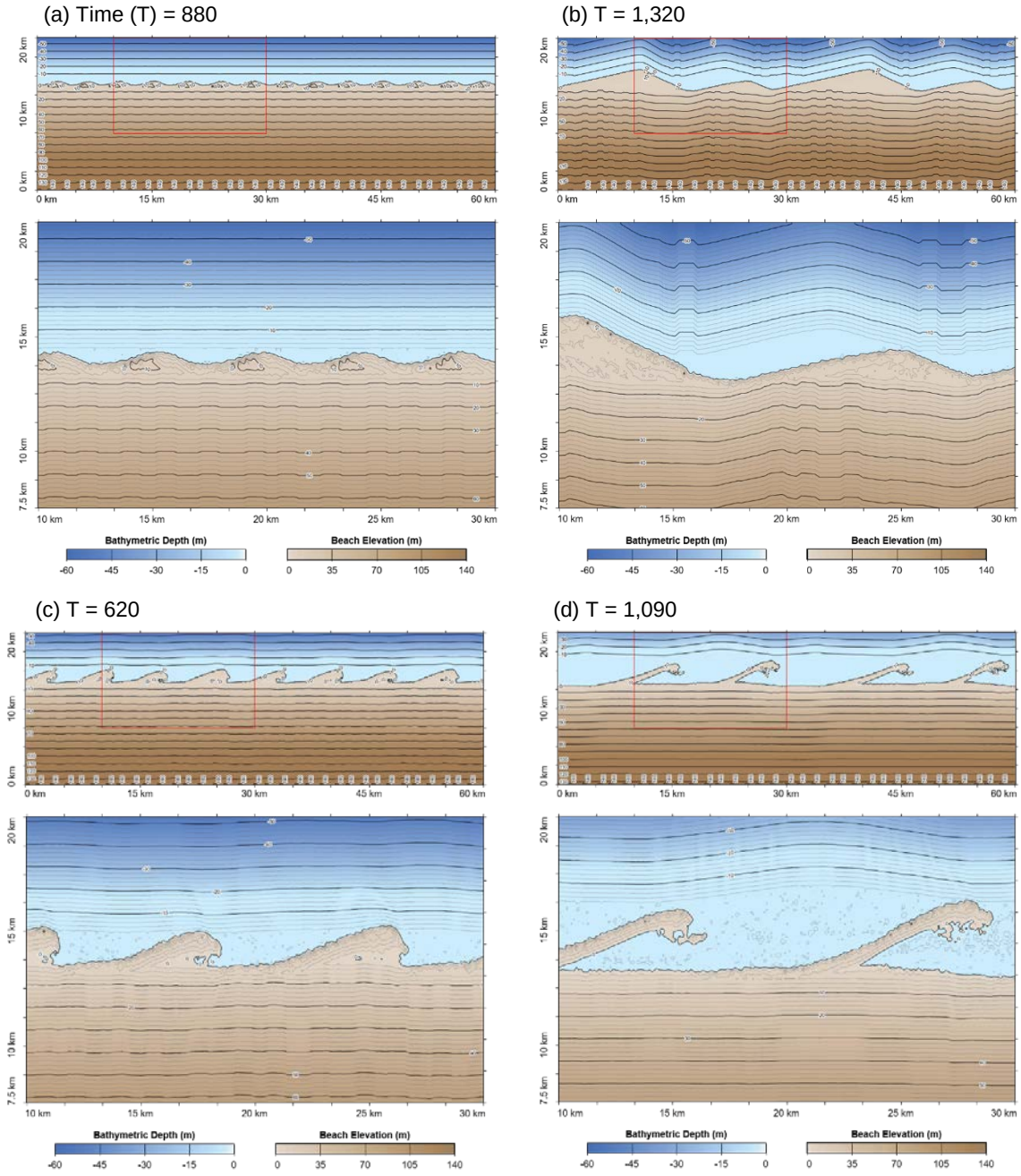

Figure 6.43 Morphology plots showing outputs of the (a) A = 0.5, U = 0.55 at T = 880 (b) A = 0.6, U = 0.6 at T = 1,320, (c) A = 0.7, U = 0.65 at T = 620 and (d) A = 0.8, U = 7 at T = 1,050.

Under symmetrical wave climate conditions (*A*) with a dominance of high angle waves (*U*), morphological memories can be found where smaller cuspate headlands are diffused and feed the growth of the larger features (Figure 6.44). With negligible longshore transport, the remnants of these features are not readily diffused, particularly when situated in the wave shadow of larger landforms. This

process is observable in results of Serizawa (2009, 2012), in the simulation of short-term cusp development.

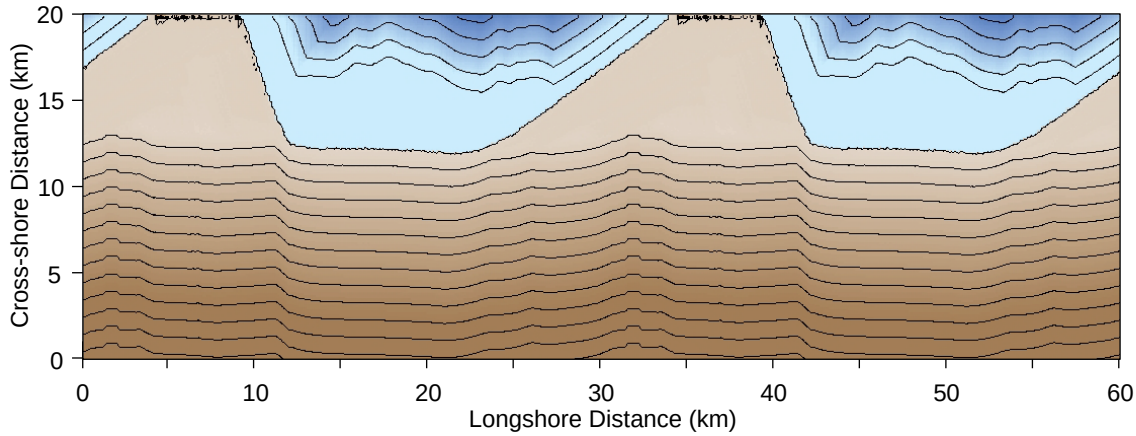

Figure 6.44 Morphology of the coastal system where the wave climate is defined by A = 0.5, U = 0.75, after 2,950 simulated years. The plot shows the remnants of previous cuspate forms in the bay of the existing features.

The identification of morphological memories in coastal systems is an important finding for several reasons. It shows that the bathymetric profiles, in particular, can provide evidence of previous coastal states, which in turn can infer historic environmental conditions (French *et al.*, 2015). Secondly, it supports the theory that the morphology and behaviour of a given coastal system may not be wholly representative of current environmental conditions, but may be influenced by historic conditions preserved in its memory (Wright and Short, 1984; French *et al.*, 2015). Finally, the bathymetric profile can influence a number of processes including sediment distribution, landform development and wave breaking processes (Masselink and Short, 1993; Nicholls *et al.*, 2012; Van Den Berg *et al.*, 2012; French *et al.*, 2015; Thomas *et al.*, 2016). Whilst it was not within the scope of this project to focus on wave breaking, it is an interesting and important topic for further work (see Chapter 8).

There is a growing interest in understanding the behaviour of coastal systems and the evolution of the nearshore due to its perceived influence on coastal

dynamics. Included in these studies should be the role of morphological memories, which are shown here to be a prevalent and persistent feature of the systems.

6.7.4 Performance of CEM2D

The evolution of both the beach profile and the bathymetry demonstrate the ability of CEM2D to simulate morphodynamics across the entire coastal profile, that has been enabled by the implementation of more complex sediment storage and handling techniques. The results show that the outputs of CEM2D are relatable to well-accepted theories of coastal profile evolution and to examples found around the shorelines of England and Wales and globally (Wright *et al.*, 1982c; Scott *et al.*, 2011). There are some limitations of the model in its ability to represent natural coastal behaviours due to parametrisation, the relatively simplistic representation of coastal processes and the presence of directional dominance in the sediment transport calculations. However, CEM2D (like CEM) is not designed to accurately represent any given system but to highlight patterns of evolution over meso spatiotemporal scales which the results presented here has demonstrated.

6.8 Conclusion

In this chapter, an analysis of how the coastal profile evolves according to the driving wave climate conditions is given. This work builds upon the findings of Chapter 5, which details the evolution of the shoreline shape as an individual entity using the same experimental set-up and wave climates as used in the previous chapter. The two-dimensional structure of CEM2D and its more complex sediment handling techniques enable the model to explore cross-shore and

longshore behaviours. This was not achievable in the one-dimensional CEM, as described in Chapter 3.

The results presented in this chapter have demonstrated the following key concepts:

- Shore-parallel contours and equilibrium coastal profiles fail to take into account the dynamic nature of the coastal profile, particularly the nearshore environment.
- The most active part of the cross-shore coastal zone is the lower beach, shoreline and upper nearshore to the seaward extent of morphological landforms. The complex sediment dynamics and morphodynamic evolution in these zones is an important component in how the systems behave and evolve; particularly in the upper nearshore.
- Typically, the dynamics and volumes of sediment transported in the active zone (as above) increases with increasing wave climate asymmetry (*A*) and the proportion of high angle waves (*U*). However, the behaviour of the systems are complex and results show that the behaviour of the systems are sensitive to the balance of cross- and longshore sediment transport
- Of further interest in future studies is the development of morphological memories in the nearshore bathymetry of coastal systems, which may be influencing their long-term evolution. The results show that remnants of previous morphological states are preserved in the nearshore environments, with their existence and location related to the dominance of cross- or longshore sediment transport and the rate of change in the systems.

- Demonstrated by the results of this chapter, CEM2D has shown to generate results that can be compared to published theories of profile change and to the behaviour and evolution of natural coastal systems.

This chapter has explored the morphodynamic behaviour of the two-dimensional coastal profile under twenty-five different wave climate conditions. In doing so, this chapter has addressed Research Objective 3 of this study:

> *"To investigate the topographic evolution of coastal systems, according to changes in environmental conditions, including the dynamics of the beach surface and nearshore profile under different wave climate conditions"* (see Chapter 2).

In the following chapter (Chapter 7), a change in water level is employed in CEM2D to explore the potential response of these environments to sea level change.

Chapter 7

Sea Level Rise:
A Driver of Change in Coastal Environments

Research Results

7.1 Introduction

In the previous two Chapters, the Coastline Evolution Model 2D (CEM2D) has been used to explore how coastal systems behave under different wave climate conditions and a fixed water level. Simulating the effects of a variable water level on coastal environments is an important function if we are to model the impact of climate change induced sea level rise on coastal evolution over meso-spatiotemporal scales (Schwartz, 2006; Masselink and Russell, 2013).

The aim of this chapter is to identify how the coastal systems behave when sea level rise is introduced into the system, in response to twenty-five different wave conditions (as per Chapter 5 and Chapter 6). The general experimental set-up used in Chapter 5 and Chapter 6 will be mirrored in this chapter (e.g. domain size, shoreline shape, coastal topography, wave climate conditions and so forth). In addition, the simulations will include two rates of water level change at 1 m and

2 m per 100 years, covering a range of predictions for future sea level rise (IPCC, 2013a). This includes an analysis of how the beach and nearshore profiles change and how rising water levels influence the evolution of landforms that develop along the shoreline.

The chapter will contribute to Research Objective 4 of this PhD thesis, as outlined in Chapter 2 and reiterated in the conclusion of this chapter in Section 7.8.

7.2 Climate Projections of Sea Level Rise

One of the most well-known and prominent effects of climate change on coastal systems is a change in the mean water level, or sea level rise (Masselink and Russell, 2013; Kopp *et al.*, 2014). As was observed over the past two centuries, the 21st century is likely to experience further increases in global mean sea level. Based on each of the RCP scenarios given in the Intergovernmental Panel on Climate Change's (IPCC) Fifth Assessment Report (AR5) (Figure 7.1), sea level projections up to 2100 have been formulated. These projections suggest that global mean sea level is likely to rise between 0.26-0.82 m by 2100 relative to 1986-2005 levels (Figure 7.1).

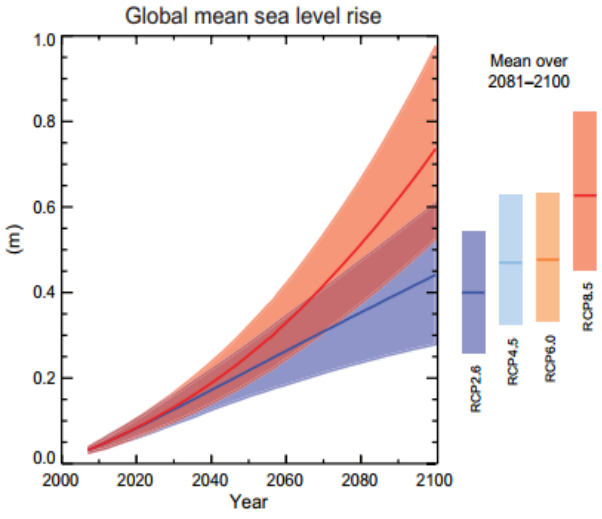

RCP	GMSLR
RCP2.6	0.26 – 0.55 m
RCP4.5	0.32 – 0.63 m
RCP6	0.33 – 0.63 m
RCP8.5	0.45 – 0.82 m

Figure 7.1 Predicted ranges of global mean sea level rise (GMSLR) (m) for 2081 - 2100, relative to 1986 – 2005 levels, according to each RCP scenarios (IPCC, 2013a, p. 24)

Sea level rise will not be felt consistently around the world. Spatial variations can be attributed to processes such as isostatic readjustment, the uneven distribution of ice mass wastage and a change in gravitational pull on the oceans by ice masses (Grinsted *et al.*, 2015). In a study of the UK's Climate Projections in 2009 (UKCP09) (Jenkins *et al.*, 2009), three sea level rise scenarios were generated to represent low, medium and high emissions. Each of the projections up to 2090-2099 and their 5th and 95th percentile ranges is presented in Table 7.1. An additional fourth scenario termed High++ (H++) was also calculated to represent a high risk but low probability projection for the UK that lies within scientific plausibility (Jenkins *et al.*, 2009; Lowe *et al.*, 2009). The H++ scenario gives an estimate for sea level rise of between 0.93-1.9 m (Lowe *et al.*, 2009).

Table 7.1 Estimates of UK mean sea level rise (m) for 2090 – 2099, relative to the period 1980 - 1999 (Lowe *et al.*, 2009, p. 27)

	5th Percentile	**Central Estimate**	**95th Percentile**
Low Emission	0.116	0.298	0.48
Medium Emission	0.131	0.369	0.607
High Emissions	0.154	0.456	0.758

Applying the high, medium and low scenarios to four locations around the UK generates slightly higher sea level rise projections than those given in Table 7.1 (Figure 7.2). This is due to more local factors which can influence changes in the water level, such as spatially variable salinity, water temperate and land movement (Jenkins *et al.*, 2009; Lowe *et al.*, 2009).

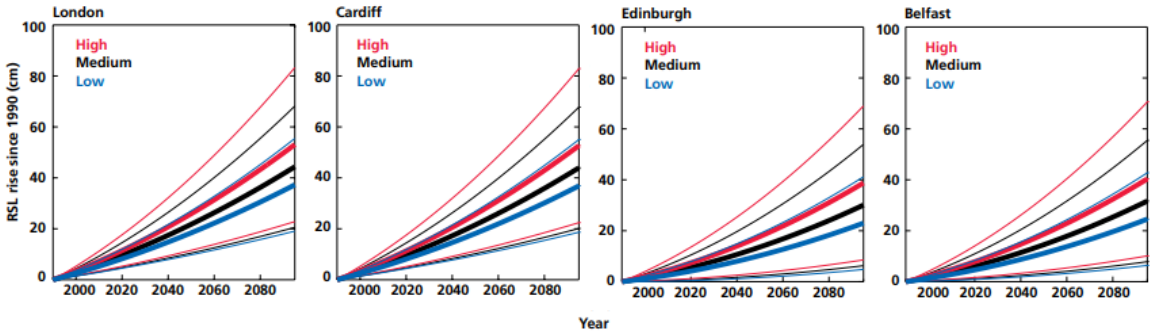

Figure 7.2 Relative sea level rise estimates over the 21st century for four cities in the UK under a high, medium and low emission scenario (2009, p. 51).

The range of sea level rise projections is a testament to the complexity of the systems at work and in the calculations. The cumulative effects of key processes, their varying inclusion in calculations and the different models and method of calculating change, as well as the natural variability and non-linearity in the systems can affect our ability to predict the behaviour of coastal systems and generate future sea level rise projections (Jenkins *et al.*, 2009; Grinsted *et al.*, 2015).

7.3 Sea Level Rise and Coastal Systems

Sea level rise, as predicted under the RCP scenarios (Figure 7.1), can affect hydrodynamic and sediment transport processes and cause a shift in behaviours in coastal systems (Kopp *et al.*, 2014; Ranasinghe, 2016). How this manifests is dependent upon site-specific environmental conditions and processes (Masselink and Russell, 2013).

It is suggested that 70% of all coastlines will experience sea level rise of within 20% of the global mean according to data given by the IPCC (Figure 7.1) (IPCC, 2013a). Komar (1991) suggested that beaches should be capable of ‘keeping pace’ with SLR over the long-term but that short-term variations in water level may not generate quasi-equilibrium states as the system takes time to adjust

(Masselink and Russell, 2013). The response is also likely to be non-linear, owing to the complex relationship between driving forces and each system will respond differently depending on the unique environmental conditions, sensitivities and resilience to change (Bray *et al.*, 1997). In general, however, coastal environments are likely to experience a change in shoreline position, erosion, submergence or progradation (Wong *et al.*, 2015).

7.3.1 Shoreline Position

It is generally accepted that along a vast majority of sandy coastlines, sea level rise will cause an increase in rates of coastal erosion, leading to shoreline recession (Dickson *et al.*, 2007; Bird, 2011). The EUROSION project commissioned in 2002 by the European Commission identified that of the 100,925 km of coastline around Europe, 15,111 km is eroding (EUROSION, 2004). More locally, it is predicted that around 28% of the coastline around England and Wales is rapidly eroding, at a rate of over 0.1 m per year (Evans *et al.*, 2004; Masselink and Russell, 2013). These figures are moderated, however, by the presence of defences which protect 45.6% of England's coastline (Masselink and Russell, 2013). Considering that not all defences can be or will be maintained into the future and not all will withstand sea level rise, the FutureCoast project predicted that approximately 67% of the coastline around England and Wales is vulnerable, with 20% likely to experience increased erosion rates in the future (Burgess *et al.*, 2004; Evans *et al.*, 2004). These figures are dependent upon the processes included in the calculations, future projections of sea level change and the level of protection afforded to given locations. It is clear to see from the data however that the general census is that coastal erosion and retreat of the shoreline is likely to be exacerbated by sea level rise (Dickson *et al.*, Walkden and Hall, 2007; Bird, 2011; Masselink and Russell, 2013).

The numerical study conducted by Dickson *et al.,* (2007) considered a range of climate change scenarios and management practices and further supported the concept that sea level rise is likely to significantly influence rates of coastal recession. The relationship between sea level rise and coastal recession is non-linear however due to the influence of other processes including increased water depth, wave breaking behaviours, sediment supply and feedbacks between coastal landforms as they independently and co-evolve (Bray and Hooke, 1997; Evans *et al.*, 2004; Dickson *et al.*, 2007). In some cases, Dickson *et al.,* (2007) noted that coastal progradation occurred in the simulated environment due to an increase in sediment supply from eroded material (Dickson *et al.*, 2007). Where there is a sufficient supply of sediment or there are protection works to artificially fix the shoreline, the coastline has the potential to remain static or prograde (Komar *et al.*, 1991; Bray *et al.*, 1997; Dickson *et al.*, 2007).

7.3.1.1 *The Bruun Rule*

One of the most commonly used methods of calculating the effect of rising sea levels on the geometry of sandy coasts is the Bruun Rule (Bruun, 1962, 1988). The rule advocates that as sea levels rise, landward ‘rollover’ will occur whereby the profile of the coast will be translated landwards and vertically upwards whilst retaining its geometric shape (Bruun, 1988). This is achieved through the erosion of sediment from the upper beach profile, which is deposited in the lower profile (Bruun, 1988; Cooper and Pilkey, 2004). The volume of material eroded equals the volume deposited in the nearshore, which increases the bed level at a rate concurrent with sea level rise (Komar *et al.*, 1991). The schematic in Figure 7.3 illustrates this process (Bruun, 1988; Komar *et al.*, 1991).

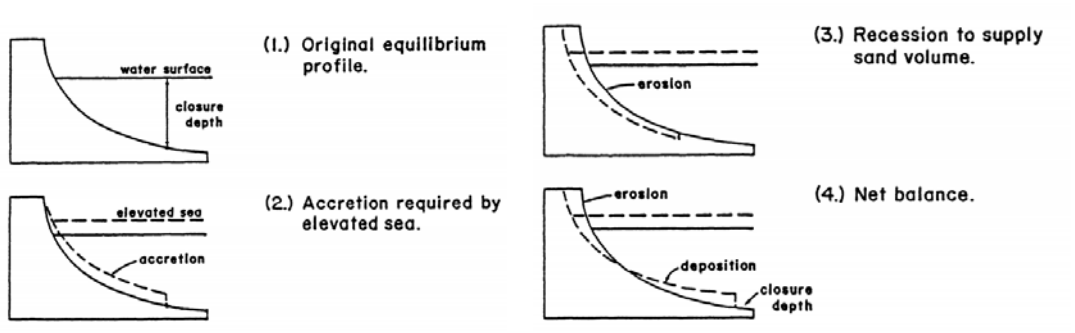

Figure 7.3 An illustration explaining the theory behind the Bruun Rule, given by Komar et al., (1991, p. 902).

The Bruun Rule is calculated using Equation 7.1:

$$R = LS \,/\, (B + h)$$

Equation 7.1

Where *R* is the horizontal recession distance, *L* is the horizontal distance from the shoreline to the depth of closure (*h*), *S* is the vertical sea level rise, *B* is the elevation of the eroded shoreline and *h* is the maximum depth of closure (Ranasinghe *et al.*, 2007). On average, according to this rule, the shoreline will retreat by approximately two orders of magnitude greater than the vertical sea level rise (Leatherman *et al.*, 2000, 2004; Wong *et al.*, 2015).

The Bruun Rule is extensively applied in coastal science and an abundance of applications can be found in the literature which supports the general concepts from which it is constructed (e.g. Schwartz, 1967; Leatherman *et al.*, 2000; Zhang *et al.*, 2004; Banno and Kuriyama, 2014). This includes, for instance, the numerical study of Banno and Kuriyama (2014) who show comparable results of shoreline retreat predicted along Hasaki's coastline (Japan) to estimations made by the Bruun Rule (Bruun, 1962).

Whilst the Bruun Rule is widely used to provide an order of magnitude estimation of coastal recession, there are several acknowledged limitations of its application. Criticisms include the Bruun rules omittance of cross-shore and longshore

sediment transport regimes, the requirement of a balanced sediment budget and assumed depth of closure, homogeneous geological conditions and an instantaneous response to changing environmental conditions (e.g. seasonal or storm conditions) (Bray and Hooke, 1997; Cooper and Pilkey, 2004; Dickson *et al.*, 2006). The Bruun rule can also only be used where the beach profile is in equilibrium, with only minor fluctuations around a mean slope angle (Bray and Hooke, 1997; Ranasinghe *et al.*, 2007). Applying the Bruun Rule to locations that are unsuitable based on the above-listed criteria can lead to either an overestimation or underestimation of shoreline recession (Ranasinghe *et al.*, 2007)

7.3.2 Coastal Flooding and Inundation

With climate change leading to sea level rise and a greater intensity of storms and storm surges, coastal flooding and inundation are likely to increase (Bray, Hooke and Carter, 1997). Submergence (or inundation) and flooding refer to similar, but distinct processes that are often used synonymously in the literature. The definitions of terms used in this thesis are taken from Flick *et al.,* (2012) who define “flooding” as the temporary covering of water onto usually dry land and “submergence” or “inundation” as the more permanent covering of water.

Rising sea levels can shift the location of the shoreline through erosional processes but also by inundating typically low-lying areas (Bray *et al.*, 1997). Further, submergence in the coastal zone can preserve its predeceasing morphologies, creating morphological memories[1] in the bathymetric profile. These preserved shorelines can be modified, reworked and removed by coastal processes over long time periods making them difficult to identify, but there are

[1] The concept of morphological memories was discussed in more detail in Chapter 6 of this thesis.

examples of their existence in nature (Shaw *et al.*, 2009). Shaw *et al.,* (2009), suggested that preserved historic shoreline morphologies are sparse, but are most likely to be found in marine waters that were previously freshwater lakes during the early Holocene. The authors give the example of the Bras d'Or Lakes in Nova Scotia, Canada that existed as a freshwater lake with a water level approximately 25 m below the present level. Shown in the multibeam bathymetry survey in Figure 7.4, the historic shoreline has been preserved in the bathymetry including features such as tombolos (A), spits (B), barriers (C, D) and barrier-enclosed lagoons (E) (see Section 7.3.3) (Shaw *et al.*, 2009).

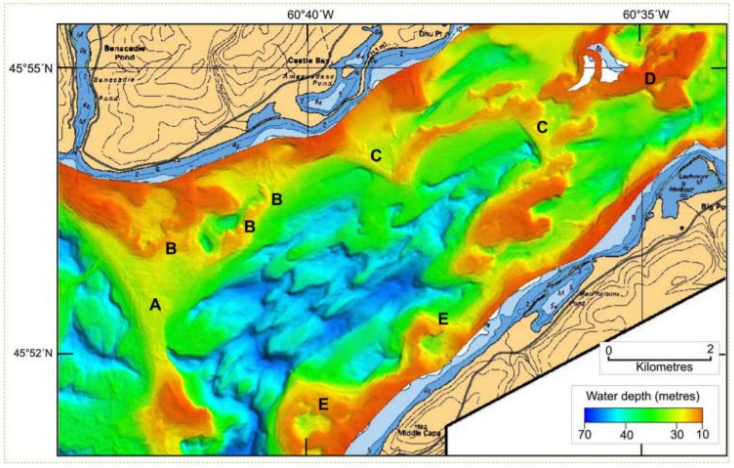

Figure 7.4 Multibeam bathymetry survey of East Bay in Bras d'Or Lake, Nova Scotia, showing submerged historic features including tombolos (A), spits (B), barriers (C, D) and barrier-enclosed lagoons (E) (Shaw *et al.*, 2009).

7.3.3 Landform Response

Coastal landforms (e.g. spits, bars, tombolos) are likely to be influenced by climate change and sea level rise (French and Burningham, 2013), but there is significantly less literature concerning the dynamics of coastal landforms compared to those which investigate the average profile of the coastline system and position of the shoreline. Much of the literature surrounding the influence of sea level rise on coastal systems cite the theory of equilibrium profiles and the work of Bruun (1962). As previously described, the Bruun Rule (Bruun, 1962) is

not designed to accommodate for cross-shore and longshore sediment transport. However, these processes are key to driving topographic changes in the coastal environment which can influence the behaviour of the systems (Mimura and Kawaguchi, 1997).

Considering previous research, there are three primary trains of thought into how depositional landforms may respond to sea level changes over mesoscales. Differing responses stem from the complex relationship between sea level change, coastal processes and landform morphodynamics, which are influenced by a host of environmental conditions such as the sediment budget and hydrodynamics. Depositional landforms could (1) migrate landward and keep pace with rising sea levels (2) prograde where there is a sufficient sediment supply (Komar *et al.*, 1991; Bray *et al.*, 1997; Dickson *et al.*, 2007; Jarmalavičius *et al.*, 2013), or (3) become submerged (Dickson *et al.*, 2007). These three responses reflect a balance between the rate of sea level rise and sediment supply, which determines the ability of the geomorphology to keep pace or adjust to the changing water level.

On a study of the response of the Curonian Spit, Lithuania, to sea level rise, Jarmalavičius *et al.*, (2013) suggest that the relatively slow rates of sea level rise (0.017 m per 100 years) observed between 1910-2010 had a marginal influence on the behaviour and development of the spit compared to processes such as longshore sediment transport. Around some sections of the feature, accretion and seaward progradation occurred due to sediment supply from longshore transport even though the sea level was rising. Whilst sea level rise played a role in coastal dynamics over the study period, it was not a significant player in comparison to, for instance, the supply of sediment and geological setting (Jarmalavičius *et al.*, 2013).

Conversely, Moore *et al.,* (2007) demonstrated that sea level rise was the primary factor in the evolution of Cape Hatteras (which forms part of the Carolina Capes) during the Holocene due to its influence on the sediment budget. The authors further predict that by 2100 under a high emissions scenario and relatively rapid rates of sea level rise, the barriers forming the tips of Cape Hatteras could be submerged.

The previously discussed example of the preserved historic shoreline in Bras d'Or Lakes (see Section 7.3.2), shows a combination of retreat and submergence processes. Initially, the response of the shoreline and depositional features, including spits and barrier, is to retreat at the rate of rising water levels. This is evidenced by the depth of landforms observed, located at 25 m below current sea level up to 10 m according to the data presented in Figure 7.4 (Shaw *et al.*, 2009). The authors suggest that landforms retreated with sea level rise until they could no longer keep pace and were hence, submerged. This submergence was induced by a lack of sediment supply to sustain the features and in the case of landform D (Figure 7.4), sediment starvation due to a disconnection from longshore sediment transport along the mainland shore (Shaw *et al.*, 2009).

7.4 Methodology

The methodology used in this chapter mirrors the experimental set-up used in Chapter 5. The reader is therefore referred to Chapter 5, Section 5.3 for a full explanation of CEM2D's initial set-up to compliment the brief overview given here.

Figure 7.5 (also Figure 5.9 in Chapter 5), shows the initial conditions used for the experiments in CEM2D. In Figure 7.6, the contours show the regular topographic and bathymetric profile of the coast at the start of each simulation.

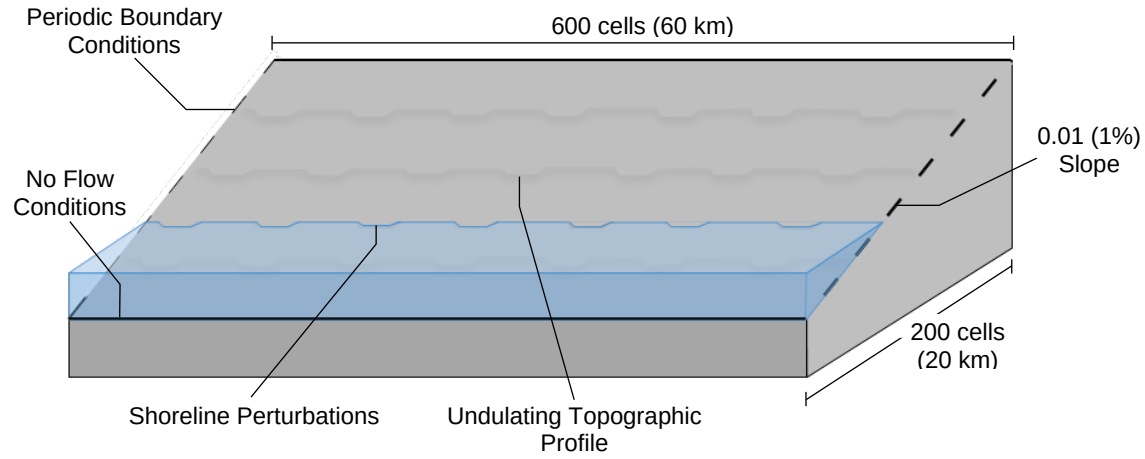

Figure 7.5 A schematic of CEM2D's model set-up and initial conditions used for simulations presented in this chapter.

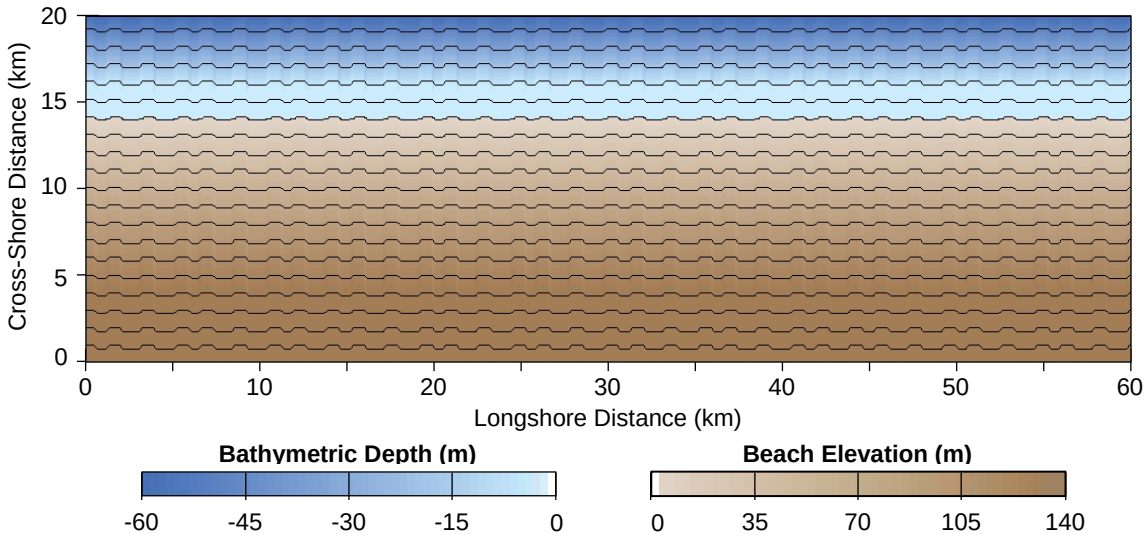

Figure 7.6 Initial Conditions of all simulations presented in this Chapter, showing bathymetric and topographic profile with 10 m contours.

A total of twenty-five simulations were run under different wave climate conditions using a four binned Probability Distribution Function (PDF) which defines the proportion of high angle waves (*U*) and the wave asymmetry (*A*). Table 7.2 (also Table 5.1 in Chapter 5) lists the wave climates used for each simulation. The wave period is kept consistent at 8 s, the wave height at 1.7 m.

Table 7.2 Wave climate ensembles used to investigate the influence of wave climate conditions on coastal morphodynamics according to the wave climate asymmetry (A) and proportional highness of waves (U).

Run Number	Asymmetry (A)	High Angle (*U*)	Run Number	Asymmetry (A)	High Angle (*U*)
1	0.5	0.55	**14**	0.8	0.65
2	0.6	0.55	**15**	0.9	0.65
3	0.7	0.55	**16**	0.5	0.7
4	0.8	0.55	**17**	0.6	0.7
5	0.9	0.55	**18**	0.7	0.7
6	0.5	0.6	**19**	0.8	0.7
7	0.6	0.6	**20**	0.9	0.7
8	0.7	0.6	**21**	0.5	0.75
9	0.8	0.6	**22**	0.6	0.75
10	0.9	0.6	**23**	0.7	0.75
11	0.5	0.65	**24**	0.8	0.75
12	0.6	0.65	**25**	0.9	0.7
13	0.7	0.65			

The primary purpose of this chapter is to investigate how a changing water level influences the behaviour and evolution of coastal systems (see Section 7.1). Therefore, we chose two rates of sea level rise based on contemporary research. A maximum value of 2 m sea level rise over 100 years was selected according to the H++ scenario of UKCP09, which defines a low probability but high-risk projection for the UK (Jenkins *et al.*, 2009; Lowe *et al.*, 2009). This exceeds the projected global values published by the IPCC (IPCC, 2013a) but remains within a plausible range. A lower rate of 1 m per 100 years was also used, as an intermediate range.

The maximum runtime of the simulations is set at 1095000 iterations to represent 3,000 years, with the rate of water level change kept consistent at a per 100-year configuration. As stated in Chapter 5, this run duration gives sufficient time for the model to spin up, to reduce the potential influence of initial conditions and to allow each of the coastal systems to reach a dynamic equilibrium according to the driving wave climate conditions. Whilst this is significantly longer than required for a mesoscale study, the results are analysed in terms of mesoscale behaviours and are used to highlight patterns of evolution over these centennial scales; it is not intended or advised that the results be used to analyse coastal systems over millennia. Furthermore, when applying a rate of sea level rise of 1 m per 100 years, according to a simplistic Bruun Rule calculation the shoreline would be predicted to recede by approximately 100 m (Bruun, 1962; Leatherman et al., 2000, 2004; Wong et al., 2015) constituting a single cell in the set-up conditions used for CEM2D in this study. By running the model for a longer period and applying a consistent rate of sea level rise per year, the response of the coastal system to a rising water level becomes more apparent and can be used to highlight rates and patterns of recession. This is important since investigating the

behaviour of coastal environments under a rising sea level over mesoscales is imperative for informing suitable and sustainable management decisions.

7.5 The Evolution of the Coastal Profile under Sea Level Rise

In this chapter, sea level rise results are directly compared against identical simulations but without sea level rise discussed in Chapter 5 and 6. The ensemble plot in Figure 7.7 (see also Appendix 7 for an enlarged print) shows final coastal morphologies for each of the twenty-five simulations listed in Table 7.2, with and without sea level rise at a rate of 1 m per 100 years and in Figure 7.8 (see also Appendix 7 for an enlarged print) with a rate of 2 m per 100 years. An outline is drawn around each pair of simulations to highlight matching sets according to the wave climate, but which differ in water level state. Each output that is shown in Figure 7.7 and Figure 7.8 measures 20 km cross-shore and 30 km longshore (exclusive of periodic boundaries) but for the subsequent analysis, the entire 60 km long system is used in the calculations.

Along the x-axis, the proportional asymmetry (*A*) of the wave climate increases from 50% to 90% (0.5-0.9) of waves approaching from the left of the domain and along the y-axis, the proportion of high angle waves (*U*) approaching the shoreline increases from 55% to 75% (0.55-0.75). Contour lines and isobaths are drawn at 10 m intervals from the water line; in each of the simulations with sea level rise the elevation data has been normalised so that the water level is at 0 m. The colour gradients remain consistent across each set of simulations with and without sea level rise.

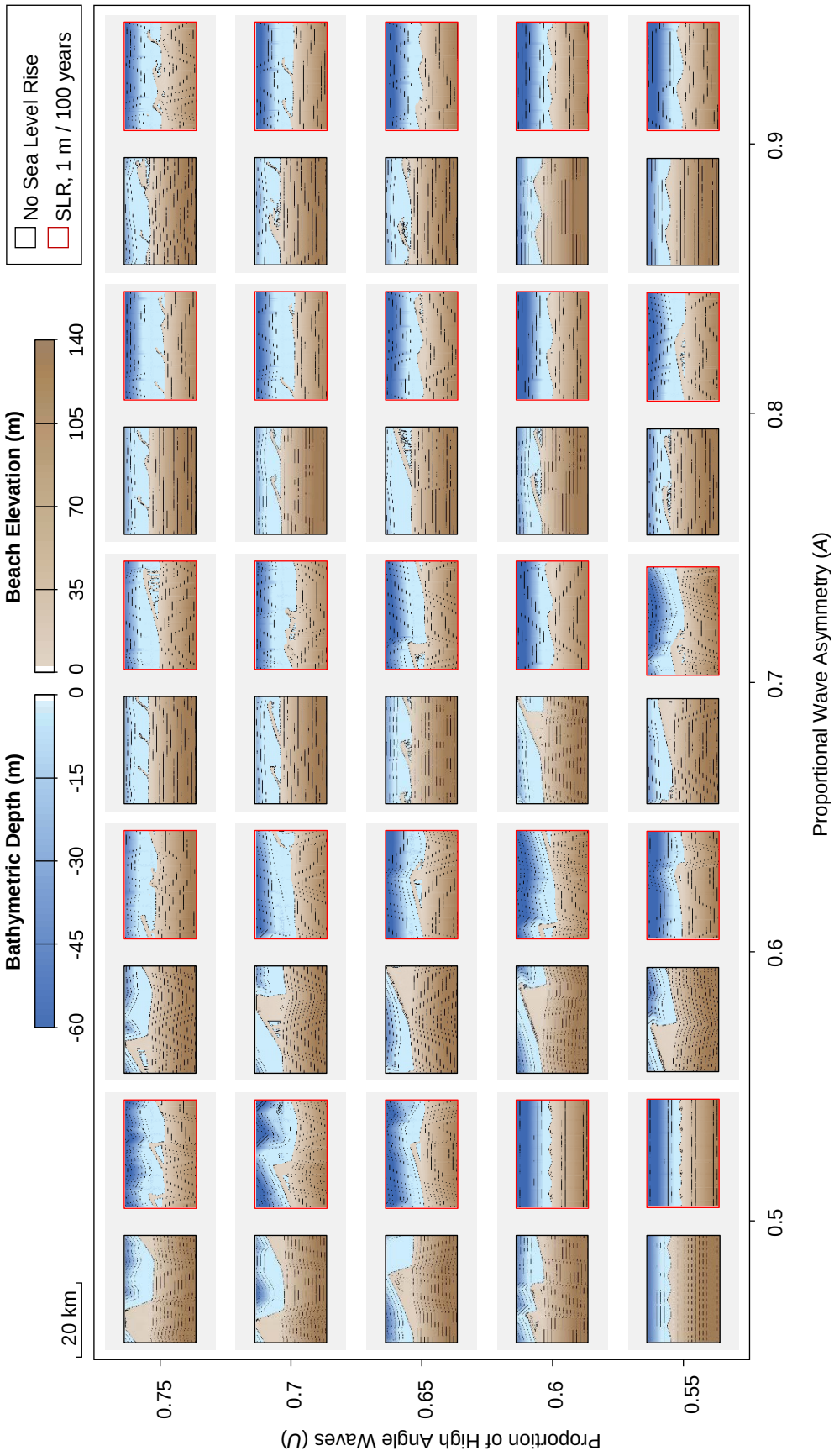

Figure 7.7 A matrix of results from CEM2D showing final shoreline morphologies as a function of the wave angle asymmetry (A) and proportion of high angle waves (U), with a static water level (black outline) and 1 m sea level rise per 100 years (red outline)

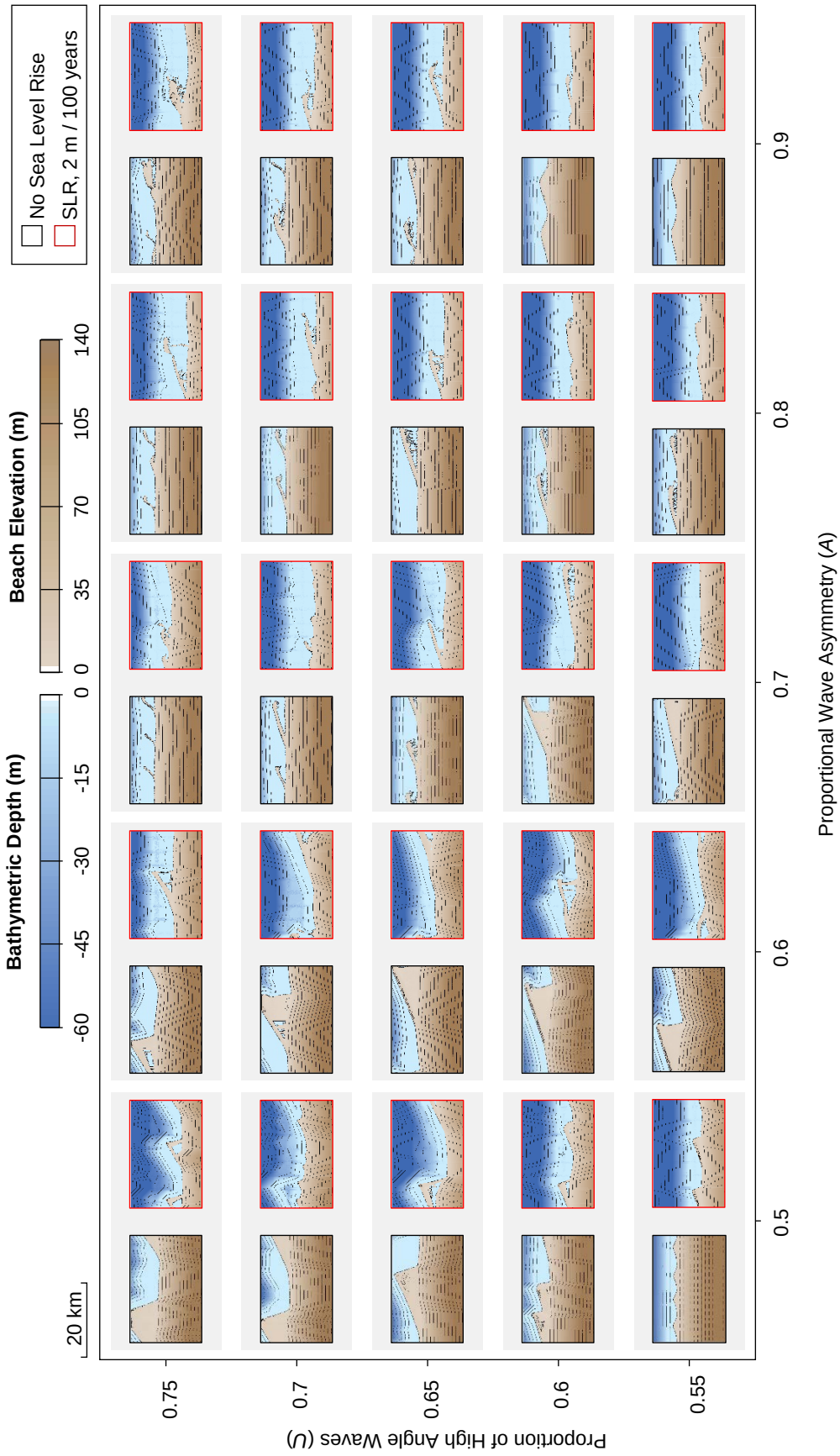

Figure 7.8 A matrix of results from CEM2D showing final shoreline morphologies as a function of the wave angle asymmetry (A) and proportion of high angle waves (U), with a static water level (black outline) and 2 m sea level rise per 100 years (red outline)

Not all simulations run for the specified 3,000 year time period. This primarily occurs when the shoreline search technique (see Chapter 3) is unable to locate a continuous shoreline and therefore, carry out the longshore sediment transport processes. This arises most commonly where the shoreline shape is complex and where features extend beyond the bounds of the domain in the cross-shore direction. Premature termination of the model has been discussed previously and is addressed in more detail in Chapter 8.

A comparison of the run duration for each simulation with 0 m, 1 m and 2 m sea level rise every 100 years is given in Figure 7.9. The data shows that the greater the wave asymmetry (*A*) and proportion of high angle waves (*U*), the shorter the run duration regardless of the water level state. However, the data also shows that the run duration tends to be longer with increasing rates of sea level rise, particularly where the wave asymmetry is greater. With the continual shift in the location of the shoreline, the likelihood that a continuous shoreline will be detected by the search technique increases.

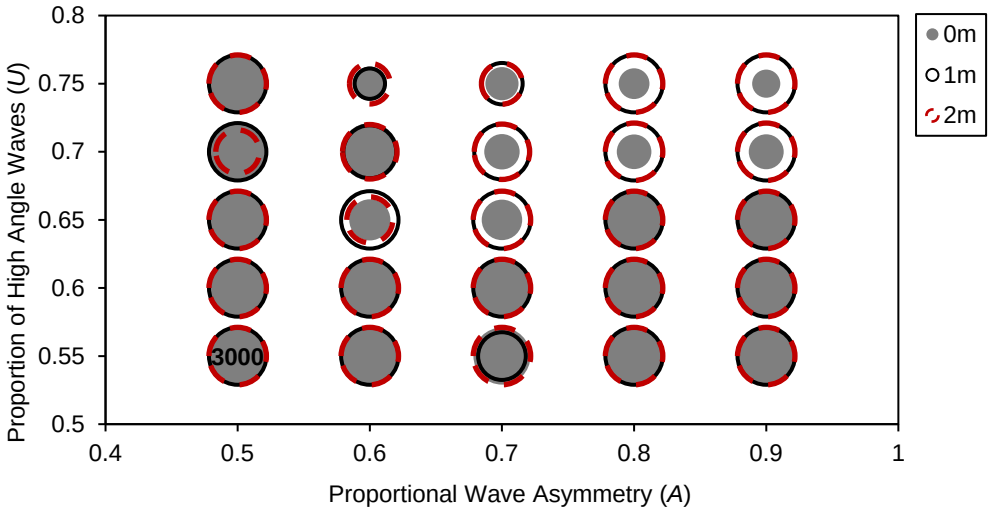

Figure 7.9 The relative run durations of each simulation with 0 m, 1 m and 2 m sea level rise per 100 simulated years, for the twenty-five wave climate scenarios. The area of the scatter points denotes the runtime, with larger circles representing longer runtimes to a maximum of 3,000.

The majority of simulations where the rate of sea level rise is at 1 m per 100 years run for the specified 3,000 year time period. Only five simulations terminate prematurely, but each of these still has run durations greater than 1,500. For a rate of rise of 2 m per 100 years, only six runs are below 3,000 years with all except where A = 0.6, U = 0.75 which again runs for at least 1,500 years.

As has been noted in previous chapters, the highly dynamic nature of the coastal profiles in some simulations means that the final morphologies given in Figure 7.7 and Figure 7.8 are not representative of the entire simulation. This is considered in the subsequent analysis, where the evolution and general behaviour of the coastal environments are considered. In Section 7.6 a more detail investigation into the temporal behaviour of the shoreline over the simulation periods is also given for four shoreline types.

A brief analysis of the results presented in Figure 7.7 and Figure 7.8 shows overall that similar patterns are observed in the evolution of the coastal systems according to the driving wave conditions, with and without sea level rise. The types of morphological features that form are comparable, categorised as cusps, sand waves, reconnecting spits and flying spits. The same relationship is observed as was described in Chapter 5 and Chapter 6, in that the asymmetry (A) of the wave climate influences the longshore skew of morphological features and the proportion of high angle waves (U) influences cross-shore sediment transport and the amplitude of features. There are, however, some interesting differences between simulations that are explored in the following sections.

7.5.1 Shoreline Shape and Coastal Morphology, with Sea Level Rise

Where the wave climate is symmetrical (A = 0.5), cuspate features form where the water level is static and where the sea level rises at a rate of 1 m or 2 m per

100 years (Figure 7.7 and Figure 7.8). Cusps which form where A = 0.5 and U = 0.55-0.65 are larger when formed under a rate of sea level rise of 2 m per year than 1 m per year, but are smaller with greater values of U.

The topographic and bathymetric profiles show similar patterns of evolution for all three water level scenarios (0 m, a rise of 1 m and 2 m per 100 years) where the wave climate is symmetrical (A = 0.5, U = 0.55-0.75). Where the amplitude of the cusps is relatively small at low values of U (0.55), the contours are planar and form gradually sloping profiles offshore. With higher values of U, the contours increasingly reflect the shape of the shoreline; this is more prominent in the bathymetric profile than across the beach surface, which gently undulates. Remnants of previous cuspate features along the shoreline are preserved in the bathymetry (particularly within the bay of larger landforms), in simulations with and without sea level rise.

With some asymmetry in the wave climate (A = 0.6, U = 0.55-0.75), sand waves form along the shoreline with and without sea level rise. With increasing rates of sea level rise and proportions of high angle waves (U), the features resemble reconnecting and flying spits as the landforms become submerged (Figure 7.7 and Figure 7.8). The updrift edge of the landforms is observed to have the highest elevation across the sand waves and remain above the water level as it rises, to create features which resemble reconnecting and flying spits. The contours of the beach and nearshore profile largely reflect the shape of the shoreline (where A = 0.6) but also store morphological memories where rates of sea level rise are 2 m per 100 years. Where rates of sea level rise are lower at 1 m per 100 years or the water level is static, shallow bays form between the shoreline features and morphological memories are not found as readily.

Where *A* = 0.7, a gradual transition is observed from sand waves to reconnecting and flying spits, with an increasing proportion of high angle waves (*U* = 0.55-0.75) (Figure 7.7 and Figure 7.8). Where the rate of sea level rise is 2 m per 100 years the transition between states occurs at lower proportions of high angle wave (*U*), than observed at a rate of 1 m per 100 years or for a static water level; sand waves form at *U* = 0.55, reconnecting spits at *U* = 0.6 and flying spits at *U* = 0.65. Thereafter, irregular flying spits form along the shoreline as the features are submerged and reform, with the influence of remnant morphologies. Irregular forms are also found under rates of sea level rise of 1 m per 100 years where the wave climate is defined by *A* = 0.7, *U* = 0.7. Under these wave climate conditions, the coast is highly dynamic and the outputs in Figure 7.7 and Figure 7.8 only represents a single moment during the transition from one landform state to another. The profile of the nearshore zone increasingly mirrors the shape of the shoreline with greater rates of sea level rise but are also influenced by remnant morphologies.

It was suggested in Chapter 5 that with a high asymmetry in the wave climate and only a slight dominance of high angle waves (*A* = 0.9, *U* = 0.55-0.6), the strong longshore current generated can drive sediment longshore and prevent the formation of features with significant amplitude. Where the coast is subject to sea level rise this effect is found with lower wave asymmetry (*A*) values: *A* = 0.8 with a rate of sea level rise at 1 m per 100 years and *A* = 0.7 at 2 m per 100 years. It is suggested therefore that the submergence of features by the increasing water level influences the ability of features to develop and sustain and the balance of the sediment budget. Under these wave climate conditions, the topography and bathymetric profiles are largely smoothed to create a gradual slope offshore.

Increasing the value of *A* further to 0.8-0.9 and with higher values of *U* between 0.65-0.75 leads to the formation of reconnecting and flying spit (with an without a rising sea level) (Figure 7.7 and Figure 7.8). For each of the water level scenarios, with increasing values of *U,* the spits show a greater irregularity in terms of their morphology, with increasing width of the neck of the spit, erratic sediment paths and isolated sediment deposits. With increasing values of *U,* the bathymetric contours increasingly mirror the shape of the shoreline regardless of whether sea level rise is employed in the simulations.

7.5.2 Cross-Shore Profile and Sea Level Rise

According to the results of seventy-five simulations (twenty-five wave climates and three water level scenarios), the average shape and morphology of the cross-shore coastal profiles are given in Figure 7.11. The results are averaged from the twenty-five different wave climate scenarios (see Section 7.4) where the water level is static (no sea level rise: NSLR) and where the coastal systems are subject to sea level rise at a rate of 1 m and 2 m per 100 years.

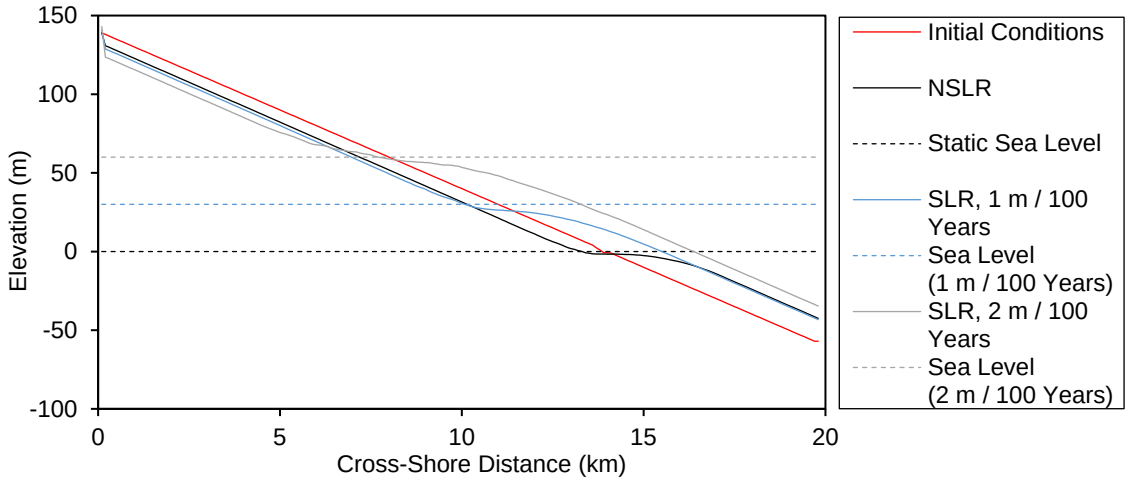

Figure 7.10 Average change in the cross-shore morphology of the simulated coastal system according to two rates of sea level rise and a base level simulation with no sea level rise (NSLR), calculated from results of seventy-five simulations. Also indicated on the plot is the location of the water level for each of the three sea level rise scenarios.

Using the average change in the cross-shore profiles with no sea level rise as a baseline (previously explored in Chapter 6), the results in Figure 7.10 show that the coast moves further landwards and upwards in response to an increase in the water level. This is achieved through the erosion of the beach and the deposition of material in the nearshore. This evolution was observed in Chapter 6 as the systems evolve from the initial shoreline position, but which is enhanced with sea level rise.

To further explore the morphological response of the coastal profile to a changing water level, the results of each simulation with varying wave climate conditions are analysed. Figure 7.11 and Figure 7.12 show the cross-shore profile of each simulated coastline according to differing wave asymmetries (*A*) and proportions of high angle waves (*U*), where the rate of sea level rise is 1 m and 2 m per 100 years respectively. The profiles are shown in three-dimensional form in Figure 7.13 and Figure 7.14 for rates of sea level rise of 1 m and 2 m per 100 years respectively. These results can be compared to the profiles given in Chapter 6, in Figure 6.16 and Figure 6.17, according to a static water level. Consistent with Chapter 6, each transect was recorded across sections of the coastal profiles where the cross-shore position of the shoreline represents the average location for the given simulation and time step. This means that the profile is not influenced by dynamic and migratory features that form along the shoreline. Unlike in Figure 7.10, the data in Figure 7.11 to Figure 7.14 has been normalised to align the water level for each of the simulations to 0 m. This processing allows the results to be compared, with model run durations in mind, in terms of how the shape of the cross-shore profiles evolves.

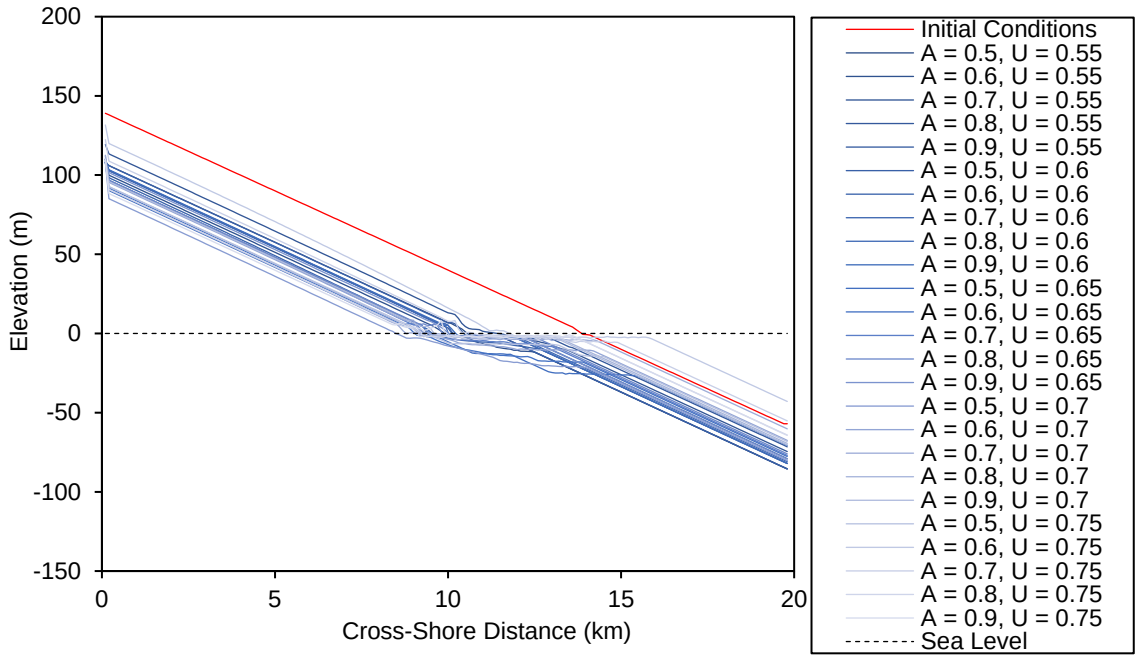

Figure 7.11 Cross-shore profiles taken for each of the twenty-five simulations shown in 2D, with a rate of sea level rise at 1 m per 100 years. The data has been normalised so the water level for each simulation is represented as 0 m.

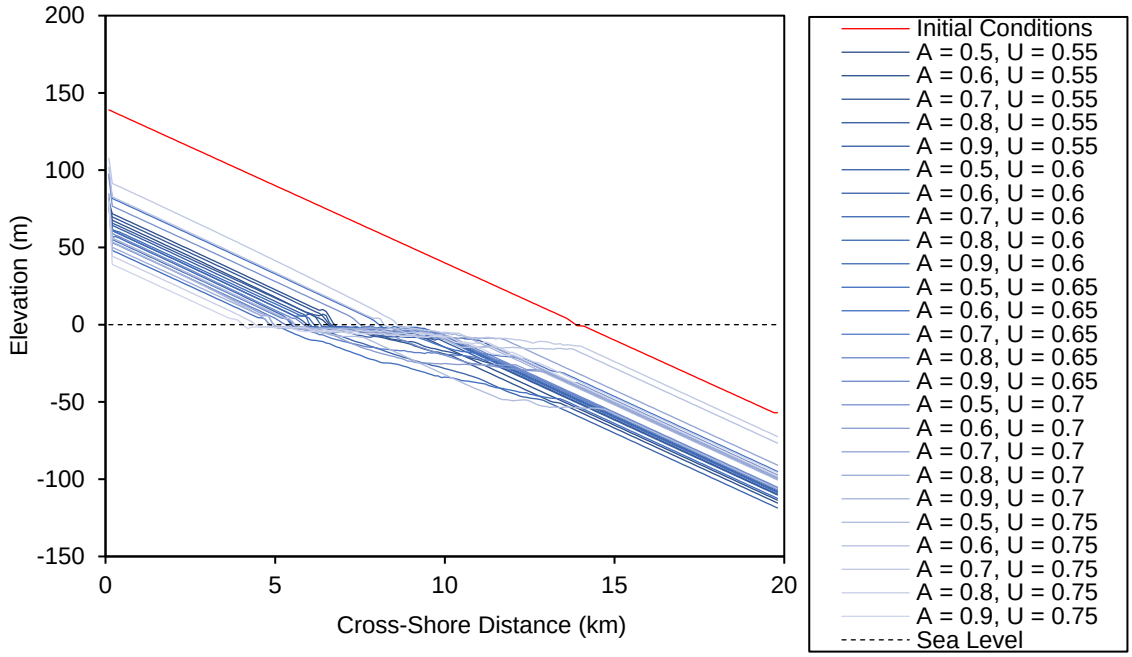

Figure 7.12 Cross-shore profiles taken for each of the twenty-five simulations shown in 2D, with a rate of sea level rise at 2 m per 100 years. The data has been normalised so the water level for each simulation is represented as 0 m.

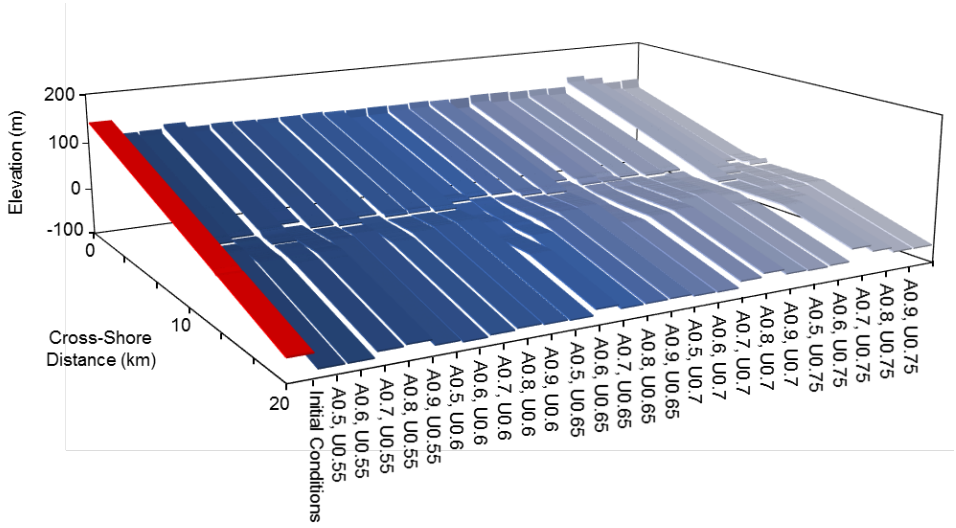

Figure 7.13 Cross-shore profiles taken for each of the twenty-five simulations shown in 3D, with a rate of sea level rise at 1 m per 100 years. The data has been normalised so the water level for each simulation is represented as 0 m, with water level shown as a white band across the transects.

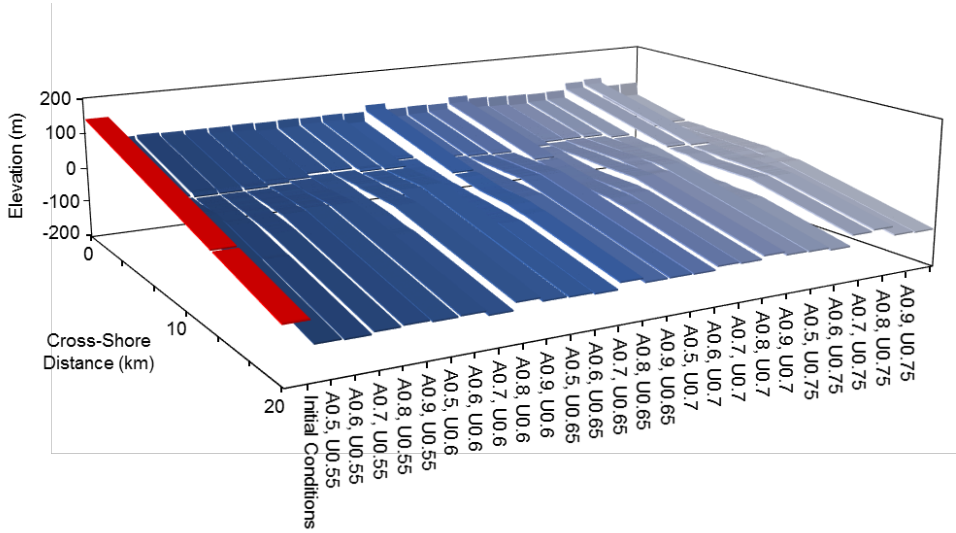

Figure 7.14 Cross-shore profiles taken for each of the twenty-five simulations shown in 3D, with a rate of sea level rise at 2 m per 100 years. The data has been normalised so the water level for each simulation is represented as 0 m, with water level shown as a white band across the transects.

The morphologies of the cross-shore coastal profiles shown in Figure 7.11 to Figure 7.14 are comparable across the varying wave climate conditions and rates of sea level rise. All coastal systems recede, but increasingly so with higher rates of sea level rise, although an average slope of 0.01 is maintained across the entire profile. A shallow nearshore shelf forms in the upper nearshore zone in each of the coastal environments for both rates of sea level rise, but to varying widths (see Section 7.5.2.2). There are no clear outliers or variations in the

response of the cross-shore coastal profile to sea level rise in terms of the shape of the profile, but the amount of material moved or redistributed differs.

The volume stacks in Figure 7.15 shows the average change (per year) in the volume of sediment in each cell across a transect, where x = 30 km, for each of the seventy-five simulations. The morphology plot at the top of the figure denotes the location where the transect is taken (shown by the red box, according to the initial conditions) and the table details the wave climate conditions for each individual volume stack (Figure 7.15). Within the volumes stack, each of the numbered sections segments five results with a single value of the proportional wave climate asymmetry (*A*) and proportions of high angle waves (*U*) from 0.55 to 0.75. For instance, segment '1' contains results where the water level is static and the wave climate conditions are defined by a wave asymmetry (*A*) of 0.5 and the proportion of high angle waves (*U*) increases from 0.55-0.75 (at increments of 0.05) from the left to the right of the section.

It is important to note that each transect in Figure 7.15 is a sum of average changes in each cell's elevation where x = 30. It can therefore only be used to analyse relative total changes in sediment volume for the entire run and not to infer the most dynamic areas of the profile. For an analysis of the most dynamic areas, temporal changes should be plotted (see Figure 7.16). To exemplify this point, in Figure 7.16 the most dynamic area of the profile is at the location of the shoreline, which in Figure 7.15 shows the lowest net change. This is because this zone fluctuates between erosional and depositional behaviours which are nullified when totalled in the volume stacks in Figure 7.15.

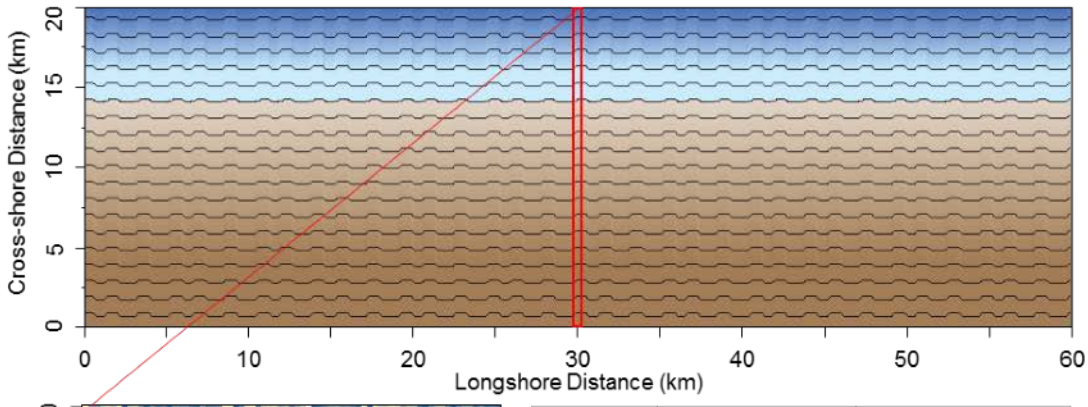

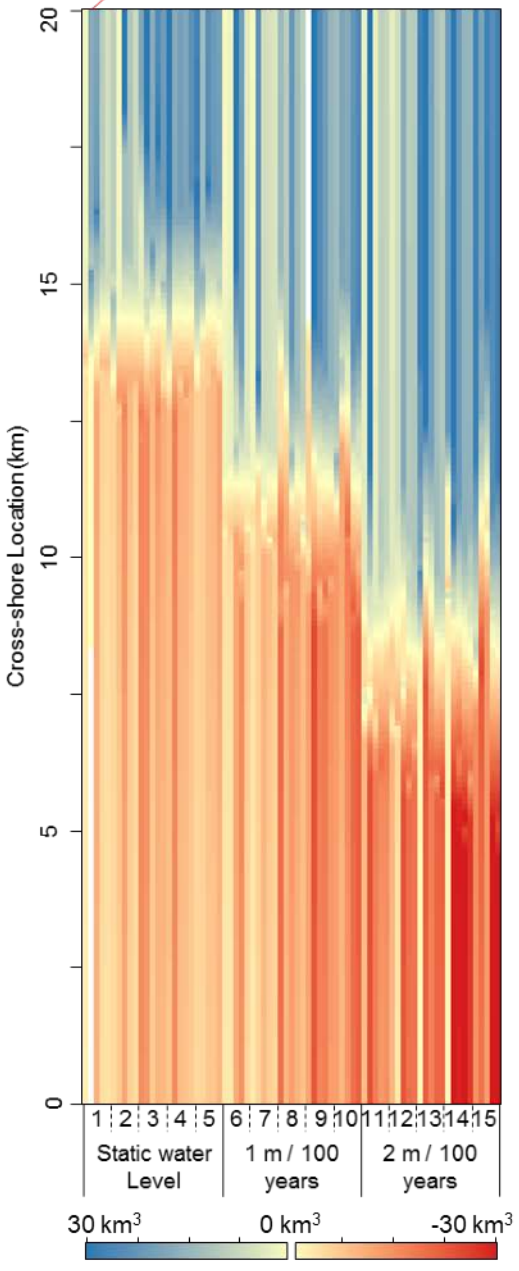

Run No.	Value *A*	Values *U* *(left to right)*
1	0.5	0.55
6		0.6
11		0.65
2	0.6	0.7
7		0.75
12		0.55
3	0.7	0.6
8		0.65
13		0.7
4	0.8	0.75
9		0.55
14		0.6
5	0.9	0.65
10		0.7
15		0.75

Figure 7.15 Volume stack showing the sum of average changes in the elevation throughout the simulation (recorded every 30-year intervals), for each cell in a single transect across the coastal profile (where x = 30 km, denoting in the morphology plot, top). Results are shown for each twenty-five wave climate conditions and for a static water level and two rates of sea level rise. The table (right) details the wave climate conditions for each of the fifteen blocks in the volume stack (left), according to the proportional asymmetry (A) and proportion of high angle waves (U).

The volume stacks in Figure 7.15 illustrate that the interface between the predominantly eroding beach surface and accretional nearshore profile shifts as the water level rises. With the increasing rate of sea level rise, there is an increase in average erosion across the beach surface, deposition in the nearshore and shoreline recession. This correlates with findings in Section 7.5.2 and Figure 7.10 which show the landward and upward movement of the cross-shore coastal profile with sea level rise. The erosional and depositional patterns are not significantly influenced by the proportion of high angle waves (*U*) approaching the shoreline, but a correlation is shown between increasing wave asymmetry and increasing sediment mobility across the profile. It was observed in Chapter 6 that recession of the shoreline from the reworking of sediment from the initial conditions decreases with increasing value of *A*, which as shown in Figure 7.15 can be attributed to the high flux and mobility of sediment under these wave climate conditions.

To explore the evolution further, the profiles given in Figure 7.11 to Figure 7.14 are examined in more detail subsequently. The profiles are analysed according to more specific changes in the beach surface and the nearshore profile as individual sections of the system.

7.5.2.1 *Beach Profile*

Figure 7.11 to Figure 7.14 show that the beach surface maintains an average slope of 0.01 (1%) regardless of the driving wave conditions or rates of sea level rise. This section of the profile shows negligible morphodynamics compared to the nearshore (see Section 7.5.2.1) even when subject to rising water levels. This supports the findings drawn from Figure 7.7 and Figure 7.8, which show that the beach surface tends to smooth and become planar throughout each of the simulations. Beach profiles for each of the runs (Appendix 8) further demonstrate

that in general, the profiles retain an average slope of 0.01. These results are comparable to those in Chapter 6, which showed minimal change in the dynamics of the beach surface under the same wave climate conditions, but with a static water level.

7.5.2.2 *Nearshore Profile*

The plots in Figure 7.11 to Figure 7.14 show that the nearshore profile and particularly the upper nearshore are the most dynamic areas of the coastal system. This is further illustrated in the volume stack in Figure 7.16 showing results where the rates of sea level rise are 1 m and 2 m per 100 years and are driven by a wave climate where A = 0.7, U = 0.65 (see Appendix 9 for volume stacks for each of the simulations). The evolutionary behaviour and morphology of this section of the coast are comparable to the results found in Chapter 6 under a no sea level rise scenario.

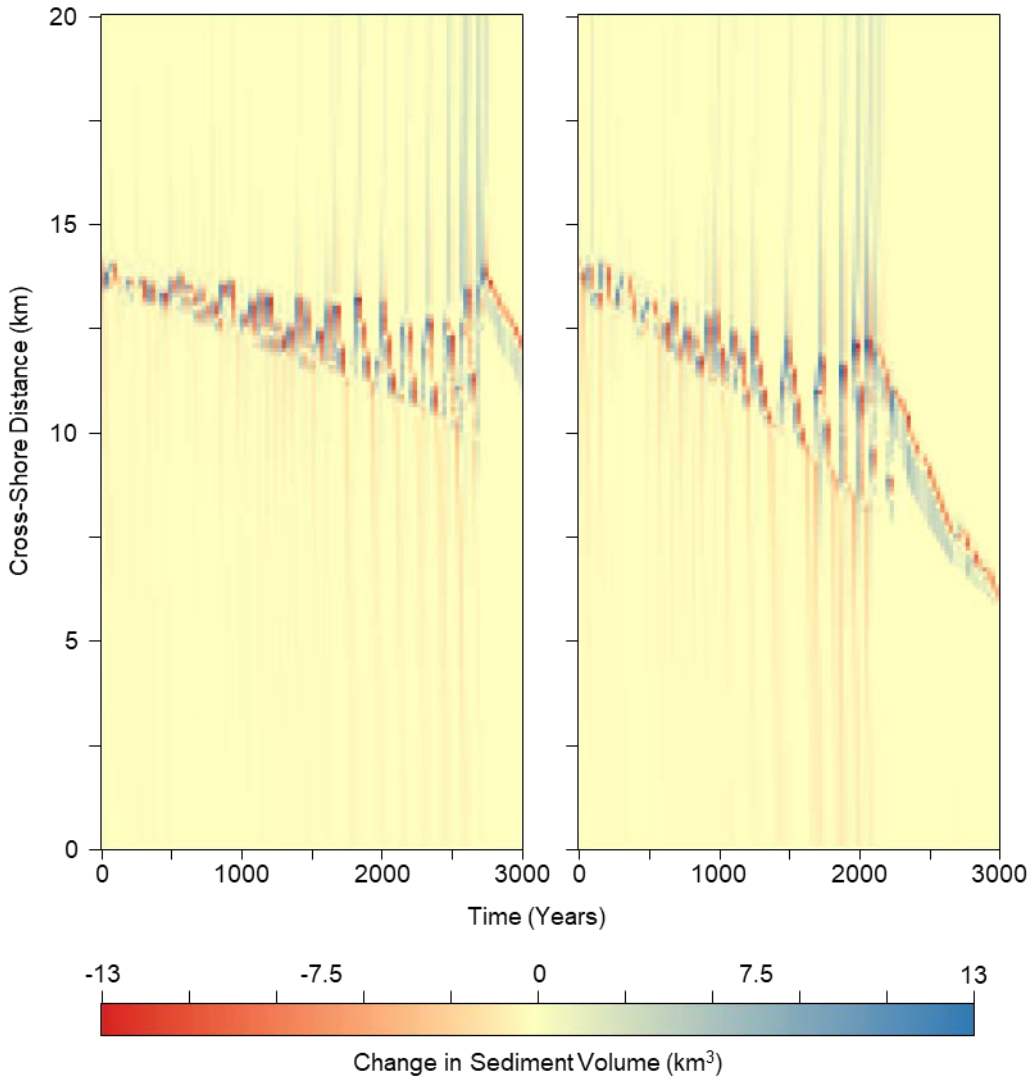

Figure 7.16 Volume stacks showing changes in sediment volume (km^3) across a transect (where x = 30 km and recorded at 30 year intervals) where A = 0.7, U = 0.65. The rates of sea level rise are (a) 1 m per 100 years and (b) 2 m per 100 years.

The average slope of the nearshore profile shows a decreasing angle over time, according to the combined results of all seventy-five simulations (Figure 7.17). The rate and extent to which the profile shallows, decreases with higher rates of sea level rise; systems subject to higher rates of sea level rise tend to show steeper profile. This is because, as the water level rises and shifts the location of the shoreline and cross-shore zone of active sediment transport, the deposited material is distributed across a wide area and does not cause a build-up of sediment in one area to the same extent as where there is no sea level rise. Where the water level is static the sediment transport processes act largely within

a fixed cross-shore section of the coastline which leads to the accumulation of material and shallowing of the profile. This effect is more greatly observed with an increasing dominance of high angle waves (*U*) (Figure 7.17). Fluctuations around the average slope angle of the nearshore profile are greater where the wave climate is highly asymmetric (*A*) and dominated by high angle waves (*U*), due to dynamic behaviour of landforms and the migration of features longshore (Figure 7.17).

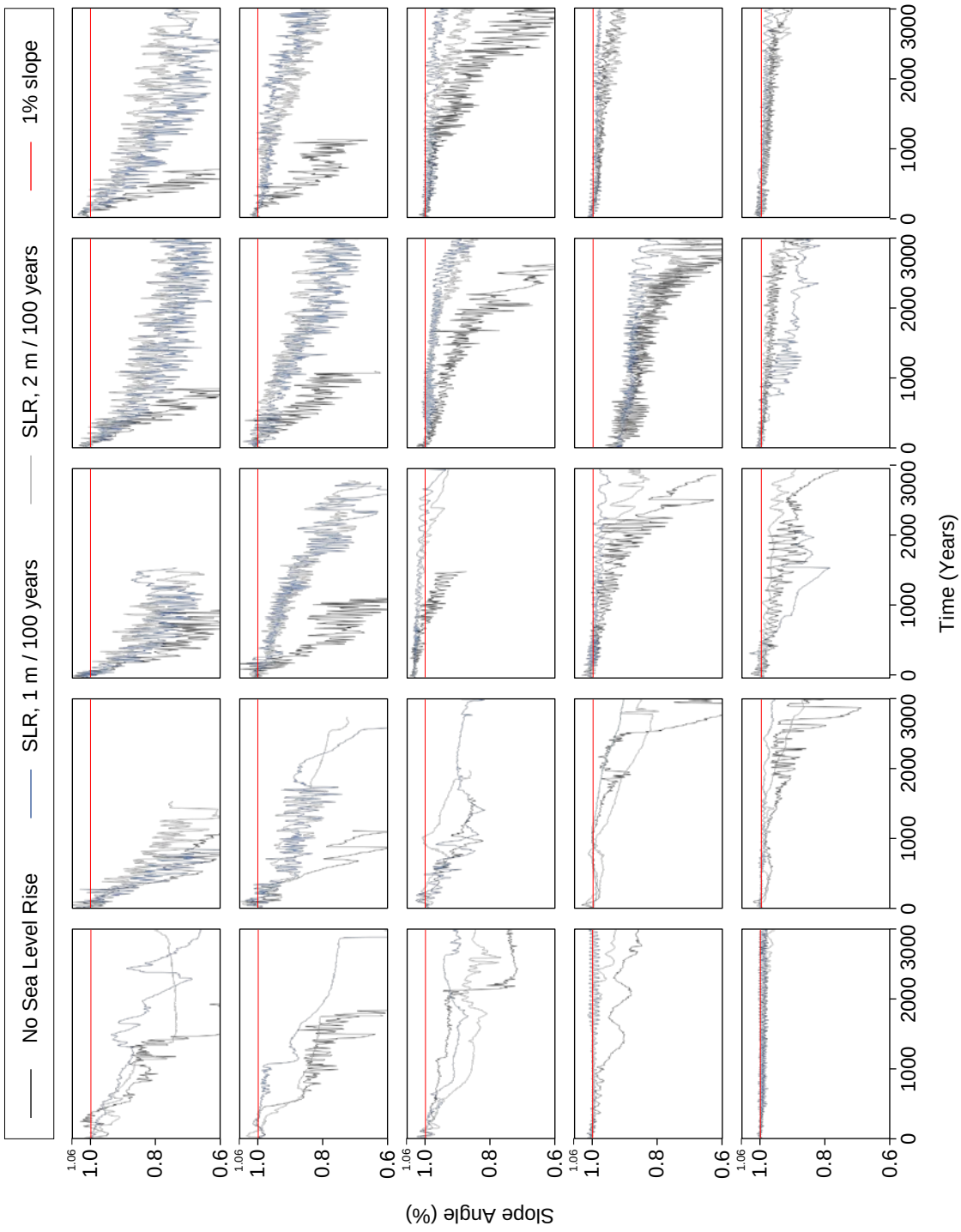

Figure 7.17 Ensemble plot showing the average cross-shore slope of the nearshore profile over the duration of the simulations, driven by twenty-five different wave climate conditions. Results are given from three sea level rise scenarios, including rise rates of 1 m and 2 m per 100 years as well as a no sea level rise state.

The shallowing of the nearshore profile is influenced by the formation of a shelf in all simulated environments, as cited previously (Figure 7.11 to Figure 7.14). The three plots in Figure 7.18 show the relationship between the shelf width and shoreline recession distance for each wave climate condition and averaged

according to the total run duration of each simulation. In Chapter 6 a relationship was found between a decreasing shoreline recession distance, decreasing shelf width and increasing wave asymmetry (*A*) under static water level conditions (Figure 7.18a, also Figure 6.19 in Chapter 6). With sea level rise at a rate of 1 m per 100 years, the shoreline recession distance remains relatively consistent regardless of the wave climate conditions and the shelf width generally shows an increasing trend with greater proportions of high angle waves (*U*) (Figure 7.18, b). With sea level rise at 2 m per 100 years, the relationship observed between recession distances, shelf width and wave climate conditions observed under a static water level, reverses (Figure 7.18). The shelf width is narrower than the recession distance in the majority of simulations and an increase in the size of the shelf and shoreline retreat is observed with increasing wave asymmetry (*A*) and proportion of high angle waves (*U*). As shown in Figure 7.15, sediment mobility increases with greater wave asymmetry which acts to reduce recession where there is no sea level rise by retaining a flux of sediment through the system. However, as demonstrated in the results here, sea level rise shifts the active geomorphic zone and the higher mobility of sediment is counterproductive in sustaining the shoreline position if the material is deposited outside of the active area and effectively lost from the most active and mobile part of the system.

An interesting relationship is observed between the recession distance and shelf width; where the water level is static the width of the shelf is greater than the recession distance, but at 2 m of sea level rise per 100 years, the recession distance is greater than the shelf width. Under static water level conditions, the location of the active cross-shore geomorphic zone is relatively constant and accretion of sediment in the nearshore largely determines the shelf width; recession of the shoreline as it adjusts to the driving wave conditions also has

some effect. With sea level rise, the active zone is constantly shifting the location of the active geomorphic zone in the nearshore and this reduces the ability of sediment to accumulate in the nearshore zone and create a wide shelf. This, relative to the rate of shoreline recession means that the shelf width is smaller than the distance over which the shoreline retreats.

It is unlikely that the model's boundary conditions influence the relationship between recession distance and shelf width. Whilst the model is governed by the principles of mass conservation and this could cause material to pile up against the nearshore slope, sufficient distance from the shoreline to the model boundary (cross-shore) was ensured to prevent this occurring. Further, some loss of material is also allowed at the offshore boundary of the model should piling occur at this boundary, according to defined criteria.

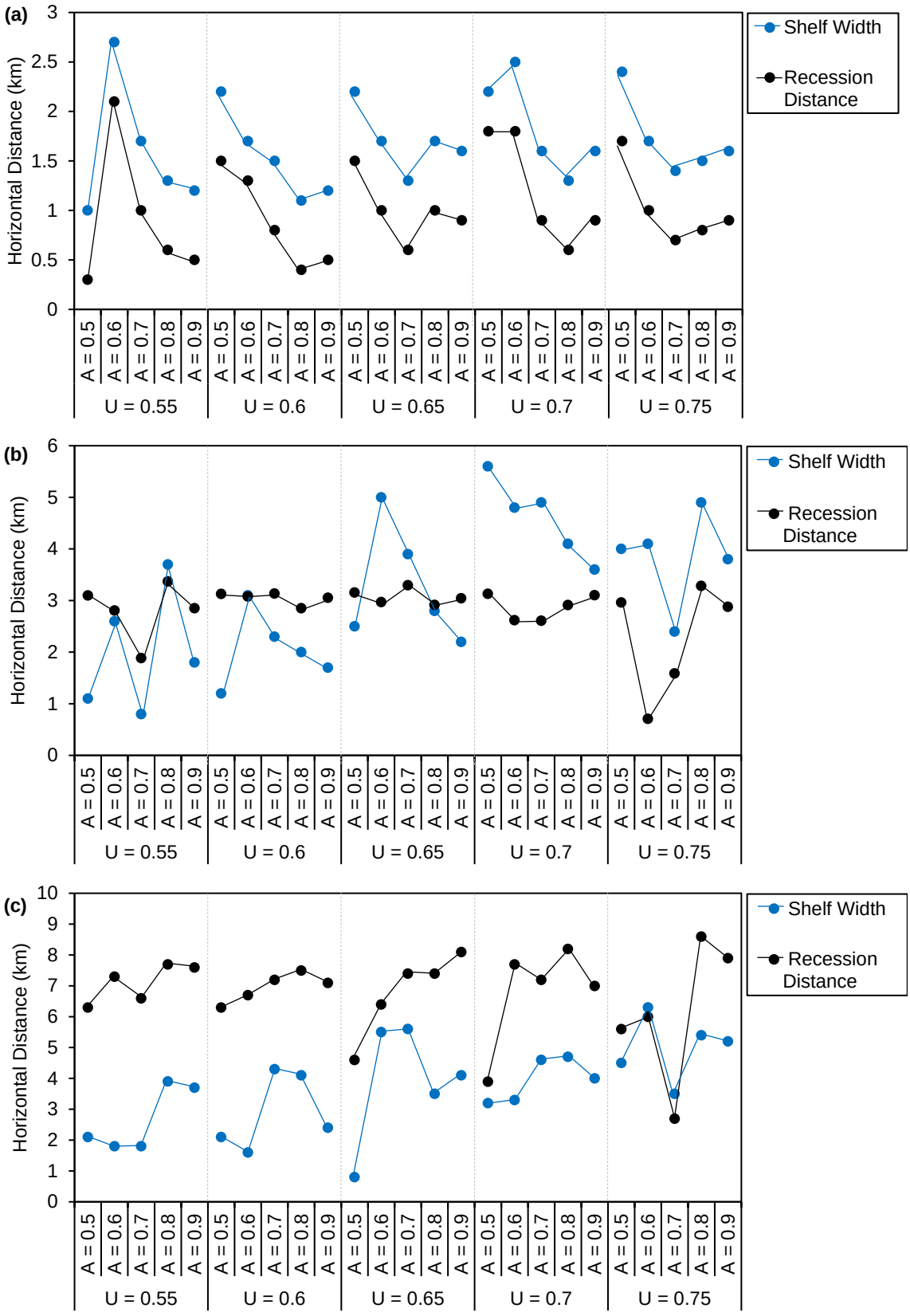

Figure 7.18 Three plot showing the relationship between the recession of the shoreline and the width of the nearshore shelf, with a static water level (a) and a sea level rise rate of 1 m (b) and 2 m (c) per 100 years.

7.5.3 Sea Level Rise induced Shoreline Change

Where the simulated environment is subject to sea level rise, the position of the shoreline recedes from its initial position. The box and whisker plot in Figure 7.19 compares the rate of shoreline recession where 1 m and 2 m sea level rise has been employed over a 100 year period. The data combines the results of the twenty-five wave climate conditions, under each rate of sea level rise.

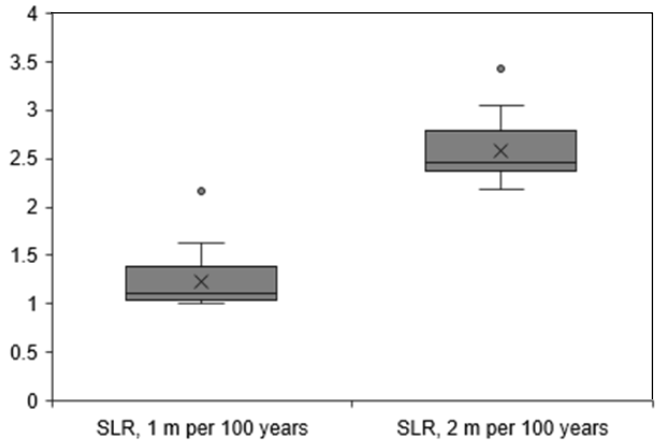

Figure 7.19 Box and whisker plot showing the rate of shoreline recession per year, driven by sea level rise at a rate of 1 m and 2 m per 100 years.

The median values of shoreline recession are recorded at 1.11 m and 2.45 m per year for a 1 m and 2 m rate of sea level rise per 100 years respectively (Figure 7.19); the mean rates measure fractionally higher at 1.23 m and 2.57 m per year. The range and interquartile range are comparable for both rates of sea level rise, but with a rate of 2 m per 100 years showing marginally greater variation in the results. The range is calculated at 0.62 m and 0.86 m respectively for a rate of 1m and 2 m rise per 100 years and the interquartile range at 0.34 m and 0.41 m respectively.

The results discussed from Figure 7.19 are exclusive of outlying values shown in each plot (see dot marker), which represent the maximum rates of recession recorded. These maximum rates measure approximately 2.16 m and 3.42 m per

year, driven by sea level rise at a rate of 1 m and 2 m per 100 years respectively. The graph in Figure 7.20 places these results in the context of all fifty simulations for both rates of sea level rise, showing the change in average shoreline position over time. The results show similar trajectories for runs with the same rate of sea level rise, although some variations are observed. Supporting the results shown in Figure 7.19, the spread of data is greater with increasing rate of sea level rise. Also of note are the simulations highlighted by the black arrow in Figure 7.20 where rates of sea level rise are at 2 m per 100 years. These results are driven by wave climate conditions where A = 0.8, U = 0.75 and where A = 0.9, U = 0.75.

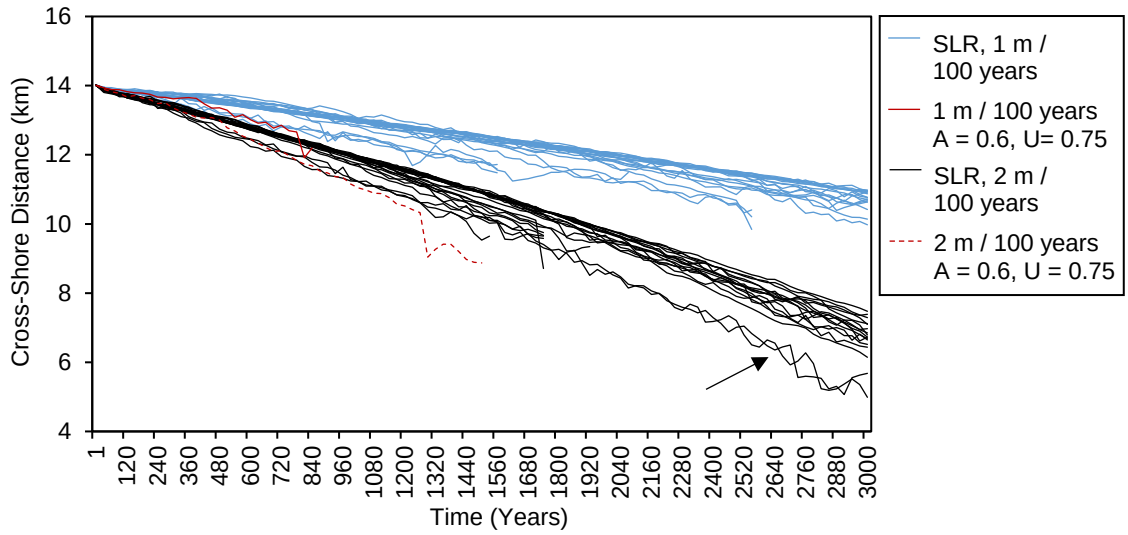

Figure 7.20 Average shoreline position over time for fifty simulations, according to sea level rise at a rate of 1 m per 100 years (blue) and 2 m per 100 years (black). The solid red line and red dashed line denote the maximum rates of recession according to 1 m and 2 m sea level rise over 100 years respectively, both driven by wave climate conditions where A = 0.6, U = 0.75.

7.6 The Response of Landforms to Sea Level Rise

As shown in the previous sections, the simulated coastal systems evolve and respond to the driving wave conditions and changes in the water level. This section focuses on the behaviour and evolution of landforms that develop along the shoreline under rates of sea level rise at 1 m and 2 m per 100 years. Their morphodynamics are compared to results generated where the water level is static (for a more detailed analysis of coastal morphodynamics under a no sea level rise scenario, see Chapter 5 and Chapter 6).

The phase space in Figure 7.21 shows responses of the simulated coastal environments to rising water levels, according to the driving wave conditions and the rate of sea level rise. The wave asymmetry (*A*) increases from 50-90% along the x-axis and the proportion of high angle waves (*U*) increases from 55-75% along the y-axis.

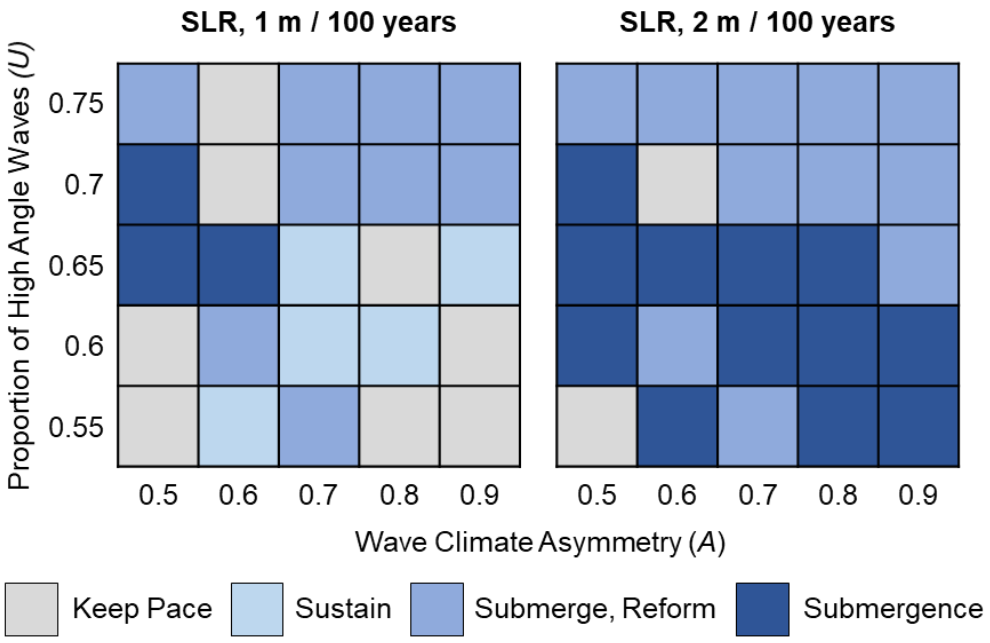

Figure 7.21 Phase space showing the response of coastal landforms to sea level change at a rate of 1 m and 2 m per 100 years, according to twenty-five different wave climate conditions.

Figure 7.21 demonstrates that the coastal landforms have varying responses to rates of sea level change. The responses have been grouped into four principle

categories that describe the most prevalent behaviour of the landform throughout the simulation. ‘Keep Pace’ denotes landforms which largely retain their planform morphology whilst receding with the shoreline as the water level rises. ‘Sustain’ shows features which show no significant periods of submergence, but their planform morphology does not wholly reflect the characteristics of the features which form with a static water level. ‘Submerge and Reform’ describes the features that cycle through periods of submersion and reformation. ‘Submergence’ denotes the features which are submerged and are not able to reform once this process has occurred.

Coastal landforms have a complex response to sea level rise at a rate of 1 m per 100 years (Figure 7.21). At the isolated extremes of highly symmetrical wave climates or highly asymmetric wave climates with a relatively equal proportion of high and low angle waves (U = 0.55), the landforms demonstrate an ability to keep pace with sea level rise. In highly asymmetric wave climates dominated by high angle waves, landforms are submerged by the rising water level but can reform. Submergence is observed principally where the wave climate is symmetrical or has only a slight asymmetry, combined with high angle wave instability.

A more defined pattern in the response of coastal landforms is observed where the rate of rise is 2 m per 100 years. At this rate of rise, fewer coastal systems are able to keep pace with the increasing water level or sustain their form. This is only achieved by those in highly symmetrical wave climates with a balance of high and low angle waves (A = 0.5, U = 0.55) or where there is a slight asymmetry and dominance of high angle waves (A = 0.6, U = 0.7). A greater number of environments succumb to submergence regardless of the wave asymmetry, but which occurs particularly where there is up to a 65% dominance of high angle.

With a greater dominance of high angle waves, the landforms are capable of cycling through periods or submergence and reformation. The balance between submergence and the ability of the landforms to reform or not is therefore dependent on high angle wave instability. High angle wave drive sediment transport along the coastline which can supply material to reform features, particularly where there is a morphological remnants in the bathymetry where a landform has been submerged previous. However, if there is not a sufficient supply of sediment driven by high angle waves this reformation cannot occur; as observed where there is a lower proportion of high angle waves approaching the shoreline.

The following results provide a largely qualitative analysis of the evolution of four coastal profiles to discuss the responses described above in greater detail (Figure 7.21). These four simulations represent the formation of the fundamental shoreline shapes, including cusps (A = 0.5, U = 0.55), sand waves (A = 0.6, U = 0.6), reconnecting spits (A = 0.7, U = 0.65) and flying spits (A = 0.8, U = 0.7). The time steps evaluated correspond with when significant morphological changes occur in each of the simulations, for instance, when the system or the morphological features along the shoreline changes from one state to another. The time steps used in the analysis, where possible, match those used in Chapter 5 and Chapter 6. It was found that significant changes in the behaviour of the model occurred at relatively similar time intervals, but additional time steps are included where the evolution patterns or rates differ. The initial conditions where T (time) = 0 is consistent across all of the runs evaluated (Figure 7.22). The shoreline exhibits regular perturbations, which are mirrored in the topographic and bathymetric profiles. In Figure 7.22, the contours are spaced at 10 m intervals with additional contours at 2 m intervals in the bottom plot.

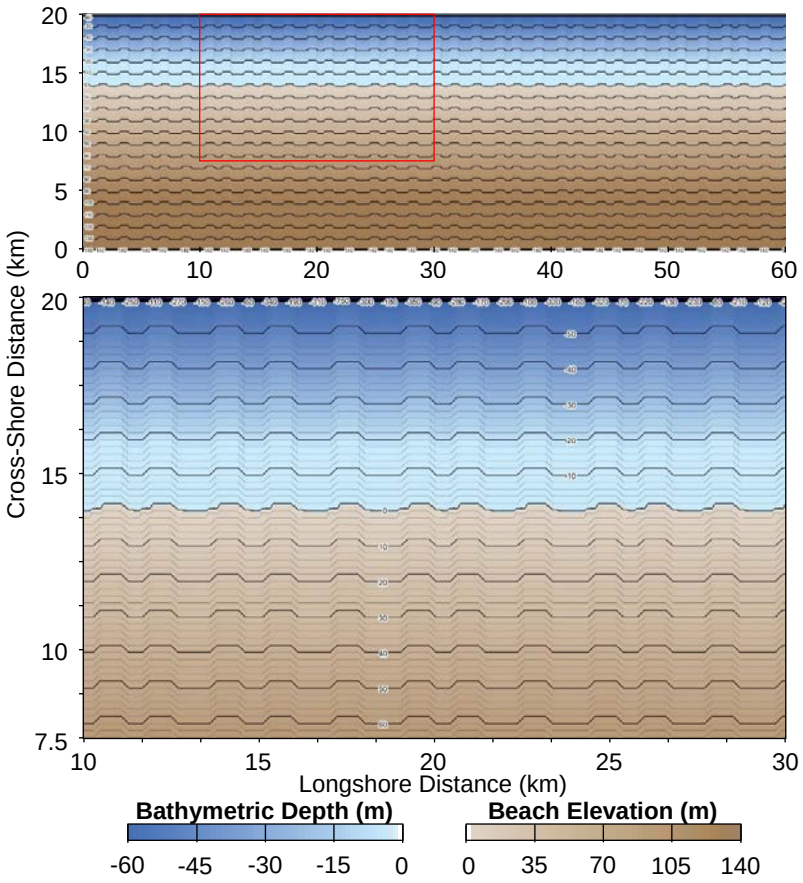

Figure 7.22 Topographic map showing the initial conditions of the coastal profile. The red square in the top image delimits the location of the study area, shown in the bottom image.

In Figure 7.23 a comparison between the average sizes (km^2) of significant landforms along the shoreline is given, for the scenarios with a static water level and with rates of sea level rise at 1 m and 2 m per 100 years. Where the wave climate is relatively symmetrical (A = 0.5, U = 0.55) or highly asymmetric (A = 0.8, U = 0.7), the largest landforms form where sea level rise is at a rate of 2 m per 100 years (Figure 7.23a and Figure 7.23d). Where A = 0.6, U = 0.6 the largest landforms evolve under a static water level (Figure 7.23b). Finally, where the wave climate is defined by A = 0.7, U = 0.65, larger features form under rates of sea level rise of 1 m per 100 years (Figure 7.23c). These relationships are considered in more detail according to each of the wave climate conditions in the following sections, which describe the temporal evolution of the coastal systems

where the water level is static, or rates of sea level rise are 1 m or 2 m per 100 years.

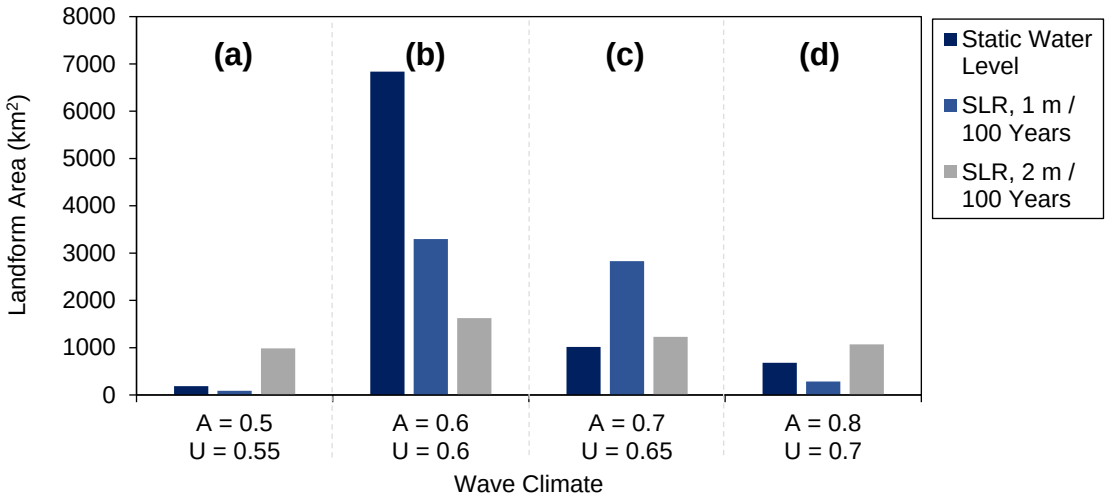

Figure 7.23 Bar chart showing the average area (km²) of significant landforms that develop along the shorelines at the end of each simulation (up to 3,000 years), under four different wave climate conditions and three water level states.

7.6.1 Cuspate Features

Where the wave climate is symmetrical and there is a marginal dominance of high angle waves (A = 0.5, U = 0.55), cuspate landforms develop along the shoreline under each of the three water level scenarios (Figure 1.7 and Figure 7.8). In Figure 7.24, the evolution of these cuspate features throughout the 3,000 year simulation period is given under a static water level and rates of sea level rise of 1 m and 2 m per 100 years.

Throughout the simulations, finite amplitude cuspate features develop and grow into larger scale landforms along the initially perturbed shoreline with and without sea level rise (Figure 7.24). The highest point of the cusps all form offset to the left of the landforms (e.g. Figure 7.24a), owing to the previously discussed directional bias in the model (see Chapter 8). As the features develop, those which form under a static water level become increasingly pointed at the tips (e.g. Figure 7.24b). Where the rate of sea level rise is at 1 m per 100 years, the features do not grow in areal size significantly but tend to keep pace with the

retreating shoreline. At a rate of sea level rise of 2 m per 100 years, the cusps merge and form large-scale features that increasingly skew towards the right of the domain between 1,940-3,000 years (e.g. Figure 7.24c).

The coastal zone between 8 m and -2 m elevation is the most morphodynamic area in all three water level scenarios. Beyond this area, the topographic and bathymetric profiles retain much of the undulating contours from the initial conditions, which over time are smoothed to create planar contours (Figure 7.24). This is with exception to where the rate of sea level rise is 2 m per 100 years, where the rapidly increasing amplitude of these features influences the bathymetric profile and the nearshore contours mirror the shape of the shoreline (e.g. Figure 7.24d).

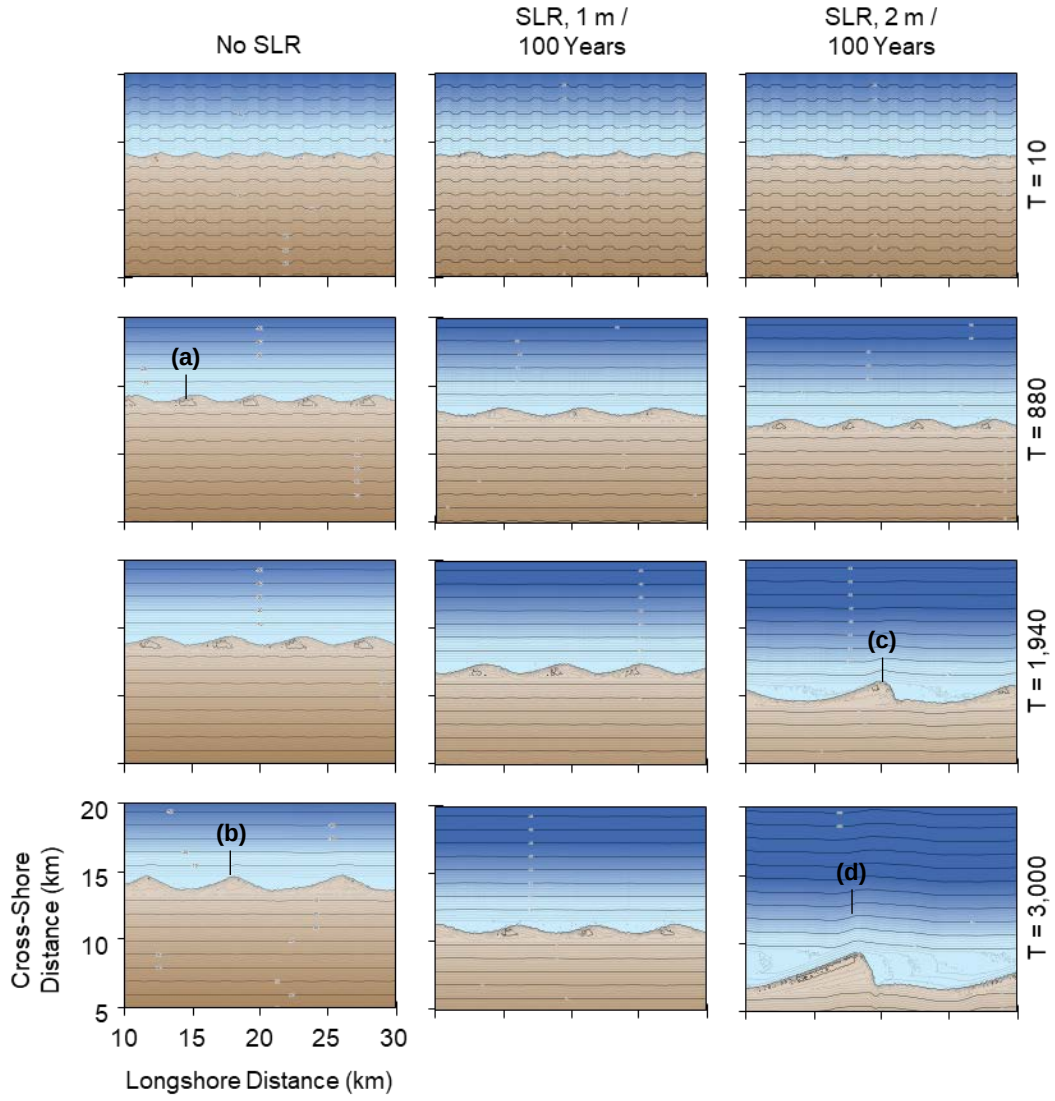

Figure 7.24 Two-dimensional temporal evolution of the coastal profile under wave climate conditions where A = 0.5, U = 0.55. Three water level scenarios are compared: no sea level rise and rates of rise at 1 m and 2 m per 100 years.

The average area (km^2) of landforms that develop under wave conditions where A = 0.5, U = 0.55 are greatest where the rate of sea level rise is 2 m per 100 years (Figure 7.23a and Figure 7.25). The increasing size of these features is not solely related to the deposition of material but the submergence of land in the bays also. As the sea level rises, low-lying areas are submerged and the shoreline retreats. If the cusps lie above the rising water level, but the surrounding shoreline retreats then their amplitude from the shoreline will increase. This is illustrated in Figure 7.25, which plots the average cross-shore position of the shoreline (solid line) and the maximum cross-shore extent of the cuspate features

(dashed line). Where the rate of sea level rise is 2 m per 100 years, the distance between the shoreline and headland increase over time, compared to rates of 1 m per 100 years or a static water level where the amplitude of landforms remains relatively consistent. In the case of sea level rise at a rate of 1 m per 100 years, the shoreline and cuspate landforms keep pace with rising sea levels and retreat landward. This is enabled by the high sediment supply to the cusps under the symmetrical wave climate conditions and elevation of the features.

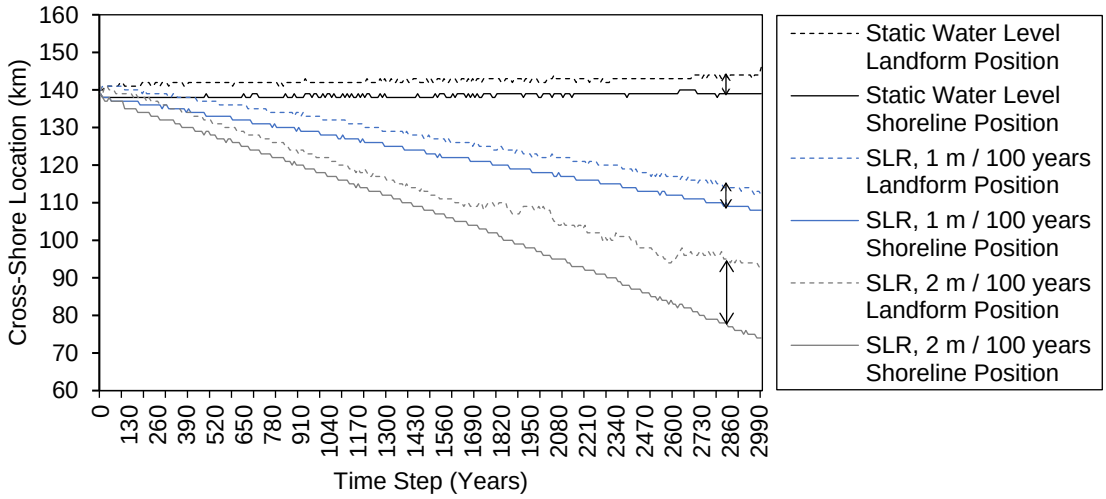

Figure 7.25 Temporal change in the cross-shore position of the shoreline and of the headland of cusps where the wave climate is defined by A = 0.5, U = 0.55. The water level is static or subject to rates of rise at 1 m or 2 m per 100 years.

7.6.2 Alongshore Sand Waves

Under wave climate conditions with a slight asymmetry (A = 0.6, U = 0.6), alongshore sand waves develop along the shoreline. The forms develop with a hooked tip where there is a static water level but which increasingly resemble flying spits with sea level rise (Figure 7.7 and Figure 7.8). The temporal evolution of these features over the 3,000 year run duration is shown in Figure 7.26 with a static water level and with rates of sea level rise at a rate of 1 m and 2 m per 100 years.

The topographic and bathymetric profiles retain the form of the initial conditions, but over time they increasingly reflect the shape of the shoreline under all water level scenarios; this is more prominent in the nearshore compared to the beach surface (e.g. Figure 7.26a). Contours close to the shoreline tend to be steeper around the headland of features and shallow bays form between the landforms. This bay has a more complex bathymetry with irregular undulations where rates of sea level rise are 2 m per 100 years (e.g. Figure 7.26b). Remnant or relic features are observed in all simulations, particularly within the bays and increasingly so with greater rates of sea level rise and longer run durations (e.g. Figure 7.26c).

Under both rates of sea level rise, the sand waves are increasingly submerged over time leading to the drowning of finite amplitude features and the formation of lagoons within the larger landforms. The lagoons grow larger over time as the water level rises and eventually drowns the downdrift edge, forming features which resemble spits (e.g. Figure 7.26d). The longshore transport of material in the updrift direction creates sediment pathways from the mainland, with the features then resembling reconnecting spits. The sediment deposits are periodically submerged and reformed as the water level continues to rise. This process occurs over a shorter run duration where rates of sea level rise are 2 m per 100 years, compared to a rate of 1 m per 100 years.

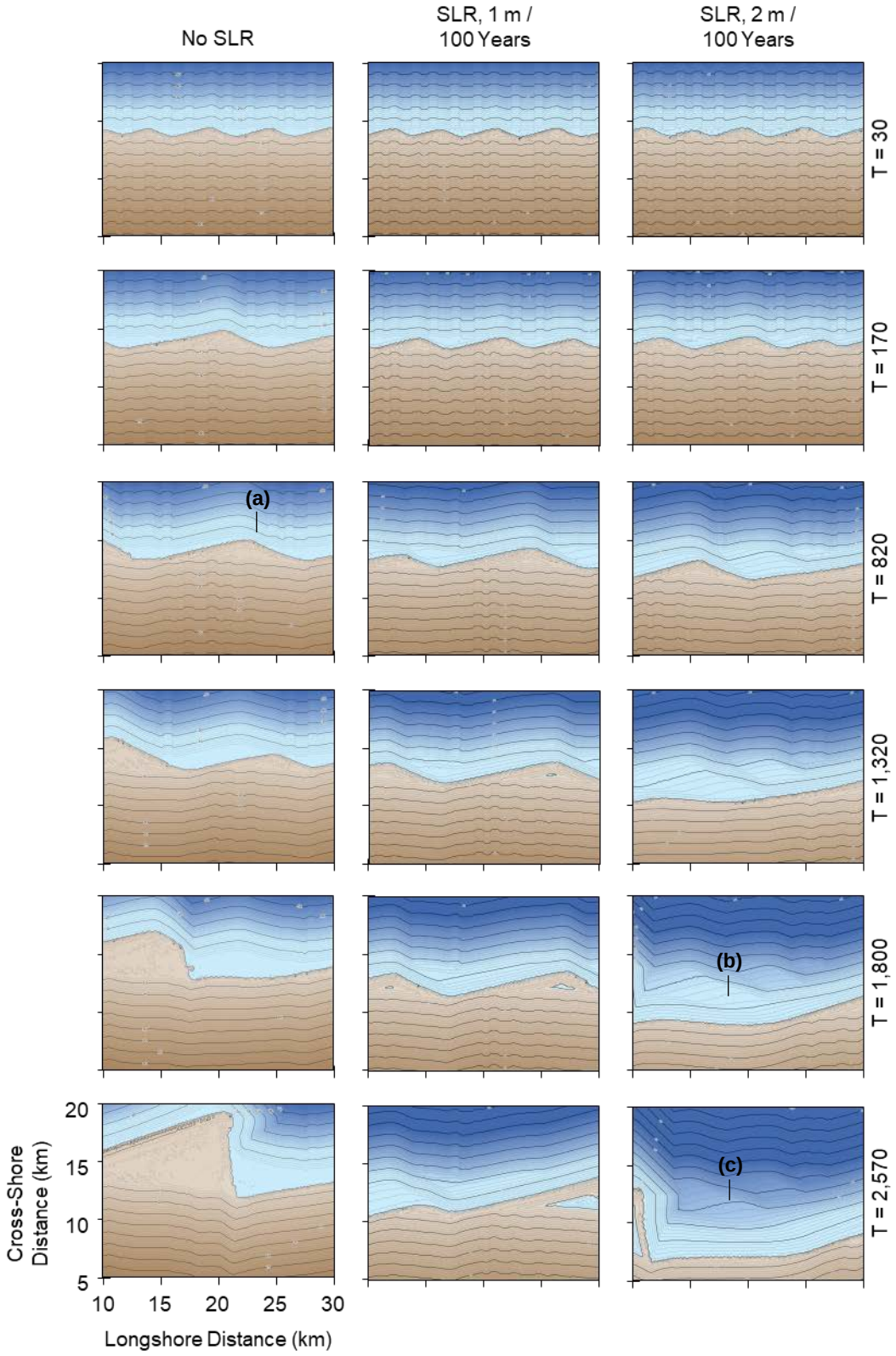

Figure continued on Page 300

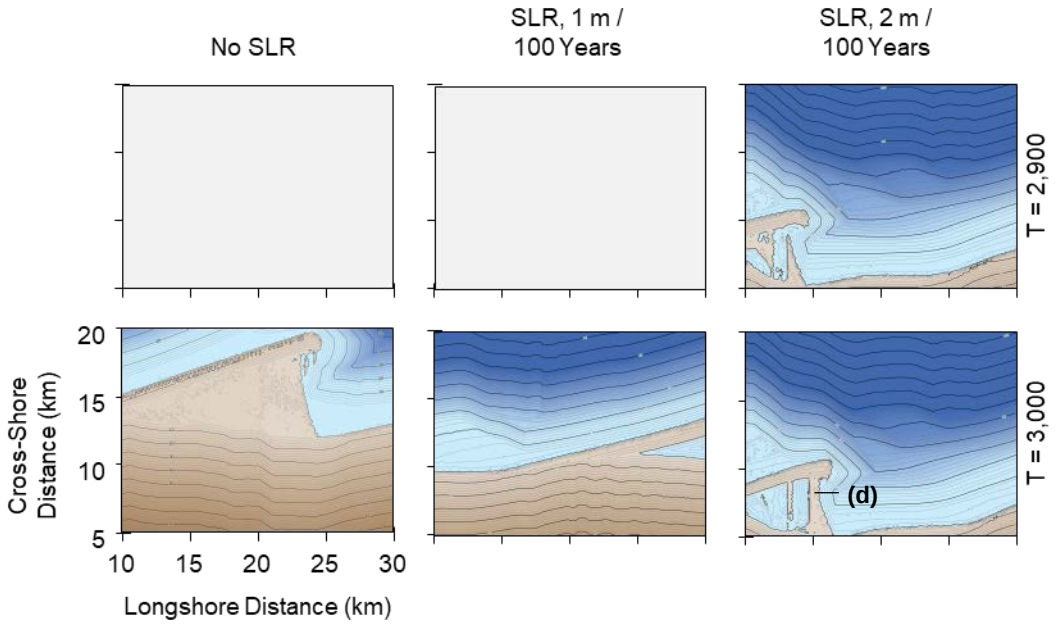

Figure 7.26 Two-dimensional temporal evolution of the coastal profile under wave climate conditions where A = 0.6, U = 0.6. Three water level scenarios are compared: no sea level rise (SLR) and SLR at a rate of 1 m and 2 m per 100 years.

The average area (km^2) of the landforms decreases with increasing rates of sea level rise (Figure 7.23b and Figure 7.27). Whilst the landforms under each sea level rise scenario are shown to increase over time (Figure 7.27), the submergence of the sand waves and formation of lagoons under rates of sea level rise reduces their total planform area. The elevation of the features is relatively low in comparison to those which form under a symmetrical wave climate, as sediment is transported longshore, making it increasingly susceptible to inundation as the sea level rises.

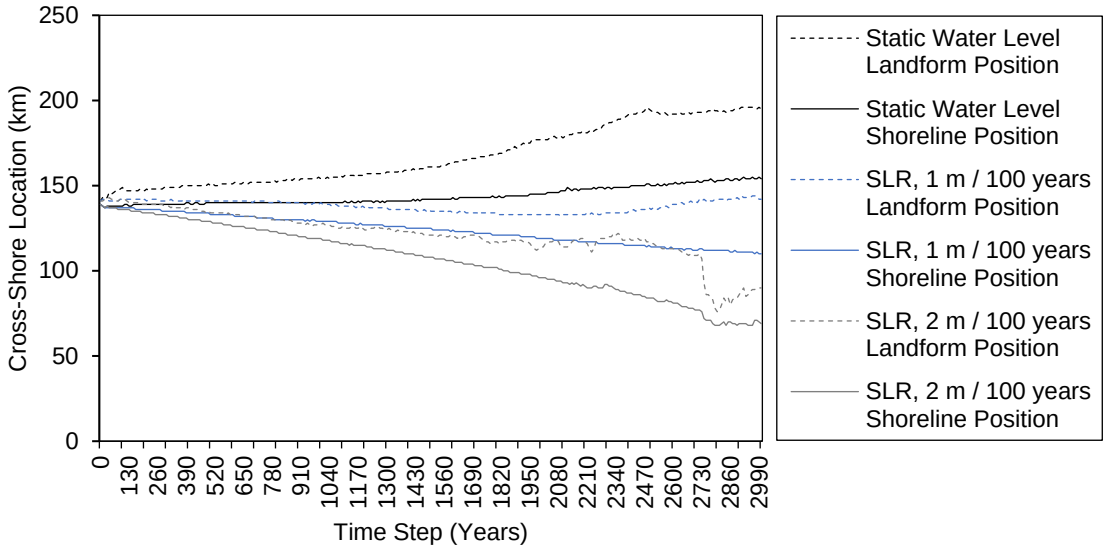

Figure 7.27 Temporal change in the cross-shore position of the shoreline and of the headland of sand waves where the wave climate is defined by A = 0.6, U = 0.6. The water level is static or subject to rates of rise at 1 m or 2 m per 100 years.

7.6.3 Reconnecting Spits

Reconnecting spits are observed to form along the shoreline where the wave climate is asymmetric (A = 0.7, U = 0.65). The evolution of these features throughout the simulations is illustrated in Figure 7.28 where the water level is static and where sea level rise is at a rate of 1 m and 2 m per 100 years. Where the water level is static, the model simulation terminates after 1,489 years for reasons given in Chapter 6. Where the coastal system is subject to sea level rise, whether at a rate of 1 m or 2 m per 100 years, the simulations run for the period of 3,000 years.

Throughout each of the simulations, the features which develop along the shoreline show a progression from cusps to sand wave and reconnecting spits (Figure 7.28). This process occurs more rapidly where the water level static as the sediment transport processes are concentrated in a relatively fixed cross-shore location. It appears to occur more readily under rates of sea level rise of 2 m per 100 years, than 1 m per 100 years owing to the effect of submergence on

the formation of reconnecting spits, similar to that observed in Section 7.6.2. At the end of each simulation after 3,000 simulated years, reconnecting spit features are found along the shoreline. At rates of sea level rise of 2 m per 100 years, the reconnecting spits go through cycles of submergence and reformation as the water level continues to rise (Figure 7.28). At lower rates of 1 m per 100 years, the evolution of the spits keeps pace with the receding shoreline and continue to evolve as the shoreline is continually relocated landwards.

The topographic and bathymetric profiles retain the initial conditions but smooth over time to create planar contours (e.g. Figure 7.28a). However, under sea level rise conditions, as the reconnecting spits increase in amplitude over time they begin to influence the profile of the contours in the upper nearshore. The undulations are particularly prevalent after 2,500 years where rates of sea level rise are at 2 m per year (Figure 7.28b). Morphological memories of the predeceasing location of the reconnecting spits are preserved in the profile as they migrate longshore, where sea level rise is at a rate of 2 m per 100 years (e.g. Figure 7.28c). At a lower rate of sea level rise (1 m per 100 years), however, the bathymetry does not store remnants of morphological features.

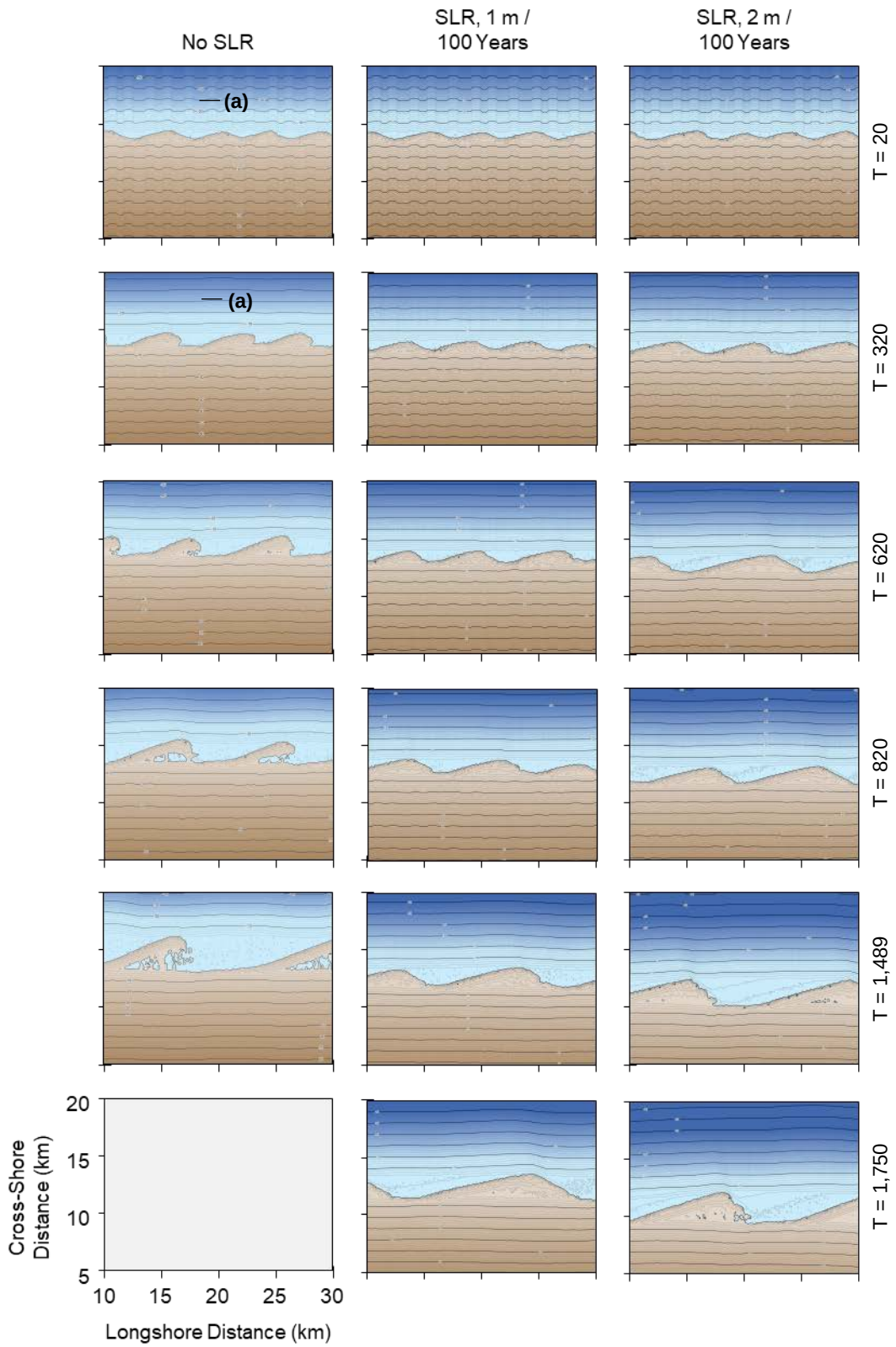

Figure continued on Page 304

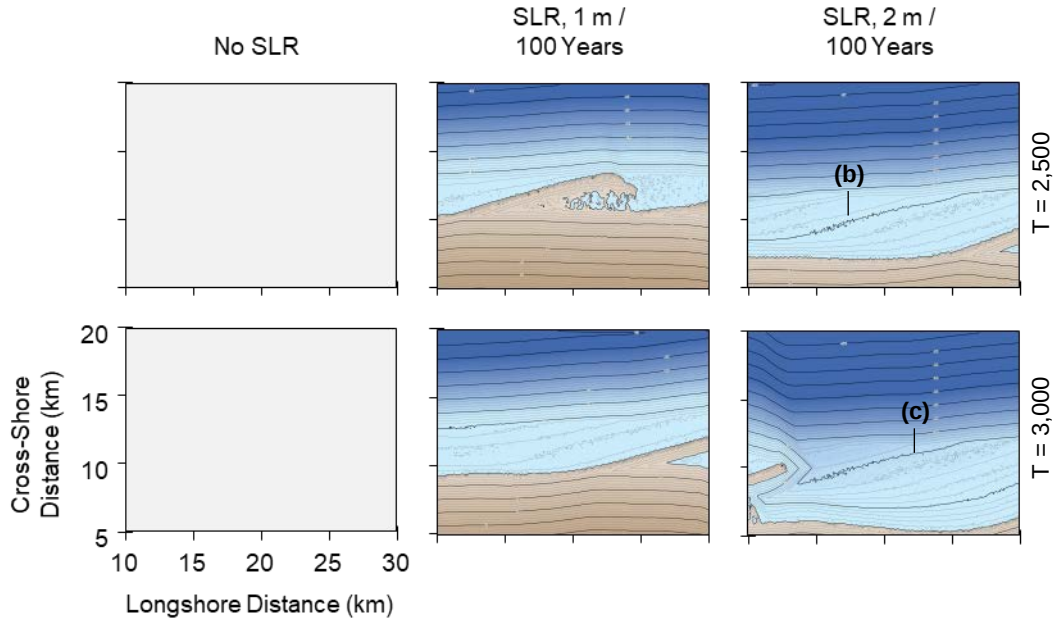

Figure 7.28 Two-dimensional temporal evolution of the coastal profile under wave climate conditions where A = 0.7, U = 0.65. Three water level scenarios are compared: no sea level rise (SLR) and SLR at a rate of 1 m and 2 m per 100 years.

The average area (km^2) of the landforms that develop along the shoreline where A = 0.7, U = 0.65, are largest where rates of sea level rise are at 1 m per 100 years (Figure 7.23, Figure 7.29). This is because at higher rates of rise the landforms are submerged and therefore the total area of land above the water level is lower. It is also important to note that the simulation with a static water level terminated prematurely, for reasons discussed in Chapter 6 and so a comparison cannot be made between the planform area of spits with and without sea level rise. The trajectory shown in Figure 7.29, however, suggests that if this simulation was to run for 3,000 years it would generate the largest landforms.

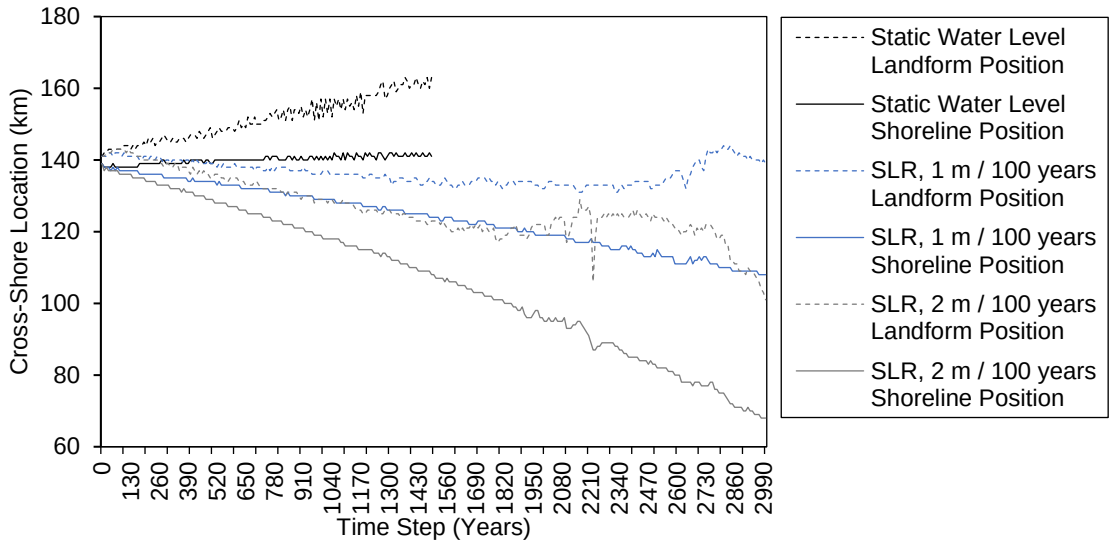

Figure 7.29 Temporal change in the cross-shore position of the shoreline and of the headland of cusps. The wave climate is defined by A = 0.7, U = 0.65 and the water level is static or subject to rates of sea level rise at 1 m or 2 m per 100 years.

7.6.4 Flying Spits

Where the wave climate is highly asymmetric, driven by conditions where $A = 0.8$, $U = 0.7$, flying spits tend to form along the shoreline where the water level is held constant (Figure 7.30). In this scenario, the simulation runs for a maximum duration of 1,090 simulated years as discussed in more detail in Chapter 6. Results of simulations under the same wave climate conditions but subject to sea level rise at a rate of 1 m and 2 m per 100 years are given in Figure 7.30; these simulations run to the maximum of 3,000 years.

Under a static water level and rates of sea level rise of 1 m and 2 m per 100 years, flying spits develop from sand waves along the shoreline (Figure 7.30). Where there is no sea level rise, the flying spits evolve more rapidly (after the initial 150 simulated years) than under a rising sea level, which takes increasingly longer time periods to form under greater rates of rise (Figure 7.30). At the lower rate of rise the flying spits keep pace with the changing water level and sustain their elongated, narrow forms as observed under a static water level (Figure 7.30a). After 3,000 simulated years however, the spits begin to become

submerged as they can no longer keep pace with the changing water level. Where the rate of rise is 2 m per 100 years the features exhibit a complex behaviour and alternate their evolution between more shore-parallel or perpendicular features as they are submerged and reform as the water level rises (e.g. Figure 7.30b).

Whilst the topographic and bathymetric profiles maintain a relatively regular sloping morphology offshore under a static or rising sea level, the flying spits form gentle undulations in the bathymetric profile where they project offshore (e.g. Figure 7.30c). A wide nearshore shelf is also formed in all simulations, which exhibits a complex morphology that has been influenced by the high sediment flux and migration of landforms (e.g. Figure 7.30d).

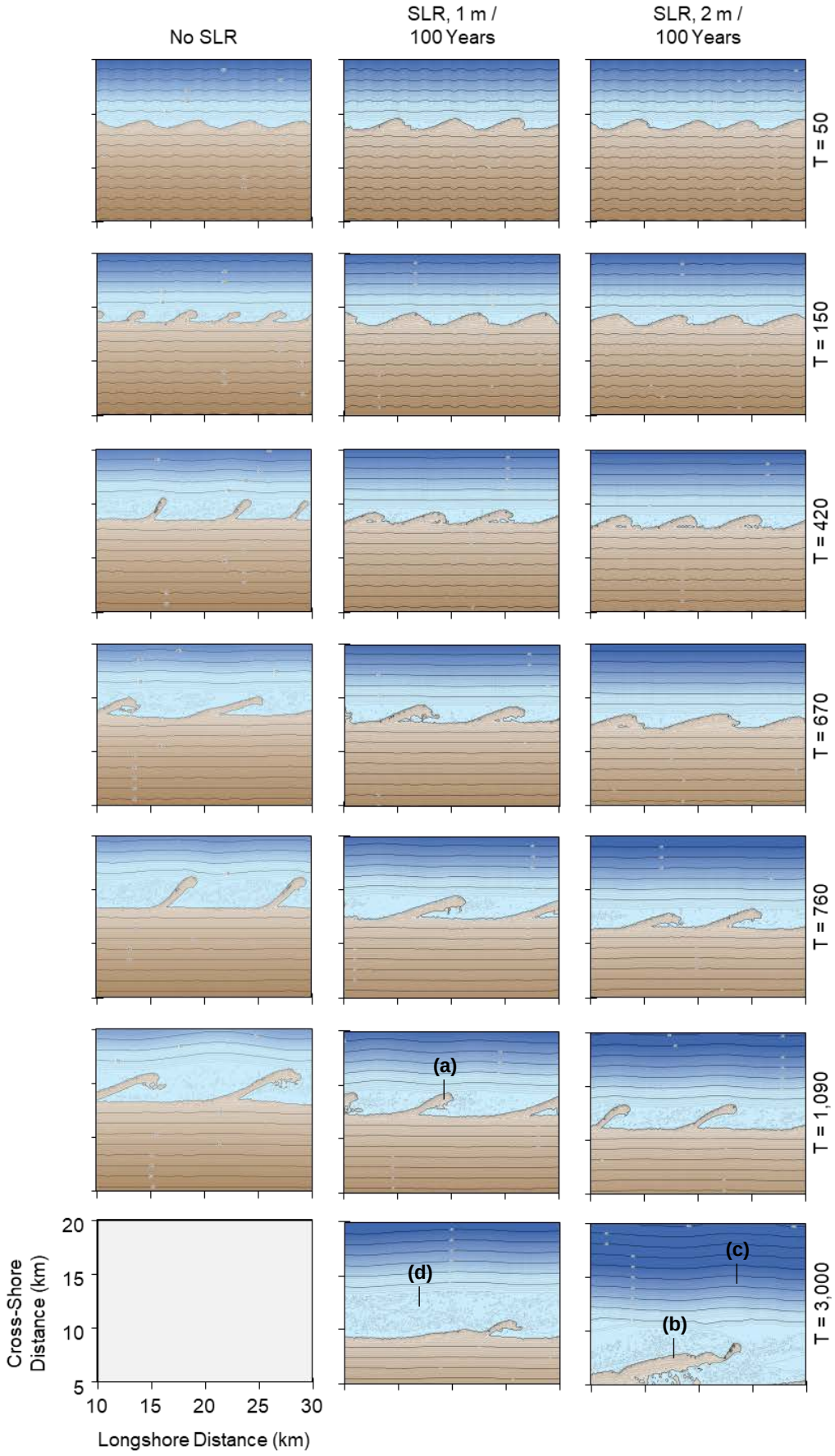

Figure 7.30 Two-dimensional temporal evolution of the coastal profile under wave climate conditions where A = 0.8, U = 0.7. Three water level scenarios are compared: no sea level rise (SLR) and SLR at a rate of 1 m and 2 m per 100 years.

As previously discussed in Section 7.6, the average area (km^2) of the landforms that develop along the shoreline where A = 0.8, U = 0.7, are largest where rates of sea level rise are at 2 m per 100 years (Figure 7.23, Figure 7.31). These findings are similar to those where the wave climate is symmetrical as discussed in Section 7.6.1 but differ from those of the other asymmetric wave climate which are presented in Section 7.6.2 and Section 7.6.3. It is important to note that the simulation with a static water level terminated prematurely for reasons discussed in Chapter 6 but if the landforms continued to evolve and develop at the rate observed, it is likely that their size and amplitude would increase beyond those with sea level rise.

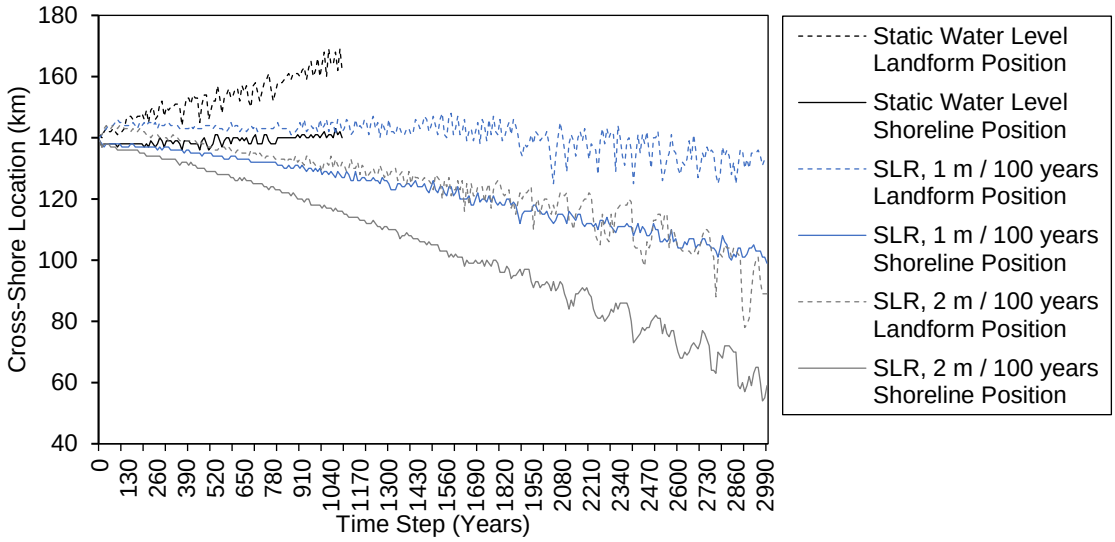

Figure 7.31 Temporal change in the cross-shore position of the shoreline and of the headland of cusps. The wave climate is defined by A = 0.8, U = 0.7 and the water level is static or subject to rates of sea level rise at 1 m or 2 m per 100 years.

7.7 Discussion

Coastal environments are understood to have a non-linear response to sea level change, as demonstrated in the results (Bray and Hooke, 1997; Evans *et al.*, 2004; Dickson *et al.*, 2007). Their response is dependent upon a combination of site-specific factors and the interaction of driving forces (Bray and Hooke, 1997), not all of which can be included in parsimonious numerical models (see Chapter 3). Acknowledging the relatively simplistic representation of the natural environment in CEM2D, the non-linearity in the response of coasts to a changing water level and sea level rise is still exposed in the results.

7.7.1 Coastal Erosion and Shoreline Retreat

Coastal erosion and shoreline retreat are commonly associated with sea level rise (Dickson *et al.*, 2007; Bird, 2011) and are shown to occur in all model results according to two rates of sea level rise: 1 m and 2 m per 100 years. For each of these scenarios, the average recession distance lies within two orders of magnitude of the rate of sea level rise (Bruun, 1962, 1988). Average recession distances measure 1.23 m per year at a sea level rise rate of 1 m per 100 years and 2.57 m at a rate of 2 m per 100 years (Figure 7.32).

With an average slope of 0.01 (1%), geometrically an average recession distance two orders of magnitude greater than sea level rise would be calculated as per the Bruun Rule (Bruun, 1962, 1988). However, much of the criticisms of the Bruun Rule are apparent in the results of individual simulations, stemming from the over or underestimation of shoreline recession; this is due to its relatively simplistic consideration for process in the coastal environment that are often site-specific (Bray and Hooke, 1997; Cooper and Pilkey, 2004; Dickson *et al.*, 2006). The results demonstrate the failure of the rule to account for the dynamic and non-linear response of coastal systems to sea level change and the range of

recession distances observed due to the influence of other environmental conditions on coastal behaviours; most notably, the wave climate.

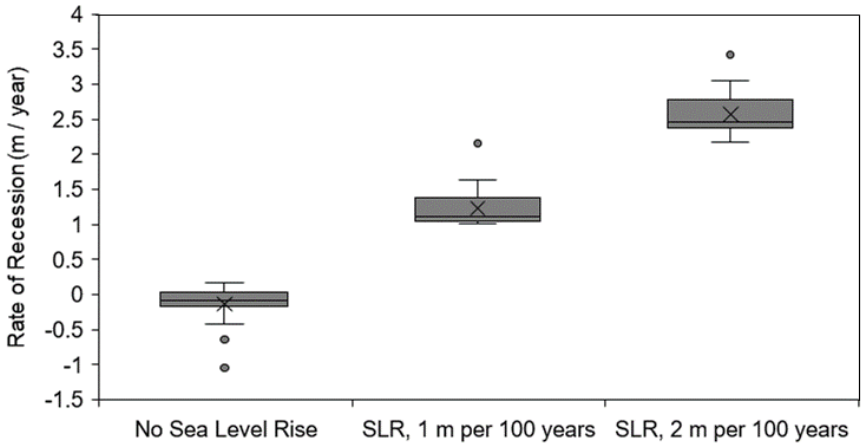

Figure 7.32 Box and whisker plot showing the rate of shoreline recession per year, driven by sea level rise at a rate of 1 m and 2 m per 100 years and a no sea level rise scenario.

Results generated under a no sea level rise scenario emphasise this point, since it is shown that even under static water level conditions some shorelines retreat as the coastal system adjusts to the environmental conditions and the sediment is reworked (Figure 7.32). Shoreline retreat is induced by a combination of other dominating processes such as wave action and sediment diffusion in these simulations, not by a change in water level. The different sediment transport patterns and the balance of cross-shore and longshore sediment transport regimes (determined by the proportional wave asymmetry (*A*) and proportion of high angle waves (*U*)) influences the response of the system to a changing water level. Taking a site-specific example, along the Holderness Coast rates of retreat are currently estimated at approximately 1-2 m per year even without considering long-term sea level change, induced by wave action and strong currents that transport material south along the geologically soft shoreline (Quinn *et al.*, 2009).

As shown in Figure 7.33, the cross-shore coastal profiles are comparable in terms of their geometry but where sea level rise occurs in the model, the profile is

positioned increasing further landwards and to a greater elevation than where there is no sea level rise. The erosion of the shoreline and of the beach surface creates a supply of material that is deposited in the nearshore (Bruun, 1988; Cooper and Pilkey, 2004), which accretes a shallow shelf. This reinforces the coastal 'rollover' theory, which suggests that the profiles will translate landward and upwards in response to sea level rise whilst retaining their cross-shore geometric shape (Bruun, 1962, 1988). However, as has already been noted, this theory provides a simplistic estimation of shoreline response and as shown in the results in this chapter; each coastal system will respond differently according to other dominate driving conditions, such as the wave climate.

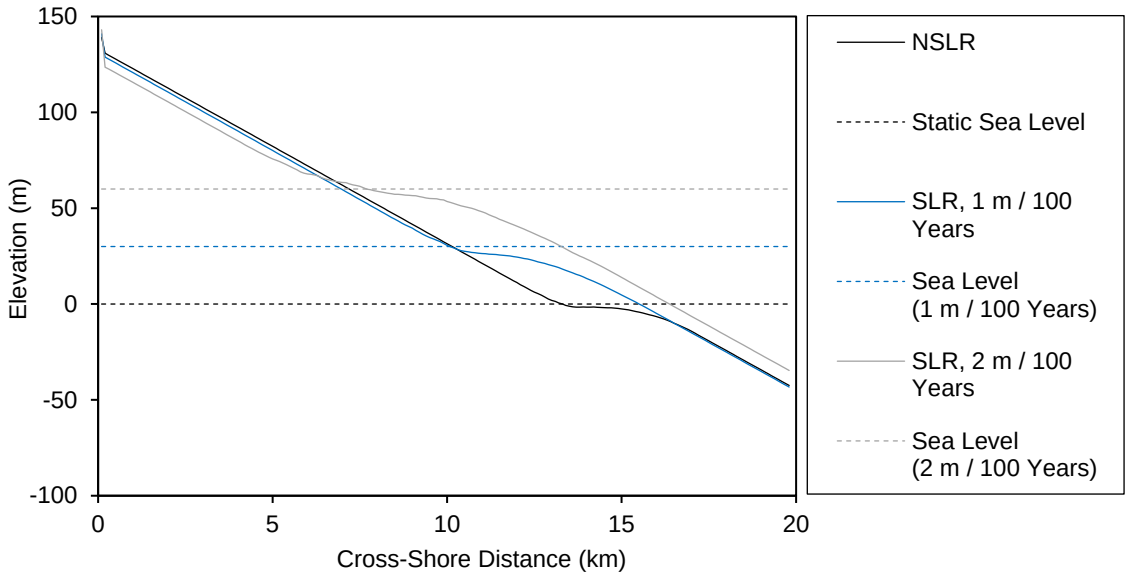

Figure 7.33 Average shape of the cross-shore morphology of the simulated coastal system according to two rates of sea level rise and a base level simulation with no sea level rise (NSLR), calculated from results of seventy-five simulations. Also indicated on the plot is the location of the water level for each of the three sea level rise scenarios.

7.7.2 Landform Response to Sea Level Rise

Four principal types of landforms are observed in the model results presented in this chapter (and across this thesis): cusps, sand waves, reconnecting spits and flying spits. Current research suggests that landforms such as these are likely to either erode, become submerged or prograde with changing water levels

depending on the specific environmental conditions of given systems (Komar *et al.*, 1991; Bray *et al.*, 1997; Dickson *et al.*, 2007; Jarmalavičius *et al.*, 2013). Whilst the results of this chapter broadly support this suggestion, the results look in greater depth at the complexities in the response of these systems to rising water levels and the geomorphic work that occurs in these systems. There is a clear relationship identified in the results between the geomorphic work that is done in the coastal environment, the energy provided by the wave climate and the ability of the system to adjust to a rising sea level.

In general, it is observed in the results, that at the slower rate of sea level rise (1 m per 100 years) the landforms can keep pace with the rising water level and at the faster rate (2 m per 100 years) the features become increasingly under threat from submergence. However, the analysis of the four exemplary landforms in Section 7.6 showed that landforms which form under different wave climate conditions have differing capacities to cope with rising water levels. Their capacity to cope and keep pace with sea level rise is highly associated with the energy derived from wave climate conditions, the mobility of sediments and the balance of cross- and long-shore sediment transport processes.

Symmetrical wave climates generate cuspate landforms with relatively high topographies, supplied with sediment from both directions along the shoreline. Their high elevation and continual sediment supply from two directions mean these features are able to keep pace with rising sea levels, even at the higher rates of rise at 2 m per 100 years (Figure 7.34). An interesting occurrence observed in the evolution of the cusps under the three sea level rise scenarios (no sea level rise, a rate of 1 m per 100 years and a rate of 2 m per 100 years), shows that their rate of growth increases with increasing rates of sea level rise (Figure 7.34a). This is due to the submergence of the relatively low-lying bays

that shifts the average shoreline back whilst the cusps retain their form, which increases the amplitude and total area of the landform. This behaviour is described in the literature relating to the progradation of shorelines (Komar et al., 1991; Bray, Hooke and Carter, 1997; Dickson et al., 2007), but the results demonstrate that this is also observed specifically in the evolution of landforms, as found along the Curonian Spit (Jarmalavičius *et al.*, 2013).

With increasing sea level rise, sediment dynamics in the nearshore is enhanced as the active geomorphic zone moves landwards, forming a more complex and irregular bathymetry (Figure 7.34b). The combination of high elevation and sufficient sediment supply driven by the wave climate conditions enables cuspate landforms to keep pace and sustain their form as sea levels rise.

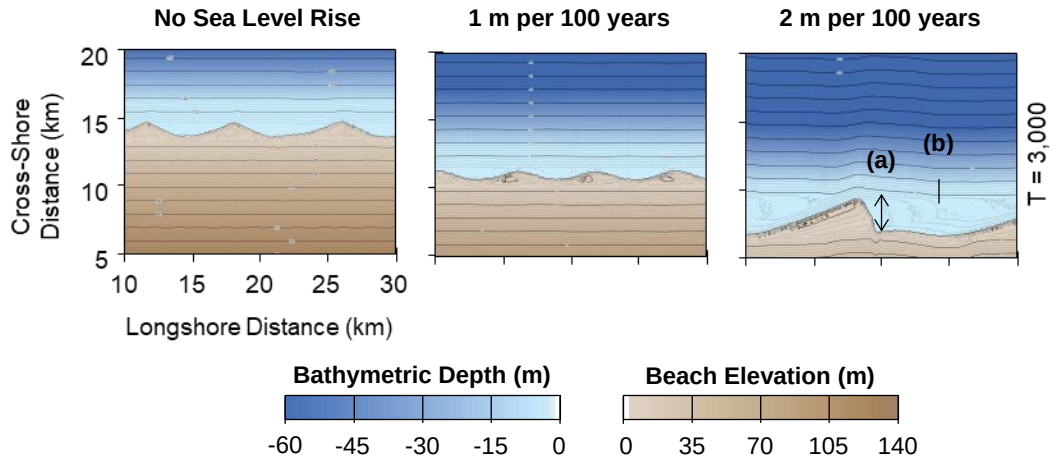

Figure 7.34 Two-dimensional temporal evolution of the coastal profile under wave climate conditions where A = 0.5, U = 0.55. Three water level scenarios are compared: no sea level rise and sea level rise at a rate of 1 m and 2 m per 100 years.

In contrast to the morphology of cusps, where there is a slight asymmetry and dominance of high angle waves, relatively low-lying sand waves form along the shoreline (Figure 7.35). The lower elevation of these features makes them more vulnerable to rising sea levels and increasingly so with greater rates of rise, leading to submergence and the formation of lagoons (Figure 7.35a). In the

example explored in this chapter (*A* = 0.6, *U* = 0.6), longshore sediment mobility and dynamics are relatively low under these wave climate conditions (Figure 6.33) and so the supply of material to feed the growth or to sustain the features is minimal. With 60% asymmetry, the results also show that submergence is more likely with an increasing proportion of high angle waves (*U*), where there is a greater movement of material offshore that can be lost from the geomorphically activity system. Increasingly noteworthy submarine features and morphological memories are observed with increasing sea level rise (Figure 7.35b), as remnant features are preserved in the bathymetry when left beyond the active geomorphic zone or the migration of features slows as their ability to keep pace with rising sea levels reduces. This also highlights the decreasing longshore mobility of sediments with increasing sea level rise and the consequence this has one the ability of these features to keep pace with rising sea levels.

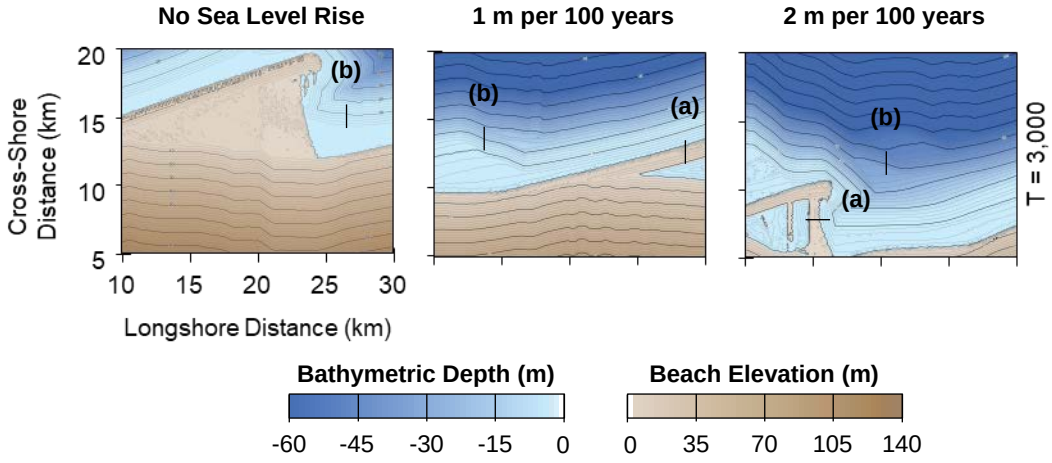

Figure 7.35 Two-dimensional temporal evolution of the coastal profile under wave climate conditions where A = 0.6, U = 0.6. Three water level scenarios are compared: no sea level rise and sea level rise at a rate of 1 m and 2 m per 100 years.

The evolution and response of reconnecting (Figure 7.36) and flying spits (Figure 7.37) to sea level rise is comparable. At lower rates of sea level rise (1 m per 100 years) these features are able to keep pace with rising sea levels (Figure 7.36a,

Figure 7.37a), but some submergence of the flying spits occurs over long run durations. However, at high rates of rise (2 m per 100 years) the features are increasingly submerged with greater wave asymmetries and proportions of high angle waves. Unlike the other landforms identified, the spits cycle through periods of submergence and reformation at the high rate of sea level rise (Dickson *et al.*, 2007). This can be attributed to the high longshore sediment mobility (Figure 6.33) induced by the wave climate. Whilst it is apparent that this high level of dynamism prevents the landforms from developing with high elevation profiles (as observed for cusps), which would lessen their vulnerability to submergence, it also means that there is a supply of entrained material to reform the features if the volume is sufficient enough to build up in the active geomorphic zone. The complexity of the morphology of reconnecting and flying spits is reflected in the submarine morphologies and remnant features left in the bathymetry of these highly geomorphically active systems, which are increasingly preserved in these environments at faster rates of sea level rise, higher wave asymmetries and greater proportions of high angle waves (Figure 7.36b, Figure 7.37b).

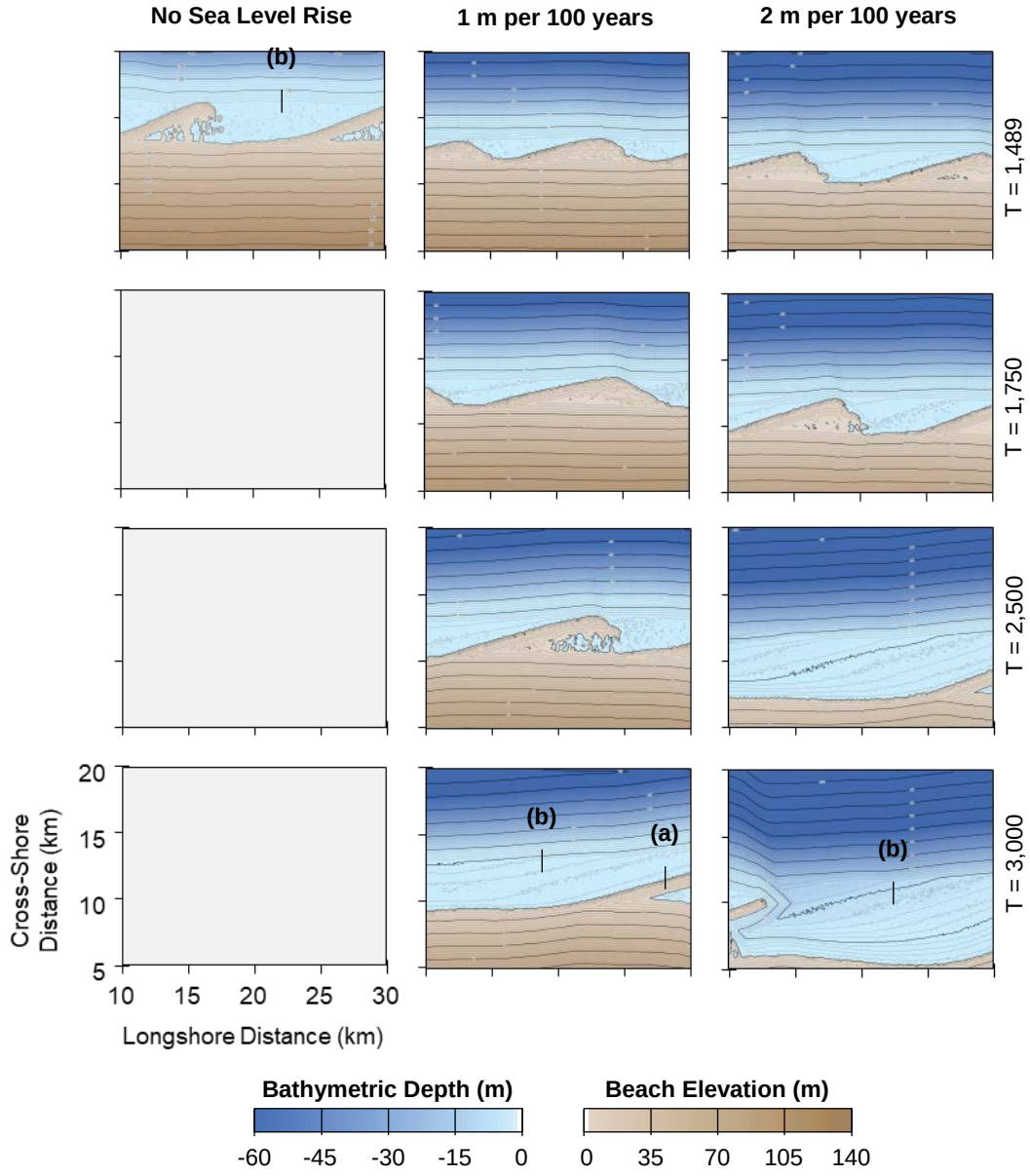

Figure 7.36 Two-dimensional temporal evolution of the coastal profile under wave climate conditions where A = 0.7, U = 0.65. Three water level scenarios are compared: no sea level rise and sea level rise at a rate of 1 m and 2 m per 100 years.

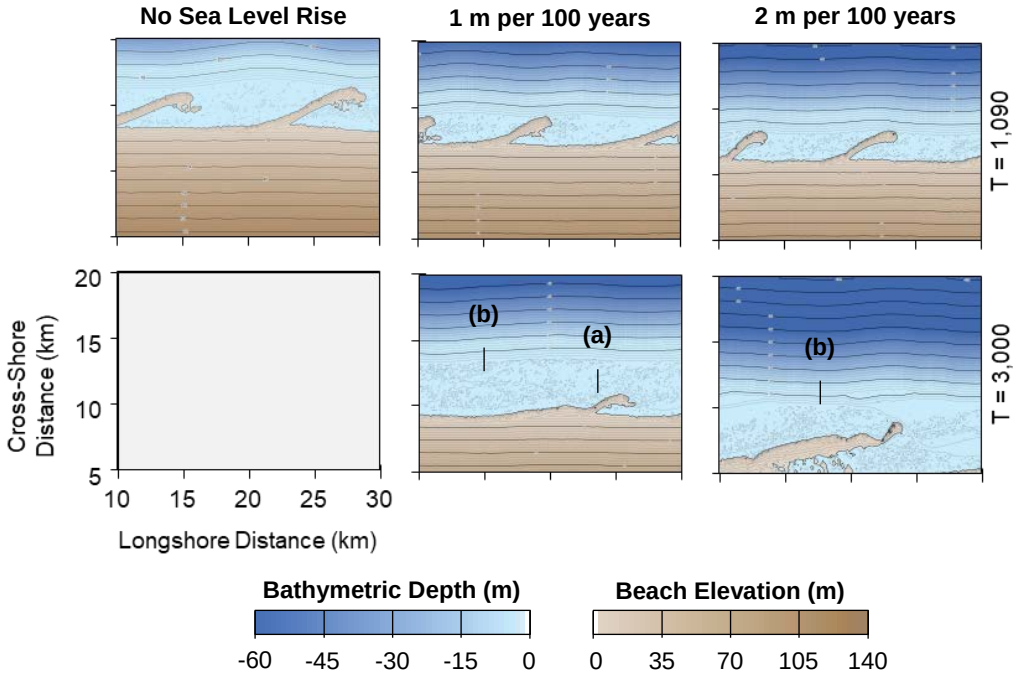

Figure 7.37 Two-dimensional temporal evolution of the coastal profile under wave climate conditions where A = 0.8, U = 0.7. Three water level scenarios are compared: no sea level rise and sea level rise at a rate of 1 m and 2 m per 100 years.

The results discussed here clearly show that the response of coastal systems to sea level rise and their ability to either keep pace or their vulnerability to submergence is highly influenced by the morphodynamics occurring in the system. These morphodynamics determine sediment mobility, pathways of transport cross- or alongshore and the morphology of the landforms that develop, including their elevation profiles. It is interesting to observe how under wave climate conditions which show relatively minimal geomorphic activity (A = 0.6, U = 0.6), this increases the vulnerability of the landforms to submergence as areas that are eroded or submerged are less likely to receive a longshore flux of sediment sufficient enough to counter the threat of inundation. However, in wave climate conditions which induce high longshore sediment mobility in longshore and cross-shore directions, this can also increase the vulnerability of landforms to some extent if the movement of material is to areas that are beyond the most active cross-shore region, as sea levels rise. There is a fine and sensitive line

between the amount of geomorphic work that is done in an area and the positive or negative influence this has on the ability of landforms to respond to sea level rise.

Although each coastal system and landform type examined show differing responses to rates of sea level rise, the wave climate remains the principle environmental condition controlling the type of feature that evolves along the shoreline. However, there are several cases where the type of feature changes, when sea level rise occurs. This is predominantly as a consequence of the submergence of landforms, which is increasingly observed in simulations at greater rates of sea level rise; an impact commonly associated with an increasing water level (Dickson *et al.,* 2007).

In a number of simulations, particularly those where the wave climate conditions are asymmetric, the submergence of landforms can lead to the formation of features not typically found under the given wave climates. For instance, where the wave climate is defined by values where $A = 0.6$, $U = 0.75$, cuspate features develop along the shoreline but as the sea level rises the majority of the landforms are submerged leaving only the updrift edge above the water level (Figure 7.38a). This resembles a flying spit feature, although its formation and evolution are not as such. However, once in this morphological state, the feature is sustained and sediment paths form between the mainland and the relic feature to create a reconnecting spit (Figure 7.38b). This demonstrates that a rising sea level could have an influence on the planform and morphology of a feature and that those found in natural systems may not be wholly representative of the driving wave conditions. The morphology of a coastal system cannot always be explained by the current environmental conditions, but are a product of the

conditions over relatively long periods of time as well as morphological remnants, as shown in the model (Wright and Short, 1984; French *et al.*, 2015).

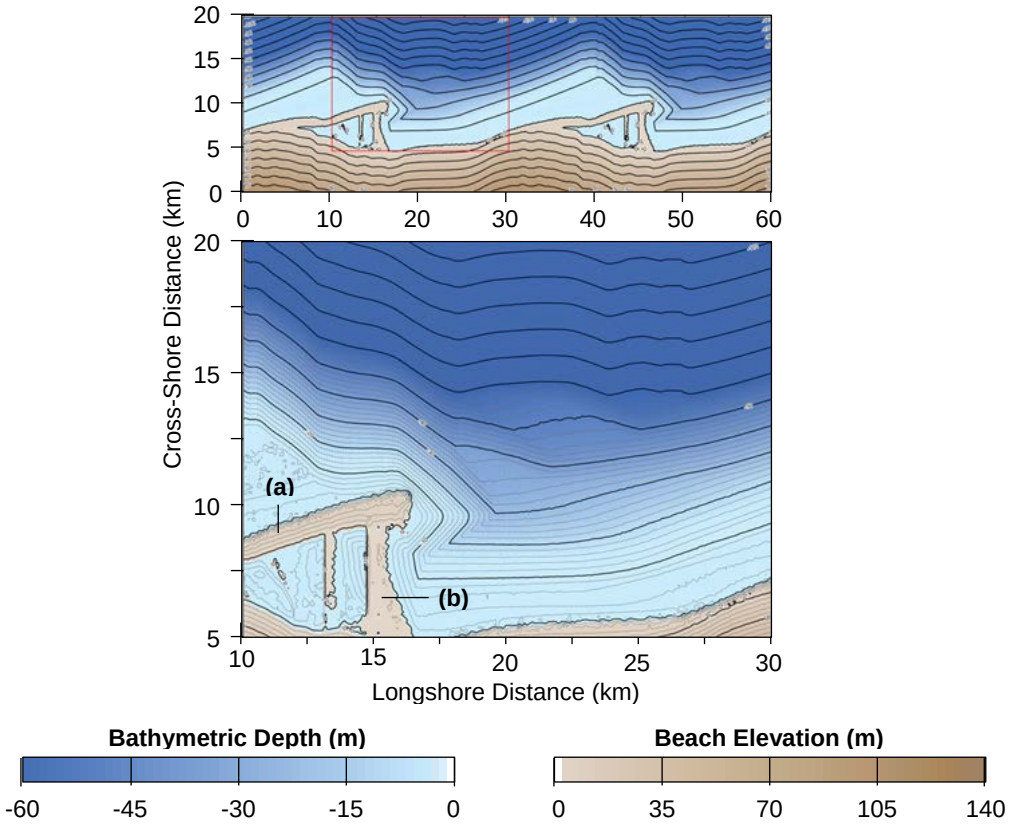

Figure 7.38 Coastal profile after 3,000 simulated years, under wave climate conditions where A = 0.6, U = 0.6 and a rate of sea level rise of 2 m per 100 years.

7.7.3 Morphological Memory

Morphological memories were observed in the results presented in Chapter 6 and are further found in the results presented here. They are increasingly observed with greater rates of sea level rise as the position of the shoreline retreats and the zone of active sediment transport also moves landwards. This leaves sections of the lower nearshore profile largely unaffected by sediment transport processes that occur along the shoreline and in the upper nearshore (Pilkey *et al.*, 1993). This zone is, therefore, able to retain a morphological profile of remnant morphologies and processes (Masselink and Short, 1993; Nicholls *et al.*, 2012; Van Den Berg *et al.*, 2012; French *et al.*, 2015; Thomas *et al.*, 2016). At a slower

rate of sea level rise, the shoreline retreats at a more gradual rate and allows time for the morphology to be adapted and remnant morphologies to be diffused. This process was observed in the Bras d'Or Lakes in Canada, where historic landforms are preserved in the bathymetry to varying extents according to the rates of sea level rise and the ability of features to sustain or keep pace (Shaw *et al.*, 2009). The landforms found in the bathymetry were shown to keep pace with rising sea level when the rate of change was relatively low and were submerged when the rate of rise increased and the supply of material was not sufficient enough to enable the features to keep pace (Shaw *et al.*, 2009).

However, it is important to note, as was discussed in Chapter 6, that these morphological memories could be artificially formed or maintained by processes in the numerical model. It is not within the scope of this research to test these results against the occurrence of morphological memories in natural systems, although they are known to exist (see Chapter 6) (Shaw *et al.,* 2009). The results should, therefore, be considered with this in mind and further research is required in this area (see Chapter 8).

7.8 Conclusion

In this chapter, an analysis is given of how coastal systems behave under a changing water level, used to represent sea level rise at a rate of 1 m and 2 m per 100 years. The results are compared to findings in Chapter 5 and Chapter 6, where the behaviour of coastal systems is analysed under a no sea level rise scenario. The following key concepts have been derived from the results of this chapter:

- The wave climate remains the principle environmental condition which determines the type of features the evolve along the shoreline (e.g. cusps), but sea level rise can influence the rate of development, their vulnerability to submergence and, in some cases, can change the morphology of the landform and its classified type.
- Landforms can transition from one state to another due to changes in sediment transport processes, or the submergence of features whilst the wave climate remains consistent. This highlights that the features observed in coastal systems cannot always be assumed to be products of the wave climate conditions. This emphasises the necessity for investigating the role of sea level rise on the morphodynamics of these systems.
- Sea level rise has a significant influence on erosion and shoreline recession. In every simulation that is subject to sea level rise at a rate of 1 m or 2 m per 100 years, the shoreline recedes in response. Average rates of recession are within two orders of magnitude the rate of rise, although the mechanisms of shoreline retreat are influenced also by the wave climate conditions.
- The rate of shoreline recession and change in shape of the cross-shore coastal profile support the Bruun Rule theory, in terms of order of magnitude change. However, variations from the rule are observed in the individual results, driven by the influence of site-specific environment conditions; namely, the wave climate conditions. These findings demonstrate that whilst the Bruun Rule can be applicable, it fails to account for more detailed morphodynamics in the system which can have an increasing influence over time, particularly in the nearshore.

- Contrary to traditional beliefs, sea level rise is also found to induce progradation in the coastal system through the development of depositional features. Where there is a sufficient supply of sediment to landforms, such as cusps formed by a symmetrical wave climate, the landforms do not only keep pace with rising sea level but are shown to increase in planform area.
- As was also found under a no sea level rise scenario (see Chapter 6), the assumption in many one-line models that the beach and nearshore profile remain shore parallel fails to account for the dynamic nature of the systems. It is observed that the most active areas of the profile along the shoreline and in the upper nearshore zone, show increasing dynamism with increasing rates of sea level rise as well as increasing wave asymmetry (*A*) and proportion of high angle waves (*U*).
- The ability of coastal systems and landforms to keep pace with sea level rise is highly influenced by the geomorphic activity occurring in the system. This influences sediment mobility, pathways of transport and the morphology of the landforms.
- Morphological memories are found in the bathymetric profile all coastal systems, where there is no sea level rise or where the rates are at 1 m or 2 m per 100 years. They are particularly prevalent with increasing rates of sea level rise.

This chapter has explored the response of coastal systems and shoreline features to sea level rise, under twenty-five wave climate conditions. In doing so, it has addressed Research Objective 4 of this study, as given in Chapter 2:

"To investigate the effects of sea level rise on the two-dimensional evolution and behaviour of coastal systems at the mesoscales, including the influence on landforms" (see Chapter 2).

In the following chapter (Chapter 8), the results of this entire study are synthesised in terms of the key findings, wider implications and limitations of this research.

Chapter 8

Synthesis and Conclusion

Key Findings, Limitations and Future Work

8.1 Introduction

The research presented in this thesis has sought to further our knowledge of the behaviour of sandy, wave-dominated coastal systems over mesoscales. A new two-dimensional exploratory model has been developed, the Coastline Evolution Model 2D (CEM2D) (Chapter 3 and Chapter 4), which has been used to investigate the role of wave climate conditions (Chapter 5 and Chapter 6) and sea level change (Chapter 7) on shoreline shape and evolution. The model was developed from the one-line CEM and provides an advanced tool capable of exploring how the shore and nearshore profile evolve according to driving environmental conditions.

In this chapter, the key research outputs from this study are synthesised, and reference is given to the wider implications of this work and the contribution it makes to the advancement of coastal science. A summary of the limitations is

also given, of which are addressed in the proposal for future work. At the close of this chapter, a brief summary is given of how the overarching aim of this research and the four research objectives of this thesis (outlined in Chapter 2) have been met.

8.2 Key Research Outputs

This research has spanned three key strands, which include (1) the development of a new numerical model, (2) its application to investigate the two-dimensional evolution of coastal systems under changing wave climate conditions and (3) the predicted response of these systems to rising sea levels. Key research outputs under each of these themes are given in this section. This is followed by a more holistic synthesis of the wider implications of this research in terms of its scientific importance (Section 8.3).

8.2.1 A New Two-Dimensional Mesoscale Coastline Evolution Model 2D (CEM2D)

The Coastline Evolution Model 2D (CEM2D) was specifically developed for this research (see Chapter 3) to address the gap between existing coastal evolutionary models that are largely designed to simulate either micro- or macro-scale behaviours (van Maanen *et al.,* 2016). This new model was built from the one-contour line Coastline Evolution Model (CEM), retaining much of its underlying principals with the morphological evolution of the systems driven by gradients in longshore sediment transport. However, developments made within CEM2D provides it with a more complex two-dimensional domain structure and the addition of cross-shore distribution mechanisms that enable it to model more complex coastal morphodynamics.

CEM2D was thoroughly tested during its development which included applying The Morris Method (Morris, 1991) as a pre-screening of the model's numerical sensitivity (see Chapter 4). This method is designed to identify the relationship between variations in input and output factor to guide the set-up of the model (Morris, 1991). The wave climate parameters, namely the angle and height of waves, were distinguished as the most influential factors to variations found in model outputs. Whilst this does not identify these factors as drivers of coastal change necessarily, it highlights that their parameterisation should be approached vigilantly. The test was used to inform calibration of the model, to ensure results aligned as accurately as achievable to natural systems and to the results of the empirically tested CEM (Ashton *et al.,* 2001, 2006a, 2006b).

The capabilities of CEM2D has been demonstrated in the results of this research and its ability to simulate fundamental shoreline shapes and coastal morphodynamic behaviours (see Chapter 5, Chapter 6 and Chapter 7). By applying sediment transport processes across an active two-dimensional domain and calculating cross-shore processes from a sediment distribution method (see Chapter 3), the complexities and functionalities of CEM2D have been significantly increased from the CEM. The model proves more inclusive of key sediment transport processes in coastal systems, that are often simplified in one-line models.

The active two-dimensional grid used in CEM2D facilitates the representation of simplified processes of water level change. The relative water level can be fluctuated at incremental or stepped intervals to represent rapid and gradual changes driven, for instance, by tides, storm surge and sea level rise (see Chapter 3). This is a key functionality of CEM2D that will become increasingly

prevalent in long-term modelling and predictions of coastal behaviours, which to-date has been largely unachievable in one-line, reduced complexity mesoscale models.

8.2.2 The Role of Wave Climates in Two-Dimensional Coastal Evolution

The first application of CEM2D served as a test of the abilities and limitations of the new model, as well as to provide an insight into fundamental coastal behaviours. A comparison of results from the empirically tested CEM (Ashton and Murray, 2006b) and CEM2D was given in Chapter 5. Both models were driven by an ensemble of twenty-five wave climates, defined according to the proportional asymmetry of waves (*A*) and the proportion of high angle waves approaching the shoreline (*U*). The results show that there are significant similarities in the outputs of CEM and CEM2D that align with the theory of high angle wave instability (Ashton *et al.*, 2001; Zenkovitch, 1959), serving as an initial validation of the new model. A relationship between the wave asymmetry (*A*) and the skew of morphological features was observed, as well as between the planform amplitude of shoreline features and the proportion of high angle waves (*U*) (Ashton *et al.*, 2001; Zenkovitch, 1959). Four fundamental shoreline shapes are generated from the results, including cusps (Figure 8.1a), sand waves (Figure 8.1b), reconnecting spits (Figure 8.1c) and flying spits (Figure 8.1d) which form under increasingly asymmetric wave climate conditions and with increasing dominance of high angle waves.

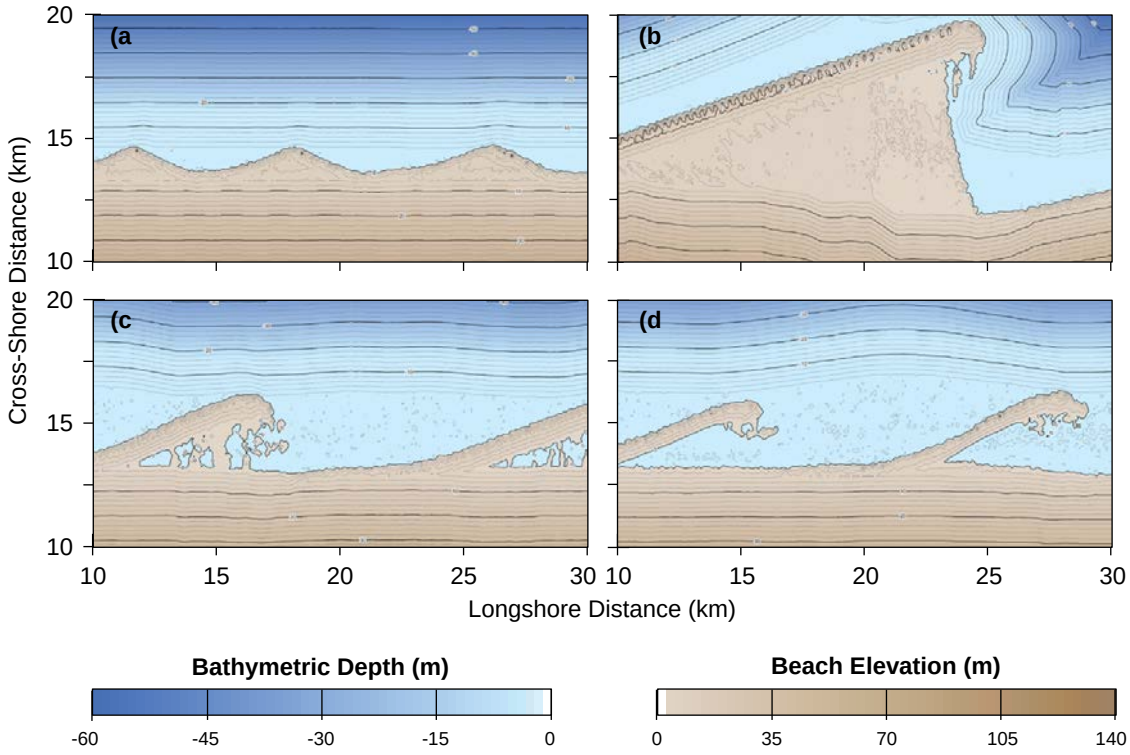

Figure 8.1 Examples of four types of landforms that evolve in CEM2D under increasing wave asymmetry (A) and proportion of high angle waves (U). This including cusps (a), sand waves (b), reconnecting spits (c) and flying spits (d).

The principal differences observed in the model-model comparison between CEM and CEM2D was the greater distinction and clarity of landforms generated in CEM2D; the shoreline features formed reinforce theories of high angle wave instability more clearly by producing a greater definition between the types of features that evolve. The features compare more accurately to natural coastal systems in CEM2D when likened to sites including the Carolina Capes (USA) and Benacre Ness (UK) (Chapter 5). With greater complexity in the modelling approach in CEM2D, as synthesised in Section 8.2.1, it can be argued that this result is due to improved process representation and greater complexity in the set-up of the modelling environment.

As CEM2D allows the simulation and evolution of the beach and nearshore in two dimensions this allows a greater richness of data to be generated over one-dimensional models, such as CEM. These two-dimensional outputs are analysed

in Chapter 6, with the results showing that the sediment dynamics in the coastal zone are complex, non-linear and can be influenced by morphological memories.

Of particular interest in the results of Chapter 6 are the dynamics of the bathymetric profile, since much of the beach surface retains a regular sloping profile offshore (Figure 8.2a). The bathymetry, however, shows varying rates of evolution with the upper nearshore being the most dynamic and highly influenced by the exchange of sediments between the shoreline and the nearshore (Figure 8.2b). The lower nearshore profile tends to be influenced to a lesser degree (Figure 8.2c) and consequently, is able to store remnants of morphological features as they evolve. These findings are in agreement with those of Pilkey *et al.,* (1993), Falqués and Calvete (2005), Hequette and Aernouts (2010) and Ortiz & Ashton (2016).

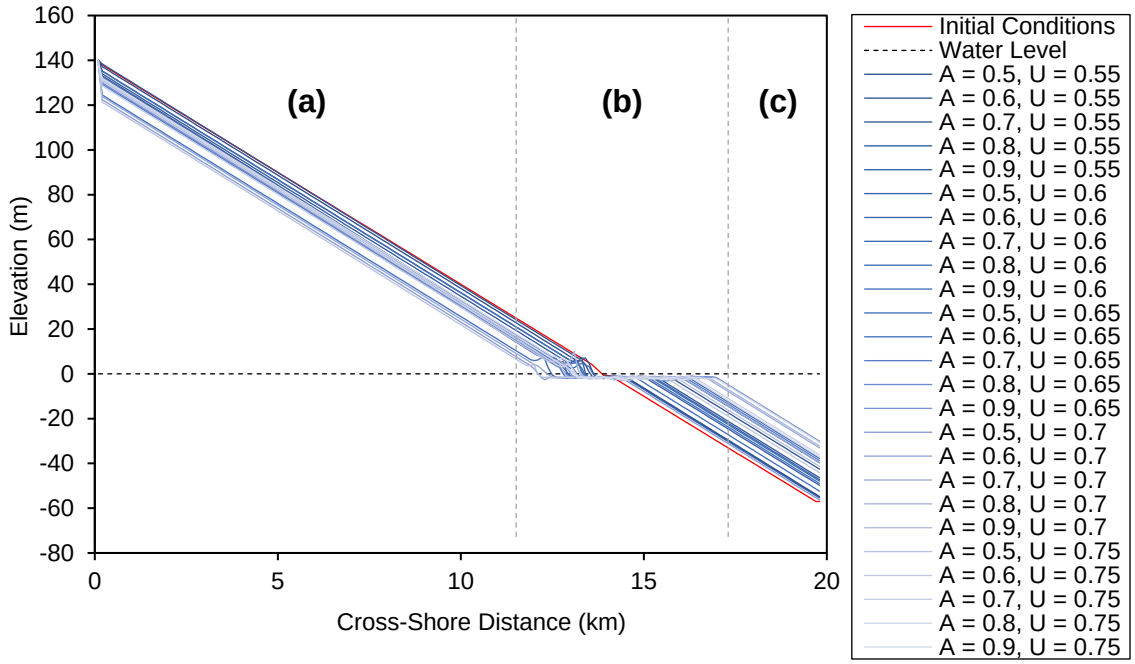

Figure 8.2 Cross-shore profiles taken for each of the twenty-five simulations shown as a 3D line graph, with water level shown as a white band across the transect. Labelled are the (a) beach surface, (b) dynamic shoreline and upper nearshore and (c) the lower nearshore.

One-line models tend to assume that offshore contours lie parallel to the shoreline, but the results in this study demonstrate that this is not always the case, particularly across the nearshore. Omitting or smoothing this zone in the representation of coastal systems could have implications for their long-term evolution (especially with fluctuating sea levels) and could explain the slight differences observed in the results between CEM and CEM2D. Whilst some of the results of CEM2D show a profile with shore-parallel contours, the majority do not exhibit this behaviour, particularly where there is a strong asymmetry in the wave climate or the system is subject to a rising sea level.

A further factor influencing the profile of the nearshore zone is the presence of morphological memories and the remnants of past coastal features. These manifest in the bathymetric profile via three different mechanisms: (1) the preservation of contours from the initial conditions, (2) the formation of a shallow shelf and (3) from remnants of previous morphologies. These features are found regardless of whether sea level rise occurs in the model environment. The types of features found are related to the balance of cross-shore and longshore sediment transport, that determines both the behaviour of the landforms that develop (e.g. migration patterns) and the sediment transport processes which determine the pathway of sediment in the nearshore.

The concept of morphological memories is not new, but few studies have investigated their existence or role in coastal evolution (Wright and Short (1984), French *et al.,* (2015) and Thomas et al., (2016)). The results of this study show that remnant features in the bathymetric profiles can be significant and their behaviour associated with the driving environmental conditions. Whilst it is not within the scope of this study to investigate their role further in terms of their

influence on shoreline dynamics, the results highlight an area of study for future research (Section 8.5).

8.2.3 The Two-Dimensional Response of Coastal Systems to Sea Level Rise

Facilitated by the development of CEM2D, the primary results of this thesis have found that the behaviour of coastal systems over mesoscales are influenced by driving environmental conditions, changes to which can induce a shift away from a quasi-equilibrium state. Hence, introducing an increasing water level into the coastal simulations results in changes to their morphodynamic behaviour and the evolution of landforms along the shoreline.

Introducing an increasing water level into the coastal simulations represents how sea level rise may influence the behaviour of these environments, as is predicted globally over the next century (IPCC, 2013a). The results of this research show that a unique response to the changing water level is found, which is dependent upon the rate of sea level rise and the wave climate conditions; the morphological response of the coast is not instantaneous or uniform (Grinsted *et al.*, 2015).

The primary response of the coastal system is to retreat and to perform a landward rollover, whereby the cross-shore profile translates landwards and upwards as the water level rises. The average rate of retreat is within two orders of magnitude of the vertical sea level rise, with a value of 1.23 m and 2.57 m per year where the rate of sea level rise is 1 m and 2 m per 100 years respectively (Figure 8.3).

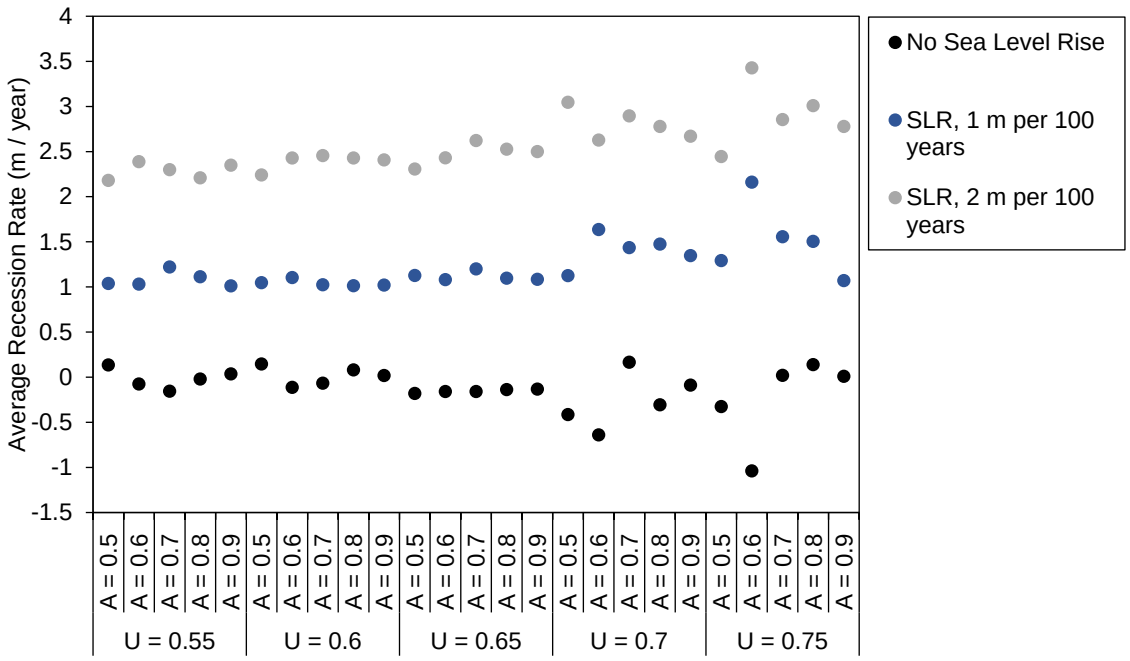

Figure 8.3 A scatter diagram showing the average rate of recession (m) per year, or average change in shoreline position where there is no sea level rise.

There are few theories or rules that can be used to predict the response of the coastal system to sea level rise, but the most commonly used is the Bruun Rule (Bruun, 1988). Whilst the theory is subject to much criticism and is flawed in its application to complex environments (Ranasinghe *et al.*, 2007) it has proven to provide an order of magnitude estimation for shoreline recession rates in the results presented in this thesis. However, variations in the distance over which the shoreline retreats and the evolution of the cross-shore profile according to the driving wave conditions demonstrates that whilst the Bruun Rule is shown to be applicable, it should be used for what it was intended and not for specific estimations of shoreline change.

In terms of the landform response to sea level rise, it is found that the wave climate remains the key driver in determining the shape and type of the coastal system that evolves in the model simulations. According to the wave climate

conditions, as discussed in Section 8.2.2, four principal shorelines shapes form under increasing wave asymmetry (*A*) and proportion of high angle waves (*U*); cusps, sand waves, reconnecting spits and flying spits (Figure 8.1). Sea level rise primarily acts to shift the position of the shoreline, alter the rate of landform development and its morphology, the landforms vulnerability to submergence and in few cases (e.g. $A = 0.5$), its ability to prograde.

A key finding from this research is the ability of coastal systems and landforms to keep pace with rising sea levels, become submerged or prograde depending on the geomorphic activity occurring. The level of geomorphic activity is a function of the wave energy delivered to the coastline, the mobility and dynamics of sediment, the transport of material cross-shore and/or longshore and the resulting morphology of the landforms. The results in Chapter 6 show that the level of geomorphic activity and sediment mobility tends to increase with increasing wave asymmetry (*A*) and the proportion of high angle waves (*U*). The increasing longshore movement of material according to the higher values of *A* and *U* and low-lying nature of the features which form in these environments is observed to reduce the ability of systems to respond to sea level change. Symmetrical wave climates form cuspate landforms with relatively high elevation profiles that are less susceptible to submergence. However, it is also observed that where there is only a slight asymmetry in the wave climate and dominance of high angle waves ($A = 0.6$, $U = 0.6$), sand waves form with relatively low elevation which makes them susceptible to submergence and also with a low longshore flux of material to sustain the landform.

It is observed that under both rates of sea level rise, the dynamics of the bathymetric profiles are similar to when there is no sea level rise. Morphological

memories are found in the majority of wave climate scenarios, predominantly in highly asymmetric wave conditions, and in all sea level rise scenarios. Remnant landforms are better preserved under greater rates of sea level rise, which acts to leave behind coastal features (Figure 8.4). As the active sediment transport and distribution zone shifts with the location of the shoreline, the less active lower nearshore is increasingly unaffected by these processes and retains its morphology.

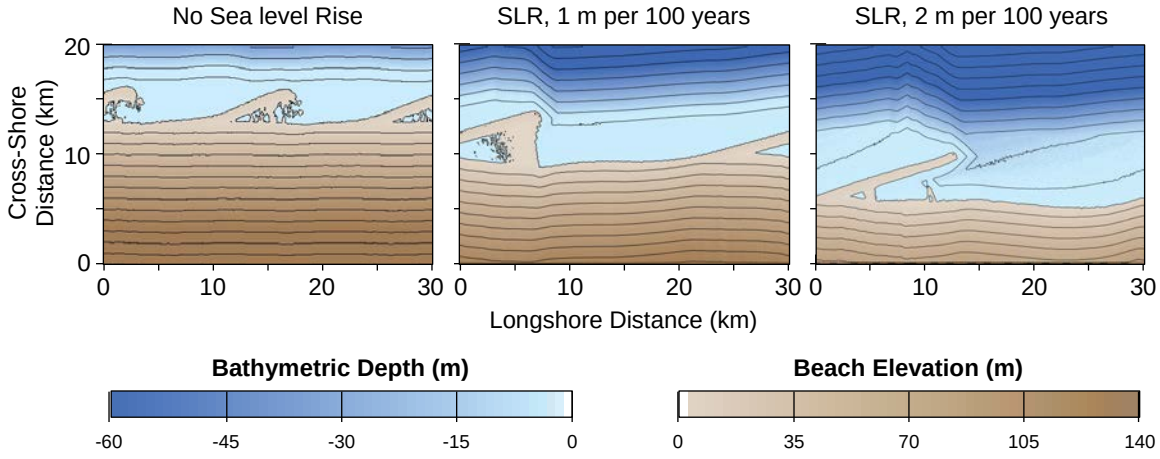

Figure 8.4 The morphology of a coastal environment under wave climate conditions defined by A = 0.7, U = 0.65 under three water level scenarios. The results show increasing preservation of morphological memories with an increasing rate of sea level rise.

In some wave climate conditions (A = 0.6, U = 0.75), sea level rise can alter the types of landforms that develop along the shoreline. This is through the partial submergence of the low-lying areas of the sand waves (which form under these wave climate conditions) which leaves the more elevated updrift edges of the original landforms above the water level. Whilst submergence of this landform can continue if the remaining feature cannot keep pace with the rising water level, in the example (Figure 8.5) the landform is sustained and sediment paths form between the mainland and the relic feature to create a reconnecting spit.

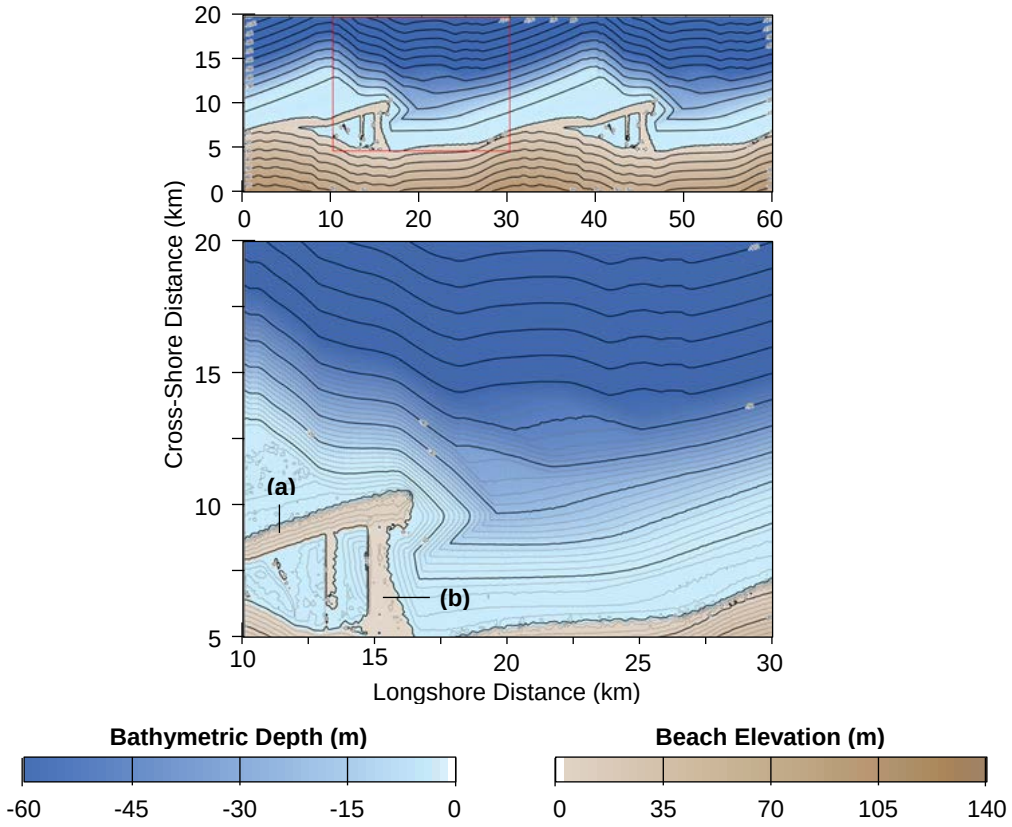

Figure 8.5 Coastal profile after 3,000 simulated years, under wave climate conditions where A = 0.6, U = 0.6 and a rate of sea level rise of 2 m per 100 years.

Landforms in highly symmetrical wave climate (A = 0.5) are shown to grow and prograde in sea level rise conditions, as has been observed in natural systems, such as along the Curonian Spit in Lithuania (Jarmalavičius *et al.*, 2013). The focus of the literature surrounding climate change and sea level rise is driven primarily by erosion and the loss of features. However, the research here shows that changes in environmental systems can have constructive impacts on landforms, of which are overlooked in the literature. Erosion of the coast in one region can lead to deposition in another due to the increase in the supply of sediment, which can act to develop landforms or form new features along the shoreline.

8.3 Key Findings and Wider Implications of this Research

The intention of research is to advance current knowledge and provide a contribution to the research field. From the key outputs given in Section 8.2, three primary implications of this research can be depicted. These relate to (1) the contribution of an advanced numerical model to the field of coastal science, (2) its application to increase our knowledge of coastal morphodynamics and (3) how this knowledge can be applied to the management of these systems. Each of these themes are discussed further in this section.

8.3.1 An Advanced Numerical Tool for Coastal Exploration

As previously ascribed in Section 8.2.1, CEM2D is an advanced tool for investigating mesoscale coastal evolution and simulating variations in longshore and cross-shore morphologies, as well as the dynamics of the one-line shoreline. As has been demonstrated in the results of this thesis (in Chapter 5, Chapter 6 and Chapter 7 in particular) these attributes allow for a more in-depth investigation into the behaviour of coastal systems. Whilst the model has been demonstrated in this thesis to provide an advancement in the field of coastal science, the model also has further applications beyond this volume of work (see Section 8.5). It advances on other existing models in the field and opens up new possibilities for research and predictions of coastal behaviours.

Attention on mesoscale coastal applications has been relatively limited to date due to the complexity of process representation and parameterisation at this scale (van Maanen *et al.,* 2016). Existing models designed for this scale are largely reduced complexity and tend to use a one-line modelling approach, in which the shoreline is represented as a single string of cells that moves according to the erosion or deposition of material (e.g. CEM (Ashton *et al.*, 2001)).

Representing the shoreline as a single contour and assuming shore-parallel bathymetric contours and a planar beach surface, as is the case in these types of models, limits their usability for applications which require the representation of a changing water level. This is particularly problematic if the desire is to model the morphodynamics of coastal environments and conduct predictive modelling exercises over timescales at which a significant change in the water level, or sea level rise occurs.

The omission of processes such as sea level rise from numerical models of coastal change is a primary factor that reduces their ability to provide reliable predictions of future behaviours (Wong *et al.*, 2015). The tool developed here overcomes this criticism and could be widely applicable to coastal regions worldwide, given suitable calibration and validation. The model bridges a gap between other tools at either end of the scale, providing a relatively complex level of detail for the mesoscale whilst retaining the computational efficiency of more simplistic models (van Maanen *et al.*, 2016).

The results demonstrate that whilst a one-line, shore-parallel approach (e.g. Ashton *et al.*, (2001)) and equilibrium coastal profile theories (Bruun, 1988; Dean, 1991) can predict general behaviours in the coastal systems, they fail to show the highly dynamic nature of coastal environments particularly in the geomorphically active nearshore zone. This morphodynamic activity could have significant implications for how the systems evolve over long timescales and so is important to consider and model. CEM2D is able to simulate these more complex morphodynamic behaviours to a greater level of detail than one-line modelling approaches that are often applied in mesoscale studies, due to the way in which it handles sediment transport over the two-dimensional domain.

The results generated by CEM2D have shown to be comparable to the results of the empirically tested CEM (Ashton *et al.*, 2001, 2006a, 2006b), to theoretical models of coastal change and to the behaviour of natural coastal systems. The results have demonstrated the ability of the model to simulate and evolve fundamental shoreline shapes (Chapter 5 and Chapter 6) and generate predictions for their response to sea level rise (Chapter 7).

Each stage of model development and testing gives confidence in the model's ability to represent and simulate processes in natural coastal systems, which gives faith in the outputs and the conclusions that are drawn. These stages also highlight the limitations of the model, which is essential for understanding its capabilities, performing appropriate analysis and interpreting the results.

CEM2D is open source and available to download for others to apply. It is intended that the model be widely used and that it be beneficial to mesoscale coastal research worldwide.

8.3.2 Coastal Morphodynamics at the Mesoscale

One of the principal aims of this thesis, outlined in Chapter 2, was to advance our scientific understanding of behavioural patterns in coastal environments. The key scientific findings of this research contribute to the understanding of the behaviour of coastal systems through reinforcing, disputing and adding to the current state of knowledge.

The key findings of this research can be summarised as follows, in the context of their wider application:

- The wave climate has a significant influence on coastal morphodynamics at the mesoscale and the formation of features along the shoreline. It

remains the key driver in the evolution of the shoreline shape, even under sea level rise conditions.

- Shoreline recession does not always occur linearly with sea level rise, but high rates of SLR lead to greater rates of recession. Shoreline recession is also influenced by the wave energy and direction of sediment transport.
- The bathymetric profile and particularly the upper nearshore is a highly dynamic zone that cannot be simulated in traditionally used one-line models, but which has the potential to influence sediment transport processes. The one-line modelling approach and equilibrium profile theories are unable to capture the dynamic behaviour of coastal systems or their response to a changing water level.
- Morphological memories can be preserved in the bathymetric profile of coastal systems, storing data about predeceasing morphologies and environmental conditions. These are particularly prevalent in systems subject to a rising sea level.
- The wave climate, rate of sea level rise and the dynamics of the bathymetric profile can all influence the way in which the coastal system behaves and evolves. The combination of these processes can lead to different responses of coastal environments to sea level change. Therefore, a single response of coastal systems to sea level rise cannot be assumed.
- The ability of the coastal system and of coastal landforms to keep pace with sea level rise is related to the energy in a system and how it is apportioned. The balance of long-shore and cross-shore sediment transport influences the elevation profile of the landforms, the rate of

sediment supply and the movement of material away from the active geomorphic zone. The factors contribute to the vulnerability of systems to submergence, their ability to keep pace with rising sea levels or their ability to prograde.

The primary findings of this research can be applied to comparable environments globally and be used to inform where further research should be focused; the model is intended to be exploratory and therefore not provide exact behaviour but rather reveal morphodynamic patterns (see Section 8.5). According to the Central Intelligence Agency (CIA), the world's coastline is approximately 356,000 km in length (Central Intelligence Agency (CIA), 2018) of which 20% are classified as sandy, open coasts (Finkl, 2004). This, therefore, means that the research presented in this thesis could be used to inform coastal science relevant for up to 71,200 km of global shorelines, dependent upon the model's suitability for site-specific conditions.

Only a select range of environmental conditions have been presented in this thesis, as necessary for the development of the model and also to demonstrate responses of coastal systems to key environmental conditions. However, for applications to coastal regions globally, the model can be set up and calibrated to more specific environments. However, it should be considered that CEM2D is exploratory in nature and so whilst different conditions can be modelled the results should be taken to represent general patterns. In each different set up of the model, it is necessary to undergo testing as was completed for this study (see Chapter 3 and Chapter 4).

8.3.3 Coastal Management

An overarching motivation for advancing coastal science is to improve our ability to manage vulnerable systems or build our resilience to potential risks. This is not to say that it is the sole purpose of research, but it can provide a purpose or motivation as well as feeding our curiosity about how the world works.

Coastal management practices are informed by the knowledge of how coastal environments behave and predictions about their future morphodynamics; whether over short, medium or long timescales. For instance, shoreline management plans (SMPs) aim to implement practices including ‘no active intervention’ or ‘hold the line’ around the coastline of England and Wales according to these three timescales of 0 to 20 (short), 20 to 50 (medium) and 50 to 100 (long) years from the present (Defra, 2006). Designing suitable and sustainable management is a challenge that must address likely behaviours over relatively long timescales, which should consider the role of climate change. Current research and numerical modelling efforts are beginning to make progress in this direction, but there is still a significant lack of research into predicting what the state of our coastal systems might be like in the future. The modelling tool and findings presented in this thesis, particularly those related to the influence of sea level rise over mesoscales (see Chapter 7), makes a significant contribution to this field.

The current version of CEM2D presented here and the findings of the overall research indicate that coastal systems do not necessarily have a linear response to changing environmental conditions and sea level rise. The Bruun Rule (Bruun, 1988) has some relevance and application to understanding shoreline retreat with and without sea level rise, as shown in the results of Chapter 7, but there are

some major limitations as has been highlighted in previous studies (Ranasinghe *et al.,* 2007). Rather, models such as CEM2D should be used to identify more specific patterns of change related to sea level rise considering a number of key processes, including the wave climate conditions which influence sediment regimes. This is not only for patterns of shoreline retreat, but as has been observed in both natural systems and the modelled results given in Chapter 7, shoreline advance can also occur with sea level rise.

Applying CEM2D to predict the morphodynamic behaviours of coastal systems over relatively long timescales relevant to management practices will inform more holistic coastal management plans that are inclusive of fundamental processes that act at these scales, including sea level change. It is becoming increasingly difficult to manage coastal environments, due to increased risk from processes such as sea level rise (IPCC, 2013a), as well as a greater vulnerability as populations and economies grow (Evans *et al.*, 2004). Not all vulnerable stretches of coastline can be protected, as it is not viable either economically or environmentally. Evans *et al.,* (2004) suggests that within 50 to 100 years' time, the majority of major infrastructures located along the coastline of England and Wales will cease to exist. Therefore, we must be able to understand how these systems evolve naturally in order to design a suitable approach. Even where engineered structures are not desirable or appropriate and an approach of 'no active intervention' is implemented, it is of interested and importance in many cases to understand the likely future state of a system in order to build informed resilience, where it is necessary.

8.4 Limitations

Models by definition are simplifications of reality that contain uncertainties and have limitations. In this section, uncertainties and limitations of CEM2D are discussed. These have been considered throughout the research and are addressed further in future work (Section 8.5).

8.4.1 Uncertainty in the Numerical Model

When attempting to parsimoniously simulate complex environments, processes and parameters are always omitted from the model (Murray, 2007). This is necessary for computational efficiency, but it is also enforced by our lack of knowledge concerning each and every process that influences a given system across all scales. Of the processes that are included, their representation is simplistic and parameterisations are coarse, which by effect induces uncertainties and errors that can propagate over long simulated timescales (Murray, 2007).

8.4.2 Process Representation: Sediment Transport

A specific source of model uncertainty stems from the sediment transport methods. Inherent from CEM, CEM2D uses the one-line approach to calculate wave-induced longshore sediment transport along the shoreline (see Chapter 3). The first step in this technique involves defining the position of the shoreline, via the shoreline search technique described in Chapter 3 and Figure 8.6 (originally Figure 3.2 in Chapter 3). The shoreline search method has proven to induce errors in the model results presented in this thesis, where repeated failed attempts to find a relatively continuous shoreline results in the termination of the simulation. The requirement for a relatively continuous shoreline also omits the inclusion of isolated sediment deposits in the calculation of longshore sediment

transport processes, such as offshore bars. Whilst in CEM2D the sediment distribution method prevents these accumulations from being static, as is the case in the CEM, wave-driven sediment transport is not calculated around the shoreline of these islands and they can therefore only evolve via the landslide-based sediment distribution technique described in Chapter 3.

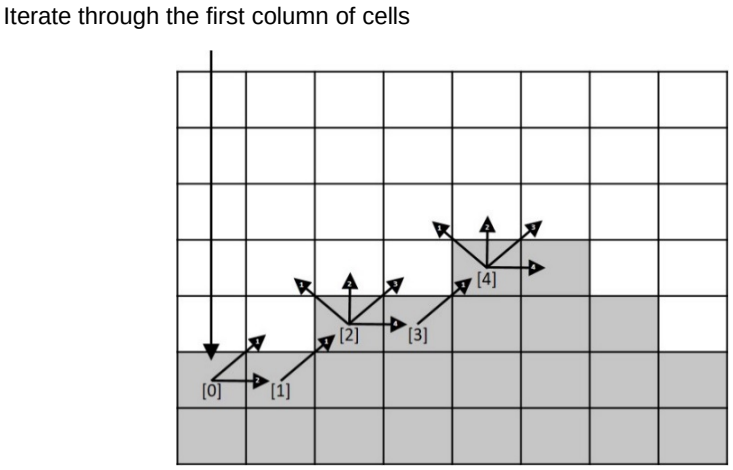

Figure 8.6 A schematic of the shoreline search technique used in CEM (and CEM2D) to map the X and Y location of shoreline cells. The shoreline cell number is given in square brackets and the number on each arrow is the iteration of the clockwise search from the shoreline cell where it originates.

Having determined the position of the shoreline, the CERC equation is used to calculate longshore sediment transport from an offshore wave climate that is transformed according to linear wave theory (see Chapter 3). This method is justifiable in the CEM where the cross-shore profile of the coast is constant, with a bathymetry that evolves parallel to the shoreline. However, the dynamic morphology and changing water depths in CEM2D warrants greater complexity in the calculation of the energy that is delivered to the shoreline, which is inclusive of terms which represent changing water depths (Chini *et al.,* 2010). In particular, this includes calculating how the water depth influences wave transformation processes in the nearshore as described in Chapter 2. Improved complexity in the calculation of wave breaking processes would generate energies along the

shoreline that are more representative of the environmental conditions in the model and which would more accurately calculate sediment transport volumes and processes.

The sediment transport methods described and critiqued above has also proven to induce directional bias in both CEM and CEM2D, which is emphasised or highlighted more clearly in the more complex outputs from CEM2D. As observed in the results, this bias causes morphological features to skew in planform towards the right side of the domain even where the wave climate is symmetrical. It is apparent that the directional bias is primarily induced from processes which scan across the domain (longshore) and which principally scan from the left to the right, as inherited from the CEM. This limitation has been accounted for in the results discussed throughout this thesis, but it is a limitation of the model nonetheless. Further investigation is required to determine how this occurrence is induced and the exact processes within the model that contribute, so that alterations to the source code can be made accordingly.

The processes with the greatest uncertainty in a numerical model are often those that have no physical equivalent but account for natural occurrences or processes that cannot be translated into numerical form. In CEM2D, uncertainty of this manner can be found in the sediment distribution method (see Chapter 3) which is employed subsequent of the shoreline search and longshore sediment transport calculation. Its primary purpose is to transport sediment from the one-line shoreline and redistribute it across the nearshore profile. It also acts to prevent anomalous cell elevations or depressions forming according to the average slope of the coastal profile. The parameterisation of the two key terms which represent the threshold and frequency of sediment distribution in the model

was thoroughly tested throughout the development of CEM2D (Chapter 3 and Chapter 4), to define suitable values that generate results representative of natural systems. One step in this process involved the completion of a sensitivity test to determine the influence of these two values on variations in the output of the model. The results of the sensitive test according to the method of Morris (1991) are given in Chapter 4. Whilst a level of uncertainty remains, the rigorous testing of the model and lack of more accurate representation of the processes at this stage in model development, validate the technique used.

8.5 Future Work

Insights from this research and limitations encountered has given insight into coastal systems and opened new avenues of research for continued work in this field. This section briefly describes some key areas of future work and applications of CEM2D.

8.5.1 Addressing Model Limitations

It is important to address the limitations of the numerical modelling techniques discussed in Section 8.4, with the intention of improving the reliability of results generated by CEM2D. The limitations relate predominantly to the representation of sediment transport processes in the model, many of which are inherited from the CEM. A review of the shoreline search technique and sediment transport methods, including longshore transport and distribution components, would improve the representation of sediment dynamics in the coastal system. It would also serve to allow further complex morphologies to be represented, including the influence of offshore sediment accumulations (e.g. bars) on shoreline evolution and the dynamics of these isolated features. It is important to consider, however,

that there is a balance to be found between model complexity and efficiency (Chau, 2010). Further development of CEM2D should be conscious of the overall purpose of the model and not surpass its intended abilities by increasing its complexity at the expense of increasing error and uncertainty.

8.5.2 Themes in Coastal Morphodynamics

The development of CEM2D provides an advancement in our ability to numerically model and predict the evolution of sandy, wave-dominated coastal systems over mesoscales. The use of the model in this thesis has been targeted at fundamental processes in coastal systems and given insight into how processes such as wave action (Chapter 5 and Chapter 6) and sea level change (Chapter 7) drive morphodynamic evolution in two-dimensions. The increased complexity of the model enables these processes to be explored and unlocks the potential to investigate further processes and process-interactions at varying scales. This could include tidal fluctuations or storm activity which can cause large-scale episodic changes along the coast (Anthony and Orford, 2002; Zhang *et al.,* 2004) (see Chapter 2).

Further exploration of the response of coastal systems to different patterns and rates of sea level rise could be explored. In this thesis, the focus has been given to investigating how linear rates of sea level rise at 1 m and 2 m per 100 years influences coastal morphodynamics. Whilst this has given an insight into the response of these systems to relatively extreme rates of sea level rise (with 2 m per 100 years representing the H++ scenario (Lowe et al., 2009)), further research could focus on a greater range of sea level changes including a lowering of current levels. Temporally variable water level fluctuations could also be

investigated to show whether coastal systems are sensitive to the mechanisms, rates and patterns of sea level change.

A theme of interest for further research is of morphological memory in coastal systems. The concept has been discussed throughout this thesis, with the occurrence of memories, or relic morphologies, identified particularly in the bathymetric profiles of results generated by CEM2D. Whilst there has been some research in this field (e.g. French *et al.,* 2015; Thomas *et al.,* 2016; Wright and Short, 1984) there is a seeming lack of investigation into the role of this phenomenon on long-term evolutionary behaviours. Further investigations could delve into the role of antecedent conditions on shoreline evolution and the resilience of different coastal environments to changes in environments conditions. This is particularly pertinent given that environmental conditions are predicted to change, influenced by climate change (IPCC, 2013a).

8.5.3 Application of CEM2D to Natural Coastal Systems

Alike the CEM, CEM2D is an exploratory model that is not intended to simulate exact behaviours in natural coastal systems and provide accurate predictions of future states (Ashton *et al.,* 2001). Rather, the models are designed to provide an insight into patterns and the response of these environments to changes in driving condition, as demonstrated in this thesis. However, results of CEM and CEM2D have been compared to natural systems including the Carolina Capes (Ashton and Murray, 2006b), the Holderness Coast (Barkwith *et al.*, 2014b), Benacre Ness and the Curonian Spit (Jarmalavičius *et al.,* 2013) to name but a few sites. More specific applications and future projections would be an insightful future step in the development and use of the new model.

The ability of CEM2D to simulate processes such as changing water levels and sea level rise is novel in a mesoscale modelling environment, with many pre-existing and accessible software's using a one-line approach at this scale (e.g. GENESIS (Hanson, 1989); and COVE (Hurst *et al.*, 2015)). The volumetric representation of the coastal morphology and integration of sediment transport processes across the two-dimensional gridded domain, as described in detail in Chapter 3, opens up opportunities to investigate the two-dimensional behaviour and evolution of coastal environments at the scale of interest. It further enables the inclusion of the increasingly important influence of sea level change as a fundamental environmental condition in natural systems. As stated in Section 8.5.2, such investigations are pertinent given the increasing effect of climate change on these vulnerable systems (IPCC, 2013a).

8.6 Conclusion

In this chapter, the research presented in this thesis has been synthesised to provide an overview of the key findings, the wider implications of the work, limitations encountered and suggestions of future work that could stem from this study. It has highlighted the main purpose of the research and how the tool developed (CEM2D) and the insights gained in the morphodynamics of coastal systems can be applied in coastal science.

The overall aim of this research was:

to improve our understanding of the morphodynamic behaviour of wave-dominated sandy coastal systems and predict their likely response to changing environmental conditions, including the wave climate and sea level rise (see Chapter 2).

Through the work completed in this thesis, insight into coastal systems and their morphodynamic behaviour has been gained by developing and applying the Coastline Evolution Model 2D (CEM2D) to understanding the influence of wave climate conditions and rates of sea level rise on the two-dimensional evolution of these systems. More specifically, the aim has been achieved by meeting the four principal research objectives, which were given in Chapter 2. Each of the Research Objectives (1-4) are addressed in Table 8.1-Table 8.4.

Table 8.1 Research Objective 1 and how it has been addressed in this thesis.

Research Objective	**Objective 1:** To develop and test a two-dimensional coastline evolution model which can be used to understand the behaviour of coastal systems according to the driving wave conditions and their likely response to climatic changes over meso-spatiotemporal scales.
Chapter Reference	Chapter 3 and Chapter 4
How has the Research Objective Been met?	This research objective has been addressed through the development of a two-dimensional meso-spatiotemporal numerical model termed the Coastline Evolution Model 2D (CEM2D). The model is based on the underlying principals of the one-line model, the Coastline Evolution Model (CEM), but sediment transport is applied over a two-dimensional grid. The model is capable of simulating the effects of different wave climate conditions and a variable water level on coastal morphodynamics.

Table 8.2 Research Objective 2 and how it has been addressed in this thesis.

Research Objective	**Objective 2:** To examine the relationship between coastal planform and wave climate conditions, which drive sediment transport processes in the environments under consideration, by comparison of the two-dimensional coastline evolution model with an existing model as well as to natural systems.
Chapter Reference	Chapter 5
How has the Research Objective Been met?	The CEM2D evolves the shoreline according to gradients in wave-driven longshore sediment transport, as per the empirically tested CEM. The model has been developed to retain this functionality and is therefore capable of modelling coastal planform evolution according to the wave climate conditions. With its additional complexity and two-dimensional structure, the results show that CEM2D is able to evolve fundamental shoreline shapes, as per the CEM, but is also able to more accurately represent natural coastal systems.

Table 8.3 Research Objective 3 and how it has been addressed in this thesis.

Research Objective	**Objective 3:** To investigate the topographic evolution of coastal systems, according to changes in environmental conditions, including the dynamics of the beach surface and nearshore profile under different wave climate conditions.
Chapter Reference	Chapter 6
How has the Research Objective Been met?	CEM2D handles sediment across a two-dimensional gridded domain, allowing a two-dimensional topographic and bathymetric profile to evolve. Using the model, this research question was addressed by analysing the evolution of the entire coastal profile according to twenty-five different wave climate conditions. Whilst the beach surface showed relatively limited evolution, the upper nearshore was highly dynamic. The results demonstrated the importance of understanding the two-dimensional behaviour of coastal systems for mesoscale modelling and reinforced the decision to develop CEM2D.

Table 8.4 Research Objective 4 and how it has been addressed in this thesis.

Research Objective	**Objective 4:** To investigate the effects of sea level rise on the two-dimensional evolution and behaviour of coastal systems at the mesoscales, including the influence on landforms.
Chapter	Chapter 7
How has the Research Objective Been met?	In light of climate change and increasing rates of sea level rise, it is essential that management practices taking into consideration the behaviour of coastal systems under a rising water level. CEM2D, with its a two-dimensional domain, is able to explore the effects of a variable water level and in this study has been used to understand coastal morphodynamics under rates of sea level rise of 1 m and 2 m per 100 years (which are within scientific plausibility). The model is used to understand the response of the shoreline and of the coastal features including cusps, sand waves, reconnecting spits and flying spits. These are generated under the twenty-five different wave climate conditions. The results show that the evolution of the shoreline is largely dictated by the wave climate conditions even under a rising water level, but that sea level rise can induce erosion, shoreline retreat, submergence and in some cases progradation in coastal environments according to the wave energy and sediment dynamics.

Bibliography

Aagaard, T. (2014) Sediment supply to beaches: Cross-shore sand transport on the lower shoreface. Journal of Geophysical Research: Earth Surface, 119, pp. 913–926.

Aagaard, T., Davidson-Arnott, R., Greenwood, B. and Nielsen, J. (2004) Sediment supply from shoreface to dunes: Linking sediment transport measurements and long-term morphological evolution. Geomorphology, 60(1–2), pp. 205–224.

Ahmed, M.R., Faizal, M., Prasad, K., Cho, Y.J., Kim, C.G. and Lee, Y.H. (2010) Exploiting the orbital motion of water particles for energy extraction from waves. Journal of Mechanical Science and Technology, 24(4), pp. 943–949.

Anthony, E.J. and Orford, J.D. (2002) Between Wave- and Tide-Dominated Coasts : the Middle Ground Revisited. Journal of Coastal Research, SI 36(36), pp. 8–15.

Ashton, A. and Murray, A.B. (2006a) High-angle wave instability and emergent shoreline shapes: 1. Modeling of sand waves, flying spits, and capes. Journal of Geophysical Research, 111(4).

Ashton, A. and Murray, A.B. (2006b) High-angle wave instability and emergent shoreline shapes: 2. Wave climate analysis and comparisons to nature. Journal of Geophysical Research: Earth Surface, 111(4).

Ashton, A., Murray, A.B. and Arnault, O. (2001) Formation of coastline features by large-scale instabilities induced by high-angle waves. Nature, 414(6861), pp. 296–300.

Ashton, A., Murray, A.B. and Littlewood, R. (2007) The response of spit shapes to wave-angle climates. In Coastal Sediment ’07, pp. 351–363.

Ashton, A., Nienhuis, J. and Ells, K. (2015) On a neck, on a spit: controls on the shape of free spits. Earth Surface Dynamics Discuss.

Ashton, A., Murray, A.B. and Ruessink, G. (2003) Initial tests of a possible explanation for alongshore sandwaves along the Dutch coast. Proceedings of the 3rd IAHR symposium. Terra Scientific Publishing Company, Tokyo, pp. 265–285.

Bakhtyar, R., Barry, D.A., Li, L., Jeng, D.S. and Yeganeh-Bakhtiary, A. (2009) Modeling sediment transport in the swash zone: A review. Ocean Engineering, 36(9–10), pp. 767–783.

Banno, M. and Kuriyama, Y. (2014) Prediction of Future Shoreline Change With Sea-Level Rise and Wave Climate Change At Hasaki, Japan. International Conference in Coastal Engineering, pp. 1–10.

Barkwith, A., Hurst, M.D., Thomas, C.W., Ellis, M.A., Limber, P.L. and Murray, A.B. (2014a) Coastal vulnerability of a pinned, soft-cliff coastline, II: Assessing the influence of sea walls on future morphology. Earth Surface Dynamics, 2(1), pp. 233–242.

Barkwith, A., Hurst, M.D., Thomas, C.W., Ellis, M.A., Limber, P.W. and Murray, A.B. (2013) Assessing the influence of sea walls on the coastal vulnerability of a pinned, soft-cliff, sandy coastline. Earth Surface Dynamics. European Geosciences Union.

Barkwith, A., Thomas, C.W., Limber, P.W., Ellis, M.A. and Murray, A.B. (2014b) Coastal vulnerability of a pinned, soft-cliff coastline – Part I: Assessing the natural sensitivity to wave climate. Earth Surface Dynamics. Copernicus GmbH, 2(1), pp. 295–308.

Beres, D.L. and Hawkins, D.M. (2001) Plackett-Burman technique for sensitivity analysis of many-parametered models. Ecological Modelling, 141(1–3), pp. 171–183.

Bird, E. (2011) Coastal Geomorphology: An Introduction. John Wiley and Sons.

Blenkinsopp, C.E., Turner, I.L., Allis, M.J., Peirson, W.L. and Garden, L.E. (2012) Application of LiDAR technology for measurement of time-varying free-surface profiles in a laboratory wave flume. Coastal Engineering, 68, pp. 1–5.

Box, G. (1979). Robustness in the strategy of scientific model building. Robustness in Statistics, 201–236.

Bray, M.J. and Hooke, J.M. (1997) Prediction of Soft-Cliff Retreat with Accelerating Sea-Level Rise. Journal of Coastal Research, pp. 453-467.

Bray, M., Hooke, J. and Carter, D. (1997) Planning for Sea-Level Rise on the South Coast of England: Advising the Decision-Makers. Transactions of the Institute of British Geographers, 22(1), pp. 13–30.

Brockmann, D. and Morgenroth, E. (2007a) Comparing global sensitivity analysis for a biofilm model for two-step nitrification using the qualitative screening method of Morris or the quantitative variance-based Fourier Amplitude Sensitivity Test (FAST). Water Science and Technology, 56(8), pp. 85-93.

Brown, J. (2013) Waves, Tides and Shallow-Water Processes: Prepared by an Open University Course Team. Elsevier.

Bruun, P. (1954) Coast erosion and the development of beach profiles. U.S. Beach Erosion Board

Bruun, P. (1962) Sea-Level Rise as a Cause of Shore Erosion. Proceedings of the American Society of Civil Engineers, pp. 117–130.

Bruun, P. (1988) The Bruun rule of erosion by sea-level rise: a discussion on large-scale two-and three-dimensional usages. Journal of Coastal Research, pp. 627-648.

Burgess, K., Jay, H. and Hosking, A. (2004) Futurecoast: Predicting the future coastal evolution of England and Wales. Journal of Coastal Conservation, 10(1), pp. 65.

Burningham, H. and French, J. (2017) Understanding coastal change using shoreline trend analysis supported by cluster-based segmentation. Geomorphology, 282, pp. 131–149.

Butt, T., Russell, P., Miles, J. and Turner, I. (2007) Sediment Transport Processes in the Swash Zone of Sandy Beaches. Journal of Coastal Research, 2007(50), pp. 636–640.

Campolongo, F., Cariboni, J. and Saltelli, A. (2007) An effective screening design for sensitivity analysis of large models. Environmental Modelling and Software. Elsevier, 22(10), pp. 1509–1518.

Carter, R.W.G. (1982) Cuspate foreland. Beaches and Coastal Geology. Dordrecht: Kluwer Academic Publishers, pp. 349–349.

Carter, R.W.G. (2013) Coastal Environments: An Introduction to the Physical, Ecological, and Cultural Systems of Coastlines. Elsevier.

Cartier, A. and Héquette, A. (2011) Estimation of longshore and cross shore sediment transport on sandy macrotidal beaches of Northern France. Proceedings of Coastal sediments, 3, pp. 2130-2143.

CEFAS (2018) WaveNet Interactive Map. Available at: http://wavenet.cefas.co.uk/Map (Accessed: 16 August 2018).

Central Intelligence Agency (CIA) (2018). The World Factbook. Available at: https://www.cia.gov/library/publications/the-world-factbook/index.html (Accessed: 18 October 2018).

Channel Coastal Observatory (2018) Hornsea. Available at: http://www.channelcoast.org/data_management/real_time_data/charts/?chart=72 (Accessed: 16 August 2018).

Chau, K.W. (2010) Modelling for Coastal Hydraulics and Engineering. CRC Press.

Chini, N., Stansby, P., Leake, J., Wolf, J., Roberts-Jones, J., and Lowe, J. (2010). The impact of sea level rise and climate change on inshore wave climate: A case study for East Anglia (UK). Coastal Engineering, 57(11), 973–984.

Cooper, J.A.G. and Pilkey, O.H. (2004) Sea-level rise and shoreline retreat: time to abandon the Bruun Rule. Global and Planetary Change, 43(3–4), pp. 157–171.

Coulthard, T. (2001) Landscape evolution models: a software review. Hydrological Processes, 15(1), pp. 165–173.

Coulthard, T.J., Neal, J.C., Bates, P.D., Ramirez, J., de Almeida, G.A. and Hancock, G.R. (2013) Integrating the LISFLOOD-FP 2D hydrodynamic model with the CAESAR model: implications for modelling landscape evolution. Earth Surface Processes and Landforms, 38(15), pp. 1897–1906.

Cowell, P.J. and Thom, B.G. (1994) Morphodynamics of coastal evolution, Coastal Evolution: Late Quaternary shoreline morphodynamics. Cambridge, United Kingdom and New York, NY, USA: Cambridge University Press.

Cukier, R.I., Fortuin, C.M., Shuler, K.E., Petschek, A.G. and Schaibly, J.H. (1973) Study of the sensitivity of coupled reaction systems to uncertainties in rate coefficients. I Theory. Journal of Chemical Physics, 59(8), pp. 3873–3878.

Dalrymple R.W., Choi K. (1978) Sediment transport by tides. In: Sedimentology. Encyclopedia of Earth Science. Springer, Berlin, Heidelberg

Davidson-Arnott, R.G.D. and Van Heyningen, A.G. (2003) Migration and sedimentology of longshore sandwaves, Long Point, Lake Erie, Canada. Sedimentology, 50(6), pp. 1123–1137.

Davis Jr., R. (2012) Coastal Sedimentary Environments. Springer Science and Business Media.

Davis Jr., R. and Dalrymple, R. (2011) Principles of Tidal Sedimentology. Springer Science and Business Media.

Davis, R.A. and Hayes, M.O. (1984) What is a wave-dominated coast? Marine Geology, 60(1–4), pp. 313–329.

Dean, R.G. (1991) Equilibrium Beach Profiles: Characteristics and Applications. Journal of Coastal Research, 7(1), pp. 53–84.

Dean, R.G. and Dalrymple, R.A. (2004a) Coastal processes with engineering applications, Cambridge University Press.

Defra. (2006) Shoreline management plan guidance Volume 1: Aims and requirements. DEFRA, 1, pp. 1–54.

DHI (2017) 'MIKE 21: Software Catalogue 2017'.

Dickson, D.M., Walkden, D.M. and Hall, P.J. (2006) Modelling the impacts of climate change on an eroding coast over the 21st Century. Available at: http://www.tyndall.ac.uk/sites/default/files/wp103.pdf (Accessed: 4 December 2018).

Dickson, M.E., Walkden, M. J.A. and Hall, J.W. (2007) Systemic impacts of climate change on an eroding coastal region over the twenty-first century. Climatic Change, 84(2), pp. 141–166.

ESRI (2018) 'Light Gray Canvas' [basemap]. Scale Not Given.'World Light Gray Canvas Base'. Available at: http://www.arcgis.com/home/item.html?id=149a9bb14d604bd18f4597b21c19fac7 (Accessed: 15 August 2018).

EUROSION (2004) Living with coastal erosion in Europe: Sediment and Space for Sustainability PART II-Maps and statistics. Available at: http://www.eurosion.org/reports-online/part2.pdf (Accessed: 3 October 2018).

Evans, E. (2004) Foresight: future flooding: scientific summary: volume I: future risks and their drivers. London: Department of Trade and Industry.

Falqués, A. and Calvete, D. (2005) Large-scale dynamics of sandy coastlines: Diffusivity and instability. Journal of Geophysical Research C: Oceans, 110(3), pp. 1–15.

Finkl, C. W. (2004) Coastal Classification: Systematic Approaches to Consider in the Development of a Comprehensive Scheme. Journal of Coastal Research, 201(1), pp. 166–213.

Finkl, C.W. (2012) Coastal Hazards. Springer Science and Business Media.

Fisher, R.L. (1955) Cuspate Spits of St. Lawrence Island, Alaska. The Journal of Geology, 63(2), pp. 133–142.

Flick, R.E., Chadwick, D.B., Briscoe, J. and Harper, K.C. (2012) “Flooding” versus “Inundation”. Eos, 93(38), pp. 365–366.

French, J.R. and Burningham, H. (2013) Coasts and climate: Insights from geomorphology. Progress in Physical Geography, 37(4), pp. 550–561.

French, J., Payo, A., Murray, B., Orford, J., Eliot, M. and Cowell, P. (2015) Appropriate complexity for the prediction of coastal and estuarine geomorphic behaviour at decadal to centennial scales. Geomorphology, 256, pp. 3-16.

French, J., Thornhill, G. and Burningham, H. (2014) ESTEEM - a New “Hybrid Complexity” Model for Prediction of Estuary Morphological Evolution at Decadal to Centennial Scales. in AGU Fall Meeting.

French, P. (2002) Coastal and estuarine management. Routledge.

Gan, Y., Duan, Q., Gong, W., Tong, C., Sun, Y., Chu, W., Ye, A., Miao, C. and Di, Z. (2014) A comprehensive evaluation of various sensitivity analysis methods: A case study with a hydrological model. Environmental Modelling and Software. Elsevier, 51, pp. 269–285.

Gelfenbaum, G. and Kaminsky, G.M. (2010) Large-scale coastal change in the Columbia River littoral cell: An overview, Marine Geology, 273(1–4), pp. 1–10.

Gravens, M.B., Kraus, N.C. and Hanson, H. (1991) GENSIS: Generalized Model for Simulating Shoreline Change. Report 2. Workbook and System User's Manual (No. CERC-TR-89-19-2). Coastal Engineering Research Centre Vicksburg MS.

Grinsted, A., Jevrejeva, S., Riva, R.E. and Dahl-Jensen, D. (2015) Sea level rise projections for Northern Europe under RCP8.5. Climate Research, 64(1), pp. 15–23.

Gulliver, F.P. (1897) Dungeness Foreland. The Geographical Journal, 9(5), pp. 536.

Hallermeier, R.J. (1978) Uses for a Calculated Linit Depth to Beach Erosion. in Proceedings of the 16th International Conference on Coastal Engineering, pp. 1493–1512.

Hanson, H. (1989) GENESIS: a generalized shoreline change numerical model. Journal of Coastal Research, pp. 1–27.

Hanson, H. and Kraus, N. (1989) GENESIS: Generalized Model for Simulating Shoreline Change. Report 1. Technical Reference (No. CERC-TR-89-19-1). Coastal Engineering Research Centre Vicksburg MS.

Hanson, H., Aarninkhof, S., Capobianco, M., Jimenez, J.A., Larson, M., Nicholls, R.J., Plant, N.G., Southgate, H.N., Steetzel, H.J., Stive, M.J.F. and de Vriend, H.D. (2003) Modelling of Coastal Evolution on Yearly to Decadal Time Scales. Journal of Coastal Research,19(4), pp. 790.

Haslett, S.K. (2009a) Coastal systems. Routledge introductions to environment series.

Hayes, M. (1979) Barrier island morphology as a function of tidal and wave regime. In Leatherman, S. (ed.) Barrier Islands from the Gulf of St. Lawrence to the Gulf of Mexico. New York: Academic Press, pp. 1–27.

Hequette, A. and Aernouts, D. (2010) The influence of nearshore sand bank dynamics on shoreline evolution in a macrotidal coastal environment, Calais, northern France. Continental Shelf Research, 30(12), pp. 1349–1361.

Hoefel, F. and Elgar, S. (2003) Wave-induced sediment transport and sandbar migration. Science (New York, N.Y.), 299(5614), pp. 1885–7.

Holthuijsen, L.H. (2007) Waves in oceanic and coastal waters. Cambridge university press.

Hurst, M., Barkwith, A., and Ellis, M. (2015). Exploring the sensitivities of crenulate bay shorelines to wave climates using a new vector-based one-line model. Journal of Geophysical Research: Earth Surface, 120(12), pp. 2586-2608.

Hurst, M.D., Barkwith, A., Ellis, M.A., Thomas, C.W. and Murray, A.B. (2015) Exploring the sensitivities of crenulate bay shorelines to wave climates using a new vector-based one-line model. Journal of Geophysical Research: Earth Surface, 120(12), pp. 2586–2608.

Hurst, M.D., Barkwith, A., Thomas, C. and Ellis, M.A. (2014) Vector-based one-line model for shoreline evolution: application to explore wave-climate control on bay morphology. In AGU Fall Meeting Abstracts.

Hutton, C.J. (2012) Modelling Geomorphic Systems: Numerical Modelling. British Society for Geomorphology Geomorphological Techniques.

Iooss, B. and Lemaître, P. (2015) A Review on Global Sensitivity Analysis Methods (pp. 101-122). Springer, Boston, MA.

IPCC. (2013a). IPCC Fifth Assessment Report (AR5) - The physical science basis. IPCC.

IPCC (2013b) Summary For Policy Makers. In: Climate Change 2013: The Physical Science Basis. Contribution of Working Group I to the Fifth Assessment Report of the Intergovernmental Panel on Climate Change. In Stocker, T. F. et al. (eds) IPCC. Cambridge, United Kingdom and New York, NY, USA: Cambridge University Press, pp. 1–29.

Jarmalavičius, D., Žilinskas, G. and Pupienis, D. (2013) Observation on the interplay of sea level rise and the coastal dynamics of the Curonian Spit, Lithuania. Geologija, 55(2).

Jenkins, G., Murphy, J., Sexton, D., Lowe, J., Jones, P. and Kilsbu, C. (2009) UKCP09 Briefing report. Met Office Hadley Centre, Exeter, UK.

Kamphuis, J. W. (1991) Alongshore Sediment Transport Rate. Journal of Waterway, Port, Coastal, and Ocean Engineering, 117(6), pp. 624–640.

Karunarathna, H., Horrillo-Caraballo, J., Kuriyama, Y., Mase, H., Ranasinghe, R. and Reeve, D.E. (2016) Linkages between sediment composition, wave climate

and beach profile variability at multiple timescales. Marine Geology, 381, pp. 194–208.

King, D.M. and Perera, B.J.C. (2013) Morris method of sensitivity analysis applied to assess the importance of input variables on urban water supply yield – A case study. Journal of Hydrology, 477, pp. 17–32.

Komar, P.D. (1971) The mechanics of sand transport on beaches. Journal of Geophysical Research, 76(3), pp. 713–721.

Komar, P.D. (1978) Angle of repose. In Sedimentology. Springer Berlin Heidelberg, pp. 25–26.

Komar, P.D. and Inman, D.L. (1970) Longshore sand transport on beaches. Journal of Geophysical Research, 75(30), pp. 5914–5927.

Komar, P.D., Lanfredi, N., Baba, M., Dean, R.G., Dyer, K., Healy, T., Ibe, A.C., Terwindt, J.H.J. and Thom, B.G. (1991) The response of beaches to sea-level changes - a review of predictive models. Journal of Coastal Research, 7(3), pp. 895–921.

Kondolf, G.M. and Piegay, H. (2016) Tools in fluvial geomorphology, 2nd edition. John Wiley and Sons.

Kopp, R.E., Horton, R.M., Little, C.M., Mitrovica, J.X., Oppenheimer, M., Rasmussen, D.J., Strauss, B.H. and Tebaldi, C. (2014) Probabilistic 21st and 22nd century sea-level projections at a global network of tide-gauge sites. Earth's Future, 2(8), pp. 383–406.

Kraus, N.C. and Harikai, S. (1983) Numerical model of the shoreline change at Oarai beach. Coastal Engineering, 7(1), pp. 1–28.

Kristensen, S.E., Drønen, N., Deigaard, R. and Fredsoe, J. (2016) Impact of groyne fields on the littoral drift: A hybrid morphological modelling study. Coastal Engineering, 111, pp. 13–22.

Larson, M., Kubota, S. and Erikson, L. (2004) Swash-zone sediment transport and foreshore evolution: Field experiments and mathematical modeling. Marine Geology, 212(1–4), pp. 61–79.

Leatherman, S.P., Zhang, K. and Douglas, B.C. (2000) Sea level rise shown to drive coastal erosion. Eos, Transactions American Geophysical Union, 81(6), pp.55-57.

Lesser, G.R., Roelvink, J.V., Van Kester, J.A.T.M. and Stelling, G.S. (2004) Development and validation of a three-dimensional morphological model. Coastal Engineering, 51(8), pp. 883–915.

Lick, W. and Mcneil, J. (2001) Effects of sediment bulk properties on erosion rates. The Science of The Total Environment, 266(1–3), pp. 41–48.

Lowe, J., Howard, T., Pardaens, A., Tinker, J., Holt, J., Wakelin, S., Milne, G., Leake, J., Wolf, J., Horsburgh, K. and Reeder, T. (2009) UK Climate Projections science report: Marine and coastal projections. Exeter, UK.

Luijendijk, A.P., Ranasinghe, R., de Schipper, M.A., Huisman, B.A., Swinkels, C.M., Walstra, D.J. and Stive, M.J. (2017) The initial morphological response of the Sand Engine: A process-based modelling study. Coastal Engineering, 119, pp. 1–14.

Martins, K., Blenkinsopp, C.E. and Zang, J. (2016) Monitoring individual wave characteristics in the inner surf with a 2-dimensional laser scanner (LiDAR). Journal of Sensors.

Martins, K., Blenkinsopp, C.E., Power, H.E., Bruder, B., Puleo, J.A. and Bergsma, E.W. (2017) High-resolution monitoring of wave transformation in the surf zone using a LiDAR scanner array. Coastal Engineering, 128, pp. 37–43.

Masselink, G. (2008) Coasts. In An Introduction to Physical Geography and the Environment, 2nd edition. Pearson, pp. 467–507.

Masselink, G. and Russell, P. (2013) Impacts of climate change on coastal erosion. MCCIP Science Review, pp. 71–86.

Masselink, G. and Short, A. (1993) The Effect of Tide Range on Beach Morphodynamics and Morphology: A Conceptual Beach Model. Journal of Coastal Research, 9(3), pp. 785–800.

Masselink, G., Hughes, M. and Knight, J. (2014) Introduction to Coastal Processes and Geomorphology, 2nd edition. Routledge.

Mccarthy, M.A., Burgman, M.A. and Ferson, S. (1995) Sensitivity Analysis for Models of Population Viability. Biological Conservation, 73, pp. 93–100.

McLean, R.F. and Kirk, R.M. (1969) Relationships between grain size, size-sorting, and foreshore slope on mixed sand - shingle beaches. New Zealand Journal of Geology and Geophysics, 12(1), pp. 138–155.

McNinch, J.E. and Luettich, R.A. (2000) Physical processes around a cuspate foreland: Implications to the evolution and long-term maintenance of a cape-associated shoal. Continental Shelf Research, 20(17), pp. 2367–2389.

Met Office (2016) 1953 east coast flood - 60 years on. Met Office, Exeter.

Mimura, N. and Kawaguchi, E. (1997) Responses of coastal topography to sea-level rise. In Proceedings of the Coastal Engineering Conference, pp. 1349-1360.

Moore, L.J., List, J.H., Williams, S.J. and Stolper, D. (2007) Modelling barrier island response to sea-level rise in the outer banks, North Carolina. In Coastal Sediments ’07: Sixth International Symposium on Coastal Engineering and Science of Coastal Sediment Process, pp. 1153–1164.

Morris, M.D. (1991) Factorial sampling plans for preliminary computational experiments. Technometrics, 33(2), pp. 161–174.

Murray, A.B. (2007) Reducing model complexity for explanation and prediction. Geomorphology, 90(3–4), pp. 178–191.

Murray, A.B., Gopalakrishnan, S., McNamara, D.E. and Smith, M.D. (2013) Progress in coupling models of human and coastal landscape change. Computers and Geosciences, 53, pp. 30–38.

Nam, P.T., Larson, M. and Hanson, H. (2009) A numerical model of nearshore waves, currents, and sediment transport. Coastal Engineering, 56(11), pp. 1084–1096.

National Trust (2015) Shifting shores – playing our part at the coast. Available at: https://www.nationaltrust.org.uk/documents/shifting-shores-report-2015.pdf (Accessed: 2 January 2019).

Nicholls, R.J., Bradbury, A., Burningham, H., Dix, J., Ellis, M., French, J., Hall, J.W., Karunarathna, H.U., Lawn, J., Pan, S. and Reeve, D.E. (2012) iCOASST–

integrating coastal sediment systems. Coastal Engineering Proceedings, 1(33), p.100.

Nicholls, R.J., Birkemeier, W.A. and Hallermeier, R.J. (1997) Application of the depth of closure concept. Coastal Engineering, pp. 3874-3887.

NOAA (2017) Tides and Water Levels. Available at: https://oceanservice.noaa.gov/education/kits/tides/tides07_cycles.html (Accessed: 23 October 2018).

NOAA (2018) Astronomical Data. Available at: https://tidesandcurrents.noaa.gov/astronomical.html (Accessed: 23 October 2018).

Norton, J. (2015) An introduction to sensitivity assessment of simulation models. Environmental Modelling and Software, 69, pp. 166–174.

Oreskes, N., Shrader-Frechette, K. and Belitz, K. (1994) Verification, validation, and confirmation of numerical models in the Earh Sciences. Science, 263(5147), pp. 641–645.

Ortiz, A.C. and Ashton, A. (2016) Exploring shoreface dynamics and a mechanistic explanation for a morphodynamic depth of closure. Journal of Geophysical Research: Earth Surface, 121(2), pp.442-464.

Pacheco, A., Horta, J., Loureiro, C. and Ferreira, Ó. (2015) Retrieval of nearshore bathymetry from Landsat 8 images: A tool for coastal monitoring in shallow waters. Remote Sensing of Environment, 159, pp. 102–116.

Park, J.-Y. and Wells, J. T. (2005) Longshore Transport at Cape Lookout, North Carolina: Shoal Evolution and the Regional Sediment Budget. Journal of Coastal Research, 211, pp. 1–17.

Pianosi, F. and Wagener, T. (2015) A simple and efficient method for global sensitivity analysis based on cumulative distribution functions. Environmental Modelling and Software, 67, pp. 1–11.

Pianosi, F., Beven, K., Freer, J., Hall, J.W., Rougier, J., Stephenson, D.B. and Wagener, T. (2016) Sensitivity analysis of environmental models: A systematic review with practical workflow. Environmental Modelling and Software, 79, pp. 214–232.

Pilkey, O.H., Young, R.S., Riggs, S.R., Smith, A.W.S., Wu, H., and Pilkey, W.D. (1993) The concept of shoreface profile of equilibrium: a critical review. Journal of Coastal Research, 9(1), pp. 255-278.

Pilkey, O., Young, R. and Cooper, A. (2013) Quantitative modeling of coastal processes: A boom or a bust for society?. The Geological Society of America, Special Pa.

Pinet, P.R. (2009) Invitation to Oceanography. Psychological Science.

Price, A.W. and Zenkovitch, V.P. (1964) Cyclic Cuspate Sand Spits and Sediment Transport Efficiency [with Discussion and Rejoinder]. The Journal of Geology, 72(6), pp. 876–880.

Quinn, J.D., Philip, L.K. and Murphy, W. (2009) Understanding the recession of the Holderness Coast, east Yorkshire, UK: a new presentation of temporal and

spatial patterns. Quarterly Journal of Engineering Geology and Hydrogeology, 42(2), pp. 165–178.

Ramming, H.-G. and Kowalik, Z. (1980) Numerical Modelling of Marine Hydrodynamics. Elsevier.

Ranasinghe, R. (2016) Assessing climate change impacts on open sandy coasts: A review. Earth-Science Reviews, pp. 320–332.

Ranasinghe, R., Watson, P., Lord, D., Hanslow, D., and Cowell, P. (2007). Sea Level Rise, Coastal Recession and the Bruun Rule. In Proceedings of Coasts and Ports '07, Melbourne, VIC, Australia.

Raynor, P. and Chatterton, J. (2014) Flood Defences Cost Money, No Defences Cost More: an Economic Case for the Humber and United Kingdom. Report Prepared on Behalf of the Humber Parlimentarians, Local Authorities and the Humber Local Enterprise Partnership. Available at: http://www.floodcba.eu/main/wp-content/uploads/Flood-Risk-Management-Investing-in-the-future-of-the-Humber-Estuary.pdf (Accessed: 28 January 2016).

Rosati, J.D. (2005) Concepts in Sediment Budgets. Journal of Coastal Research, 212, pp. 307–322.

Rosen, P.S. (1975) Origin and processes of cuspate spit shorelines. Geology and Engineering. Academic Press, pp. 77–92.

Saltelli, A. (2002) Sensitivity Analysis for Importance Assessment. Risk Analysis, 22(3), pp. 579–590.

Saltelli, A., Ratto, M., Andres, T., Campolongo, F., Cariboni, J., Gatelli, D., Saisana, M. and Tarantola, S. (2008) Global sensitivity analysis: the primer. John Wiley & Sons.

Sawczyński, S. and Kaczmarek, L.M. (2014) Sediment transport in the coastal zone. Technical Sciences/University of Warmia and Mazury in Olsztyn.

Schwartz, M. (2006) Encyclopedia of Coastal Science. Springer Science & Business Media.

Schwartz, M.L. (1967) The Bruun Theory of Sea-Level Rise as a Cause of Shore Erosion. The Journal of Geology, 75(1), pp. 76–92.

Scott, T., Masselink, G. and Russell, P. (2011) Morphodynamic characteristics and classification of beaches in England and Wales. Marine Geology, 286(1–4), pp. 1–20.

Serizawa, M., Uda, T. and Miyahara, S. (2012) Prediction of development of sand spits and cuspate forelands with rhythmic shapes caused by shoreline instability using BG model. Coastal Engineering, 1(33), pp. 35.

Serizawa, M., Uda, T., San-nami, T. and Furuike, K. (2007) Three-dimensional model for predicting beach changes based on Bagnold's concept. Coastal Engineering, 5, pp. 3155-3167.

Shaw, J., Fader, G.B. and Taylor, R.B. (2009) Submerged early Holocene coastal and terrestrial landforms on the inner shelves of Atlantic Canada. Quaternary International, 206(1–2), pp. 24–34.

Short, A.D. (1996) The role of wave height, period, slope, tide range and embaymentisation in beach classifications: a review. Revista Chilena de Historia Natural, 69(4), pp. 589–604.

Short, A.D. (2006) Australian Beach Systems—Nature and Distribution. Journal of Coastal Research, 221, pp. 11–27.

Shu, G. and Collins, M. (1998) Equilibrium coastal profiles: I. Review and synthesis. Chinese Journal of Oceanology and Limnology, 16(2), pp.97-107.

Skinner, C.J., Coulthard, T.J., Parsons, D.R., Ramirez, J.A., Mullen, L. and Manson, S. (2015) Simulating tidal and storm surge hydraulics with a simple 2D inertia based model, in the Humber Estuary, U.K. Estuarine, Coastal and Shelf Science, 155, pp. 126–136.

Skinner, C.J., Coulthard, T.J., Schwanghart, W., Wiel, M.J. and Hancock, G. (2018) Global Sensitivity Analysis of Parameter Uncertainty in Landscape Evolution Models. Geoscientific Model Development, 11(12), pp.4873-4888.

Slott, J.M., Murray, A.B., Ashton, A. and Crowley, T.J. (2006) Coastline responses to changing storm patterns. Geophysical Research Letters, 33(18).

Solomon, S., Qin, D., Manning, M., Averyt, K. and Marquis, M. eds., 2007. Climate change 2007-the physical science basis: Working group I contribution to the fourth assessment report of the IPCC (Vol. 4). Cambridge University Press.

Soulsby, R. L. (2006) Simplified calculation of wave orbital velocities, HR Wallingford Report Tr155.

Spencer, T., Brooks, S.M., Evans, B.R., Tempest, J.A. and Möller, I. (2015) Southern North Sea storm surge event of 5 December 2013: Water levels, waves and coastal impacts. Earth-Science Reviews, 146, pp. 120–145.

Stewart, C.J. and Davidson-Arnott, R.G.D. (1988) Morphology, formation and migration of longshore sandwaves; Long Point, Lake Erie, Canada. Marine Geology, 81(1–4), pp. 63–77.

Thomas, C.W., Murray, A.B., Ashton, A., Hurst, M.D., Barkwith, A.K. and Ellis, M.A. (2016) Complex coastlines responding to climate change: do shoreline shapes reflect present forcing or remember the distant past? Earth Surface Dynamics, 4(4), pp.871-884.

Thomas, T.J. and Dwarakish, G.S. (2015) Numerical Wave Modelling – A Review. Aquatic Procedia, 4, pp. 443–448.

Trenhaile, A.S. and Lakhan, V.C. (1989) Applications in Coastal Modeling. Volume 49. Elsevier.

Tucker, G.E. and Hancock, G.R. (2010) Modelling landscape evolution. Earth Surface Processes and Landforms, 35(1), pp. 28–50.

Tucker, G.E. and Slingerland, R.L. (1994) Erosional dynamics, flexural isostasy, and long-lived escarpments: A numerical modeling study. Journal of Geophysical Research: Solid Earth, 99(6), pp. 12229–12243.

Uda, T. and Yamamoto, K. (1991) Experimental study on formative process of a compound spit. Japanese Geomorphological Union, 12, pp. 357–365.

Valters, D. (2016) Modelling Geomorphic Systems: Landscape Evolution. Geomorphological Techniques, 12(1880), pp. 1–24.

Valvo, L.M., Murray, A.B. and Ashton, A. (2006) How does underlying geology affect coastline change? An initial modeling investigation. Journal of Geophysical Research: Earth Surface, 111(2).

Van Den Berg, N., Falqués, A. and Ribas, F. (2011) Long-term evolution of nourished beaches under high angle wave conditions. Journal of Marine Systems, 88(1), pp. 102–112.

Van Den Berg, N., Falqués, A. and Ribas, F. (2012) Modeling large scale shoreline sand waves under oblique wave incidence. Journal of Geophysical Research: Earth Surface, 117(3).

Van Maanen, B., Nicholls, R.J., French, J.R., Barkwith, A., Bonaldo, D., Burningham, H., Murray, A.B., Payo, A., Sutherland, J., Thornhill, G. and Townend, I.H. (2016) Simulating mesoscale coastal evolution for decadal coastal management: A new framework integrating multiple, complementary modelling approaches. Geomorphology, 256, pp. 68–80.

Wainwright, J. and Mulligan, M. (2013) Environmental Modelling: Finding Simplicity in Complexity. John Wiley and Sons.

Wang, J., Gao, W., Xu, S. and Yu, L. (2012) Evaluation of the combined risk of sea level rise, land subsidence, and storm surges on the coastal areas of Shanghai, China. Climatic Change, 115(3–4), pp. 537–558.

Warren, I.R. and Bach, H.K. (1992) MIKE 21: a modelling system for estuaries, coastal waters and seas. Environmental Software, 7(4), pp. 229–240.

Willgoose, G., Bras, R.L. and Rodriguez-Iturbe, I. (1991) Results from a new model of river basin evolution. Earth Surface Processes and Landforms, 16(3), pp. 237–254.

Wolf, J. (2008) Coupled wave and surge modeling and implications for coastal flooding. Advances in geosciences, 17, pp. 19–22.

Wong, P.P. et al. (2015) 'Coastal systems and low-lying areas', in Climate Change 2014 Impacts, Adaptation and Vulnerability: Part A: Global and Sectoral Aspects, pp. 361–410. doi: 10.1017/CBO9781107415379.010.

Wong, P.P., Losada, I.J., Gattuso, J.P., Hinkel, J., Khattabi, A., McInnes, K.L., Saito, Y., Sallenger, A., Nicholls, R.J., Santos, F. and Amez, S. (2015). Coastal systems and low-lying areas. In Climate Change 2014 Impacts, Adaptation and Vulnerability: Part A: Global and Sectoral Aspects (pp. 361–410).

Woodroffe, C.D. (2002) Coasts: Form, Process and Evolution. Cambridge University Press.

Wragg, S. (2014) Hull City Council Flood Investigation Report: December 2013 City Centre Tidal Surge Event. Report to the Environment and Transport Overview and Scrutiny Committee, Hull City Council, 4th February 2014. Available at: https://cmis.hullcc.gov.uk/CMIS/Document.ashx?czJKcaeAi5tUFL1DTL2UE4zNRBcoShgo=09mkr6mrOzl87tgw6I3CSqQ4lTiCFmPyYzJLNMUI1HVY5UC6zpXOBA%3D%3DandrUzwRPf%2BZ3zd4E7Ikn8Lyw%3D%3D=pwRE6AGJFLDNlh225F5QMaQWCtPHwdhUfCZ%2FLUQzgA2uL5jNRG4jdQ%3D%3DandmCTIbCubSFfXsDGW9IXnl (Accessed: 16 December 2015).

Wright, L.D. (1982a) Field observations of long-period, surf-zone standing waves in relation to contrasting beach morphologies. Marine and Freshwater Research, 33(2), pp. 181–201.

Wright, L.D. and Short, A.D. (1984) Morphodynamic variability of surf zones and beaches: A synthesis. Marine Geology, 56(1–4), pp. 93–118.

Wright, L.D., Guza, R.T. and Short, A.D. (1982b) Dynamics of a high-energy dissipative surf zone. Marine Geology, 45(1–2), pp. 41–62.

Wright, L.D., Thorn, B.J. and Chappell, J. (1978) Morphodynamic Variability of High-Energy Beaches. Coastal Engineering, 68, pp. 1180–1194.

Wright, L. D., Chappell, J., Thom, B.G., Bradshaw, M.P. and Cowell, P. (1979) Morphodynamics of reflective and dissipative beach and inshore systems: Southeastern Australia. Marine Geology, 32(1–2), pp. 105–140.

Wright, L.D., Nielsen, P., Short, A.D. and Green, M.O. (1982c) Morphodynamics of a macrotidal beach. Marine Geology, 50(1–2), pp. 97–127.

Yang, J. (2011) Convergence and uncertainty analyses in Monte-Carlo based sensitivity analysis. Environmental Modelling and Software, 26(4), pp. 444–457.

Young, R.S. (1999) Seasonal variability of the global ocean wind and wave climate. International Journal of Climatology, 19(9), pp. 931–950.

Young, R.S., Pilkey, O.H., Bush, D.M. and Thieler, E.R. (1995) A discussion of the generalized model for simulating shoreline change (GENESIS). Journal of Coastal Research, pp. 875–886.

Zangiabadi, E., Edmunds, M., Fairley, I.A., Togneri, M., Williams, A.J., Masters, I. and Croft, N. (2015) Computational Fluid Dynamics and Visualisation of Coastal Flows in Tidal Channels Supporting Ocean Energy Development. Energies, 8, pp. 5997–6012.

Zenkovitch, V.P. (1959) On the Genesis of Cuspate Spits along Lagoon Shores. The Journal of Geology, 67(3), pp. 269–277.

Zhang, K., Douglas, B.C. and Leatherman, S.P. (2004) Global Warming and Coastal Erosion. Climatic Change, 64(1-2), pp. 41–58.

Ziliani, L., Surian, N., Coulthard, T.J. and Tarantola, S. (2013) Reduced-complexity modeling of braided rivers: Assessing model performance by sensitivity analysis, calibration, and validation. Journal of Geophysical Research: Earth Surface, 118(4), pp. 2243–2262.

Appendices

Table of Appendices

Appendix 1

Variations of the Sediment Distribution Method

Cited in Chapter 3

1.1 Introduction

In Chapter 3 the development of the Coastline Evolution Model 2D (CEM2D) is presented. A sediment distribution method was implemented in the model to distribute material across the model domain from the shoreline. Inherent from the CEM, CEM2D initially calculate the flux of material along the one-dimensional shoreline, which in the two-dimensional CEM2D needs to be distributed across the shoreline to prevent material from creating significant piles of sediment of depression. The method secondarily then acts to prevent pilling or depressions occurring across the whole domain.

The chosen method is described in section Chapter 3, but numerous techniques were evaluated as part of the model development process. In this appendix, a

number of methods that were tested are described. It is important to note that this is not an exhaustive list, but it describes that primary methods evaluated.

1.2 The Active Shoreface Method

This technique was designed to distribution sediment from shoreline across the active shoreface. The first stage in this process is to define the active shoreface zone, of which two principle methods were evaluated.

1. The active shoreface was defined as a given distance from the shore, calculated according to the approximate location of the depth of closure (Figure 1.1a).
2. The active shoreface was defined by the bathymetric profile. From the shoreline, shoreface cells were defined whilst the profile continued to slope seawards, according to given thresholds. Peaks in the bathymetry marked the extent of the active shoreface (Figure 1.1b).

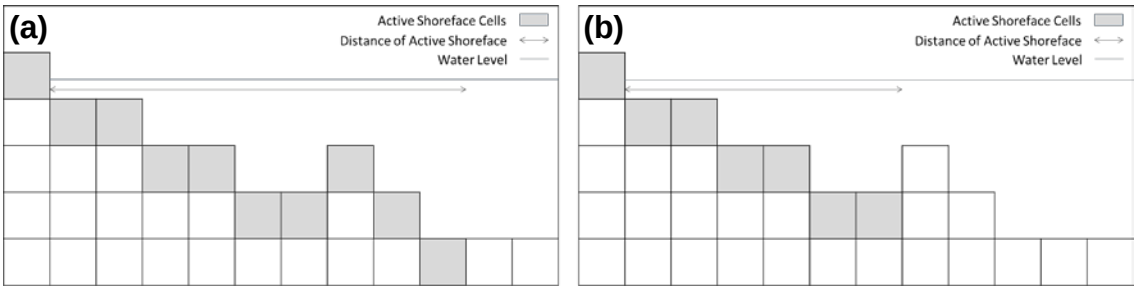

Figure 1.1 Cross-sectional schematic of the Coastline Evolution Model 2D (CEM2D) illustrating two methods tested during model development, for defining the active shoreface: (a) by a given distance and (b) by the bathymetric profile.

Both methods shown in Figure 1.1 are required to select a directional path to see the active shoreface. Three different methods of defining the direction the methods take from the shoreline were evaluated:

1. Perpendicular to the local shoreline orientation of each cell using all eight directions

2. Perpendicular to the local shoreline orientation in four directions
3. Directly offshore or to the centre of a bay according to the shoreline shape.

Once the active shoreface was defined by either method in Figure 1.1, sediment was distributed in one of three ways:

1. Linearly: the total volume of sediment transport was divided equally between the shoreline cell and the active shoreface cells
2. Linear Regression: the volume of sediment deposited in active shoreface cells was reduced in the offshore direction, using linear regression
3. Percentage Regression: the volume of sediment deposited in active shoreface cells was reduced offshore by a given percentage.

Each combination of methods described above to describe the definition of the active shoreline, the directional path of the active shoreface and the sediment distribution method proved too complex for CEM2D. Unnatural peaks and troughs developed in the simulations, instabilities occurred in the model and the shoreline shapes produced did not reflect those observed in nature (Ashton *et al.*, 2001, 2006a, 2006b).

1.3 Conclusion

For the reasons described in this Appendix, the more simplistic sediment distribution method described in Chapter 3 was chosen. This method also comes with caveats as discussed in Chapter 3 and in Chapter 8, but it is capable of simulating fundamental shoreline shapes and is comparable to results of the CEM which has been empirically tested. It proved the most effective method at this stage of model development and generated credible results.

1.4 References

Ashton, A. D. and Murray, A. B. (2006a) High-angle wave instability and emergent shoreline shapes: 1. Modeling of sand waves, flying spits, and capes. Journal of Geophysical Research, 111(4).

Ashton, A. D. and Murray, A. B. (2006b) High-angle wave instability and emergent shoreline shapes: 2. Wave climate analysis and comparisons to nature. Journal of Geophysical Research: Earth Surface, 111(4).

Ashton, A. D., Murray, A. B. and Arnault, O. (2001) Formation of coastline features by large-scale instabilities induced by high-angle waves. Nature, 414(6861), pp. 296–300.

Appendix 2

CEM2D Source Code Sample

Cited in Chapter 3

A sample of CEM2D's source code is given here, but the full document can be found at https://doi.org/10.5281/zenodo.2604988.

```
//
//
// Modified version of the Coastline Evolution Model
(CEM), originally developed by originally developed by
Ashton et al. (2001), Ashton and Murray (2006) and
Valvo et al. (2006)
//
//

using System.IO;
using System;
using System.Drawing;
using System.Collections;
using System.ComponentModel;
using System.Windows.Forms;
using System.Data;
using System.Text;
using System.Net;
using System.Xml;
using System.Text.RegularExpressions;
using System.Linq;
using System.Drawing.Drawing2D;
using System.Collections.Generic;


namespace CEM1
{
    /// <summary>
    /// Summary description for Form1.
    /// </summary>
    public class Form1 : System.Windows.Forms.Form
    {
        private System.Drawing.Bitmap
m_objDrawingSurface;

        //JMW

[System.Runtime.InteropServices.DllImport("gdi32.dll")]
        public static extern long BitBlt(IntPtr
hdcDest, int nXDest, int nYDest, int nWidth, int
nHeight, IntPtr hdcSrc, int nXSrc, int nYSrc, int
dwROP);

        private System.ComponentModel.IContainer
components;

        //Jorge variables
        public static double sedOut = 0;
//amount of sediment at outlet, plotted
        public static double waterOut = 0;
//amount of water at outlet, plotted
        public static int plotType = 0;
        public static double magnifyValue = 0;
        public static int updateClick = 0;
        private double[] zoomFactor = { .25, .33, .50,
.66, .80, 1, 1.25, 1.5, 2.0, 2.5, 3.0 };
        private double[] contrastFactor = { 1, 1.2,
1.4, 1.6, 1.8, 2.0, 2.2, 2.4, 2.6, 2.8, 3 };
        private double contrastMultiplier = 0;
        public int imageCount = 0;
        public int imageCount2 = 1;
        public string kml = "";
        public string KML_FILE_NAME =
"animation\\animation.kml";
        int save_time2, save_interval2 = 0;
        public string startDate, kmlTime;
        public DateTime googleTime;
        public string[] DateArray;
        public string[] DateArray2;


        // toms global variables
        const Single g = 9.81F;
        const Single kappa = 0.4F;
        double time_1=1;
        double save_time=0;
        int input_type_flag=0;
// 0 is water input from points, 1 is input from
hydrograph or rainfall file.
        double saveinterval=1000;
        int counter=0;
        Timer gameClock;
        int xmax, ymax;
        double xll, yll;
        const int ACTIVE_FACTOR=1;
        const int TRUE = 1;
        const int FALSE = 0;
        double DX=5;
        double root=7.07;
        double fiveroot=10.04;
        double time_factor;
        double baseflow=0.00000005;
//end of hyd model variables usually 0.0000005 changed
2/11/05
        public static double cycle=0;
        double init_cycle=0;
        double output_file_save_interval=60;
        int graphics_scale = 5;
// value that controls the number of bmp pixels per
model pixel for the output images.
```

Appendix 3

An Analysis of Results from CEM and CEM2D, Wave Climates

Cited in Chapter 5

3.1 Introduction

In Chapter 5, CEM2D is used to investigate the planform evolution of coastal systems under different driving wave climate conditions. A model-model comparison of CEM and CEM2D is given and the results are compared to the behaviour of natural coastal systems. In this appendix, an in-depth analysis of the results from this investigation are presented, from which the principal results given in Chapter 5 are drawn. This is intended to support the findings of Chapter 5 and provide additional detail that may be of interest to the reader.

3.2 Simulating Fundamental Coastal Shapes; a Comparison of Results from CEM and CEM2D

Comparable simulations were run using the parent model CEM and the developed CEM2D to explore similarities and differences in the outputs of the model. Results from both CEM and CEM2D are compared to show the influence of wave climate conditions on the evolution of one-dimensional shorelines. The results can be used as a form of validation for CEM2D against the empirically tested CEM, but also to highlight where CEM2D is able to generate more accurate results when compared to natural systems due to its increased complexity.

The ensemble plot in Figure 1 shows final coastal morphologies produced from CEM, where the asymmetry (A) and proportional highness of waves (U) have been varied according to the values in Chapter 5, Table 5.1. The ensemble in Figure 2 shows results from simulations using CEM2D, with a comparable model set-up as CEM. Both results demonstrate a sensitivity of shorelines to different wave climate scenarios, as previously demonstrated by Ashton and Murray (2006). However, there are a number of differences in the results and patterns of behaviour in the modelled environment. The results of each set of simulations from the models are reviewed subsequently followed by an analysis and suggested reasoning behind the differences observed.

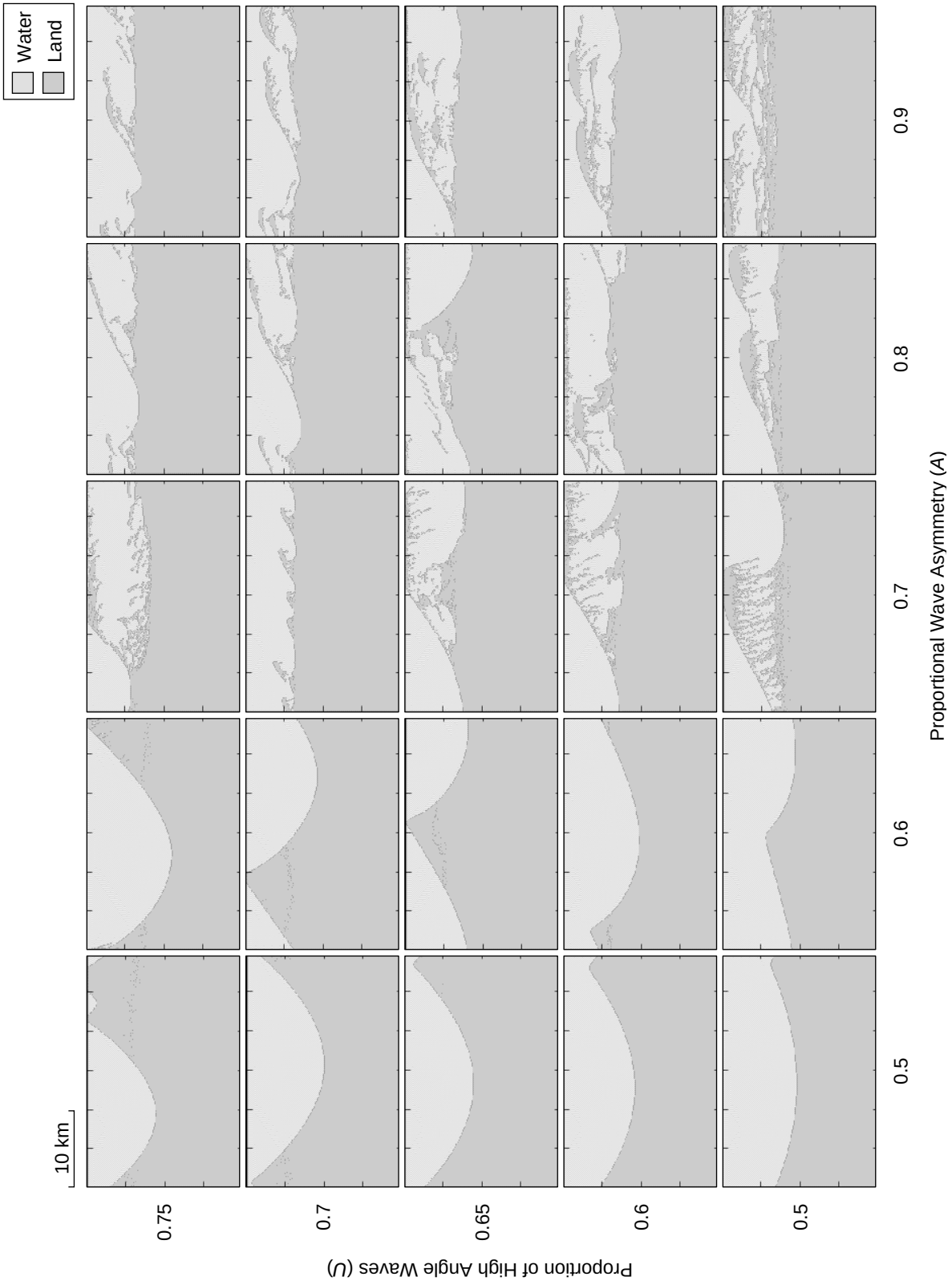

Figure 1 A matrix of results from CEM showing final shoreline morphologies as a function of the wave angle asymmetry (A) and proportion of high angle waves (U) approaching the coast relative to the local shoreline orientation. The outputs measure 20 km width and 30 km in length and are not inclusive of the periodic boundaries.

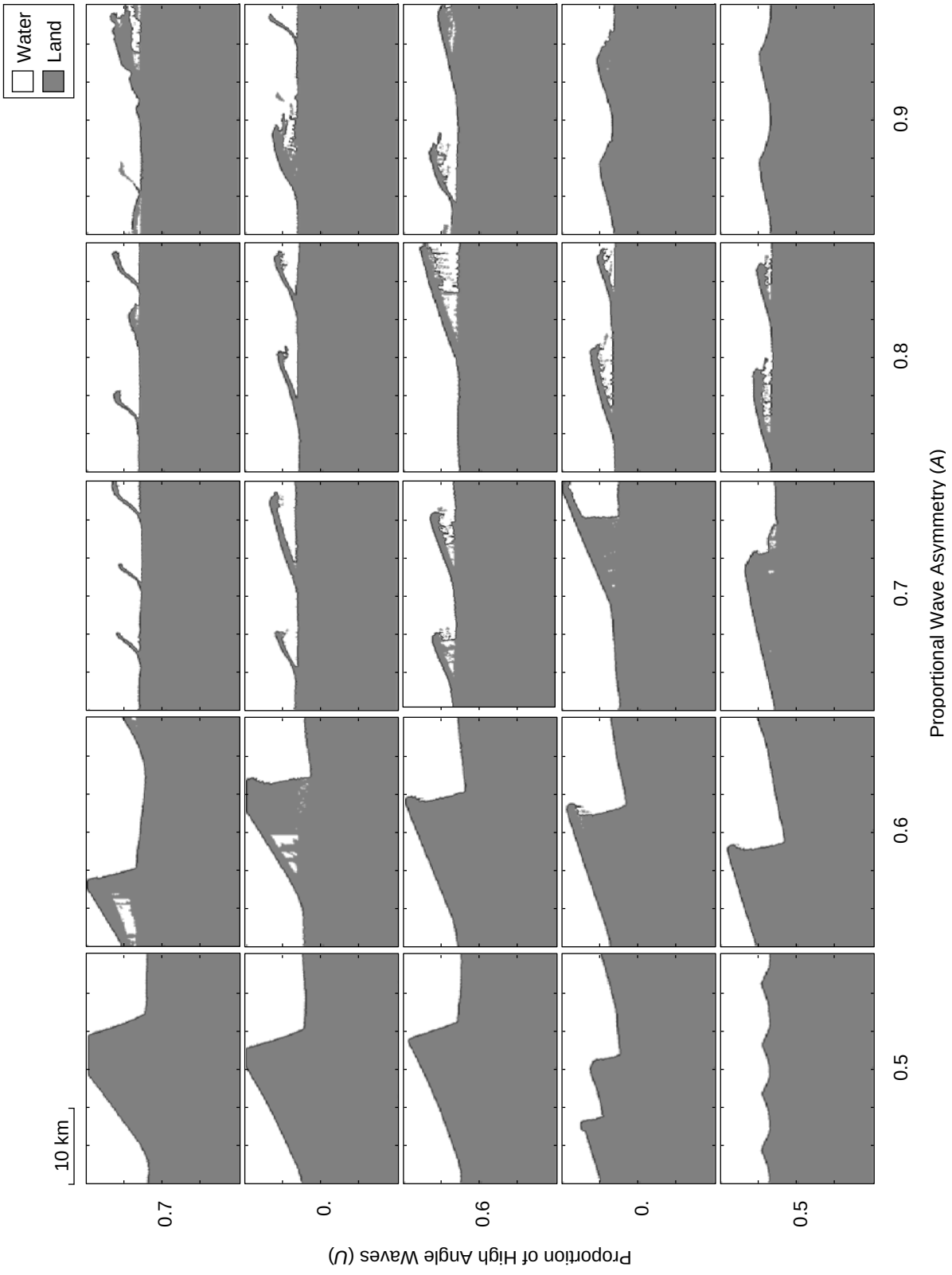

Figure 2 A matrix of results from CEM2D showing final shoreline morphologies as a function of the wave angle asymmetry (A) and proportion of high angle waves (U) approaching the coast relative to the local shoreline orientation. The outputs measure 20 km width and 30 km in length and are not inclusive of the periodic boundaries.

3.2.1 CEM

According to the wave climate conditions, CEM produces four principle shoreline shapes; cuspate bumps, alongshore sand waves, reconnecting spits and flying spits, although there is little distinction between the latter two types (Figure 1). A detailed description of these features and their likely formation in natural systems is given in Chapter 2. The reproduced simulations show some similarities and differences between the comparable results described by Ashton and Murray (2006).

Across the phase space in Figure 1, there is less distinction between reconnecting and flying spit features compared to the findings of Ashton and Murray (2006). Rather, a smooth transition and evolution between these two types of features exist. As observed by Ashton and Murray (2006), spits dominate the top right half of plot where the wave climate is asymmetrical and there is a dominance of high angle waves. With increasing asymmetry and proportion of high angle waves, the features show a greater resemblance to flying spits that disconnect from the mainland. Cuspate features and sand waves dominate the bottom left half of the plot, where the asymmetry and proportional highness of waves are generally low.

Whilst the majority of simulations completed the 3,000-year maximum simulation period, only one of the ten simulations that produced flying spit features ran for the specified number of model iterations. Four of these simulations ran for less than 1,000 simulated years. Only two simulations produce features classified as reconnecting spits (distinct from flying spits) and so the data is also limited for identifying trends in the development and evolution of these forms. The premature termination of the models has been discussed throughout the thesis

and is primarily attributed to the shoreline search technique being unable to locate a continuous shoreline.

In respect of the data availability and the varying maximum run durations, a trend is observed in the development patterns of the three main types of landforms observed. Figure 3 compares the areal size of landforms using representative simulations for each type of feature discussed.

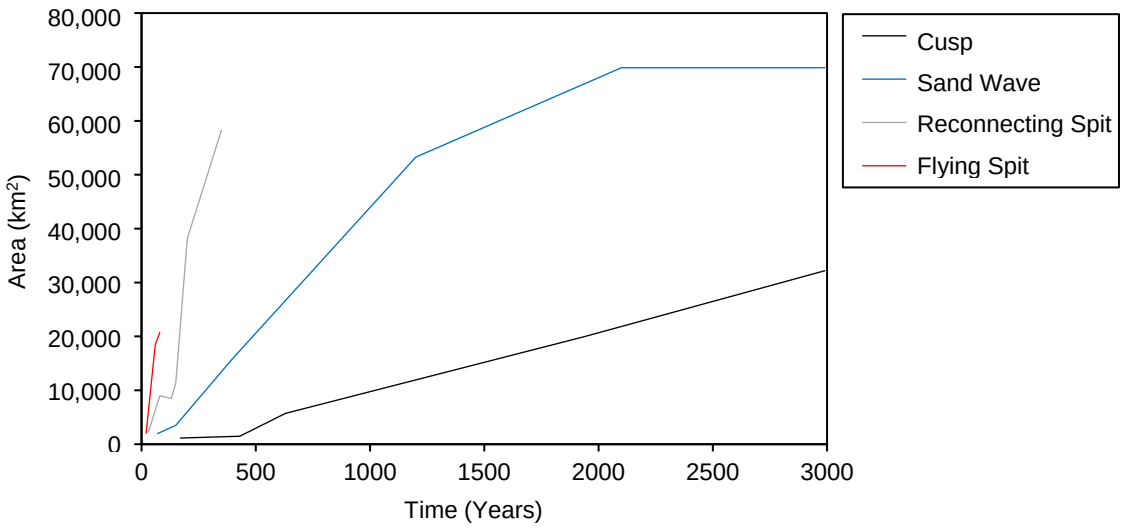

Figure 3 A graph showing the change in the average areal size of landforms over the simulation period, for four simulations using CEM that produce morphologies representative of cusps, sand waves, reconnecting spits and flying spits.

Over time, there is an increase in the area of all landforms observed; cusps, sand waves and spits (Figure 3). With greater asymmetry and proportions of high-angle waves, the rate of growth increases. In the example, cuspate landforms grow at an average rate of 10.73 km^2 per simulated year with a total landform size after 3,000 years of 32,190 km^2 and sand waves at a rate of 23.28 km^2 per year with an average areal size of 69,860 km^2 after 3,000 years. After 2,100 years the sand wave reaches a dynamic equilibrium and no significant changes in its planform area occur. Similar observations cannot be made for the spit features due to the

lack of data, but an observed increase in areal size over time is apparent. The rate of increase is more rapid than observed for cusps and sand waves, with reconnecting spits exhibiting a rate of 166.57 km^2 per year and flying spits a rate of 259.44 km^2 per year. Whilst the initial rate of flying spit growth outcompetes reconnecting spits, it plateaus after 300 simulated years as the features retain an equilibrium form and migrate until prematurely terminating due to model instability.

The point at which the simulations terminate prematurely, or reach a dynamic equilibrium, as is the case for sand waves, marks the point where the wavelength of landforms reaches its maximum. This is with exception to the cusps, which show a gradual increase in areal size over time. The maximum wavelength is limited by the size of the modelling domain, which influences sediment availability and growth potential. As shown in Figure 4 the wavelength increases with increasing wave asymmetry and proportion of high angle waves.

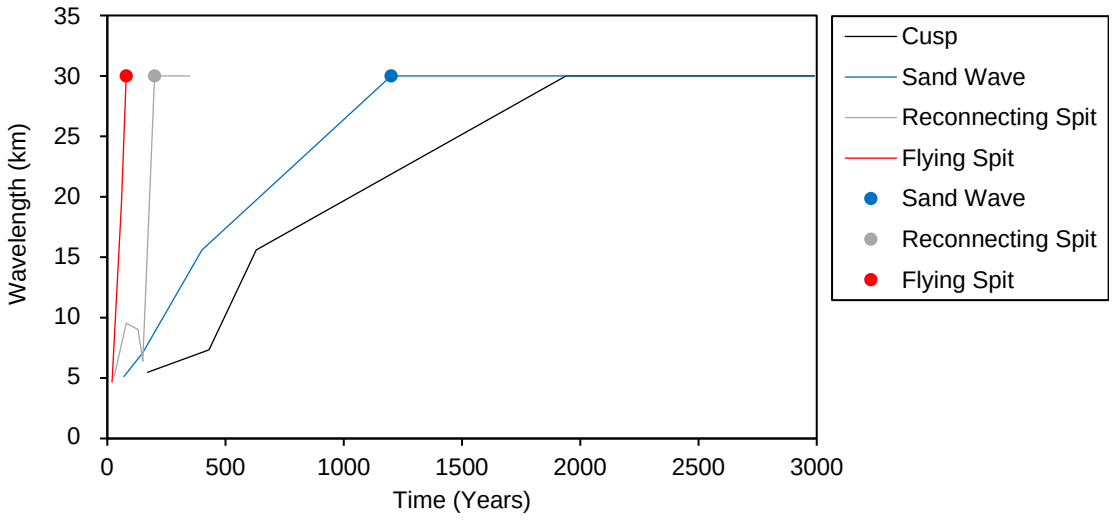

Figure 4 A graph showing the average wavelength of landforms over time, for four simulations using CEM that produce morphologies representative of cusps, sand waves, reconnecting spits and flying spits. The markers denote for each simulation where a reduction in areal growth of features is observed, according to Figure 3, except in the case of cusps which show a gradual growth over time.

The aspect ratio of features describes the relationship between their wavelength and amplitude. A value of 1 is attributed to landforms with an equal wavelength to amplitude ratio, <1 denotes a feature with greater wavelength and >1 a feature with greater amplitude. As shown in Figure 5, all features exhibit a morphology with greater wavelength over amplitude with this ratio weighted towards the wavelength with increasing wave asymmetry and proportion of high angle waves. For cusps and sand waves, throughout the simulation, there is a slight increase in aspect ratio from 0.08 (T = 430) to 0.1 and from 0.14 to 0.21 respectively. As features merge the balance of waves approaching from the left and right of the domain drive both longshore and cross-shore sediment transport to maintain the aspect ratio, but once a single feature remains its amplitude increases as it builds in the cross-shore direction. Even though the evolution of cuspate landforms and sand waves differ, their behaviour here is similar.

Although there is limited data to show the evolution of spit features, the results in Figure 5 show a sharp increase followed by a sharp decrease in aspect ratio for the reconnecting spit. This denotes that during the initial 150 simulated years the amplitude of the shoreline features grows at a greater rate than the wavelength, but thereafter, the wavelength increases to its maximum of 30 km. Conversely, for flying spits the aspect ratio decreases throughout the simulation, as features merge rapidly and increase in wavelength relative to their cross-shore evolution.

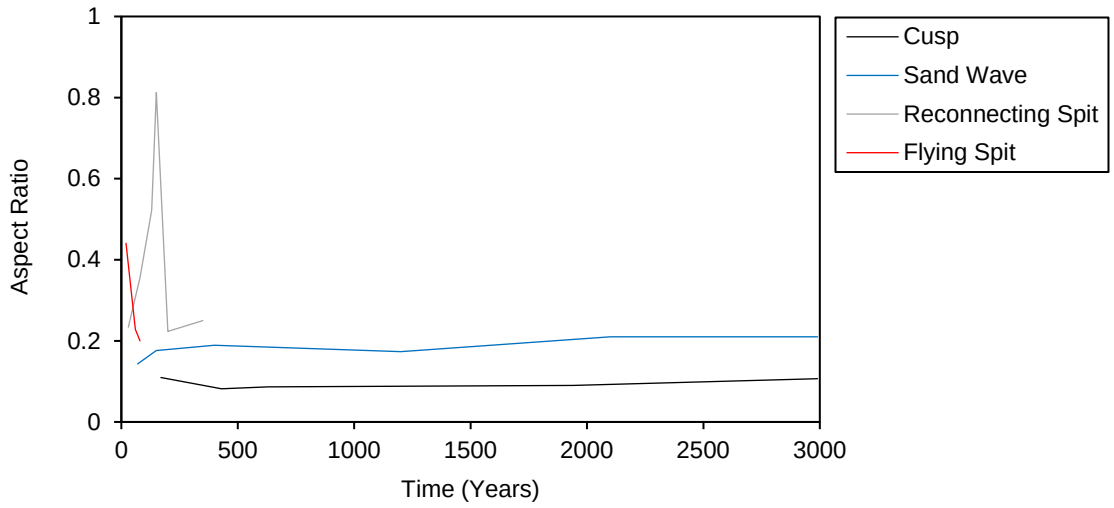

Figure 5 A graph showing the average aspect ratio of landforms over time, for four simulations using CEM that produce morphologies representative of cusps, sand waves, reconnecting spits and flying spits.

The results discussed so far indicate how increasing the asymmetry and proportional highness of waves increases the rate of landform growth, in terms of its planform area and wavelength. It also influences cross-shore and longshore sediment transport, that can evolve the morphology of landforms, particularly with regards to their aspect ratio. Attention is focused subsequently on two sets of simulations that look at the separate influence of wave asymmetry and proportion of high angle waves on shoreline shape.

1.1.1.1 *Wave Angle Asymmetry (A)*

This section focuses on the simulations presented in Figure 1 where 60% of waves approach from a high angle (*U = 0.6*) and the wave asymmetry ranges from 50% - 90% (*A = 0.5-0.9*). Not all of these simulations ran for the specified time period of 3,000 years but were terminated prematurely due to instabilities occurring in the model. For runs with 70% and 80% asymmetry, the simulations were terminated after 720 and 240 years respectively. In both simulations, one reconnecting spit feature dominated the shoreline and formed a multitude of islands and sediment trails in the mature stages of its development, which created

a complex shoreline shape and sediment transport patterns that are beyond the understanding and capabilities of CEM2D. Analysing the results of these simulations takes this into consideration.

Under a wave climate where the proportion of high angle waves dominates by 10% over low angle waves (*U = 0.6)*, with increasing wave asymmetry landforms show a progression from cuspate landforms to spit-like features (Figure 6).

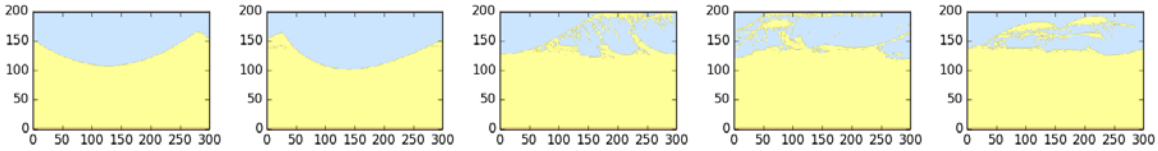

Figure 6 Outputs from CEM where U = 0.6 and A ranges from 0.5 to 0.9. In all outputs T = 3,000 except where A = 0.7 (T = 720) and A = 0.9 (T=240)

Under a symmetrical wave climate (*A = 0.5, U = 0.6)*, cuspate features form along the shoreline and where there is a slight asymmetry with 60% of waves approaching from the left of the domain (*A = 0.6, U = 0.6*), alongshore sand waves form (Figure 6). With a 70% directional dominance, Ashton and Murray (2006) described the formation of sand wave features but in the reproduced results, reconnecting spits form as can be seen in Figure 6. Where the wave asymmetry is increased further to 80–90%, reconnecting spit features form in the model. However, their development is not contained within narrow and structured spit projections as observed by Ashton and Murray (2006), rather islands and reconnecting sediment paths exist between the primary spit neck and the shore (Figure 6). A high level of dynamism is observed in the reproduced simulations as the wave asymmetry increases.

Concurrent with findings of Ashton and Murray (2006), under asymmetric wave climates, waves approaching from the dominant direction drive sediment transport alongshore and cause erosion of the updrift slope of perturbations and deposition downdrift. With increasing asymmetry, deposition at the tip of landforms creates shadow zones downdrift and spit hooks are formed at the tips (Ashton and Murray, 2006).

The rate of landform growth differs depending on the asymmetry of the wave climate and the types of features that form. As shown in Figure 7, the average planform area of landforms and their rate of growth tends towards an increase with asymmetry. Similarities are observed in these metrics with features of the same type; cusps and sand waves which form under 50% and 60% asymmetry have a growth rate of approximately 52 km^2 per year between 300 and 1200 simulated years; this is a greater rate than discussed previously for simulations where A = 0.6, U = 0.6, as this was averaged over the entire model duration. During this period of time, the finite amplitude landforms reach relative stability and begin merging and migrating to form one large-scale feature. Hereafter, a breakpoint is observed where the simulation with 60% asymmetry continues to develop at a rate of 18 km^2 per year compared with 4.5 km^2 per year for landforms forming under 50% wave asymmetry. With greater asymmetry, the mechanism for formation is driven by longshore sediment transport which causes erosion of the updrift flank and feeds the growth of the sand wave cusp at a high rate compared to the cuspate feature.

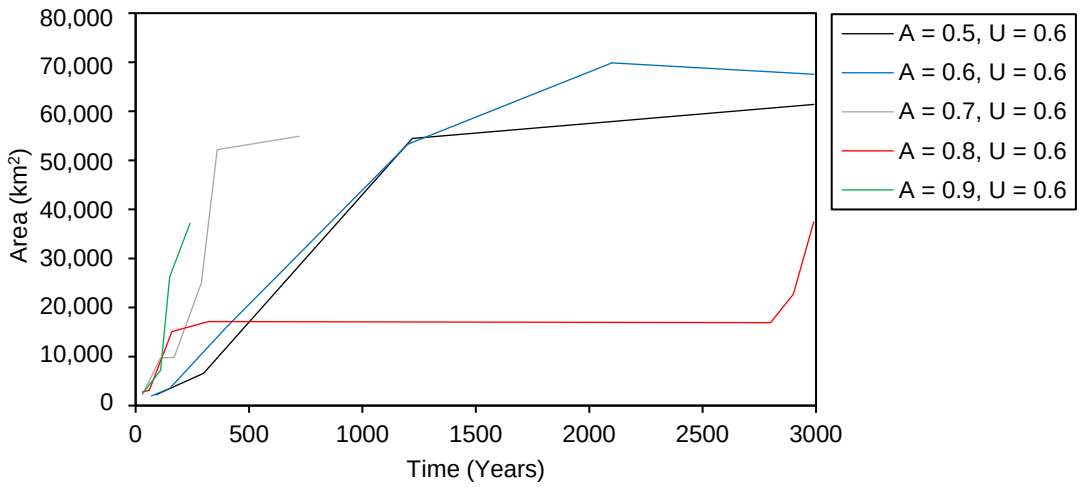

Figure 7 A graph showing the average area of landforms over time, for four simulations using CEM2D where U is held constant at 0.6 and A ranges from 0.5 to 0.9.

With 70% and 90% asymmetry, reconnecting spits form along the shoreline and show more rapid rates of growth compared to the cusps and sand waves. A rate of areal growth of 151 km^2 is calculated under a 70% wave asymmetry up to 360 years and 165 km^2 for 90% asymmetry to 240 years. After 360 simulated years, with 70% wave asymmetry the growth rate of the reconnecting spit reduces as all features merge into one larger landform.

Where there is 80% asymmetry, a different pattern is observed in the development of features compared to those discussed previously. Whilst the initial growth of the spits relatively rapid in the first 300 simulated years, hereafter wave shadowing effects influence longshore transport and prevent the migration and merging of large-scale features. Comparison of simulations with 70%, 80% and 90% wave asymmetry illustrates why shadowing to this extent occurs only with 80% asymmetry. Increasing asymmetry induces greater rates of longshore transport. Where 70% of waves are coming from the left of the domain, some sediment is driven updrift by 30% of waves into areas shadowed under the dominant wave regime, reducing the shadowing effect and driving cross-shore

growth. With 90% asymmetry and particularly where the proportion of high angle waves is relatively low at 60%, spits are less pronounced cross-shore and develop parallel to the shoreline, a shorter longshore shadow distance. Between these asymmetry values, with 80% of waves approaching from the left of the domain, the spits grow cross-shore and are fed with some sediment from the left of the domain but also exhibit rapid longshore migration. The shadow zones are large due to the size of the features and so the ability of waves approaching from the left to transport sediment into predominately shadowed zones is limited.

It is noted that the development of features in the simulation where *A = 0.8, U = 0.6* are affected by methods in the numerical model. This is particularly in relation to the shoreline search and sediment transport techniques (as described in Chapter 3). In this simulation, a large volume of the reconnecting spit is detached from the mainland and is not detected in the shoreline search as illustrated in Figure 8. The red line in Figure 8 marks the position of the one-line shoreline, along which sediment transport occurs. Only once this shoreline accretes and reattaches with the islands after 281 simulated years, is the spit able to continue its evolution (see Figure 8).

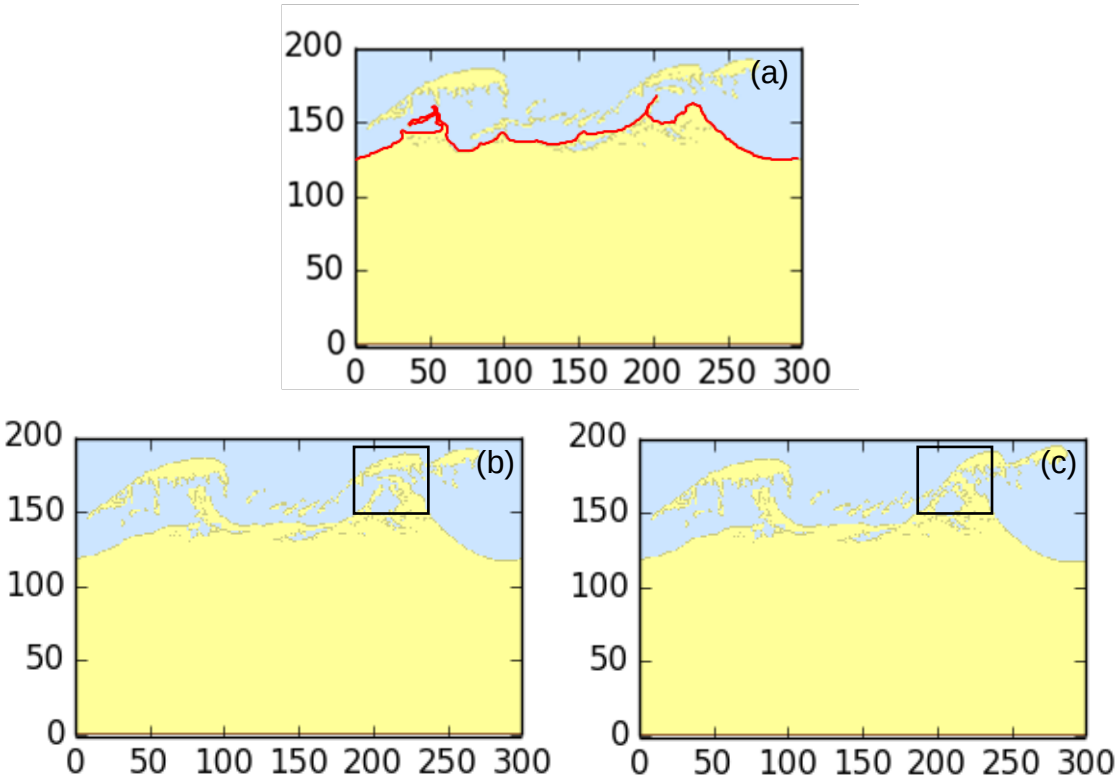

Figure 8 A time series of images from CEM, where A = 0.8, U = 0.6. Image (a) shows the model output at 500 simulated years with the position of the shoreline according to the model's algorithm marked in red. Image (b) shows model outputs at 2800 simulated years and (c) at 2810 simulated years. The black box in images (b) and (c) shows where the reconnecting spit is detached (b) and then reconnects with the shoreline (c).

The pattern of change in the size of landforms over time corresponds with the change in wavelength, as shown in Figure 9. Plotted is the point at which the growth in the area of features reduces, which maps onto where the wavelength of features stabilises (after approximately 320 simulated years where *U = 0.8)* or where the maximum wavelength, determined by the domain size, is reached. The average wavelength of landforms in all simulations increases over time until the maximum size is reached, with relative rates consistent with that observed for the increase in planform area (Figure 7).

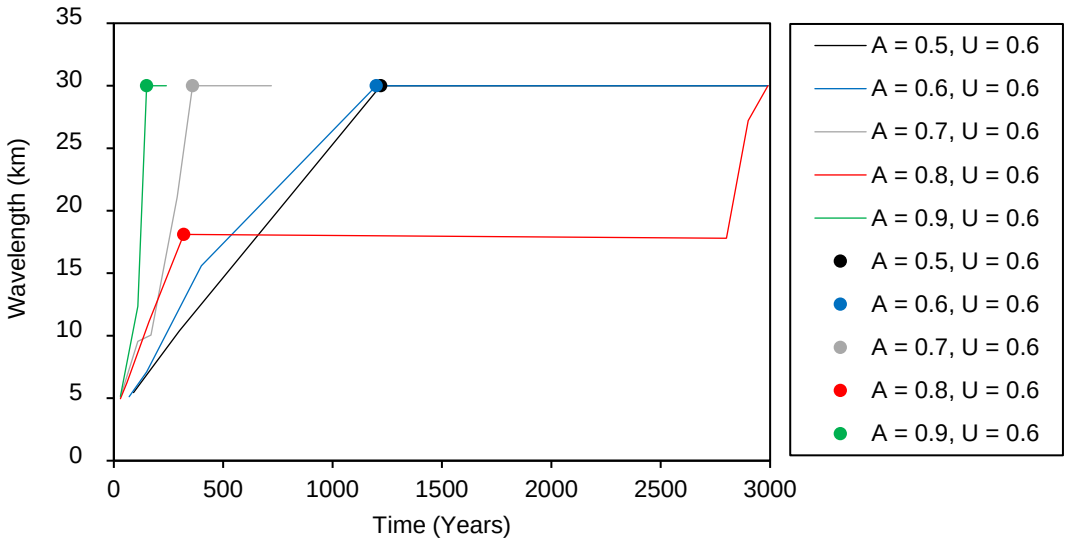

Figure 9 A graph showing the average wavelength of landforms over time, for four simulations using CEM where U is held constant at 0.6 and A ranges from 0.5 to 0.9. The markers show for each simulation where this is a significant reduction in the areal growth rate of landforms, according to Figure 7.

A trend is observed whereby the greater the wave asymmetry, the quicker the shoreline reaches a dynamic equilibrium (Table 1). It is assumed in the results that where the area or wavelength stabilise or where the maximum wavelength is reached, landforms have reached dynamic equilibrium.

Table 1 A table detailing the time step when each CEM simulation reaches a dynamic equilibrium, where U = 0.6 and A ranges from 0.5 to 0.9

Simulation *(according to A and U values)*	**Time to reach dynamic equilibrium** *(simulated years)*
A = 0.5, U = 0.6	1220
A = 0.6, U = 0.6	1200
A = 0.7, U = 0.6	360
A = 0.8, U = 0.6	320
A = 0.9, U = 0.6	150

As shown in Figure 10, the aspect ratio of features that form under a symmetrical or slightly asymmetric climate where A = 0.6, increases gradually throughout the simulation. This suggests a greater increase in cross-shore amplitude compared to the wavelength. The increase is marginal however, from 0.18-0.19 where *A* = 0.5 and from 0.14-0.21 where *A* = 0.6. Where *A* = 0.7, the aspect ratio initially increases rapidly as features merge. The wavelength is reduced and minimal change is observed for the amplitude of the sand waves that form. A similar pattern is observed where *A* = 0.8, which shows a sharp increase in aspect ratio initially which then gradually decreases as the spits extent offshore. Conversely, where *A* = 0.9 a rapid decrease in aspect ratio is observed. Initially, features grow rapidly offshore which increases their amplitude and decreases aspect ratio. As the features merge and the wavelength grows and their aspect ratio begins to increase.

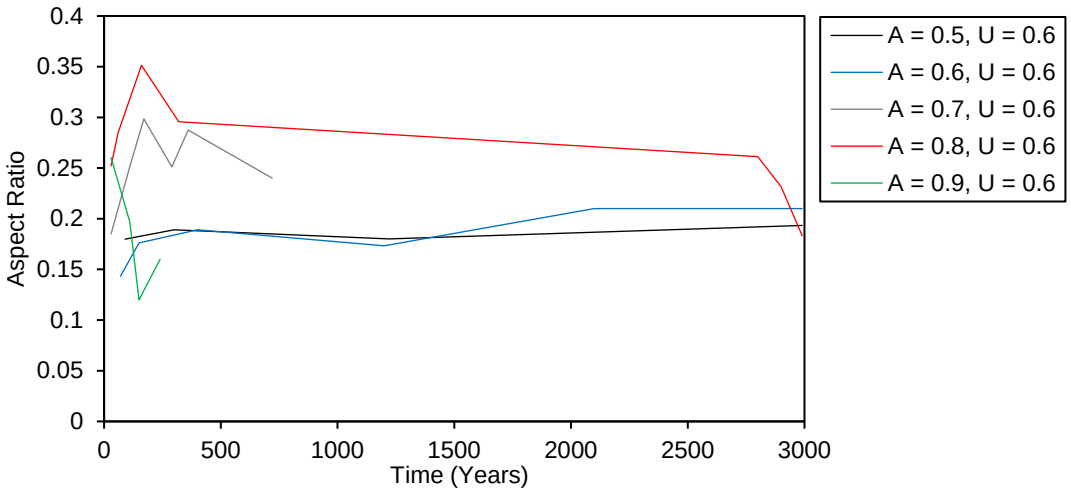

Figure 10 A graph showing the average aspect ratio of landforms over time, for four simulations using CEM where U is held constant at 0.6 and A ranges from 0.5 to 0.9.

With increasing wave asymmetry the average, relative rate at which landforms migrate alongshore according to the dominant approach direction increases (Figure 11). The rate of migration is recorded towards the end of the simulation

period when the landforms show an equilibrium form. Where the wave climate is symmetrical (*A = 0.5*) minimal longshore translation of the cuspate features are observed, although some movement is tracked at an average rate of 1.6 m per year. A similar rate is observed where *A = 0.*6, which generates relatively symmetrical sand wave features that show minimal direction skew of migration longshore (rate: 7 m per year). Considerably high rates of migration are observed where *A = 0.7-0.9*, from 80-110 m per year. Under these wave climate conditions reconnecting spit features form which exhibit dynamism in both the longshore and cross-shore directions, under a wave climate with strong directional dominance from the left of the domain.

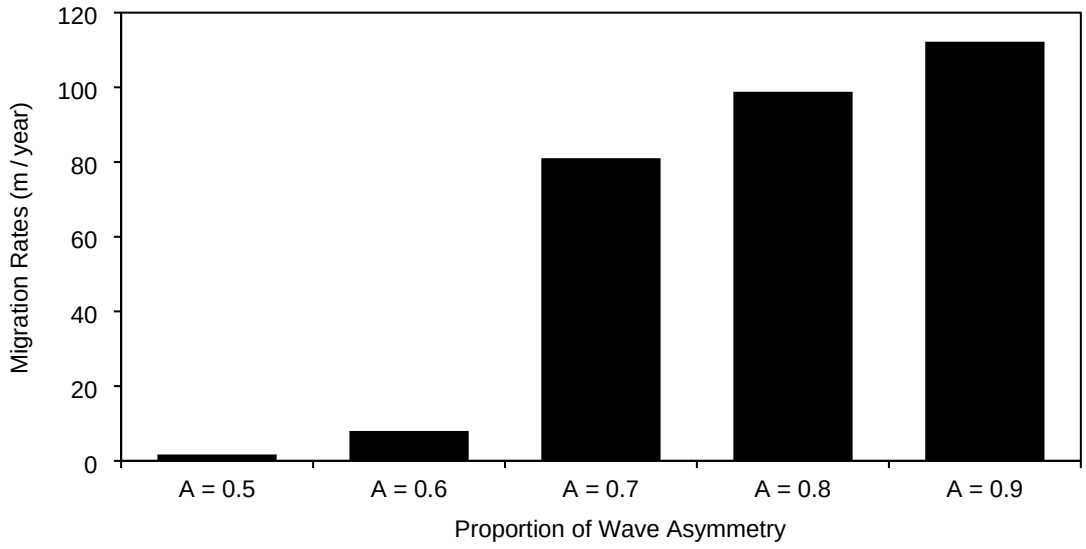

Figure 11 A graph showing the average rate of landform migration, according to the asymmetry (A) or the wave climate.

1.1.1.2 *The Proportion of High Angle Waves (U)*

This section focuses on the simulations presented in Figure 1 where the wave climate is symmetrical (*A = 0.5*) and the proportion of high angle waves ranges from 55-75% (*U = 0.55-0.75*).

Where the wave climate is symmetrical (*A = 0.5)* and $\geq$ 55% of waves approach the shore from a high angle (*U* $\geq$ *0.55)*, cuspate features form along the shoreline (Figure 1). With a greater proportion of high angle waves (*U*), the cusps increase in amplitude and extend further offshore. Concurrent with Ashton and Murray's (2006) findings, these features develop through a mechanism unlike the other landforms discussed in this Chapter. Larger features grow at a greater rate, fed by sediment transported under high-angle waves and transported in both directions. These landforms shadow the smaller cusps, which are eventually diffused in the low energy bays. The time series images in Figure 12 illustrates this process under a wave climate where *A = 0.5, U = 0.75.* In Figure 12b six low amplitude cusps of relatively equal proportions occupy the shoreline. After 130 simulated years (Figure 12c), four cusps remain with larger landforms intersected by smaller cusps. These smaller cusps diffuse in the bay of the larger features and after 230 simulated years (Figure 12d), two cusps remain.

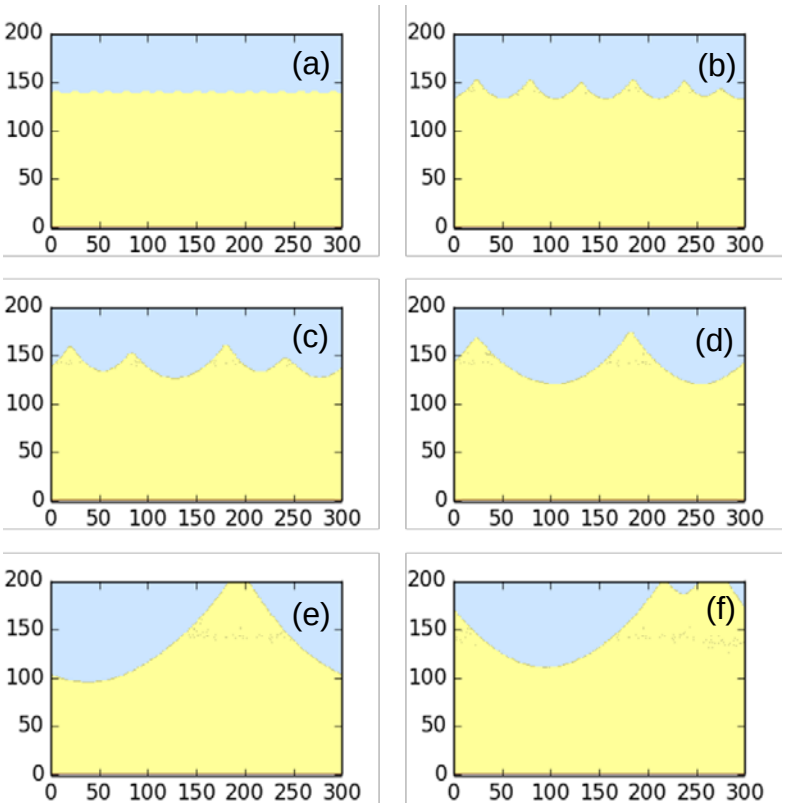

Figure 12 A time series of CEM outputs where A = 0.5 and U = 0.75, illustrating the process of cuspate formation along the shoreline. Images are presented where significant changes have occurred in the simulation: image (a) is 0 simulated years (T = 0), (b) T = 40, (c) T = 130, (d) T = 270, (e) T = 1100 and (f) T = 3000.

Under a symmetrical climate (*A = 0.5*), the planform size of cuspate features increases with increasing proportion of high angle waves (Figure 13). A pattern is observed in the rate of this formation, where features reach a peak or equilibrium size and thereafter, their growth rate is significantly reduced. On average, this point is reached at between 750-1250 simulated years (Figure 13). The point at which the growth of features decelerates is coincident with the merging of landforms into one relatively large feature. As multiple individual cusps form from the initial perturbations along the shoreline at T = 0, their average size increases rapidly as they each merge until a single landform remains and becomes relatively stable. However, this breakpoint is not observed where *A* = 0.5, U = 0.55 (Figure 13). The rate of net sediment transport is lower due to the

balance of diffusional and anti-diffusional wave approaches, which drives a slower and more gradual rate of landform formation and transition (Figure 13).

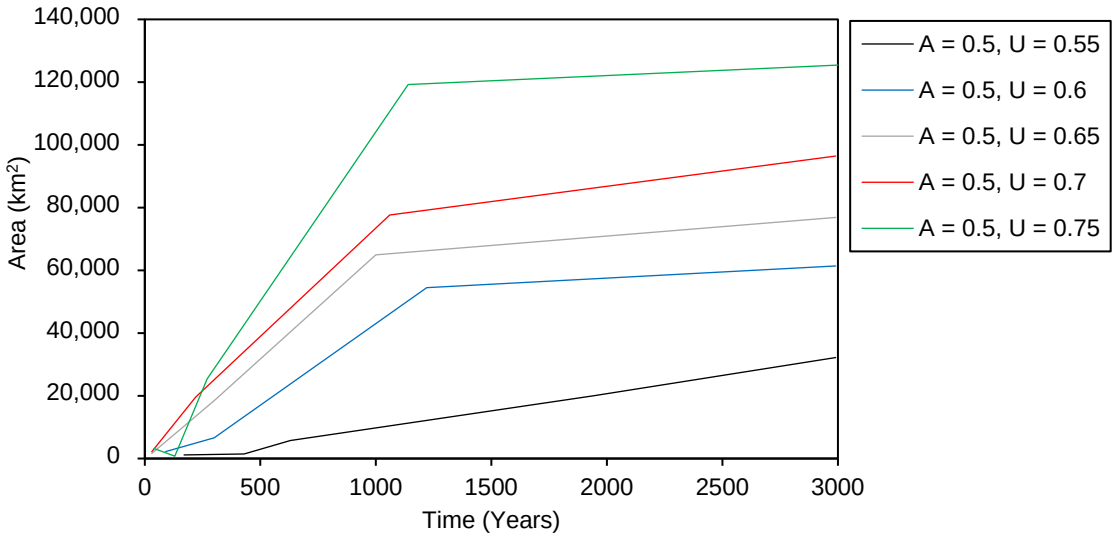

Figure 13 A graph showing the average area of landforms over time, for four simulations using CEM where A is held constant at 0.5 and U ranges from 0.55 to 0.75.

Figure 14 maps the change in wavelength over time with markers to denote where a decrease in the rate of landform growth is observed (see Figure 13). The position of the markers is coincident with where landforms reach their maximum achievable wavelength of 30 km according to the size of the analysed domain. To this point, the wavelength of all cuspate features gradually increases as features merge and the number of landforms along the shoreline reduces.

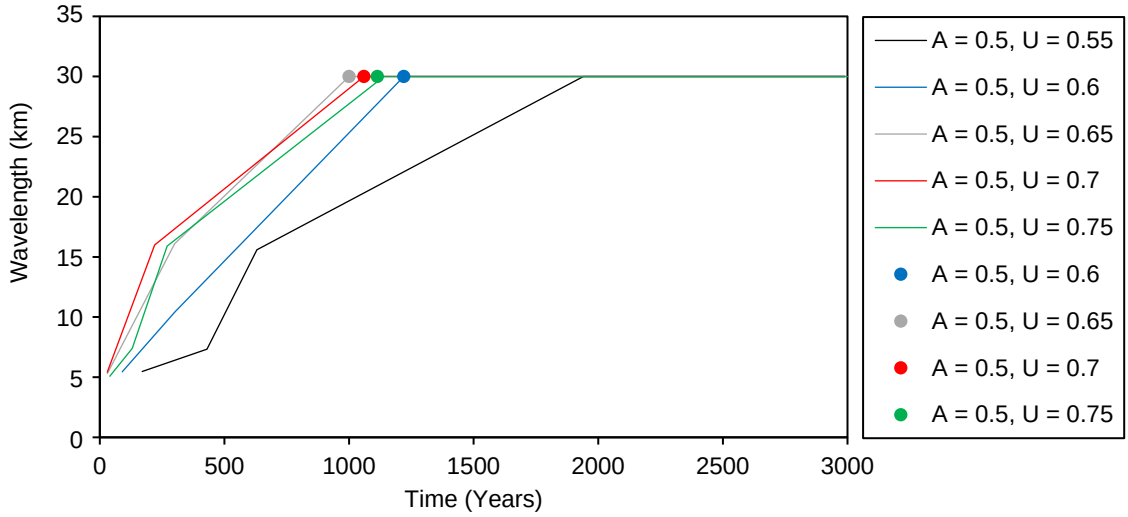

Figure 14 A graph showing the average wavelength of landforms over time, for four simulations using CEM where A is held constant at 0.5 and U ranges from 0.55 to 0.75. The markers show for each simulation, where there is a significant reduction in the areal growth rate of features. This is with exception to where A = 0.5, U = 0.5, which grow gradually.

The greater the proportion of high angle waves, the quicker the increase in wavelength and thus the development of the landforms over time. However, beyond a given proportion of high angle waves, wave shadowing influences the rate and patterns of sediment transport and wavelength growth. Table 2 details the time step when each of these simulations reaches its maximum wavelength, denoting that a single feature remains along the shoreline. From this point, the single feature in each simulation is sustained as it has reached a dynamic equilibrium.

Table 2 A table detailing the time step when each simulation reaches a dynamic equilibrium

Simulation *(according to A and U values)*	**Time to reach dynamic equilibrium** *(simulated years)*
A = 0.5, U = 0.55	1940
A = 0.5, U = 0.6	1220
A = 0.5, U = 0.65	1000
A = 0.5, U = 0.7	1060
A = 0.5, U = 0.75	1114

As shown in Table 2, the time taken for the shoreline to reach dynamic equilibrium according to the development of a single stable feature decreases as the proportion of high angle waves increases from 0.55-0.65. However, for the proportions of 0.7-0.75, a decrease in the rate of landform development and wavelength growth is observed.

Comparing the amplitude of cusps in the simulations listed in Table 2, the features extend further offshore with increasing proportions of high angle waves (Figure 15). High angle waves drive cross-shore sediment transport, which will move sediment to the tips of the landforms. However, as the landforms grow they create a wave shadow in the bay which reduces sediment transport and slows the process of landform development towards an equilibrium form. There is a balance between increased sediment transport rates which induce landform growth and wave shadowing effects as the features extend further offshore.

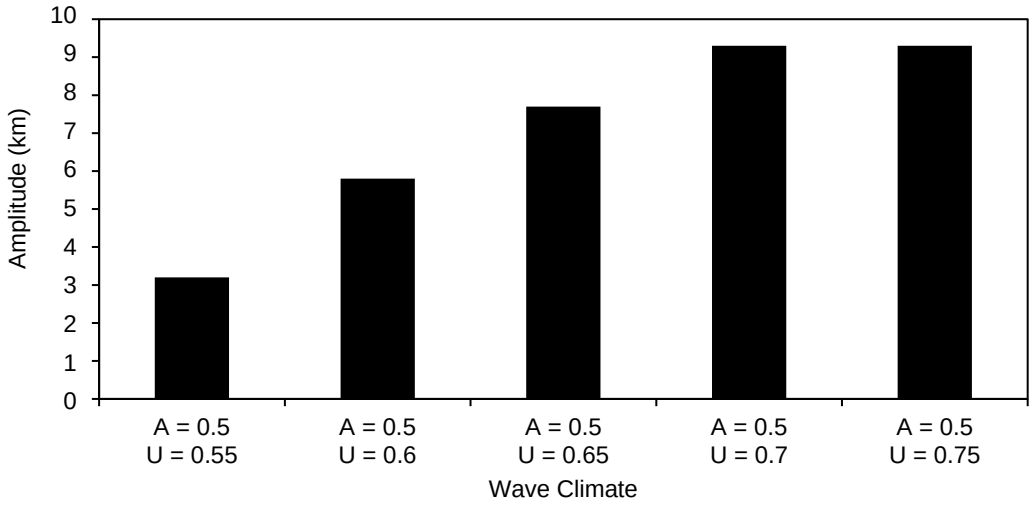

Figure 15 A graph showing the average amplitude of landforms that develop under a symmetryical wave climate, where A = 0.5 and U varies from 0.55 to 0.75.

A comparison of time series images in Figure 16 illustrates this process, showing outputs from CEM between T = 700-750 where *U* varies from 0.55 to 0.75. Where *U = 0.55* and *U = 0.6* more than one feature exists along the shoreline. Where *U = 0.65* a finite amplitude cusp is observable in the bay of the larger landform where T = 700, but is diffused by T = 750 leaving a single features along the shoreline (Figure 16). For simulations where *U = 0.7 and U = 0.65* the rate at which landforms merge reduces with an increasing proportion of high angle waves. In these simulations, two cuspate features are clearly visible along the shoreline. The features extend further offshore compared to the other results.

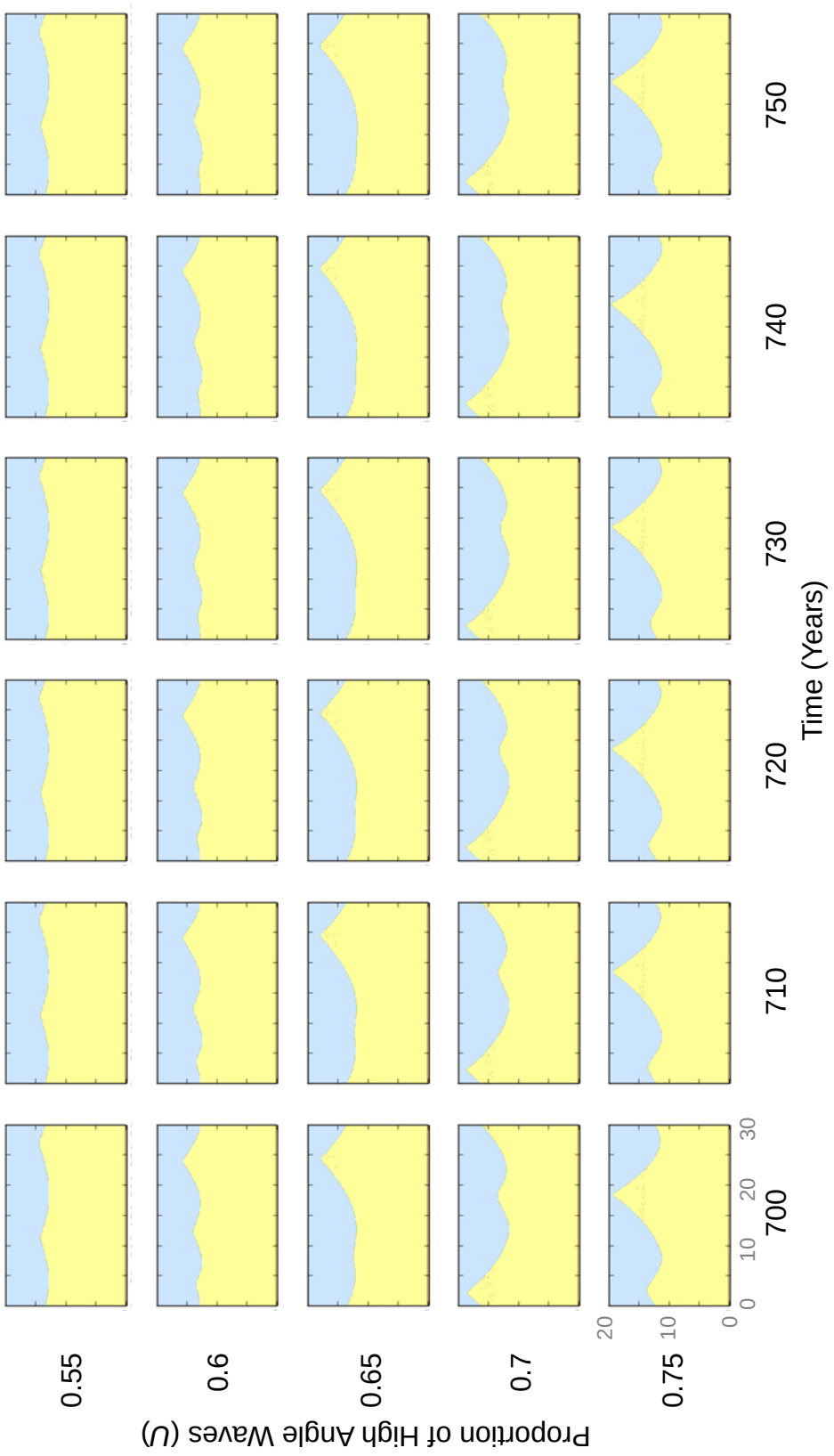

Figure 16 A time series of images illustrating the time period in which each shoreline under differing proportions of high angle waves reaches ds dynamic equilibrium. The size of the domains are given in grey (km).

As shown in Figure 17, the aspect ratio of cusps is greater with an increasing proportion of high angle waves. This is concurrent with the understanding that high angle waves induce cross-shore sediment transport and elongate the tips of cusps. Whilst there is a slight increase in aspect ratio over time for the majority of simulations presented in Figure 17, it remains relatively constant throughout the simulations.

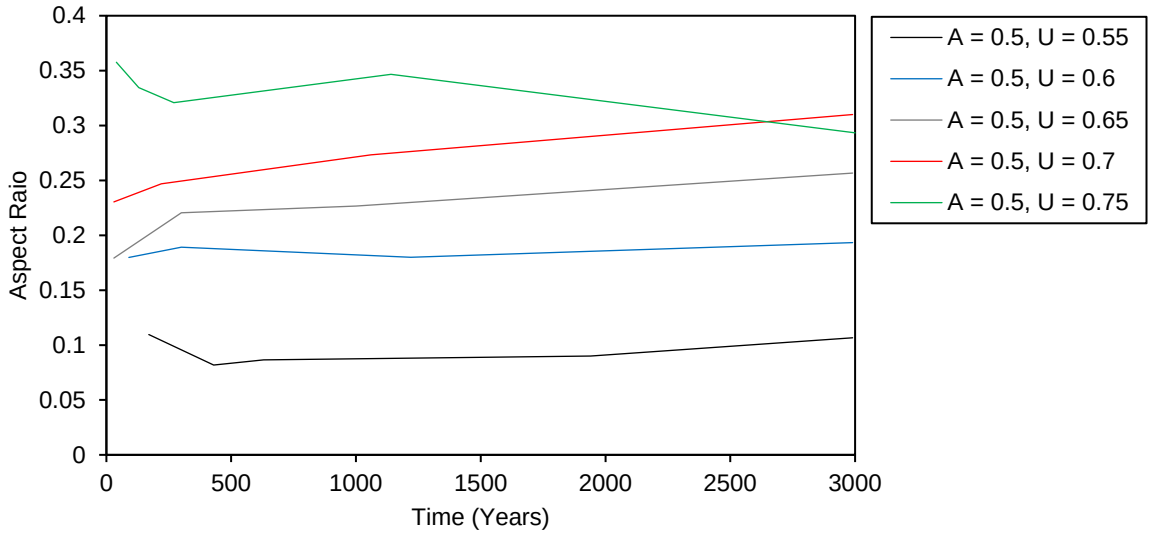

Figure 17 A graph showing the average aspect ratio of landforms over time, for four simulations using CEM where A is held constant at 0.5 and U ranges from 0.55 to 0.75.

3.2.2 CEM2D

Simulations have been run using CEM2D, using a similar experimental set-up to the CEM as presented in Section 3.2.1. The outputs of CEM2D are shown in the matrix in Figure 2, with increasing wave asymmetry along the x-axis and increasing proportion of high angle waves along the y-axis. Four principle shoreline shapes are observed, according to the wave climate conditions, including cusps, sand waves, flying spits and reconnecting spits.

Across the phase space (Figure 2), cuspate and finite amplitude sand waves occur where either the proportion of high angle waves is low or where the

proportion of approaching wave angles is symmetrical. With increasing asymmetry and proportion of high angle waves, flying and reconnecting spit features form along the shoreline.

Many of the simulations presented in Figure 2 terminate prematurely, due to the features developing beyond the capabilities of the model to analyse their form and continue transporting sediment according to the wave regime. There is a trend which shows that with increasing proportions of high angle waves and increasing wave asymmetry, model runs terminate increasingly earlier than those with lower *A* and *U* values (Figure 18).

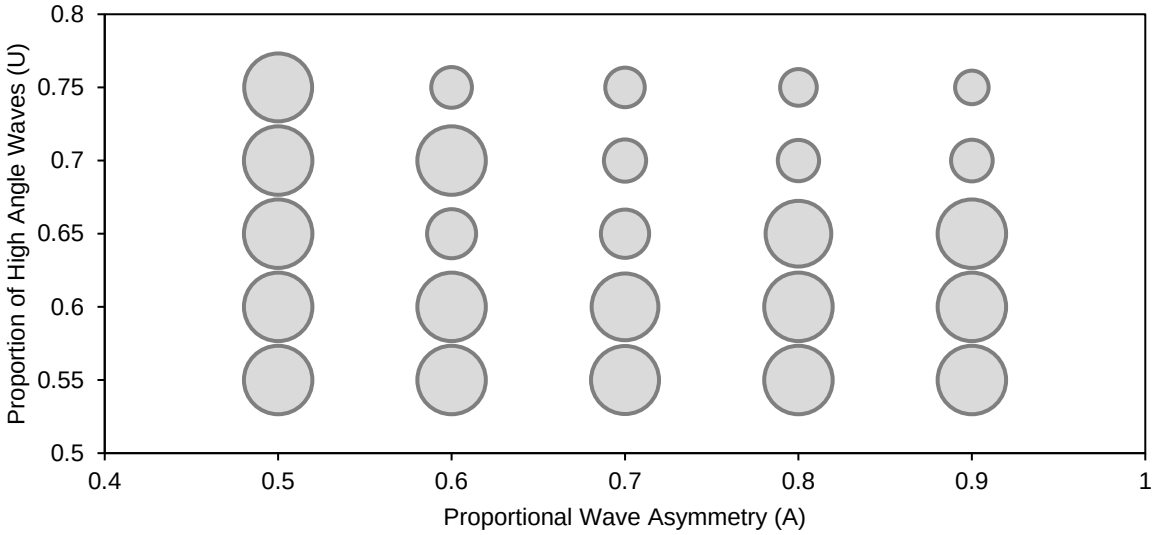

Figure 18 A plot showing the relative run durations of simulations where A ranges from 0.5 to 0.9 and U ranges from 0.55 to 0.75. The diameter of the scatter points denotes the runtime, with larger circles representing longer runtimes to a maximum of 3,000 simulated years.

The differing runtimes for each simulation in indicative of the development patterns of the shorelines under the wave regimes input into the model, but a further more detailed exploration is required to understand their evolutionary behaviour. Taking four representative simulations that generate cuspate coastline (*A = 0.5, U = 0.55)*, sand waves features (*A = 0.6, U = 0.6)*, reconnecting

spits (*A = 0.7, U = 0.65)* and flying spits (*A = 0.8, U = 0.7)*, an analysis of how each type of feature develops and evolves over time. The representative simulations used, match those used in Section 3.2.1 with results from CEM.

Using these four representative simulations, Figure 19 shows how the planform area of each feature increases over time. A trend also suggests that increasing proportions of high angle waves and wave asymmetry, larger landforms evolve. For instance, the average size of cuspate features at the end of the simulation period is 1857 km^2, compared with flying spits which exhibit a size of 76,500 km^2 after 1090 simulated years when the run terminates. Although the area of the sand wave at the end of the simulation period is much greater at an average of 94,520 km^2, this simulation ran for the maximum 3000 year period. If the flying spit continued to evolve for the maximum time, its trajectory could surpass the rate of the sand wave's development. The simulation which generates reconnecting spit features is an exception to the rule and develops over a smaller spatial area than the trend would predict. At the end of the run period of 1490 simulated years, it covers an area of approximately 11,340 km^2.

Cuspate features evolve and develop at a steady rate, whilst the sand wave features have periods of differing growth rates (Figure 19). The sand waves exhibit a relatively linear evolution until they grow to an area of approximately 94,520 km^2. Thereafter, the size of the landform is sustained throughout the remainder of the simulation. Whether a similar behaviour occurs for spit features is unknown, since these simulations terminate prematurely. analysed

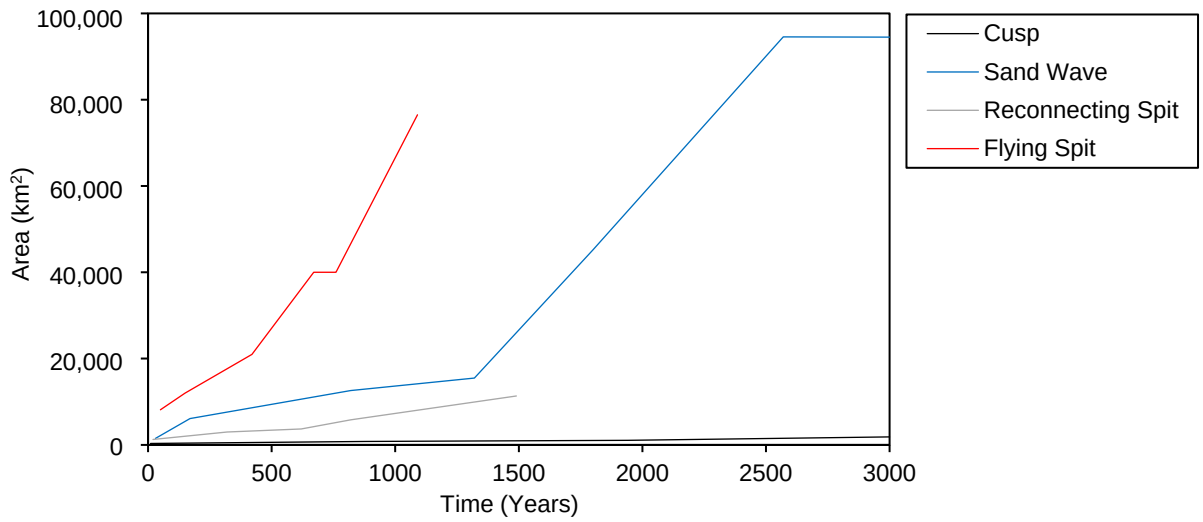

Figure 19 A graph showing the average area of landforms over time, for four simulations using CEM2D that produce planform morphologies representative of cusps, sand waves, reconnecting spits and flying spits.

The wavelength of the four representative landforms is also indicative of their evolution over time. According to the size of the analysed domain, the maximum wavelength achievable in the simulations is 30 km. In Figure 20, the wavelength growth for each representative simulation is presented. Each result shows an increase in the wavelength over time, with a steady growth occurring for cuspate landforms and a more rapid evolution for sand waves. The relatively short simulation period for reconnecting and flying spit features limits the ability to compare results, but a relatively comparable gradual increase in wavelength growth is observed. Plotted onto this figure is the point at which the sand wave reaches its maximum areal size.

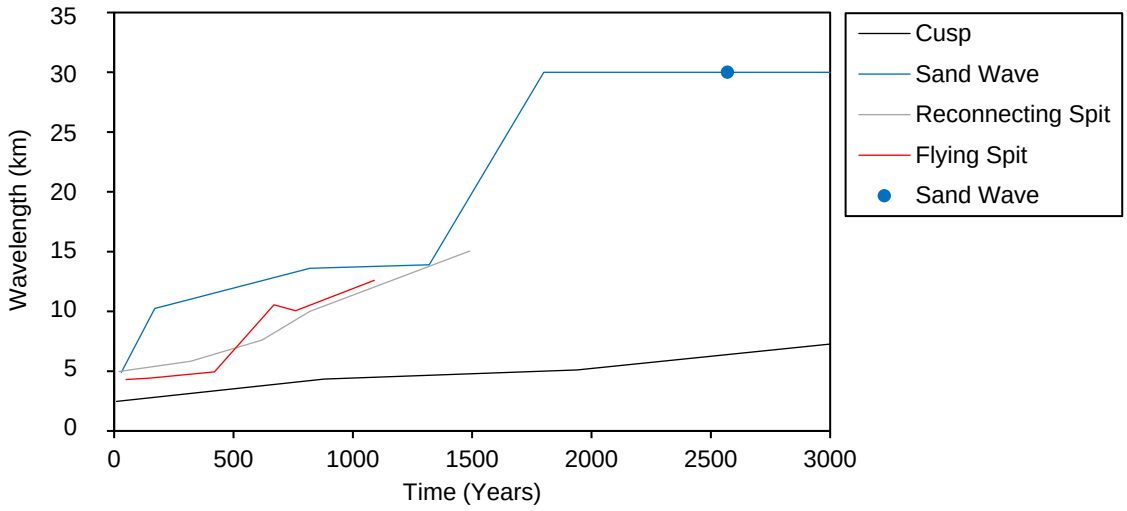

Figure 20 A graph showing the average wavelength of landforms over time, for four simulations using CEM2D that produce morphologies representative of cusps, sand waves, reconnecting spits and flying spits. The point marks where the sand wave reaches it's largest areal size.

Unlike the results presented in Section 3.2.1, there is no apparent correlation between the time frame where the landform reaches the maximum wavelength and its growth rate plateaus. In the results presented in this section using CEM2D, the wavelength of the sand waves reaches 30 km after approximately 1800 simulated years but the size of the feature continues to grow up to approximately 2570 simulated years. As shown in the time series in Figure 21, after 1600 simulated years (T = 1600), two features exist along the shoreline with a wavelength of approximately 14.5 km and an amplitude of the larger landform of approximately 3.1 km. Where T = 1800 one landform remains and the wavelength reaches 30 km with an approximate amplitude of 3.5 km. Maintaining this wavelength, as the maximum achievable within the limits of the domain, the sand wave increases in areal size and amplitude, to 7.4 km where T = 2600.

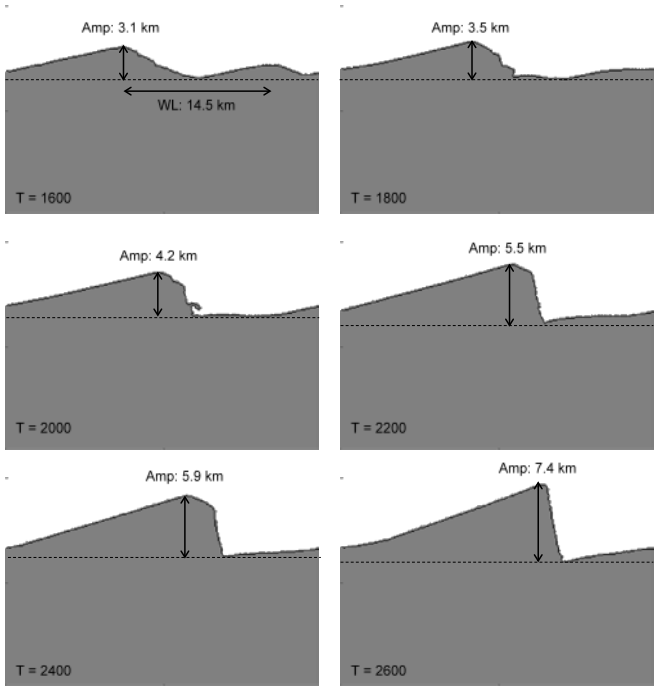

Figure 21 A time series of images showing how sand waves (generated under a wave climate where A = 0.6, U = 0.6) grow in amplitude (Amp) over time whilst sustaining an average wavelength (WL) of 30 km after 1800 simulated years (T). The dashed line marks the approximate location of the base of the landforms.

The aspect ratio further describes the relationship between wavelength and landform amplitude. As shown in Figure 22, after an initial spin-up period the aspect ratio increases with greater wave asymmetry and proportion of high angle waves. A coincidence is observed between the aspect ratio and the point at which the areal size of the sand wave stabilises and where the maximum wavelength is achieved, as shown in Figure 22. The data reinforce the concept that once the sand wave reaches the maximum wavelength where T = 1800, accretion offshore extends the amplitude of the feature which increases the aspect ratio up to where T = 2570 and the landform reaches a dynamic equilibrium (Figure 22).

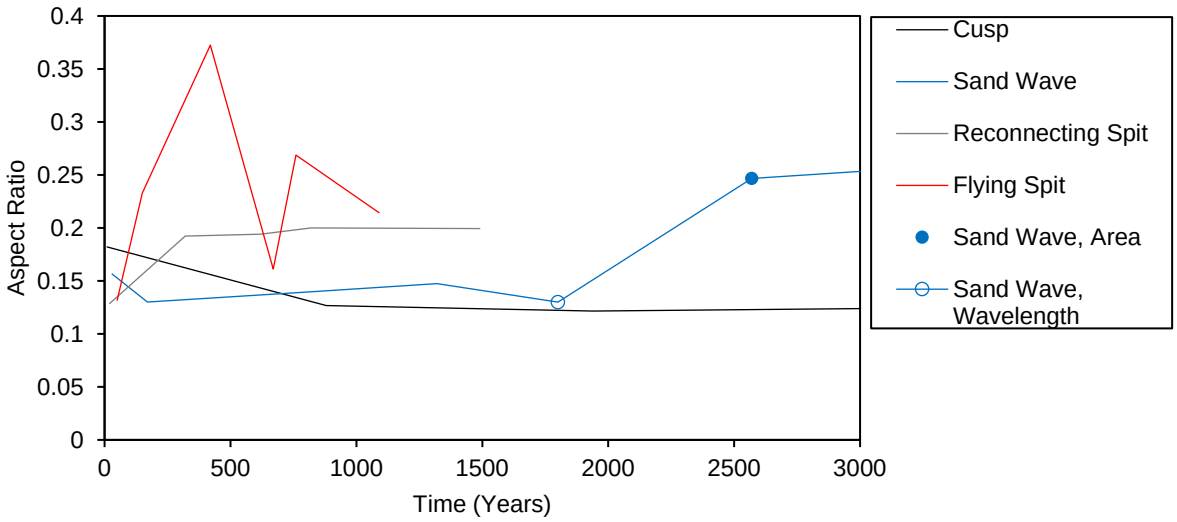

Figure 22 A graph showing the aspect ratio of landforms over time, for four simulations using CEM2D that are representative of cusps, sand waves, reconnecting spits and flying spits. The markers denote where the sand wave reduces its rate of growth (filled circle) and where it reaches the maximum wavelength (outline circle) as per Figure 19 and Figure 20 respectively.

As shown in Figure 22, the aspect ratio of the cuspate features decreases gradually over time from 0.18-0.12 between 10 and 3000 simulated years. This suggests that the wavelength increases at a rate greater than the amplitude over time. This is observable in the results which show that cusps diffuse, reducing the count along the shoreline and increasing the wavelength, yet due to the balance of low and high angle waves, there is a limited extension of the features offshore. Conversely, reconnecting spits show a gradual increase in aspect ratio over time, from 0.12-0.19 between 10 and 1490 simulated years when the run terminates (Figure 22). The greater proportion of high angle waves drives cross-shore sediment transport and the extension of landforms offshore. The simulation generating flying spit features also show a general increase in aspect ratio, but with some fluctuation throughout the simulation. With high wave asymmetry and proportion of high angle waves, wave shadowing and migration patterns could be influencing the longshore and cross-shore sediment transport patterns. Phases of growth are observed where landforms initially extend offshore (Figure 23, T =

420) but as they migrate longshore and smaller landforms are engulfed by the larger features, the wavelength increases (Figure 23, T = 670). As the larger landforms persist and continue to grow, they develop cross-shore due to the dominance of high angle waves (Figure 23, T = 760) but again merge as they migrate to increase the wavelength (Figure 23, T = 1090).

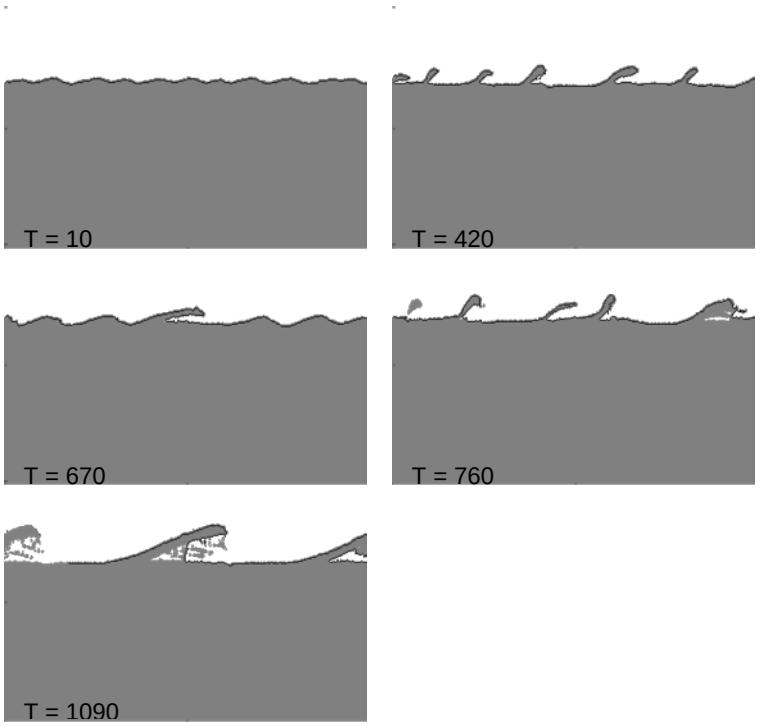

Figure 23 A time series of images showing how flying spits (generated under a wave climate where A = 0.8, U = 0.7) evolve in phases where the amplitude and wavelength increases successively over time (T).

The results discussed highlight that a relationship exists between the rate and pattern of landform evolution along shorelines and the proportional wave asymmetry and highness of waves. Attention is focused subsequently on two series of simulations that look at the separate influence of wave asymmetry and the proportion of high angle waves on the behaviour of the shoreline.

3.2.2.1 *Wave Angle Asymmetry (A)*

To investigate the influence of wave asymmetry (*A*), a set of simulations varying this parameter from proportions of 0.5-0.9 have been completed, whilst holding the proportion of high angle waves (*U*) constant at 0.6.

With increasing wave asymmetry, there is a progression in the shape of landforms from cusps to flying spit features, as shown in Figure 24, but where *A = 0.9*, cuspate sand wave features form. As explored further in Section 3.2.2.2 (below), where *A = 0.5, U = 0.6,* the landforms show a directional skew similar to the sand wave features, although their formation is likened to that of cusps and are therefore considered as such in this analysis. The observed skew in their form is explained in the above-cited section in relation to bias in the model as opposed to representing natural phenomenon.

With 90% of waves approaching the coast from the left of the domain, there is a strong longshore sediment transport component (*where A = 0.9, U = 0.6*). As shown in Figure 24, the shoreline takes a cuspate form in the model simulation. These types of features typically form in highly symmetrical waves climates and so their formation here is of interest.

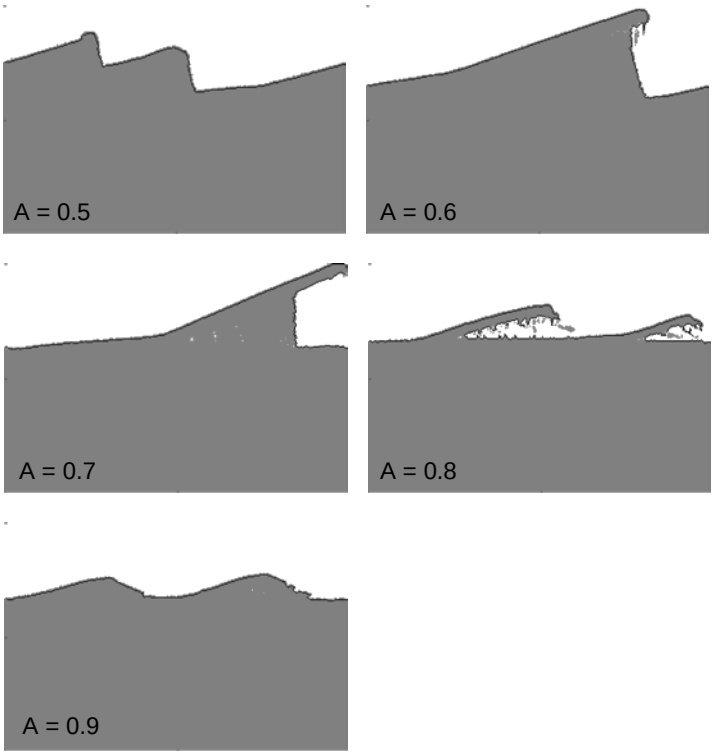

Figure 24 A time series of images showing the shorelines shapes that are generated under wave climates where the proportional asymmetry ranges from 0.5 to 0.9 and the proportion of high angle waves is held constant at 0.6.

An analysis of time series images of the evolution of the shoreline where *A = 0.9, U = 0.6* shows how the mechanisms responsible for sediment transport do not correspond with cuspate coastlines. The shoreline evolves through building shore-parallel spits which reconnect with the mainland and create cuspate-like bumps. The image in Figure 25 taken after 2540 simulated year's shows evidence of these spits along the shoreline. The output presented in Figure 24 is therefore not wholly representative of the long-term behaviour of this shoreline and the wave climate conditions can be associated with forming shallow reconnecting spits. These spits are shallower, in term of their proximity to the shoreline than those that form where *U = 0.6* to *0.8*. This is attributed to the high asymmetric climate and only slight dominance of high angle waves, which in combination drive a strong longshore transport component and have a greater smoothing

effect on perturbations than climates where there is increased cross-shore transport induced by greater wave symmetry.

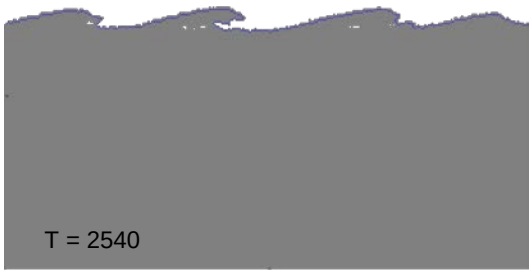

Figure 25 An image showing an output of CEM2D after 2540 simulated years (T), where the coastal system is driven by a wave climate where A = 0.9, U = 0.6.

As shown in Figure 26 for each simulation there is a slight increase in the planform area of landforms over time. Similar trajectories are followed for the simulations with proportional asymmetries greater than 70% (A = 0.7). This trajectory shows an average rate of areal landform growth at 2.9 km^2 per year over the 3,000-year simulation. The rate of landform growth is greater where the proportional wave asymmetry is 50% (10 km^2 per year) and 70% (11 km^2 per year) but is greatest at 60% (31 km^2 per year). The slight dominance of high angle waves and waves approaching from the left of the domain transport sediment longshore, forming skewed features along the shoreline. Waves approaching from the alternate angles and directions move sediment in the opposite direction. These processes working in unison and the colliding of sediment pathways drives sediment offshore and features extend seaward as a result. Hence, rather than smoothing the shoreline and diffusing sediment, under these wave climate conditions large planform sand wave evolve as shown in Figure 24 and Figure 26.

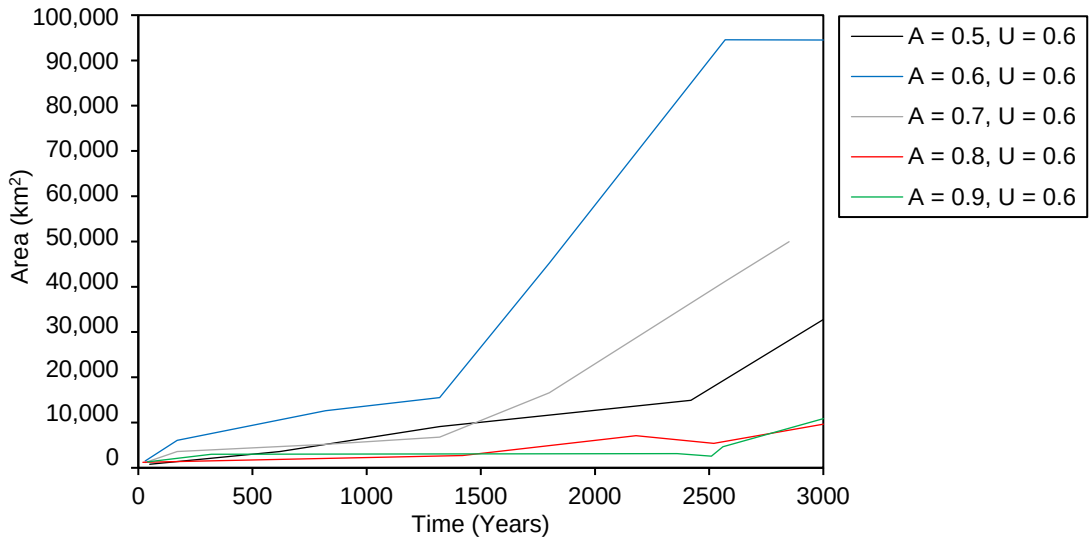

Figure 26 A graph showing the average planform area of landforms over time, for four simulations using CEM2D where U is held constant at 0.6 and A ranges from 0.5 to 0.9.

The change in wavelength of features along the shorelines also follows a positive trend (Figure 27). Wave climates with high asymmetry $A \geq 0.8$ or are symmetrical where $A = 0.5$ show similar trajectories and gradual increases in wavelength over time. Where $A = 0.8\text{-}0.9$, the wavelength increases from an average of 4.7 km after 10 simulated years to 13.7 km at the end of the 3,000 year simulation period. Where $A = 0.5$ the initial rate of wavelength growth is greater than observed from the shorelines under high wave asymmetries, but a similar average increase occurs throughout the simulation from approximately 3.9 km to 15 km.

Where $A = 0.6$ and where $A = 0.7$ the high amplitude spit features develop at a greater rate in terms of their wavelength after the first 1,300 simulated years, relative to the other features plotted in Figure 27. During the first half of the simulations, the landforms develop gradually and form finite amplitude features along the shoreline. As the landforms grow and build seaward wave shadowing influence increases and the growth rate increases rapidly (see Figure 26), including the wavelength (Figure 27). The point at which the rate of areal growth

of these spits increases, as plotted in Figure 26, is marked by scattering points in Figure 27.

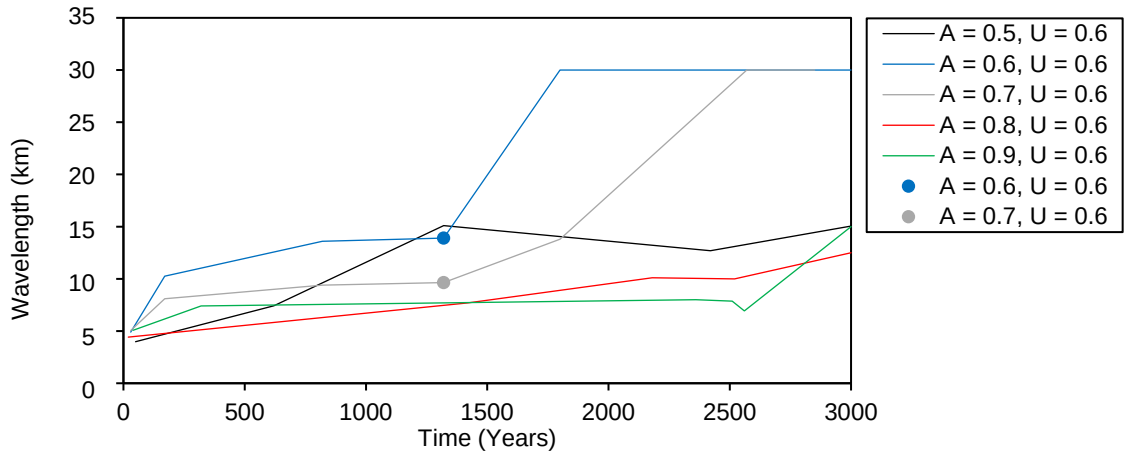

Figure 27 A graph showing the average wavelength of landforms over time, for four simulations using CEM2D where U is held constant at 0.6 and A ranges from 0.5 to 0.9. Markers denote the point in time where the area of landforms shows a significant increase in the rate of growth as per Figure 26.

Figure 28 shows the change in aspect ratio over time of features that form where the proportional asymmetry varies from 0.5-0.9 and the proportion of high angle waves is held constant at 0.6. During the first 1,500 simulated years, the aspect ratio of landforms remains relatively constant between 0.1 and 0.15, denoting features with larger wavelengths over amplitude. After this period, there is a gradual increase in ratio to an average of 0.2 to 0.3 as the landforms accrete cross-shore, excluding where A = 0.9 (Figure 28). For this highly asymmetric wave climate, the strong longshore sediment transport processes act to smooth the shoreline and develop spits that are near-parallel to the shoreline, as shown in Figure 25.

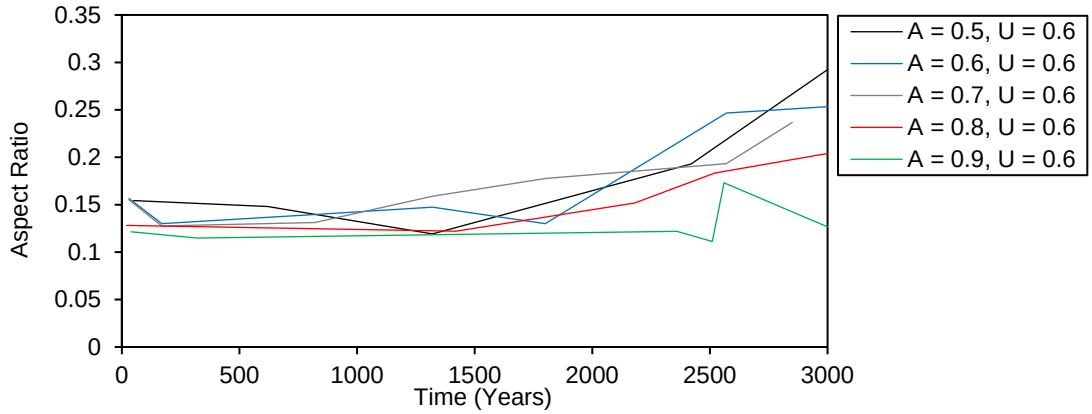

Figure 28 A graph showing the average aspect ratio of landforms over time, for four simulations using CEM2D where U is held constant at 0.6 and A ranges from 0.5 to 0.9.s

A comparison of average, relative rates of landform migration demonstrate that with increasing wave asymmetry the features migrate quicker longshore (Figure 29). Where the wave climate is symmetrical (*A = 0.5*), minimal migration of the cuspate features are observed, although some movement is noted at a rate of approximately 1.7 m per year. A slightly greater rate of 5 m is observed for the sand wave features that form with a slight asymmetry in the wave climate (*A = 0.6*), which drives some longshore sediment transport. A much high rate of migration occurs with increasing asymmetry, from 100 m per year to 2,300 m per year where *A = 0.7* and *A = 0.9* respectively. Under these wave climate conditions the dominant wave direction driver a strong longshore current of sediment, forming spit features that migration longshore.

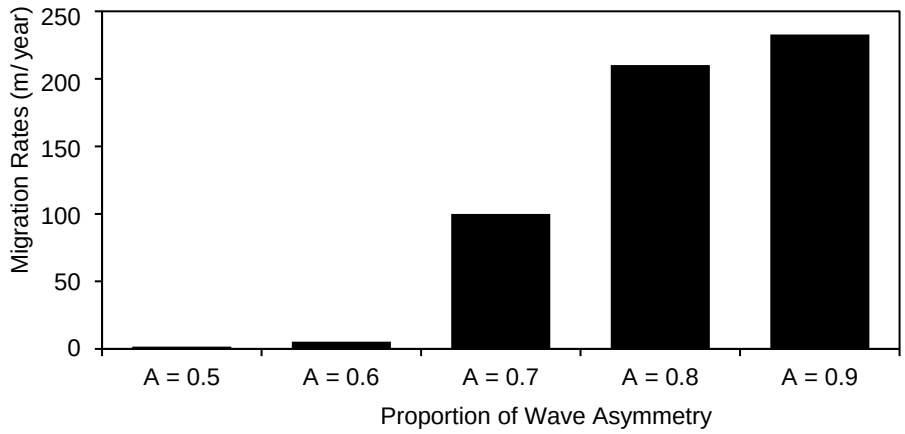

Figure 29 A graph showing the average rate of landform migration, according to the asymmetry (A) or the wave climate.

3.2.2.2 *The Proportion of High Angle Waves (U)*

To investigate the influence of high angle waves (*U*), a set of simulations varying this parameter from proportions of 0.55- 0.75 have been completed, whilst holding the wave asymmetry (U) constant at 0.5 denoting a symmetrical wave climate.

Where the wave climate is symmetrical (*A = 0.5)* and the proportion of high angle waves is $\leq$ 60% (where *U = 0.55 or 0.6),* uniform cuspate features form along the shoreline (Figure 2). With increasing proportions of high-angle waves (e.g. where *U = 0.65, 0.7 or 0.75)*, the cuspate features show a slight skew towards the right side of the domain. However, the formation of all features under a symmetrical climate, regardless of high-wave proportions, is similar to the mechanism responsible for cusp formations in the CEM as described previously (see Section 3.2.1). It can be assumed therefore that whilst the features skew where high angle wave proportions are > 60%, these features are cuspate in behaviour as opposed to resembling sand waves. Their skewed planform is seemingly unrelated to longshore transport in the symmetrical climate, rather to diffusional processes in the model and bias that favours transport from the left to right of the domain due to the design of the numerical modelling. Once a feature begins to skew, it can activate other processes such as wave shadowing which exaggerates the skew of cusp tips toward the right of the domain. Numerical modelling bias is a recognised limitation of CEM2D that has been investigated and discussed further in Chapter 8.

Considering all features under a symmetrical wave climate (A = 0.5) to be cuspate, with increasing proportions of high angle waves these landforms grow in amplitude and extend offshore. This is illustrated in Figure 30, which shows

outputs from simulations where A = 0.5 and U ranges from 0.55-0.75. The outputs show results after 950 simulated years, since beyond this point the features with a greater proportion of high angle waves begin to skew, as discussed in Section 3.2.2, which influences their cross-shore growth rate (Figure 30).s

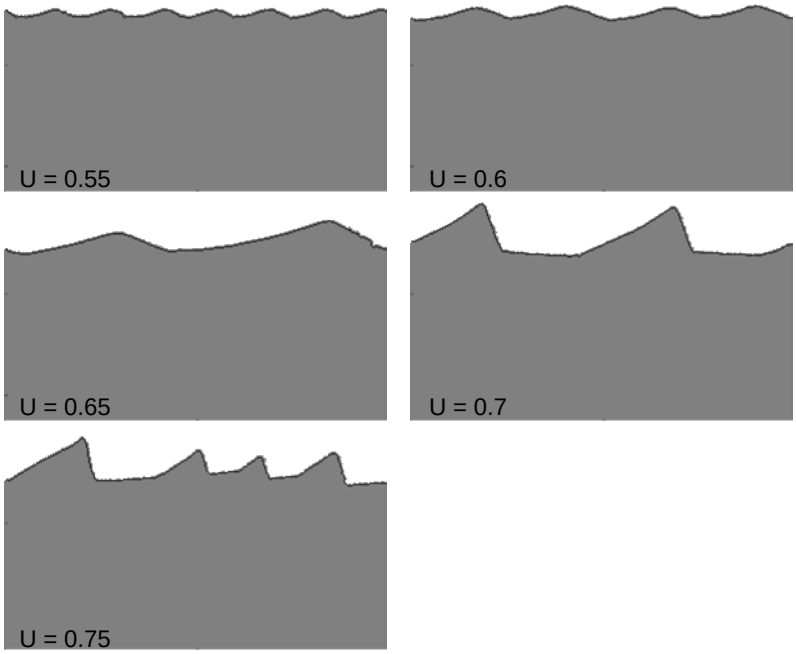

Figure 30 A series of images showing the difference in amplitude of cuspate landforms that form under a symmetrical wave climate (A = 0.5) with an increasing proportion of high angle waves (U).

Over the simulation period, the shoreline features shown in Figure 30 increase in planform area (Figure 31). The greater the proportion of high angle waves, the greater the rate of growth. The features which form under wave climates with $\leq$ 70% proportion of high angle waves show a gradual increase over time. The average landform size increases from approximately 400 km^2 after 10 simulated years to 1850 km^2 after 3,000 simulated years where U = 0.55, and to approximately 83,200 km^2 where U = 0.7 (Figure 31). Spit features that form where U = 0.75 show a less gradual rate of evolution, growing rapidly at a rate of 84 km^2 per year between 1020 and 1620 simulated years, but reduces significantly to 14.26 km^2 thereafter (Figure 31).

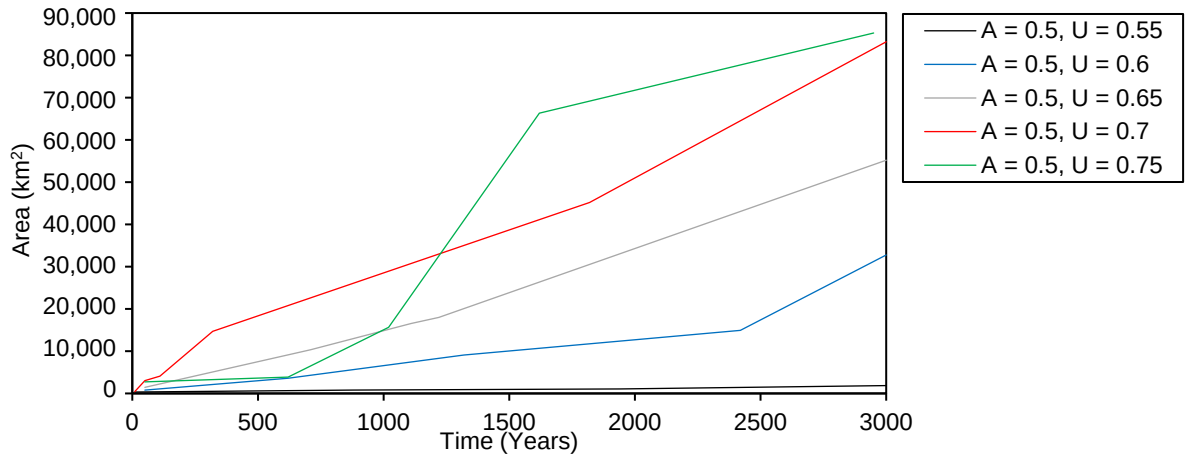

Figure 31 A graph showing the average area of landforms over time, for four simulations using CEM2D where A is held constant at 0.5 and U ranges from 0.55 to 0.75.

The change in growth rate of the cusps which forms in an environment dominated by high angle waves (where *U = 0.75*, Figure 31) is coincident with the point at which the wavelength reaches the maximum extent according to the length of the analysed domain (30 km) (Figure 32). The domain size affects the evolution of this landform, unlike the other features plotted in Figure 32.

The wavelength increases over time for all features plotted in Figure 32, indicating the development of these landforms in the model runs. The greater the proportion of high angle waves the quicker the rate of wavelength growth; where *U = 0.55* the average rate of wavelength increase is 0.0016 km per year and where *U = 0.75*, the average rate is 0.008 km per year. Although where *U = 0.75* the rate of landform development is the most rapid of those observed, there is a lag time during the first 620 simulated years where the wavelength between features remains relatively consistent (Figure 32). During this period the cusps develop cross-shore and fewer low-angle waves act to diffuse smaller features, which would otherwise reduce the count of cusps along the shoreline and increase the

wavelength.

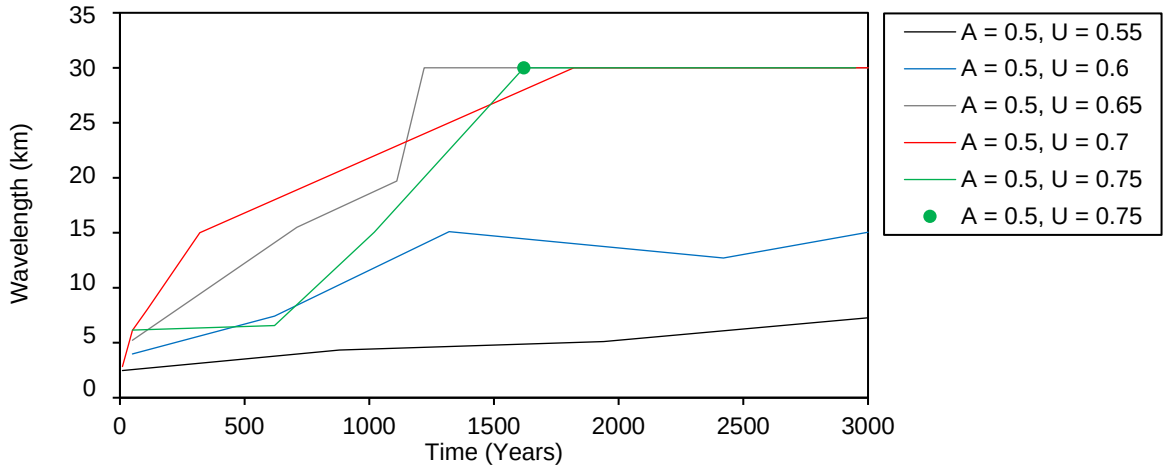

Figure 32 A graph showing the average wavelength of landforms over time, for four simulations using CEM2D where A is held constant at 0.5 and U ranges from 0.55 to 0.75. The markers show for each simulation, where there is a significant reduction in the areal growth rate of features, according to Figure 31.

3.3 Conclusion

This appendix has provided some additional analysis of the results of simulations from CEM and CEM2D, under different driving wave conditions. The results show how the coastal systems behave in each of the models and particularly the development of landforms over time according to their shape, area, wavelength and aspect ration. This analysis can be considered alongside the more synthesised analysis given in Chapter 5.

3.4 References

Ashton, A.D., and Murray, A.B. (2006) High-angle wave instability and emergent shoreline shapes: 1. Modeling of sand waves, flying spits, and capes. *Journal of Geophysical Research*, 111(4).

Appendix 4

Figures 5.11 and Figure 5.12, Enlarged

Cited in Chapter 5

4.1 Introduction

In Chapter 5, CEM and CEM2D are applied to understanding the influence of wave climate conditions on shoreline behavior. An ensemble of twenty-five simulations were run for each model, with the results presented in matrices in Figure 5.11 and 5.12 from CEM and CEM2D respectively. In this appendix, the figures are enlarged to show the results more clearly.

4.1 Results from CEM

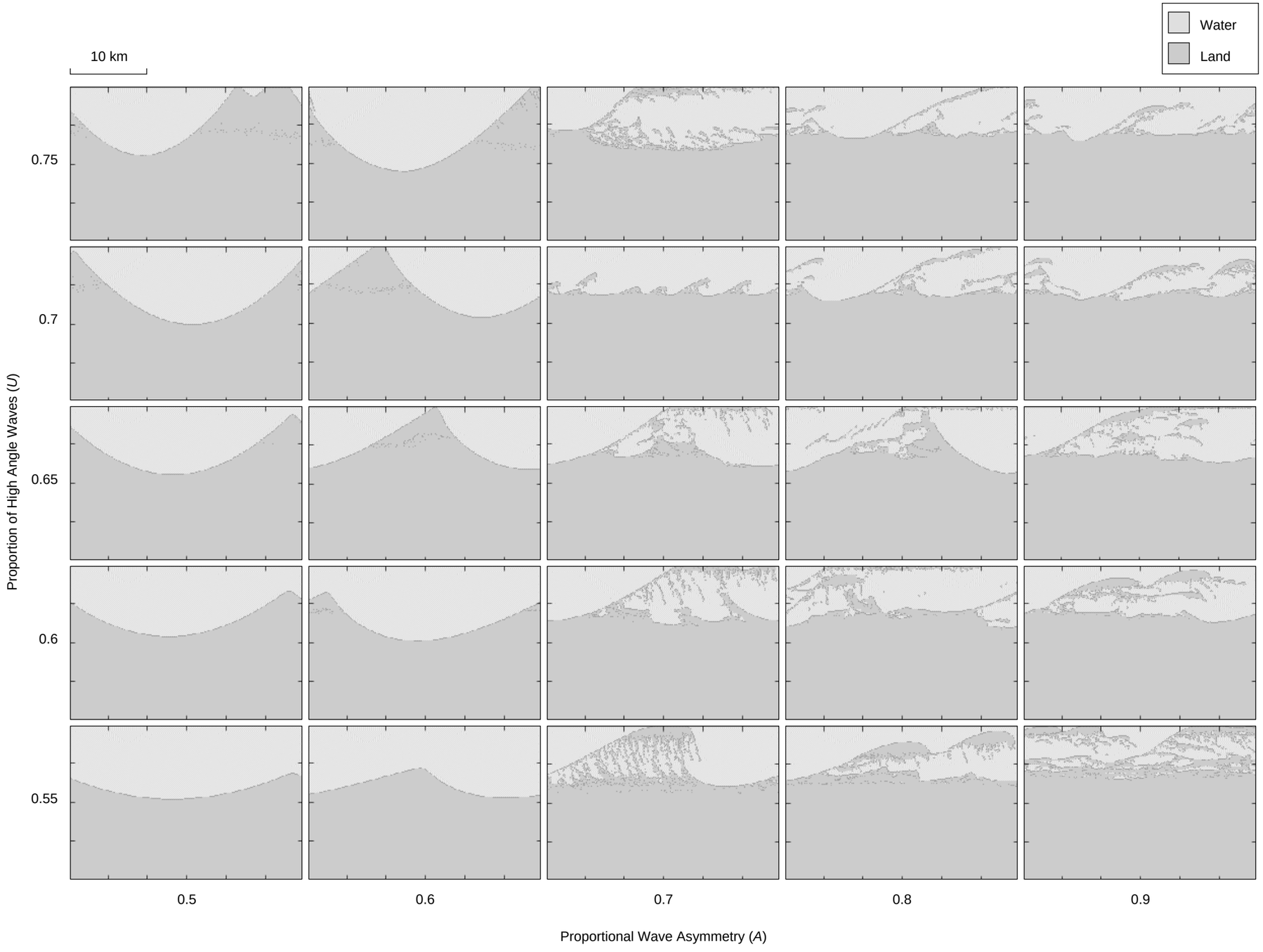

Figure 1 A matrix of results from CEM showing final shoreline morphologies as a function of the wave angle asymmetry (A) and proportion of high angle waves (U) approaching the coast relative to the local shoreline orientation.

The outputs measure 20 km width and 30 km in length and are not inclusive of the periodic boundaries.

4.2 Results from CEM2D

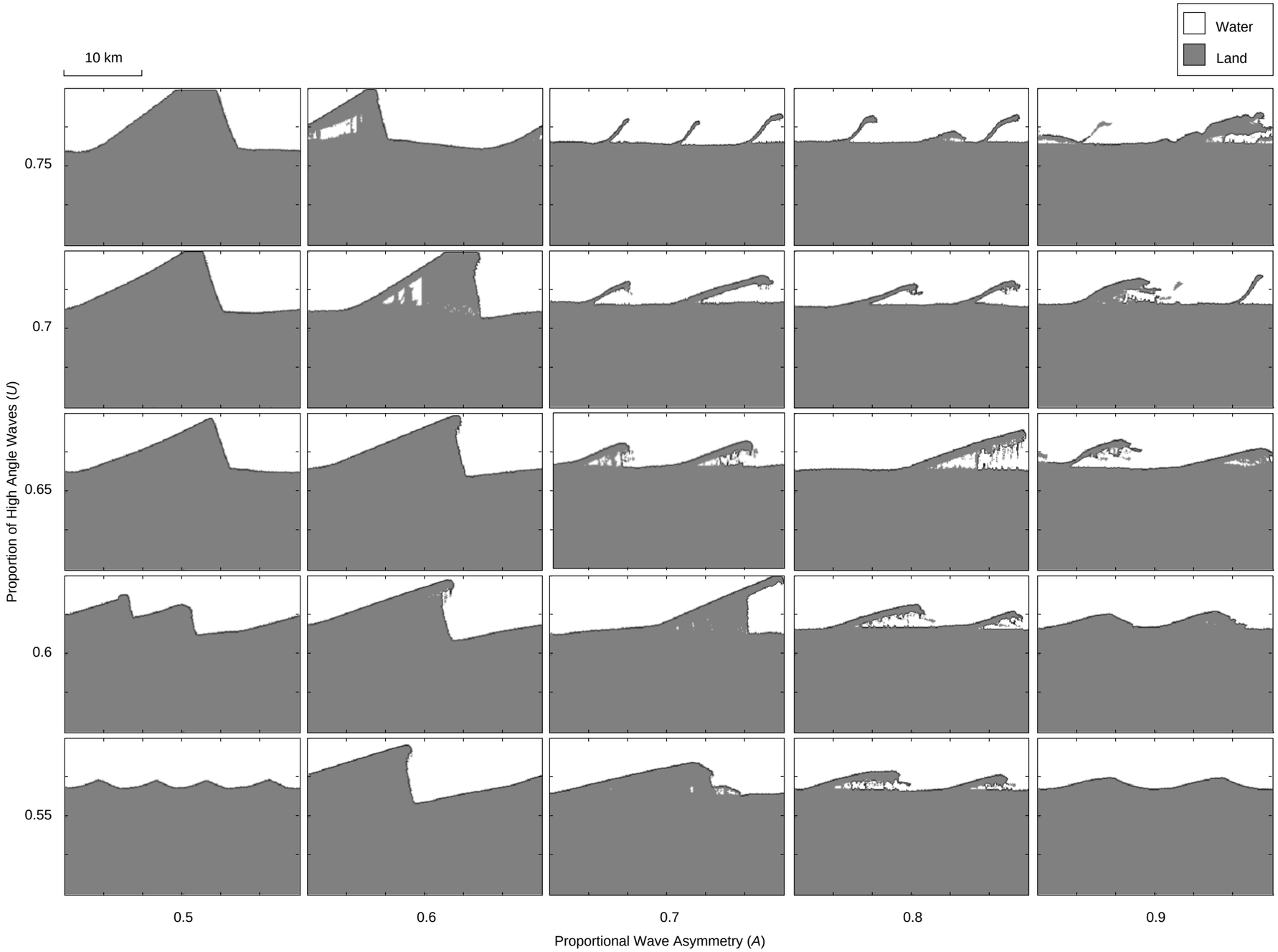

Figure 2 A matrix of results from CEM2D showing final shoreline morphologies as a function of the wave angle asymmetry (A) and proportion of high angle waves (U) approaching the coast relative to the local shoreline orientation. The outputs measure 20 km width and 30 km in length and are not inclusive of the periodic boundaries.

Appendix 5

Figure 6.12, Enlarged

Cited in Chapter 6

5.1 Introduction

In Chapter 6, the CEM2D was applied to understanding the influence of wave climate conditions on the two-dimensional behavior of coastal systems, including the dynamics of the beach surface and nearshore profile. An ensemble of twenty-five simulations were run for this investigation, with the results presented in a matrix in Figure 6.12. In this appendix, the figure is enlarged to show the results more clearly.

5.1 Results from CEM2D

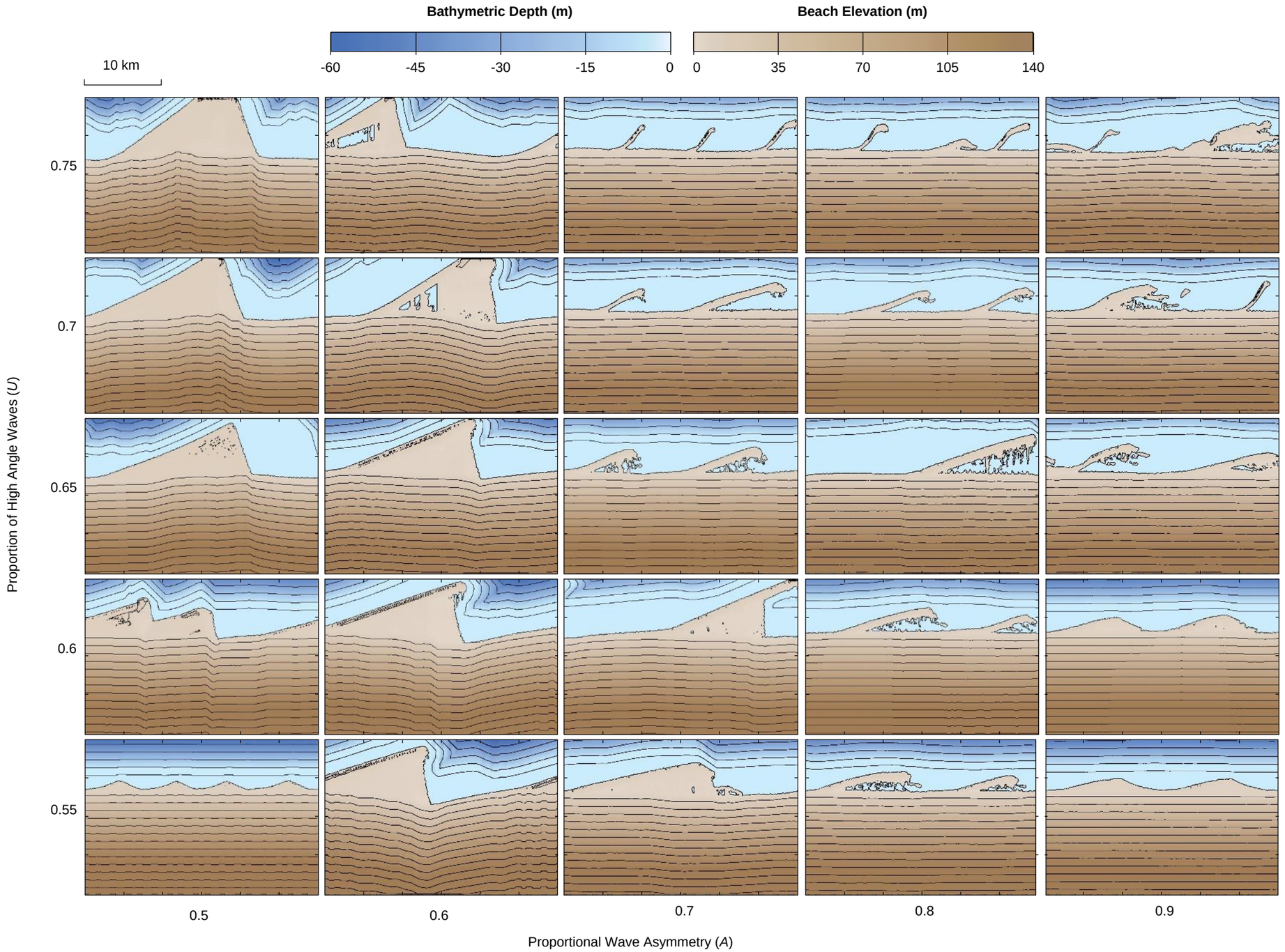

Figure 1 A matrix of results from CEM2D showing two-dimensional final shoreline morphologies as a function of the wave angle asymmetry (A) and proportion of high angle waves (U) approaching the coast relative to the local shoreline orientation.

The outputs measure 20 km width and 30 km in length and are not inclusive of the periodic boundaries.

Appendix 6

Volume Stacks for CEM2D, without Sea Level Rise

Cited in Chapter 6

6.1 Introduction

In Chapter 6 volume stacks are used to depict the most dynamic regions of the coastal profile. These stacks show the change in sediment volume of each cell of the cross-section (where x = 30 km), recorded every 30 simulated years; this provides 100 datasets for each 3,000 year simulation. The volume stacks for each of the twenty-five simulations (without sea level rise) are given in this appendix (see Figure 1), to accompany the results presented in Chapter 6. The matrix in Figure 1 is organized with increasing proportional wave asymmetry (*A*) along the x-axis at increments of 0.1 and increasing proportion of high angle waves (*U*) along the y-axis, at increments of 0.05.

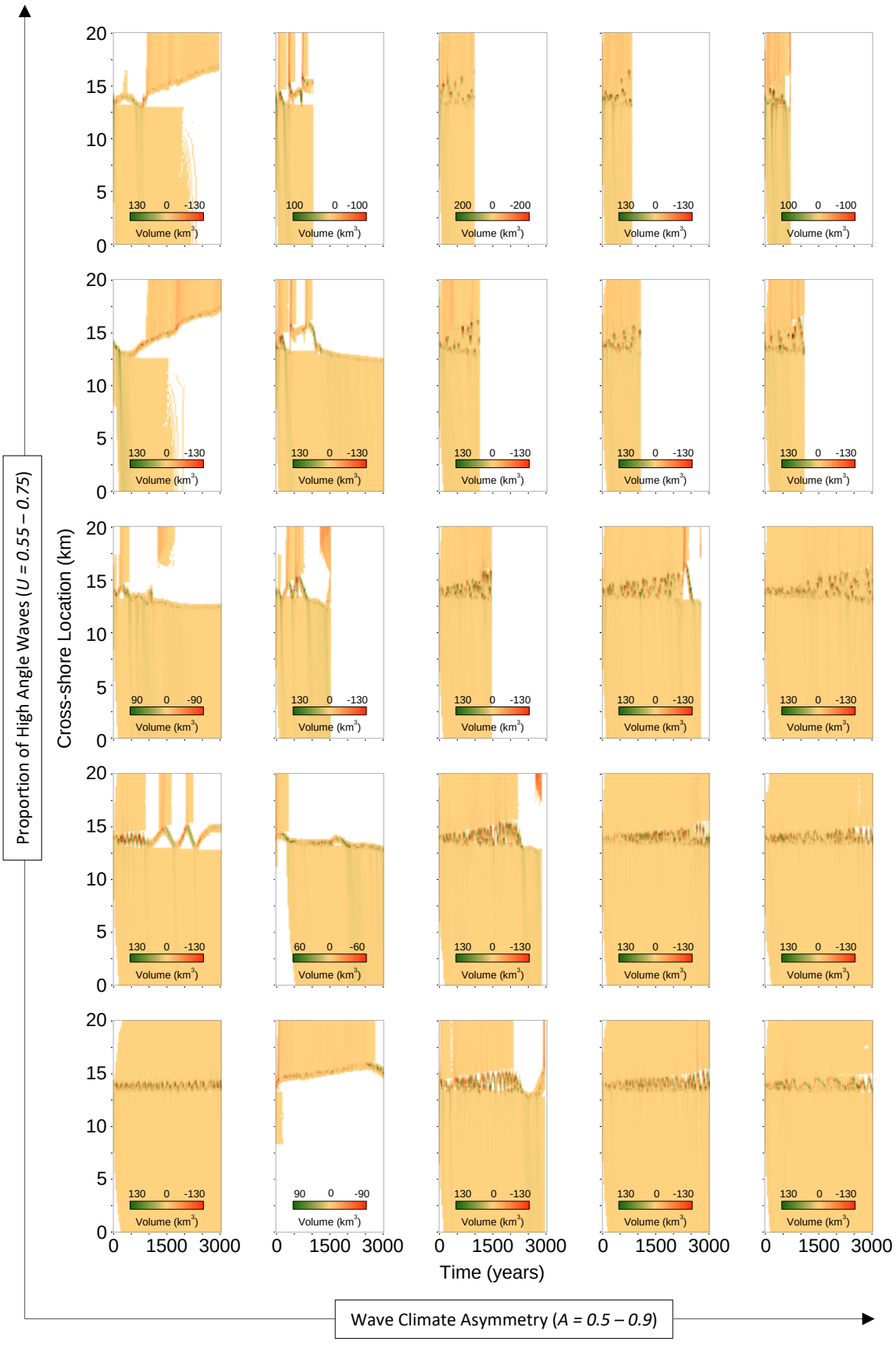

Figure 1 Volume stack of change in sediment volume (km3) cross-shore over 3,000 simulated years, recorded where x = 30 km every 30 simulated years for each wave climate condition.

Appendix 7

Figures 7.7 and Figure 7.8, Enlarged

Cited in Chapter 7

7.1 Introduction

In Chapter 7, CEM and CEM2D are applied to understanding the influence of sea level rise on shoreline behavior. An ensemble of twenty-five simulations were run for each model, with the results presented in matrices in Figure 7.7 and 7.8 from according to rates of sea level rise of 1 m and 2 m per 100 years respectively. In this appendix, the figures are enlarged to show the results more clearly.

7.1 Sea Leve Rise at a Rate of 1 m per 100 Years

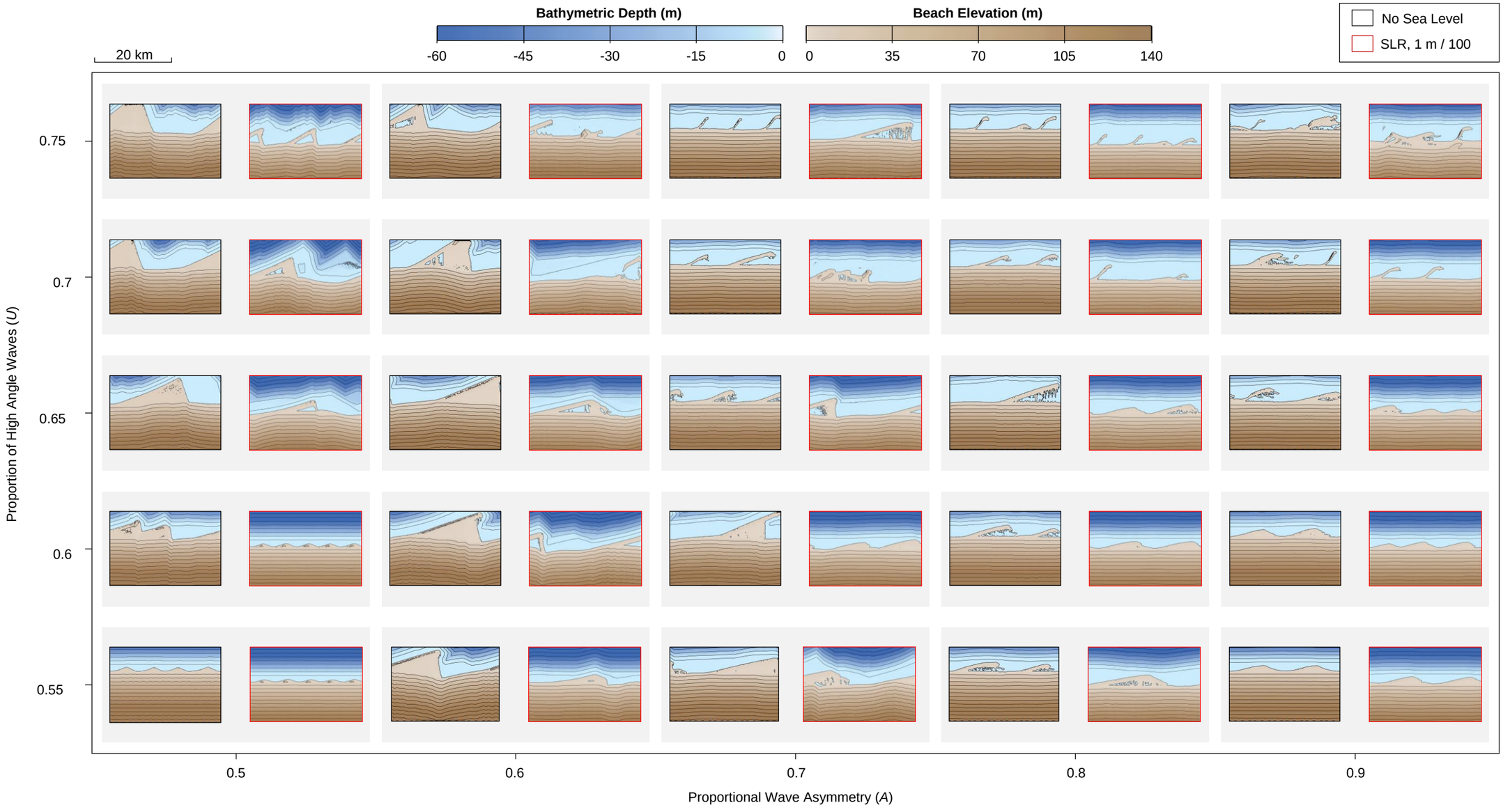

Figure 1 A matrix of results from CEM2D showing final shoreline morphologies as a function of the wave angle asymmetry (A) and proportion of high angle waves (U) approaching the coast relative to the local shoreline orientation, subject to sea level rise at a rate of 1 m per 100 years.

The outputs measure 20 km width and 30 km in length and are not inclusive of the periodic boundaries.

7.2 Sea Leve Rise at a Rate of 2 m per 100 Years

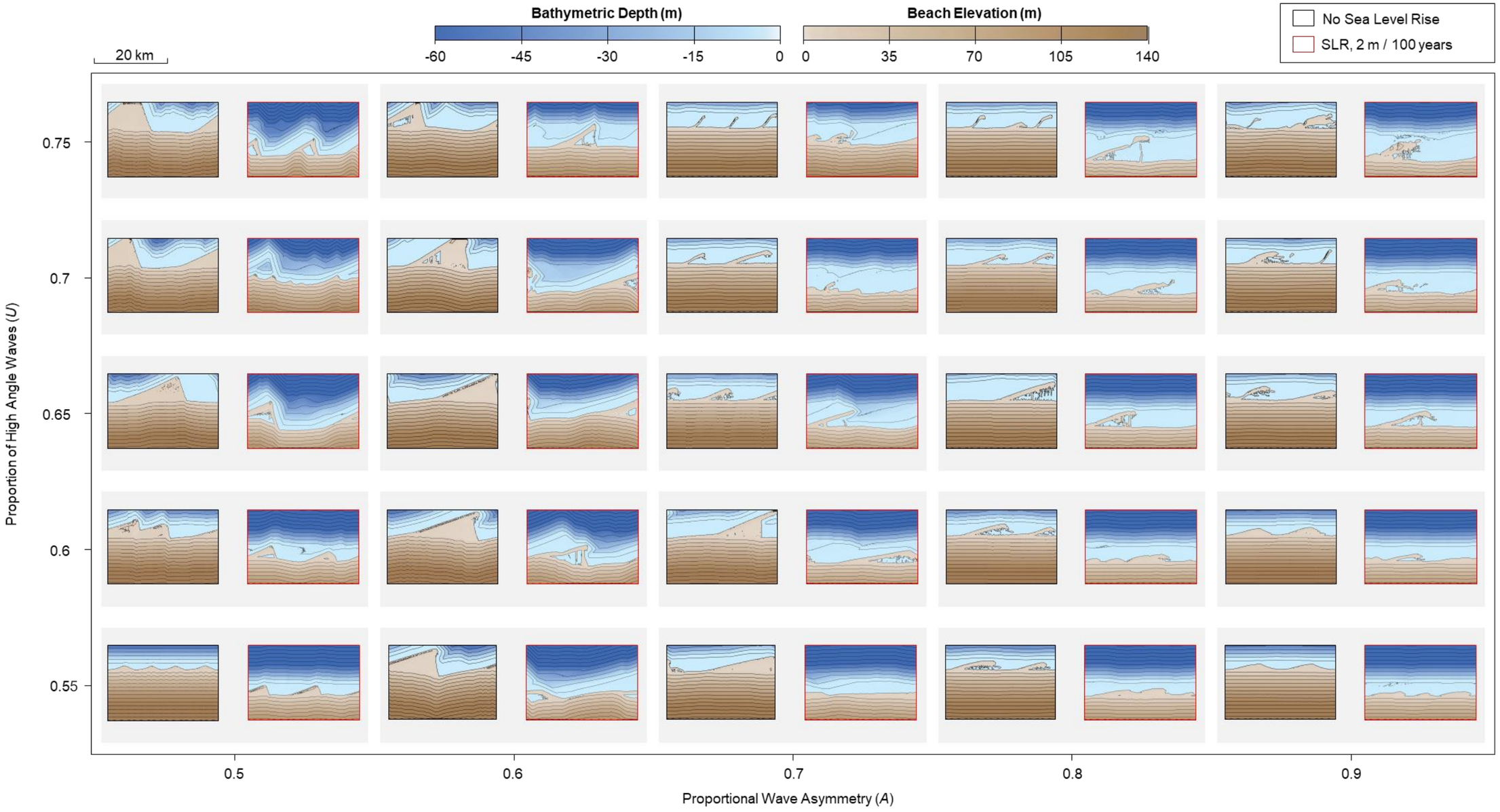

Figure 2 A matrix of results from CEM2D showing final shoreline morphologies as a function of the wave angle asymmetry (A) and proportion of high angle waves (U) approaching the coast relative to the local shoreline orientation, subject to sea level rise at a rate of 2 m per 100 years.

The outputs measure 20 km width and 30 km in length and are not inclusive of the periodic boundaries.

Appendix 8

A Comparison of Beach Profile Change with and without Sea Level Rise

Cited in Chapter 7

8.1 Introduction

In Chapter 7, CEM2D is used to investigate the planform evolution of coastal systems under different driving wave climate conditions and sea level rise, at rates of 1 m and 2 m per 100 years. Included in this investigation is an analysis of how the beach profile changes over time in response to the rising water levels. As was noted in Chapter 7, limited morphological evolution occurs across the beach profile and so minimal discussion is given in the chapter. In this appendix, the results of the beach profile analysis are given in more detail to provide additional information that may be of interest to the reader.

8.2 Evolution of the Beach Profile with Sea Level Rise

Beach profiles recorded over time for each of the twenty-five wave climate conditions with a static water level and sea level rise at a rate of 1 m per 100 years and 2 m per 100 years, are given in Figure 1. Similar profiles are observed for the static water level and sea level rise scenarios. The profiles fluctuate around a 0.01 (1%) slope and tend to show an increase in slope angle initially before shallowing towards, or marginally beyond, the average slope angle. It is also observed that the average profile of the beach is slightly steeper with increasing wave asymmetry (*A*) and proportion of high angle waves (*U*).

Where the wave climate is relatively symmetrical, with only a slight asymmetry induced either by a slight directional (*A* = 0.6, *U* = 0.55 – 0.75) or high angle (*A* = 0.5, *U* = *0.65 – 0.75*) dominance, the change in beach profile over time differs according to the rate of sea level rise or no sea level rise scenario (Figure 1). In particular, the beach surface is shown to become shallower over time, induced by the dominant cross-shore sediment transport mechanisms that distributed material from the beach surface in the nearshore. For all other wave climate scenarios the change in slope of the beach surface overtime is comparable where the water level is static and where rates of sea level rise are 1 m and 2 m per 100 years. It is also observed that with an increasing proportion of high angle waves (*U*), the average slope of the profile also increases marginally; for example from 0.99% where *A* = 0.7, *U* = 0.55 to 1.02% where *A* = 0.7, *U* = 0.75 under a no sea level rise scenario (Figure 1).

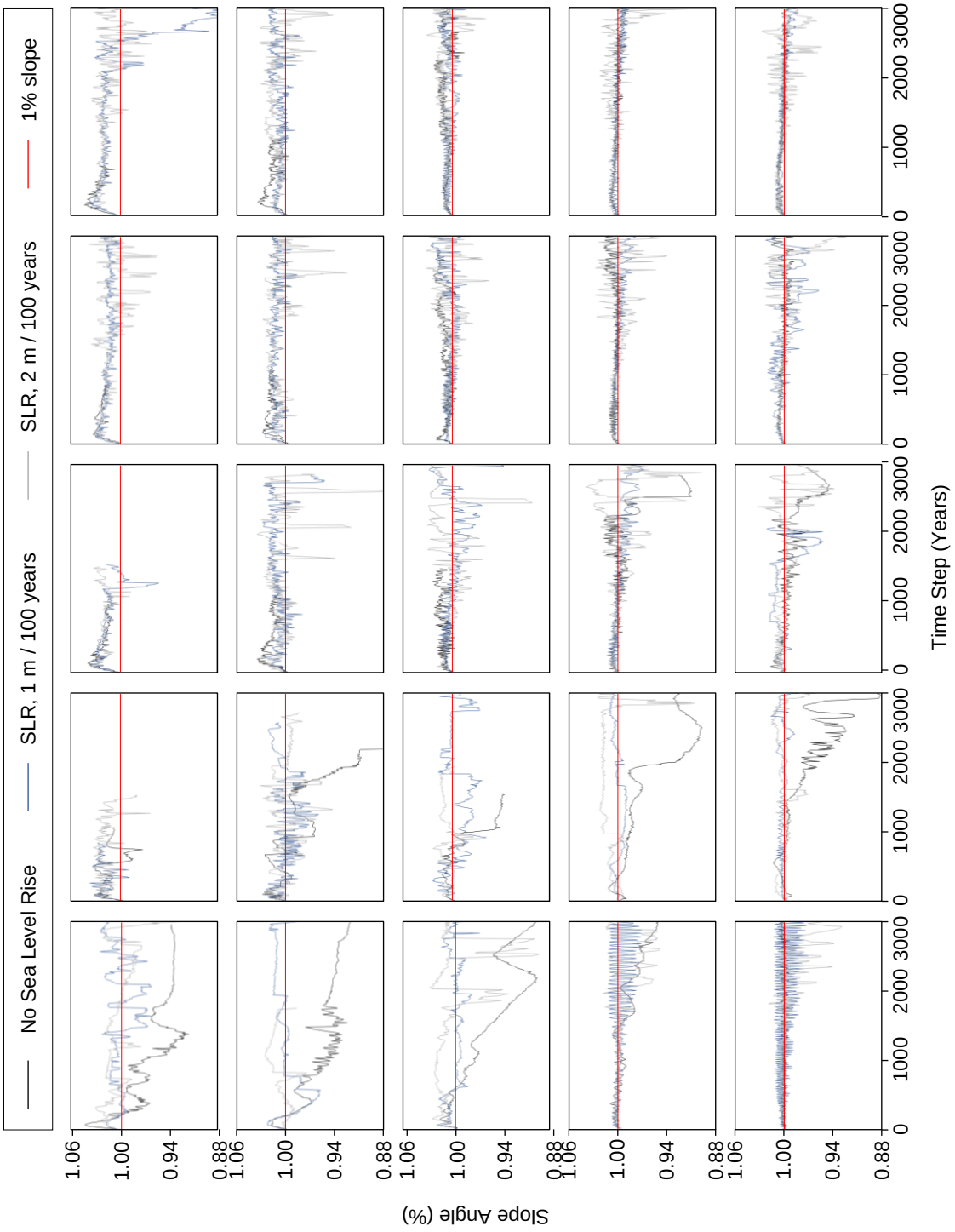

Figure 1 Ensemble plot showing the average cross-shore slope of the beach over the duration of the simulations, driven by twenty-five different wave climate conditions. Results are given from three sea level rise scenarios, including rise rates of 1 m and 2 m per 100 years as well as a no sea level rise state.

Appendix 9

Volume Stacks for CEM2D, with Sea Level Rise

Cited in Chapter 7

9.1 Introduction

In Chapter 7 volume stacks are used to depict the most dynamic regions of the coastal profile. These stacks show the change in sediment volume of each cell of the cross-section (where x = 30 km), recorded every 30 simulated years; this provides 100 datasets for each 3,000 year simulation. The volume stacks for each of the twenty-five simulations (with sea level rise) are given in this appendix (see Figure 1), to accompany the results presented in Chapter 6. The matrix in Figure 1 is organized with increasing proportional wave asymmetry (*A*) along the x-axis at increments of 0.1 and increasing proportion of high angle waves (*U*) along the y-axis, at increments of 0.05.

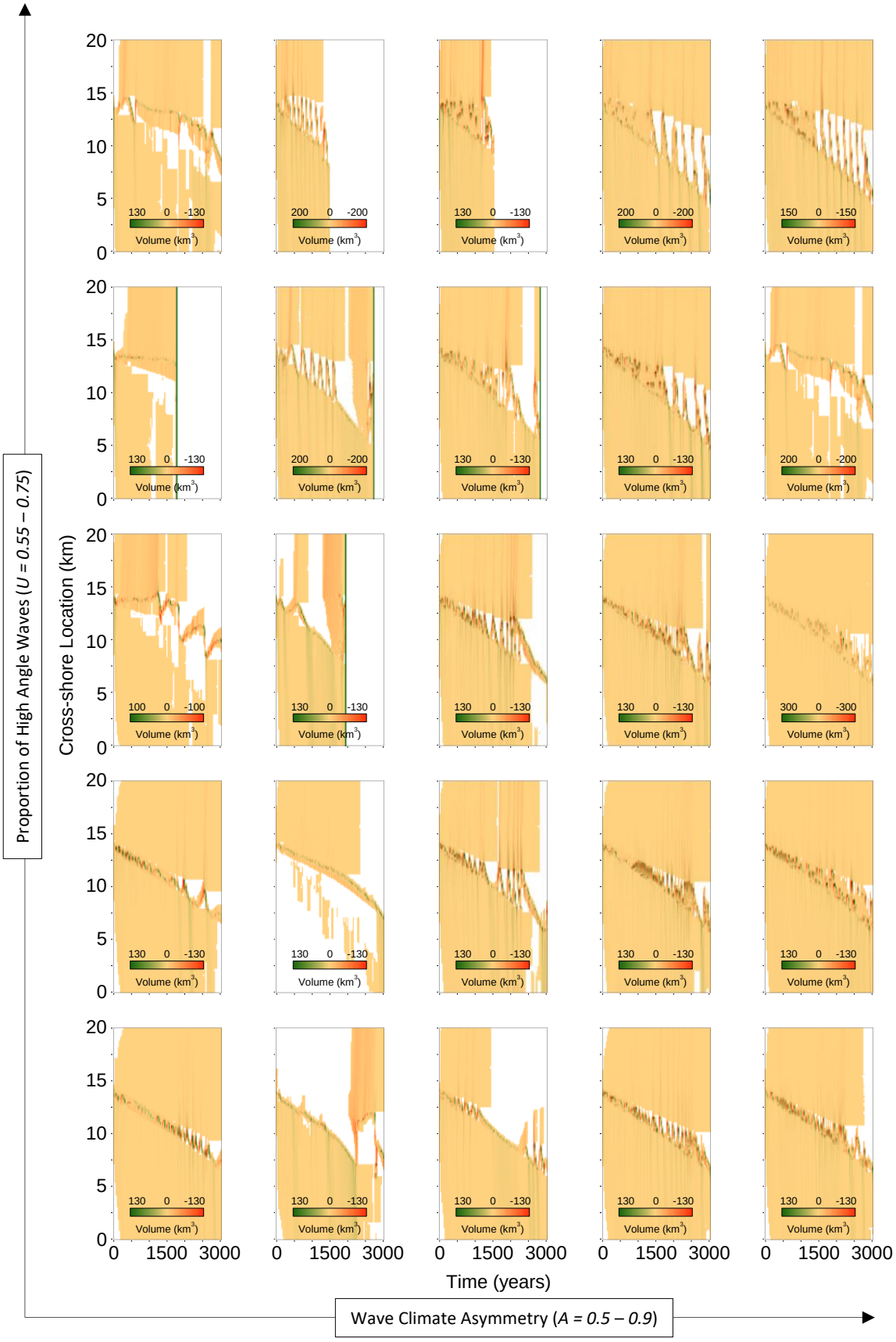

Figure 1 Volume stack of change in sediment volume (km3) cross-shore over 3,000 simulated years, recorded where x = 30 km every 30 simulated years for each wave climate condition.